NOTE TO USERS

Page(s) not included in the original manuscript are unavailable from the author or university. The manuscript was microfilmed as received.

352

This reproduction is the best copy available.

UMI

University of Alberta

Plane Turbulent Jets in Shallow Tailwater
and
Their Application to Energy Dissipation

by

Samir Ali Ead ©

A thesis submitted to the
Faculty of Graduate Studies and Research
in partial fulfillment of the requirements for the degree of
Doctor of Philosophy

in

Water Resources Engineering
Department of Civil and Environmental Engineering
Edmonton, Alberta
Spring 1999

National Library
of Canada

Acquisitions and
Bibliographic Services

395 Wellington Street
Ottawa ON K1A 0N4
Canada

Bibliothèque nationale
du Canada

Acquisitions et
services bibliographiques

395, rue Wellington
Ottawa ON K1A 0N4
Canada

Your file Votre référence

Our file Notre référence

The author has granted a non-exclusive licence allowing the National Library of Canada to reproduce, loan, distribute or sell copies of this thesis in microform, paper or electronic formats.

L'auteur a accordé une licence non exclusive permettant à la Bibliothèque nationale du Canada de reproduire, prêter, distribuer ou vendre des copies de cette thèse sous la forme de microfiche/film, de reproduction sur papier ou sur format électronique.

The author retains ownership of the copyright in this thesis. Neither the thesis nor substantial extracts from it may be printed or otherwise reproduced without the author's permission.

L'auteur conserve la propriété du droit d'auteur qui protège cette thèse. Ni la thèse ni des extraits substantiels de celle-ci ne doivent être imprimés ou autrement reproduits sans son autorisation.

0-612-39523-5

Canada

University of Alberta
Library Release Form

Name of Author:	Samir Ali Ead
Title of Thesis:	Plane Turbulent Jets in Shallow Tailwater and Their Application to Energy Dissipation
Degree:	Doctor of Philosophy
Year this Degree Granted:	1999

Permission is hereby granted to the University of Alberta library to reproduce single copies of this thesis and to lend or sell such copies for private, scholarly, or scientific research purposes only.

The author reserves all other publication and other rights in association with the copyright in the thesis, and except as herein before provided, neither the thesis nor any substantial portion thereof may be printed or otherwise reproduced in any material form whatever without the author's prior written permission.

Samir Ali Ead

110 RH, Michener Park
Edmonton, Alberta
Canada, T6H 4M4

Date: 18 Dec. 98

University of Alberta

Faculty of Graduate Studies and Research

The undersigned certify that they have read, and recommend to the Faculty of Graduate Studies and Research for acceptance, a thesis entitled "**Plane Turbulent Jets in Shallow Tailwater and Their Application to Energy Dissipation**" submitted by **Samir Ali Ead** in partial fulfillment of the requirements for the degree of **Doctor of Philosophy in Water Resources Engineering**.

Dr. N. Rajaratnam
(Supervisor)

Dr. P. M. Steffler

FE Hicks
Dr. F. E. Hicks

Dr. J. Leonard

Dr. S. J. Stanley

Dr. W. H. Hager
(External Examiner)

Date: 10th Dec1998

بِسْمِ اللهِ الرَّحْمَنِ الرَّحِيمِ

أَوَلَمْ يَرَ الَّذِينَ كَفَرُوا أَنَّ السَّمَاوَاتِ
وَالأَرْضَ كَانَتَا رَتْقًا فَفَتَقْنَاهُمَا وَجَعَلْنَا مِنَ الْمَاءِ
كُلَّ شَيْءٍ حَيٍّ أَفَلَا يُؤْمِنُونَ .

(سورة الأنبياء — آية ٣٠)

In the Name of Allah the Most Gracious, the Most Merciful

"Do not those who disbelieve see that the
heavens and the earth were joined together,
then We (God Almighty) tore them asunder?
And We made of water every living thing.
Will they not then believe?"

The Quran, 21:30

Abstract

This thesis is written in the paper format. It includes three contributions and this abstract presents a brief summary of these three contributions.

The first contribution introduces a new design concept for energy dissipation below flow regulators. Instead of using a single-leaf sluice gate, a double-leaf gate design has been suggested. The two leaves were arranged in such a way that a plane turbulent jet issued at an angle towards the water surface through the opening between the two leaves. The bottom leaf remains fixed while the top leaf (control leaf) is moved up and down to regulate the flow. By using this arrangement, the high velocity supercritical stream was deflected away from the bed to the water surface. Besides minimizing erosion, a lifting device of smaller capacity is adequate for operating the control leaf. Existing regulators can be modified by adding an upward sloping sill just below the gate. Twenty one experiments were conducted for different offset ratios, submergence ratios, width ratios, angles of inclination and Froude numbers. The flow patterns, velocity decay, momentum decay and bed shear stress were studied experimentally. The main characteristics of the deflected jet and the surface jet were also investigated and compared with those of free and submerged jumps, and surface jets. The new dissipator performs well in comparison with free and submerged jumps.

The second contribution presents a theoretical and experimental study of plane turbulent surface jets with finite tailwater depth. The momentum flux and the rise in the water surface elevation at the section where the surface jet attaches to the bed were evaluated theoretically. Nine experiments with different Froude numbers and offset ratios, were conducted to observe and quantify the growth of the surface jet, the decay of the velocity scale and the momentum flux and the variation of the volume flux. The

momentum flux of the forward flow in the surface jet was found to decay appreciably with the distance from the nozzle. This decay is shown to be due to the entrainment of the return flow which has negative momentum and also due to the increase in the tailwater depth, further away from the nozzle, which produces this return flow. This study has contributed to an understanding of the behavior of turbulent surface jets when the ambient fluid has a limited extent.

The third contribution presents a theoretical and laboratory study of plane turbulent wall jets in shallow tailwater. The momentum flux, in terms of that at the nozzle, was evaluated theoretically. A theoretical expression for the depression in the water surface elevation at the gate (housing the nozzle) was also obtained. An extensive set of experiments, with different Froude numbers and tailwater depth ratios, was conducted to observe and quantify the growth of the wall jet, the decay of the velocity scale and the momentum flux and the variation of the volume flux. Also, experiments were conducted to measure the bed shear stress and the length of the re-circulating flow region and to evaluate the drop in the water surface elevation at the wall. The depression in the water surface elevation in the vicinity of the wall produced return flow with negative momentum which resulted in a considerable decay of the momentum flux of the forward flow in the wall jet. Expressions describing the different flow characteristics of the wall jet, based on the experimental observations, were developed. The experimental and the corresponding theoretical results agreed quite well. This study has contributed to an understanding of the behavior of turbulent wall jets when the receiving water body has a limited extent.

ACKNOWLEDGMENTS

First and foremost I am thankful to Allah the Almighty (God) for his grace and Mercy.

I would like to express my sincere gratitude to my supervisor Dr. N. Rajaratnam for his patience, support and continuous encouragement throughout the course of this study. Dr. Rajaratnam devoted his time and effort to make this study a success. I consider it a matter of great privilege and a rare opportunity to work under his supervision.

I wish to extend my thanks to Dr. W. H. Hager, my external examiner, for his time and effort in reading this thesis thoroughly and making many helpful comments and suggestions.

Thanks are due to Mr. Sheldon Lovell for his help in the construction and maintenance of the experimental arrangement.

I would like to acknowledge the financial support provided by the Natural Sciences and Engineering Research Council of Canada through an operating grant to my supervisor.

Special thanks are to my wife, Shazy, and to my children, Ahmed, Maha and Rana, for their patience, encouragement and support during this study.

My thanks also go to my mother, brother and sisters for always being there.

Table of Contents

Chapter 1

Introduction 1
1.1 General 1
1.2 Organization of the Thesis 2
1.3 References 4

Chapter 2

Literature Review 5
2.1 Introduction 5
2.2 Energy Dissipators 5
2.3 Hydraulic Jump Stilling Basins 7
  2.3.1 Classical hydraulic jump 8
  2.3.2 Forced hydraulic jump 9
2.4 Plane Turbulent Jets in Deep Tailwater 11
  2.4.1 Plane turbulent free jets 11
  2.4.2 Plane turbulent surface jets 14
  2.4.3 Plane turbulent wall jets 16
2.5 Turbulent Jets in Close Proximity of Boundaries 21
2.6 References 32

Chapter 3

Experimental Arrangement and Instrumentation Techniques 39
3.1 Introduction 39
3.2 Experimental Arrangement 39
  3.2.1 The flume 39
  3.2.2 Pressure transducers 40
  3.2.3 Data acquisition system 41
3.3 Velocity Measurements 42
  3.3.1 Prandtl tube 42
  3.3.2 Pitch probe 43
3.4 Bed Shear Stress Measurements 46
  3.4.1 Introduction 46
  3.4.2 Preston tube technique 48
3.5 The Experiments 49

3.6 Experimental Errors and Uncertainties 49
  3.6.1 Introduction and basic concepts 49
  3.6.2 Estimate of uncertainty 53
3.7 References 58

Chapter 4
A Double-Leaf Gate for Energy Dissipation Below Regulators 66
4.1 Introduction 66
4.2 Dimensional Analysis 67
4.3 Experimental Study 69
  4.3.1 Experimental arrangement 69
  4.3.2 Experiments 70
4.4 Experimental Results and Analysis 71
  4.4.1 Flow patterns 71
    4.4.1.1 Width ratio w/W = 1.00 and θ = 30 degrees 72
    4.4.1.2 Width ratio w/W = 1.00 and θ = 10 degrees 74
    4.4.1.3 Width ratio (w/W) < 1.00 and θ = 10 degrees 75
    4.4.1.4 Hysteresis effects 76
  4.4.2 Velocity profiles 77
  4.4.3 Reverse flow 79
  4.4.4 Velocity decay 80
  4.4.5 Inclined jet 83
  4.4.6 Surface jet 85
  4.4.7 Surface-jet discharge 86
  4.4.8 Surface-jet momentum flux 87
  4.4.9 Bed shear stress 88
    4.4.9.1 Pattern A 89
    4.4.9.2 Pattern B 90
    4.4.9.3 Pattern C 91
4.5 Conclusions and Recommendations 92
4.6 References 94

Chapter 5
Plane Turbulent Surface Jets in Shallow Tailwater 161
5.1 Introduction 161
5.2 Theoretical Considerations 162
5.3 Dimensional Analysis 168
5.4 Experimental Study 169
    5.4.1 Experimental arrangement 169
    5.4.2 Experiments 170
5.5 Experimental Results and Analysis 170
    5.5.1 Eddy length 170
    5.5.2 Velocity profiles 172
    5.5.3 Reverse flow 172
    5.5.4 Surface jet 173
    5.5.5 Velocity and length scales 174
    5.5.6 Surface-jet discharge 176
    5.5.7 Surface-jet momentum flux 178
5.6 Engineering Significance 179
5.7 Conclusions 181
5.8 References 182

Chapter 6
Plane Turbulent Wall Jets in Shallow Tailwater 229
6.1 Introduction 229
6.2 Theoretical Considerations 231
    6.2.1 Neglecting the bed shear stress 232
    6.2.2 Considering the bed shear stress 234
6.3 Dimensional Analysis 238
6.4 Experimental Study 239
    6.4.1 Experimental arrangement 239
    6.4.2 Experiments 240
6.5 Experimental Results and Analysis 241
    6.5.1 Eddy length 241
    6.5.2 Velocity profiles 242
    6.5.3 Wall jet 243
    6.5.4 Velocity and length scales 244
    6.5.5 Wall-jet discharge 246

6.5.6 Bed shear stress........ 248
6.5.7 Wall-jet momentum flux........ 249
6.6 Conclusions........ 251
6.7 References........ 251

Chapter 7

Conclusions and Recommendations........ 293

Appendix

1. A Double Leaf Gate for Energy Dissipation Below Regulators 298
1.1 Velocity Measurements along Vertical Sections at x-stations........ 298
1.2 Velocity Measurements for the Inclined Jet........ 310
1.3 Bed Shear Stress Measurements........ 315
1.4 Variation of Velocity Scale, Length Scale, Jet Discharge and Momentum Flux with Distance........ 318
2. Plane Turbulent Surface Jets in Shallow Tailwater........ 334
2.1 Velocity Measurements along Vertical Sections at x-stations........ 334
2.2 Variation of Velocity Scale, Length Scale, Jet Discharge and Momentum Flux with Distance........ 343
3. Plane Turbulent wall Jets in Shallow Tailwater........ 353
3.1 Velocity Measurements along Vertical Sections at x-stations........ 353
3.2 Bed Shear Stress Measurements........ 359
3.3 Variation of Velocity Scale, Length Scale, Jet Discharge and Momentum Flux with Distance........ 360

List of Tables

Table	Title	Page
3.1	Explicit equations for Patel's calibration curves for Preston tube.............	63
3.2	Primary details of experiments of a double-leaf gate (series A)..............	64
3.3	Primary details of experiments of the plane turbulent surface jets...........	65
3.4	Primary details of experiments of the plane turbulent wall jets (series A)..	65
4.1	Primary details of experiments (series A)..	97
5.1	Primary details of experiments	184
6.1	Primary details of experiments (series A)......................................	254

List of Figures

Figure **Title** **Page**

2.1 Definition sketch of plane turbulent free jets.. 38

2.2 Definition sketch of plane turbulent surface jets.. 38

2.3 Definition sketch of plane turbulent wall jets.. 38

3.1 Experimental flume.. 59

3.2 Typical calibration of pressure transducers.. 60

3.3 Prandtl tube.. 60

3.4 Pitch probe.. 61

3.5 Calibration curves for the pitch probe.. 62

4.1 Definition sketch of double-leaf gate dissipator.. 98

4.2 Modification to existing regulators.. 98

4.3 Experimental flume.. 99

4.4 Pitch probe.. 100

4.5 Prandtl tube.. 101

4.6(a-c) (a) Pattern A.. 102

(b) Pattern B.. 103

(c) Pattern C.. 104

4.7(a-c) Flow patterns A, B & C for double-leaf gate dissipator.. 105

4.8(a-d) Boundaries of the flow patterns

(a) $\theta=30^\circ$, $Z_o/b_o=30.00$.. 106

(b) $\theta=30^\circ$, $Z_o/b_o=13.50$.. 106

(c) $\theta=30^\circ$, $Z_o/b_o=6.75$.. 107

(d) $\theta=10^\circ$, $Z_o/b_o=13.50$.. 107

4.9 Jet trajectories.. 108

4.10 Oscillating zones.. 109

4.11 Width ratio w/W=0.50.. 110

4.12(a-n) (a) Typical velocity profiles for pattern C 111

(b) Typical velocity profiles for pattern B 111

(c-d)Typical velocity profiles for pattern A 112

(e)Typical velocity profiles for pattern AB.. 113

(f)Typical velocity profiles for pattern A.. 113

(g-h) Typical velocity profiles for pattern A.. 114

(i-j) Typical velocity profiles for pattern A 115
(k-l) Typical velocity profiles for pattern A 116
(m-n) Typical velocity profiles for pattern A 117
4.13 Reverse flow near the bed (x=2m) 118
4.14(a-d) (a-b) Variation of the depth-averaged reverse velocity with distance 119
(c-d) Variation of the depth-averaged reverse velocity with distance 120
4.15(a-n) (a-b) Maximum velocity decay in flow pattern A 121
(c-d) Maximum velocity decay in flow pattern A 122
(e-f) Maximum velocity decay in flow pattern A 123
(g-h) Maximum velocity decay in flow pattern A 124
(i-j) Maximum velocity decay in flow pattern A 125
(k-l) Maximum velocity decay in flow patterns A, B & C 126
(m-n) Maximum velocity decay in flow patterns A & AB 127
4.16 Consolidated plot for all the maximum-velocity decay profiles in flow pattern A 128
4.17 Comparison between the double-leaf gate and the baffle wall dissipators 129
4.18(a-b) Comparison between the double-leaf gate, the free and the submerged jumps 130
4.19(a-b) Comparison between the double-leaf gate, the free and the submerged jumps 131
4.20 Locus of the maximum velocity 132
4.21(a-j) (a-b) Velocity distributions for the inclined jet (Expt. 3)
(a) Typical velocity profiles 133
(b) Similarity profile 133
(c-d) Velocity distributions for the inclined jet (Expt. 9)
(c) Typical velocity profiles 134
(d) Similarity profile 134
(e-f) Velocity distributions for the inclined jet (Expt. 12)
(e) Typical velocity profiles 135
(f) Similarity profile 135
(g-h) Velocity distributions for the inclined jet (Expt. 14)
(g) Typical velocity profiles 136
(h) Similarity profile 136

(i-j) Velocity distributions for the inclined jet (Expt. 16)
(i) Typical velocity profiles.. 137
(j) Similarity profile.. 137
4.22 Consolidated non-dimensional plot for the velocity distribution in the inclined jet.. 138
4.23 Maximum-velocity decay with distance along the inclined jet...... 139
4.24(a-ab) (a-b) Velocity distribution in surface jet (Expt. 2)
(a) Velocity profiles.. 140
(b) Similarity profile.. 140
(c-d) Velocity distribution in surface jet (Expt. 3)
(c) Velocity profiles.. 141
(d) Similarity profile.. 141
(e-f) Velocity distribution in surface jet (Expt. 4)
(e) Velocity profiles.. 142
(f) Similarity profile.. 142
(g-h) Velocity distribution in surface jet (Expt. 8)
(g) Velocity profiles.. 143
(h) Similarity profile.. 143
(i-j) Velocity distribution in surface jet (Expt. 9)
(i) Velocity profiles.. 144
(j) Similarity profile.. 144
(k-l) Velocity distribution in surface jet (Expt. 12)
(k) Velocity profiles.. 145
(l) Similarity profile.. 145
(m-n) Velocity distribution in surface jet (Expt. 14)
(m) Velocity profiles.. 146
(n) Similarity profile.. 146
(o-p) Velocity distribution in surface jet (Expt. 15)
(o) Velocity profiles.. 147
(p) Similarity profile.. 147
(q-r) Velocity distribution in surface jet (Expt. 16)
(q) Velocity profiles.. 148
(r) Similarity profile.. 148
(s-t) Velocity distribution in surface jet (Expt. 17)
(s) Velocity profiles.. 149
(t) Similarity profile.. 149

	(u-v) Velocity distribution in surface jet (Expt. 18)	
	(u) Velocity profiles	150
	(v) Similarity profile	150
	(w-x) Velocity distribution in surface jet (Expt. 19)	
	(w) Velocity profiles	151
	(x) Similarity profile	151
	(y-z) Velocity distribution in surface jet (Expt. 20)	
	(y) Velocity profiles	152
	(z) Similarity profile	152
	(aa-ab) Velocity distribution in surface jet (Expt. 21)	
	(aa) Velocity profiles	153
	(ab) Similarity profile	153
4.25	Consolidated non-dimensional plot for the velocity distribution in the surface jet	154
4.26(a-b)	Growth rate of the surface-jet half-width	
	(a) b_o is the length scale	155
	(b) b_{so} is the length scale	155
4.27(a-b)	Variation of the surface-jet discharge, Q/Q_o, with distance, x/b_o	
	(a) Effect of the offset ratio Z_o/b_o	156
	(b) Effect of the inclination angle θ and the width ratio w/W	156
4.28(a-b)	Variation of the surface-jet momentum flux, M_{-}/M_o, with distance, x/b_o	
	(a) Effect of the offset ratio Z_o/b_o	157
	(b) Effect of the inclination angle θ and the width ratio w/W	157
4.29(a-c)	Shear stress distribution for pattern A	
	(a) Variation of shear stress with distance	158
	(b) Similarity profile	158
	(c) Study of shear stress and length scales	158
4.30(a-b)	Shear stress distribution for pattern B	159
4.31(a-d)	(a-b) Shear stress distributions for pattern C	160
	(c-d) Study of shear stress and length scales for pattern C	160
5.1(a-b)	(a) Definition sketch	185
	(b) Flow pattern	185
5.2	Water surface elevation ($F_o = 4.0$, $Z_o/b_o=10$)	186
5.3	Variation of (ϕ) with the offset ratio (η)	187

5.4 Variation of (θ) with the offset ratio (η) for different Froude numbers........ 184
5.5 Variation of (M_∞/M_o) with the offset ratio (η) for different Froude numbers........ 189
5.6 Variation of (F_p/M_o) with the offset ratio (η) for different Froude numbers........ 190
5.7 Experimental flume........ 191
5.8 Streamlined entrance to produce an uniform jet of thickness b_o.... 192
5.9 False floor to produce an offset distance of Z_o........ 193
5.10 Prandtl tube........ 194
5.11(a-d) (a) Surface jet ($F_o = 7.20$, $Z_o/b_o = 100$)........ 195
(b) Surface jet ($F_o = 4.80$, $Z_o/b_o = 50$)........ 195
(c) Surface jet ($F_o = 4.80$, $Z_o/b_o = 25$)........ 196
(d) Surface jet ($F_o = 4.00$, $Z_o/b_o = 10$)........ 196
5.12(a-i) (a) Typical velocity profiles (Expt. 1)........ 197
(b) Typical velocity profiles (Expt. 2)........ 198
(c) Typical velocity profiles (Expt. 3)........ 199
(d) Typical velocity profiles (Expt. 4)........ 200
(e) Typical velocity profiles (Expt. 5)........ 201
(f) Typical velocity profiles (Expt. 6)........ 202
(g) Typical velocity profiles (Expt. 7)........ 203
(h) Typical velocity profiles (Expt. 8)........ 204
(i) Typical velocity profiles (Expt. 9)........ 205
5.13 Variation of the eddy length with the offset ratio........ 206
5.14(a-b) (a) Variation of the depth-averaged reverse velocity with distance. 207
(b) Effect of the offset ratio on the magnitude and the location of the maximum reverse velocity........ 208
5.15(a-b) Velocity distribution in partially-developed flow ($x/b_o = 6$)
(a) Velocity profiles........ 209
(b) Similarity profile........ 209
5.16(a-r) (a-b) Velocity distribution in fully-developed flow (Expt. 1)
(a) Velocity profiles........ 210
(b) Similarity profile........ 210
(c-d) Velocity distribution in fully-developed flow (Expt. 2)

(c) Velocity profiles 211
(d) Similarity profile 211
(e-f) Velocity distribution in fully-developed flow (Expt. 3)
(e) Velocity profiles 212
(f) Similarity profile 212
(g-h) Velocity distribution in fully-developed flow (Expt. 4)
(g) Velocity profiles 213
(h) Similarity profile 213
(i-j) Velocity distribution in fully-developed flow (Expt. 5)
(i) Velocity profiles 214
(j) Similarity profile 214
(k-l) Velocity distribution in fully-developed flow (Expt. 6)
(k) Velocity profiles 215
(l) Similarity profile 215
(m-n) Velocity distribution in fully-developed flow (Expt. 7)
(m) Velocity profiles 216
(n) Similarity profile 216
(o-p) Velocity distribution in fully-developed flow (Expt. 8)
(o) Velocity profiles 217
(p) Similarity profile 217
(q-r) Velocity distribution in fully-developed flow (Expt. 9)
(q) Velocity profiles 218
(r) Similarity profile 218
5.17 Consolidated non-dimensional plot for the velocity distribution in the surface jet 219
5.18(a-d) (a) Variation of the maximum jet velocity, u_m, with distance 220
(b) Variation of u_m/U_o with x/b_o 221
(c) Variation of $(U_o/U_m)^2$ with x/b_o 222
(d) Effect of the offset ratio on the breakdown distance 223
5.19 Variation of the jet half-width with distance 224
5.20(a-c) (a) Variation of the surface jet discharge with distance 225
(b-c) Effect of Z_o/b_o on the magnitude and the location of the maximum discharge 226
5.21 Variation of the surface jet momentum flux with distance 227
5.22 Modified regulators 228
5.23 Modified spillways 228

6.1(a-c)	(a) Definition sketch	255
	(b) Flow pattern	255
	(c) Typical velocity distribution	255
6.2	Water surface elevation ($F_o = 8$, $y_t/b_o = 25$)	256
6.3(a-b)	(a) Variation of θ with η for various Froude numbers F_o, with and without shear stress	257
	(b) Variation of θ with η for various shear coefficients ε	258
6.4 (a-b)	(a) Variation of η_f with F_o for various values of ε	259
	(b) Variation of η_f with ε for various values of F_o	260
6.5	Variation of (M_{-}/M_o) and ($F_{\delta w}/ M_o$) with (η)	261
6.6	Experimental flume	262
6.7	Streamlined entrance to produce an uniform jet of thickness b_o	263
6.8	Prandtl tube	264
6.9(a-d)	(a) Wall jet ($F_o = 8$, $y_t/b_o = 25$)	265
	(b) Wall jet ($F_o = 8$, $y_t/b_o = 35$)	265
	(c) Wall jet ($F_o = 8$, $y_t/b_o = 40$)	266
	(d) Wall jet ($F_o = 8$, $y_t/b_o = 50$)	266
6.10	Variation of the eddy length, L_e/b_o, with (η-η_f)	267
6.11(a-f)	(a) Typical velocity fields of wall jets in shallow tail waters (Expt. 1)	268
	(b) Typical velocity fields of wall jets in shallow tail waters (Expt. 2)	269
	(c) Typical velocity fields of wall jets in shallow tail waters (Expt. 3)	270
	(d) Typical velocity fields of wall jets in shallow tail waters (Expt. 4)	271
	(e) Typical velocity fields of wall jets in shallow tail waters (Expt. 5)	272
	(f) Typical velocity fields of wall jets in shallow tail waters (Expt. 6)	273
6.12(a-b)	Velocity distribution in partially-developed flow ($x/b_o = 6$)	
	(a) Velocity profiles	274
	(b) Similarity profile	274

6.13(a-l) (a-b) Velocity distribution in fully-developed flow (Expt. 1)
(a) Velocity profiles........ 275
(b) Similarity profile........ 275
(c-d) Velocity distribution in fully-developed flow (Expt. 2)
(c) Velocity profiles........ 276
(d) Similarity profile........ 276
(e-f) Velocity distribution in fully--developed flow (Expt. 3)
(e) Velocity profiles........ 277
(f) Similarity profile........ 277
(g-h) Velocity distribution in fully-developed flow (Expt. 4)
(g) Velocity profiles........ 278
(h) Similarity profile........ 278
(i-j) Velocity distribution in fully-developed flow (Expt. 5)
(i) Velocity profiles........ 279
(j) Similarity profile........ 279
(k-l) Velocity distribution in fully-developed flow (Expt. 6)
(k) Velocity profiles........ 280
(l) Similarity profile........ 280
6.14 Consolidated non-dimensional plot for the velocity distribution in the wall jet........ 281
6.15(a-d) (a) Variation of the maximum jet velocity, u_m, with distance........ 282
(b) Variation of u_m/U_o with x/b_o........ 283
(c) Variation of $(U_o/U_m)^2$ with x/b_o........ 284
(d) Effect of the tailwater depth ratio on the breakdown distance........ 285
6.16 Variation of the jet half-width with distance........ 286
6.17(a-c) (a) Variation of the wall jet discharge with distance........ 287
(b-c) Effect of y_t/b_o on the magnitude and the location of the maximum discharge........ 288
6.18(a-d) (a-b) Variation of the bed shear stress with distance........ 289
(c-d) Variation of the bed shear stress with distance........ 290
6.19 Determination of the shear force coefficient ε........ 291
6.20 Variation of the wall jet momentum flux with distance........ 292

Notations[*]

Symbol	Description
A	flow pattern [4], function of the offset ratio [5], function of the tailwater depth ratio [6];
A', B', C'	functions of the offset ratio [5], functions of the tailwater depth ratio [6];
AB	flow pattern [4];
B	flow pattern [4], function of the offset ratio [5], constant equal to 0.82 [6];
b	length scale [2,4,5,6];
b_A, b_B, b_C	shear stress length scales [4];
b_o	slot width [2,3,4,5,6];
b_s	length scale for surface jet [4];
b_τ	shear stress length scale [6];
b_u, b_l	length scales for inclined jet [4];
C	flow pattern [4], function of the offset ratio [5];
C_1, C_2, C_3	constants [2];
C_f	skin friction coefficient = $\tau_o/(\rho U_o^2/2)$ [2];
C_{fm}	skin friction coefficient = $\tau_m/(\rho U_o^2/2)$ [4];
C_{fo}	skin friction coefficient = $\tau/(\rho U_o^2/2)$ [6];
d	external diameter of the Preston tube [3];
Δp	dynamic pressure [3];
E	kinetic energy of the flow at any section [2];

---

[*] The number in square brackets [ ] denote relevant chapter number

E_o	the value of E at the slot [2];
F_1	supercritical Froude number in hydraulic jump [2];
$F_{\delta w}$	loss in the hydrostatic pressure force at the wall [6];
F_o	supercritical Froude number at the slot [3,4,5,6];
$F_{p\infty}$	maximum increase of the hydrostatic pressure force [5];
F_τ	integrated bed shear stress, per unit width, from the slot till the jet surfaces [6];
$F_{\tau x}$	integrated bed shear stress, per unit width, over a distance x from the slot [6];
g	acceleration due to gravity [2,3,4,5,6];
h_1, h_2, h_3	piezometric pressure heads sensed by the pitch probe tubes [3];
h_{c1}	lower critical baffle height [2];
h_{c2}	upper critical baffle height [2];
h_o	static piezometric pressure head [3];
h_s	strip height [5];
k_1,k_2,k_3,k_4,k_5	calibration coefficients that are functions of the pitch or yaw angle θ [3];
L	the horizontal distance from the gate to the point where the velocity is $0.5U_o$ [4];
L_e	length of recirculating flow region (eddy length) [5,6];
l	distance measured across the inclined jet from the point of u_m [4];
M	momentum flux at a distance x from the wall [2], surface jet momentum flux at a distance x from the wall [4,5], wall jet momentum flux at a distance x from the gate [6];
M_∞	momentum flux at the section where the jet occupies the whole depth [5,6];

M_o	jet momentum flux at the slot [2,4,5,6];
M_s	momentum flux through a single strip of the forward flow [5];
m	constant equals to $Cot(\theta_o/2)$ [2];
p	mean pressure at any point [2];
Q	jet discharge at a distance x measured from the slot [2], discharge [3], surface jet discharge per unit width [5], wall jet discharge per unit width [6];
Q_m	maximum value of Q [5,6];
Q_o	value of Q at the slot [2,5,6];
Q_s	volume flux through a single strip of the forward flow [5];
q	jet discharge per unit width [2,4];
q_o	value of q at the slot [4];
R	Reynolds number [2,4,5,6], hydraulic radius [3], Result [3];
S	channel slope [3], submergence ratio = $[(y_t - Z_o)/h_o]$ [4], submergence factor = $[(y_t - y_2)/y_2]$ [6];
U	mean velocity [3];
U_1, U_2	mean velocities at depths of y_1 and y_2 [3];
U_o	velocity issuing from the slot [2,3,4,5,6];
$-\overline{uv}(y)$	Reynolds stress [3];
u	time-averaged velocity at any point [2,3,4,5,6];
u_*	shear velocity [2,3];
u_1, u_2	upper and lower velocities of a single strip in the forward flow [5];
u_m	maximum value of u [2,4,5,6];
u_r	depth-averaged reverse velocity [4,5];
u_{rm}	maximum value of u_r [5];

V	velocity vector [3], uniform velocity of the flow when the jet occupies the whole depth [5,6];
V_1	the average velocity at the toe of the hydraulic jump [2];
v	time-averaged velocity in y-direction [2];
v_e	entrainment velocity [2];
W	flume width [3,4,5,6];
W_R	uncertainty interval [3];
w	opening width [4];
$\bar{x}$	longitudinal distance measured from the slot [2];
$\bar{x}_o$	length of the potential core [2];
x	longitudinal distance measured from the virtual origin [2], longitudinal distance measured from the gate [4,5,6];
x_{M1}	the distance after which the momentum flux starts to decay [6];
x_{M2}	the distance at which the momentum flux approaches zero [6];
x_o	distance from the baffle front to the gate [2], longitudinal distance to the point of maximum surface velocity [4], the distance at which the velocity and length scales breakdown [5,6];
x_{oA}, x_{oB}, x_{oC}	characteristic lengths for shear stress [4];
x_{Qm}	longitudinal distance at which the surface-jet discharge is maximum [5], distance at which the wall jet discharge is maximum [6];
x_{rm}	the distance at which the maximum reverse velocity occurs [5];
y	coordinates [2], height above the bed [3,4,5,6];
y_1	initial depth of the hydraulic jump [2], vertical distance above the bed [3];
y_2	subcritical sequent depth of the hydraulic jump [2,6], vertical distance above the bed [3];

y_o	depth of flow [3,4,5], depth of flow (equal to $Z_o+b_o+\delta_x$) [5];
y_t	tailwater depth [2,3,4,5,6];
Z_o	height of the lower edge of the slot above the bed [2,3,4,5];
α_e	entrainment coefficient [2];
δ	boundary layer thickness [2,6];
δ_m	maximum value of δ_x [5];
δ_w	drop in the water surface elevation at the wall [6];
δ_x	increase of water surface elevation at a distance x from the gate [5];
ε	function of the offset ratio [5], shear force coefficient at a longitudinal distance L_e from the slot = F_τ/M_o [6];
ε_x	shear force coefficient at a longitudinal distance x from the slot = $F_{\tau x}/M_o$ [6];
ϕ	function of the offset ratio and the Froude number [5], function of the shear force coefficient and the Froude number [6];
γ	specific weight of water [5,6];
η	y/b [2], offset ratio = Z_o/b_o [5], tailwater depth ratio = y_t/b_o [6];
η_f	the value of η in the free hydraulic jump [6];
κ	Von Karman constant [3];
μ	dynamic viscosity [4,5,6];
ν	kinematic viscosity = μ/ρ [2,3,5,6];

θ	pitch or yaw angle [3], deflection angle [4], δ_J/b_o [5], δ_w/b_o [6];
θ_f	the value of θ in the free hydraulic jump = $(\eta_f - 1)$ [6];
θ_w	the angle the wall makes with the jet axis [2];
ρ	density of water [2,3,4,5,6];
τ	shear stress at depth y above the bed [3], bed shear stress [4,6];
τ_l	laminar shear stress [2];
τ_m	maximum value of τ [4,6];
τ_{md} & τ_{mu}	maximum value of t for pattern C [4];
τ_o	wall shear stress [2,3];
τ_t	turbulent shear stress [2];

Chapter 1

Introduction

1.1 General

Retaining structures (like dams and regulators) are hydraulic structures built on water ways to control large volumes of water under high pressures. The release of the retained water (over spillways, through outlet conduits or gates) is associated with tremendous amount of energy at the base or downstream of these structures. The resulting flow usually takes the form of a turbulent jet. This turbulent jet can be plane or axisymmetric depending on the shape of the outlet. Also, the jet can be a free jet, surface jet or wall jet depending on the relative locations of the rigid boundaries and the free surface with respect to the jet. The tremendous amount of kinetic energy carried by turbulent jets can cause erosion in tailwater channels, partial or complete failure of hydraulic structures, generation of tailwater waves and scour. Energy dissipators are devices used to protect the tailwater channel by dissipating the excess hydraulic energy in the turbulent jets. A comprehensive understanding of the behavior of a turbulent jet in a particular problem enables the engineer to design a suitable energy dissipator for such problem.

Tollmien (1926) and Görtler (1942) performed the first theoretical studies on turbulent jets while Förthmann (1936) performed the first experimental work (Abramovich, 1963). Since then, a tremendous amount of work on turbulent jets has been published. The two books written by Abramovich (1963) and Rajaratnam (1976) present an extensive treatment of turbulent jets.

Although the available knowledge on turbulent jets is claimed to be comprehensive, there are many practical problems in hydraulic engineering in which the behavior of turbulent jets is still not well understood. This thesis presents three contributions on the behavior of plane turbulent jets in shallow tailwater.

1.2 Organization of the Thesis

In this thesis, the results of theoretical and experimental studies on three practical problems dealing with the behavior of plane turbulent jets in shallow tailwater are presented. Each piece of work is introduced in a separate chapter. Following is a brief introduction to each chapter.

Chapter 2 presents a review of previous theoretical and experimental investigations related to the present study. This chapter starts with an introduction followed by a brief description of the different types of energy dissipators including the classical and the forced hydraulic jump stilling basins. It also introduces previous studies on plane turbulent jets in tailwaters of unlimited extent. Also, the available studies on turbulent jets issuing in the close proximity of boundaries are reviewed.

Chapter 3 describes the experimental arrangement, instrumentation and techniques used in the present study. Primary details of experiments are given. A brief review of experimental errors and uncertainties is also presented.

Chapter 4 presents the results of an experimental study on a double-leaf gate as an energy dissipator. The main objective of this study was to introduce a simple and efficient energy dissipator downstream of flow regulators. Section 4.1 is an introduction for this chapter. In the introduction, the disadvantages of the hydraulic jump stilling basins are mentioned. Also, a brief description of the new model is explained. In section 4.2, the main non-dimensional parameters affecting the flow characteristics in the double-leaf gate model are figured out using dimensional analysis.

The details of the experiments are given in section 4.3. The main characteristics of the inclined jet, the surface jet and the reverse flow are presented in section 4.4. Conclusions and recommendations for future research work are given in section 4.5.

Chapter 5 presents a theoretical and an experimental study of plane turbulent surface jets in shallow tailwater. The main objective of this study was to show that the behavior of plane turbulent surface jets in shallow tailwater is significantly different than that in deep tailwater. The reverse pressure gradient associated with the surface jet causes more than 90% of the momentum flux to decay. Section 5.1 is an introduction with a brief review of previous studies. Section 5.2 shows a theoretical approach where the momentum loss and piezometric-pressure increase are evaluated. Dimensional considerations and experimental arrangement are presented in sections 5.3 and 5.4 respectively. In section 5.5, the eddy length, similarity of the velocity profiles, breakdown in the velocity and length scales, the surface jet discharge variation and decay of momentum flux, are evaluated experimentally. The conclusions of this study are formulated in section 5.6.

Chapter 6 presents a theoretical and an experimental analysis of the effects of the tailwater shallowness on the different characteristics of the plane turbulent wall jet. Section 6.1 introduces, in brief, some of the previous studies in which the momentum flux was assumed preserved. Experimental studies showing momentum decay in turbulent jets out of a wall and in turbulent jets in channels of limited depth, are also presented in the same section. Section 6.2, theoretical approach, started with an explanation of the difference between the surface and plane turbulent jets regarding the formation of the tailwater depth in each of the two problems. The tailwater depth in the surface jet is dependent on the jet characteristics. In plane jets, the tailwater depth is an independent variable. Formulations for the momentum decay and the water surface depression at the gate, with and without the inclusion of bed shear stress, are shown in the same section. Dimensional analysis, experimental arrangement, experimental results and analysis and conclusions are shown in sections 6.3 to 6.6 respectively.

Chapter 7 presents a general discussion on the three contributions presented in Chapters 4 to 6. For each of these contributions, a brief summary and suggestions for future research are made.

1.3 References

Abramovich, G. N. (1963). "The theory of turbulent jets." English translation published by M.I.T. Press, Massachusetts, 671p.

Förthmann, E. (1936). "Turbulent jet expansion." English translation NACA TM-789. (Original Paper in German, 1934. Ing. Archiv., 5).

Görtler, H. (1942). "Berechnung von Aufgaben der freien Turbulenz auf Grund eines neuen Näherungsansatzes. ZAMM, 22, pp. 244-254.

Rajaratnam, N. (1976). Turbulent Jets. Elsevier Publishing Co., The Netherlands, 304p.

Tollmien, W. (1926). "Berechnung turbulenter Ausbreitungsvorgänge." Z. angew. Math. Mech. 6, pp. 468-478; [English Transl. NACA TM 1085 (1945)].

Chapter 2

Literature Review

2.1 Introduction

This chapter contains four sections. In section 2.2, energy dissipators are defined and classified and the way the kinetic energy is dissipated, in each of them, is introduced in brief. Advantages and disadvantages of the hydraulic jump stilling basins are discussed in section 2.3. Sections 2.2 and 2.3 help in the understanding and evaluation of the double-leaf gate energy dissipator introduced in chapter 4. In section 2.4, plane turbulent jets in deep tailwater are presented. Equations of motion and empirical relationships, based on experimental observations, are described. Section 2.5 shows experimental observations and results for turbulent jets issuing in the close proximity of boundaries. Sections 2.4 and 2.5 are prerequisite for the understanding and evaluation of the present study (mainly chapters 5 & 6).

2.2 Energy Dissipators

Energy dissipators are devices used to dissipate kinetic energy and are used in places where excess kinetic energy could cause serious damage such as erosion, partial or complete failure of hydraulic structures and generation of tailwater waves. Vischer and Hager (1995) mentioned that the process of energy dissipation in hydraulic engineering can be usefully classified into two cases. Firstly, a particle of water within a water current where energy dissipation occurs because of the energy dissipating eddies which are generated in zones of large velocity gradients. They added that, to achieve a considerable loss of energy, it is important to create high turbulence zones. Secondly, a particle of water moving in a stream of air where energy dissipation occurs due to the air resistance exerted on the drop of water. The energy loss is large if the water drop is small and the relative velocity between the drop and the ambient air is large. Following is a brief description of the different types of energy dissipators as classified by Vischer and Hager (1995).

Energy dissipation by expansion and deflection: In sudden expansions an impact loss occurs when a faster current impacts with a slower one, inducing separation zone/s of large velocity gradients. Sudden expansions are used in most of the energy dissipators as the outflow velocity, in such structures, is much less than the inflow velocity. Classical hydraulic jumps and forced hydraulic jumps are good examples of this type of dissipators.

Energy dissipation by counterflow: Counterflow is the principal of directing two or more jets against each other to dissipate their energy. For the impact losses to be maximum, the different jets should be more or less of the same size. Koch (1968) studied two jets of similar size and velocity. They impacted at a small angle and then united to form a single jet. He noticed that the impact yielded poor results as the generated velocity gradients were small. Uymaz (1988) studied scour below a vertical gate in the case of simultaneous flow over and under the gate. He found that the final depth of scour is smaller as compared to the cases of flow only under or over the gate, although more water can be discharged in the former case. He concluded that the overtopping of a sluice gate is not critical from the downstream scour point of view.

Energy dissipation by rough channels and cascades: Hydraulic energy can be effectively dissipated in a short distance in channels with considerable roughness. A short baffled apron can form an effective roughness in a canal or spillway drop. Peterka (1963) recommended baffle heights equal to 0.8 of the critical depth of the design discharge for a baffle apron slope of 50%. A good example of energy cascades is the stepped spillway. A study of stepped spillways as energy dissipators was conducted by Chamani (1997).

Energy dissipation with vortex devices: Although vortex devices have been known for a long time (Thoma, 1930), they have been recently applied in hydraulic engineering. A vortex chamber is a cylindrical tank with a tangential inlet and an axial outlet. In the vortex chamber, the inflow creates a strong vortex and the outflow is a rotating and hollow water jet with an air core. Therefore, a considerable part of its energy is dissipated. The same principle is applied in vortex tubes where the flow is guided tangentially into the tube and then proceeds axially in a helical path along the wall where the energy is mainly dissipated by wall friction.

Energy dissipation by air entrainment: In most of energy dissipators, the loss of kinetic energy occurs due to a mixing process between fast and slow currents. It has been found that when a fast current entrains air, the mixing process does not consume as much energy if compared with the mixing of two water currents. As water is 800 to 900 times denser than air, it is logical to have an insignificant loss of kinetic energy when water jets entrain ambient air.

Energy dissipation by jet diffusion: It is mentioned above that air entrainment is not efficient in dissipating the excess energy of water jets. This is in the case of normal air entrainment which results in air bubbles flowing in a stream of water. However, if much air entrainment occurs in such a way that the water stream is transformed into a spray, a significant amount of kinetic energy can be dissipated. The drops of water in such a spray are strongly affected by air drag. More dissipation is anticipated with smaller water drops especially when their speed is high relative to the surrounding air. The classic example of the energy dissipation by spray action, or jet diffusion, is the flip bucket spillway. For the flip buckets to be successful as spray generators, they might need additional splitting devices to be installed on their crests or on the buckets to increase diffusion especially when the supercritical stream is relatively thick.

2.3 Hydraulic Jump Stilling Basins

In chapter 4, a double-leaf gate energy dissipator downstream of regulators, will be introduced. As the classical and forced hydraulic jump stilling basins have been widely used downstream of regulators, it has been essential to discuss them in some details.

2.3.1 Classical hydraulic jump

Hydraulic jumps have been widely used as energy dissipators on different types of hydraulic structures. The hydraulic jump is a rapid transition from supercritical to subcritical flow. A jump is called a classical jump when it is formed in a smooth, wide and horizontal rectangular channel. In the classical hydraulic jump, the water depth increases abruptly from an initial depth of y_1 to a sequent depth of y_2 at which the water surface becomes level. The supercritical Froude number is $F_1 = V_1/(gy_1)^{0.5}$ where V_1 is the average velocity at the toe of the jump where the water depth is y_1. A relation between the sequent and the initial depths of the classical hydraulic jump could be obtained by applying the momentum equation between the beginning and end sections of the hydraulic jump. At these two sections, velocity distributions were assumed uniform, the pressure distributions were assumed hydrostatic and the turbulent velocity fluctuations were neglected. The integrated boundary shear stress, between the beginning and end sections, was also neglected. The ratio of the sequent to initial depths, y_2/y_1, considering the above assumptions, is given by the equation

$$\frac{y_2}{y_1} = \frac{1}{2}\left[\sqrt{1+8F_1^2} - 1\right] \tag{2.1}$$

The above equation is the well-known Belanger equation.

The flow in the hydraulic jump, two-phase flow due to air entrainment, is highly turbulent with pressure and velocity fluctuations. A substantial amount of the kinetic energy is dissipated in the hydraulic jump mainly due to turbulence production and dissipation in the surface roller which extends from the toe of the jump to a section very close to the end of the jump. The efficiency of the hydraulic jump as an energy dissipator depends on the type of the jump, which is mainly dependent on the supercritical Froude number, the tailwater depth and the bed slope. The advantage of using the hydraulic jump as an energy dissipator is that dissipation occurs in the distance between the beginning and end sections of the jump which is relatively short (almost 6 times the sequent depth, y_2). Disadvantages in using the hydraulic jump as an energy dissipator is that the hydraulic jump is always associated with wave formation in the downstream tailwater. Also, the formation of the hydraulic jump is sensitive to the tailwater depth. In other words, for a classical jump to occur downstream of a gate, the tailwater depth in the channel should be equal to the sequent depth y_2 that corresponds with y_1 and F_1. If the tailwater depth is less than the sequent depth, the jump is called a "repelled jump" and usually occurs downstream of the stilling basin (on the unprotected stream bed) causing serious erosion problems and a considerable amount of damage could happen. If the tailwater depth is greater than the sequent depth, the jump becomes submerged. The "submerged jump" is not as efficient as the classical jump regarding its ability to dissipate the excess energy. Therefore, using the hydraulic jump as an energy dissipator has been always critical especially when the downstream conditions are not fixed. For regulators built on irrigation canals, the tailwater depth always varies according to the irrigation demands and using the hydraulic jump as the energy dissipation element in such situations is unacceptable.

2.3.2 Forced hydraulic jump

In order to keep the hydraulic jump within the stilling basin, for a range of tailwater levels, an external force is required. This force could be in the form of baffle blocks, baffle walls (see for example Rajaratnam, 1967 and Peterka, 1963), or a favorable slope to the basin floor. According to the momentum balance equation, the external force allows the jump to occur for lower values of tailwater depth. Rajaratnam (1968) found that for a given classical jump and a roughness height of about 0.5 y_1, the required tailwater depth is about 0.8 y_2. But, the existence of such blocks might create a cavitation problem (as mentioned by Rajaratnam (1995) and Hager (1992)). Baffle walls may also be used with deeply submerged sluice gates to deflect the high velocity stream to the free surface. Wu and Rajaratnam (1995) mentioned that using baffles in deeply submerged flows for the aforementioned reason is not always successful. For some flow conditions, a reattached high velocity wall jet might form. This will be discussed in some detail later in this chapter.

More details about the evaluation of hydraulic jumps as energy dissipators are available in Elevatorski (1959), Peterka (1963), Rajaratnam (1967) and Hager (1992).

It seems from the above brief description of the different types of energy dissipators that they could be reclassified according to the types of jets used in them. All inflows to the different types of energy dissipators take the form of a turbulent jet whose momentum is partially dissipated in a mixing process. This turbulent jet might be a free jet, a surface jet, a wall jet, a radial jet, an oscillating jet, a counter-current jet, a split jet or a rotating jet. Plane free, surface and wall jets, are the most common types used in hydraulic engineering. In the following section, plane turbulent jets in deep tailwater will be presented. In Section 2.5, the behavior of turbulent jets in the close proximity of boundaries (either rigid boundaries or the free surface) will be discussed.

2.4 Plane Turbulent Jets in Deep Tailwater

2.4.1 Plane turbulent free jets

A plane turbulent free jet, as defined by Rajaratnam (1976), is a jet of water coming out of a plane slot into a large body of water. The height of the jet is $2b_o$ and its uniform velocity at the slot is U_o. The free jet mixes violently with the surrounding fluid creating turbulence and the jet itself grows thicker (see Fig. 2.1). In the axial direction, the jet flow can be divided into two regions, the developing flow region and the developed flow region. The developing flow region is a wedge-like region with a constant velocity equal to U_o. This wedge is known as the potential core and is surrounded by mixing layers on top and bottom. The length of the potential core is about $12b_o$. In the developed flow region, turbulence penetrates to the axis and as a result the maximum jet velocity, which is the centerline velocity, starts to decay. If $u = u(x,y)$ is the mean velocity in the axial direction, Förthmann (1936) found that the distributions of the axial velocity $u(y)$ with y, at different x-stations, were similar with u_m and b, at each station, chosen as the velocity and length scales respectively. The maximum velocity u_m is equal to the value of u at the centerline and b is the value of y where u is equal to half the maximum velocity u_m. In order to benefit from this property of similarity and to use it for predicting the mean velocity field in any particular problem, the velocity and length scales should be predictable. The equations of motion of the plane turbulent free jet in the axial direction were given by Rajaratnam (1976) as

$$u\frac{\partial u}{\partial x} + v\frac{\partial u}{\partial y} = \frac{-1}{\rho}\frac{\partial p}{\partial x} + \frac{1}{\rho}\frac{\partial \tau_t}{\partial y} \tag{2.2}$$

$$\frac{\partial u}{\partial x} + \frac{\partial v}{\partial y} = 0 \tag{2.3}$$

where u and v are the mean velocities in x and y directions respectively, p is the mean pressure at any point and τ_t is the turbulent shear stress. Rajaratnam (1976) integrated the above equations for a plane turbulent jet issuing into a large body of water and expanding under zero pressure gradient (i.e. $\partial p/\partial x = 0$). The integration results showed that the axial momentum of the jet is preserved. Rajaratnam (1976) also found that the maximum velocity u_m is inversely proportional to the square root of x ($u_m \propto x^{-1/2}$) and the jet half width b is directly proportional to x ($b \propto x$).

Förthmann (1936) conducted the first experimental study on plane turbulent free jets. The thickness of the jet $2b_0$ was equal to 30mm with a length equal to 650mm. These dimensions could assure two dimensional flow, especially in the central region of the flume. It was mentioned before that Förthmann's (1936) results showed similar distributions of the velocity profiles when u_m and b were chosen as the velocity and length scales respectively. Further measurements on plane free jets were made by Albertson et al. (1950), Zijnen (1958) and Heskestad (1965). Zijnen (1958) found that the similarity profile of the velocity distribution at any x-station could be represented by a Gaussian distribution as

$$u/u_m = \exp\left(-0.693\eta^2\right) \qquad (2.4)$$

where η is equal to y/b. Dimensional analysis shows that the decay of the maximum velocity u_m in terms of that at the nozzle U_o can be given as

$$\frac{u_m}{U_o} = \frac{C_1}{\sqrt{x/b_o}} \tag{2.5}$$

To evaluate C_1, Abramovich (1963), using the experimental results of Förthmann (1934) and others, found this constant to be 3.78 and Görtler (1942) found it to be 3.39. Also, this constant was given a value of 3.52 and 3.24 in the experiments conducted by Zijnen (1958) and Albertson et al. (1950). Rajaratnam (1976) concluded, based on the aforementioned values, that this constant could be given an average value of 3.50 for all practical purposes. For the evaluation of the length scale b, it was found that $b = C_2 . x$ and the constant C_2 was given values of 0.097 and 0.114 by Abramovich (1963) and Görtler (1942), respectively. Rajaratnam (1976) commented that the value of 0.097 was found to be better than the value of 0.114 for the constant C_2. He added that C_2 could be given a value of 0.10 for convenience.

If Q_o is the jet discharge at the nozzle and Q is the jet discharge at a distance x measured from the nozzle, experiments showed that Q/Q_o is greater than unity and assumes very large values for large values of x. The jet discharge increases because of the considerable amount of the surrounding fluid that the jet entrains as it travels forward. The discharge variation with distance could be described by the following equation

$$\frac{dQ}{dx} = 2v_e = 2\alpha_e u_m \tag{2.6}$$

where v_e is the entrainment velocity and α_e is the entrainment coefficient. The above equation shows that the entrainment velocity, at any x-station, is directly proportional to the maximum velocity at this station. Using the value of $C_2 = 0.10$, Rajaratnam (1976) found that the entrainment coefficient α_e was equal to 0.053.

The discharge at any section Q, in terms of the discharge at the nozzle Q_o, may be written as

$$\frac{Q}{Q_o} = C_3 . \sqrt{x / b_o} \tag{2.7}$$

The coefficient C_3 was evaluated by Albertson et al. (1950) and was found to be equal to 0.44. If E is the kinetic energy of the flow at any section and E_o is the value of E at the slot, Albertson et al. (1950) and Rajaratnam (1976), using $C_1 = 3.50$ and $C_2 = 0.10$, evaluated E/E_o as

$$\frac{E}{E_o} = \frac{2.64}{\sqrt{x / b_o}} \tag{2.8}$$

2.4.2 Plane turbulent surface jets

Fig. 2.2 shows a plane turbulent surface jet of thickness b_o and uniform velocity U_o. The jet length and the ambient depth are assumed to be much larger than the slot width. As soon as the jet leaves the slot, a shear layer develops. The section at which the shear layer meets the water surface is the end of the potential core and downstream of this section the flow is developed. The length of the potential core is approximately $12b_o$.

The equations of motion for the plane turbulent surface jets could be written as

$$u\frac{\partial u}{\partial x}+v\frac{\partial u}{\partial y}=\frac{-1}{\rho}\frac{\partial p}{\partial x}+\frac{1}{\rho}\frac{\partial \tau_t}{\partial y} \tag{2.9}$$

$$\frac{\partial u}{\partial x}+\frac{\partial v}{\partial y}=0 \tag{2.10}$$

where u and v are the velocities in the x and y directions, respectively, and τ_t is the turbulent shear stress.

The experimental observations of Rajaratnam (1969) and Vanvari and Chu (1974) showed that the velocity profiles u(y) at different x-stations are similar. The maximum velocity u_m, at, or very close to, the free surface was chosen as the velocity scale and b, which is the vertical distance between the point of u_m and that of $0.5u_m$, was chosen as the length scale. Rajaratnam and Humphries (1984) mentioned that the similarity profile of the velocity distributions could be satisfactorily described by the exponential equation

$$u/u_m = \exp\left(-0.693\eta^2\right) \tag{2.11}$$

where η is equal to y/b. Integrating Eq. 2.9, with respect to y, for a plane turbulent surface jet with zero pressure gradient (i.e. $\partial p/\partial x = 0$), Eq. 2.9 could be reduced to

$$\frac{d}{dx}\int_0^{\infty}\rho u^2 dy=0 \tag{2.12}$$

According to Eq. 2.12, the momentum flux of the surface jet in the longitudinal direction would be preserved.

Using simple dimensional considerations with the equations of motion in the integral form, it could be shown that $u_m \propto x^{-1/2}$ and $b \propto x$.

Experimental results of Vanvari and Chu (1974) and Rajaratnam and Humphries (1984) showed that the maximum velocity u_m, in terms of the uniform velocity at the nozzle U_o, could be described as

$$\frac{u_m}{U_o} = \frac{3.1}{\sqrt{x/b_o}} \tag{2.13}$$

They also showed that the length scale b grows linearly with the longitudinal distance measured from the virtual origin which is located roughly $10b_o$ behind the nozzle. The rate of growth was about 0.07 which is about 0.7 times that of the plane free jets. The length scale b, in terms of the slot width b_o, could be written as

$$\frac{b}{b_o} = 0.07\frac{x}{b_o} = 0.07\frac{\overline{x}}{b_o} + 0.7 \tag{2.14}$$

where $\overline{x}$ and x are the longitudinal distances measured from the nozzle and the virtual origin, respectively. Also, based on the above results, the coefficient of entrainment α_e was estimated to be 0.037.

2.4.3 Plane turbulent wall jets

A plane turbulent wall jet, as defined by Rajaratnam (1976), is a jet of thickness b_o and uniform velocity U_o issuing from a rectangular slot tangentially to a flat plate submerged in a semi-finite expanse of the fluid (see Fig. 2.3). As soon as the jet leaves the slot, a shear layer develops on the fluid side while a boundary layer develops on the wall side. The section at which the two layers meet is the end of the potential core and downstream of this section the flow is developed. Experimental observations of the variation of the axial velocity u(y) with y, at different x-stations, showed that the velocity profiles have the same shape at the different stations. Förthmann's (1936) data showed that, at any x-station, the axial velocity u increases from zero at the wall to reach its maximum value u_m at a distance of $y = \delta$ and then decreases to reach zero at large y. The boundary layer is the region between $y = 0$ and $y = \delta$. The region above the boundary layer is known as the free mixing region. To check for the similarity of the velocity profiles, the maximum velocity u_m was chosen as the velocity scale and the length scale b was taken as the distance, above the flume bed, at which the axial velocity $u = 0.5u_m$ and $\partial u/\partial y$ is negative. Using the experimental observations of Förthmann (1936), Rajaratnam (1976) found that the velocity profiles were similar. Rajaratnam (1976) also wrote the equations of motion for the plane turbulent wall jets in the form

$$u\frac{\partial u}{\partial x} + v\frac{\partial u}{\partial y} = \frac{-1}{\rho}\frac{\partial p}{\partial x} + \frac{1}{\rho}\frac{\partial \tau}{\partial y} \tag{2.15}$$

$$\frac{\partial u}{\partial x} + \frac{\partial v}{\partial y} = 0 \tag{2.16}$$

In Eq. 2.15, $\tau = \tau_l + \tau_t$, where τ_l and τ_t are, respectively, the laminar and the turbulent shear stresses.

Rajaratnam (1976) integrated Eq. 2.15, with respect to y, for a plane turbulent wall jet with zero pressure gradient (i.e. $\partial p/\partial x = 0$). Hence, Eq. 2.15 could be reduced to the form

$$\frac{d}{dx}\int_0^\infty \rho u^2\,dy = -\tau_0 \qquad (2.17)$$

where $\tau_0 = \tau_0(x)$ is the wall shear stress at a distance x measured from the virtual origin. Eq. 2.17 shows a momentum decay in the longitudinal direction. The rate of momentum decay at any x-station is equal to the wall shear stress at that station. According to Eq. 2.17, if the bed shear stress is to be neglected in a particular problem, the momentum flux in the longitudinal direction would be preserved. Using dimensional considerations along with the equations of motion in the integral form, Rajaratnam (1976) found that $u_m \propto x^{-1/2}$, $b \propto x$ and $\tau_0 \propto 1/x$.

Concerning the experimental results, Förthmann (1936) was the first to conduct experiments on plane turbulent wall jets. The slot width and length were 30 mm and 650 mm, respectively. He found that the velocity distributions are similar for x greater $20b_o$. Other experiments on turbulent plane jets have been conducted by Zerbe and Selna (1946), Sigalla (1958), Myers et al. (1961), Schwarz and Cosart (1961). Myers et al. (1961) and Schwarz and Cosart (1961) which showed that the velocity distribution in the boundary layer could be described by a power law with an exponent of 1/14. Moreover, Myers et al. (1961) found that the velocity distribution in the boundary layer could be represented by the logarithmic law in the form

$$u/u_* = 5.6\log(yu_*/\nu) + 4.9 \qquad (2.18)$$

where $u_* = (\tau_o/\rho)^{0.5}$ is the shear velocity. Other values of the coefficients in Eq. 2.18 were reported by Mathieu and Tailland (1963). Rajaratnam (1976) mentioned that the velocity distributions of the entire wall jet, at different x-stations, were found to be similar in the experimental studies performed by Förthmann (1936), Sigalla (1958), Myers et al. (1961) and Schwarz and Cosart (1961). An empirical equation was given by Verhoff (1963) to describe the similarity profile as

$$u/u_m = 1.48\eta^{1/7}\left[1 - \mathrm{erf}(0.68\eta)\right] \tag{2.19}$$

Rajaratnam and Subramanya (1968), using most of the available observations on the decay of the maximum velocity along with those of Rajaratnam (1965), found that the maximum velocity u_m in terms of that at the nozzle U_o could be described by the following equation

$$\frac{u_m}{U_o} = \frac{3.5}{\sqrt{x/b_o}} \tag{2.20}$$

Rajaratnam (1976), using the observations of Sigalla (1958), Schwarz and Cosart (1961), Myers et al. (1961), found that the length scale b_o grows linearly with the longitudinal distance measured from the virtual origin, which is located roughly $10b_o$ behind the nozzle, as

$$\frac{b}{b_o} = 0.068\frac{x}{b_o} = 0.068\frac{\bar{x}}{b_o} + 0.68 \tag{2.21}$$

where $\bar{x}$ and x are the longitudinal distances measured from the nozzle and the virtual origin, respectively. The rate of growth of the length scale was found to be about 0.068 which is very close to that of the surface jet but only 0.7 times that of the free jet.

Shear stress observations of Myers et al. (1961) showed that the variation of the skin friction coefficient $C_f = \tau_o/\rho U_o^2/2$ could be expressed by the equation

$$C_f = \frac{\tau_o}{\rho U_o^2/2} = \frac{0.20}{(x/b_o).R^{1/12}} \tag{2.22}$$

where τ_o is the wall shear stress and $R = U_o b_o/\nu$ is the Reynolds number.

Based on the above relations of the velocity and length scales and the similarity profile of the velocity distribution, Rajaratnam (1976) found that the forward flow discharge Q at any section, in terms of that at the nozzle Q_o, may be written as

$$Q/Q_o = 0.248\sqrt{\overline{x}/b_o} \tag{2.23}$$

Using Eq. 2.20 with Eq. 2.23, it could be shown that the entrainment coefficient α_e is equal to 0.035, which is very close to that of the surface jet but only about 0.7 that of the free jet.

Regarding the developing region, Rajaratnam (1976) mentioned that the growth of the boundary layer δ could be described by the equation

$$\delta/\overline{x} = 0.37/(U_o\overline{x}/\nu)^{1/5} \tag{2.24}$$

Assuming that the mixing region spreads inwards at an angle of 5°, Rajaratnam (1976) found that the length of the potential core could be described by the equation

$$0.0875\left(\frac{\bar{x}_o}{b_o}\right)+0.37\left(\frac{\bar{x}_o}{b_o}\right)^{4/5}\cdot\frac{1}{R^{1/5}}=1.0 \qquad (2.25)$$

Rajaratnam (1965) showed also that, in the developing region, the flow rate Q in terms of the flow rate at the slot Q_o could be written as

$$\frac{Q}{Q_o}=\left[1+0.04\frac{\bar{x}}{b_o}+0.0046\left(\frac{\bar{x}}{b_o}\right)^{0.8}\right] \qquad (2.26)$$

Also, the entrainment velocity v_e could be expressed as

$$v_e=\frac{dQ}{d\bar{x}}=0.04U_o+0.0037\frac{U_o}{\left(\bar{x}/b_o\right)^{0.2}} \qquad (2.27)$$

Neglecting the second term on the R.H.S of Eq. 2.27, the entrainment coefficient α_e is equal to 0.04.

2.5 Turbulent Jets in Close Proximity of Boundaries

In this section, the differences between the classical turbulent jets in deep tailwater and those that issue in the close proximity of boundaries are revealed. For example, it might be reasonable to assume a constant momentum flux in turbulent jets in deep receiving water bodies (Schlichting (1960), Rajaratnam (1976)). But, it would be unrealistic, as will be explained in the next chapters, to assume that the momentum flux is preserved in a turbulent jet in shallow tailwater. Following are some applications where turbulent jets issue close to rigid boundaries or to the free surface.

Johnson (1990) mentioned that recent shallow-water discharge observations indicated that the classical integral method of analysis, which has been successfully applied to a range of unconfined and partially confined receiving water situations (see for example Rajaratnam (1976)), has to be treated with caution. This caution results from the fact that in shallow tailwaters there is a possibility of reattachment of the jet to different boundaries (Coanda effect) and the presence of internal jumps in some outfall flow patterns.

Johnson (1990) added that the general near-field characteristics of jets entering relatively deep tailwater are reasonably understood and could be represented by using the integral method of analysis where Reynolds stress closure was provided by some suitable entrainment assumptions. The close proximity of both the bed and the free surface has a great influence on the near field flow patterns in cases of buoyant (density of the jet is different from density of the receiving water) and nonbuoyant jets (jet and receiving water have the same density) entering shallow tailwater. To varying degrees, the presence of induced eddies, internal jumps, and significant pressure variations related to water surface oscillations all serve to complicate the fundamental entertainment processes that are commonly associated with turbulent jets entering unconfined environments. These additional processes are usually unsteady, unstable, and produced by nonlinear effects, which indicate that their mathematical models pose a considerable challenge. Recent research has shown that within certain parameter ranges in shallow tailwater conditions, existing theory and analysis for fully and partially unconfined conditions can be used. In other ranges, however, such analysis is uncertain and meaningful predictions can only be clarified through the analysis of data from experimental studies that quantitatively describe the aforementioned additional mixing processes.

Johnson (1990) studied experimentally a plane jet emerging from a slot of width b_o with velocity U_o. The centerline of the slot was a distance Z_o above the flume bed. The tailwater depth y_t in the channel was such that the free surface was (y_t-Z_o) above the slot centerline. Johnson (1990) mentioned that when the jet emerges from a horizontal slot into a shallow tailwater it would, in general, curve either towards the channel bed or towards the free surface. It has been necessary in some engineering conditions to define the conditions under which the jet would deflect to the surface rather than the channel bed and vice versa. Dimensional analysis showed that this feature of the flow is dependent on three non-dimensional parameters which are the Froude number $U_o/(gb_o)^{0.5}$, the offset ratio Z_o/b_o and the submergence ratio $(y_t-Z_o)/b_o$.

The experimental observations of Coates (1976) showed, as mentioned by Johnson (1990), that for a given Froude number and offset ratio, if the submergence depth is gradually increased, the jet would change from a surface jet to a bed jet at a particular value of the submergence ratio. For the same offset ratio but at a different Froude number, the change from surface-type jet to bed-type jet would occur at a different submergence ratio.

Johnson and Halliwell (1986) argued that the above simple description is not complete. They noticed that at large values of the submergence ratio, the Coanda effect was apparent and the jet attached to the channel bed. Decreasing the submergence ratio, the jet remained as a bed jet until the submergence ratio reached a particular value where a distinct changeover occurred and the jet attached to the free surface rather than the bed. The jet remained attached to the free surface with further reduction of the submergence ratio. On the other hand, when they repeated their observation while increasing the submergence ratio gradually, they found that the changeover condition from surface jet to bed jet occurred at larger values of the submergence ratio. Further study showed that there was indeed a region where the jet could attach either to the bed or to the free surface for the same non-dimensional flow-defining parameters. This phenomenon was anticipated by Bourque and Newman (1960). They worked on a two-dimensional jet emerging from a slot and reattaching to an adjacent flat plate. Bourque and Newman (1960) commented that the flow exhibited a hysteresis phenomenon.

Bakhmeteff and Feodoroff (1957), as mentioned by Johnson (1990), investigated the plane turbulent jet problem experimentally. They described the various flow patterns that were observed as the tailwater depth increases. They worked on the whole range of submergence starting from the free flow conditions till the jet was totally submerged. Five discharge regimes were observed: free nappe flow, plunging repelled jump, direct repelled undular jump, springing vein, and tranquil flow. They explained that these regimes were dependent on the kineticity ($\lambda = q^2 g^{-1} b_o^{-3}$), which is a form of the Froude number. For plunging repelled jump ($\lambda = 3\text{-}4$), undular jump ($\lambda = 1\text{-}3$), and tranquil flow ($\lambda < 1$).

Rajaratnam and Subramanya (1968) studied, experimentally, the diffusion characteristics of a submerged plane turbulent jet issuing from a nozzle located over an abrupt drop in the bed. They studied in detail the growth of the wall jet beyond the impingement region. They concluded that, after a certain distance downstream of the reattachment line, the velocity profiles were similar and the similarity profile was the same as that of the classical wall jet. They found that beyond a certain point the maximum-velocity decay profiles were similar to the classical wall jet decay. They also found that when the jet issued tangential to the bed, it behaved in the same way as the classical wall jet regarding the velocity profiles and the decay of the maximum velocity. The only difference was the length scale which grew at a faster rate than that of the classical wall jet. Also, Rajaratnam and Subramanya (1968) measured the bed shear stress and found that the shear stress distributions were similar when represented in a dimensionless form.

Dodds (1960), as mentioned by Sawyer (1962), introduced a simple model of the cavity flows of a curved two-dimensional reattaching turbulent jet using plausible assumptions regarding the bifurcation of the jet at reattachment. He had expressions relating the cavity pressure and cavity length to the jet momentum per unit jet width and the geometry of the boundaries. A spread parameter, which is a measure of the rate of spread, was involved in these expressions and was connected with the entrainment properties of the inner edge of the jet.

Sawyer (1962) conducted an experiment to determine the flow pattern, the cavity pressure and cavity length for a flow under a curved two-dimensional turbulent jet discharging parallel to a flat plate at some height above the bed. This work, as mentioned by Sawyer, was performed to give some experimental backing to the simple model proposed by Dodds (1960) and Bourque (1959) and to find the value of the spread parameter involved in their expressions. Sawyer (1962) mentioned that a stable flow pattern was achieved and the mechanism of that stable flow pattern was that the entrainment of fluid, by the turbulent jet, near the bed caused a pressure difference across the jet, curving the jet towards the bed. On striking the bed, the jet bifurcated. The reverse flow, or the volume gained by the cavity, balanced the volume entrained, or the volume lost from the cavity. Sawyer (1962) commented that this balance, between the quantity of air entrained by the jet from the cavity and the quantity of reversed flow at reattachment, was not exact. The experiments showed that there was a secondary flow that fed air from outside into the cavity. However, near the center of the slot length, it was estimated that this lack of balance was negligible and the flow approached very closely to two-dimensional conditions.

Also, Sawyer (1962) expressed the curvature of the jet as the ratio of the pressure difference across the jet to the jet momentum. By determining the geometry of the jet centerline, assumptions regarding the jet velocity profile and rate of spread (as measured by the spread parameter) led to an expression for the amount of air entrained by the jet along its inner edge, which was taken to be the volume flow fed back into the cavity at reattachment. Hence, the division of the volume flow of the jet at reattachment was determined. Assumptions regarding the velocity profile shapes of the initial reversed flow and the initial attached downstream flow, with the aid of a momentum balance equation at reattachment point, were used to determine the division of momentum flow at reattachment. Concerning the velocity profile, Sawyer assumed that the velocity profile of the jet was similar to that of a two-dimensional plane jet. Sawyer also used Dodd's (1960) assumption that the initial reversed flow and initial downstream flow had velocity profiles similar to that of a half Görtler (1942) jet profile. It was assumed also that the pressure inside the cavity was constant so that there was a constant pressure difference acting across the jet.

Sawyer (1962) concluded that the variations of the pressure difference across the jet and the length of the cavity with the height of slot from the bed agreed quite well with those predicted by Dodds (1960) analysis in that they were consistent with a choice of spread parameter which was constant at the value of 15. Sawyer also commented that the value of the spread parameter for which the analysis was in best agreement with the results was not, in fact, the true value of the spread parameter for the curved jet. The discrepancy between the two values was a measure of the collective errors in the various assumptions made in the analysis. Thus, the choice of the spread parameter to be 15 was considered, by Sawyer, to be the fixing of a convenient empirical constant in order that the results could be applied to give reasonably accurate predictions of the cavity length and cavity pressure. Sawyer (1962) also mentioned that the difference in the rate of entrainment between the inner and outer edges of the jet due to curvature effects did not affect the growth rate of the jet as a whole. The difference in the entrainment rates was responsible only for the locus of the maximum velocity not to be a streamline.

Reichardt (1942) found experimentally, as mentioned by Sawyer (1962), that the value of the spread parameter for the two-dimensional plane jet was 7.67. Sawyer (1962) expected that the value of this parameter relevant to entrainment along the inner edge of the curved jet would be higher than 7.67 due to suppression of turbulent mixing, as a consequence of curvature.

Townsend (1956) mentioned that the mechanism of entrainment was intimately connected with the growth of turbulent shear flow, and it was possible to use entrainment properties in the setting up of mean flow equations for such flows. It was mentioned also by Sawyer (1962) that the entrainment properties of a curved two-dimensional turbulent jet were expected to differ from those of the corresponding plane jet. Momentum transport arguments indicated that the entrainment along the inner edge was reduced whereas entrainment along the outer edge was enhanced. Sawyer (1962) also argued that the curvature of the jet enhanced the mixing properties of the jet. He described a small parcel of fluid that is transported from a higher velocity region to a lower velocity region nearer to the outside edge of the jet. Sawyer argued that if this parcel of fluid arrived with some excess velocity over its surroundings, it would be subjected to a greater centrifugal force than its surroundings. But its surroundings were subjected to centrifugal forces and pressure forces which just balanced in the mean. Hence it was expected that the parcel of fluid would experience a total force tending to move it further outwards, which implied a more vigorous mixing than that which occurred with no curvature. A reverse argument holds for the mixing at the inner edge where mixing is expected to be relatively weak.

If a turbulent wall jet is obstructed by a baffle wall, it could either be deflected to the free surface or, for some flow conditions, it might reattach to the flume bed.

Wu and Rajaratnam (1995) studied the effect of two dimensional baffles on submerged hydraulic jumps. They classified the flow into two different stable flow states, the deflected surface jet state and the reattaching wall jet state. They also stated that, in the deflected surface jet state, the main flow is deflected to the water surface to form a surface jet downstream of the baffle, thereby deflecting the high velocity supercritical stream away from the bed to the surface to protect the channel bed. On the other hand, the deflected jet might induce a wave attack on the banks of the downstream channel. In the reattaching wall jet state, the main flow passes over the baffle to impinge and reattach to the bed immediately downstream the baffle.

Wu and Rajaratnam (1995) also added that, for a given tailwater depth and baffle position, two critical baffle heights exist (h_{c1} and h_{c2}) which are independent of the gate opening or gate Froude number. If the baffle height is smaller than h_{c1}, the flow will be in the stable reattaching wall jet state. If the baffle height is larger than h_{c2}, the flow will be in the stable deflected surface jet state. If the baffle height is between h_{c1} and h_{c2}, the flow can be stable in either state, depending on the initial flow state, and the flow can change from one state to the other by external interference. For the relation between the two critical depths h_{c1} and h_{c2} Wu and Rajaratnam (1995) stated that h_{c1} was about 0.02 of the tailwater depth y_t and the regression equation for h_{c2} could be written as

$$\frac{h_{c2}}{y_t} = 0.0382 - 0.0078\left(\frac{x_o}{y_t}\right) + 0.0261\,\mathrm{Sin}^2\left(\frac{x_o}{y_t}\right) \tag{2.28}$$

where x_o is the distance from the baffle front to the gate and y_t is the tailwater depth.

Based on the results of detailed measurements, Wu and Rajaratnam (1995) concluded that, in the region upstream of the baffle, the forward velocity profiles were found to be similar in their lower part and could be described by the corresponding plane turbulent wall jet curve. These velocity profiles were not similar in the upper part due to the effect of the strong surface eddy formed upstream of the baffle. In the deflected surface jet state, the maximum velocity decayed continuously to reach its minimum value somewhere below the water surface and then speeded up, due to the existence of a surface hump, till it hit the water surface. After this, the maximum velocity in the surface jet decayed continuously. In the reattaching wall jet state, the maximum velocity decayed all the way from the gate. For the same boundary conditions, the decay of the maximum velocity was faster in the deflected surface jet state than that of the reattaching wall jet state. The scales for the surface jet (the maximum surface velocity, the surface hump height, the location of the maximum surface velocity and the location of the top of the surface hump) were generally affected by the following four variables: tailwater depth, gate Froude number, baffle location and baffle height.

For turbulent jets discharged from slots or orifices in walls into large ambients at rest, it has been generally assumed (Albertson et al. (1950), Schlichting (1960), Rajaratnam (1976)) that the momentum flux would be preserved. In some experimental investigations (Miller and Comings (1957); Goldschmidt and Eskinazi (1966); Heskestad (1965) and Kotsovinos (1975)), it has been noticed that the momentum flux decayed to some extent at large distances from the origin of the jets.

Based on an approximate integral analysis, Kotsovinos (1978) developed an equation to describe the variation of the momentum flux with the longitudinal distance from the nozzle producing the jet. He estimated the various terms in the momentum balance equation and concluded that the induced outer flow was the main reason of the momentum decay in plane jets out of a wall. Discussing Kotsovinos's results, Schneider (1985) commented that Kotsovinos's (1978) approximation breaks down with infinite distances from the orifice. He added that this breakdown was due to the fact that Kotsovinos (1978) did not consider the reactive effect of the decrease of the momentum flux on the induced flow. Kotsovinos's (1978) momentum decay equation was given as

$$\frac{M(x)}{M_o} = 0.983 - 0.06931 \ln\left(\frac{x}{6b_o}\right) \qquad (2.29)$$

Schneider (1985) noticed that in turbulent jets the assumption of constant momentum flux is in apparent agreement with the experimental results of Bradbury (1965). However, other researches showed that the theory and the experimental results were not in agreement. Miller and Comings (1957) showed that the maximum velocity decay was slightly larger than that predicted by the classical boundary layer theory whereas the jet width was in agreement with theory. Schneider (1985) commented that the above observations suggest that the momentum decays slowly with distance from the orifice. It should be noted, as mentioned in Schneider (1985), that Miller and Comings (1957) performed their experiments with a nozzle located in a wall perpendicular to the jet axis, while such wall did not exist in Bradbury's (1965) experiments which indicated that the existence of the wall might be the reason for such momentum decay. The problem became even more controversial when Hussain and Clark (1977) concluded that the total momentum flux (including the mean momentum flux due to velocity fluctuations) increased with increasing distance and was not completely balanced by the mean static pressure integral.

Schneider (1985) studied laminar and turbulent plane and axisymmetric jets emerging from orifices in plane or conical walls to determined the entrainment of the momentum and the discharge into a jet. In that study the problem of the jet flows at large distances from an orifice in a wall was studied by coupling the jet flow with the induced outer flow. The momentum flux in the jet boundary layer was considered to be a slowly-varying function of the distance, and the coupling is established by accounting for the momentum flux from the induced outer flow into the jet (entrainment of momentum). Schneider (1985) benefited from the observations of Taylor (1958), Wygnanski (1964), Rubin and Falco (1968) and Kraemer (1971) who studied the induced outer flows with and without walls. It could be concluded that the streamlines of the outer flow enter the turbulent jet at an angle of $0.5\theta_w$ where θ_w is the angle the wall makes with the jet axis (θ_w would be $\pi/2$ in case of an infinite plane wall perpendicular to the jet axis). For turbulent (plane or axisymmeyric) flow, the analysis provided answers to the questions concerning the invariance of the momentum flux, and unveiled the source of previous discrepancies. Schneider (1985) found that in turbulent jets out of a wall, the axial velocity decayed more rapidly than that predicted by the classical boundary layer solutions. Also, the momentum flux vanished with infinite distance from the orifice. Schneider's analysis explained the reason of the discrepancies found in the previous experimental data on turbulent jets. For a plane turbulent jet out of a wall, Schneider's analysis predicted that the momentum M would slowly vary as

$$\frac{M(x)}{M_o} = \left(\frac{x_o}{x}\right)^{\frac{\alpha_e}{2}.m} \tag{2.30}$$

where α_e is the entrainment coefficient. Schneider (1985) mentioned that the entrainment coefficient is equal to 0.085 in plane turbulent jets as found by Tollmien (1926) and Reichardt (1942), m is a constant equal to $\cot(\theta_w/2)$ for plane turbulent jets and x_o is a constant of integration. For the particular case of a plane turbulent jet issuing from a vertical upstream wall, $m' = 1$ and Eq. 2.30 becomes

$$\frac{M(x)}{M_o} = \left(\frac{x_o}{x}\right)^{\frac{\alpha_f}{2}} \tag{2.31}$$

Swean Jr. et al.(1989) studied the variation of momentum and mass fluxes as well as the growth for plane turbulent surface jets with limited depth of tailwater. They conducted 10 experiments to study the effect of the finite depth of tailwater on the characteristics of the surface jet and to observe the variation of the momentum and volume fluxes and the breakdown of the surface jet due to the limited depth of the ambient. They also used the experimental results of Vanvari and Chu (1974) and Rajaratnam and Humphries (1984). Their results showed a momentum decay and a breakdown (or variation from that of jets in infinite ambient) in the velocity and length scales due to the jet confinement. The study of Swean Jr. et al. (1989) provided a general understanding of the problem of surface jets with a finite depth of tailwater. However, their analysis did not consider the adverse pressure gradient in the momentum balance.

2.6 References

Abramovich, G. N. (1963). "The theory of turbulent jets." English translation published by M.I.T. Press, Massachusetts, 671p.

Albertson, M. L., Dai. Y. B., Jensen, R. A. & Rouse, H. (1950). "Diffusion of submerged jets." Trans. ASCE. 115, 639-664.

Bakhmeteff, B. A., and Feodoroff, N. V. (1957). "Patterns of flow through horizontal slits." Ixth Int. Congress Appl. Mech., 1: 1 (1957).

Bourque, C. (1959). M.Sc. Thesis, University of Laval. Also Aero. Quart. 11, p. 201.

Bourque, C., and Newman, B. G. (1960). "Reattachment of a two-dimensional, incompressible jet to an adjacent flat plate." Aero. Quart. 11, 201.

Bradbury, L. J. S. (1965). "The structure of a self-preserving turbulent plane jet." J. Fluid Mech. 23, pp. 31-64.

Chamani, M. (1997). "Skimming flow in a model of a stepped spillway." Ph.D. Thesis, University of Alberta.

Coates, A. D. (1976). "The numerical and experimental studies on the dynamics of fluids." Ph.D. Thesis, Heriot-Watt University, Edinburgh.

Dodds, J. I. (1960). Ph.D. Thesis, Cambridge University.

Elevatorski, E. A. (1959) "Hydraulic energy dissipators." McGraw-Hill, New York.

Förthmann, E. (1936). "Turbulent jet expansion." English translation NACA. TM-789. (Original Paper in German, 1934. Ing. Archiv., 5).

Görtler, H. (1942). "Berechnung von Aufgaben der freien Turbulenz auf Grund eines neuen Näherungsansatzes. ZAMM, 22, pp. 244-254.

Goldschmidt, V., and Eskinazi, S. (1966). "Two phase turbulent flow in a plane jet." Trans. ASME, Series E, J. Appl. Mech., 33(4), 735-747.

Hager, W. H. (1992). "Energy dissipators and hydraulic jump." Kluwer Academic Publishers, Dordrecht, 288p.

Heskestad, G. (1965). "Hot wire measurements in a plane turbulent jet." Trans. ASME, Series E, J. Appl. Mech., 32(4), 721-734.

Hussain, A. K. M. F. and Clark, A. R. (1977). "Upstream influence on the near field of a plane turbulent jet." Phys. Fluids 20, 1416-1426.

Johnson, A. J., and Halliwell, A. R. (1986). "Jet behavior in shallow receiving water." Proc. Instn. Civ. Engrs., Part 2, 81:549.

Johnson, J. A. (1990). "Jet outfalls entering shallow tailwaters." Encyclopedia of Fluid Mechanics (1986-1993), Vol. 10 (Surface and ground water flow phenomena), Chapter 7, pp. 267-294.

Koch, K. (1968). "Die gegenseitige Strahlablenkung auf horizontaler Sohle." Bericht 18, Versuchsanstalt für Wasserbau, Technische Universität München: München.

Kotsovinos, N. E. (1975). "A study of the entrainment and turbulence in a plane turbulent jet." W. M. Keck Lab. Hydr. Water Resources, Calif. Inst. Tech. Rept. KH R-32.

Kotsovinos, N. E. (1978). "A note on the conservation of the axial momentum of a turbulent jet." J. Fluid Mech., 87(7), pp. 55-63.

Kraemer, K. (1971). "Die Potentialströmung in der Umgebung von Freistrahlen." Z. Flugwiss. 19, pp. 93-104.

Mathieu, J. and Tailland, A. (1963). "Etude d'un jet plan dirigé trangentiellement à une paroi" C. R., Acad. Sci., Paris, 257, pp. 44-47.

Miller, D. R., and Comings, E. W. (1957). "Static pressure distribution in the free turbulent jet." J. Fluid Mech., 3(10), pp. 1-16.

Myers, G. E., Schauer, J. J and Eustis, R. H. (1961). "The plane turbulent wall jet." I, Jet development and friction factor, Tech. Rep., 1, Department of Mechanical Engineering, Stanford University. (Also published in Trans. ASME., J. Basic Eng., 1963).

Peterka, A. J. (1963). "Hydraulic design of stilling basins and energy dissipators." Engrg. Monograph 25, U.S.D.I. Bureau of Reclamation: Denver, Col.

Rajaratnam, N. (1965). "Flow below a submerged sluice gate as a wall jet problem." Proc. 2nd Aus. Conf. on Hydraulics and Fluid Mechanics, Auckland, New Zealand, pp. 131-146.

Rajaratnam, N. (1967). "Hydraulic jumps.", Advances in Hydroscience, Vol. 4, pp. 198-276.

Rajaratnam, N. (1968). "Hydraulic jumps on rough beds." Trans. Engineering Institution of Canada 11(A-2), pp. 1-8.

Rajaratnam, N. (1969). "Diffusion of a supercritical stream on a stagnant pool." Trans. Engrg. Inst. Of Canada, Vol. 12, No. A-1, pp. 1-5.

Rajaratnam, N. (1976). Turbulent Jets. Elsevier Publishing Co, The Netherlands, 304p.

Rajaratnam, N. (1995). "Almanac of energy dissipation mechanisms." IAHR, Hydraulic Structures Design Manual, 9, Energy Dissipators, Chapter 3, pp. 23-42.

Rajaratnam, N. and Subramanya, K. (1968). "Plane turbulent reattached wall jets." J. Hydraulics Div., ASCE, Vol. 94, No. HY1, pp. 95-112.

Rajaratnam, N., and Humphries, J. A. (1984). "Turbulent non-buoyant surface jet." J. Hydr. Res., 22(2), pp. 103-115.

Reichardt, H. (1942). "Gesetzmässigkeiten der freien Turbulenz." VDI-Forschungsheft, p. 414.

Rubin, S. G. and Falco, R. (1968). "Plane laminar jet. AIAA J.6, pp. 186-187.

Sawyer, R. A. (1962). " The flow due to a two-dimensional jet issuing parallel to a flat plate." J. Fluid Mech. 9(4), pp. 543-560.

Schlichting, H. (1960). "Boundary layer theory." 4th Edn. McGraw-Hill: New York.

Schneider, W. (1985). "Decay of momentum flux in submerged jets." J. Fluid Mech., 154(5), pp. 91-110.

Schwarz, W. H. and Cosart, W. P. (1961). "The two-dimensional turbulent wall jet." J. Fluid Mech., 10, pp. 481-495.

Sigalla, A. (1958). "Measurements of skin friction in a plane turbulent wall jet." J. R. Aeronaut., Soc. 62, pp. 873-877.

Swean Jr, T. F., Ramberg, S. E., Plesniak, M. W. Stewart., M. B. (1989). "Turbulent surface jet in channel of limited depth." J. Hydr. Engrg., ASCE, 115(12), pp. 1587-1606.

Taylor, G. I. (1958). "Flow induced by jets." J. Aero. Sci. 25, pp. 464-465.

Thoma, D. (1930). "Die Rückstromdrossel." VDI-Zeitschrift 74:1098.

Tollmien, W. (1926). "Berechnung turbulenter Ausbreitungsvorgänge." Z. angew. Math. Mech. 6, pp. 468-478; [English Transl. NACA TM 1085 (1945)].

Townsend, A. A. (1956). "The structure of turbulent shear flow." Cambridge University Press, 315 pp.

Uyumaz, A. (1988). "Scour downstream of vertical gate." J. Hydr. Engrg., Vol. 114, No. 7, pp. 811-816.

Vanvari, M. R., and Chu, V. H. (1974). "Two-dimensional turbulent surface jets of low Richardson number." Tech. Report No. 74-2 [FML], Fluid Mech. Lab., Dept. of Civ. Engrg. and Appl. Mech., McGill Univ., Montreal, Canada.

Verhoff, A. (1963). "The two-dimensional turbulent wall jet with and without an external stream." Rep. 626, Princeton Univ.

Vischer, D. L., and Hager, W. H. (1995). "Energy dissipators." IAHR, Hydraulic Structures Design Manual, 9, Chapter 2, pp. 9-22.

Wu, S. and Rajaratnam, N. (1995). "Effect of baffles on submerged flows" J. Hydr. Engrg., ASCE, 121(9), pp. 644-652.

Wygnanski, I. (1964). "The flow induced by two-dimensional and axisymmetric turbulent jets issuing normally from an infinite plane surface." Aeron. Q. 15, pp. 373-380.

Zerbe, J. and Selna, J. (1946). "An empirical equation for the coefficient of heat transfer to a flat surface from a plane heated air jet directed tangentially to the surface." NACA, TN, 1070.

Zijnen, B. G. Van der Hegge (1958). "Measurements of the velocity distribution in a plane turbulent jet of air." Appl. Sci. Res., Sect. A, 7, pp. 256-276.

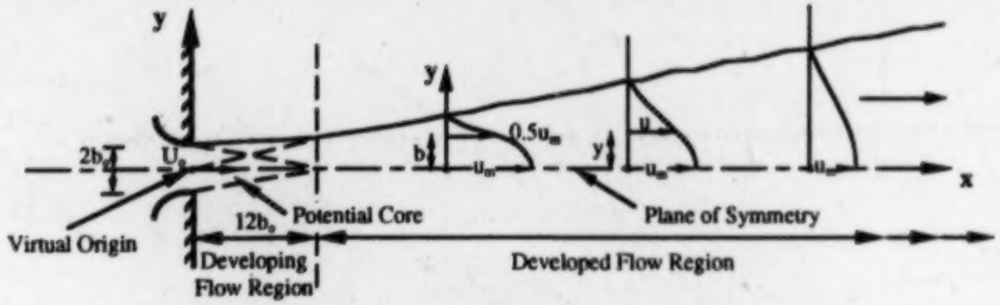
y
y
0.5u_m
u
b
y
2b_o
U_o
u_m
u_m
u_m
x
12b_o
Potential Core
Plane of Symmetry
Virtual Origin
Developing Flow Region
Developed Flow Region

Fig. 2.1 Definition sketch of plane turbulent free jets

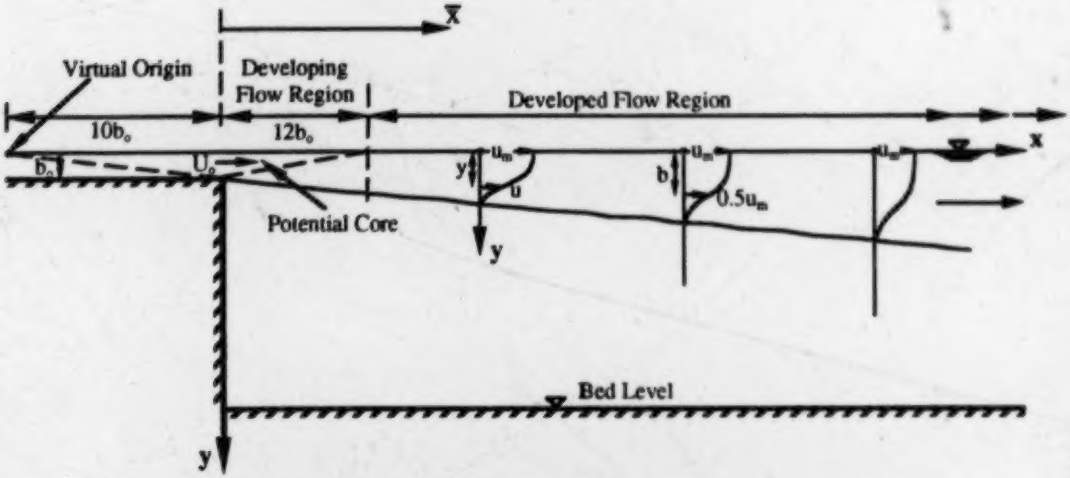
x̄
Virtual Origin
Developing Flow Region
Developed Flow Region
10b_o
12b_o
x
b_o
U_o
u_m
u_m
u_m
y
u
b
0.5u_m
Potential Core
y
Bed Level
y

Fig. 2.2 Definition sketch of plane turbulent surface jets

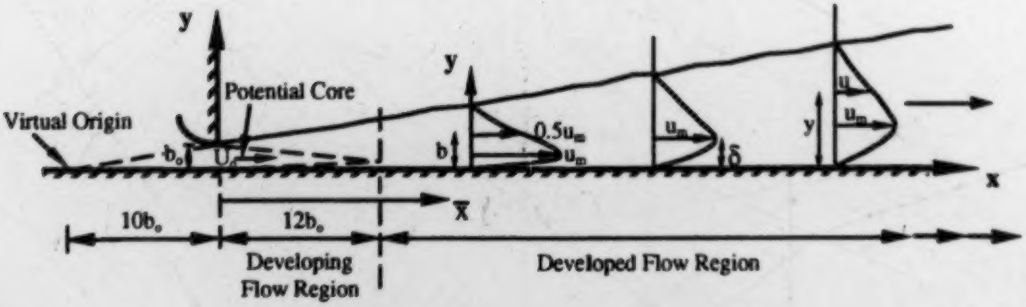
y
y
Potential Core
Virtual Origin
0.5u_m
u_m
u
u_m
y
b
δ
b_o
U_o
x
x̄
10b_o
12b_o
Developing Flow Region
Developed Flow Region

Fig. 2.3 Definition sketch of plane turbulent wall jets

Chapter 3

Experimental Arrangement and Instrumentation Techniques

3.1 Introduction

This chapter describes the laboratory equipment and the experimental procedure used with the double-leaf gate dissipator, the plane turbulent surface jets and the plane turbulent wall jets. The experimental study was carried out at the T. Blench Hydraulics Laboratory, University of Alberta.

3.2 Experimental Arrangement

3.2.1 The flume

All of the experiments were conducted in a straight rectangular flume, 0.446 m wide, 0.60 m deep and 7.6 m long, with a smooth aluminum bottom and plexiglas sides (see Fig. 3.1). The flume was supported on a pivot and a scissors jack which was operated manually to adjust the slope of the flume in the longitudinal direction. A head gate installed at the flume entrance was used to create the required flow. In the double leaf gate dissipator, the head gate was split into two leaves. The upper leaf was located upstream of the lower one to create an opening which produced an inclined jet. A single-leaf head gate was used to create the plane surface and wall jets. Streamlined lip(s) were fixed on the gate to produce a supercritical stream with a thickness equal to the gate opening, b_o. A tail gate, installed at the downstream end of the flume, was used to control the tailwater depth in the flume. False floors, with the same width as the flume, were used in the surface jet experiments to change the offset distance and to create the required offset ratio. A traverse system was mounted on the flume to hold the different probes and the point gauge. It could be moved manually in the longitudinal, as well as in the transverse, direction. A manometer board was fixed on one of the flume side walls and was connected to the probe(s) in use.

Water was supplied to the head tank of the flume from an underground sump. The head tank was 3.40 m long and the width of the head tank decreased gradually from 1.20 m, at the upstream end, to 0.446 m (the flume width) as shown in Fig. 3.1. Two pumps were used to supply the head tank with the required discharge. The discharge was measured by a magnetic flow meter located in the supply line.

3.2.2 Pressure transducers

Variable reluctance differential pressure transducers (Validyne model DP45-16 Northridge, Calif) were used in the experiments to measure the pressure difference. The range of the these transducers was ±1.4 inch (35.56 mm) of water. Thus, the maximum velocity that these transducers could measure was 0.83 m/s. The accuracy of these transducers, as given by the manufacture, was 0.25% of the full scale (2.8 inches) which is ±0.1778 mm of water or 0.059 m/s. Validyne CD379 portable digital transducer demodulators were used to display the readings of the pressure transducers. The signals from the demodulators were then fed into a computer equipped with a data acquisition system for further analysis.

The transducers were calibrated by applying known heads of water of up to ± 1 inch (±25.4 mm) with 0.1 inch increments of the pressure head. The adjustment of the demodulators was dependent on the type of the probe connected to the transducer. In case of a Prandtl tube, the positive side of the transducer was connected to the total head tube and the negative side was connected to the static head tube. With this connection the demodulator would show positive readings all the time. Hence, the demodulator was adjusted, using the zero and the span screws on the demodulator, to give zero volt for zero pressure head and +1 volt for +1 inch pressure head. With the Pitch probe (three holes probe) the situation was different as the pressure difference between any two holes could be either positive or negative. Therefore, the demodulators had to be adjusted for both the positive as well as the negative sides. In this case, the demodulators were adjusted to give zero volts for zero pressure head and ± 1 volt for ± 1 inch pressure head.

After adjusting the demodulators, the transducers had to be calibrated between the upper and the lower limits (from -1 inch pressure head to +1 inch pressure head). An incremental pressure head of 0.1 inch was applied. Fig. 3.2 shows the results of three calibration tests conduced at the beginning of the main experiments (Double-leaf gate, Surface jets and Wall jets). Also, the transducers were tested and re-calibrated, if necessary, at the beginning of each run within the main experiments. Fig. 3.2 shows that the transducers had a linear response to the applied pressure difference.

3.2.3 Data acquisition system

A data acquisition system consisting of a Macintosh IIfx computer equipped with a data acquisition board and several programs written in the LabView language, was used. Different programs were available for use with different probes. The input to these programs was the calibration equations of the probes and the pressure transducers, and the output was the magnitude and the direction of the velocity vector, the piezometric pressure and the shear stress. The arithmetic means and the standard deviations of all quantities measured were displayed on strip charts on the screen in real time and then saved in an open file. These programs allowed the user to set the total number of samples required at each point and the sampling rate or frequency. For the experiments conducted in this study, a total of 5000 samples were recorded, at each point in the flow, at a frequency of 40 Hz. It should be mentioned that when the pressure difference was outside the transducers' range (±25.4 mm), the pressure connections were switched to a manometer board and the differential pressure head results were obtained manually from the manometer and entered into the computer.

3.3 Velocity Measurements

Two probes were used for the measurement of the velocity in this study. A Prandtl tube (or Pitot-static tube) was used, when the direction of flow was known, to measure one-dimensional velocity. A pitch probe was used in two-dimensional flows. The sizes of these probes, their equations and experimental connections are presented in this section.

3.3.1 Prandtl tube

A Prandtl tube with an external diameter of 3.0 mm was used to measure one dimensional velocity in the longitudinal direction. It was used in the double-leaf gate experiment only after the jet surfaced and moved parallel to the flume bed. It was also used in the surface jet and wall jet experiments. The Prandtl tube was also used as a Preston tube for measuring the bed shear stress (Preston (1954); Patel (1965)).

Fig. 3.3 shows a Prandtl tube with an external diameter of 3 mm connected to one transducer. Also included in the same connection was a manometer for use in cases where the pressure difference was outside the transducer range (± 25.4 mm). The positive side of the transducer was connected to the total pressure hole of the Prandtl tube and the negative side was connected to the static pressure hole of the Prandtl tube. When the pressure difference was outside the transducer range, the clamps on the transducer-probe tubes were closed and the clamps on the manometer-probe tubes were opened and the pressure difference was obtained from the manometer (see Fig. 3.3).

3.3.2 Pitch probe

A pitch probe was used in the double-leaf gate experiment to measure the velocity in the inclined jet from the slot till the jet surfaced. It was used because of the two dimensional nature of the flow within this region. The flow is considered two-dimensional when the magnitude and direction of the velocity are unknown but the plane containing the velocity vector is determinable (either exactly or approximately). The velocity vector was measured in the centerline plane parallel to the flume side walls. The lateral component of the velocity was neglected as it was very small compared to the longitudinal and the vertical components especially in the middle third of the flume. The pitch probe used in this study was made of three tubes of external diameters of 1.0 mm and was made and calibrated at the T. Blench Hydraulics Laboratory, University of Alberta.

Fig. 3.4 shows the pitch probe used in this study. It consisted of three stainless steel tubes rigidly soldered together. The nose of the probe was machined so that the face of the central tube is perfectly flat and the side tubes were chamfered at an angle of 45°. Three transducers were used in the pitch probe connection. The positive side of each transducer was connected to one of the pitch probe holes and the negative side was connected to a reference level. Hence, each traducer was used to measure the pressure difference between one of the pitch probe holes and the corresponding reference level. If the pressure difference sensed by a transducer, as displayed in the corresponding demodulator, was outside the transducer range (± 25.4 mm), the corresponding reference level was adjusted (either raised or lowered) to bring the pressure difference within the transducer range. The three reference tubes were directly connected to three glass tubes on the manometer board. After adjusting the reference levels, the levels were read in the corresponding glass tubes on the manometer board and then typed into the computer.

Rajaratnam and Muralidhar (1967) discussed the theory of pitch probes based on simple pressure head equations. Assume a pitch probe is placed in a two dimensional flow in the plane containing the velocity vector V, see Fig. (3.5), at an angle θ with the velocity vector . Therefore, the piezometric pressure heads sensed by the three tubes of the pitch probe could be written as

$$h_1 = h_o + K_1 \frac{V^2}{2g} \tag{3.1}$$

$$h_2 = h_o + K_2 \frac{V^2}{2g} \tag{3.2}$$

$$h_3 = h_o + K_3 \frac{V^2}{2g} \tag{3.3}$$

where h_o is the static piezometric pressure head at the point under consideration and K_1, K_2, and K_3 are calibration coefficients and are functions of the pitch angle θ. Combining the above equations, it could be shown that

$$\frac{h_2 - h_3}{h_2 - h_1} = \frac{K_2 - K_3}{K_2 - K_1} = K_4 \tag{3.4}$$

and

$$V = \frac{\sqrt{2g(h_2 - h_1)}}{\sqrt{K_2 - K_1}} = K_5\sqrt{2g(h_2 - h_1)} \tag{3.5}$$

where new coefficients, K_4 and K_5 were introduced. Rotating the pitch probes through known angles (in the range of zero to 60 degrees) in the potential core of a plane turbulent jet produced by a deeply submerged sluice gate, Rajaratnam and Muralidhar (1967) determined the calibration curves for the coefficients K_1 to K_5 as functions of the pitch angle θ. Rajaratnam and Muralidhar's (1967) measurements showed that the calibration curves were symmetrical about the zero pitch angle (i.e. any calibration coefficient had the same value at the corresponding positive and negative angles). Fig. 3.5 shows the calibration results.

The data acquisition system used the above equations and those describing the relations shown in Fig. 3.5 to solve for the velocity vector (the magnitude and direction of the velocity). Following are the steps followed in the calculation of the velocity vector.

1. The pressure differences between each tube, of the pitch probe, and the corresponding reference level were measured by the differential pressure transducers;
2. Knowing the reference levels, the pressure heads (h_1, h_2 and h_3) at the nose of the three tubes, were calculated;
3. The differential pressure heads, (h_2-h_3) and (h_2-h_1) were calculated;
4. Eq. 3.4 was used to obtain K_4;
5. Having K_4, θ (the direction of the velocity vector) could be evaluated from Fig. 3.5;
6. Having θ, K_5 could be evaluated from Fig. 3.5;
7. Having K_5, the magnitude of the velocity vector, V, could be obtained from Eq. 3.5;

8. One of the equations (Eq. 3.1, Eq. 3.2 or Eq. 3.3) could be used along with the corresponding pressure head h_1, h_2 or h_3 to obtain the static piezometric pressure head, h_o.

3.4 Bed Shear Stress Measurements

3.4.1 Introduction

The main factor in the evaluation of an energy dissipator is its ability to minimize erosion of the downstream bed. Therefore, measuring the bed shear stress in the first experiment (double-leaf gate energy dissipator) was essential. In the plane turbulent surface jet experiment, the bed shear stress was neglected as it was caused by the reverse flow which was relatively weak. In the plane turbulent wall jet experiment, the bed shear stress was measured and included in the momentum balance equation. Several methods have been used to measure shear stress, τ_o, or friction velocity, $u_* = (\tau_o/\rho)^{0.5}$, as stated by Nezu and Nakagawa (1993)

1. In normal and uniform flow, u_* may be evaluated as follows

$$u_* = \sqrt{gRS} \tag{3.6}$$

where R is the hydraulic radius and S is the channel slope.

2. u_* can be determined using a measured mean velocity profile with the consideration of the logarithmic law as

$$u_* = \frac{U_2 - U_1}{5.75 \log\left(\frac{y_2}{y_1}\right)} \tag{3.7}$$

where U_1 and U_2 are, respectively, the mean velocities at depths of y_1 and y_2 above the bed. In Eq. 3.7 the value of the Von Karman constant, κ, was assumed to be 0.4.

3. Measuring the Reynolds stress distribution, $-\overline{uv}(y)$, u_* can be determined as

$$\frac{\tau}{\rho} \equiv -\overline{uv} + \nu\frac{\partial U}{\partial y} = u_*^2\left(1 - \frac{y}{y_0}\right) \tag{3.8}$$

where U is the mean velocity, y is the height, above the channel bed, of the point under consideration, y_o is the flow depth and ν is the kinematic viscosity of water.

4. The velocity distribution measured in the viscous sublayer, if it exists, can be used to determine u_* as follows

$$\frac{U}{u_*} = \frac{yu_*}{\nu} \tag{3.9}$$

5. Bed shear stress can be measured directly using a Preston tube.

Nezu and Nakagawa (1993) mentioned that the accuracy of the first method depends directly on small deflections of the channel bed and of the water surface. Also, the friction velocity determined from Eq. 3.6 is not a local but an overall value. They added that the difficulty of obtaining measurements within the viscous sublayer, makes method 4 extremely difficult to use. The third method is mostly used for turbulent studies and needs accurate turbulence measurements. Method 2 has been used in open channel flows but Nezu and Nakagawa (1993) commented that u_* must be evaluated from method 3 to check the validity of assuming $\kappa = 0.4$ in method 2.

We were left with the Preston tube technique, mentioned in method 5, for measuring the local bed shear stress for the type of flows studied in this research.

3.4.2 Preston tube technique

Preston (1954), based on the existence of the law of the wall, found a relation between the dynamic pressure (the difference between the total pressure head sensed by a total head tube, or the so-called Preston tube, resting on the bed and the static pressure head). If τ_o is the wall shear stress, Δp is the dynamic pressure, d is the external diameter of the Preston tube and ρ and υ are, respectively, the fluid density and kinematic viscosity. Simple dimensional analysis showed that

$$\frac{\tau_o d^2}{4\rho\upsilon^2} = F\left(\frac{\Delta p d^2}{4\rho\upsilon^2}\right) \tag{3.10}$$

Many researches have been performed to determine the function F and the calibration of Patel (1965) is considered to be the most definitive one. In the present study, the shear stress on a smooth bed was evaluated based on Patel's (1965) results. It should be noted that Patel's original equations were not always explicit and this needed a trial and error procedure which was not convenient. Hence, explicit equations were derived from the original equations as shown in Table. 3.1, where the trial and error procedure was eliminated and the bed shear stress could be calculated easily. In the present study, a Prandtl tube (Pitot-static tube) was used as a Preston tube to measure the dynamic pressure Δp which was sensed by a transducer and sent as a signal to the data acquisition system for the calculation of the shear stress using the modified equations shown in Table. 3.1.

3.5 The Experiments

In the present study, three research topics have been examined which are the study of a double-leaf gate as an energy dissipator, plane turbulent surface jets in shallow tailwater and plane turbulent wall jets in shallow tailwater. A number of experiments were conducted for each study. Tables 3.2, 3.3 and 3.4 show the details of the experiments conducted in each of the three research topics respectively. In the double-leaf gate energy dissipator, twenty one experiments were conduced as shown in Table 3.2. The effect of the offset ratio Z_o/b_o, submergence ratio $(y_t-Z_o)/b_o$, width ratio w/W, the Reynolds number R and the Froude number F_o, on the different characteristics of the flow were studied. Other experiments (series B) were conducted to classify the different flow patterns and to check for the existence of hysteresis effects. In the plane turbulent surface jets in shallow tailwater, nine experiments were conducted as shown in Table 3.3. The flow characteristics were investigated for different values of the offset ratio Z_o/b_o, the Reynolds number R and the Froude number F_o. Data from six experiments was included in the analysis of the plane turbulent wall jets in shallow tailwater and the details of these experiments are shown in Table 3.4. The first two experiments were conducted in the present study while experiments 3 to 6 were conducted (in the same flume) by Wu and Rajaratnam (1995). A further series of experiments (series B) were conducted to measure the drop in the water surface elevation at the gate, from that of the tailwater as well as the length of the surface eddy. Specific details about the experiments are provided in chapters 4, 5 and 6.

3.6 Experimental Errors and Uncertainties

3.6.1 Introduction and basic concepts

Concerning the reliability estimates of experimental results, two categories of experiments exist: single-sample and multiple-sample experiments. A given experiment is of the multiple-sample type if a sufficiently large number of measurements are taken (replications), by different observers, using various methods, instruments and sometimes more than one laboratory, such that statistical evaluation of the results can be made. On the other hand, a single-sample experiment is the one in which uncertainties are not found from such repetition.

The majority of engineering experiments, including the present work, are of the single-sample type. Even multiple-sample experiments are, in part, single-sample, due to the presence of several factors reducing the effect of repetition. Generally, measurements taken by a single observer do not provide consistent results and even measurements taken by different observers might not be completely independent. The same equipment can give different results when used by different observers and equipment of different designs, used by the same observer, usually give different results.

Kline and McClintock (1953) and Kline (1985) introduced a useful and practical way of describing uncertainties in basic variables for engineering single-sample experiments. Also included in their analysis is how uncertainties propagate into other dependent variables. Following is a brief description of their analysis.

The difference between the true and the measured values of a certain variable is called an *error* . The *uncertainty* of such measurement is defined as what the observer thinks, with a certain degree of confidence, the expected error might be. Although the error is a fixed quantity, the associated uncertainty can vary substantially. A *variable* is a basic quantity measured directly and the *result* is obtained from the basic variables after calculations and/or corrections. *Propagation of uncertainty* is the way in which uncertainties in the basic variables affect the uncertainties of the results.

Errors are usually classified into three groups which are accidental (or random) errors, fixed errors, and mistakes. *Accidental errors* are those varying errors which occur without a known reason. Their sources are unrecoverable such as instrumental friction and time lag, personal observation power and many others. ***Fixed errors*** are those which cause repeated readings to be in error by the same amount with no apparent reason. If the reason is known, as a dent on the probe, it can be fixed and hence the error is removed. With undetected reasons, fixed errors remain in the measurements. ***Mistakes*** are completely faulty readings of scales, watches, and other measuring devices. These errors are usually detectable on inspection as "way-out" and are rejected. In error analysis, it is usually assumed that all the fixed errors and mistakes have been detected and removed and hence, only the random errors are considered.

The accidental (or random) errors were found, in most of the cases, to have a normal (Gaussian) distribution. In single-sample experiments, because measurements are not repeated, no measure of errors is obtained and hence the distribution function can not be established. Consequently, the experimenter has to rely on his/her past experience and judgment. He/she can think of what would happen if the experiment was repeated a very large number of times. Kline and McClintock (1953) proposed that a good and concise way to describe the uncertainty in a variable is to specify the most likely value (usually the arithmetic mean of several readings) and an uncertainty interval with a specified confidence level. If the arithmetic mean of an observed variable is m and the uncertainty interval is W, the observed variable can be described as

$$\text{Variable} = m \pm W \text{ (confidence or probability level)} \qquad (3.11)$$

the following is an example of Eq. 3.11

$$\text{Velocity} = 1.5 \pm 0.05 \text{ m/s } (95\%)$$

Based on this statement, the experimenter believes that the true value of the velocity is probably 1.5 m/s and if a large number of observations are taken, 95% of them will fall within ±0.05 m/s of the mean value. The uncertainty interval, W, is not a variable but a fixed value selected so that the experimenter could estimate that, with assumed confidence level (here 95%), the error is less than ±W.

In most experiments, it is essential to calculate the uncertainty in the results from the estimates of uncertainty in the measurements. Kline and McClintock (1953) described a method to compute the propagation of uncertainty into a result R. Assume that the result R is a function of n independent variables $X_1, X_2, \ldots X_n$ and the corresponding uncertainty intervals for these variables are $W_{X1}, W_{X2}, \ldots, W_{Xn}$, with the same confidence levels. the result R can be expressed in a functional form as

$$R = R(X_1, X_2, \ldots\ldots\ldots X_n) \tag{3.12}$$

The uncertainty interval of the result, W_R, is described as

$$W_R = \sqrt{\left(\frac{\partial R}{\partial X_1} W_{X1}\right)^2 + \left(\frac{\partial R}{\partial X_2} W_{X2}\right)^2 + \ldots\ldots\ldots \left(\frac{\partial R}{\partial X_n} W_{Xn}\right)^2} \tag{3.13}$$

Eq. 3.13 has been successfully used for uncertainty analysis in fluid mechanics. Sometimes Eq. 3.12 takes the form

$$R = X_1^{m_1} X_2^{m_2} \ldots\ldots\ldots\ldots X_n^{m_n} \tag{3.14}$$

Then by using Eq. 3.14 in Eq. 3.13, a more useful form of Eq. 3.13 is obtained as follows

$$\frac{W_R}{R} = \sqrt{\left(m_1 \frac{W_{X1}}{X_1}\right)^2 + \left(m_2 \frac{W_{X2}}{X_2}\right)^2 + \text{..........}\left(m_n \frac{W_{Xn}}{X_n}\right)^2} \tag{3.15}$$

From this equation, the share of uncertainty for each variable in the total uncertainty of the result can be detected. If improvement in accuracy is necessary, the most effective instruments or measurements can be chosen. Uncertainty measurements can provide necessary information to accurately find which instrument has to be improved.

3.6.2 Estimate of uncertainty

The possible sources of errors for the measured variables in the experiments conducted in the present study are presented in this section. Also, the uncertainties of the results are calculated based on Eq. 3.15. The confidence level for all uncertainty estimates was taken as 95% (or 19 to 1 odds or 1 in 20 chance).

The main dimensions of the flume were measured by a scale to the nearest 1 mm and hence the estimated uncertainty was ±0.5 mm. The depth of flow was calculated from the water surface and bed elevations using a scale to the nearest 1 mm. The uncertainty in measuring the bed level was ±0.5 mm whereas that of the water surface was ±2 mm (due to the existence of surface waves). If the water depth is y_o and the water surface and bed levels are respectively L_s and L_b then

$$y_o = L_s - L_b \tag{3.16}$$

Differentiating Eq. 3.16 w.r.t L_s and L_b and substituting the results along with the uncertainty estimates of the surface and bed levels in Eq. 3.13, the uncertainty of the water depth can be estimated as follows

$$W_{y_o} = \pm\sqrt{(1\times 2)^2 + (-1\times 0.5)^2} = \pm 2.06\,\text{mm} \tag{3.17}$$

A vernier was used to measure the slot width b_o to the nearest 0.1 mm. So, the estimated uncertainty in this measurement was ±0.1 mm. The uncertainty in the discharge measurement was estimated to be ±0.1 l/s. Using the above uncertainty estimates, the uncertainty in the jet velocity at the slot U_o and the average velocity V, after the jet occupied the whole depth, can be calculated, as an example, in experiment 1 in the plane turbulent wall jet study (see Table 3.4) as follows

$W = 446 \pm 0.5$ mm;
$b_o = 10 \pm 0.1$ mm;
$y_o = 500 \pm 2.06$ mm;
$Q = 11.15 \pm 0.1$ l/s;
$U_o = Q/(W.b_o) = 2.50$ m/s;
$V = Q/(W.y_o) = 0.05$ m/s.

Then using Eq. 3.15 we get

$$\frac{W_{U_o}}{U_o} = \sqrt{\left(1\times\frac{0.1}{11.15}\right)^2 + \left(-1\times\frac{0.5}{446}\right)^2 + \left(-1\times\frac{0.1}{10}\right)^2} \tag{3.18}$$

or

$$\frac{W_{U_o}}{U_o} = \sqrt{(8.044 + 0.126 + 10.000).10^{-5}} = 1.35\% \tag{3.19}$$

and

$$\frac{W_V}{V} = \sqrt{\left(1\times\frac{0.1}{11.15}\right)^2 + \left(-1\times\frac{0.5}{446}\right)^2 + \left(-1\times\frac{2.06}{500}\right)^2} \tag{3.20}$$

or

$$\frac{W_V}{V} = \sqrt{(8.044+0.126+1.697).10^{-5}} = 1\% \qquad (3.21)$$

With U_o = 2.50 m/s and V = 0.05 m/s, Eq. 3.19 and Eq. 3.21 show that the uncertainties in U_o and V are respectively 0.03375 m/s and 0.0005 m/s. The above example shows that the accuracy of U_o can be enhanced by improving the discharge and the slot width measurements. It shows also that the accuracy of U_o is not much affected by the accuracy in measuring the flume width. To make V more accurate, focus should be given mainly to the discharge measurements. The accuracy of V is less affected by the water depth measurement and the effect of the flume width accuracy is almost negligible.

The accuracy of the pressure transducers used in this study, based on the manufacturer's specifications, was ±0.25% of the full scale and this included the effects of linearity, hysteresis and repeatability. The range of the pressure head that these transducers could measure was ±1.4 inches. However, the calibration of the transducers in the lab showed higher accuracy. For the unidirectional flows, the transducers were calibrated between zero and 1 inch (full scale = 1 inch = 25.4 mm). For the two-dimensional flows, the transducers were calibrated between -1 inch and +1 inch (full scale = 2 inches = 50.8 mm). Therefore, the uncertainty in the differential pressure head measurements in the one dimensional and two dimensional flows were respectively ±0.0635 mm and ±0.127 mm.

As was mentioned before, the velocity in the uni-directional flows was measured with a Prandtl tube (Pitot-static tube). In the two-dimensional flows, a pitch probe was used. Accuracy of the velocities measured with a Prandtl tube depended mainly on the accuracy of measuring the differential pressure head, the probe alignment, turbulence and wall effects. The Prandtl tubes are sensitive to an error in alignment of more than ±5 degrees. The accuracy in alignment of the probe could be estimated to be within ±2 degrees. No correction was made for turbulence and wall effects. Therefore, in estimating uncertainties in the velocity measurements using a Prandtl tube, only errors from pressure transducers (or manometer) were considered. Eq. 3.15 can be used to predict uncertainties in the velocity measurements as follows.

Differential pressure head (transducer) = $h \pm 0.0635$ mm

Differential pressure head (manometer) = $h \pm 2$ mm

where h is the differential pressure head in mm sensed by the transducer or measured by a manometer. Assuming the velocity measurement, u, depends only on the differential pressure head accuracy, Eq. 3.15 can be written as

$$\frac{W_u}{u} = \frac{1}{2}.\frac{W_h}{h} = \frac{g.W_h}{u^2} \qquad (3.22)$$

where g is the acceleration due to gravity. Using transducers, it was mentioned before that $W_h = \pm 0.0635$ mm in one dimensional flow velocity measurements. Assuming velocity u of 0.1, 0.2, 0.3 and 1.0 m/s, Eq. 3.22 shows uncertainties, W_u/u of 6.2%, 1.6%, 0.7% and 0.06% respectively. Eq. 3.22 shows that the uncertainty in the velocity measurements is inversely proportional to the magnitude of the velocity. In other words, the larger uncertainties in the velocity measurements should exist in the reverse flow zone where the velocities were relatively low. However, the overall uncertainty could be less than the calculated one due to the large number of samples (5000 samples) taken at each point. The corresponding estimates in case of using manometers could be easily obtained by repeating the above calculations for $W_h = \pm 2$ mm.

In two dimensional flows, velocity was measured with a pitch probe. In the present study, the pitch probe was only used in the double-leaf gate experiment to measure the velocity in the inclined jet from the slot till the jet surfaced. Different types of errors made it difficult to estimate uncertainties in the velocities measured with the pitch probe. Sources of errors in these measurements may include the presence of velocity and/or pressure gradients across the three holes of the probe, calibration curve fitting, probe misalignment, blockage error and existence of a third component of the velocity normal to the plane containing the probe. Errors because of using pitch probes were less, in this study, as the velocity measurements were taken in the plane of symmetry. Also, the pitch probe was not used near the boundaries where strong velocity gradients exist. Calculating the combined effects of the above-mentioned errors on the resultant accuracy of the velocity measurements would be a study by itself. However, rough estimates could be made to give an idea about the size of these errors based on flow visualization, inspection of velocity measurements and past experience. For small pitch angles (less than 15 degrees), pitch probes are considered to be as accurate as Prandtl tubes (Pitot-static tubes). With larger pitch angles, more uncertainty in the velocity measurements is expected. The uncertainty in the measurement of the probe angle was ±0.5 degrees. The uncertainty in the measurement of the attack angle or pitch angle (see Fig. 3.5) could be estimated to be within ±2 degrees. The effect of the pressure and velocity gradients on the velocity measurements could not be roughly estimated.

It was mentioned before that the bed shear stress was measured with a Prandtl tube sitting on the smooth bed of the flume. The uncertainty in the probe alignment was ±2 degrees. Neglecting the turbulence and the wall effects, only the errors in measuring differential pressure heads, using pressure transducers, may be considered. If the uncertainty in measuring the differential pressure head, using pressure transducers, is $W_h = \pm 0.0635$ mm, Eq. 3.13 can be used, along with the relations shown in Table 3.1, to predict uncertainties in measuring the bed shear stress.

3.7 References

Kline, S. J. (1985). "The purposes of uncertainty analysis." ASME Journal of Fluids Engineering, Vol. 107, pp. 153-160.

Kline, S. J. and McClintock, F. A. (1953). "Describing uncertainties in single-sample experiments." Mechanical Engineering, Vol. 75, pp. 3-8.

Nezu, I., and Nakagawa, H. (1993). "Turbulence open-channel flows." IAHR Monograph Series, A.A Balkema Publishers.

Patel, V. C. (1965). "Calibration of the Preston tube and limitations on its use in pressure gradients." J. Fluid Mech., Vol. 23, pp. 185-208.

Preston, J. H. (1954). "The determination of turbulent skin friction by means of Pitot tubes." J. Royal Aero. Soc., Vol. 54, pp. 109-121.

Rajaratnam, N., and Muralidhar, D. (1967). "Yaw and pitch probes." Hydraulic Instrumentation Series, Dept. of Civil Engrg., University of Alberta.

Wu, S. and Rajaratnam, N. (1995). "Free jumps, submerged jumps and wall jets." J. Hydr. Res., 33(2), pp. 197-212.

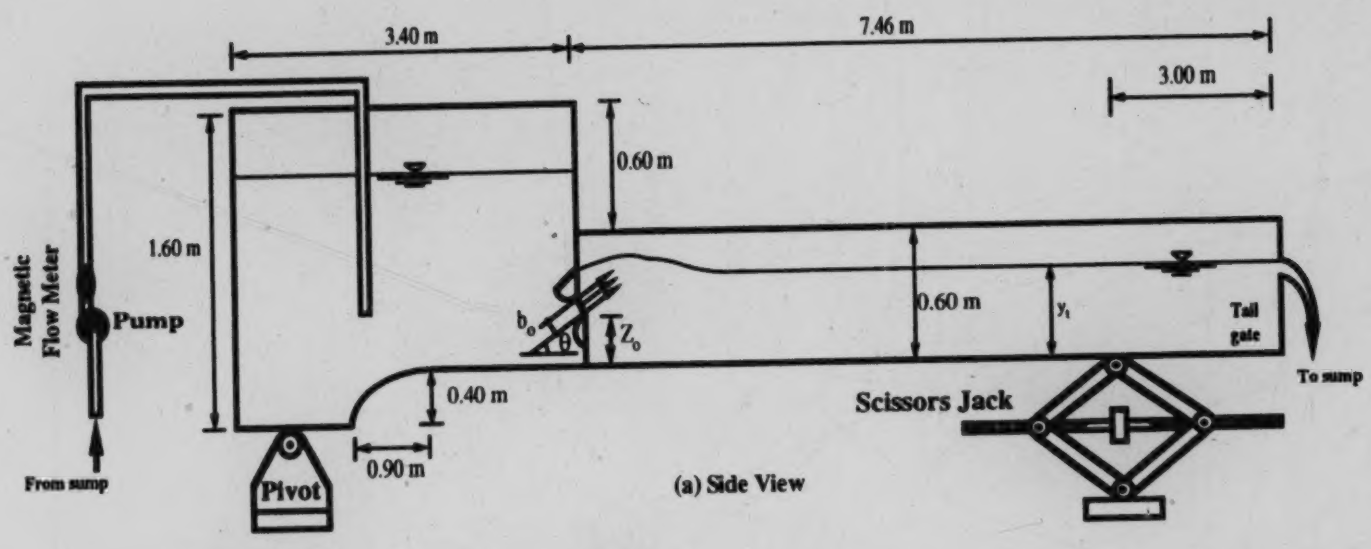
3.40 m
7.46 m
3.00 m
0.60 m
1.60 m
Magnetic Flow Meter
Pump
From sump
b_o
θ
Z_o
0.60 m
y_t
Tail gate
To sump
0.40 m
0.90 m
Pivot
Scissors Jack

(a) Side View

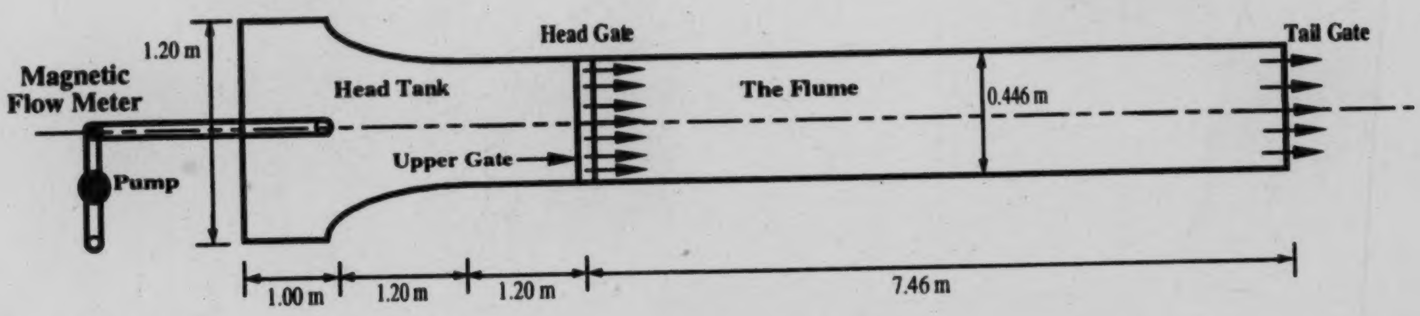
1.20 m
Magnetic Flow Meter
Pump
Head Tank
Head Gate
Upper Gate
The Flume
0.446 m
Tail Gate
1.00 m
1.20 m
1.20 m
7.46 m

(b) Plan View

Fig. 3.1 Experimental flume

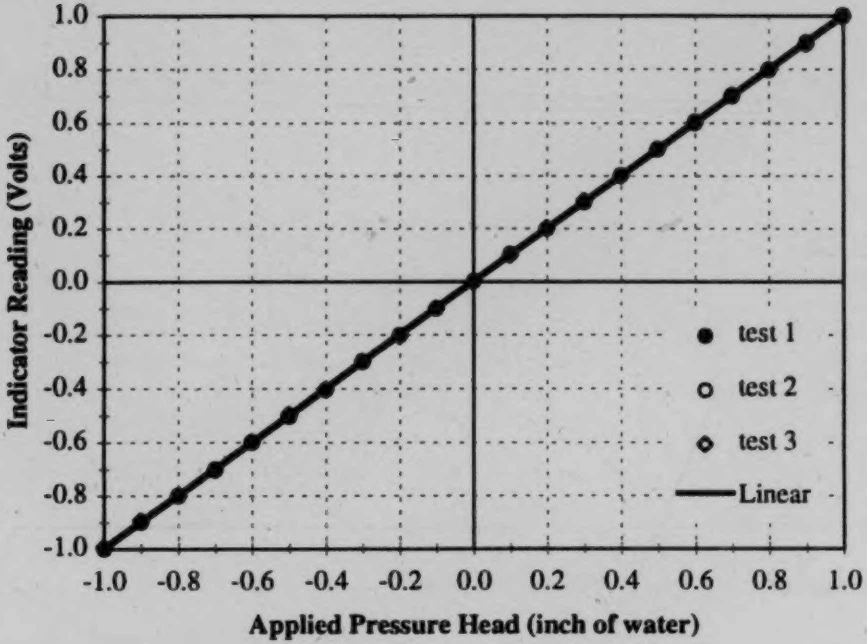

Fig. 3.2 Typical calibration of pressure transducers

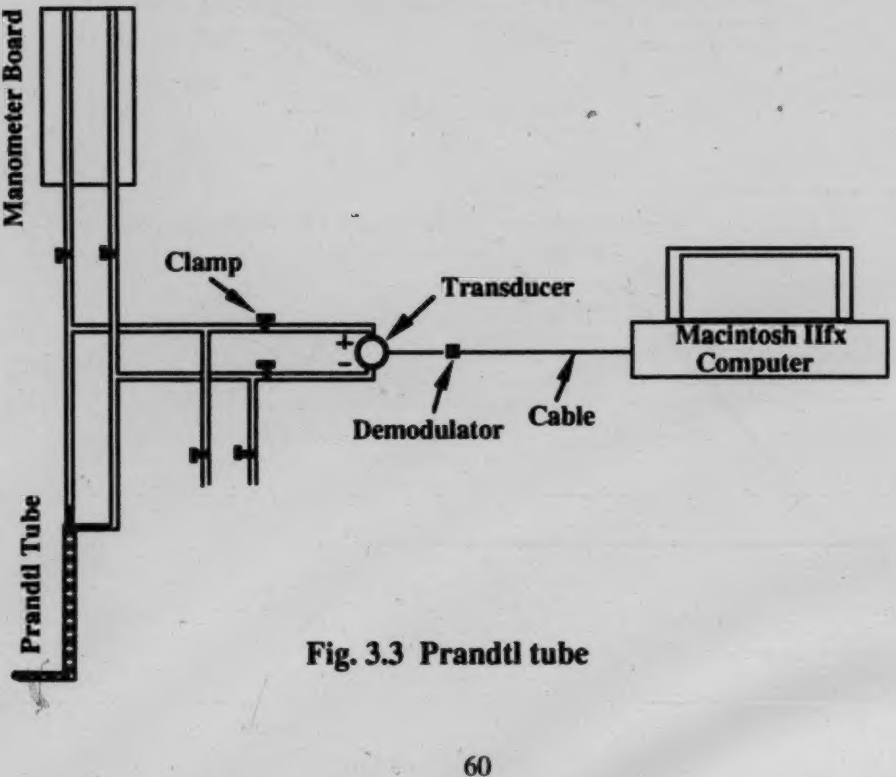
Manometer Board
Clamp
Transducer
+
-
Macintosh IIfx Computer
Demodulator
Cable
Prandtl Tube

Fig. 3.3 Prandtl tube

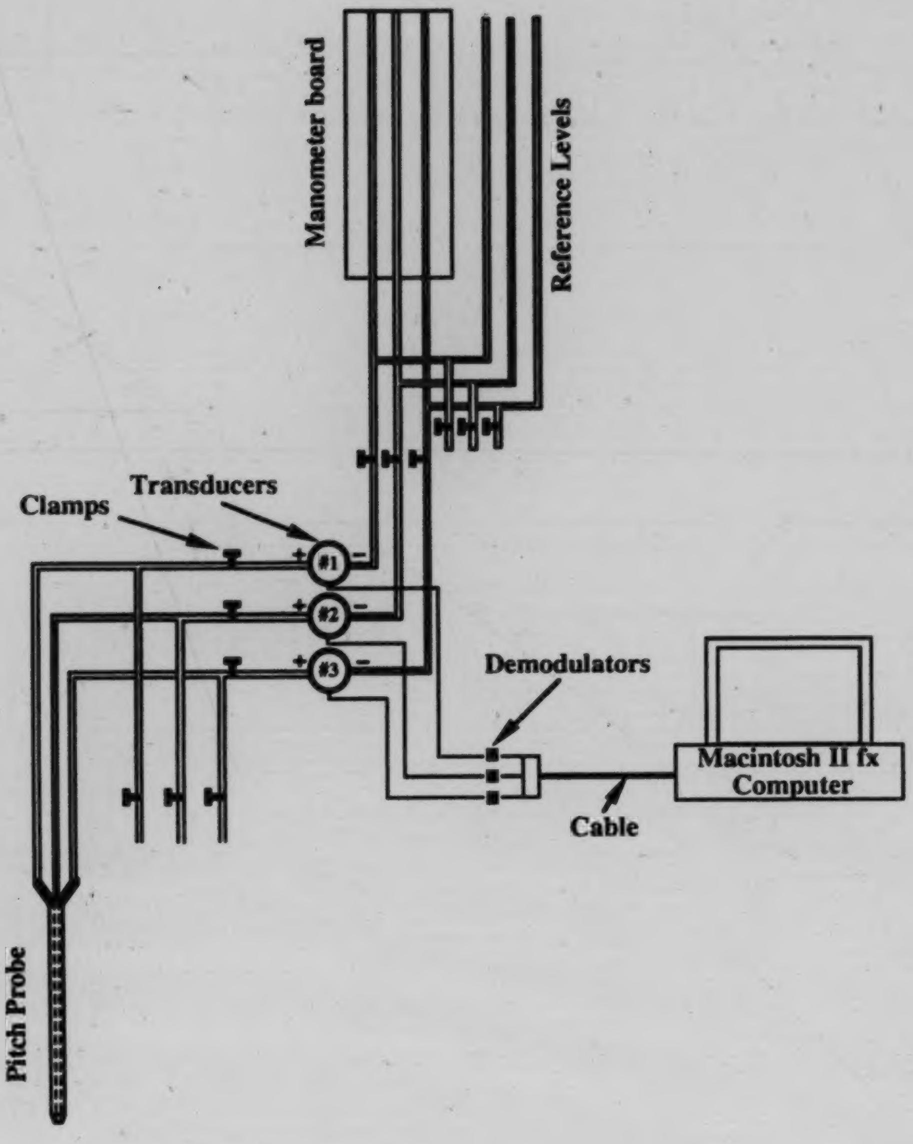
Manometer board
Reference Levels
Transducers
Clamps
#1
#2
#3
Demodulators
Macintosh II fx Computer
Cable
Pitch Probe

Fig. 3.4 Pitch probe

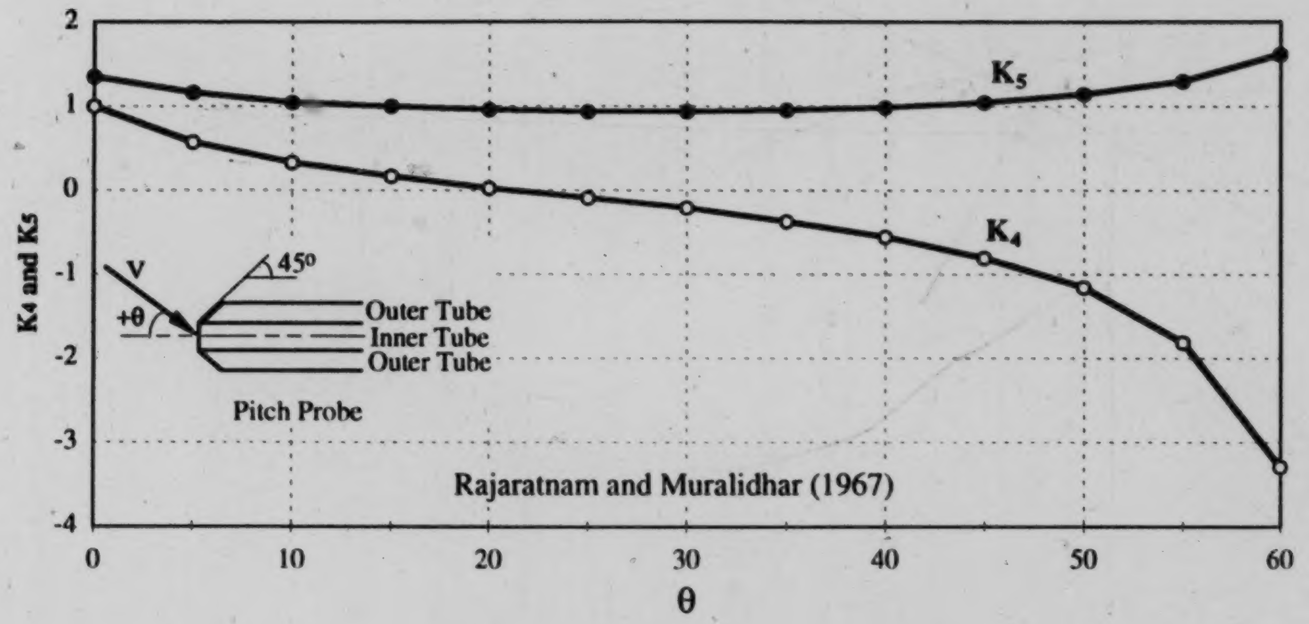

Rajaratnam and Muralidhar (1967)

Fig. 3.5 Calibration curves for the pitch probe

Table 3.1 Explicit equations for Patel's calibration curves for Preston tube

	Region 1	**Region 2**	**Region 3**
Original equations (Patel, 1965)	$y_* = 0.5x_* + 0.037$	$y_* = 0.8287 - 0.1381x_* + 0.1437x_*^2 - 0.006x_*^3$	$x_* = y_* + 2\log(1.95y_* + 4.1)$
Range of validity (Patel, 1965)	$y_* < 1.5$	$1.5 < y_* < 3.5$	$3.5 < y_* < 5.3$
Range in terms of τ_{o*}	$\tau_{o*} < 32$	$32 < \tau_{o*} < 3{,}162$	$3{,}162 < \tau_{o*} < 199{,}526$
y_* in terms of x_*	$y_* = 0.5x_* + 0.037$	$y_* = 0.8287 - 0.1381x_* + 0.1437x_*^2 - 0.006x_*^3$	$y_* = -0.96562 + 0.71911x_* + 0.017594x_*^2 - 0.00053x_*^3$
x_* in terms of y_*	$x_* = -0.074 + 2y_*$	$x_* = -0.61306 + 3.0882y_* - 0.57057y_*^2 + 0.055727y_*^3$	$x_* = 1.3272 + 1.2866y_* - 0.024433y_*^2 + 0.00106y_*^3$
Range in terms of x_*	$x_* < 2.926$	$2.926 < x_* < 5.59$	$5.59 < x_* < 7.619$
Range in terms of Δp_*	$\Delta p_* < 843$	$843 < \Delta p_* < 389{,}045$	$389{,}045 < \Delta p_* < 41{,}591{,}061$
$\Delta p/\tau_o$ in terms of x_*	$\Delta p/\tau_o = 0.918 + 3.482x_* - 2.996x_*^2 + 1.6358x_*^3$	$\Delta p/\tau_o = 114.58 - 111.19x_* + 35.967x_*^2 - 2.826x_*^3$	$\Delta p/\tau_o = 10.706 + 2.748x_* + 2.881x_*^2 + 0.0215x_*^3$

Note: $x_* = \log\left(\frac{\Delta p d^2}{4\rho\upsilon^2}\right) = \log(\Delta p_*)$ and $y_* = \log\left(\frac{\tau_o d^2}{4\rho\upsilon^2}\right) = \log(\tau_{o*})$

Table 3.2 Primary details of experiments of the double-leaf gate (series A)

Expt. (1)	θ (2)	b_o (mm) (3)	Z_o (mm) (4)	y_t (mm) (5)	W(mm) (6)	w(mm) (7)	U_o (m/s) (8)	F_o (9)	Z_o/b_o (10)	$(y_t-Z_o)/b_o$ (11)	w/W (12)	R (13)	Pattern (14)
1	30	9	270	270	446	446	1.43	4.80	30.00	0.00	1.00	12836	C
2	30	9	270	279	446	446	1.43	4.80	30.00	1.00	1.00	12836	B
3	30	9	270	473	446	446	1.43	4.80	30.00	22.50	1.00	12836	A
4	30	9	270	540	446	446	1.43	4.80	30.00	30.00	1.00	12836	A
5	30	9	270	270	446	446	2.14	7.20	30.00	0.00	1.00	19254	C
6	30	9	270	279	446	446	2.14	7.20	30.00	1.00	1.00	19254	B
7	30	9	270	338	446	446	2.14	7.20	30.00	7.50	1.00	19254	B
8	30	9	270	405	446	446	2.14	7.20	30.00	15.00	1.00	19254	AB
9	30	9	270	540	446	446	2.14	7.20	30.00	30.00	1.00	19254	A
10	30	9	270	279	446	446	3.09	10.40	30.00	1.00	1.00	27812	B
11	30	9	270	338	446	446	3.09	10.40	30.00	7.50	1.00	27812	B
12	30	9	270	540	446	446	3.09	10.40	30.00	30.00	1.00	27812	A
13	30	20	270	270	446	446	1.06	2.40	13.50	0.00	1.00	21261	C
14	30	20	270	540	446	446	1.06	2.40	13.50	13.50	1.00	21261	A
15	30	20	135	405	446	446	1.06	2.40	6.75	13.50	1.00	21261	A
16	30	20	0	270	446	446	1.06	2.40	0.00	13.50	1.00	21261	A
17	30	20	0	270	446	446	1.59	3.60	0.00	13.50	1.00	31892	A
18	30	20	270	540	446	446	2.13	4.80	13.50	13.50	1.00	42523	A
19	10	20	270	540	446	446	2.13	4.80	13.50	13.50	1.00	42523	A
20	10	20	270	540	446	357	2.13	4.80	13.50	13.50	0.80	42523	A
21	10	20	270	540	446	223	2.13	4.80	13.50	13.50	0.50	42523	A

Table 3.3 Primary details of experiments of the plane turbulent surface jets

Expt. (1)	b_o (mm) (2)	Z_o (mm) (3)	y_s (mm) (4)	W(mm) (5)	U_o (m/s) (6)	F_o (7)	Z_o/b_o (8)	$(y_s-Z_o)/b_o$ (9)	R (10)
1	5	500	505	446	1.60	7.2	100	1.00	8000
2	10	500	510	446	0.75	2.4	50	1.00	7500
3	10	500	510	446	1.50	4.8	50	1.00	15000
4	10	500	510	446	2.25	7.2	50	1.00	22500
5	10	300	310	446	1.88	6.0	30	1.00	18800
6	20	500	520	446	2.13	4.8	25	1.00	42600
7	10	200	210	446	0.90	2.9	20	1.00	9000
8	10	100	110	446	1.25	4.0	10	1.00	12500
9	10	50	60	446	0.50	1.6	5	1.00	5000

Table 3.4 Primary details of experiments of the plane turbulent wall jets (series A)*

Expt. (1)	b_o (mm) (2)	W (mm) (3)	U_o (m/s) (4)	F_o (5)	y_t (mm) (6)	y_2 (mm) (7)	$\eta = y_t/b_o$ (8)	$S = \eta/\eta_f - 1$ (9)	R (10)
1	10	446	2.50	8.0	500	108	50	3.63	25000
2	10	446	1.25	4.0	500	52	50	8.68	12500
3	10	446	1.72	5.5	440	73	45	5.04	17200
4	15	446	2.86	7.5	530	151	35	2.51	42900
5	15	446	2.86	7.5	460	151	30	2.05	42900
6	15	446	2.86	7.5	390	151	25	1.59	42900

* Experiments 3, 4, 5 and 6 were conducted by Wu and Rajaratnam (1995)

Chapter 4

A Double-Leaf Gate for Energy Dissipation Below Regulators[1]

4.1 Introduction

Hydraulic jumps have been widely used for energy dissipation below hydraulic structures. The formation of a hydraulic jump is very sensitive to the tailwater condition and as a result a specific tailwater level has to be maintained for a jump to form at a required location for any given flow rate. If the tailwater is raised above this specific level, the jump becomes submerged and if it is lowered below that level, the jump becomes repelled. Different types of hydraulic jumps have been evaluated as energy dissipators as summarized by Elevatorski (1959), Peterka (1963), Rajaratnam (1967) and Hager (1992). For regulators that are constructed in irrigation systems, the downstream water levels generally vary according to the irrigation demands and the hydraulic jump solution is generally unsuitable. Baffle walls and baffle blocks have been used in hydraulic jump stilling basins either to force the jump to form just downstream of the gate, if the tailwater depth is less than the sequent depth, or to deflect the high velocity stream to the free surface, if the tailwater depth is greater than the sequent depth. But baffles might be exposed to cavitation damage for relatively high velocity jets and further, they are not suitable for some flow conditions under which a reattached high velocity wall jet might form, as mentioned by Wu and Rajaratnam (1995).

This study introduces a new concept of a double-leaf gate as an energy dissipator which has the same advantage as the baffles of directing the high velocity stream to the free surface, without the risk of cavitation damage (see Fig. 4.1). Further, the performance of this scheme is independent of the tailwater fluctuations and as a result it can be used with variable tailwater conditions. In the double-leaf gate, the two leaves are arranged in such a way that a jet issues at an angle towards the water surface through the opening between the two leaves. The bottom leaf remains fixed while the top leaf (control leaf) is moved up and down to regulate the flow. Although only the upper gate is used for regulation, the lower one can also be lifted, when necessary, to flush out accumulated sediment deposits. In addition to being simple and efficient as an energy dissipator, splitting the vertical gate into two portions will be of benefit in decreasing the capacity, weight and size of the overhead gate control structure. (In the double-leaf gate dissipator a concrete apron is still required to satisfy the percolation length and to prevent erosion whenever the bottom gate is raised).

---

[1] The main content of this chapter has been published in the Journal of Hydraulic Engineering of the American Society of Civil Engineers, Vol. 124, No. 11, pp.1134-1145, 1998.

Fig. 4.1 shows a double-leaf gate where b_o is the opening width, Z_o is the height of the lower edge of the slot above the bed; U_o is the velocity of the jet issuing from the opening; y_t is the tailwater depth and θ is the angle of inclination of the jet. In this design, the upper gate is located upstream of the lower one to create the opening which produces the inclined jet. The Froude number of the jet is $F_o = U_o/(gb_o)^{0.5}$; S equal to $(y_t-Z_o)/b_o$ is the submergence ratio of the jet, defined as the ratio of the depth of water above the lower edge of the opening to the opening width; and Z_o/b_o is the offset ratio. Existing regulators can be modified using this idea by adding an upward sloping sill just under the gate as shown in Fig. 4.2.

4.2 Dimensional Analysis

Considering the problem illustrated in Fig. 4.1, any property (m) of the flow can be expressed as a function of various parameters of the flow, fluid properties and channel dimensions as

$$m = f(U_o, g, b_o, Z_o, w, W, y_1, \theta, \rho, \mu) \tag{4.1}$$

where w and W are the opening and the flume widths, respectively. The above relation can be represented in a dimensionless form as

$$M = f'\left[\frac{U_o}{\sqrt{gb_o}}, \frac{\rho U_o b_o}{\mu}, \frac{w}{W}, \frac{w}{b_o}, \frac{y_1 - Z_o}{b_o}, \frac{Z_o}{b_o}, \theta\right] \tag{4.2}$$

Eq. 4.2 shows that any property of the flow can be expressed as a function of the Froude number, the Reynolds number, the width ratio, the aspect ratio, the submergence ratio, the offset ratio and the deflection angle of the jet. For large values of the Reynolds number, $R = \rho U_o b_o/\mu$, where ρ and μ are, respectively, the mass density and dynamic viscosity of the fluid, viscosity is known to have negligible effects. Also, the aspect ratio of the jet w/b_o ranged between 11.15-22.30 which is large enough for the jet flow to be considered two-dimensional especially in the middle third of the flume where the measurements were taken. Hence, Eq. 4.2 becomes

$$M = f''\left[\frac{U_o}{\sqrt{gb_o}}, \frac{w}{W}, \frac{y_1 - Z_o}{b_o}, \frac{Z_o}{b_o}, \theta\right] \tag{4.3}$$

Experiments were conducted for different Froude numbers, width ratios, submergence ratios, offset ratios and two deflection angles of θ (30° and 10°).

4.3 Experimental Study

4.3.1 Experimental arrangement

This concept of double-leaf gate energy dissipator was studied in the laboratory in a flume, 0.446 m wide, 0.60 m deep and 7.6 m long, with aluminum bottom and plexiglas sides (see Fig. 4.3). Two pumps were used to supply the flume with the required discharge. The discharge was measured by a magnetic flow meter located in the supply line. Water entered the flume through an opening between two aluminum gates. The upper gate was located upstream of the lower one in such a way that the jet issued from the opening towards the water surface at a certain angle. Two streamlined lips were fixed on the upper and lower gates to produce a supercritical stream with a thickness equal to the gate opening b_o. A tail gate was used to control the tailwater depth in the flume.

Two systems were used for measuring the time-averaged velocity and bed shear stress. In one system a pitch probe was used whereas in the other, a Prandtl tube was used (see Fig. 4.4 and Fig. 4.5). The pitch probe was made of three tubes of external diameters of 1.0 mm and was made and calibrated in the Hydraulics laboratory. The pitch probe was used in measuring the velocity distribution in the jet directed towards the water surface. This probe was always placed normal to the jet and was used in measuring the velocity profiles across the jet. The Prandtl tube with an external diameter of 3.0 mm, was used in measuring the velocity distribution along vertical sections in the jet after it surfaced. The Prandtl tube was also used as a Preston tube for measuring the bed shear stress (Preston (1954); Patel (1965)).

Three transducers (Validyne model DP45-16 Northridge, Calif) were used in the experiments to measure the pressure differences. The output ends of the transducers were connected to a flat cable that was connected to a Macintosh IIfx computer. In cases where the pressure differences were within the range of the transducers (±1 inch), two transducers were used. The first one was connected between the middle and the upper tubes of the pitch probe while the other was connected between the middle and the lower tubes. In cases where the pressure differences were outside the transducers range, each transducer had to be connected between one of the tubes and a reference level and the reference was adjusted at each point to make the pressure difference, between the two sides of the transducer, within its range. The Prandtl tube was used in measuring the velocities downstream of the point of collision, with the free surface or the bed, and used also to measure the bed shear stress. Usually, one transducer was required to connect the static and the total head tubes of the Prandtl tube. In cases where the pressure difference at a point was outside the transducer range, the two tubes were switched to a manometer board to measure the pressure difference and then calculate the velocity at that point.

The computer took samples from the transducers at a certain sampling rate, couples every sequence of two signals to obtain the magnitude of the velocity, attack angle and the pressure in case of the pitch probe or the magnitude of the velocity in case of the Prandtl tube. The computer displayed the results on a strip chart on the screen in real time. When the required number of samples were taken (usually 5000 samples were recorded at each point with a sampling rate of 40 samples/second) the computer processed all the samples to obtain the mean value and the standard deviation for each variable and saved the results in an open file. The computer programs used in the experiments were written in LabView language.

4.3.2 Experiments

A total of 21 experiments (series A) were conducted and the primary details of these experiments are shown in Table 4.1. Eighteen of these experiments (Expt.1-Expt.18) were conducted for a deflection angle of θ equal to 30 degrees and a width ratio of 1.00. Three experiments (Expt.19-Expt.21) were conducted for a deflection angle of θ equal to 10 degrees and width ratios of 1.00, 0.80 and 0.50 respectively. The values of the various parameters (b_o, Z_o, y_t, w, U_o) were selected to achieve a wide and a practical range of the offset ratio, the submergence ratio, the width ratio and the Froude number. Four offset ratios of 0.00, 6.75, 13.50 and 30.00 were used. The submergence ratio S was varied from zero to about 30. Three width ratios of 1.00, 0.80 and 0.50 were studied. Experiments were conducted for Froude numbers equal to 2.40, 3.60, 4.80, 7.20 and 10.40. The Reynolds number of the jet was in the range of 12000 to 43000. Two conditions had to be satisfied in the selection of the deflection angle θ. The first was to avoid the jet reattachment to the rigid boundaries (the flume bed or the gate). The second was to have a reasonable horizontal component of the jet velocity. A deflection angle of θ equal to 30 degrees satisfied these two conditions. Other experiments (series B) were conducted to classify the different flow patterns and to check for the existence of any hysteresis effects.

4.4 Experimental Results and Analysis

4.4.1 Flow patterns

Preliminary experiments (series B) were conducted to determine the different flow patterns for a range of the Froude number and the submergence ratio. The different flow patterns are shown in Fig. 4.6(a-c) and Fig. 4.7(a-c). Two deflection angles of 30 and 10 degrees were used. For the 30 degrees' angle, experiments were performed with one width ratio of 1.00 and four offset ratios of 30.00, 13.50, 6.75 and 0.00. For the 10 degrees angle, experiments were performed with three width ratios of 1.00, 0.80, 0.50 and one offset ratio of 13.50. For each angle, offset ratio and width ratio, the critical submergence ratios at which the flow changed from one pattern to another were determined through the following steps. (1) Open the tail gate completely and start the pump to obtain the desired discharge. (2) Slowly raise the tail gate in small increments and wait for the flow to become stable. (3) Determine the tailwater elevations at which the flow changes from one pattern to another. (4) Lower the tail gate slowly in small increments and wait for the flow to become stable. (5) Repeat step (3) to see as to whether hysteresis effects existed.

4.4.1.1 Width ratio w/W = 1.00 and θ = 30 degrees

For experiments conducted with $w/W = 1.00$ and $\theta = 30$ degrees, three stable flow patterns were observed as shown in Fig. 4.6(a-c) and Fig. 4.7(a-c). Fig. 4.8(a-c) show the classification of these flow patterns according to the submergence ratio $S = (y_t-Z_o)/b_o$, Froude number $F_o = U_o/(gb_o)^{0.5}$ for three values of the offset ratio Z_o/b_o of 30.00, 13.50 and 6.75 respectively. Starting with the tailwater at or below the lower edge of the opening (i.e. $S \leq 0$), the jet issued as a free jet and plunged into the tailwater where it impinged on the bed at a certain section (see Fig. 4.6(c) & Fig. 4.7(c)). At the line of impingement, the jet bifurcated into one jet traveling downstream and another jet traveling upstream. The forward flowing jet proceeded as a wall jet whereas the backward flow diffused in the confined pool under the jet. This flow was referred to as pattern C. When the tailwater was raised above the lower edge of the slot, the air cavity under the jet started to fill, inducing an upward pressure on the jet. This pressure raised the jet trajectory and consequently the line of impingement started to move downstream (see Fig. 4.9). With further increase in the tailwater depth, the plunging jet changed into a surface jet as shown in Fig. 4.6(b) & Fig. 4.7(b) and was referred to as pattern B. The upward pressure on the jet increased with increasing tailwater depth until the jet started to oscillate and this flow was referred to as pattern AB. In the oscillating zone, the jet oscillated between the angle of the slot and an enhanced angle. At the angle of the slot, the upward pressure became maximum and pushed the jet towards the gate while at the steeper angle, the pressure under the jet was relieved allowing the jet to return back to its original direction and so on. The oscillating pattern AB produced strong surface waves and should be excluded from design unless a suitable wave suppresser is used. These oscillations were totally suppressed with a piece of wood placed on the water surface where the jet surfaced. With a further increase of the tailwater, water started to accumulate above the jet producing a downward force that balanced the upward pressure and finally the jet stopped oscillating and pattern A started to form (see Fig. 4.6(a) & Fig. 4.7(a)). In flow pattern A, the jet issued with the slot angle, kept its initial direction until it reached a certain point after which the jet path became steeper with the angle of the jet increasing to about 45 degrees. Finally, the jet hit the water surface at a certain line and then proceeded as a surface jet. In the stable flow pattern A, two eddies formed, one above and another below the jet, as shown in Fig. 4.7(a). The upper eddy was confined by the jet, the water surface and the gate whereas the lower eddy was bounded by the jet on the top and the channel bed. Pattern B also showed a surface jet but the jet from the slot was not submerged near the gate.

This design of the double-leaf gate dissipator would be used mainly in rivers and main canals where the sluices are submerged enough for pattern A to exist during operation. The other flow patterns were covered only to account for operations during canal filling, emptying or other special operations. In these streams, the tailwater variations, due to the different water requirements, should be within zone A. It can be noticed from Fig. 4.8(a-c) that the oscillating zones are relatively wide which may require the sluices to be deeply submerged so that pattern A can form. Hence, it was of great importance to modify[2] the model in such a way that the oscillating zones are eliminated, or at least minimized, and hence pattern A can form with less submergence.

---

[2] Modification of the model has been tentatively accepted at the 1st Minia Conference for Advanced Trends in Engineering, MICATE'99, Minia, Egypt.

Two methods were tried, first by decreasing the deflection angle (i.e. using $\theta<30$ degrees) and the other by having the jet ventilated (i.e. $w/W<1$).

4.4.1.2 Width ratio w/W = 1.00 and θ = 10 degrees

One experiment (Expt. !9) was conducted with $w/W = 1.00$, $Z_o/b_o = 13.50$ and $\theta = 10$ degrees. Some observations were also taken for an offset ratio equal to zero. For $Z_o/b_o = 13.50$, the same behavior of the jet was repeated as it issued with the original angle (i.e. 10 degrees) until it assumed a larger angle at a later stage as with the case of the 30 degrees jet. With $\theta = 10$ degrees, the upper cavity was larger and this helped in minimizing the oscillating zone. Other than this benefit, the different flow characteristics for the two angles were quite similar. For $Z_o/b_o = 0.00$, the 10 degrees jet tended to reattach to the bed by the Coanda effect. Therefore, the 10 degrees angle can only be used in the prototypes of relatively large offset ratios. As the 30 degrees angle is suitable for both the small and the large offset ratios, it is recommended for double-leaf gate dissipators. However, more experiments are needed to determine the minimum angle that can be used in the double-leaf gate dissipators. It is important to note that at a certain angle and offset ratio the jet reattaches to the bed only when the submergence exceeds a certain limit. In the recommended study, each angle should be studied with different offset ratios. For each combination of an angle and an offset ratio, the minimum submergence at which the jet reattaches to the bed should be determined. This study will help the designers to select the suitable angle when the ranges of the offset ratio and the submergence ratio are known in the prototype. (Note that the offset ratio and the submergence ratio change not only with Z_o and y_t but also with the change of the opening according to the irrigation demands).

4.4.1.3 Width ratio (w/W) < 1.00 and θ = 10 degrees

It was mentioned earlier that raising the tailwater above the slot level was associated with an increase in the upward pressure induced on the jet, resulting in jet oscillation. As the jet occupied the whole width of the flume, the downstream water could not accumulate above the jet until the water surface elevation reached the crest of the jet trajectory. Raising the tailwater above the crest level resulted in the accumulation of water above the jet and hence an increase in the downward pressure. The jet stopped oscillating when a balance in the upward and downward pressures was reached. To overcome this pressure unbalance in the oscillating zone, two experiments (Expt. 20 and Expt. 21) were conducted with width ratios equal to 0.8 and 0.5 (see Fig. 4.11 for w/W=0.50) and an offset ratio of 13.50. In these experiments, the jet occupied part of the flume width leaving two gaps, or ventilation zones, between the jet and the side walls (see Fig. 4.11). As soon as the tailwater elevation exceeded the slot level, the water under the jet moved up through the side gaps and accumulated above the jet. No oscillations (pattern AB) were observed in these two experiments. In this design, i.e. w/W < 1.00, only flow patterns A, B and C existed (see Fig. 4.8(d)). The tailwater had to be above the lower edge of the slot for patterns B and A to form. If the only concern is to eliminate the oscillating zone, a width ratio of 0.8 (or even 0.9) is adequate. Other advantages of having a width ratio less than unity will be discussed later. The modified double-leaf gate dissipator, with w/W < 1.00, can be used in shallow tailwater streams as well as deep ones. It should be noted that in shallow-tailwater streams the formation of the classical hydraulic jump is difficult and to form just downstream of the gate, the jump should be forced by baffle blocks or baffle walls or by any other means. Therefore, double-leaf gate basins are strongly recommended to be used, instead of common basins, in such streams.

4.4.1.4 Hysteresis effects

Preliminary experiments (series B) were conducted to classify the different flow patterns and the results of these experiments are shown in Fig. 4.7(a-c) and Fig. 4.8(a-d). In these experiments, the tailwater depth was varied in such a manner as to observe the different flow patterns. The critical submergence ratios, at which the flow changed from one pattern to another, were found with the tailwater depth increased in small steps. Experiments were also performed with decreasing tailwater depth to see as to whether hysteresis effects were present. For the experiments with the 9 mm slot width, switching of the flow pattern from C to B and from B to C occurred when the tailwater level was at the upper and lower edges of the slot respectively as shown in Fig. 4.8(a) thus showing minor hysteresis effects. However, appreciable hysteresis effects were present for the 20 mm slot as shown in Fig. 4.8(b-c). With raising the tailwater, the jet switches from pattern C to pattern A with the oscillatory regime AB existing in between and flow pattern B did not exist. When the tailwater was lowered, the situation became different as pattern B set in at the lower limit of the oscillating zone. The jet switched to the plunging pattern (C) when the water level fell to the lower edge of the slot. The difference in behavior between the 9 mm and the 20 mm jets was perhaps due to the relatively larger momentum flux in the 20 mm jets. In weak jets, if the minor hysteresis through the opening is overlooked, a specific flow pattern is formed for each combination of the Froude number and the submergence ratio, whether the tailwater was raised or lowered. In large momentum jets, the original state of the jet is the third factor in determining the flow pattern. While raising the tailwater and assuming the jet is originally of the plunging type, it prefers to stay as a plunging jet for as maximum submergence as possible. The same occurs while lowering the tailwater and assuming the jet is originally of pattern B as it also tries to keep its state for as minimum submergence as possible. The ventilated jets did not show any hysteresis effects as shown in Fig. 4.8(d). For the oscillating jet regime, the maximum height reached by the jet increased with the Froude number. To delineate the range of the oscillating jet, the variation of the tailwater depth normalized with ($U_o^2 \sin^2\theta /2g$) was plotted against the Froude number as shown in Fig. 4.10 where the range of the tailwater through which the oscillation occurs decreased as the offset ratio decreased. No oscillations were observed for Z_o/b_o equal to zero. The ventilated jets suffered neither oscillations nor hysteresis effects because the upward and the downward pressures acting on the jet were in balance at any tailwater level. In conclusion, the unbalance between the upward and the downward pressures acting on the jet is assumed to be the main reason causing the jet oscillations as well as the hysteresis effects.

4.4.2 Velocity profiles

Time-averaged velocity profiles were obtained for the whole flow field including the inclined jet from the slot, the surface jet for flow patterns A, B and AB and the wall jet on the bed for pattern C and also in the recirculating flow regions for several experiments. A total of 14 experiments were conducted and the details of these experiments are shown in Fig. 4.12(a-n) and are included in table 4.1. These observations were taken for the different Froude numbers (F_o = 2.40, 3.60, 4.80, 7.20 and 10.40), six submergence ratios (S = 0.00, 1.00, 13.50, 15.00, 22.50 and 30.00) and four offset ratios (Z_o/b_o = 0.00, 6.75, 13.50 and 30.00). The velocity profiles in the inclined jet from the slot are discussed later. Velocity measurements could not be obtained in the strong shear layer separating the forward and the backward flows because the flow within this layer was very turbulent. In this layer the velocity fluctuations were larger than the local mean velocity. Hence, velocities within this layer were predicted by linear interpolation.

Fig. 4.12(a) shows the velocity profiles for pattern C where the jet plunged into the tailwater till it hit the bed at a certain line and then moved as a wall jet. Fig. 4.12(b) shows the velocity profiles for pattern B where the jet issued from the slot as a curved surface jet and then proceeded as a horizontal surface jet. For flow patterns C and B which are shown in Figs. 4.12(a and b), respectively, the Froude number is the same but the tailwater in pattern C was at the lower edge of the slot whereas in pattern B, the tailwater was at the upper edge. Fig. 4.12(c-n) show flow pattern A except for Fig. 4.12(e) which shows flow pattern AB. In flow pattern A, the jet issued from the opening with a certain angle and then assumed a larger angle at a later stage. After the jet surfaced it proceeded as a surface jet. These figures show the velocity profiles for the surface jet as well as the reverse flow. In the surface jet the maximum velocity is located at, or very close, to the free surface and the velocity distribution seems to be linear. The velocity distribution of the return flow is almost uniform except near the bed and at the jet edges. The velocity profiles of pattern AB, shown in Fig. 4.12(e), are very similar to those of pattern A. In pattern AB, the velocity measurements were affected by the jet oscillation especially in the far field where the mean velocities were relatively small and could easily be affected by the flow unsteadiness. Fig. 4.12(k-n) show pattern A for the Froude number, the submergence ratio and the offset ratio are equal to 4.80, 13.50 and 13.50 respectively. Fig. 4.12(k) and Fig. 4.12(l) are for the same width ratio of w/W = 1.00 but the deflection angles, in the two experiments, were 30 and 10 degrees respectively. The velocity profiles shown in Fig. 4.12(k and l) are almost identical indicating that the deflection angle has almost no effect on the velocity characteristics of the surface jet if the Froude number, the submergence ratio, the offset ratio and the width ratio are kept constant. Fig. 4.12 (l-n) show the effect of the width ratio on the velocity distributions. In these three figures the width ratios w/W are 1.00, 0.80 and 0.50 respectively while the other variables are the same. These figures show that the decrease in the width ratio is associated with a faster decay of the maximum velocity.

4.4.3 Reverse flow

The reverse flow underneath the surface jet is driven by an adverse pressure gradient. This flow is the source of the entrained fluid required for the expansion of the surface jet (see Fig. 4.13 for the reverse flow near the bed). The velocity profiles shown in Fig. 4.12(c-n) indicate that the velocity in the reverse flow below the surface jet is almost uniform except near the bed and at the jet edges. Fig. 4.14(a-d) show the variation of the depth-averaged reverse velocity u_r for different Froude numbers, submergence ratios, offset ratios, inclination angle and width ratios. Fig. 4.14(a) shows that the depth-averaged reverse velocity increases as the Froude number increases, and as the offset ratio decreases but is only slightly affected by the submergence factor as long as the flow pattern remains the same. For the oscillating jet flow pattern AB, u_r was found to have significantly smaller values, especially in the far field. Fig. 4.14(b) shows the longitudinal variation of (u_r/U_o) for patterns A and AB. The maximum value of the normalized reverse velocity is affected by the offset ratio. For $Z_o/b_o = 30.00$, this maximum value is about 10% U_o whereas it is 14% and 18% for $Z_o/b_o = 13.50$ and 6.75 respectively. Fig. 4.14(c-d) show the effect of the jet angle θ and the width ratio w/W on the depth-averaged reverse velocity distributions. It can be shown that the deflection angle θ does not have a significant effect on the depth-averaged reverse velocity distributions. Decreasing the width ratio from 0.80 to 0.50 was associated with a little decrease in the depth-averaged reverse velocity downstream of the peak of the profile. In conclusion, the normalized depth-averaged reverse-velocity distributions are mainly affected by the offset ratio, Z_o/b_o. For $Z_o/b_o = 30.00$, the normalized depth-averaged velocity distributions can be represented by the following equation

$$\frac{u_r}{U_o} = 3.0951 * 10^{-6}\left(\frac{x}{b_o}\right)^2 - 0.0007\left(\frac{x}{b_o}\right) - 0.0557 \qquad (4.4)$$

with a value of the correlation coefficient r^2 of 0.89

The corresponding equation for $Z_o/b_o = 13.50$ is

$$\frac{u_r}{U_o} = 1.466 * 10^{-5}\left(\frac{x}{b_o}\right)^2 - 0.0014\left(\frac{x}{b_o}\right) - 0.0955 \qquad (4.5)$$

with a value of the correlation coefficient r^2 of 0.93

4.4.4 Velocity decay

For each velocity profile, the maximum velocity u_m may be considered as an important characteristic and as a scale. Fig. 4.15(a-n) show the decay of the maximum velocity u_m at any section with the longitudinal distance measured from the slot for flow patterns A, B, C and AB. Half of these plots are presented in a dimensionless form to show the decay of the maximum velocity u_m in terms of the velocity of the jet at the slot U_o with the normalized distance from the gate x/b_o along with the corresponding curves for plane turbulent wall jets and surface jets (Rajaratnam 1976; Rajaratnam and Humphries 1984). As flow pattern A has been recommended for operation in the prototype, more focus was given to pattern A compared to the other flow patterns. A study of the above mentioned figures shows that, in flow pattern A, the decay of the maximum velocity occurs in three stages. The first stage is the decay in the inclined jet, from the slot to the surfacing of the jet. The maximum velocity in this stage decays very rapidly. This zone may be considered the most efficient zone in dissipating the energy of the jet and up to 80% of the issuing velocity can decay within this zone. The fast decay in this region is due to the high entrainment rate of curved turbulent jets. The second stage starts at the section of minimum velocity and indicates an increase due to the fall from the surface hump, which forms at the location where the inclined jet surfaces, and ends at the section of the next maximum. The velocity decays again in the third stage due to the turbulent mixing in the surface jet. This stage shows a very slow decay in comparison with the first stage. It may also be noticed that the decay of the maximum velocity in the last stage is very similar to that of the plane surface and wall jets. The overall decay was found to be more than that of the surface and wall jets in the range of x/b_o of 220. It was mentioned earlier that the factors that affect the flow characteristics are the Froude number, the offset ratio, the submergence ratio, the inclination angle, the width ratio and, of course, the flow pattern.

Figs. 4.15(a-n) were designed in such a way that only one parameter is changing while the other parameters are kept constant. Figs. 4.15(a-b) show experiments 4, 9 and 12 where the flow is of pattern A. The changing parameter in the three experiments was the Froude number which was equal to 4.8, 7.2 and 10.4 in the three experiments respectively. Fig. 4.15(b) shows that the Froude number has no effect on the decay of the maximum velocity if U_o and b_o are used as the velocity and length scales respectively. Figs. 4.15(c-d) show experiments 3 and 4 where the flow is also of pattern A. The changing parameter was the submergence ratio equal to 22.5 and 30.0 respectively. Figs. 4.15(c-d) show that the submergence ratio has no effect on the velocity decay (as long as the change in the submergence does not change the pattern of flow). Figs. 4.15(e-f) shows experiments 14, 15 and 16 (pattern A) where the changing parameter was the offset ratio which had the values of 13.50, 6.75 and 0.00 in the three experiments respectively. Figs. 4.15(e-f) show that the change in the offset ratio can affect the velocity decay significantly. The smaller the offset ratio, the faster is the velocity decay. This might be explained that decreasing the offset ratio is associated with an increase in the velocity of the return flow which in turn causes the main flow velocity to decay faster. The changing parameter in Figs. 4.15(g-h) was the inclination angle of the jet. This figure shows experiments 18 and 19 (pattern A) where the inclination angle of the jet θ was equal to 30 and 10 degrees respectively. It can be seen from Figs. 4.15(g-h) that changing the inclination angle does not have any significant effect on the velocity decay. The last parameter to be considered was the width ratio w/W. Figs. 4.15(i-j) show experiments 19, 20 and 21 where the width ratio was equal to 1.0, 0.8 and 0.5 respectively. Figs. 4.15(i-j) show that the smaller the width ratio the faster is the maximum velocity decay. This seems logical as decreasing the width ratio enhances the mixing of the jet with its surroundings which results in a faster decay of its maximum velocity.

The maximum velocity decay in the flow patterns A, B and C are shown in Figs. 4.15(k-l) where all the other parameters, except for the submergence ratio, were kept constant. At $x/b_0 \approx 220$, u_m/U_o was almost identical in flow patterns A and B. Flow pattern C showed a faster decay. At $x/b_o \approx 120$, u_m/U_0 was nearly one third that of flow patterns A and B. Figs. 4.15(m-n) show experiments 9 and 8 for flow patterns A and AB respectively. It is clear that the maximum velocity decay in both flow patterns is almost the same. A consolidated plot for all the maximum velocity decay profiles in flow pattern A is shown in Fig. 4.16.

To evaluate the double-leaf gate as an energy dissipator, comparisons with well-known dissipators were essential. Fig. 4.17 shows a comparison between the decay of the maximum velocity in the double-leaf gate dissipator for flow pattern A with the results of Wu and Rajaratnam (1995) for a surface jet produced with a baffle wall for submerged flow. For a Froude number equal to 7.20, Fig. 4.17 shows that in the first stage, the decay of the maximum velocity in the present study is much faster. The overall decay for greater distances is almost the same in both the experiments.

Comparisons of the maximum velocity decay in the double-leaf gate dissipator with those of the free and the submerged hydraulic jumps are shown in Figs. 4.18(a-b) and 4.19(a-b). In Figs. 4.18(a-b), U_o was taken as the velocity scale and b_o as the length scale whereas in Figs. 4.19(a-b), the length scale was taken as L, where L is the horizontal distance from the gate to the point where the velocity is $0.5U_o$. Fig. 4.18(a) shows that the maximum velocity decay in the first stage of the double-leaf gate dissipator is similar to that of the free jump whereas in the far field, the free jump basin appears to be more efficient. However, the overall decay in the two cases is comparable. The double-gated jet is much more efficient than the submerged jump, especially in the first stage of decay as shown in Fig. 4.18(b). With L as a length scale, Figs. 4.19(a-b) show a better similarity between the double-leaf gate dissipator, the free and the submerged jump stilling basins. As b_o is relatively small, L is considered to be more reliable and hence the maximum velocity decay for the present study is considered, in general, to be very similar to that of free and submerged jumps.

4.4.5 Inclined jet

Fig. 4.20 shows the locus of the maximum velocity along with the water surface profiles for pattern A in experiments 4, 9 and 12 respectively. The jet issues from the slot with an initial angle θ of 30 degrees. The jet keeps its initial direction until it reaches a certain point after which the jet path becomes steeper with the angle of the jet increasing to about 45 degrees. It was noticed that the point at which the jet changes its direction is very close to the end of the first stage of the maximum velocity decay. This bending of the jet is similar to the Coanda effect of jets located near boundaries. This aspect of the curved jet has been attributed to the pressure difference across the jet. Changing the direction was also explained by Sawyer (1962).

Some observations were also taken for a deflection angle of $\theta = 10$ degrees. For the large offset ratios, the same behavior of the jet was observed as it issued with the original angle until it assumed a larger angle at a later stage as with the case of the 30 degrees jet. With $\theta = 10$ degrees, the upper cavity was larger and this minimized the oscillating zone. Other than this, the different flow characteristics for the two angles were quite similar. For the small offset ratios, the 10 degrees jet tended to reattach to the bed by the Coanda effect. Therefore, the 10 degrees angle can only be used with prototypes having large offset ratios. As the 30 degrees angle is suitable for both small and large offset ratios, it is recommended for use in double-leaf gate dissipators.

Fig. 4.21(a-j) show the velocity distributions and the similarity profiles for the inclined jet for experiments 3, 9, 12, 14 and 16 respectively. In these plots, each group of data points are for a certain Froude number, submergence ratio, offset ratio, width ratio and distance from the slot. The velocity distributions in the five experiments mentioned above, along with the Gaussian distribution for the simple submerged plane jet, are represented in Fig. 4.22. The maximum velocity within each section was chosen to be the velocity scale. The jet half width b was taken as the length scale which is the inclined distance across the jet between the point of u_m and the point of $0.5u_m$. As the velocity distribution was not symmetrical about the jet centerline, two length scales were used, one for the upper half b_u of the velocity distribution and the other length scale b_l for the lower half. It was found that b_l is approximately 0.90 b_u. The maximum velocity decay with distance in the inclined jet zone is shown in Fig. 4.23 along with the relevant plots for the plane wall and surface jets. Fig. 4.23 shows that the maximum velocity starts to decay earlier and the rate of decay is faster in the inclined jet than those of the plane wall and surface jets. The best fit to the data showed an exponential decay for the maximum velocity and can be described by the equation

$$\frac{u_m}{U_o} = 1.0642 * e^{-0.0467\left(\frac{x}{b_o}\right)} \qquad (4.6)$$

Rajaratnam and Humphries (1984) described the decay of the maximum velocity in the plane surface jets using the following equation

$$\frac{u_m}{U_o} = \frac{3.1}{\sqrt{x/b_o}} \tag{4.7}$$

The corresponding equation for the plane wall jet is

$$\frac{u_m}{U_o} = \frac{3.5}{\sqrt{x/b_o}} \tag{4.8}$$

4.4.6 Surface jet

Fig. 4.24(a-ab) show the velocity distributions and the similarity profiles for the surface jet for flow patterns A, B and AB. These figures represent experiments 2, 3, 4, 8, 9, 12, 14, 15, 16, 17, 18, 19, 20 and 21 respectively. Each figure shows the surface jet velocity distributions for a specific Froude number, offset ratio, submergence ratio, width ratio and inclination angle. The plots shown in each figure are for different longitudinal distances from the slot. In these figures, the maximum velocity, u_m, which occurs at, or very close to, the free surface is the velocity scale and b_s is the length scale which is equal to the distance where the normalized velocity is equal to 0.5. Fig. 4.25 shows a consolidated non-dimensional plot of all the experiments along with the Gaussian distribution. The forward velocity profiles are approximately similar. This similarity profile seems to be almost linear and a similar observation has been made by Wu and Rajaratnam (1995). The deviation of the similarity profile from the Gaussian distribution that describes the velocity profiles in the simple surface jet might be due to the shallow tailwater conditions. Some scatter in the results can be observed in the lower portion of Fig. 4.25. Swean Jr. et al. (1989) mentioned that the distortion in the lower portion of the forward flow occurs in the region of the jet where the reverse flow velocity is approaching the magnitude of the jet velocity and the breaking down of the jet behavior is expected.

Fig. 4.26(a-b) show the growth of the surface jet half-width b_s. In Fig. 4.26(a), the jet half-width was normalized by the slot width b_o and x_o is the value of x where the maximum surface velocity occurred. It can be noticed from Fig. 4.26(a) that, at the beginning of the surface jet, the jet half-width ranged between 2.5 to 10 times the slot width. It can be shown also that the jet half-width increases with the Froude number increase, with the width ratio decrease and is slightly affected by the submergence and offset ratios. In the analysis of Schneider (1985), It was concluded that the jet half-width is not highly affected by the degree of the downstream constraint. In Fig. 4.26(b), the jet half-width at the first station, b_{so}, was used as the length scale. It can be shown that the growth rate is nearly the same as that of the classical surface jet (Rajaratnam and Humphries, 1984) over some distance after which the growth of the jet becomes very weak. The reason of this break down is perhaps due to the weak entrainment ability of the jet due to the jet confinement by the downstream shallow tailwater conditions. The characteristics of this breakdown will be studied in details in the next two chapters.

4.4.7 Surface-jet discharge

Fig. 4.27(a-b) show the variation of the surface jet discharge intensity Q for flow pattern A, in terms of the discharge intensity at the slot Q_o, with the dimensionless distance measured from the gate. As the entrainment rate is relatively high in the inclined-jet region, the dimensionless discharge reaches its maximum value at the point of impingement with the free surface. Downstream of this point, the degree of the jet confinement becomes larger as the jet grows. Hence, the entrainment rate becomes weaker in the surface jet resulting in a decrease in the jet discharge. The underlying recirculation region ends where the ratio $Q/Q_o = 1$. Fig. 4.27(a) shows the effect of the offset ratio Z_o/b_o on the discharge variation. For Z_o/b_o was equal to 30.0, the maximum value for Q/Q_o was about 4.5. This value was about 3.5 and 1.5 for Z_o/b_o was equal to

13.5 and 0.0 respectively. This indicates the significant effect of the offset ratio on the variation of the jet discharge with distance. Wu and Rajaratnam (1995), in studying the effect of baffles on submerged flows, found that the maximum discharge ratio is as high as 2.50 while the same ratio was found to be about 4.00 in the study done by Swean Jr. et al. (1989). It can be concluded that the decrease in the offset ratio, or the degree of the jet confinement, is associated with a significant decrease in the jet-discharge ratio. This seems reasonable as the reverse flow, that is required to supply the entrained fluid, is affected by the jet confinement.

The effect of the inclination angle θ and the width ratio w/W on the discharge variation is shown in Fig. 4.27(b). In experiments 18 and 19, the width ratio was 1.0 and the inclination angle was 30 and 10 degrees, respectively. In experiments 19, 20 and 21, the inclination angle was 10 degrees and the width ratio was 1.0, 0.8 and 0.5 respectively. Fig. 4.27(b) shows that the inclination angle does not have any significant effect on the discharge variation. The inclination angle only affected the longitudinal distance to the peak where this distance was found to be inversely proportional to the inclination angle. The surface-jet discharge was affected significantly by the changes in the width ratio. The maximum value of Q/Q_o was about 5.0, 4.0 and 3.0 for the width ratio was equal to 0.5, 0.8 and 1.0 respectively.

4.4.8 Surface-jet momentum flux

The presence of a strong reverse flow approximately parallel to the surface jet would reduce the momentum flux in the surface jet. Assuming a linear velocity distribution for the surface jet, it can be shown that:

$$\frac{M}{M_o} = \left(\frac{2}{3}\right)\left(\frac{U_m}{U_o}\right)\left(\frac{Q}{Q_o}\right) = \left(\frac{2}{3}\right)\left(\frac{U_m}{U_o}\right)^2\left(\frac{b_s}{b_o}\right) \qquad (4.9)$$

where $\bar{M}$ is the momentum flux in the surface jet at any station and M_o is the momentum flux at the slot. The above relation confirms the decay of the momentum flux as the growth rate of the length scale b, is very weak and the velocity decays rapidly (as mentioned earlier). Fig. 4.28(a-b) show the variation of the dimensionless momentum flux M/M_o versus the dimensionless distance x/b_o and a significant reduction in the momentum flux can be seen. Considerable momentum losses in free jets were also found in the data obtained by Goldschmidt and Eskinazi (1966), Heskestad (1965), Miller and Comings (1957) and Kotsovinos (1975) as presented in Kotsovinos (1978). This phenomenon was found also in surface jets as analyzed by Swean Jr. et al. (1989). Kotsovinos (1978) mentioned that the main reason for the momentum losses is the jet interaction with the reverse flow. Fig. 4.28(a) shows the effect of the offset ratio on the momentum decay. This figure shows three offset ratios of 30.0, 13.5 and 0.00 where it is easy to see that the surface-jet momentum flux decays faster for smaller offset ratios. Fig. 4.28(b) shows the effect of the inclination angle and the width ratio on the momentum decay. Neither the angle nor the width ratio had a significant effect on the momentum decay. As decreasing the width ratio resulted in an increase in the discharge ratio and a faster decay in the maximum velocity (see sections 4.4.7 and 4.4.4), it was logical that the momentum flux would not be affected by the width ratio changes (see Eq. 4.9).

4.4.9 Bed shear stress

One main consideration in this study was to prevent erosion of the downstream bed. It was therefore important to consider the bed shear stress in the downstream channel for the different flow patterns. A Prandtl tube was used as a Preston tube to measure the bed shear stress.

4.4.9.1 Pattern A

Fig. 4.29(a-c) show the variation of the bed shear stress for pattern A for four Froude numbers, three submergence ratios, three offset ratios, three width ratios and two inclination angles. In this flow pattern, it was found that the bed shear stress τ reached a maximum value of τ_m at a distance of x_{oA} from the gate and was symmetrical on either side of the maximum (see Fig. 4.29(a-b)). Fig. 4.29(a) shows the variation of the bed shear stress with the distance from the gate. Fig. 4.29(b) shows the variation of the dimensionless shear stress τ/τ_m with the dimensionless distance $(x-x_{oA})/b_A$ where b_A is the longitudinal distance between the point of τ_m and that of $0.5\tau_m$. The effect of the offset ratio on the coefficient of skin friction $C_{fo} = \tau_m/(\rho U_o^2/2)$ and the normalized longitudinal distance to the peak x_{oA}/b_o is shown in Fig. 4.29(c). The coefficient of skin friction was found to vary mainly with the offset ratio. It was found to decrease from about 0.0003 for $Z_o/b_o = 0.0$ to 0.00007 for $Z_o/b_o = 30.0$. Also, the normalized longitudinal distance to the peak x_{oA}/b_o was found to depend mainly on the offset ratio. The variation of the coefficient of skin friction C_{fo} and the longitudinal distance to the peak x_{oA}/b_o with the offset ratio are described by Eq. 4.10 and Eq. 4.11 respectively

$$C_{fo} = 0.289 * 10^{-3} * e^{-0.0468\left(\frac{Z_o}{b_o}\right)} \qquad (r^2 = 0.88) \qquad (4.10)$$

$$\frac{x_{oA}}{b_o} = 19.63 + 3.60\frac{Z_o}{b_o} \qquad (r^2 = 0.95) \qquad (4.11)$$

4.4.9.2 Pattern B

Fig. 4.30(a-b) show the bed shear stress distribution for pattern B for three different Froude numbers and two different submergence ratios. Similar to flow pattern A, the bed shear stress τ reached a maximum value of τ_m at a distance of x_{oB} from the gate but was asymmetrical about its maximum value. For the Froude number F_o = 10.40, the bed shear stress was found to decrease dramatically with the submergence ratio increasing from 1.0 to 7.5 (see Expt. 10 & 11). Hence, it is recommended, in the case of the large Froude numbers, to keep the slot slightly submerged to suppress the bed shear stress. In Fig. 4.30(b), the bed shear stress is normalized by its maximum value τ_m and the longitudinal distance from the location of the maximum shear stress is normalized by b_B which is the distance, to the left of the peak, between the point of the zero shear and that of the maximum shear. Fig. 4.30(b) shows that the bed shear stress distributions are almost similar. The similarity profile can be represented by the following equation:

$$\frac{\tau}{\tau_m} = 0.90 - 0.18\left(\frac{x - x_{oB}}{b_B}\right) - 0.63\left(\frac{x - x_{oB}}{b_B}\right)^2 + 0.49\left(\frac{x - x_{oB}}{b_B}\right)^3 - 0.10\left(\frac{x - x_{oB}}{b_B}\right)^4 \tag{4.12}$$

It should be mentioned that, in flow pattern B the strong turbulent layer separating the forward and the backward flows was very close to the bed. Hence, the bed shear stress could not be measured for $Z_o/b_o < 30$ and consequently the variation of the bed shear and the length scales with the offset ratio could not be evaluated in this flow pattern.

4.4.9.3 Pattern C

Fig. 4.31(a-d) show the bed shear stress distribution for pattern C for three different Froude numbers, two different offset ratios and the same submergence. Fig. 4.31(a) shows that the bed shear stress increased from zero at the line of impingement located at a distance of x_{oC} from the gate to a maximum value of τ_{md} downstream with another maximum value τ_{mu} on the upstream side of the impingement line with a distance of b_c between these two maximums. A normalized distribution of the shear stress variation is shown in Fig. 4.31(b) by choosing the maximum positive shear stress as the shear scale. The length scale, b_c, was taken as the longitudinal distance between the maximum negative and positive shear and x_{oC} is the distance, measured from the gate, to the point of impingement with the bed or the point of zero shear. The skin friction coefficient corresponding to τ_{md} varied mainly with the offset ratio Z_o/b_o, decreasing from about 0.004 for $Z_o/b_o = 14.0$ to about 0.0008 for $Z_o/b_o = 30.0$. Further, τ_{mu} was equal to 0.75 τ_{md}. The variation of the skin friction $C_{fo} = \tau_{md}/(\rho U_o^2/2)$ with the offset ratio is shown in Fig. 4.31(c). Eq. 4.13 describe this relation.

$$C_{fo} = 15.64 * 10^{-3} * e^{-0.1\left(\frac{Z_o}{b_o}\right)} \qquad (r^2 = 0.78) \qquad (4.13)$$

It was found that b_c/Z_o and x_{oC}/Z_o varied mainly with the Froude number. These relations are shown in Fig. 4.31(c-d) and are described by Eq. 4.14 and Eq. 4.15 respectively.

$$\frac{x_{sc}}{Z_o} = 0.385\, F_o \qquad (r^2 = 0.95) \tag{4.14}$$

and the variation of b_c/Z_o with the Froude number is given as

$$\frac{b_c}{Z_o} = 0.43\, F_o - 0.053 F_o^2 \qquad (r^2 = 0.92) \tag{4.15}$$

4.5 Conclusions and Recommendations

This study introduces a new design concept for energy dissipation below regulators. In the new design, a high velocity jet is deflected to the free surface by means of a double-leaf gate with the upper gate located upstream of the lower to create the opening which produces the inclined jet.

Dimensional analysis showed that the dimensionless variables involved in this problem are the Froude number, the width ratio, the submergence ratio, the offset ratio and the inclination angle of the jet.

Based on a laboratory study, four flow regimes were defined. Pattern A occurs with a relatively large submergence. The jet moves towards the water surface and after impinging on it, proceeds as a surface jet. Pattern B occurs with relatively small submergence. The jet penetrates the free surface and returns back to proceed also as a surface jet. In this flow pattern, the jet is not submerged at the gate. In pattern C, the jet plunges into the tailwater and after impingement on the bed, travels as a wall jet. In between zones A and B, the jet oscillates due to unbalanced pressure across the jet. The jet oscillation, i.e. pattern AB, does not exist in the models with the width ratio less than 1.0. Flow pattern A is recommended for design and can easily be achieved in flow regulators.

Velocity distributions and bed shear stresses were measured. The velocity distributions for the inclined jet are similar and the similarity profile is the same as that of the plane turbulent jet. The velocity profiles of the surface jet are also similar but the distribution is almost linear due to the confinement of the spreading jet by the shallow tailwater. The decay of the maximum velocity was studied and compared with that for free and submerged jumps. The decay process was divided into three stages of the deflected jet in which the decay was rapid; the convergence stage in which the falling jet speeds up; and the surface jet stage in which the maximum velocity decays rather slowly. It was found that the decay of the maximum velocity in the double-leaf gate design is as effective as that in free and submerged jumps.

The shallow tailwater condition affects the main characteristics of the surface jet. It decreases the entrainment rate and as a result the growth rate of the length scale becomes very weak. Further, this confinement enhances the rate of the velocity decay. The momentum flux in the jet is not preserved due to the entrainment of the fluid traveling towards the gate with appreciable horizontal velocity.

Bed shear stress in the downstream channel were found to have certain characteristic distributions. In flow pattern A, the shear stress increases until it reaches a peak value and then decreases. The distribution is symmetrical about the peak. In pattern B, the distribution looks like that of pattern A but is not symmetrical. In pattern C, the shear stress increases from zero at the line of impingement to two maximum values, one on either side. The shear stress in pattern A was very small compared with that for pattern C.

Considering the lifting of the gates in a flow regulator, the weight of the gate in kg/m^2 varies widely depending on the head and the gate size. However, a single gate can weigh up to several tons. There are some flow regulators on rivers that have more than 100 vents. If a double-leaf gate design is used instead of single-leaf gates, up to 50% of the power and height of the lifting device can be saved. These savings can be added to the advantage of having minimum scour downstream of this type of regulators. Also, in this type of regulators, a short apron can be used if adequate sheet piles are installed. The apron for hydraulic jump dissipators tends to be longer. For modifying existing regulators an upward sloping sill may be installed under the gate.

The ventilation of the jet (i.e. using jets with $w/W<1.00$) is very important and is highly recommended in the prototype. It eliminates the oscillating zone and leads to a faster decay of the maximum velocity. With the jet ventilated, the double-leaf gate regulator can be used in deep as well as in shallow tailwater streams.

Experiments with $Z_o/b_o = 0.0$ indicated that the jet issued as in pattern A and was stable in this flow pattern unless it was forced towards the bed. In the later case, the jet changed into a wall jet and remained stable in this pattern. However, the design with the gate opening at the bed needs further study, especially for the effect of the angle on the jet stability.

Gate vibration is a serious problem that can cause structural damage and all precautions have to be taken to prevent vibration of the leaves in the prototype. Although the 30 degrees jet was found to be suitable for the large as well as the small offset ratios, more angles have to be checked especially the 45 degrees angle.

4.6 References

Bakhmeteff, B. A. and Feodoroff, N. V. (1941). "Discussion of energy loss at the base of a free overfall." Trans. ASCE, Vol. 108, pp. 1364-1373.

Elevatorski, E. A. (1959) "Hydraulic energy dissipators." McGraw-Hill, New York.

Goldschmidt, V., and Eskinazi, S. (1966). "Two phase turbulent flow in a plane jet." Trans. ASME, Series E, J. Appl. Mech., 33(4), 735-747.

Hager, W. H. (1992). "Energy dissipators and hydraulic jump." Kluwer Academic Publishers, 288p.

Heskestad, G. (1965). "Hot wire measurements in a plane turbulent jet." Trans. ASME, Series E, J. Appl. Mech., 32(4), 721-734.

Kotsovinos, N. E. (1975). "A study of the entrainment and turbulence in a plane turbulent jet." W. M. Keck Lab. Hydr. Water Resources, Calif. Inst. Tech. Rept. KH R-32

Kotsovinos, N. E. (1978). "A note on the conservation of the axial momentum of a turbulent jet." J. Fluid Mech., 87(7), pp. 55-63.

Liu, H. K. (1949). "Diffusion of flow from submerged sluice gate." Thesis presented to the State Univ. of Iowa, Iowa, in partial fulfillment of the requirements for the degree of M. Sc., 32p.

Long, D, Rajaratnam, N. and Steffler, P. M. (1990). "LDA study of flow structure in submerged hydraulic jump" J. Hydr. Res., 28(4), pp. 437-460.

Miller, D. R., and Comings, E. W. (1957). "Static pressure distribution in the free turbulent jet." J. Fluid Mech., 3(10), pp. 1-16.

Narasimhan, S. and Bhargava, V. P. (1976). "Pressure fluctuations in submerged jump." J. Hydr. Div., ASCE, 102(3), pp. 339-350.

Ohtsu, I., Yasuda, Y. and Awazu, S. (1990). "Free and submerged hydraulic jumps in rectangular channels." Report of the Research Institute of Science and Technology, Nihon University, No. 35, Feb. 1990, 50 p.

Patel, V. C. (1965). "Calibration of the Preston tube and limitations on its use in pressure gradients." J. Fluid Mech., Vol. 23, pp. 185-208.

Peterka, A. J. (1963). "Hydraulic design of stilling basins and energy dissipators." Engrg. Monograph 25, U.S.D.I. Bureau of Reclamation: Denver, Col.

Peterka, A. J. (1963). "Hydraulic design of stilling basins and energy dissipators." Engrg. Monograph 25, U.S.D.I. Bureau of Reclamation: Denver, Col.

Rajaratnam, N. (1965). "The hydraulic jump as a wall jet." J. Hydr. Div., ASCE, 91(5), pp. 107-132.

Rajaratnam, N. (1967). "Hydraulic jumps.", Advances in Hydroscience, Vol. 4, pp. 198-276.

Rajaratnam, N. (1976). Discussion of "pressure fluctuations in submerged jump." J. Hydr. Div., ASCE, 102(12), pp. 1785-1787.

Rajaratnam, N. and Subramanya, K (1967). "Diffusion of rectangular wall jets in wider channels.", Contributions to Turbulent Wall Jets in Hydraulic Engineering and Other Related Problems, Dept. of Civil Engineering, Univ. of Alberta, Edmonton, Canada.

Rajaratnam, N., and Humphries, J. A. (1984). "Turbulent non-buoyant surface jet." J. Hydr. Res., 22(2), pp. 103-115.

Rouse, H. Siao, T. T. and Nagaratnam, S. (1959). "Turbulence characteristics of the hydraulic jump." Trans. ASCE, Vol. 124, pp. 926-966.

Sawyer, R. A. (1962). " The flow due to a two-dimensional jet issuing parallel to a flat plate." J. Fluid Mech. 9(4), pp. 543-560.

Schneider, W. (1985). "Decay of momentum flux in submerged jets." J. Fluid Mech., 154(5), pp. 91-110.

Schröder, R. (1963). "Die turbulente Strömung im freien Wechselsprung." Habilitationsschrift, Mitteilung 59, Institut fur Wasserbau und Wasserwirtschaft, TU Berlin, Berlin.

Swean Jr, T. F., Ramberg, S. E., Plesniak, M. W. Stewart., M. B. (1989). "Turbulent surface jet in channel of limited depth." J. Hydr. Engr., ASCE, 115(12), pp. 1587-1606.

Wu, S. (1994). "Four contributions to the application of turbulent jet theory in hydraulic engineering." PhD thesis, University of Alberta, Edmonton, Alberta, Canada.

Wu, S. and Rajaratnam, N. (1995). "Effect of baffles on submerged flows" J. Hydr. Div., ASCE, 121(9), pp. 644-652.

Table 4.1 Primary details of experiments (series A)

Expt. (1)	θ (2)	b_o (mm) (3)	Z_o (mm) (4)	y_t (mm) (5)	W(mm) (6)	w(mm) (7)	U_o (m/s) (8)	F_o (9)	Z_o/b_o (10)	$(y_t-Z_o)/b_o$ (11)	w/W (12)	R (13)	Pattern (14)
1	30	9	270	270	446	446	1.43	4.80	30.00	0.00	1.00	12836	C
2	30	9	270	279	446	446	1.43	4.80	30.00	1.00	1.00	12836	B
3	30	9	270	473	446	446	1.43	4.80	30.00	22.50	1.00	12836	A
4	30	9	270	540	446	446	1.43	4.80	30.00	30.00	1.00	12836	A
5	30	9	270	270	446	446	2.14	7.20	30.00	0.00	1.00	19254	C
6	30	9	270	279	446	446	2.14	7.20	30.00	1.00	1.00	19254	B
7	30	9	270	338	446	446	2.14	7.20	30.00	7.50	1.00	19254	B
8	30	9	270	405	446	446	2.14	7.20	30.00	15.00	1.00	19254	AB
9	30	9	270	540	446	446	2.14	7.20	30.00	30.00	1.00	19254	A
10	30	9	270	279	446	446	3.09	10.40	30.00	1.00	1.00	27812	B
11	30	9	270	338	446	446	3.09	10.40	30.00	7.50	1.00	27812	B
12	30	9	270	540	446	446	3.09	10.40	30.00	30.00	1.00	27812	A
13	30	20	270	270	446	446	1.06	2.40	13.50	0.00	1.00	21261	C
14	30	20	270	540	446	446	1.06	2.40	13.50	13.50	1.00	21261	A
15	30	20	135	405	446	446	1.06	2.40	6.75	13.50	1.00	21261	A
16	30	20	0	270	446	446	1.06	2.40	0.00	13.50	1.00	21261	A
17	30	20	0	270	446	446	1.59	3.60	0.00	13.50	1.00	31892	A
18	30	20	270	540	446	446	2.13	4.80	13.50	13.50	1.00	42523	A
19	10	20	270	540	446	446	2.13	4.80	13.50	13.50	1.00	42523	A
20	10	20	270	540	446	357	2.13	4.80	13.50	13.50	0.80	42523	A
21	10	20	270	540	446	223	2.13	4.80	13.50	13.50	0.50	42523	A

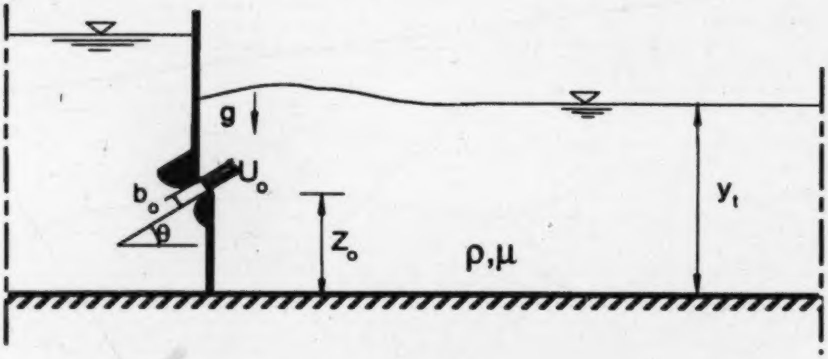
g
U_o
b_o
θ
Z_o
ρ,μ
y_t

Fig. 4.1 Definition sketch of double-leaf gate dissipator

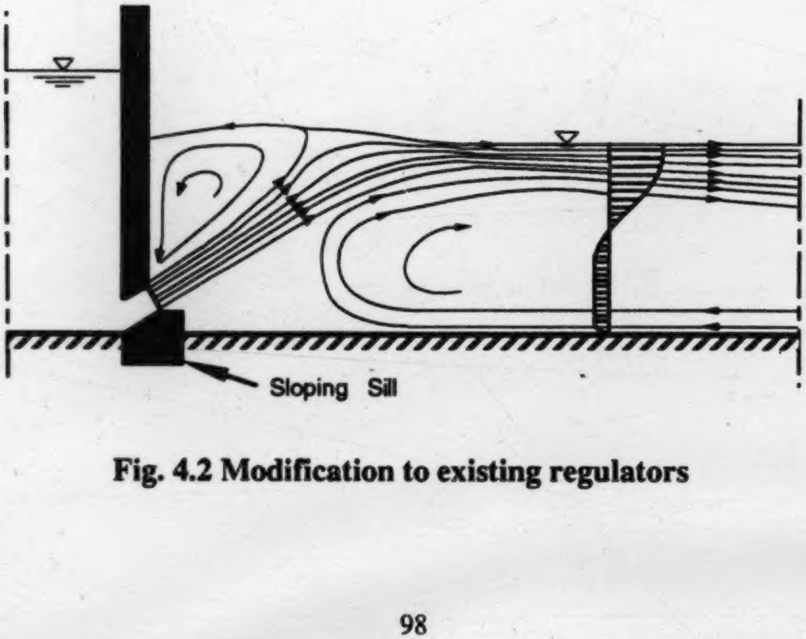
Sloping Sill

Fig. 4.2 Modification to existing regulators

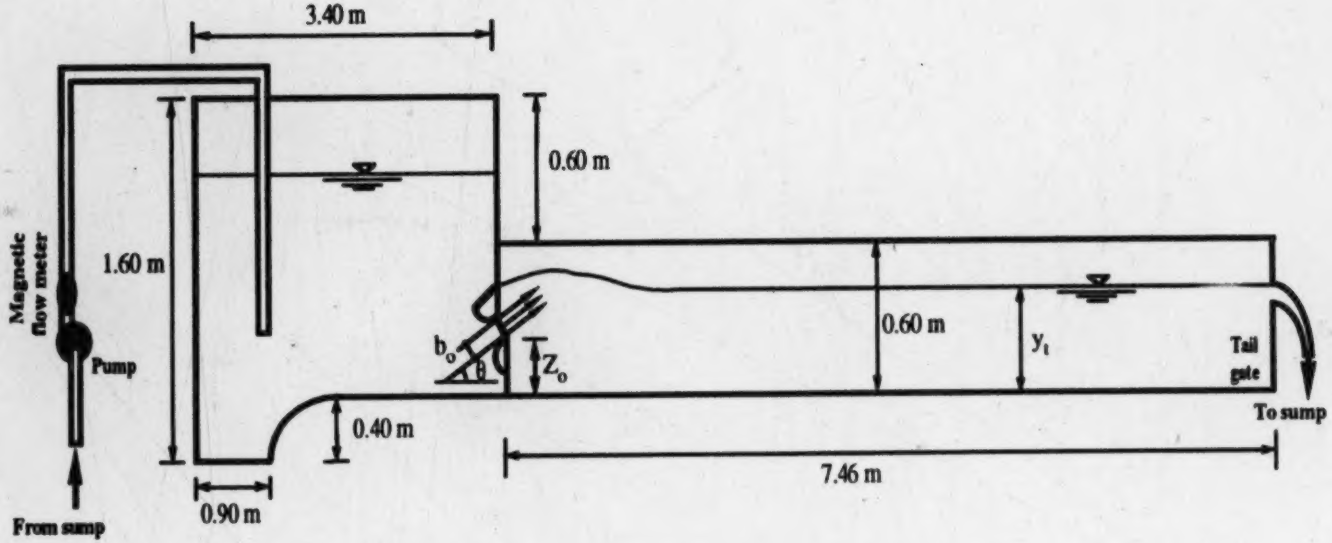
3.40 m
0.60 m
Magnetic flow meter
1.60 m
Pump
From sump
0.90 m
0.40 m
b_o
θ
Z_o
0.60 m
y_t
Tail gate
To sump
7.46 m

Fig. 4.3 Experimental flume

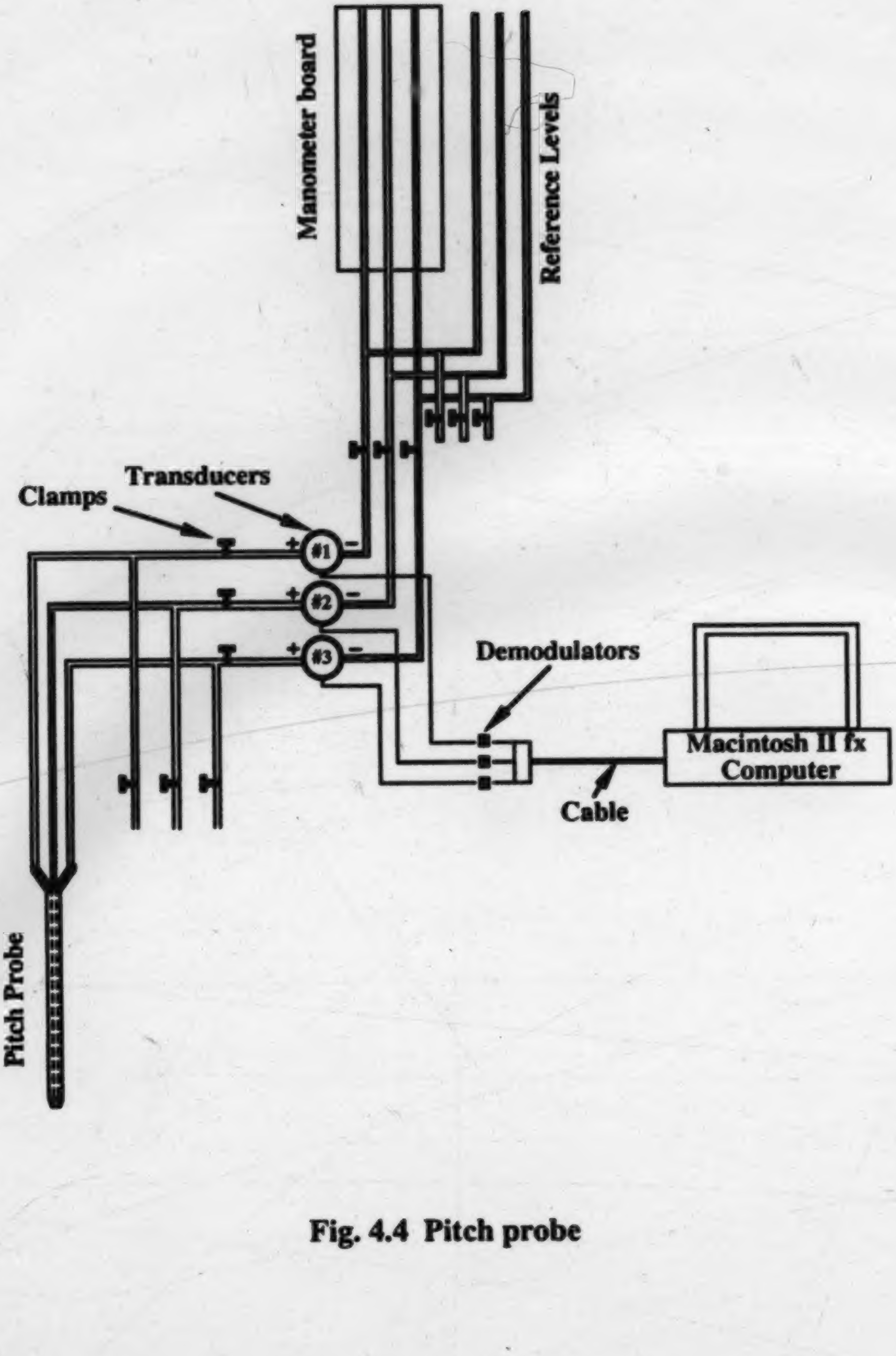
Manometer board
Reference Levels
Transducers
Clamps
#1
#2
#3
+
−
Demodulators
Macintosh II fx Computer
Cable
Pitch Probe

Fig. 4.4 Pitch probe

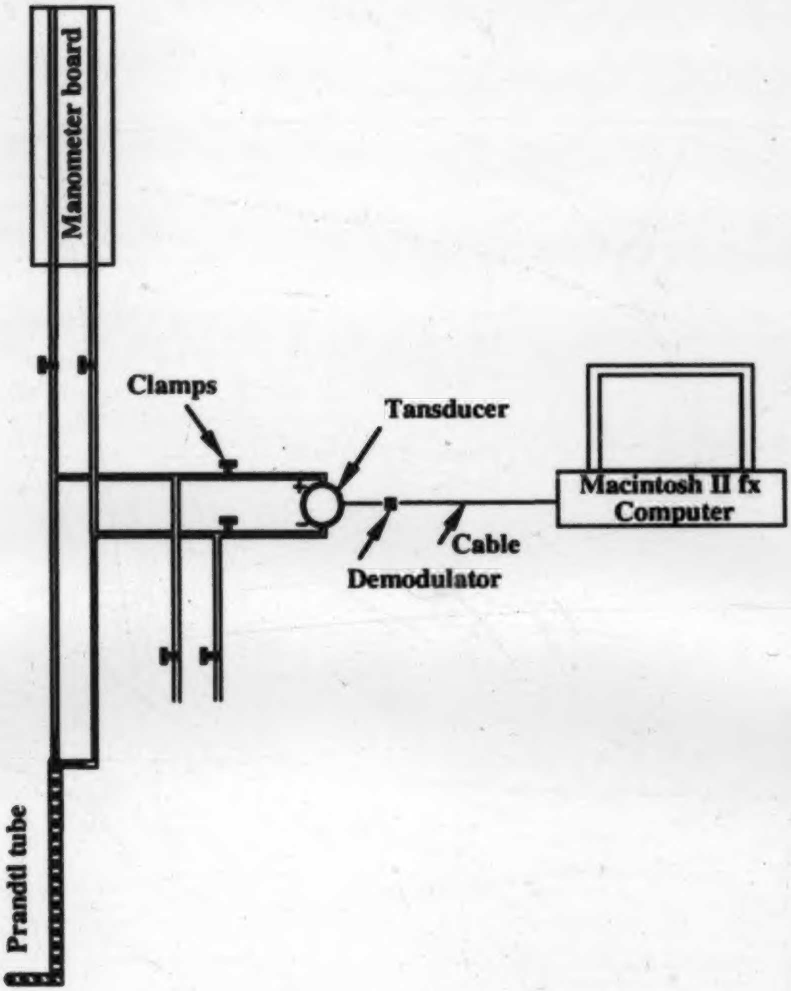
Manometer board
Clamps
Tansducer
Macintosh II fx Computer
Cable
Demodulator
Prandtl tube

Fig. 4.5 Prandtl tube

Fig. 4.6(a) Pattern A

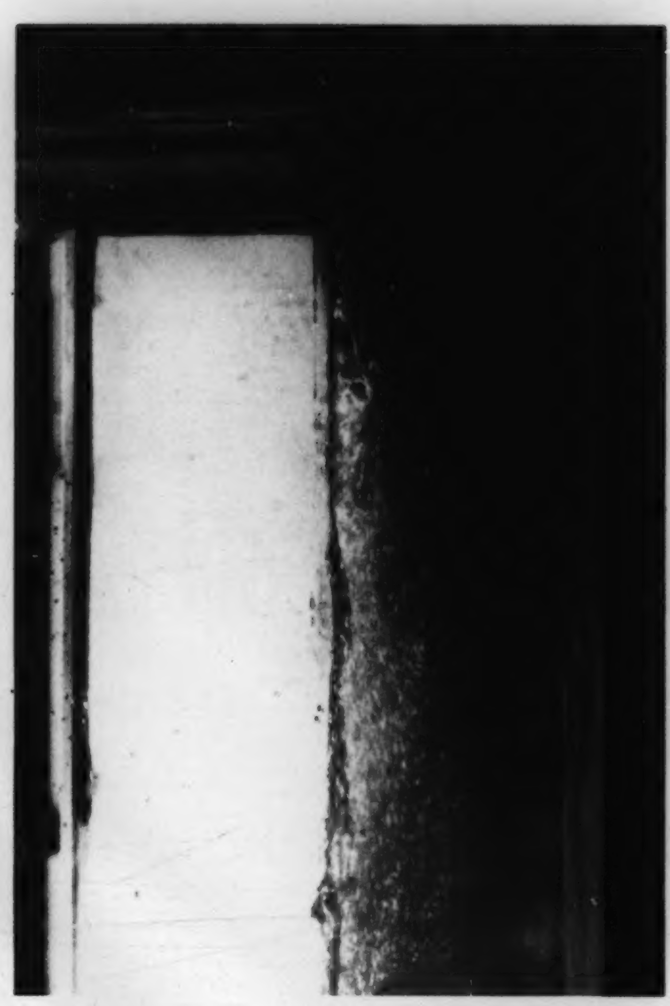

Fig. 4.6(b) Pattern B

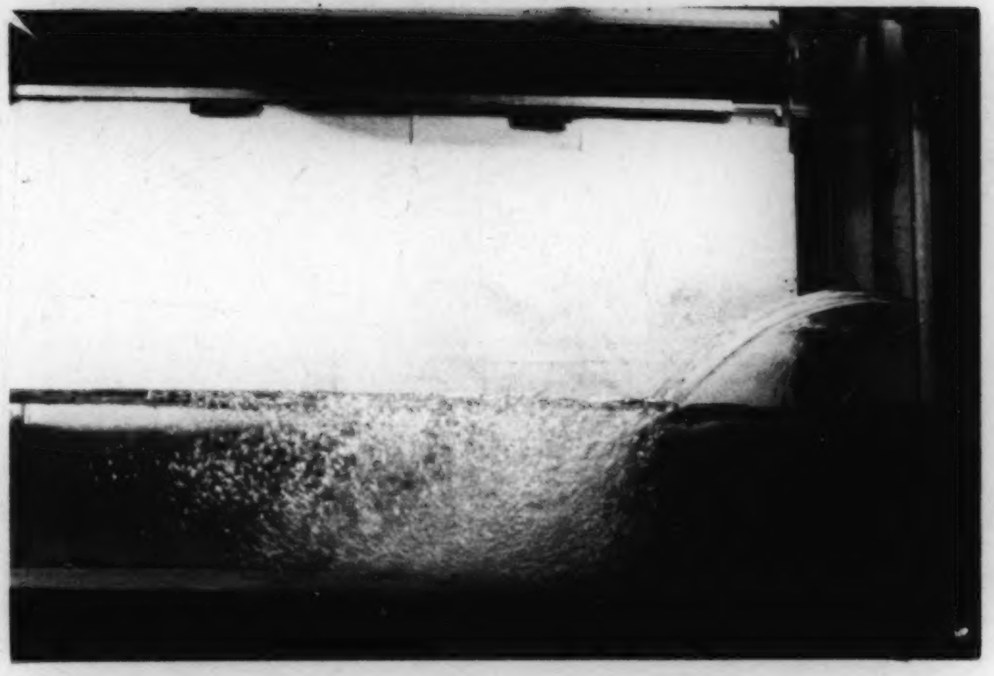

Fig. 4.6(c) Pattern C

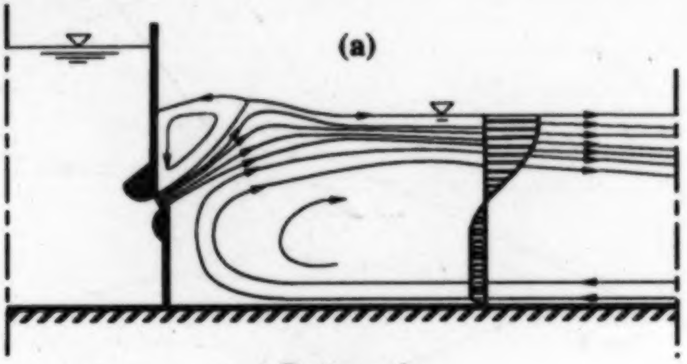

Pattern A

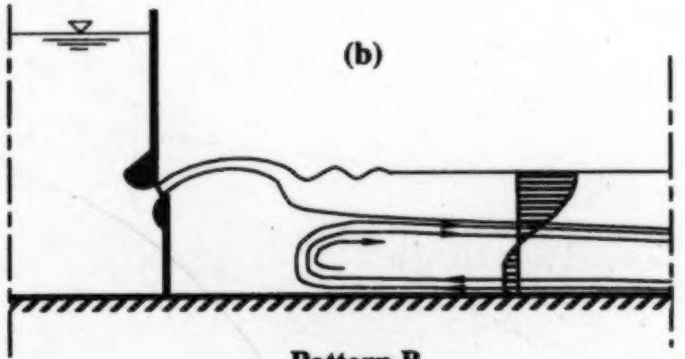

Pattern B

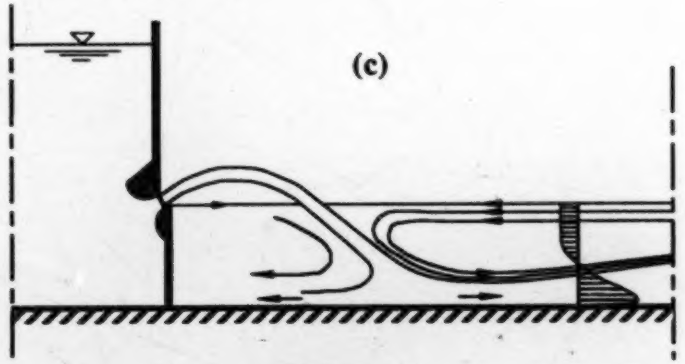

Pattern C

Fig. 4.7(a-c) Flow patterns A, B & C for double-leaf gate dissipator

b_o = 9mm, Z_o/b_o = 30.00, w/W = 1.00, θ = 30°

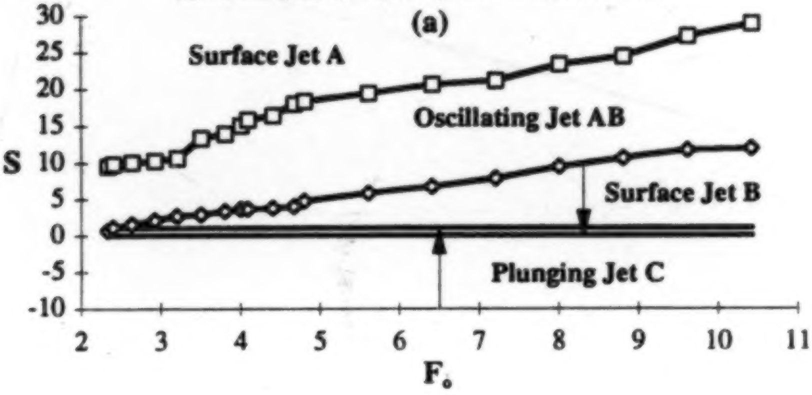

b_o = 20mm, Z_o/b_o = 13.50, w/W = 1.00, θ = 30°

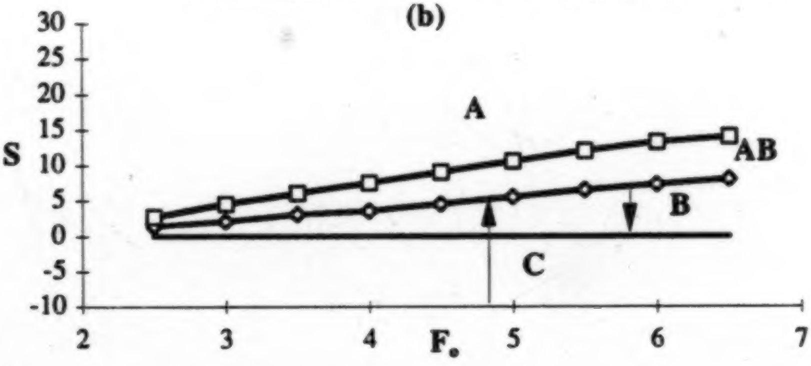

Fig. 4.8(a-b) Boundaries of the flow patterns
(a) θ=30°, Z_o/b_o=30.00; and (b) θ=30°, Z_o/b_o=13.50

$b_o = 20mm, Z_o/b_o = 6.75, w/W = 1.00, \theta = 30°$

(c)

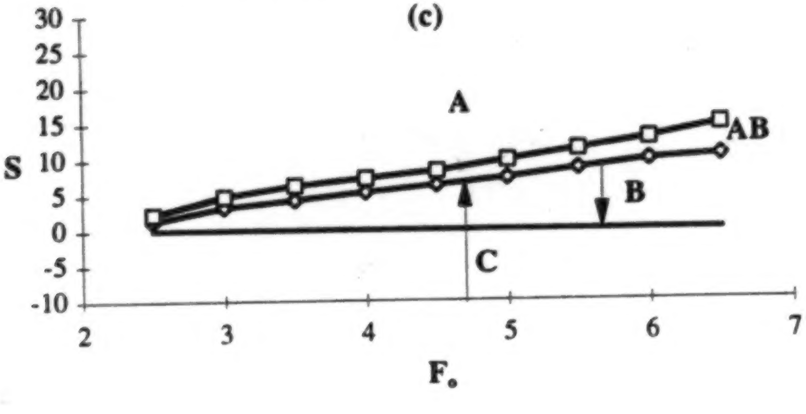

$b_o = 20mm, Z_o/b_o = 13.50, w/W = 0.80, \theta = 10°$

(d)

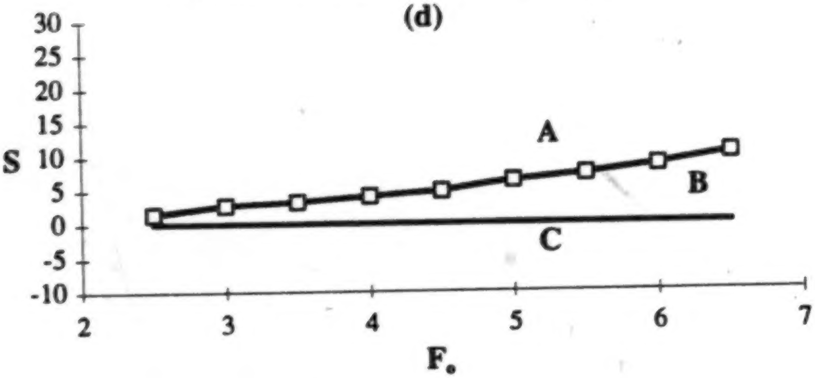

Fig. 4.8(c-d) Boundaries of the flow patterns
(c) $\theta=30°$, $Z_o/b_o=6.75$; and (d) $\theta=10°$, $Z_o/b_o=13.50$

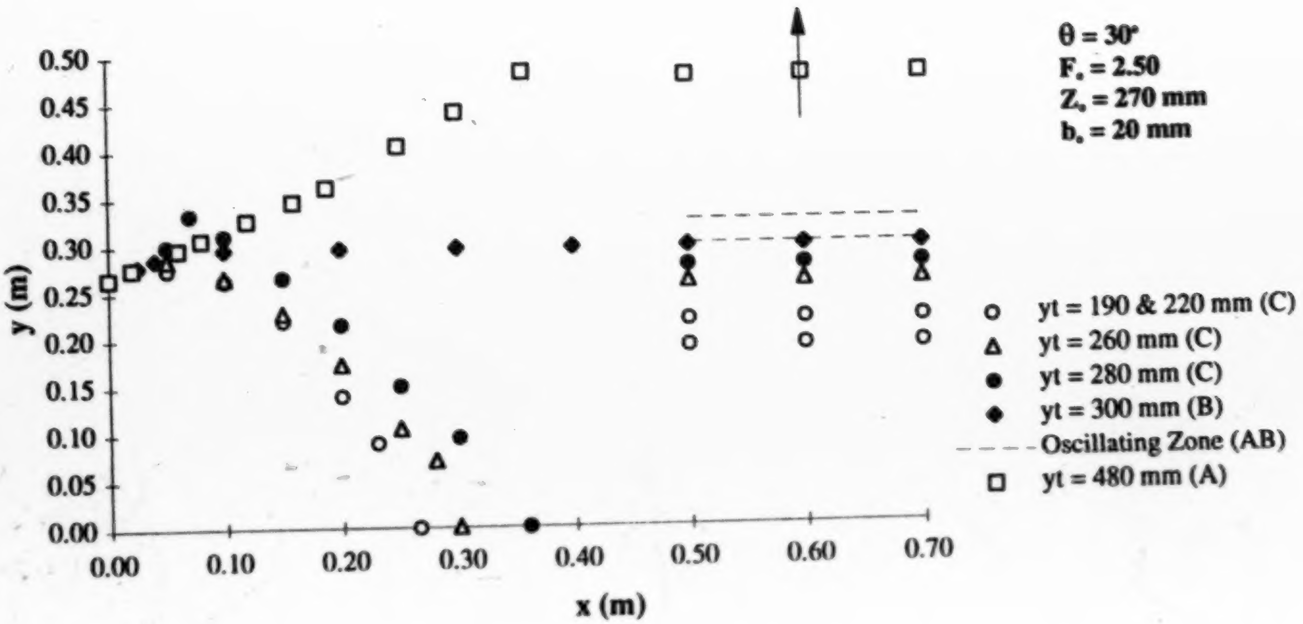

Fig. 4.9 Jet trajectories

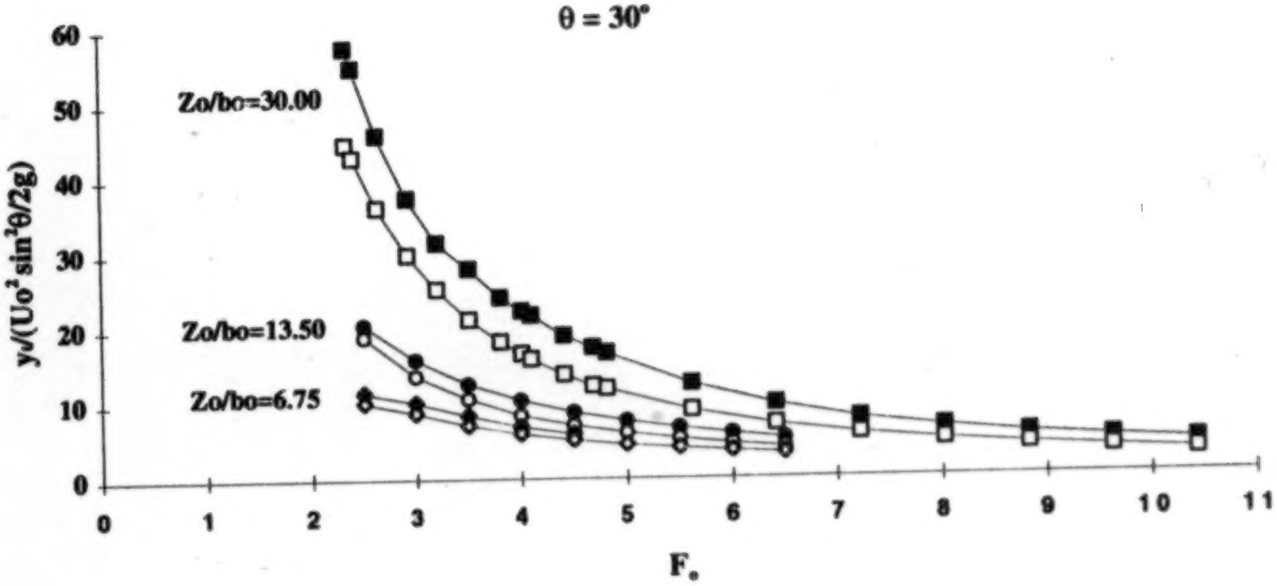

Fig. 4.10 Oscillating zones

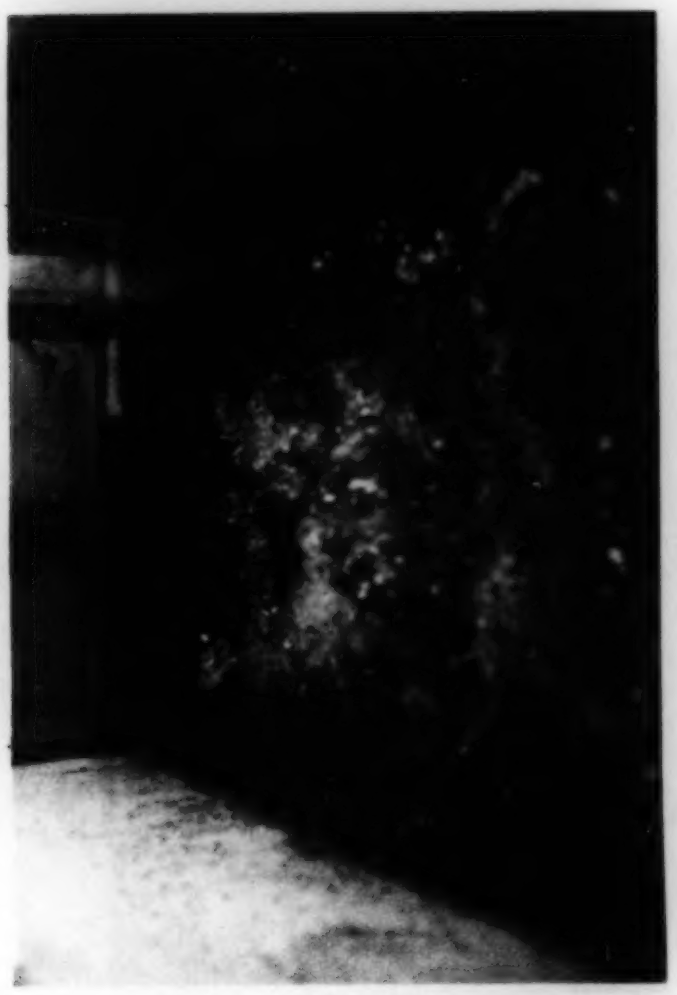

Fig. 4.11 Width ratio w/W = 0.50

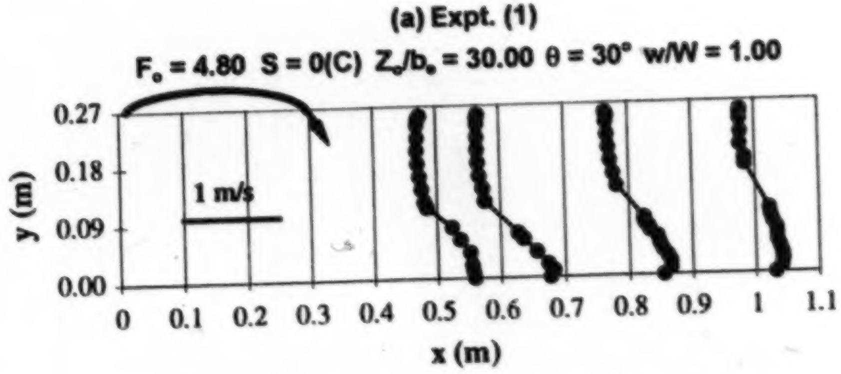

Fig. 4.12(a) Typical Velocity Profiles for Pattern C

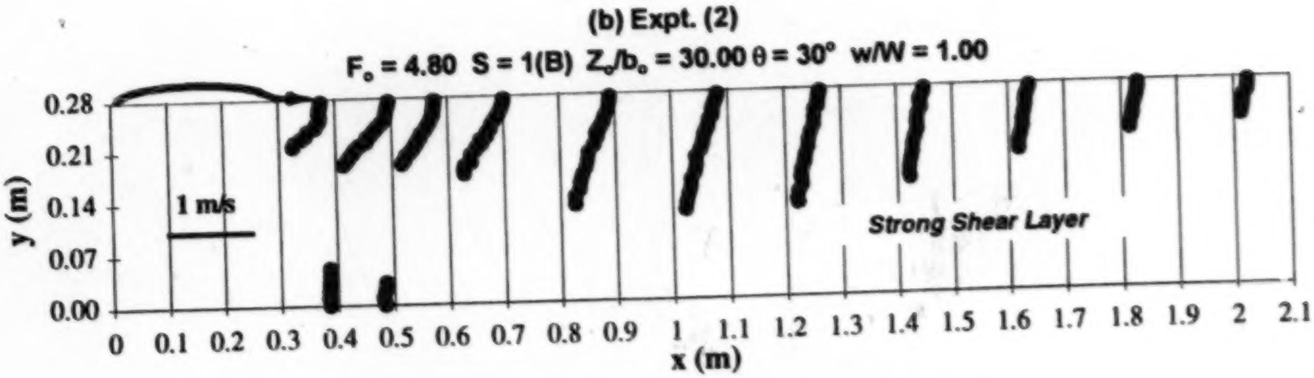

Fig. 4.12(b) Typical Velocity Profiles for Pattern B

(c) Expt. (3)

$F_o = 4.80$ & $S = 22.50(A)$ $Z_o/b_o = 30.00$ $\theta = 30°$ $w/W = 1.00$

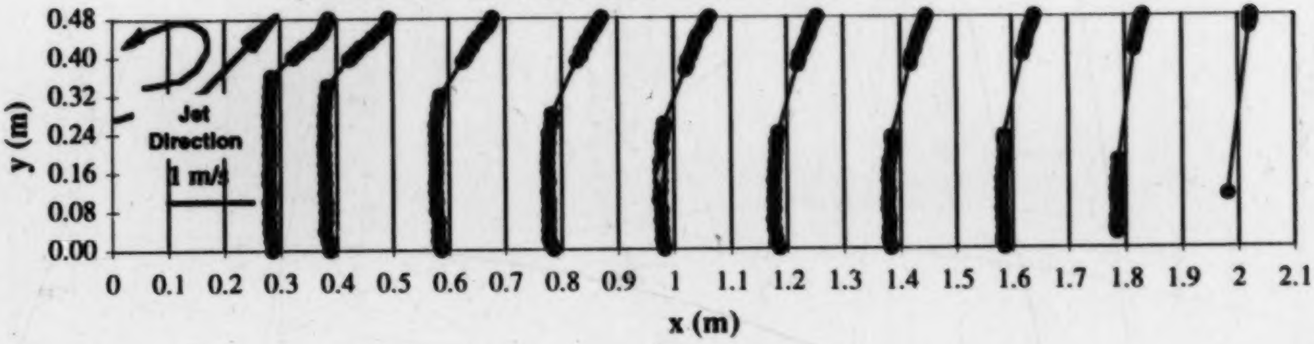

(d) Expt. (4)

$F_o = 4.80$ $S = 30.00(A)$ $Z_o/b_o = 30.00$ $\theta = 30°$ $w/W = 1.00$

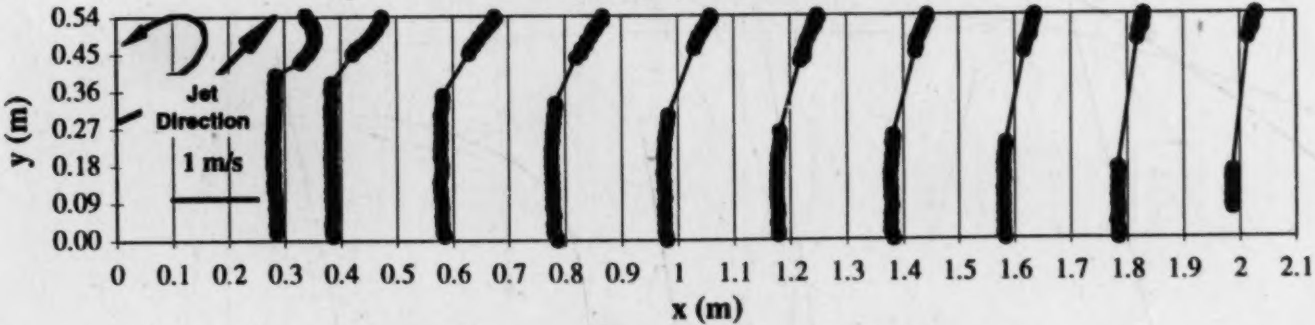

Fig. 4.12(c-d) Typical Velocity Profiles for Pattern A

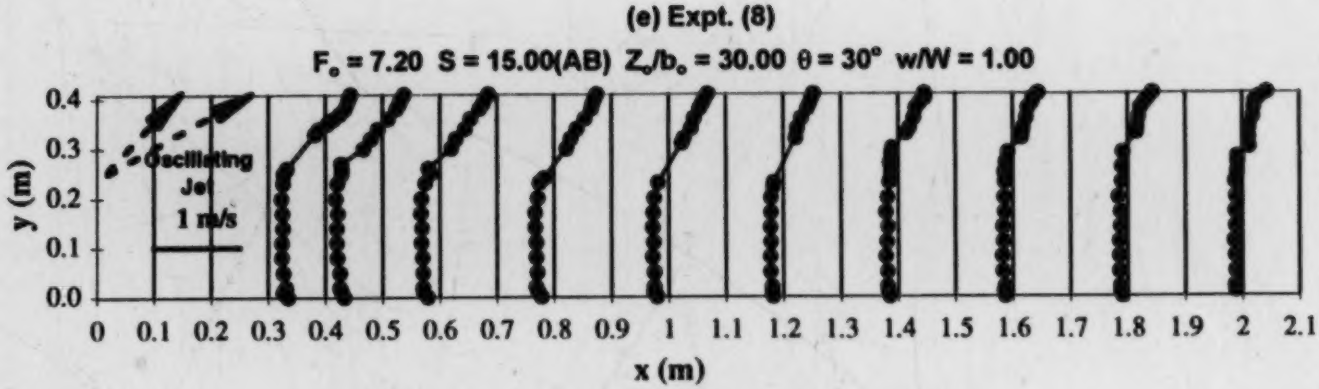

(e) Expt. (8)

$F_o = 7.20$ $S = 15.00$(AB) $Z_o/b_o = 30.00$ $\theta = 30°$ $w/W = 1.00$

Fig. 4.12(e) Typical Velocity Profiles for Pattern AB

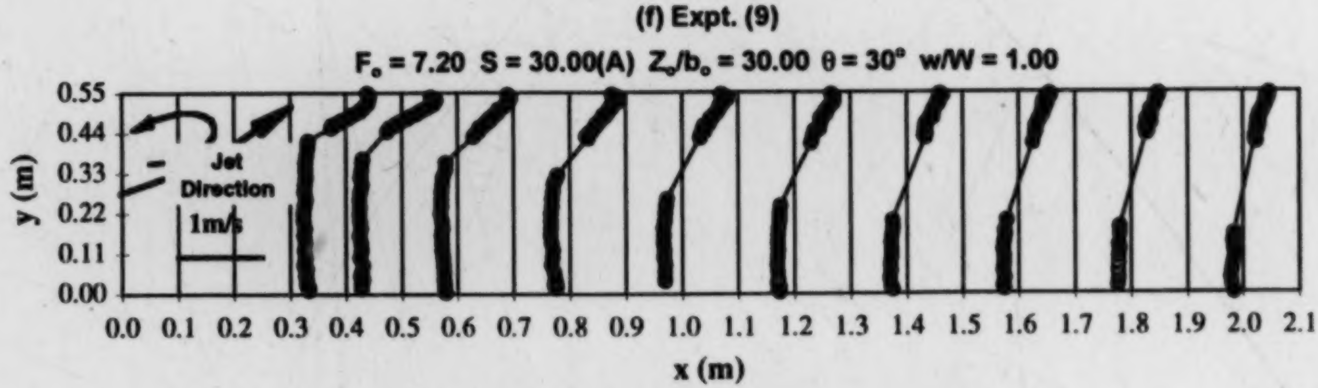

(f) Expt. (9)

$F_o = 7.20$ $S = 30.00$(A) $Z_o/b_o = 30.00$ $\theta = 30°$ $w/W = 1.00$

Fig. 4.12(f) Typical Velocity Profiles for Pattern A

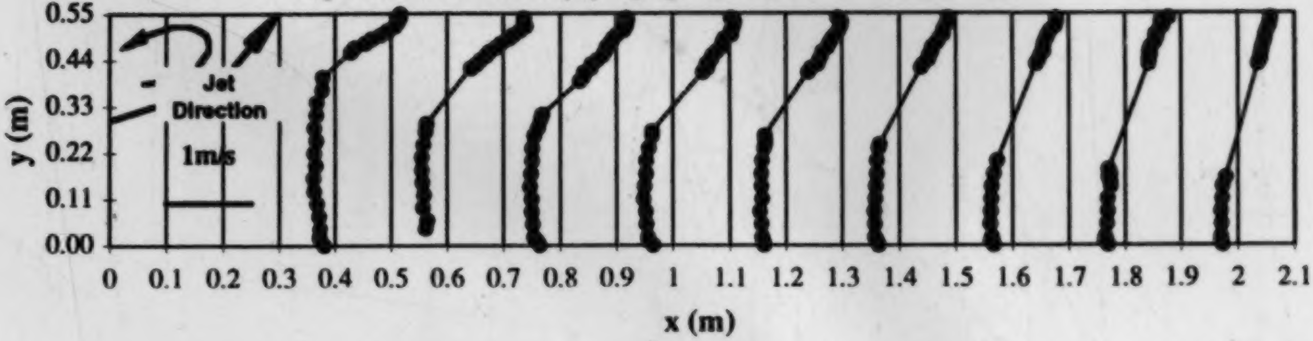
(g) Expt. (12)

$F_o = 10.40$ $S = 30.00(A)$ $Z_o/b_o = 30.00$ $\theta = 30°$ $w/W = 1.00$

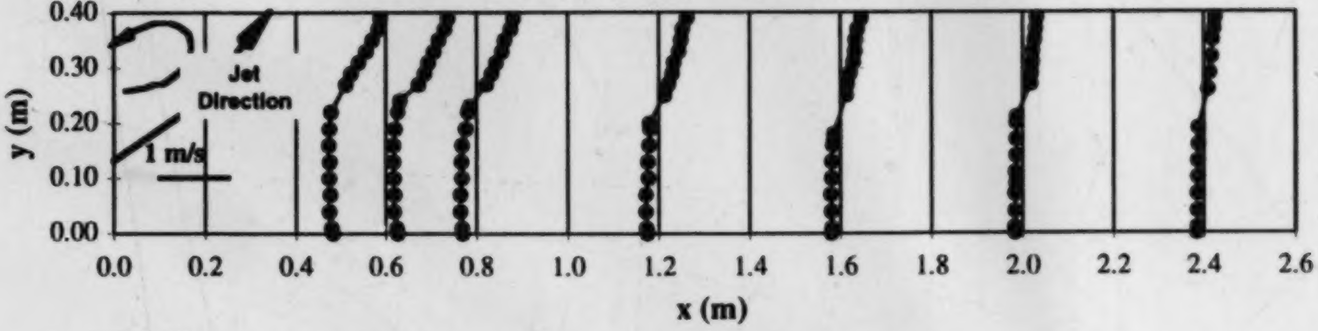
(h) Expt. (15)

$F_o = 2.40$ $S = 13.50(A)$ $Z_o/b_o = 6.75$ $\theta = 30°$ $w/W = 1.00$

Fig. 4.12(g-h) Typical Velocity Profiles for Pattern A

(i) Expt. (16)

$F_o = 2.40$ $S = 13.50$(A) $Z_o/b_o = 0.00$ $\theta = 30°$ $w/W = 1.00$

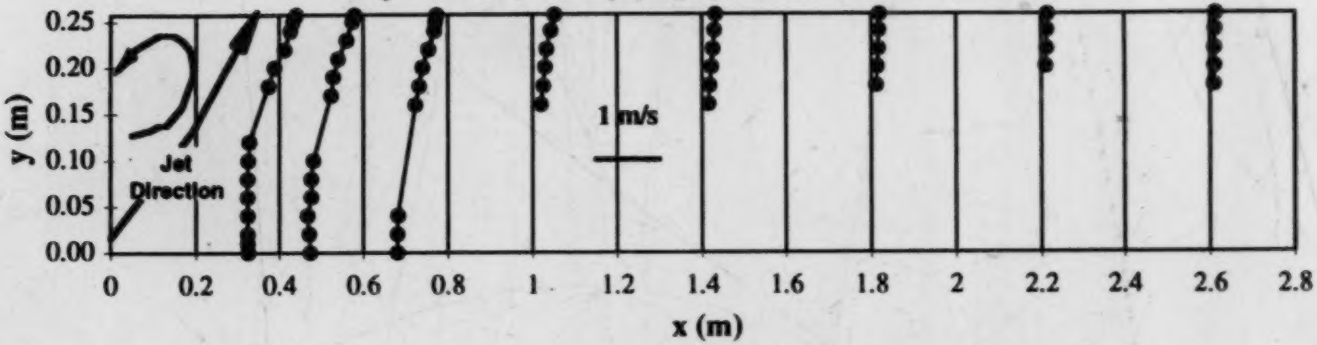

(j) Expt. (17)

$F_o = 3.60$ $S = 13.50$(A) $Z_o/b_o = 0.00$ $\theta = 30°$ $w/W = 1.00$

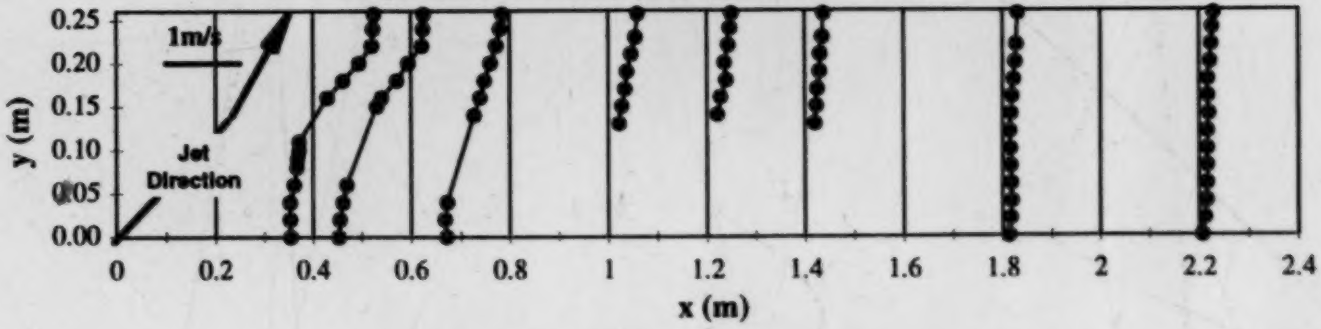

Fig. 4.12(i-j) Typical Velocity Profiles for Pattern A

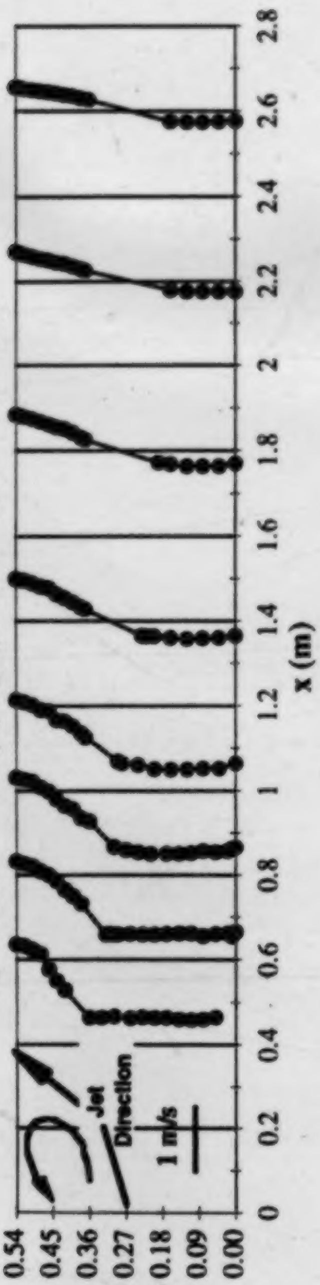

(k) Expt. (18)

$F_o = 4.80$ $S = 13.50(A)$ $Z_o/b_o = 13.50$ $\theta = 30°$ $w/W = 1.00$

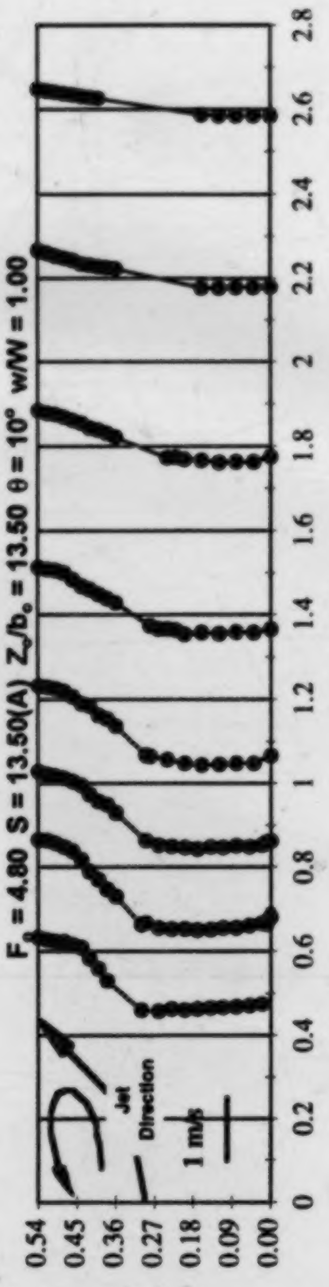

(l) Expt. (19)

$F_o = 4.80$ $S = 13.50(A)$ $Z_o/b_o = 13.50$ $\theta = 10°$ $w/W = 1.00$

Fig. 4.12(k-l) Typical Velocity Profiles for Pattern A

(m) Expt. (20)

$F_o = 4.80$ $S = 13.50(A)$ $Z_o/b_o = 13.50$ $\theta = 10°$ $w/W = 0.80$

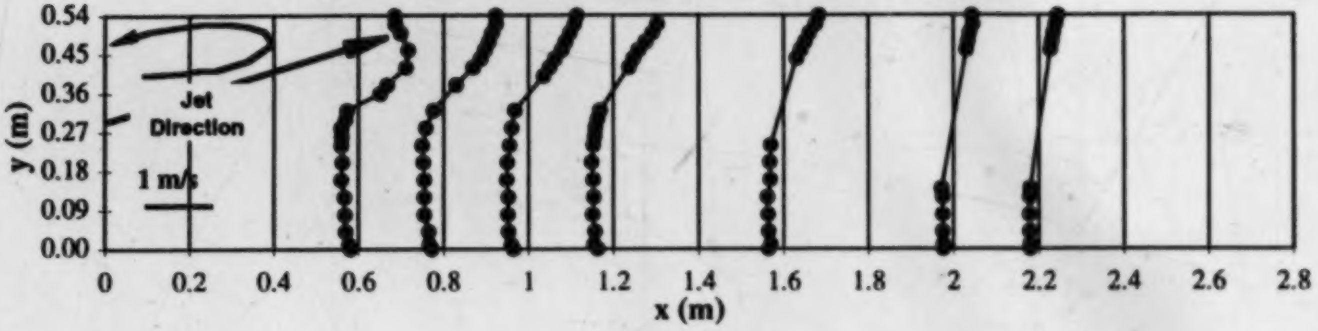

(n) Expt. (21)

$F_o = 4.80$ $S = 13.50(A)$ $Z_o/b_o = 13.50$ $\theta = 10°$ $w/W = 0.50$

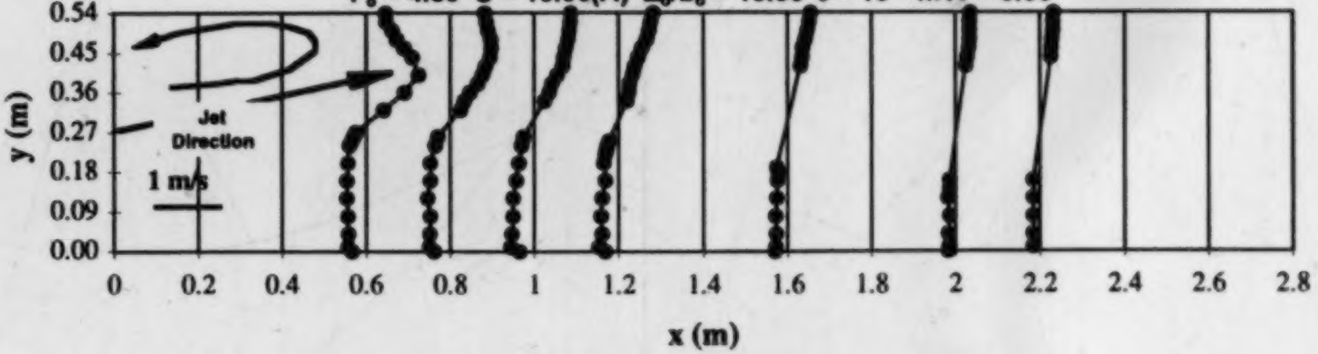

Fig. 4.12(m-n) Typical Velocity Profiles for Pattern A

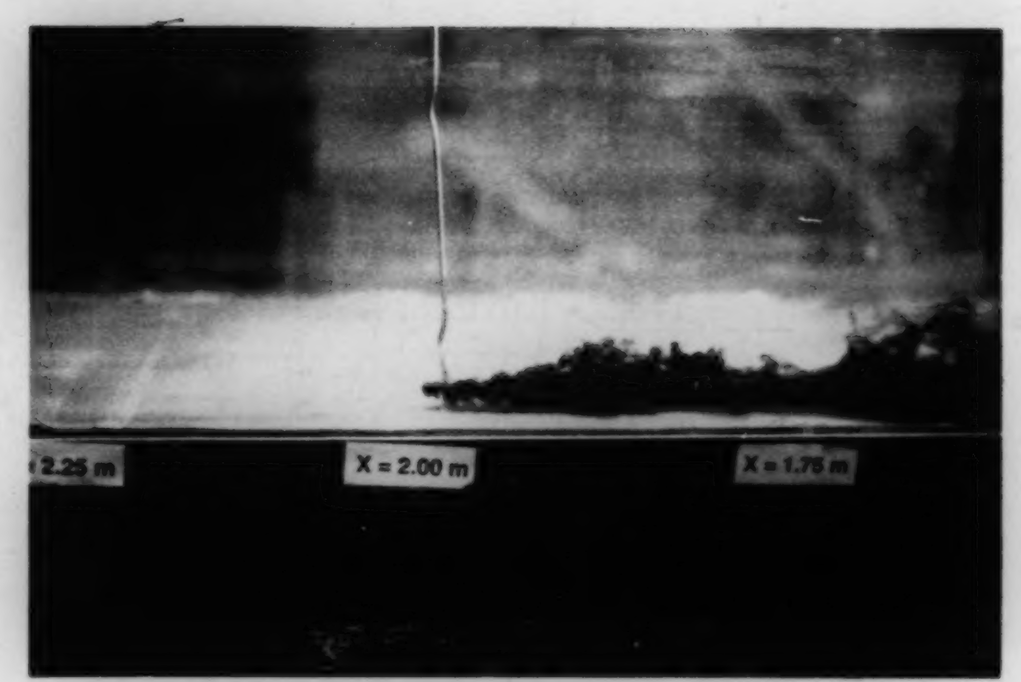
2.25 m
X = 2.00 m
X = 1.75 m

Fig. 4.13 Reverse flow near the bed (x = 2 m)

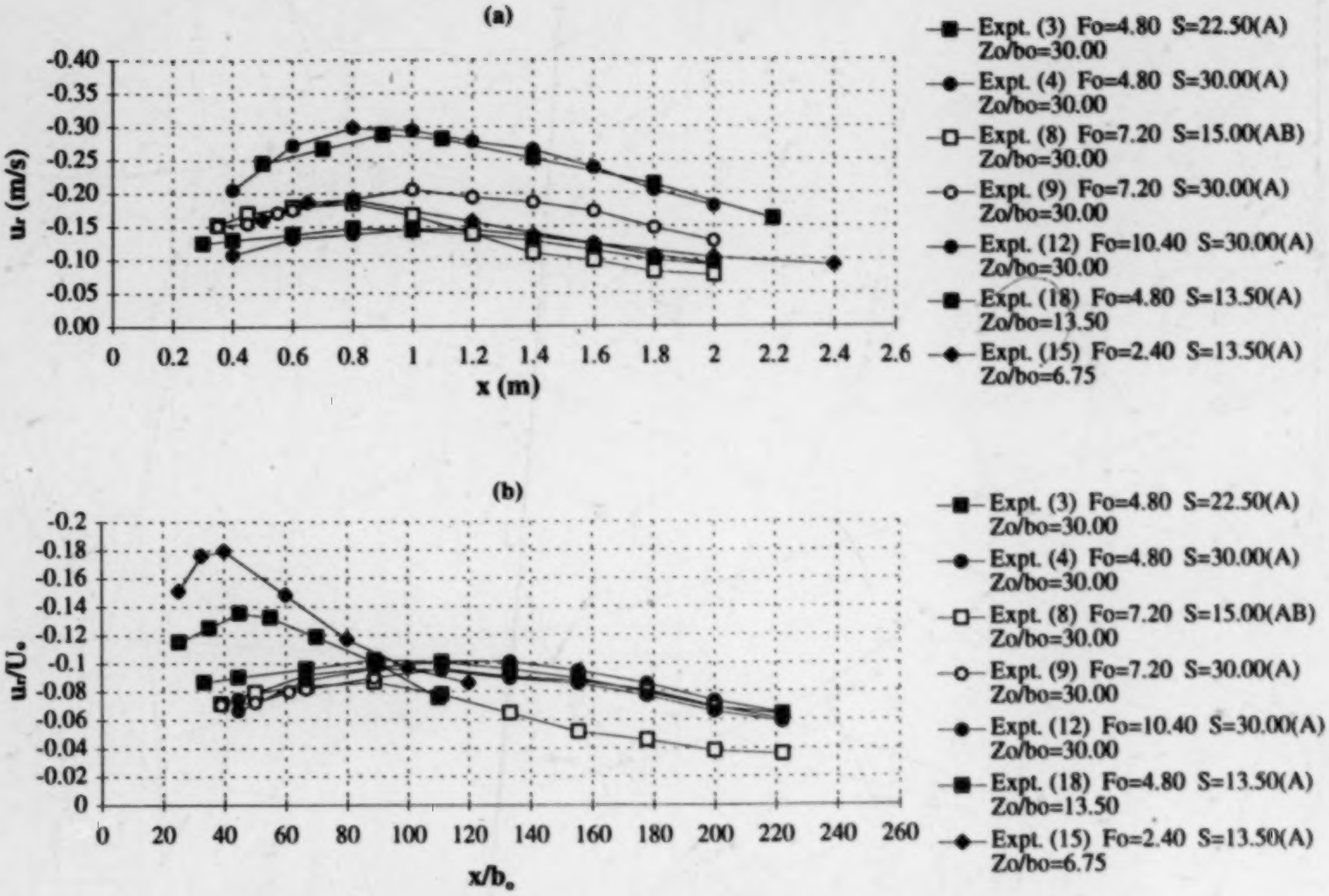

Fig. 4.14(a-b) Variation of the depth-averaged reverse velocity with distance

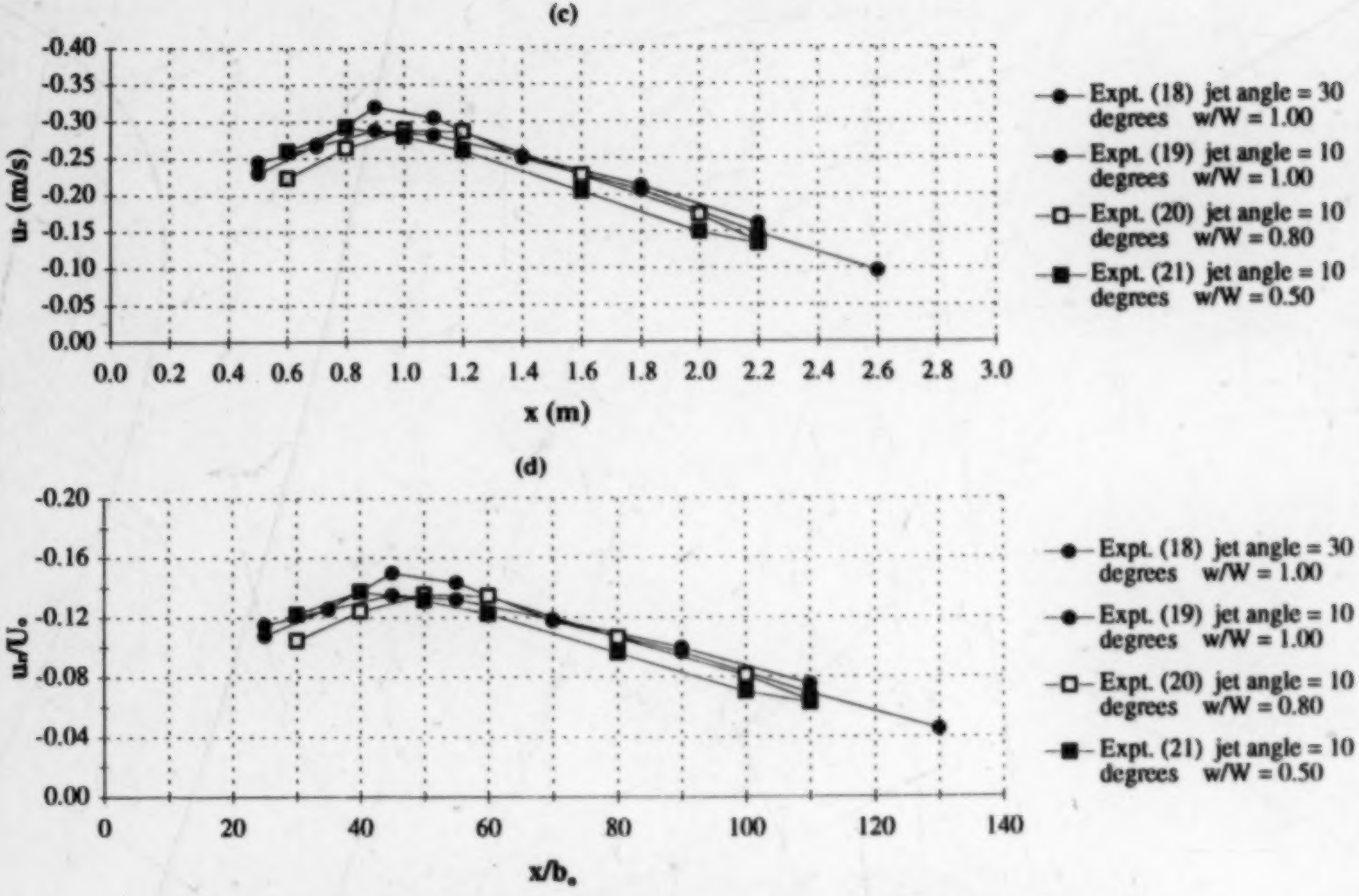

Fig. 4.14(c-d) Variation of the depth-averaged reverse velocity with distance

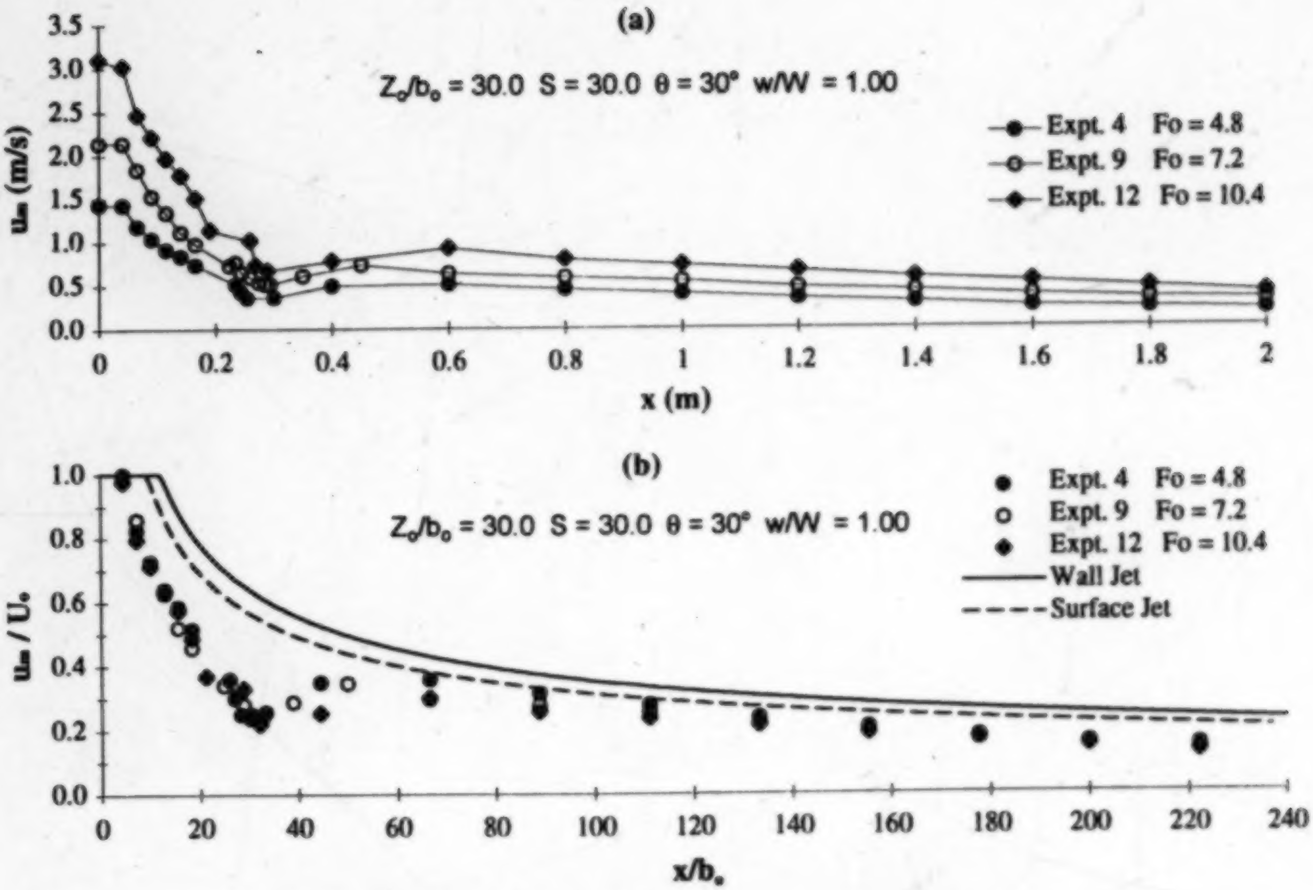

Fig. 4.15(a-b) Maximum-velocity decay in flow pattern A

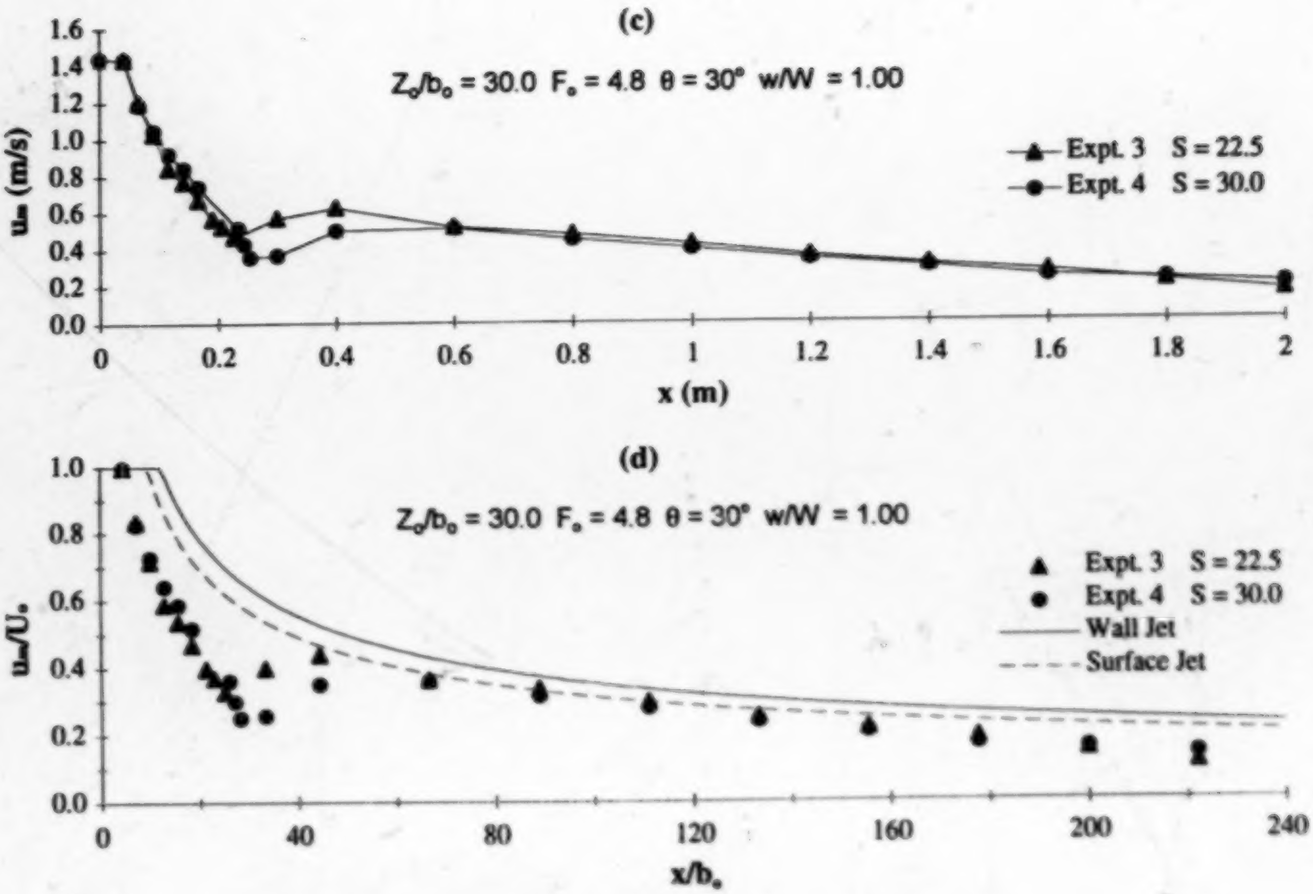

Fig. 4.15(c-d) Maximum-velocity decay in flow pattern A

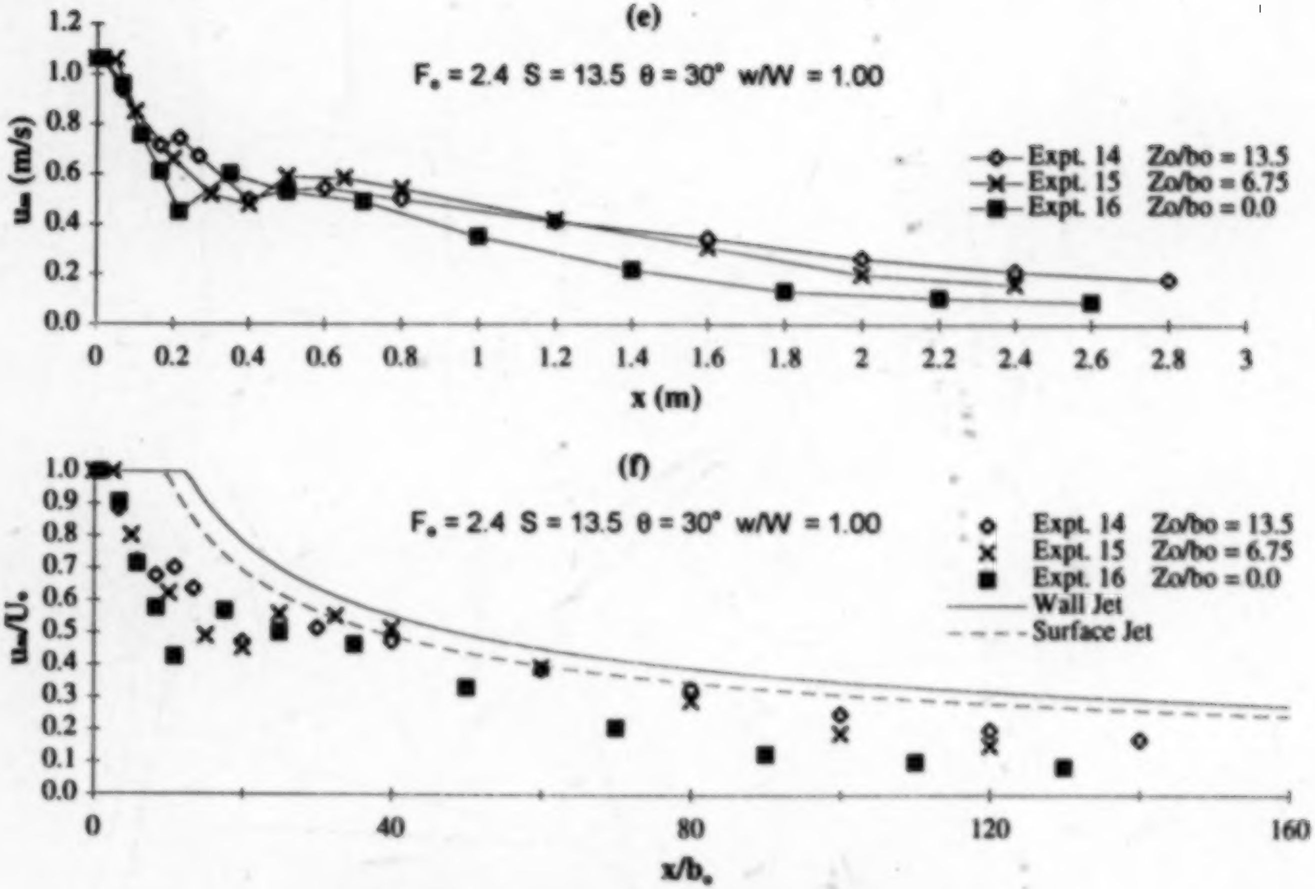

Fig. 4.15(e-f) Maximum-velocity decay in flow pattern A

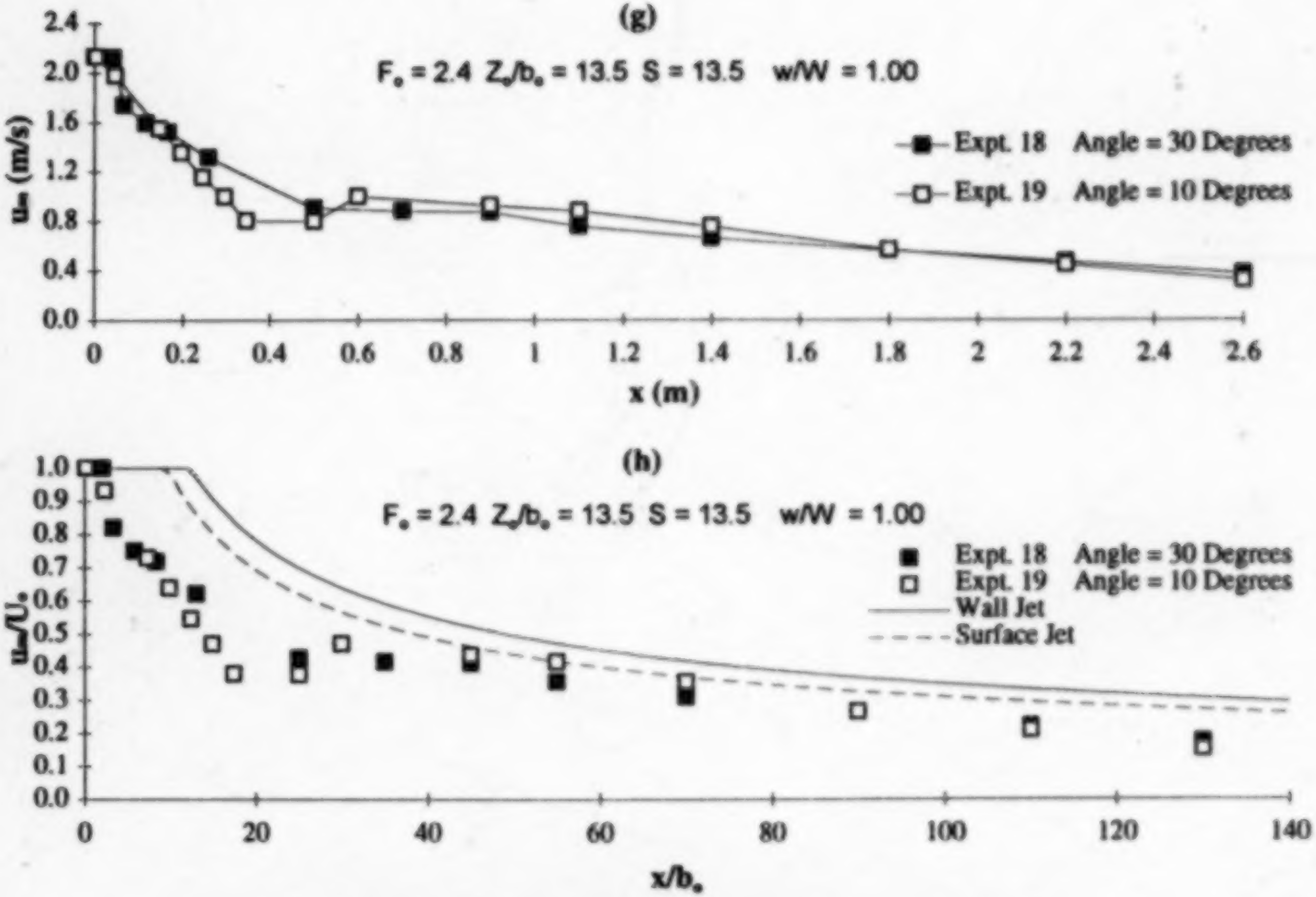

Fig. 4.15(g-h) Maximum-velocity decay in flow pattern A

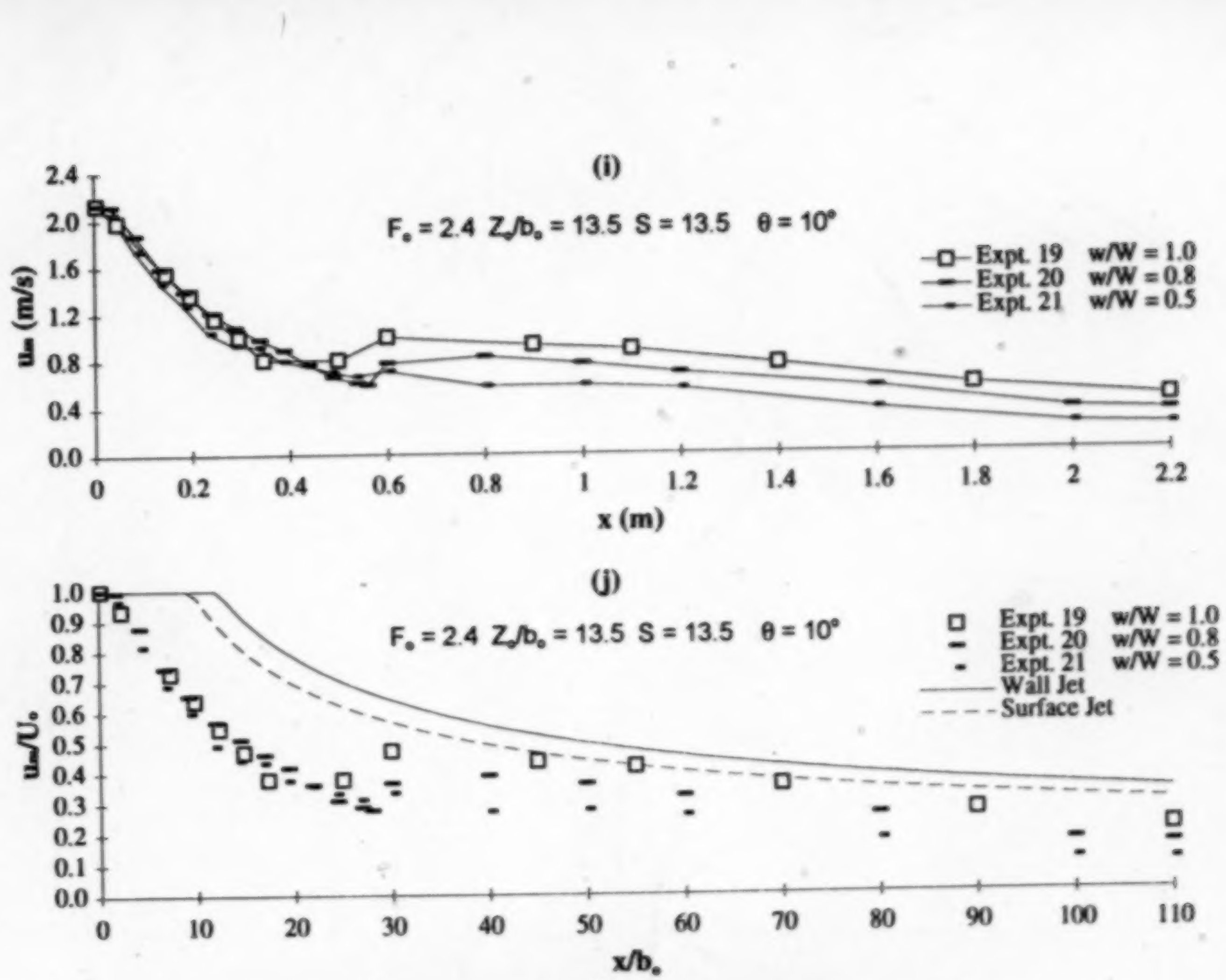

Fig. 4.15(i-j) Maximum-velocity decay in flow pattern A

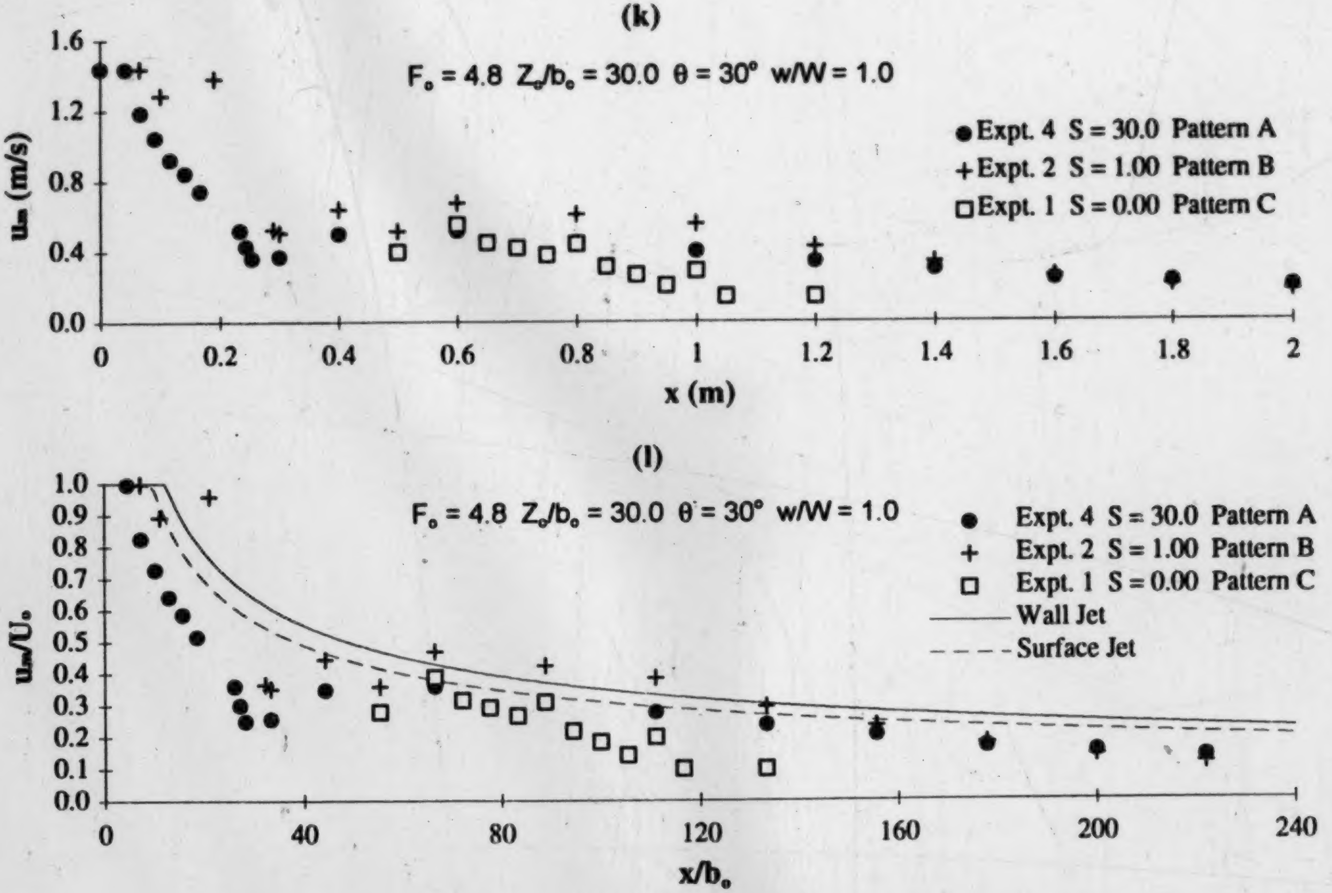

Fig. 4.15(k-l) Maximum-velocity decay in flow pattern A, B & C

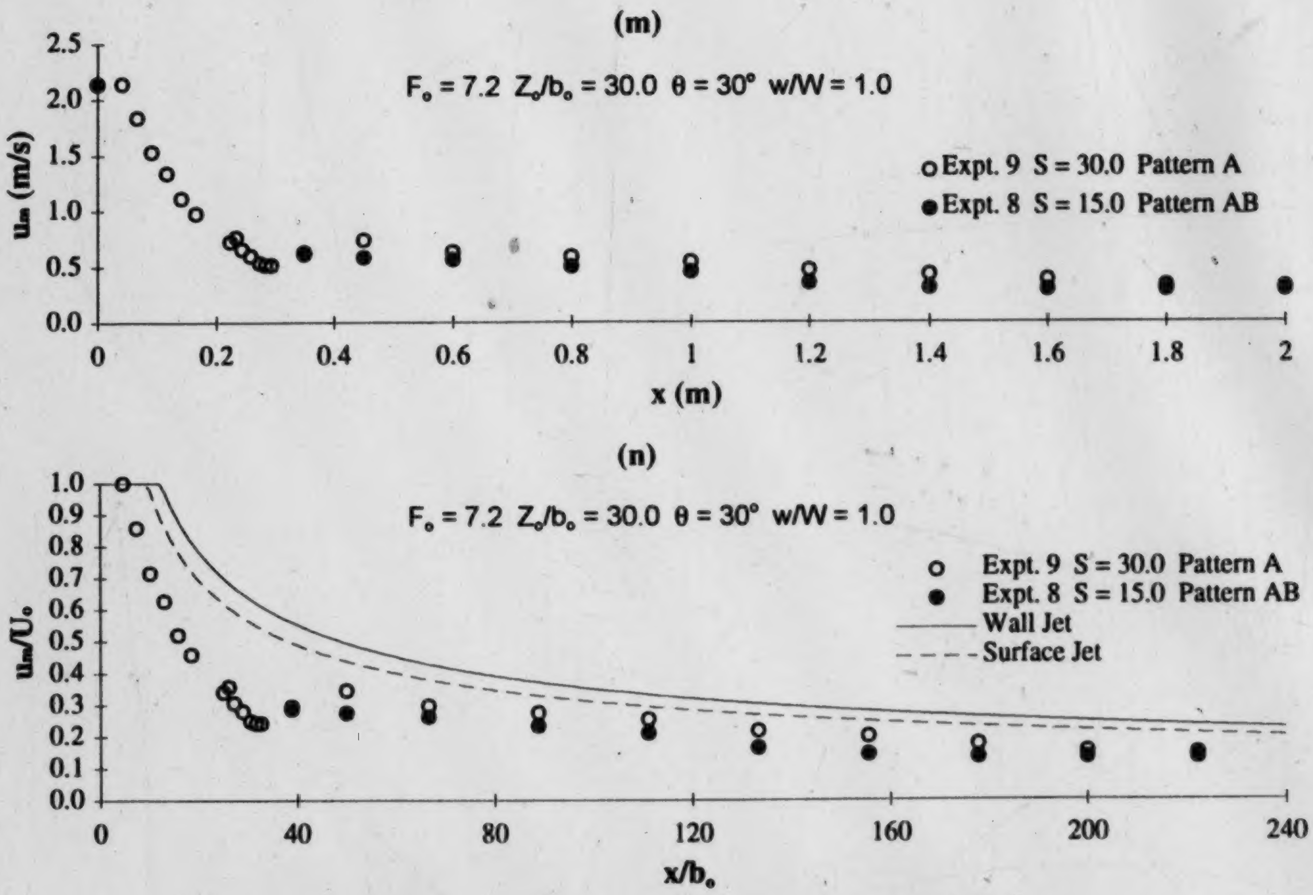

Fig. 4.15(m-n) Maximum-velocity decay in flow pattern A & AB

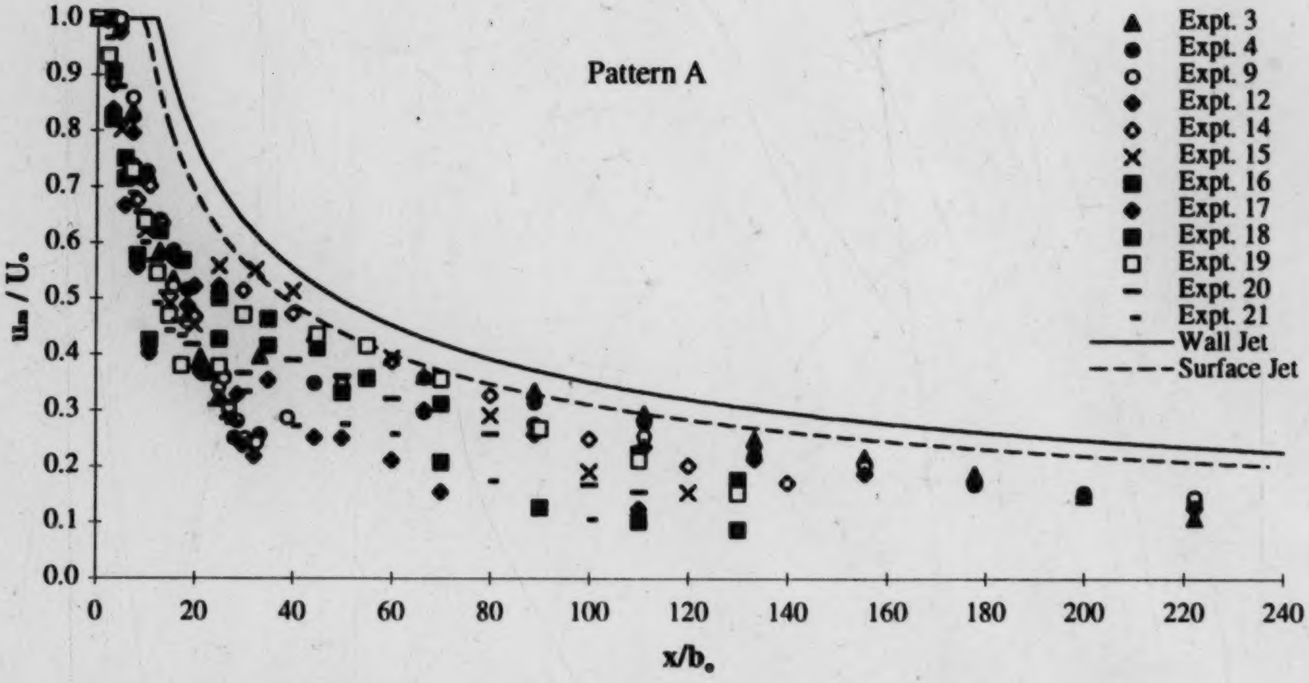

Fig. 4.16 Consolidated plot for all the maximum-velocity decay profiles in flow pattern A

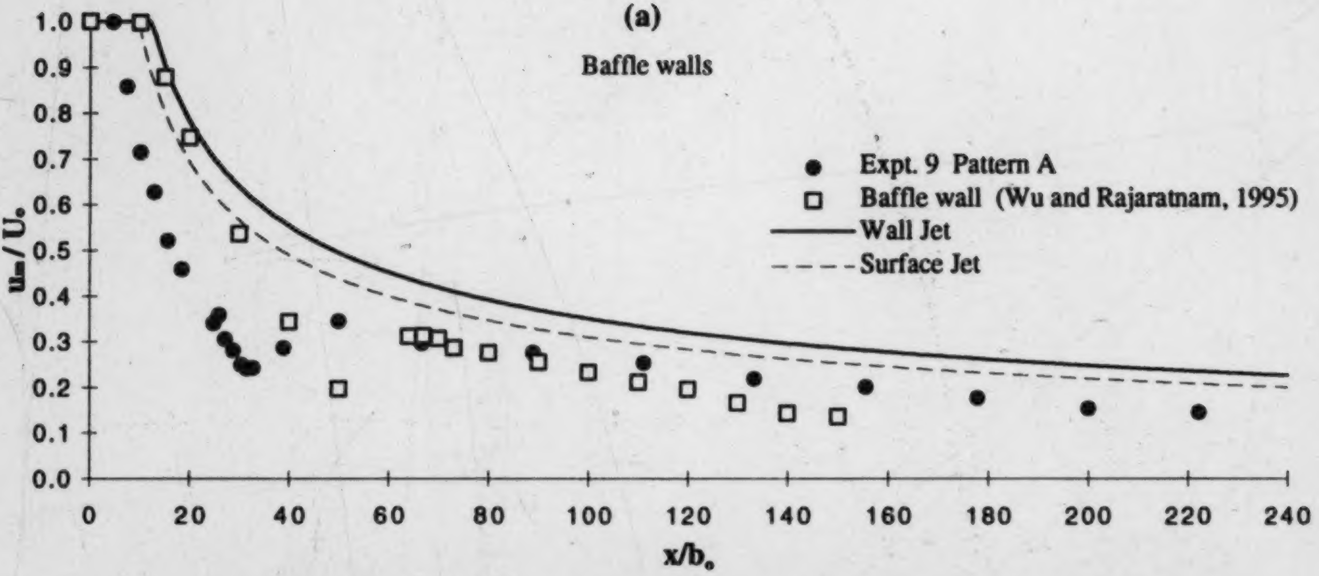

Fig. 4.17 Comparison between the double-leaf gate and the baffle wall dissipators

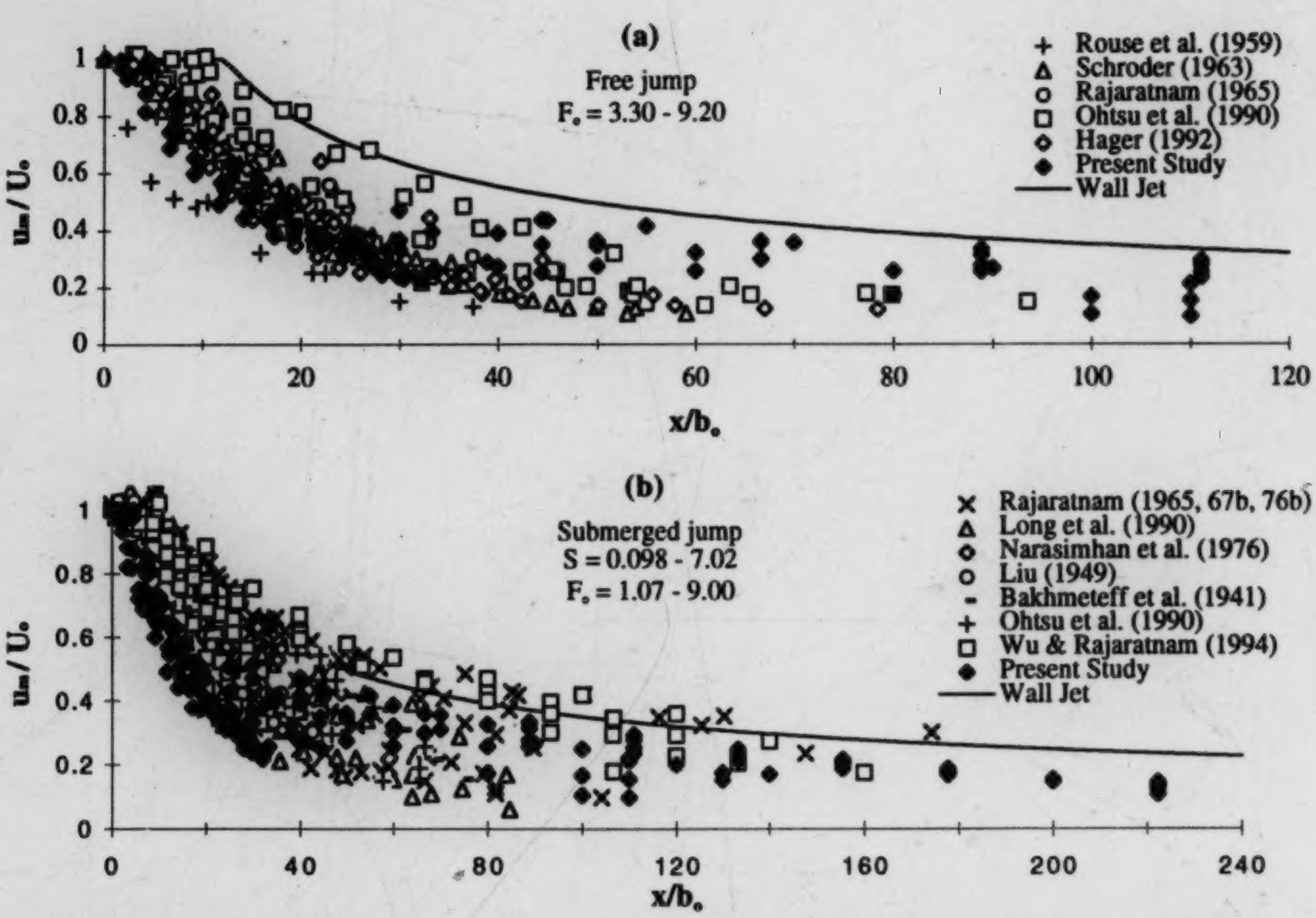

Fig. 4.18(a-b) Comparison between the double-leaf gate, the free and the submerged jumps

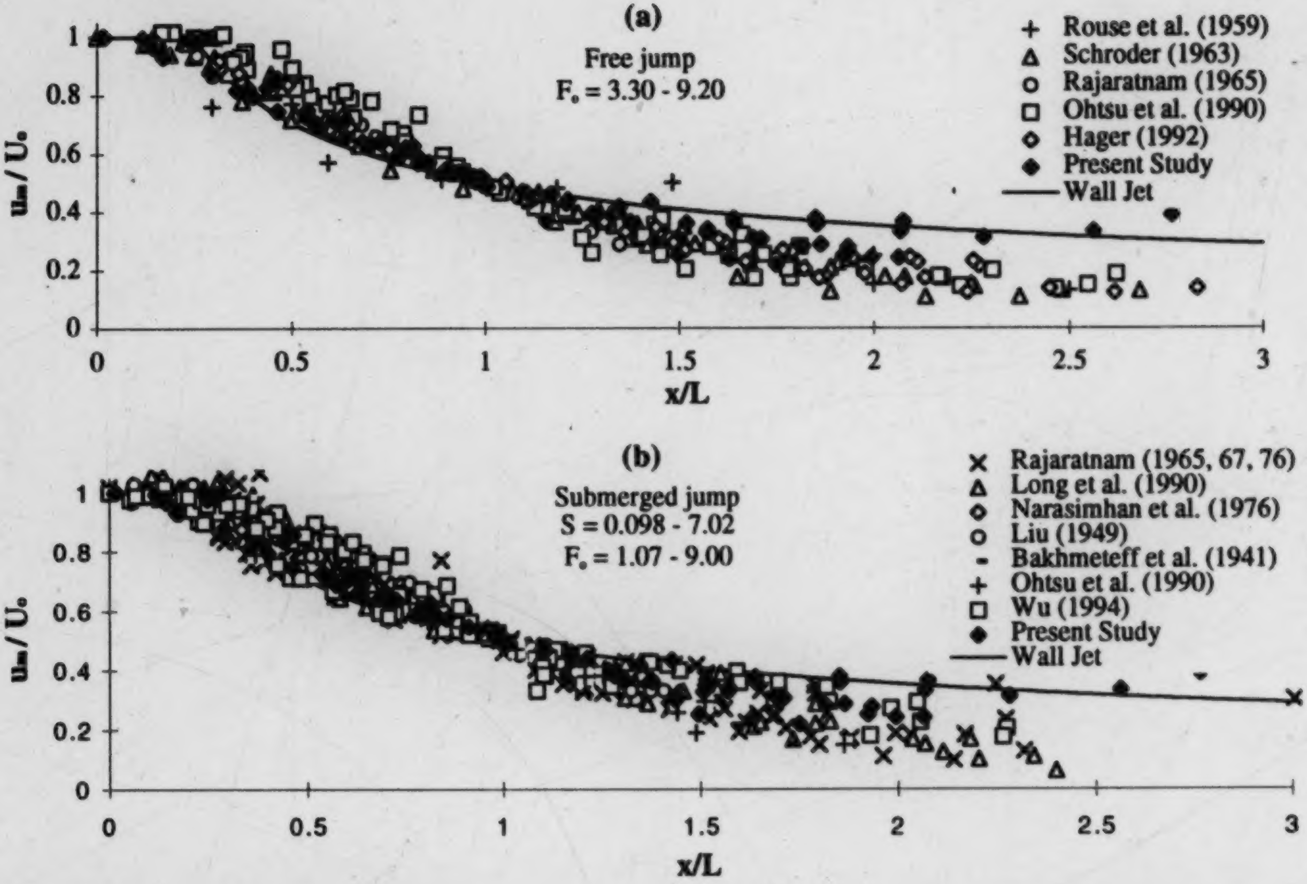

Fig. 4.19(a-b) Comparison between the double-leaf gate, the free and the submerged jumps

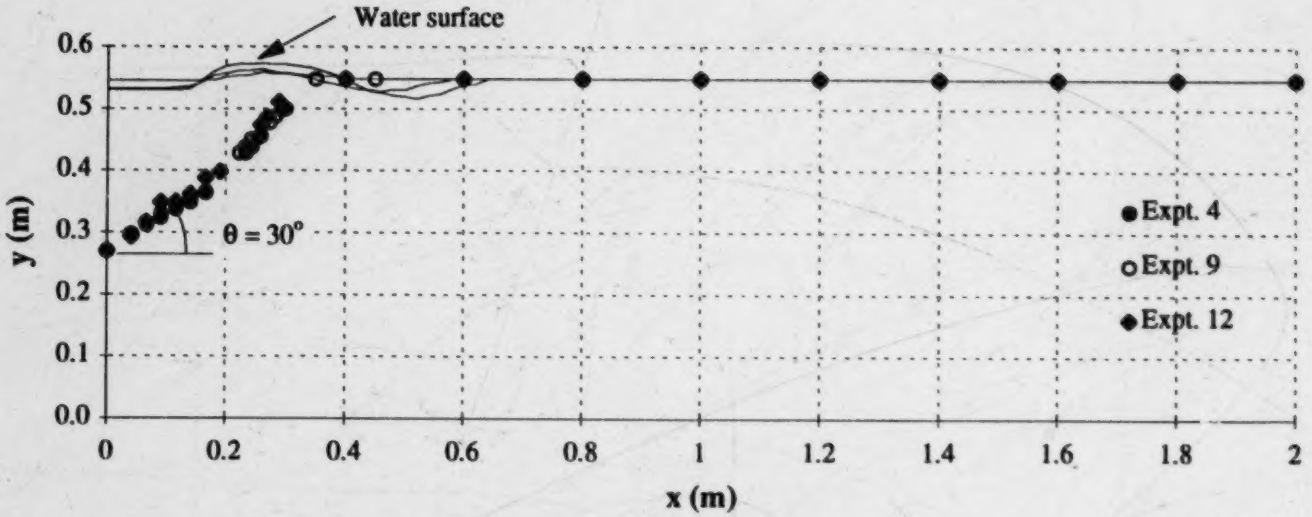

Fig. 4.20 Locus of the maximum velocity

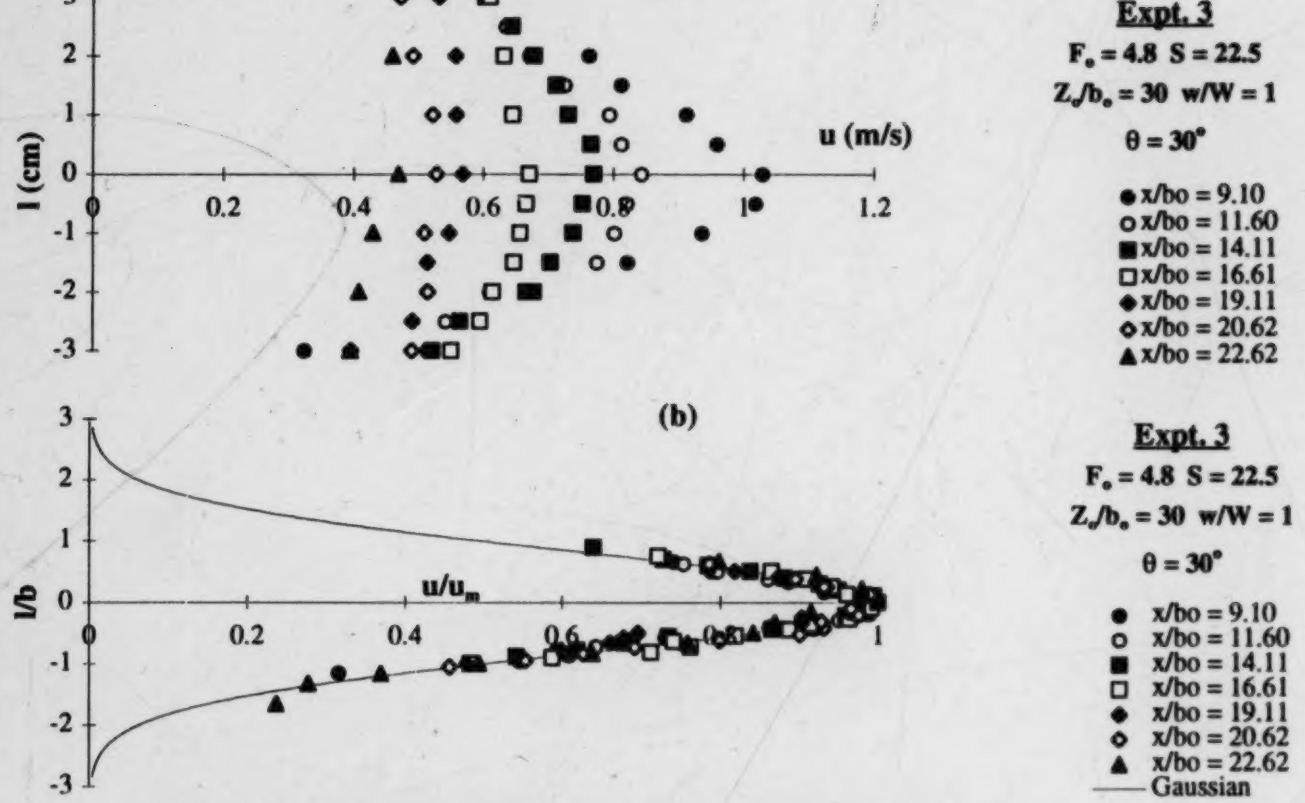

Fig. 4.21(a-b) Velocity distributions for the inclined jet (Expt. 3)
(a) Typical velocity profiles; (b) Similarity profile

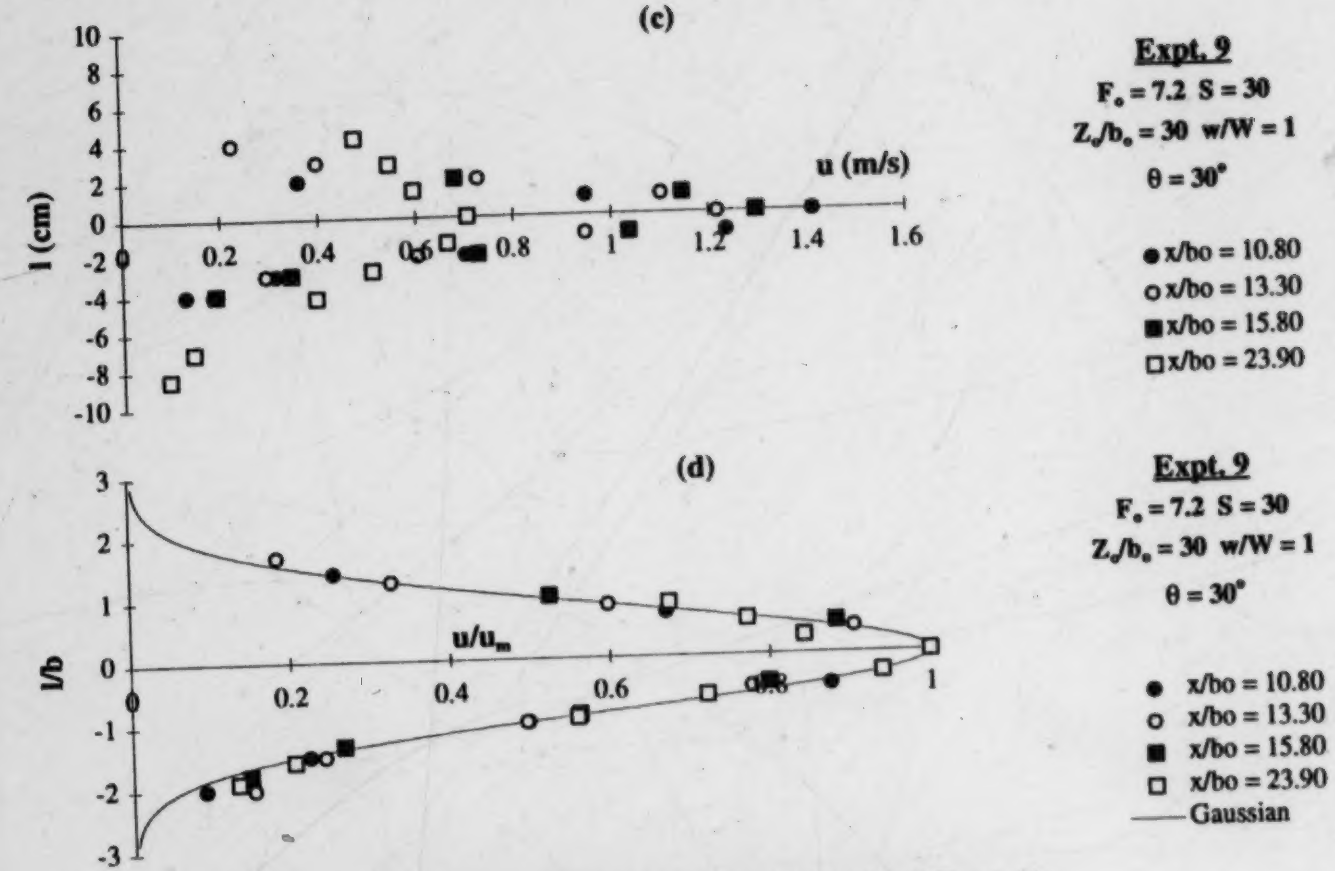

Fig. 4.21(c-d) Velocity distributions for the inclined jet (Expt. 9)
(c) Typical velocity profiles; (d) Similarity profile

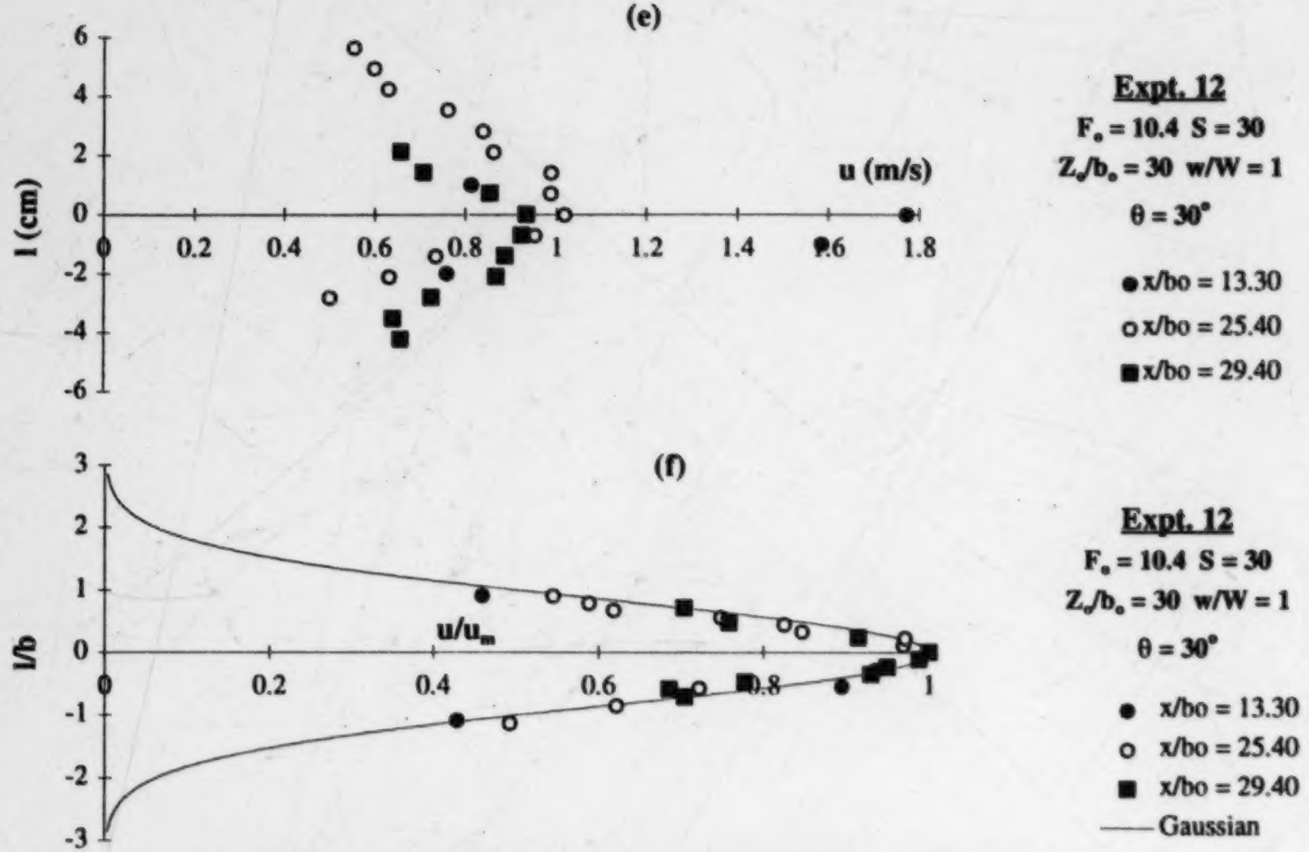

Fig. 4.21(e-f) Velocity distributions for the inclined jet (Expt. 12)
(e) Typical velocity profiles; (f) Similarity profile

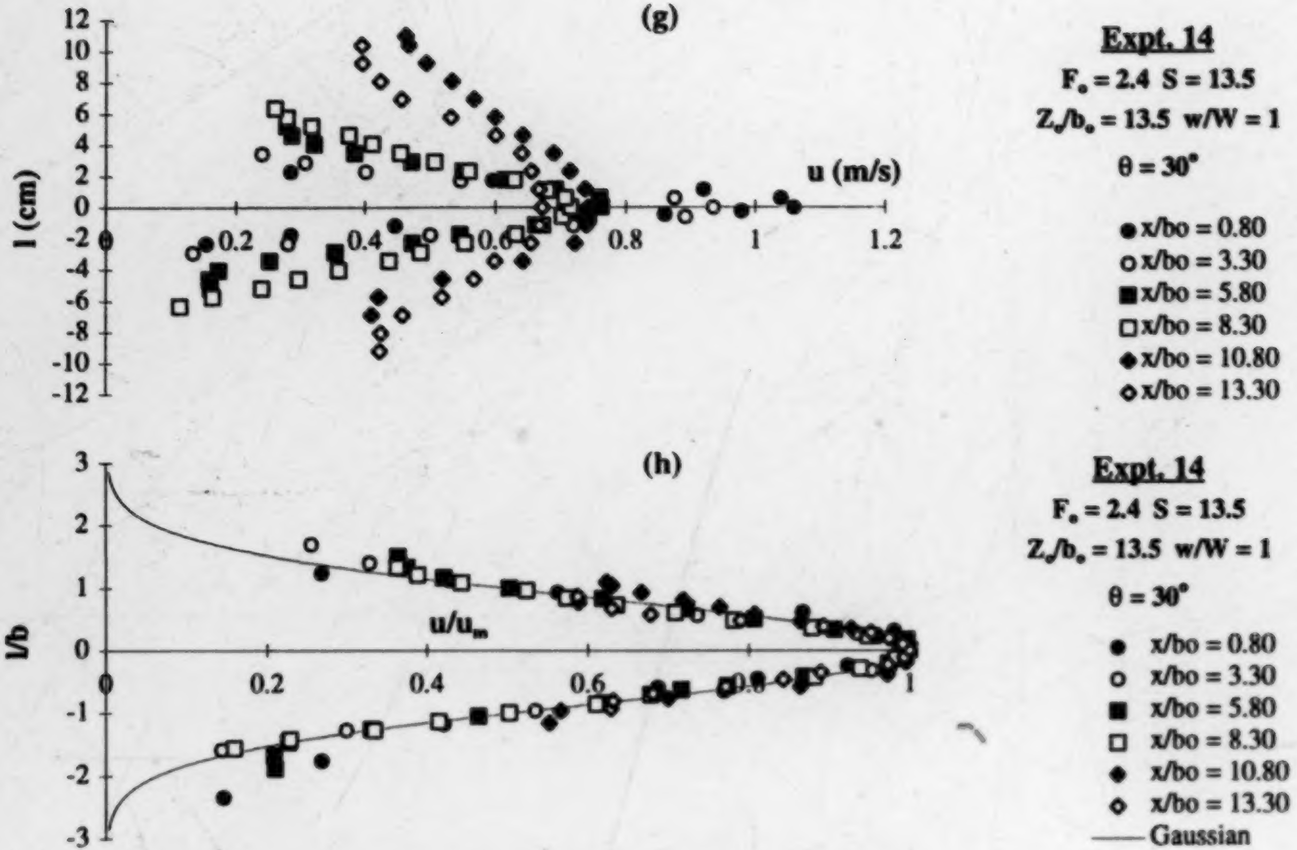

Fig. 4.21(g-h) Velocity distributions for the inclined jet (Expt. 14)
(g) Typical velocity profiles; (h) Similarity profile

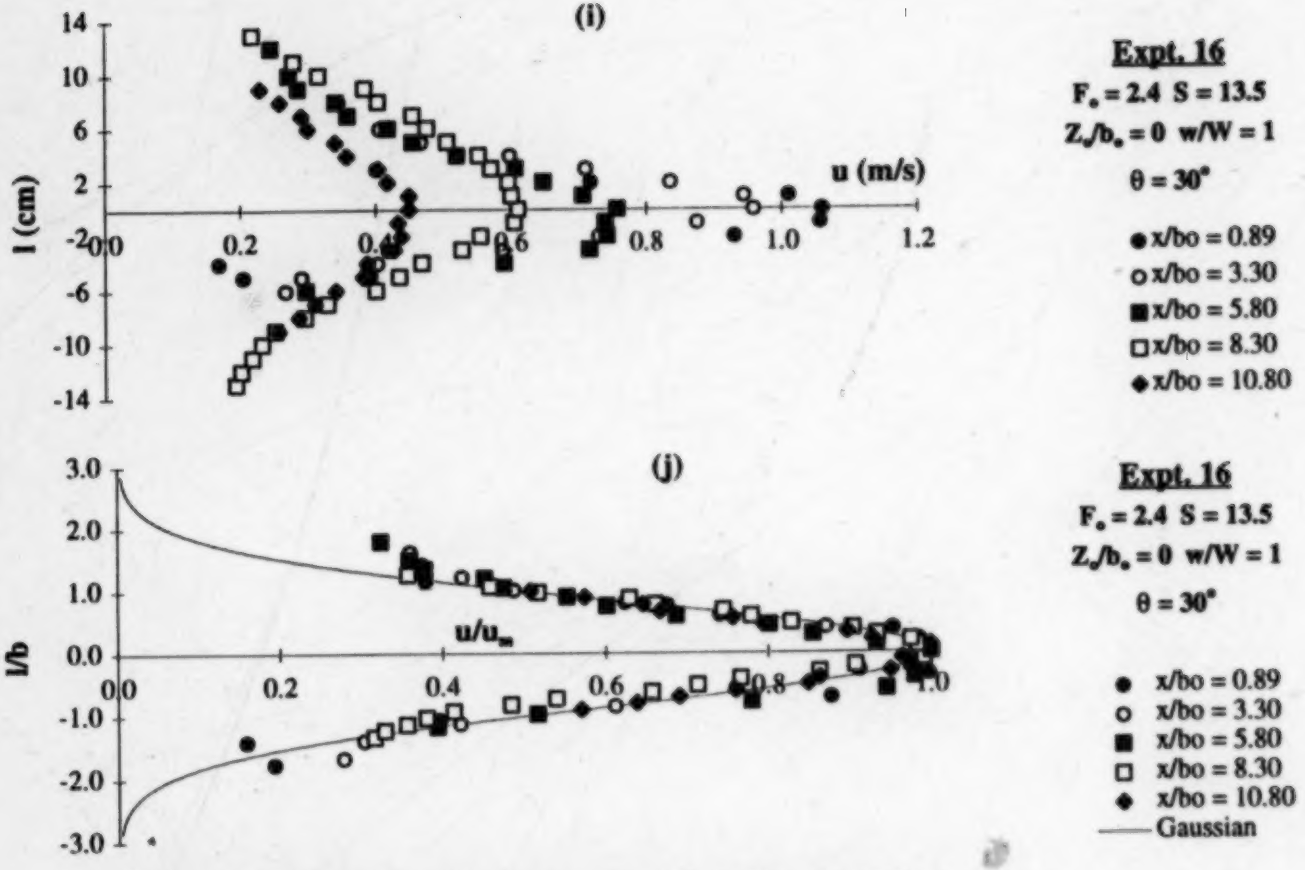

Fig. 4.21(i-j) Velocity distributions for the inclined jet (Expt. 16)
(i) Typical velocity profiles; (j) Similarity profile

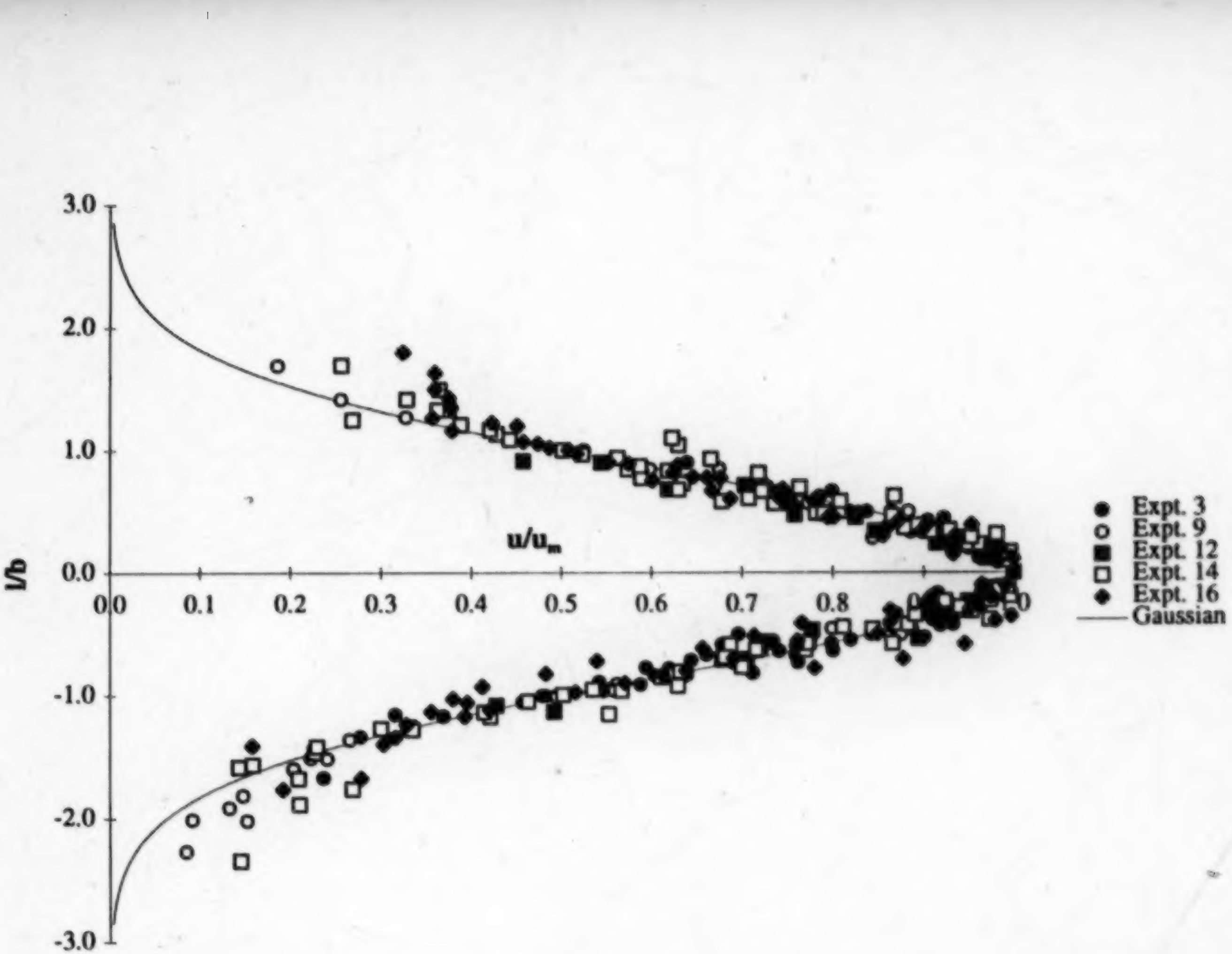

Fig. 4.22 Consolidated non-dimensional plot for the velocity distribution in the inclined jet

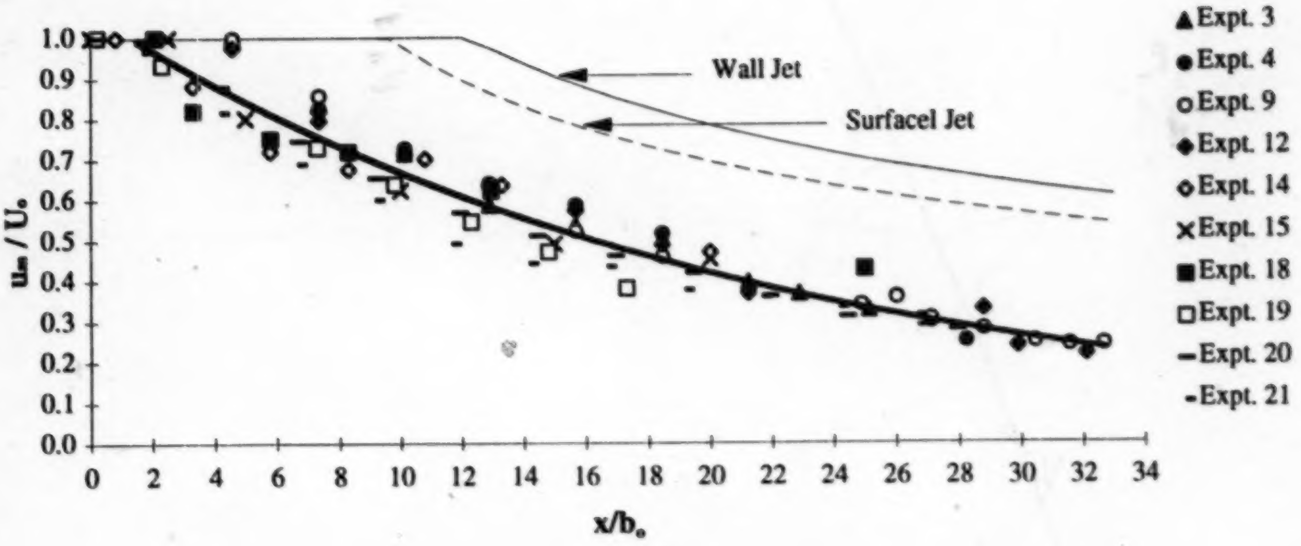

Fig. 4.23 Maximum-velocity decay with distance along the inclined jet

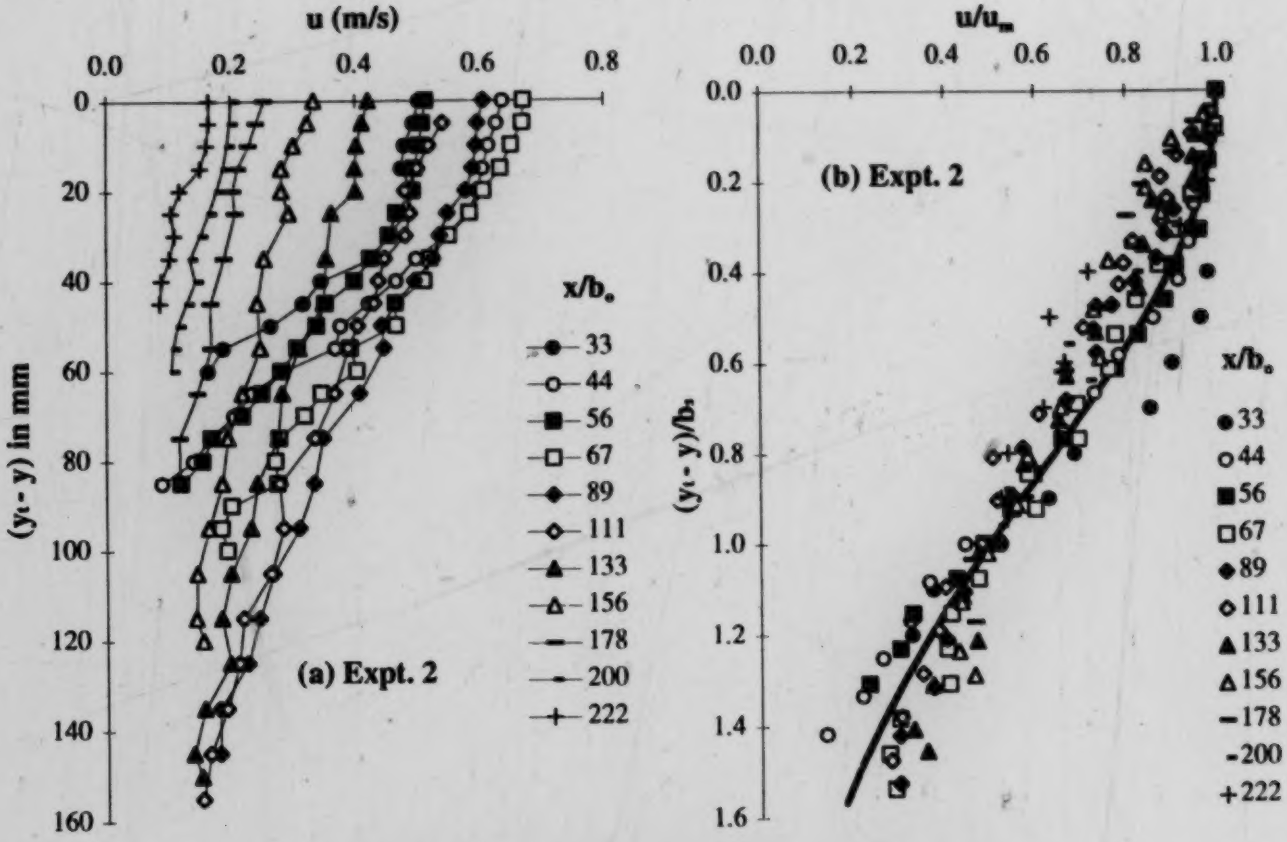

Fig. 4.24(a-b) Velocity distribution in surface jet (Expt. 2)
(a) Velocity profiles; and (b) Similarity profile

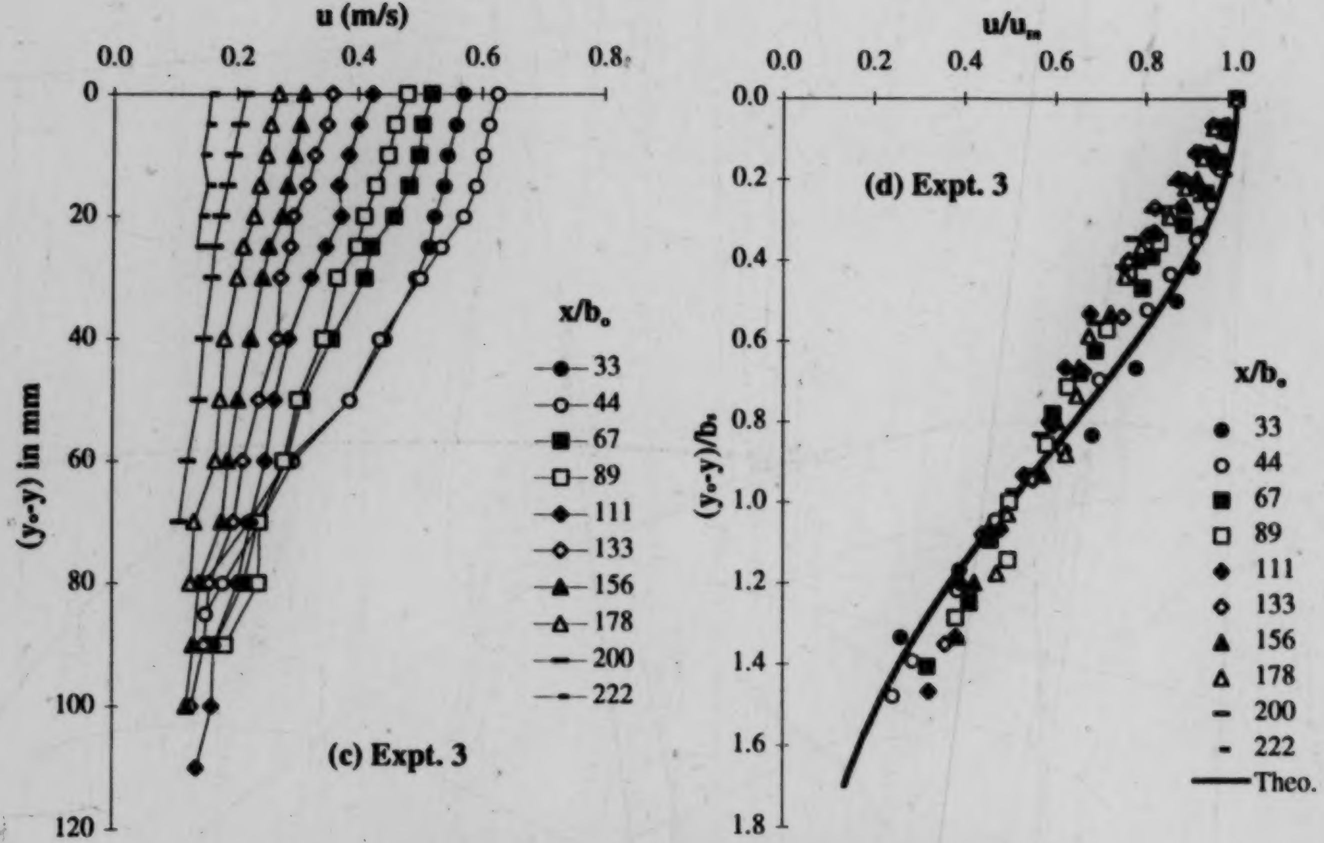

Fig. 4.24(c-d) Velocity distribution in surface jet (Expt. 3)
(c) Velocity profiles; and (d) Similarity profile

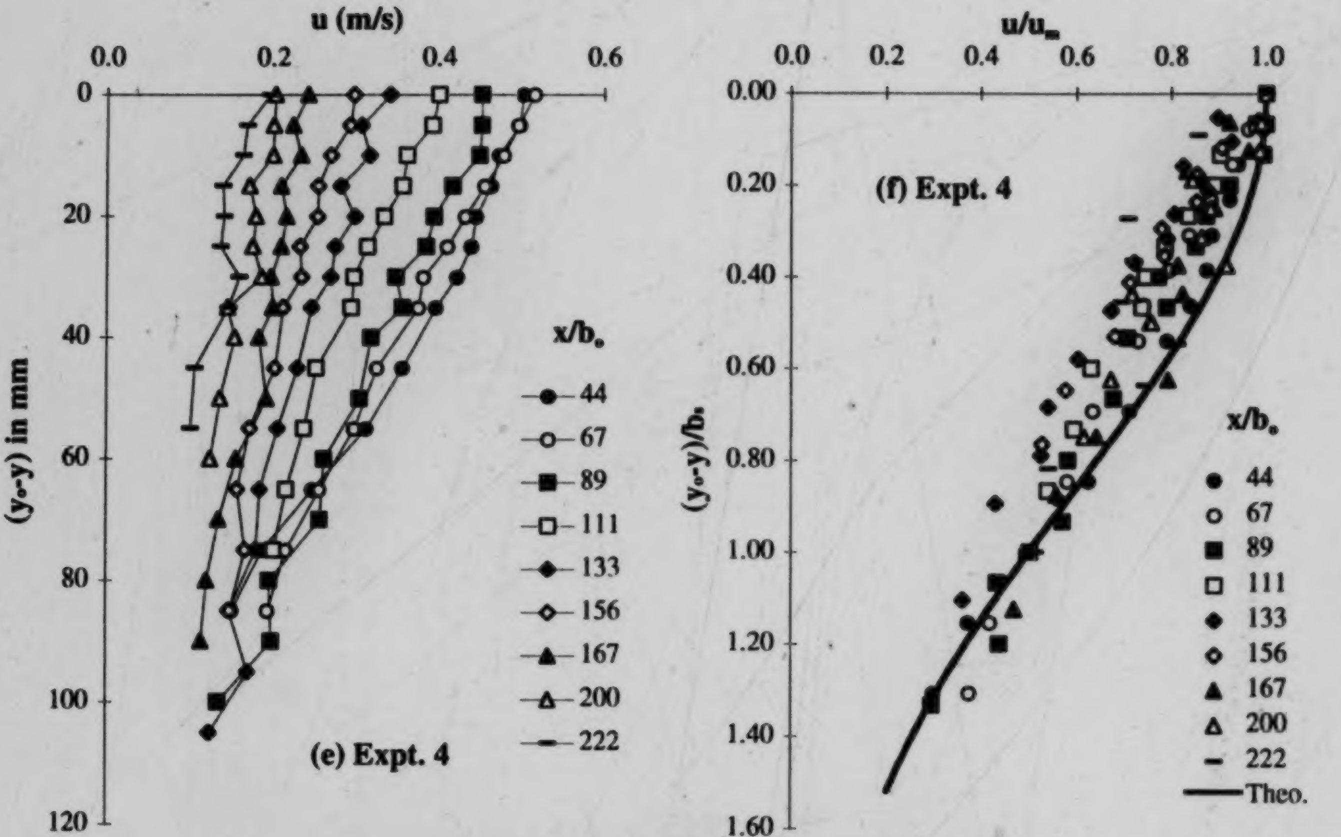

Fig. 4.24(e-f) Velocity distribution in surface jet (Expt. 4)
(e) Velocity profiles; and (f) Similarity profile

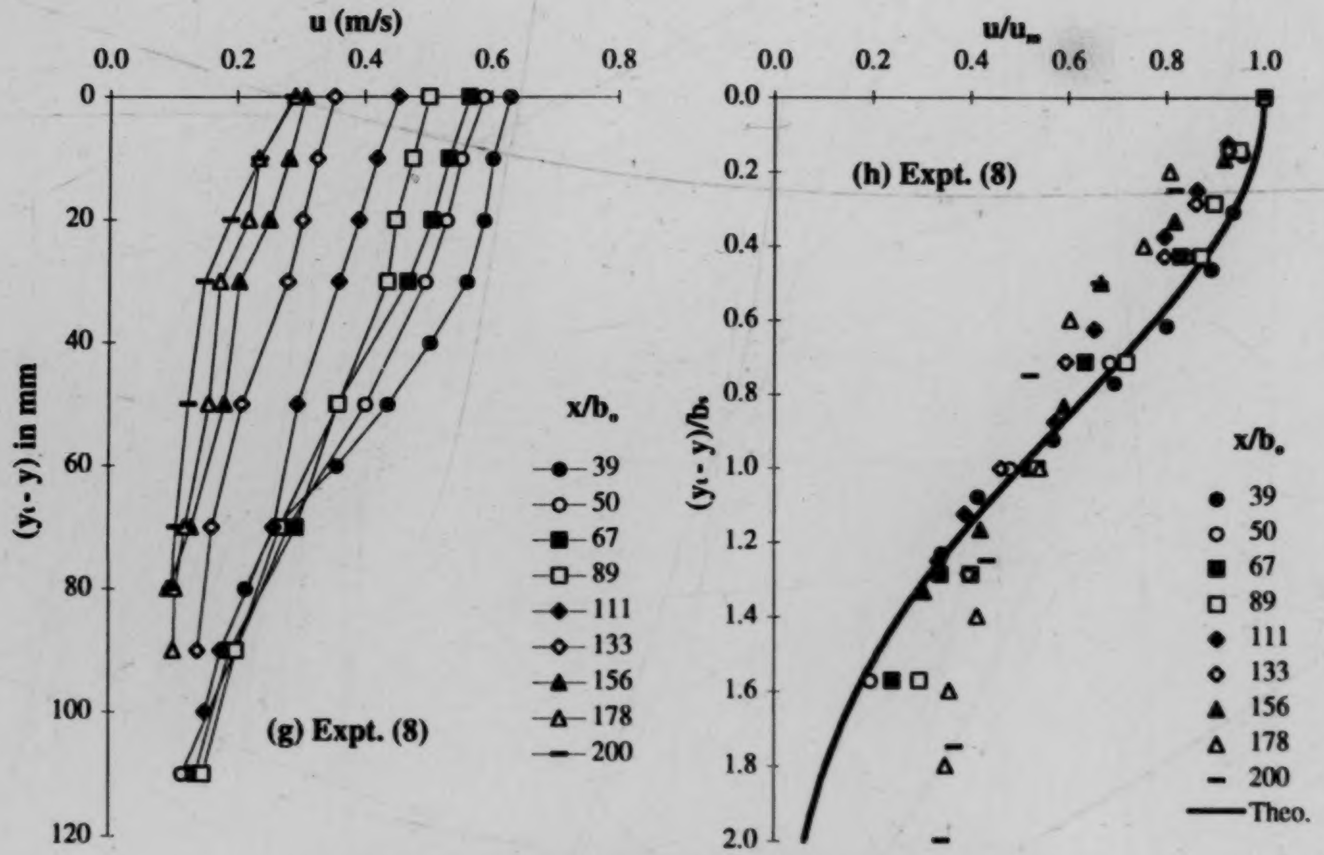

Fig. 4.24(g-h) Velocity distribution in surface jet (Expt. 8)
(g) Velocity profiles; and (h) Similarity profile

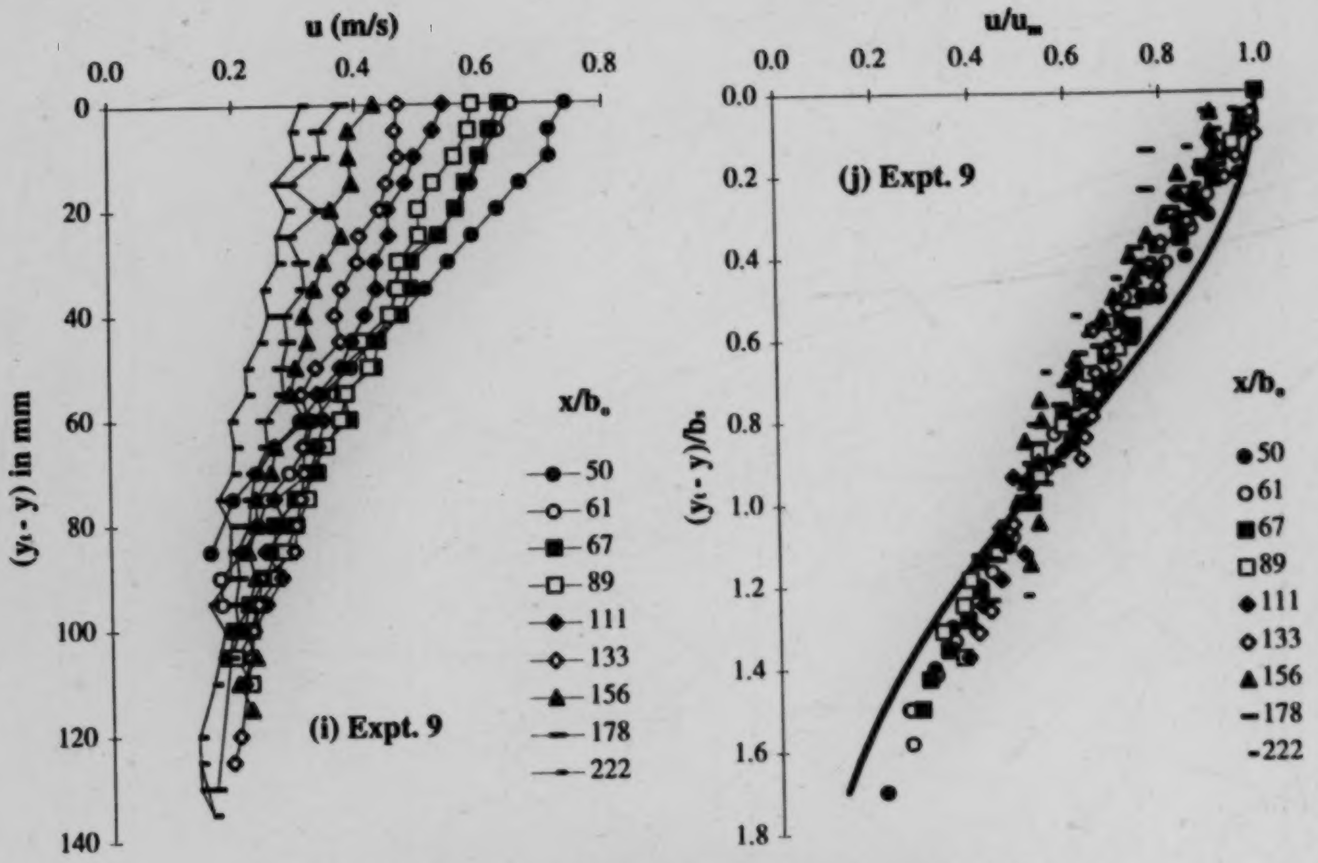

Fig. 4.24(i-j) Velocity distribution in surface jet (Expt. 9)
(i) Velocity profiles; and (j) Similarity profile

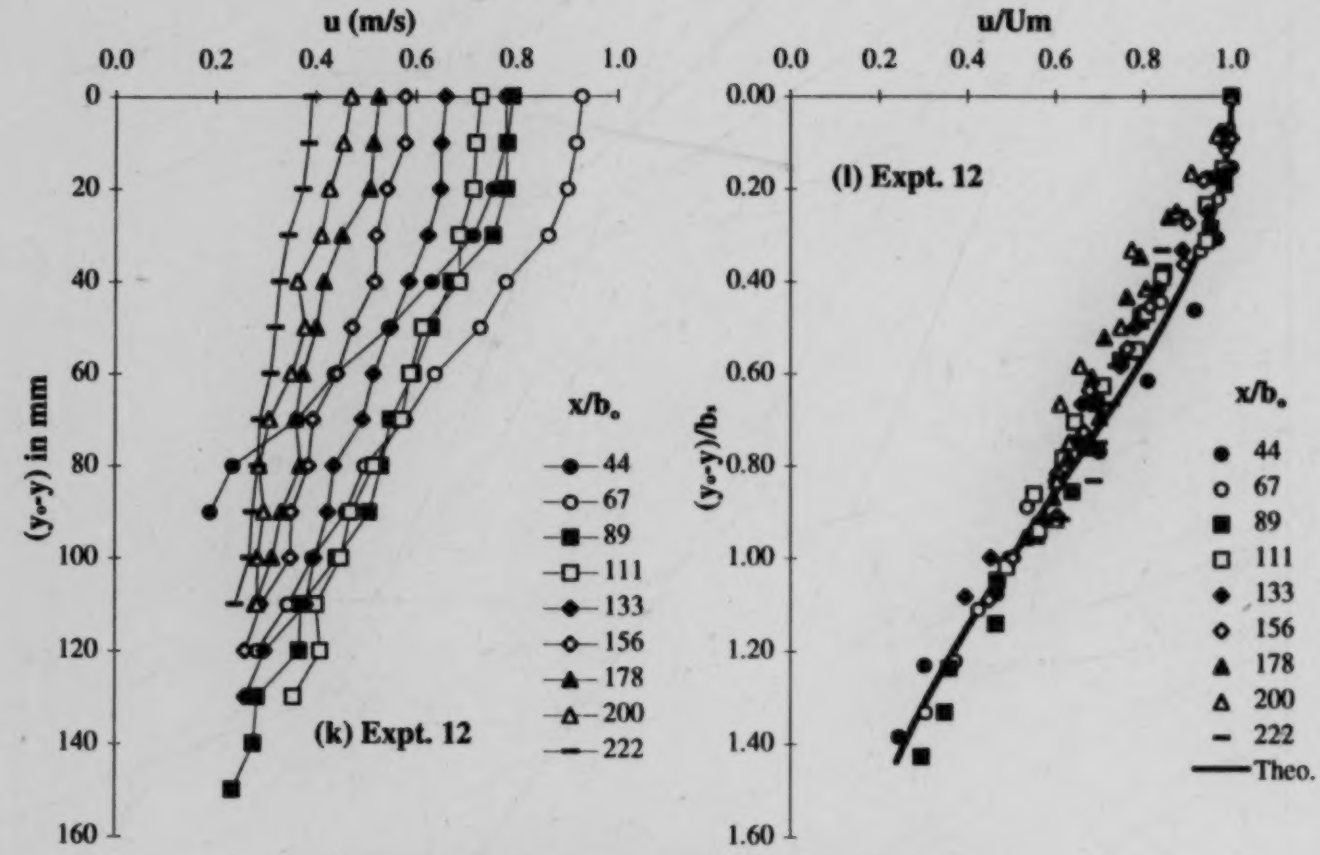

Fig. 4.24(k-l) Velocity distribution in surface jet (Expt. 12)
(k) Velocity profiles; and (l) Similarity profile

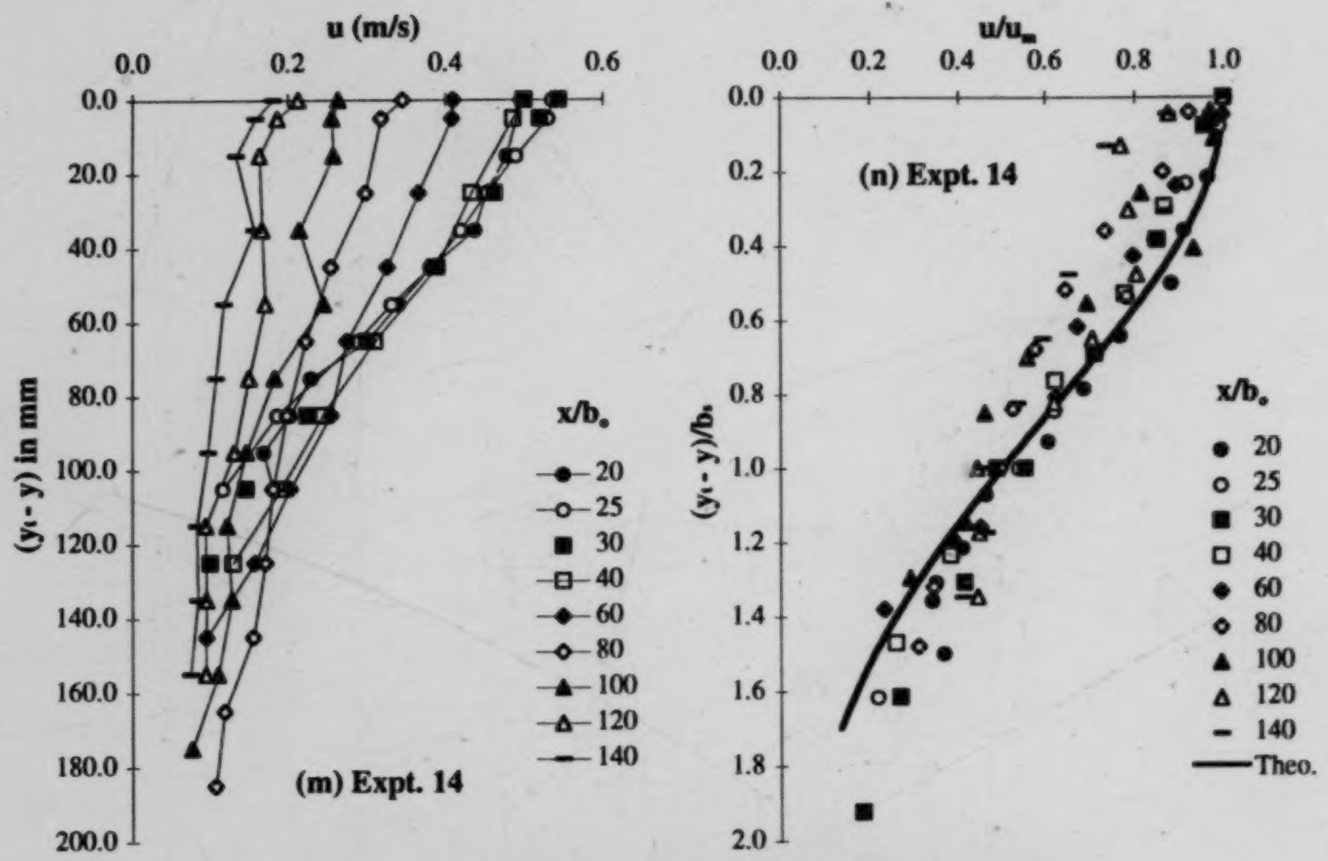

Fig. 4.24(m-n) Velocity distribution in surface jet (Expt. 14)
(m) Velocity profiles; and (n) Similarity profile

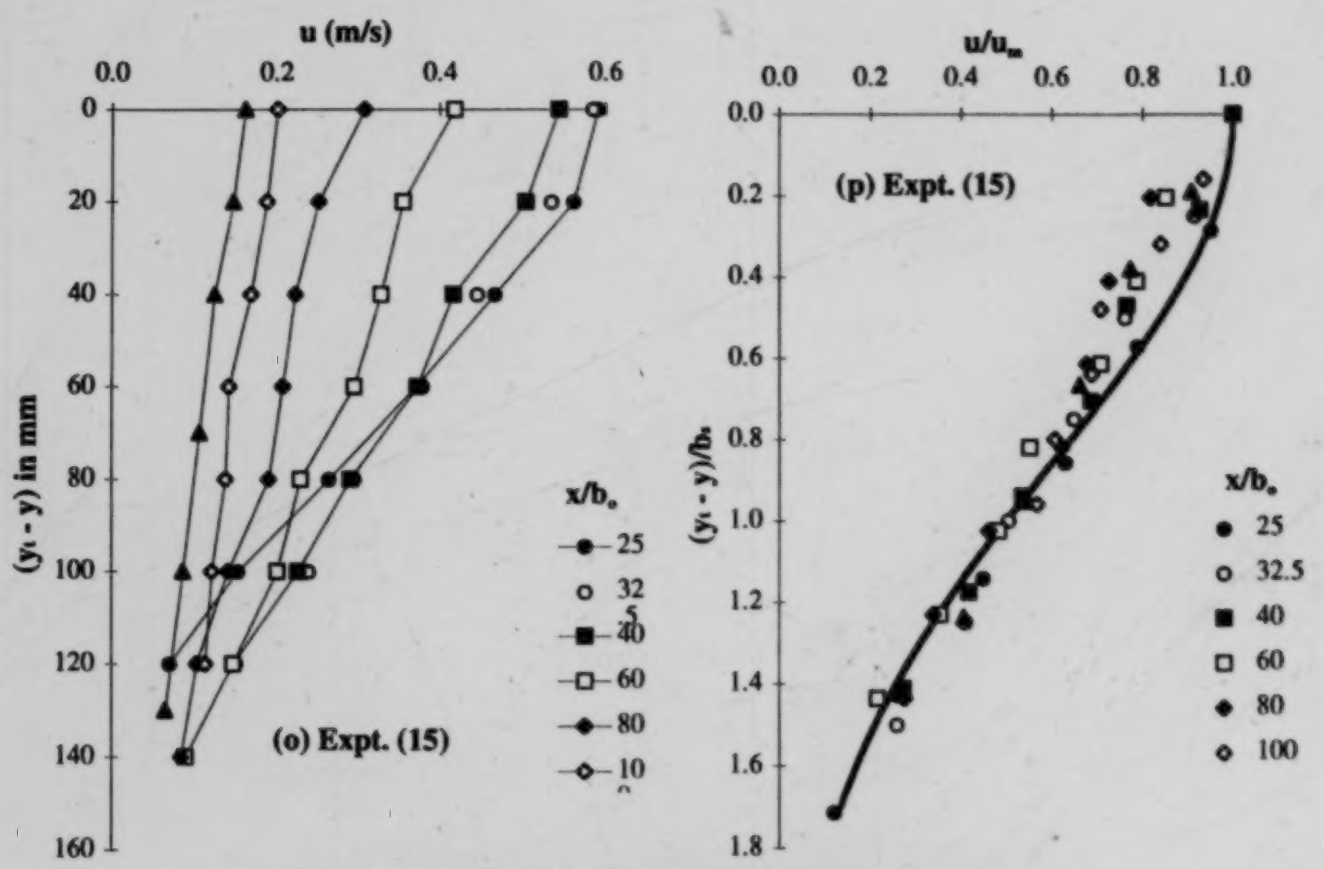

Fig. 4.24(o-p) Velocity distribution in surface jet (Expt. 15)
(o) Velocity profiles; and (p) Similarity profile

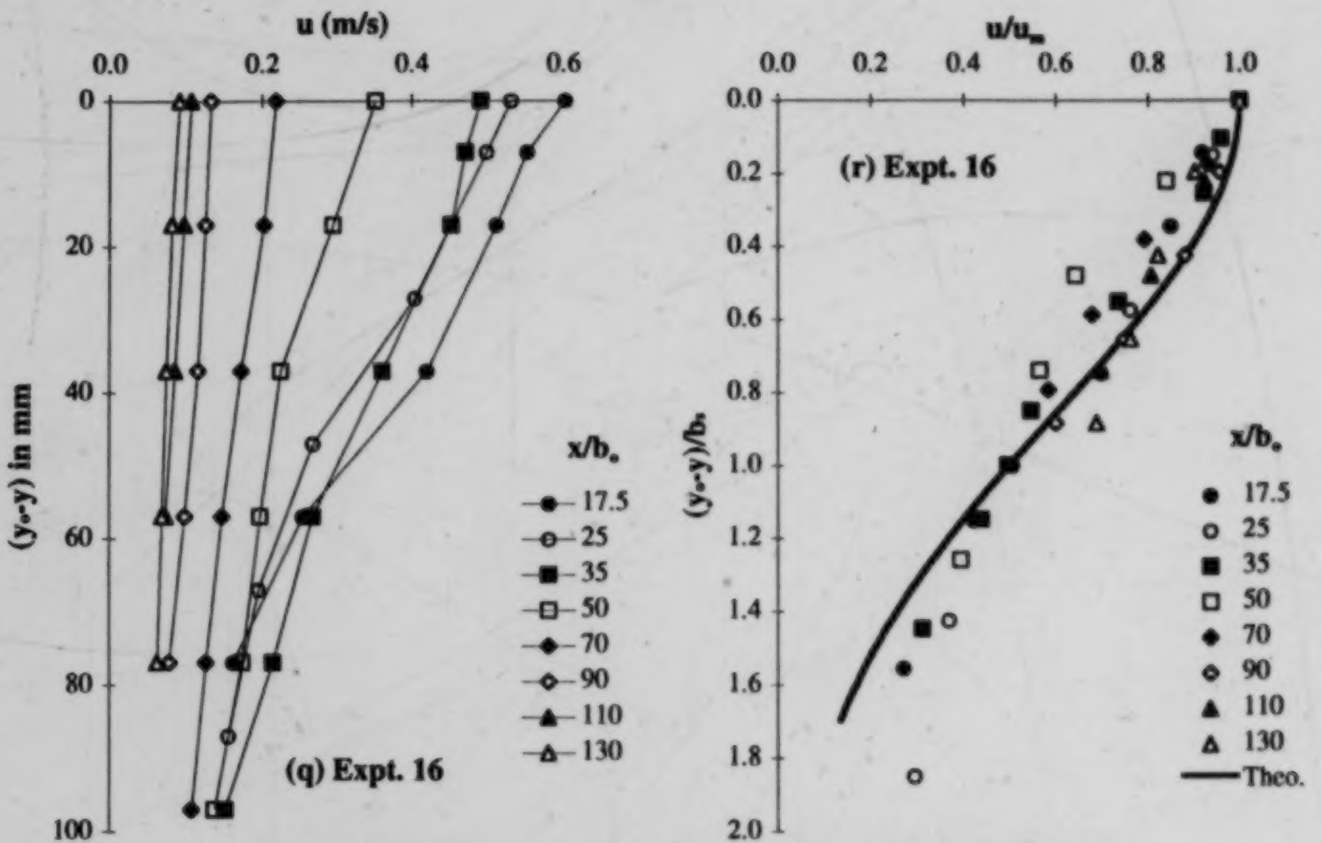

Fig. 4.24(q-r) Velocity distribution in surface jet (Expt. 16)
(q) Velocity profiles; and (r) Similarity profile

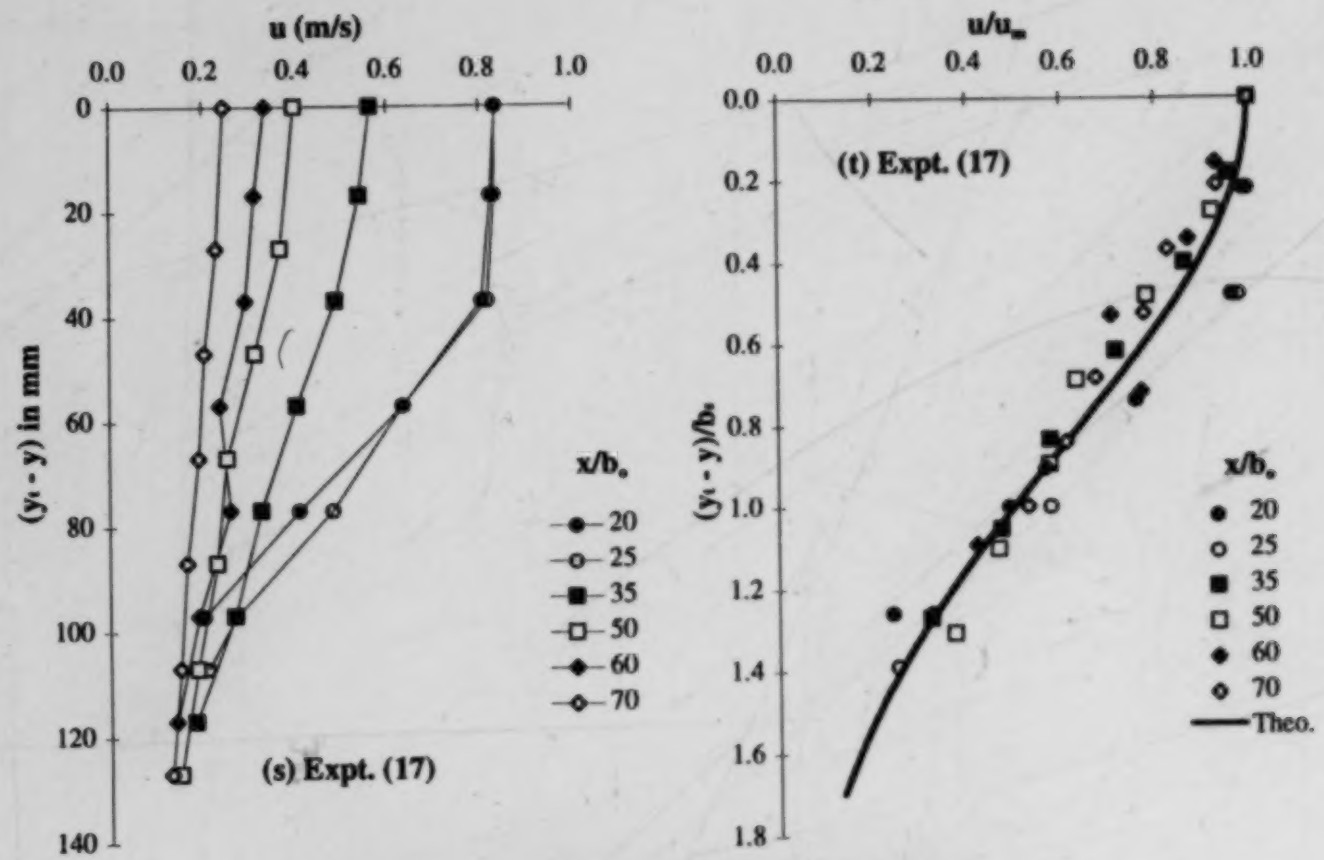

Fig. 4.24(s-t) Velocity distribution in surface jet (Expt. 17)
(s) Velocity profiles; and (t) Similarity profile

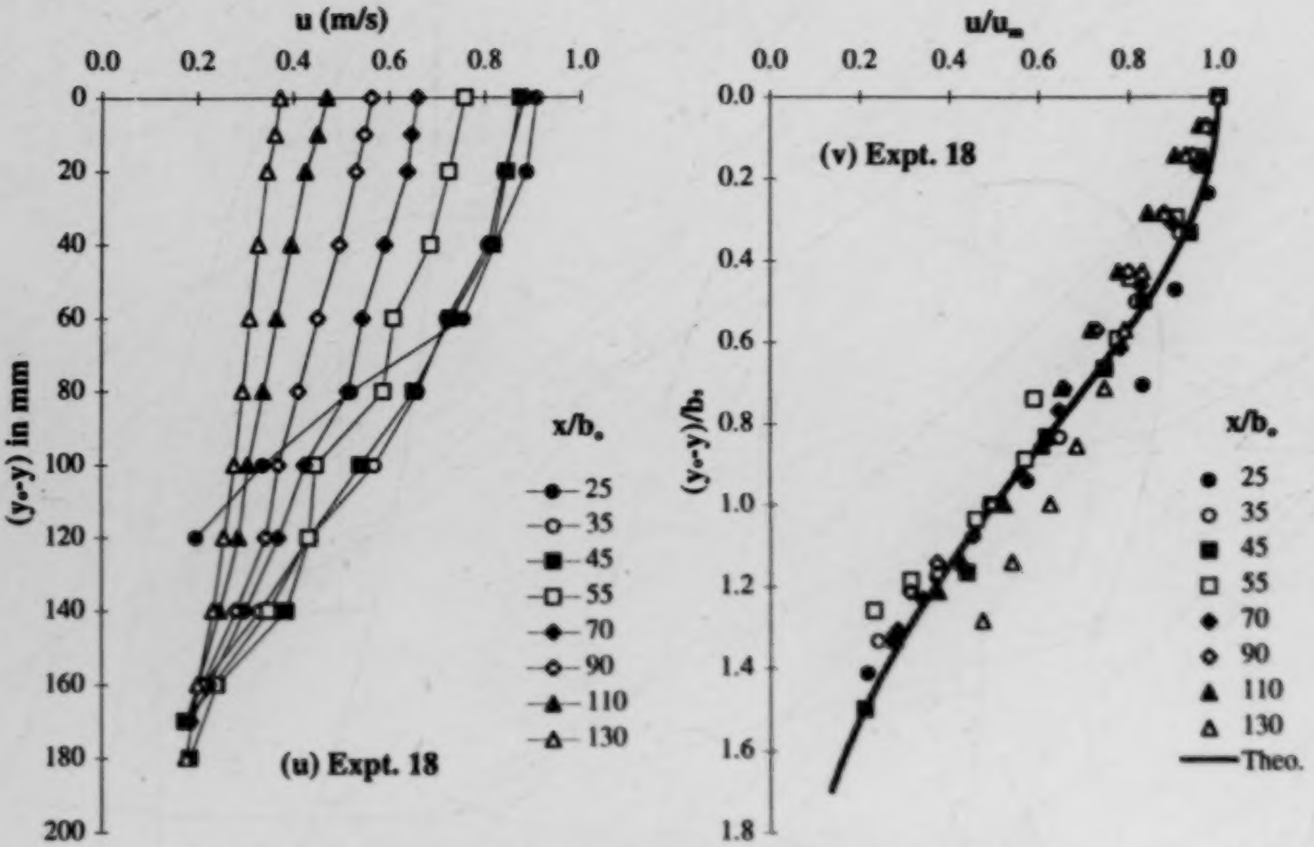

Fig. 4.24(u-v) Velocity distribution in surface jet (Expt. 18)
(u) Velocity profiles; and (v) Similarity profile

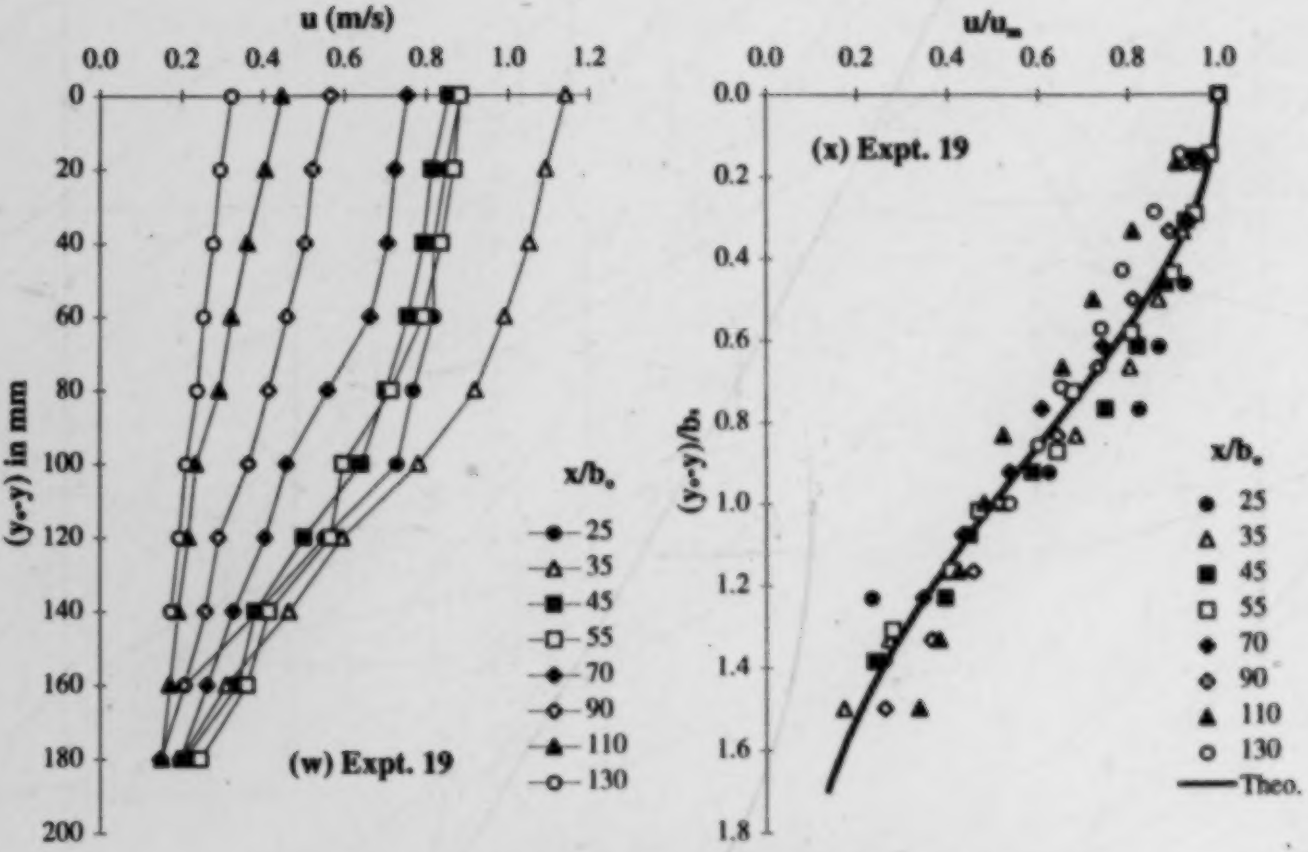

Fig. 4.24(w-x) Velocity distribution in surface jet (Expt. 19)
(w) Velocity profiles; and (x) Similarity profile

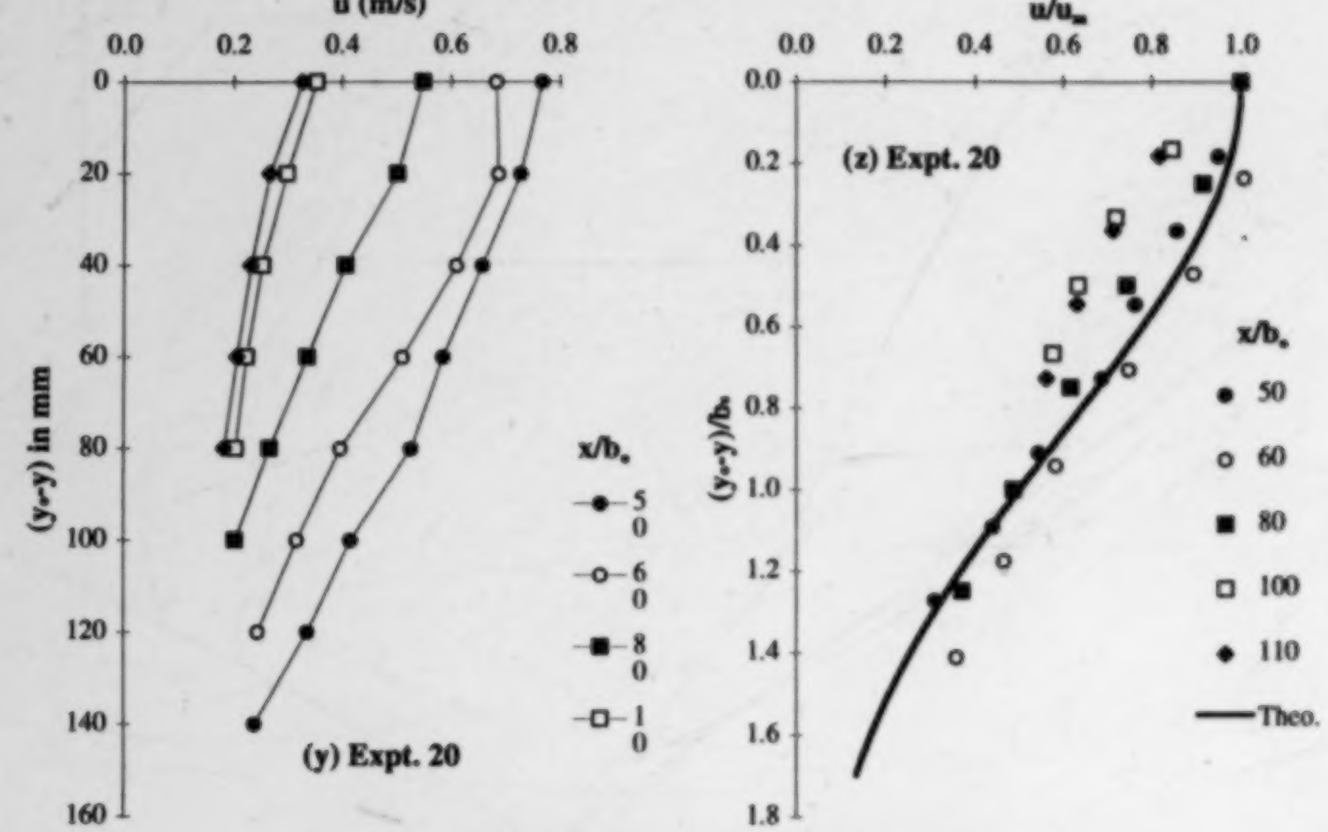

Fig. 4.24(y-z) Velocity distribution in surface jet (Expt. 20)
(y) Velocity profiles; and (z) Similarity profile

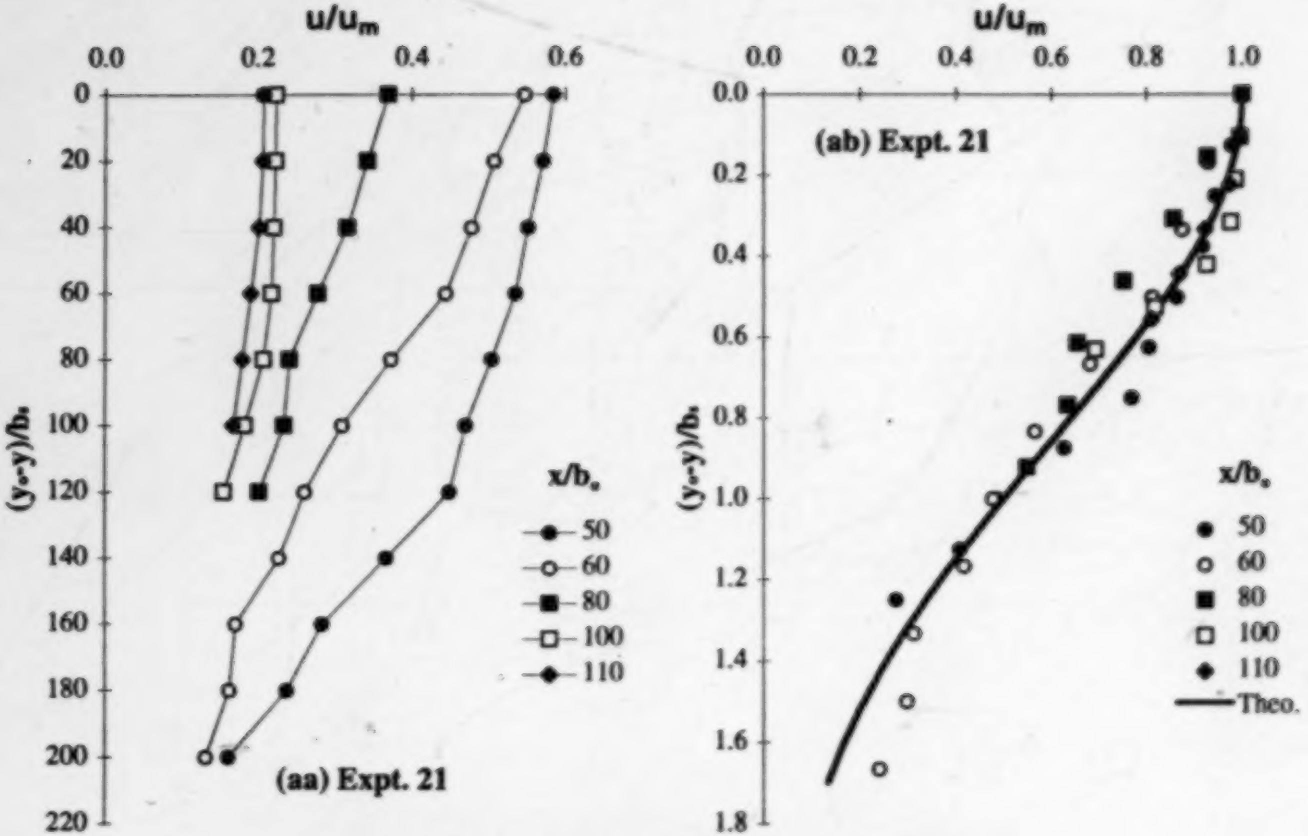

Fig. 4.24(aa-ab) Velocity distribution in surface jet (Expt. 21)
(aa) Velocity profiles; and (ab) Similarity profile

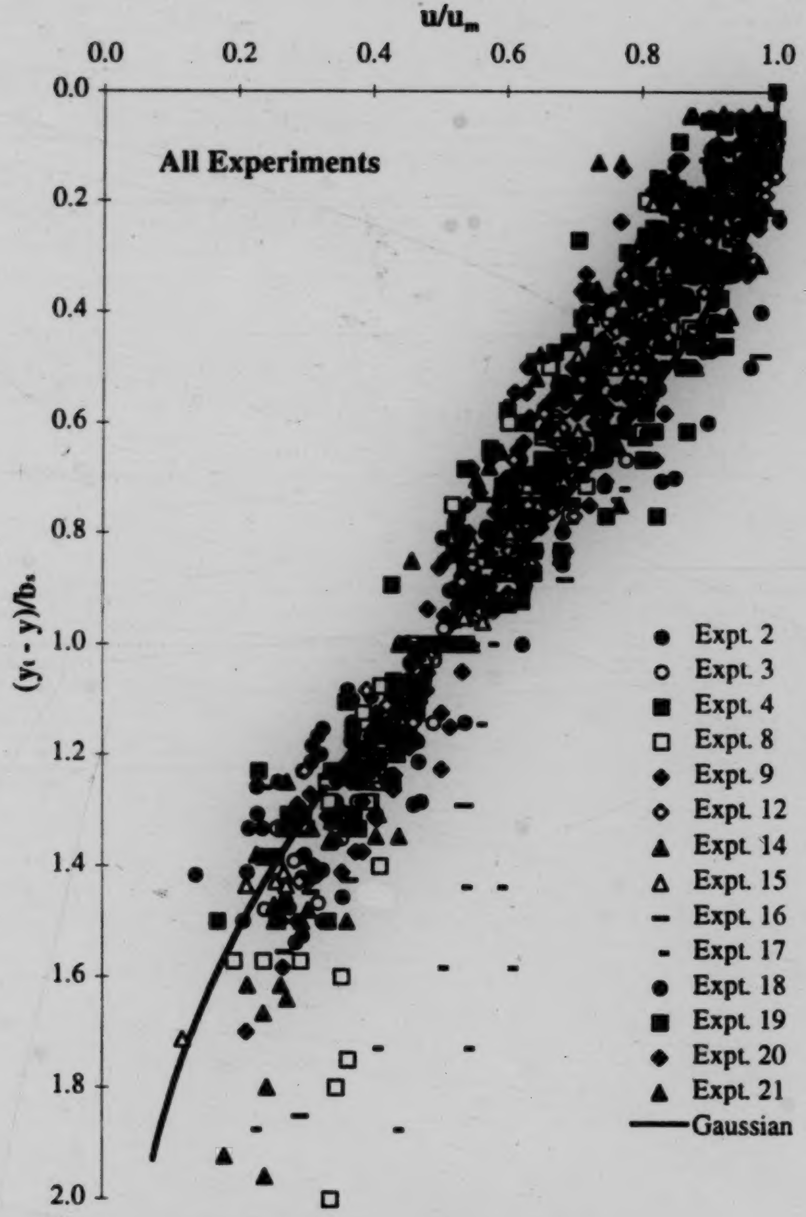

Fig. 4.25 Consolidated non-dimensional plot for the velocity distribution in the surface jet

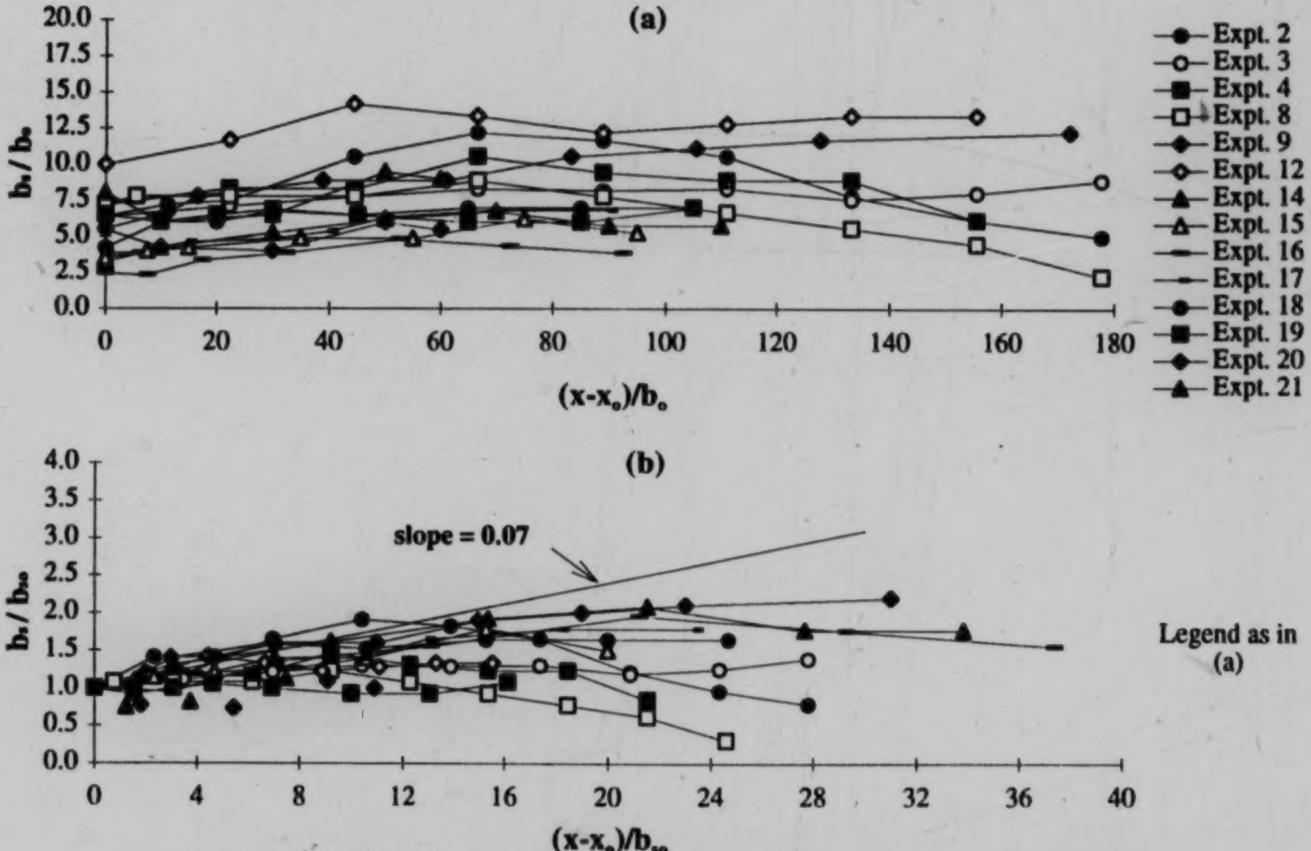

Fig. 4.26(a-b) Growth rate of the surface jet half-width: (a) b_o is the length scale; and (b) b_{so} is the length scale

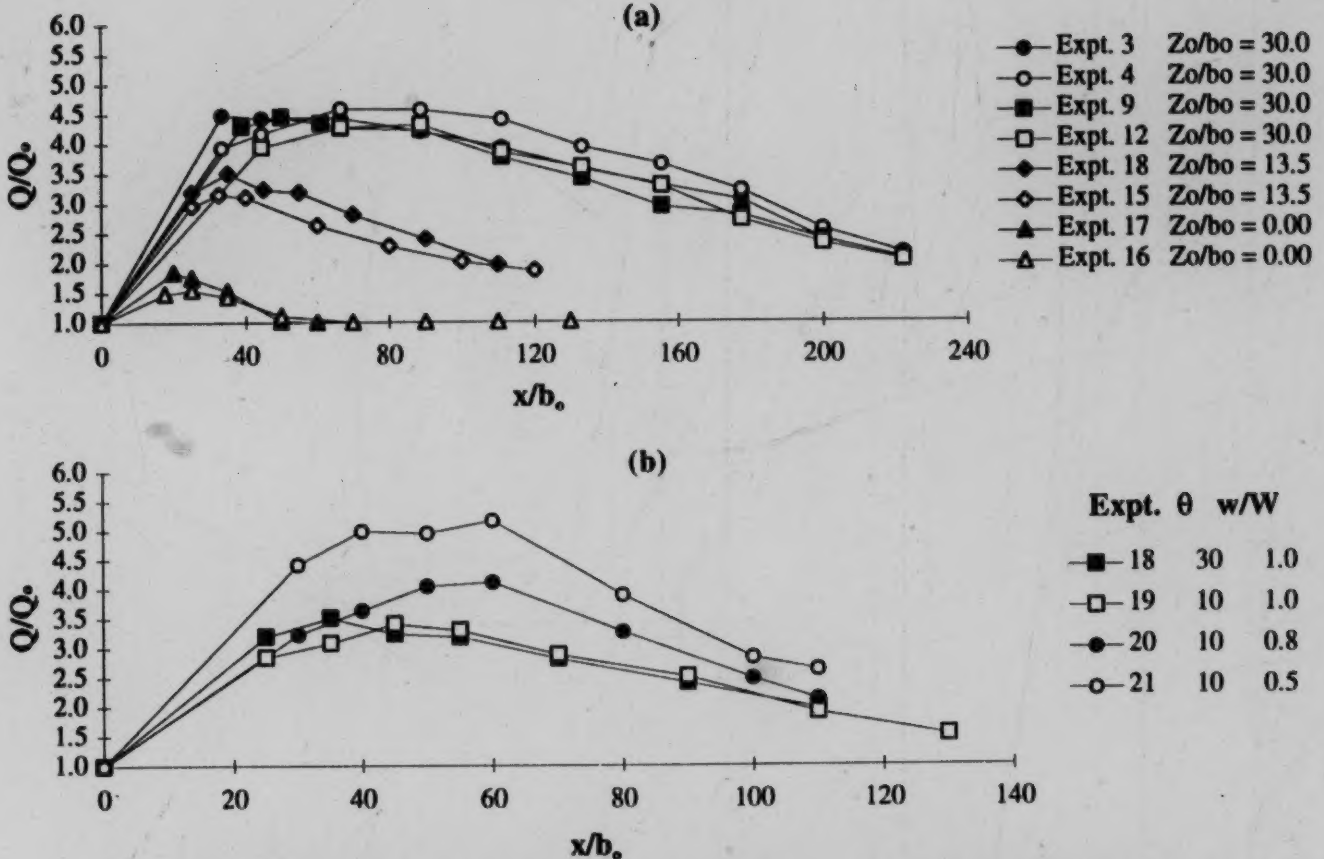

Fig. 4.27(a-b) Variation of the surface-jet discharge, Q/Q_o, with distance, x/b_o
(a) Effect of the offset ratio Z_o/b_o; & (b) Effect of the inclination angle θ and the width ratio w/W

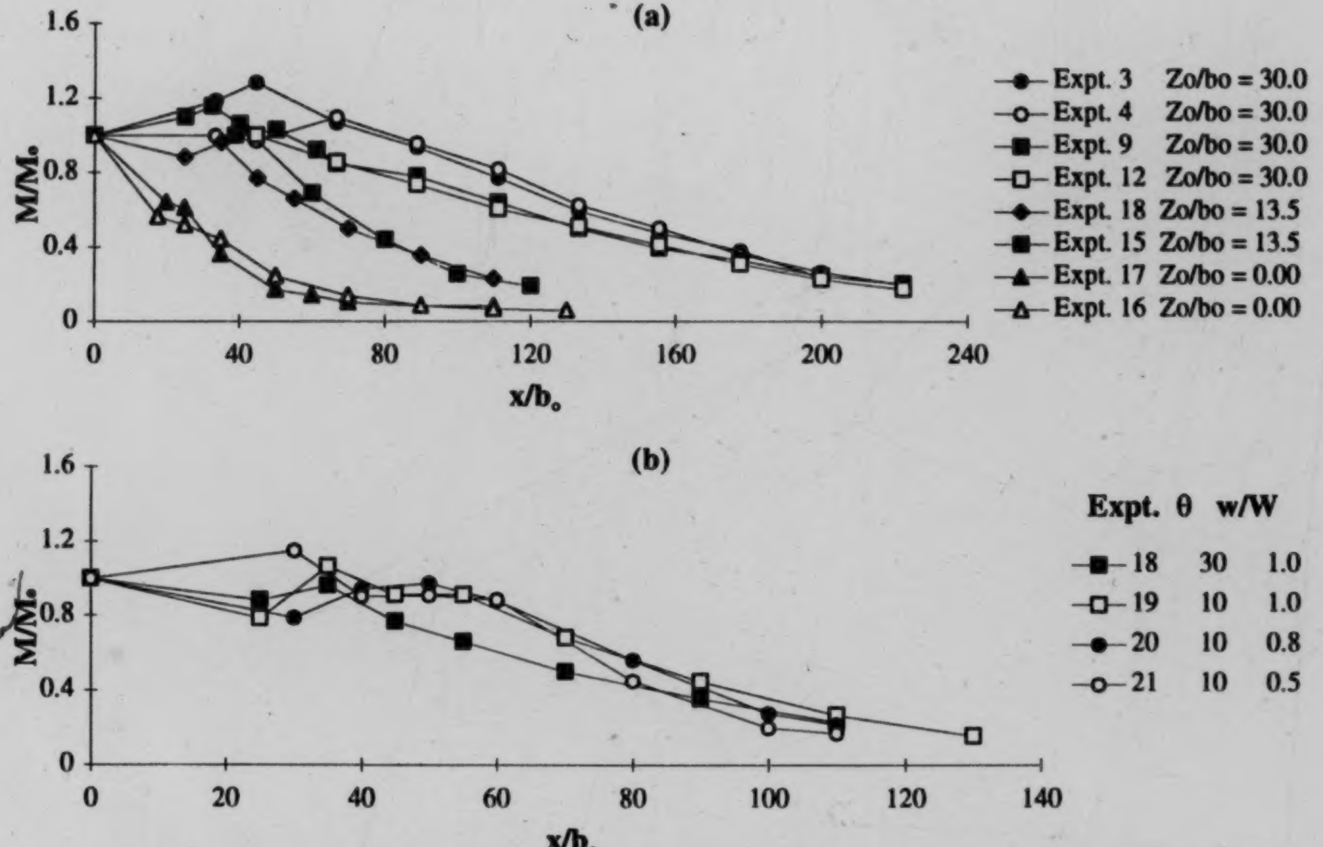

Fig. 4.28(a-b) Variation of the surface-jet momentum flux, M/M$_o$, with distance, x/b$_o$
(a) Effect of the offset ratio Z$_o$/b$_o$; & (b) Effect of the inclination angle θ and the width ratio w/W

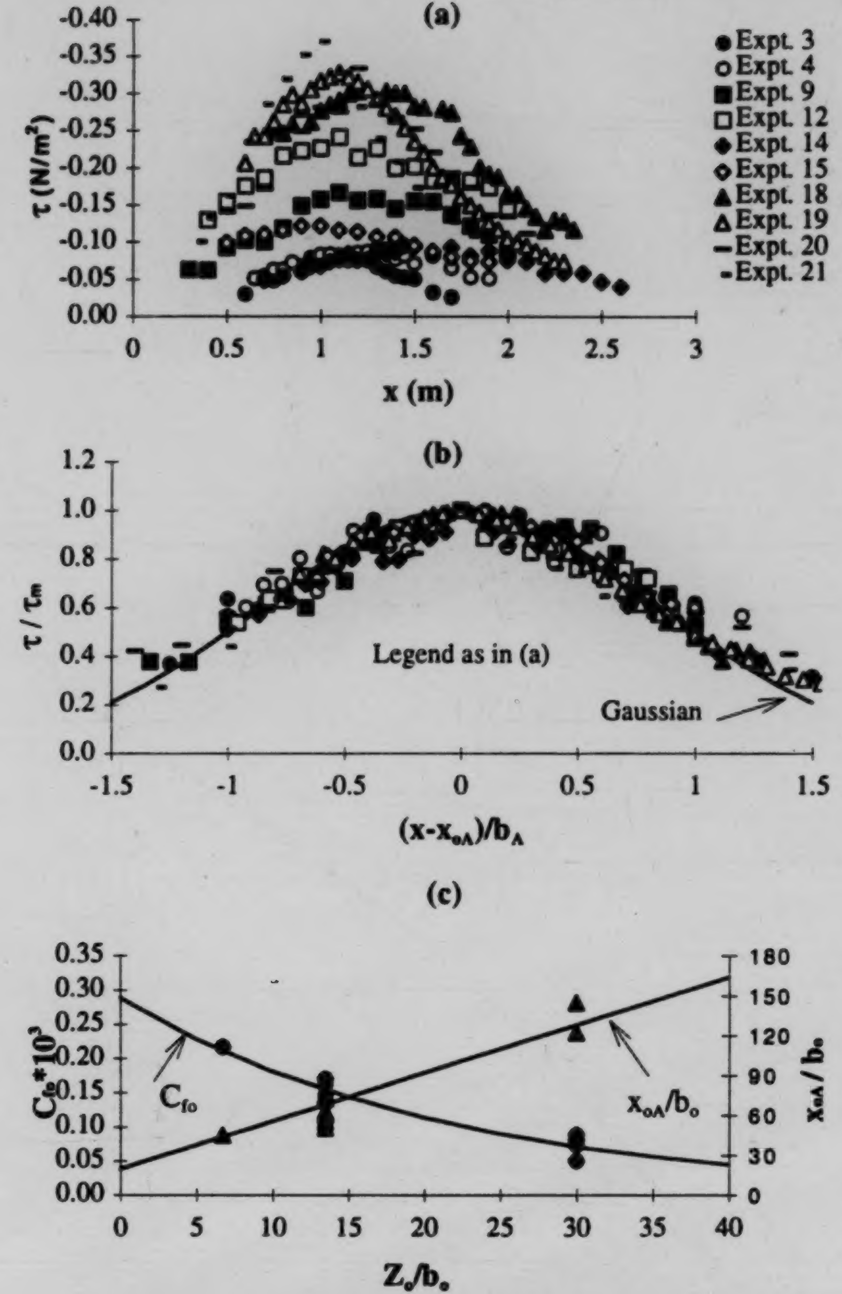

Fig. 4.29(a-c) Shear stress distribution for pattern A (a) Variation of shear stress with distance; (b) Similarity profile; and (c) study of shear stress and length scales

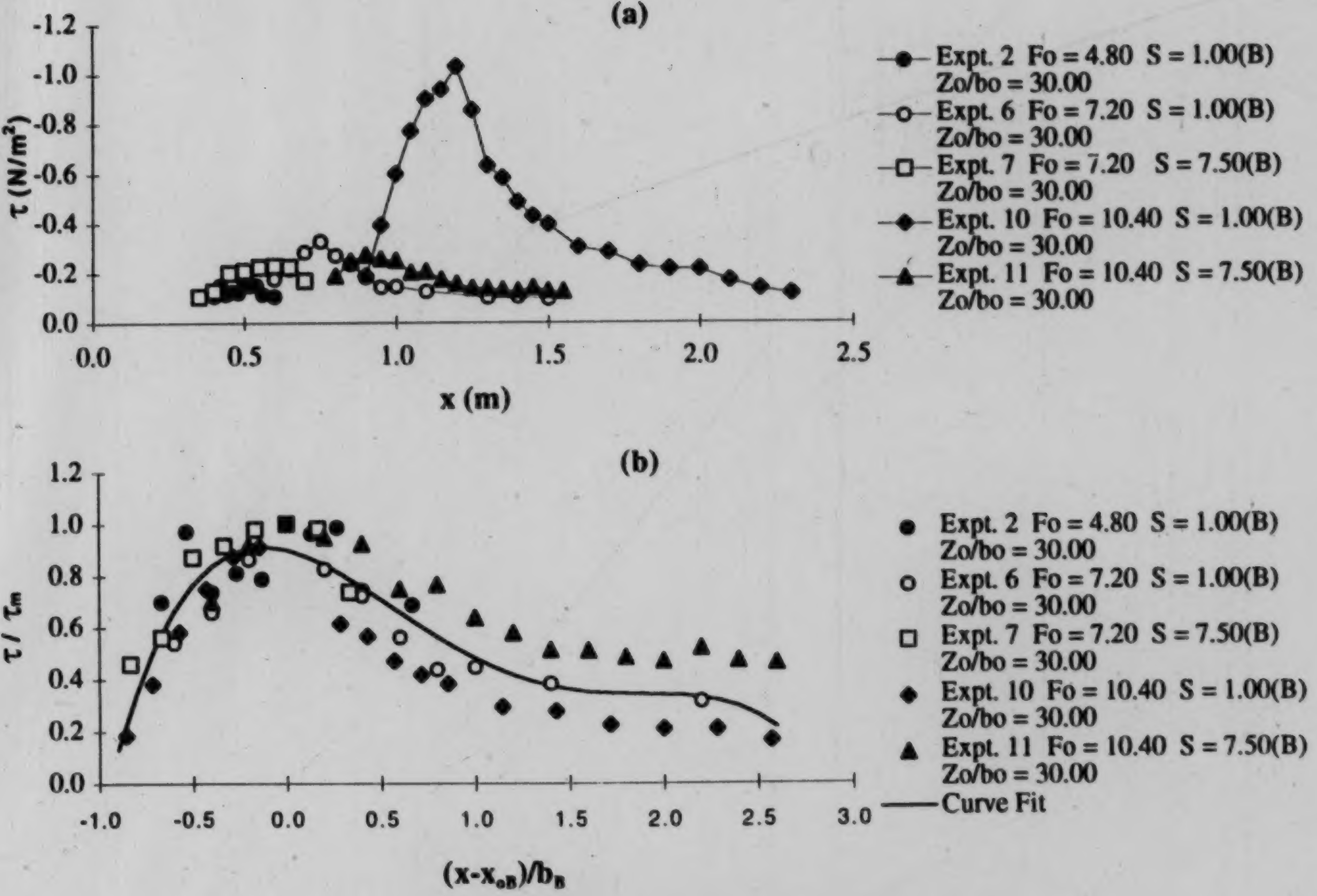

Fig. 4.30(a-b) Shear stress distribution for pattern B

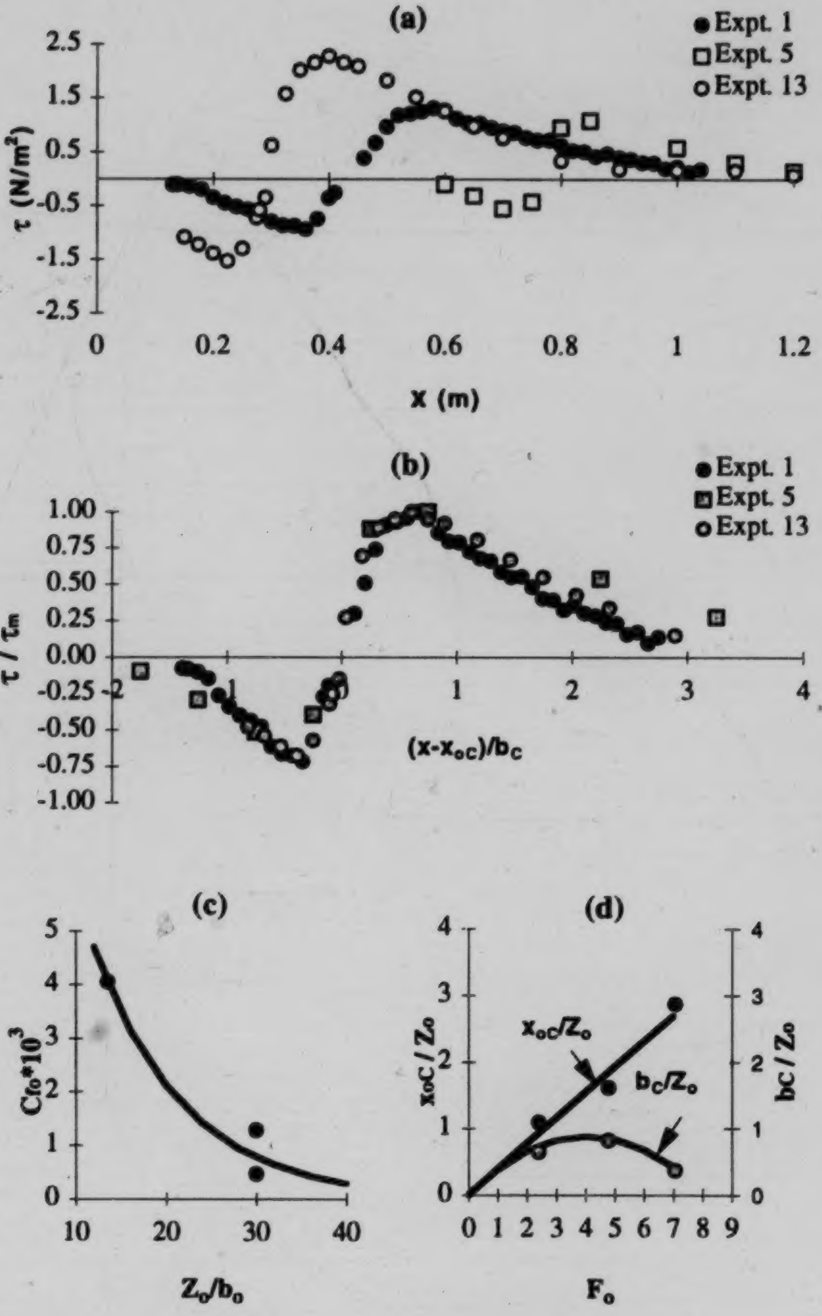

Fig. 4.31 (a-b) Shear stress distributions for Pattern C
(c-d) Study of shear stress and length scales for pattern C

Chapter 5

Plane Turbulent Surface Jets in Shallow Tailwater[*]

5.1 Introduction

For turbulent jets discharged from slots or orifices in walls into large ambients at rest, it has been generally assumed (Albertson et al. (1950), Schlichting (1960), Rajaratnam (1976)) that the momentum flux would be preserved. In some experimental investigations (Miller and Comings (1957); Goldschmidt and Eskinazi (1966); Heskestad (1965) and Kotsovinos (1975)), it has been noticed that the momentum flux decayed to some extent at large distances from the origin of the jets. Kotsovinos (1978) mentioned that the momentum flux could decay to about 80% of that at the source at a longitudinal distance equal to 100 b_o for plane turbulent jets where b_o is the slot width. Kotsovinos (1978) attributed this loss of momentum flux to the negative momentum carried by the entrained fluid which approached the jet at an angle of about $\pi/4$ radians from the forward direction of the jet. Based on an approximate integral analysis, Kotsovinos (1978) developed an equation to describe the variation of the momentum flux with the longitudinal distance from the nozzle producing the jet. Schneider (1985) attempted to explain this decay of momentum flux by combining the analysis of the jet with the flow in the region surrounding the jet. He coupled the jet and the induced outer flow through momentum and volume balances.

Swean Jr. et al. (1989) studied the variation of momentum and mass fluxes as well as the growth for plane turbulent surface jets with limited depth of tailwater. They conducted 10 experiments to study the effect of the finite depth of tailwater on the characteristics of the surface jet and to observe the variation of the momentum and volume fluxes and the breakdown of the surface jet due to the limited depth of the ambient. They also used the experimental results of Vanvari and Chu (1974) and Rajaratnam and Humphries (1984). Their results showed a momentum decay and a break down (or variation from that of jets in infinite ambient) in the velocity and length scales due to the jet confinement. The study of Swean Jr. et al. (1989) provides a general understanding of the problem of surface jets with a finite depth of tailwater. However, their analysis did not consider the adverse pressure gradient in the momentum balance. As the depth of flow increases gradually in the longitudinal direction, it is important to include the excess pressure due to this increasing depth.

---

[*] The main content of this chapter has been submitted to the Journal of Hydraulic Engineering of the American Society of Civil Engineers for possible publication.

This chapter presents the results of a theoretical and an experimental study of turbulent surface jets with finite depth of tailwater. It was conducted to investigate the nature of the jet growth, the decay of the maximum velocity, the variation of the momentum and volume fluxes in the forward flow region of the surface jet, and the effect of the depth of tailwater on these properties. With the double-leaf gate energy dissipator introduced in chapter 4, the jet velocity and the momentum flux were found to decay dramatically. To understand the reasons behind this decay, it was important to study the behavior of turbulent jets of simpler geometry in shallow tailwater. In this chapter, the plane turbulent surface jet was chosen for this purpose. The plane turbulent surface jet issued from the opening with the inclination angle and the submergence ratio equal to zero. Hence, the plane turbulent surface jet, presented in this chapter, is considered to be a special case of the inclined turbulent jet presented in chapter 4.

5.2 Theoretical Considerations

Assume a plane turbulent surface jet of thickness b_o with a flow rate per unit width of Q_o and momentum flux per unit width of M_o entering a rectangular channel horizontally at a height of Z_o above the bed of the channel as shown in Fig. 5.1(a). Let U_o be the velocity of the jet at the nozzle. The downstream control gate is adjusted so that the depth of flow at the nozzle is equal to (Z_o+b_o) and so that the surface jet enters the channel horizontally. My experimental observations (presented later) have shown that the water surface rises gradually as the distance x from the gate or nozzle increases, and that this increase is important for flows with finite depth of tailwater. Assume that δ_∞ is the maximum rise in the water surface elevation (see Fig. 5.1(a) and Fig. 5.2) and let δ_x be the corresponding rise at a section located at a longitudinal distance of x from the gate. The maximum value of δ_x would be δ_∞ which would occur at the section where the jet attaches to the bed. It appears that the longitudinal adverse pressure gradient is created to produce the return flow underneath the surface jet, for the jet entrainment.

Assuming hydrostatic pressure distributions on the wall containing the nozzle and at the downstream section where the expanding surface attaches to the bed, and that the velocity distribution at the nozzle and the downstream section is uniform (see Fig. 5.1(b)) and neglecting the integrated bed shear stress caused by the reverse flow, the continuity and the momentum equations could be written as

$$U_o b_o = V.\,(Z_o + b_o + \delta_\infty) \tag{5.1}$$

$$M_o - M_\infty = \gamma\delta_\infty (Z_o + b_o) + 0.5\gamma\delta_\infty{}^2 \tag{5.2}$$

where V and M_∞ are respectively the uniform velocity and the momentum flux at the downstream section, and M_o is the momentum flux at the nozzle.

Multiplying Eq. 5.1 by $\rho U_o V$ and rearranging, Eq. 5.1 is rewritten as

$$\frac{M_\infty}{M_o} = \frac{1}{(1 + Z_o/b_o + \delta_\infty/b_o)} = \frac{1}{(1+\eta)+\theta} \tag{5.3}$$

where η is the offset ratio equal to Z_o/b_o and $\theta = \delta_\infty/b_o$.

Dividing Eq. 5.2 by M_o and rearranging, Eq. 5.2 becomes

$$1-\frac{M_\infty}{M_o}=\frac{2\theta(1+\eta)+\theta^2}{2F_o^{\,2}} \tag{5.4}$$

Solving equations 5.3 and 5.4, we obtain a cubic equation in θ as

$$\theta^3+3(1+\eta)\theta^2+2\left[(1+\eta)^2-F_o^{\,2}\right]\theta-2\eta F_o^{\,2}=0 \tag{5.5}$$

Eq. 5.5 has three real roots, one is positive and the other two are negative. Since the experiments showed positive values for δ_∞ (see Fig. 5.2), the positive root of Eq. 5.5 was only considered as the relevant physical solution. However, the negative roots (that represent a depression in the water elevation) may be relevant for other problems. The positive root of Eq. 5.5 can be written as

$$\theta=\frac{2}{\sqrt{3}}\sqrt{(1+\eta)^2+2F_o^{\,2}}\,\cos(\phi/3)-(1+\eta) \tag{5.6}$$

The negative roots of Eq. 5.5 are

$$\theta=\frac{-1}{\sqrt{3}}\sqrt{(1+\eta)^2+2F_o^{\,2}}\,\left[\cos(\phi/3)+\sqrt{3}\,\sin(\phi/3)\right]-(1+\eta) \tag{5.7}$$

and,

$$\theta = \frac{-1}{\sqrt{3}}\sqrt{(1+\eta)^2 + 2F_o^{\,2}}\ \left[\cos(\phi/3) - \sqrt{3}\,\sin(\phi/3)\right] - (1+\eta) \qquad (5.8)$$

where ϕ is a function of η and the Froude number F_o at the nozzle equal to $[U_o/(gb_o)^{0.5}]$ and is described by the equation

$$\phi = \tan^{-1}\left(\sqrt{\frac{\left[(1+\eta)^2 + 2F_o^{\,2}\right]^3}{27F_o^{\,4}} - 1}\right) \qquad (5.9)$$

With the exception of relatively small values of η ($\eta<10$ as shown in Fig. 5.3), ϕ is equal to $\pi/2$. Using this value of ϕ, Eq. 5.6 reduces to

$$\theta = \sqrt{(1+\eta)^2 + 2F_o^{\,2}} - (1+\eta) \qquad (5.10)$$

Eq. 5.7 and Eq. 5.8 respectively reduce to

$$\theta = -\sqrt{(1+\eta)^2 + 2F_o^{\,2}} - (1+\eta) \qquad (5.11)$$

$$\theta = -(1+\eta) \qquad (5.12)$$

It was mentioned before that the positive root would only be considered as the relevant solution. Hence, to estimate θ for the different values of η and F_o, Eq. 5.10 was considered as the solution of Eq. 5.5.

Further, M_∞ can be evaluated by combining Eq. 5.3 and 5.10 as

$$\frac{M_\infty}{M_o} = \left((1+\eta)^2 + 2F_o^2\right)^{-1/2} \qquad (5.13)$$

It is interesting to note that substituting in Eq. 5.5 with $\eta = 0$, (the supercritical jet is on the bed), results in a quadratic equation. Solving this quadratic equation

$$\theta = 0.5\left(\sqrt{1+8F_o^2} - 3\right) \qquad (5.14)$$

which is closely related to the well-known Belanger equation. Eq. 5.5 could be simplified if the second term on the right hand side of Eq. 5.2 is neglected. For this assumption to be valid, δ_∞ should be small compared to (Z_o+b_o). With this simplification, Eq. 5.5 reduces to

$$(1+\eta)\theta^2 + \left[(1+\eta)^2 - F_o^2\right]\theta - \eta F_o^2 = 0 \qquad (5.15)$$

The positive root for this equation is

$$\theta = \frac{+\sqrt{\left[(1+\eta)^2 - F_o^2\right]^2 + 4\eta(1+\eta)F_o^2} - \left[(1+\eta)^2 - F_o^2\right]}{2(1+\eta)} \qquad (5.16)$$

Using Eq. 5.3 with Eq. 5.16, the momentum flux M_∞ becomes

$$\frac{M_\infty}{M_o} = \frac{1}{(1+\eta)+\theta} = \frac{-\sqrt{\left[(1+\eta)^2 - F_o^{\,2}\right]^2 + 4\eta(1+\eta)F_o^{\,2}} + \left[(1+\eta)^2 + F_o^{\,2}\right]}{2F_o^{\,2}} \qquad (5.17)$$

Let $F_{p\infty}$ be the maximum excess in the hydrostatic pressure force at the downstream section caused by the maximum increase of the depth of δ_∞ in the water surface elevation. Assuming that the decrease in the momentum flux is only due to $F_{p\infty}$, it can be shown that

$$\frac{F_{p\infty}}{M_o} = 1 - \frac{M_\infty}{M_o} = \frac{0.5\theta^2 + \theta(1+\eta)}{F_o^{\,2}} \qquad (5.18)$$

Equation (5.10) was solved along with equation (5.18) to evaluate $F_{p\infty}$. Again, by neglecting the term $(0.5\gamma\delta_\infty^{\,2})$ in equation (5.2), a simpler relation for $F_{p\infty}$ could be obtained as follows

$$\frac{F_{p\infty}}{M_o} = 1 - \frac{M_\infty}{M_o} = \frac{\theta(1+\eta)}{F_o^{\,2}} = \frac{\sqrt{\left[(1+\eta)^2 - F_o^{\,2}\right]^2 + 4\eta(1+\eta)F_o^{\,2}} - \left[(1+\eta)^2 - F_o^{\,2}\right]}{2F_o^{\,2}} \qquad (5.19)$$

Based on these theoretical formulations, the variation of θ, which is equal to the maximum rise in the water surface elevation in terms of the slot width, with the offset ratio η, is shown in Fig. 5.4 as solutions of Eq. 5.10 and 5.16, with and without considering the term $(0.5\gamma\delta_\infty^{\,2})$, respectively. Fig. 5.4 shows the variation for the jet Froude number F_o from 1.6 to 7.2 and it may be observed that both equations give almost the same value for θ if the offset ratio exceeds a certain value. This value of η

was found to increase with the Froude number and is equal to 20 for $F_o = 7.2$ and falls to about 5 for $F_o = 1.6$. For any given Froude number, θ decreases as the offset ratio increases. For the offset ratio equal to 100, θ decreases from about 0.5 for $F_o = 7.2$ to almost zero for $F_o = 1.6$.

Eq. 5.13 and Eq. 5.17 were plotted in Fig. 5.5 to show the variation of the dimensionless momentum flux with the offset ratio η for the different Froude numbers. Fig. 5.5 shows that both equations exhibit the same momentum decay for offset ratios equal to or greater than 25. Further, F_o appears to have no effect on the momentum decay for η greater than about 25. Fig 5.4 also shows that the momentum flux in terms of that at the nozzle, is equal to 0.040, 0.020, 0.013 and 0.010 respectively for η equal to 25, 50, 75 and 100. Eq. 5.18 is plotted in Fig. 5.6 to show the variation of $F_{p\infty}/M_o$ with η. For the offset ratio equal to 25, 50, 75 and 100, $F_{p\infty}/M_o$ is equal to 0.960, 0.980, 0.987 and 0.990 respectively.

5.3 Dimensional Analysis

Considering the problem illustrated in Fig. 5.1(a), any property (m) of the flow can be expressed as a function of various parameters of the flow, fluid and channel dimensions as

$$m = f(U_o, g, b_o, Z_o, \rho, \mu) \qquad (5.20)$$

The above relation can be represented in a dimensionless form as follows

$$M = f'\left[\frac{U_o}{\sqrt{g b_o}}, \frac{\rho U_o b_o}{\mu}, \frac{Z_o}{b_o}\right] \qquad (5.21)$$

The above relation shows that any property of the flow can be expressed as a function of the Froude number, the Reynolds number and the offset ratio. For large values of the Reynolds number, $R = \rho U_o b_o/\mu$, where ρ and μ are, respectively, the mass density and viscosity of the fluid, viscosity is known to have negligible effects. Hence, Eq. 5.21 becomes

$$M = f^{*}[F_o, \eta] \tag{5.22}$$

Eq. 5.22 shows that the main variables affecting the different characteristics of the flow are the Froude number and the offset ratio.

5.4 Experimental Study

5.4.1 Experimental arrangement

Surface jets were produced in a flume, 0.446 m wide, 0.60 m deep and 7.6 m long, with aluminum bottom and Plexiglas sides (see Fig. 5.7). Two pumps were used to supply the head-tank feeding the flume. The discharge was measured by a magnetic flow-meter located in the supply line. Water entered the flume through an opening between two aluminum gates, provided with streamlined entrances thereby producing an uniform jet with a thickness of b_o (see Fig. 5.8). A tailgate was used to control the tailwater depth in the flume. In all the experiments the tailgate was adjusted so that the jet issued from the slot horizontally. False floors of different heights were used to produce the required offset distance Z_o (see Fig. 5.9).

A Prandtl tube with an external diameter of 3.0 mm was used to measure the time-averaged longitudinal velocity u (see Fig. 5.8 & Fig. 5.10). Velocity distributions of the forward and backward flows were measured along vertical sections at different longitudinal distances from the nozzle producing the jet. Velocity measurements were also made, when needed, downstream of the line of the jet attachment to the bed. All the measurements were taken in the middle third of the flume.

One transducer (Validyne model DP45-16 Northridge, Calif) was used in the experiments to measure the pressure difference indicated by the Prandtl tube. The output of the transducer was connected to a Macintosh IIfx computer. When the pressure difference was outside the transducer range (±25.4 mm), the pressure connections were switched to a manometer board (see Fig. 5.10). The computer displayed the results on a strip chart on the screen in real time. When the required number of samples (usually 5000) were recorded at each point with a sampling rate of 40 samples/s, the computer processed all the samples to obtain the mean value and the standard deviation for each variable and saved the results in an open file. The computer programs used in the experiments were written in LabView Language.

5.4.2 Experiments

A total of 9 experiments were conducted and the primary details of these experiments are shown in Table 5.1. The values of the various parameters (b_o, Z_o, U_o) were selected to achieve a wide range of the offset ratio and the Froude number. Seven offset ratios of 5, 10, 20, 25, 30, 50 and 100 were used. Experiments were conducted for Froude numbers equal to 1.60, 2.40, 2.90, 4.00, 4.80, 6.00 and 7.20. The Reynolds number of the jet was in the range of 5000 to 43000. Fig. 5.11(a-d) show the surface jets produced with the offset ratio equal to 100, 50, 25 and 10 respectively.

5.5 Experimental Results and Analysis

5.5.1 Eddy length

As soon as the jet issues from the slot, a recirculating flow region starts to develop between the jet and the flume bed (see Fig. 1(b)). The normalized eddy length L_e/b_o was equal to 50, 80, 140, 160, 200, 320 and 640 for offset ratios Z_o/b_o equal to

5, 10, 20, 25, 30, 50, 100 respectively. The eddy lengths were predicted either from the typical velocity profiles shown in Fig. 5.12 or by using dye injection. Dye injection was used where velocity measurements could not be taken near the bed as in experiments 2, 4 and 6.

If L_e is the length of the recirculating region (or the eddy length), it could be written that

$$L_e = f[U_o, b_o, \rho, \mu, Z_o] \tag{5.23}$$

Using the π theorem, it can be shown that

$$\frac{L_e}{b_o} = f'\left[\frac{Z_o}{b_o}, \frac{\rho U_o b_o}{\mu}\right] \tag{5.24}$$

For large values of the Reynolds number, viscous effects may be neglected and Eq. 5.24 reduces to

$$\frac{L_e}{b_o} = f''\left[\frac{Z_o}{b_o}\right] \tag{5.25}$$

The experimental results are shown plotted in Fig. 5.13 with L_e/b_o versus Z_o/b_o. Fig. 5.13 shows a linear relationship between the eddy length L_e and the offset distance Z_o. The best-fit linear equation shows that L_e is 6.50 times Z_o. Rajaratnam (1969) found this constant to be about 7.50.

5.5.2 Velocity profiles

Time-averaged velocity profiles were obtained for the whole flow field including the surface jet and the recirculating flow regions for several experiments. Fig. 5.12(a-i) show velocity profiles for Expt. 1 to Expt. 9 respectively and the details of these experiments are included in table 5.1. These observations were taken for seven Froude numbers (F_o = 1.60, 2.40, 2.90, 4.00, 4.80, 6.00 and 7.20 and seven offset ratios (Z_o/b_o = 5, 10, 20, 25, 30, 50 and 100). These figures show the velocity profiles for the surface jet as well as the reverse flow. Intensive velocity measurements were taken especially in the surface jet zone for the precise calculation of the volume and the momentum fluxes. In the surface jet, the maximum velocity is located at, or very close to the free surface and the velocity distribution seems to be linear. The velocity distribution of the return flow is almost uniform except near the bed and at the jet edges. Velocity measurements could not be obtained in the strong shear layer separating the forward and the backward flows because the flow within this layer was very turbulent. In this layer the velocity fluctuations were larger than the local mean velocity. Hence, mean velocities within this layer were predicted by linear interpolation.

5.5.3 Reverse flow

It is believed that the reverse flow underneath the surface jet is driven by the adverse pressure gradient (see Fig. 5.2). This reverse flow is the source of the entrained fluid required for the expansion of the surface jet. It may be observed from Fig. 5.12(a-i) that the mean velocity in the reverse flow below the surface jet is almost uniform except near the bed and at the jet edges. Fig. 5.14(a) shows the variation of the depth-averaged reverse-velocity in terms of the velocity at the opening u_r/U_o with the dimensionless longitudinal distance from the opening x/b_o for the different Froude numbers and offset ratios. Experiments 2, 3 and 4 were conducted for the same offset ratio and for three different Froude numbers (2.40, 4.80 and 7.20 respectively). The variation of the reverse-velocity was almost identical in the three experiments indicating that the dimensionless reverse velocity does not depend on the Froude number. The observations shown in Fig. 5.14(a) indicate that this variation depends only on the offset ratio. The maximum value of the reverse-velocity, u_{rm}, decreases as the offset ratio increases as shown in Fig. 5.14(b) and is described by the equation

$$\left(\frac{u_{rm}}{U_o}\right) = 11 * 10^{-4}\left[\left(\frac{Z_o}{b_o}\right) - 175\right] \quad (r^2 = 0.95) \tag{5.26}$$

If x_{rm} is the value of x where u_{rm} occurs, x_{rm}/b_o was found to increase with the offset ratio as shown in Fig. 5.14(c) and this variation is described by the equation

$$\left(\frac{x_{rm}}{b_o}\right) = 2.65\left[\left(\frac{Z_o}{b_o}\right) + 7.65\right] \quad (r^2 = 0.99) \tag{5.27}$$

These equations show that for offset ratios equal to 5 and 100, the normalized maximum reverse velocity is 0.19 and 0.08, respectively, and the normalized locations of these values are about 33.50 and 285.25, respectively.

5.5.4 Surface jet

The velocity measurements in the surface-jet zone shows that the maximum velocity u_m occurs at or very near the free surface. To test for the similarity of the forward-flow velocity distributions, the maximum velocity, u_m, at any station was chosen as the velocity scale. The length scale, b, is the distance between the point of u_m and that of $0.5u_m$. Fig. 5.15(a-b) show the velocity distributions and the similarity profiles in the partially-developed flow region. In this figure, u/u_m was plotted against

$(y_o-y)/b$ where y_o is the depth of flow at any station and y is the height, above the flume bed, of the point under consideration. This plot represents a station located approximately in the middle of the developing region (at $x/b_o = 6$). Within the potential core, the flow is uniform whereas outside the potential core the distribution of the velocity is almost linear.

The velocity distributions and the similarity profiles in the fully-developed flow region ($x/b_o \geq 12$) are shown in Fig. 5.16(a-r). These figures represent Expt. 1 to Expt. 9 respectively. The plots shown in each figure are for different longitudinal distances from the slot. Fig. 5.17 shows a consolidated non-dimensional plot of all the experiments. A study of these profiles established that the velocity distributions are similar. The similarity profile is almost linear. This linear velocity distribution has been observed earlier by Wu and Rajaratnam (1995) and can also be observed in the results of Swean Jr et al. (1989). There is some scatter in the data near the bottom of the forward flow region and this could be due to the interaction with the backward flow and the resulting turbulence.

5.5.5 Velocity and length scales

Having found that the velocity profiles in the forward flow are similar, it is necessary to study the variation of the velocity scale, u_m, and the length scale, b, with the distance x. Fig. 5.18(a) shows the decay of the maximum velocity with the longitudinal distance from the nozzle. The maximum velocity at the nozzle was varied from 0.5 to 2.25 m/s and u_m was measured for x up to about 3.20 m. At the last section, the maximum velocity was in the range of 0.04-0.35 m/s. Fig. 5.18(b) shows the decay of the maximum velocity u_m at any section in terms of the velocity of the jet at the nozzle U_o with the normalized distance from the gate x/b_o. The decay of the maximum velocity shows the existence of two stages. The first stage represents the plane surface jet with large depth of tailwater and starts at the end of the development region. The decay of the normalized velocity scale in this region can be described by the following equation

$$\frac{u_m}{U_o} = \frac{4.20}{\sqrt{x/b_o}} \tag{5.28}$$

The second stage of the velocity decay starts at a distance x_o from the gate, where the observations begin to deviate from the curve describing Eq. 5.28 and the maximum velocity decays more rapidly. This behavior can be noticed more easily in Fig. 5.18(c) which shows the variation of $(U_o/u_m)^2$ with x/b_o where Eq. 5.28 would plot as a straight line. The decay of the maximum velocity in this stage can be described by the following quadratic equation

$$\frac{u_m}{U_o} = A\left(\frac{x}{b_o}\right)^2 + B\left(\frac{x}{b_o}\right) + C \tag{5.29}$$

where the coefficients A, B are C are functions of the offset ratio, Z_o/b_o as

$$A = 0.006\left(\frac{Z_o}{b_o}\right)^{-1.94} \qquad (r^2 = 0.95) \tag{5.30}$$

$$B = -0.258\left(\frac{Z_o}{b_o}\right)^{-1.14} \qquad (r^2 = 0.95) \tag{5.31}$$

$$C = 2.964\left(\frac{Z_o}{b_o}\right)^{-0.37} \qquad (r^2 = 0.86) \tag{5.32}$$

The value of x_o, was also found to be a function of the offset ratio (see Fig. 5.18(d)) and is described by the equation

$$\left(\frac{x_o}{b_o}\right) = -0.02\left(\frac{Z_o}{b_o}\right)^2 + 4.00\left(\frac{Z_o}{b_o}\right) + 6.25 \quad (r^2 = 0.99) \qquad (5.33)$$

These considerations show that as the tailwater depth decreases, the length of the first stage of decay decreases and the maximum-velocity decay will be more rapid. It was also found that the Froude number does not have any significant effect on the velocity decay.

A breakdown in the growth of the length scale, b, occurred in all the 9 experiments, as shown in Fig. 5.19. The location of this breakdown, where the rate of growth begins to deviate from the linear growth rate of surface jets on deep tailwater, was very close to the location where the corresponding breakdown occurred in the velocity scale variation and can also be described by Eq. 5.33. The original growth rate of the jet half-width was 0.065 which is somewhat smaller than the value of 0.070 found by Rajaratnam and Humphries (1984). After the breakdown, the jet half-width grew at a rate which varied from 0.007 to 0.033.

5.5.6 Surface-jet discharge

For every experiment, at each section where velocity observations were made, the forward flow rate Q and the momentum flux M per unit width were calculated as the sum of the fluxes through thin strips (whose thickness varied from 2.5 to 20 mm). If the upper and the lower ordinates of a single strip are u_1 and u_2 respectively, the discharge and the momentum fluxes per unit width through this strip were calculated using the following relations

$$Q_s = \frac{1}{2}(u_1 + u_2).h_s \tag{5.34}$$

$$M_s = \left[\frac{1}{3}(u_1 - u_2)^2 + u_1 u_2\right].h_s \tag{5.35}$$

where Q_s, M_s and h_s are the discharge, the momentum and the height of the strip respectively.

Fig. 5.20(a) shows the variation of the relative discharge Q/Q_o in the surface jet with distance x/b_o and a number of interesting observations could be made from a study of Fig. 5.20(a). Firstly, the relative discharge increases with the relative distance at the same rate as that of the surface jet with large tailwater up to a certain section and then deviates from it, to reach eventually the value of one. Secondly, the maximum value of the relative discharge decreases from about 4 for $Z_o/b_o = 100$ to 1.5 for $Z_o/b_o = 5$. If x_{Qm}, is the longitudinal distance where the relative discharge reaches the maximum value, x_{Qm}/b_o decreases from about 200 for $Z_o/b_o = 100$ to about 20 for $Z_o/b_o = 5$. The variation of Q/Q_o with x/b_o is not dependent on the Froude number and could be represented by a cubic equation of the form

$$\frac{Q}{Q_o} = A'\left(\frac{x}{b_o}\right)^3 + B'\left(\frac{x}{b_o}\right)^2 + C'\left(\frac{x}{b_o}\right) + 1 \tag{5.36}$$

where the coefficients A', B' and C' are functions of the offset ratio, Z_o/b_o as follows

$$A' = 0.0003\left(\frac{Z_o}{b_o}\right)^{-1.85} \quad (r^2 = 0.98) \tag{5.37}$$

$$B' = -0.009\left(\frac{Z_o}{b_o}\right)^{-1.00} \quad (r^2 = 0.99) \tag{5.38}$$

$$C' = 0.07\left(\frac{Z_o}{b_o}\right)^{-0.18} \quad (r^2 = 0.95) \tag{5.39}$$

For a surface jet with very large value of Z_o/b_o, the variation of Q/Q_o with x/b_o should be independent of the offset ratio and for such a jet, Q/Q_o = constant.$(x/b_o)^{0.50}$. This equation is shown plotted in Fig. 5.20(a) with the value of the constant chosen as 0.35.

Fig. 5.20(b-c) show the variation of the maximum value of the relative flow Q_m/Q_o and the distance where this occurs x_{Qm}/b_o with the offset ratio Z_o/b_o and these variations could be described by the equations

$$\frac{Q_m}{Q_o} = -3.4*10^{-4}\left(\frac{Z_o}{b_o}\right)^2 + 0.064\left(\frac{Z_o}{b_o}\right) + 1.00 \quad (r^2 = 0.97) \tag{5.40}$$

$$\frac{x_{Qm}}{b_o} = -9.2*10^{-3}\left(\frac{Z_o}{b_o}\right)^2 + 2.914\left(\frac{Z_o}{b_o}\right) \quad (r^2 = 0.99) \tag{5.41}$$

5.5.7 Surface-jet momentum flux

It was mentioned earlier that the surface jet loses a substantial portion of the momentum flux as it travels downstream when the depth of tailwater is relatively shallow. Fig. 5.21 shows the variation of the normalized momentum flux of the surface jet with the normalized distance from the nozzle for different offset ratios. A relatively simple function was found to describe this variation and is written as

$$\frac{M}{M_o} = \cos\left[\left(\frac{\pi}{\varepsilon}\right)\left(\frac{x}{b_o}\right)\right] \tag{5.42}$$

where ε is a function of the offset ratio and is given by the equation

$$\varepsilon = 8.80\left(\frac{Z_o}{b_o} + 13.40\right) \qquad (r^2 = 0.98) \tag{5.43}$$

It can be seen also from Fig. 5.21 that the Froude number has no effect on the momentum-distribution profiles. It should be remembered that the great percentage of the momentum that is lost is converted into pressure in the form of a water depth increase. Fig. 5.21 shows that the losses in the normalized momentum flux are 0.95, 0.94, 0.97, 0.95 and 0.92 for the offset ratios equal to 100, 50, 30, 20 and 10 respectively. As these measurements were taken at or downstream of the point of the jet reattachment to the bed, these values of the normalized momentum flux should be comparable to the corresponding theoretical values shown in Fig. 5.5 which are 0.99, 0.98, 0.97, 0.95 and 0.92 respectively. It is interesting to see the agreement between the predicted and the measured values.

5.6 Engineering Significance

Based on the results presented in this chapter, plane turbulent surface jets in shallow tailwater may be recommended to be used, in practice, as energy dissipators. One application of the new dissipators is to be used in flow regulators. In a flow regulator, a sluice gate is usually used where a supercritical jet issues under the gate, tangential to the channel bed. To minimize downstream scour, a long concrete apron is required. Also, baffle blocks (or walls) may be needed for a higher efficiency of the basin. In deeply submerged flow regulators, the flow discharge is mainly dependent on the head difference between the upstream water level and the downstream tailwater. The location of the opening does not have any significant effect on the flow discharge. In this case, a double-leaf gate can be used with the supercritical jet issuing in-between the two gates, as a surface jet (see Fig. 5.22). The lower gate is adjusted to Z_o above the downstream bed level while the upper gate is moved up or down till the required opening/discharge is reached. In the new arrangement, the turbulent jet is lifted away from the stream bed to the water surface. According to the theoretical and experimental analyses discussed earlier, when the jet attaches to the channel bed, a great portion of the momentum flux is already lost and a uniform velocity is attained. Between the gate and the attachment section, the channel bed is only affected by the reverse flow which is relatively weak and lining the channel bed, in this recirculating zone, with relatively coarse material might be enough to prevent any sediment motion. If a suitable sheet pile wall is installed below the gate for percolation requirements, only a very short concrete seat is required. Also, splitting the vertical gate into two portions will be of benefit in decreasing the capacity, weight and size of the overhead gate control structure as it is required to control either the upper or the lower gate at a time instead of controlling a complete sluice gate. In conclusion, the new basin is simple, short, efficient and economic and is recommended for deeply submerged flow regulators to replace existing basins.

This model may also be used in spillways with relatively shallow tailwater (see Fig. 5.23). The concrete apron of the spillway will be Z_o above the channel bed. This model may be applied on a small scale first and the results should be compared with those of a similar basin (like the submerged bucket basin) before being generally used.

In the above applications, given the thickness of the opening in the flow regulator (or the anticipated thickness of the supercritical stream at the toe of the spillway), the supercritical Froude number and the tailwater depth in the downstream channel, Z_0 and δ_∞ can be easily calculated for design purposes (using Eq. 5.6 or Eq. 5.16 with the relation $y_t = Z_0 + b_0 + \delta_\infty$).

5.7 Conclusions

For turbulent surface jets in shallow tailwater, it has been shown theoretically and experimentally that the momentum flux is not preserved. In the theoretical study, the momentum loss and the piezometric-pressure increase were evaluated at a section just downstream of the line of the jet attachment to the bed. The experimental results showed that the length of the return-flow region is about 6.50 times the offset distance. The velocity profiles in the surface jet were found to be similar, in the developing as well as in the developed regions. Two stages were seen to exist in the decay of the maximum velocity. The rate of the velocity decay in the first stage was independent of the relative depth of the tailwater whereas the faster rate in the second stage depended on it. The length of the first stage of velocity decay was directly proportional to the offset ratio. The length scale of the jet grew at a rate of 0.065 in the early stage and the rate of growth was much smaller in the second stage. The volume flux in the surface jet with limited tailwater was affected significantly. The decay of the momentum flux in the surface jet with the distance from the nozzle was observed and correlated with the offset ratio and the relative longitudinal distance. On the whole, the results from this study highlight the effect of limited tailwater depth on the behavior of plane turbulent surface jets. Based on the momentum and velocity decay results, surface jets in shallow tailwater may be recommended to be used as energy dissipators. Two applications were discussed, flow regulators and spillways.

5.8 References

Albertson, M. L., Dai. Y. B., Jensen, R. A. & Rouse, H. (1950). "Diffusion of submerged jets." Trans. ASCE. 115, 639-664.

Goldschmidt, V., and Eskinazi, S. (1966). "Two phase turbulent flow in a plane jet." Trans. ASME, Series E, J. Appl. Mech., 33(4), 735-747.

Heskestad, G. (1965). "Hot wire measurements in a plane turbulent jet." Trans. ASME, Series E, J. Appl. Mech., 32(4), 721-734.

Kotsovinos, N. E. (1975). "A study of the entrainment and turbulence in a plane turbulent jet." W. M. Keck Lab. Hydr. Water Resources, Calif. Inst. Tech. Rept. KH R-32.

Kotsovinos, N. E. (1978). "A note on the conservation of the axial momentum of a turbulent jet." J. Fluid Mech., 87(7), pp. 55-63.

Miller, D. R., and Comings, E. W. (1957). "Static pressure distribution in the free turbulent jet." J. Fluid Mech., 3(10), pp. 1-16.

Rajaratnam. N. (1969). "Diffusion of a supercritical stream on a stagnant pool." Trans. Engr. Inst. of Canada, 12(A-1), 1-5.

Rajaratnam, N. (1976). "Turbulent Jets." Elsevier Publishing Co, The Netherlands, 304p.

Rajaratnam, N., and Humphries, J. A. (1984). "Turbulent non-buoyant surface jet." J. Hydr. Res., 22(2), pp. 103-115.

Schlichting, H. (1960). "Boundary layer theory." 4th Edn. McGraw-Hill: New York.

Schneider, W. (1985). "Decay of momentum flux in submerged jets." J. Fluid Mech., 154(5), pp. 91-110.

Swean Jr, T. F., Ramberg, S. E., Plesniak, M. W. Stewart., M. B. (1989). "Turbulent surface jet in channel of limited depth." J. Hydr. Engrg., ASCE, 115(12), pp. 1587-1606.

Vanvari, M. R., and Chu, V. H. (1974). "Two-dimensional turbulent surface jets of low Richardson number." Tech. Report No. 74-2 [FML], Fluid Mech. Lab., Dept. of Civ. Engrg. and Appl. Mech., McGill Univ., Montreal, Canada.

Wu, S. and Rajaratnam, N. (1995). "Effect of baffles on submerged flows" J. Hydr. Engrg., ASCE, 121(9), pp. 644-652.

Table 5.1 Primary details of experiments

Exp. (1)	b_o (mm) (2)	Z_o (mm) (3)	y_t (mm) (4)	W(mm) (5)	U_o (m/s) (6)	F_o (7)	Z_o/b_o (8)	$(y_t-Z_o)/b_o$ (9)	R (10)
1	5	500	505	446	1.60	7.2	100	1.00	8000
2	10	500	510	446	0.75	2.4	50	1.00	7500
3	10	500	510	446	1.50	4.8	50	1.00	15000
4	10	500	510	446	2.25	7.2	50	1.00	22500
5	10	300	310	446	1.88	6.0	30	1.00	18800
6	20	500	520	446	2.13	4.8	25	1.00	42600
7	10	200	210	446	0.90	2.9	20	1.00	9000
8	10	100	110	446	1.25	4.0	10	1.00	12500
9	10	50	60	446	0.50	1.6	5	1.00	5000

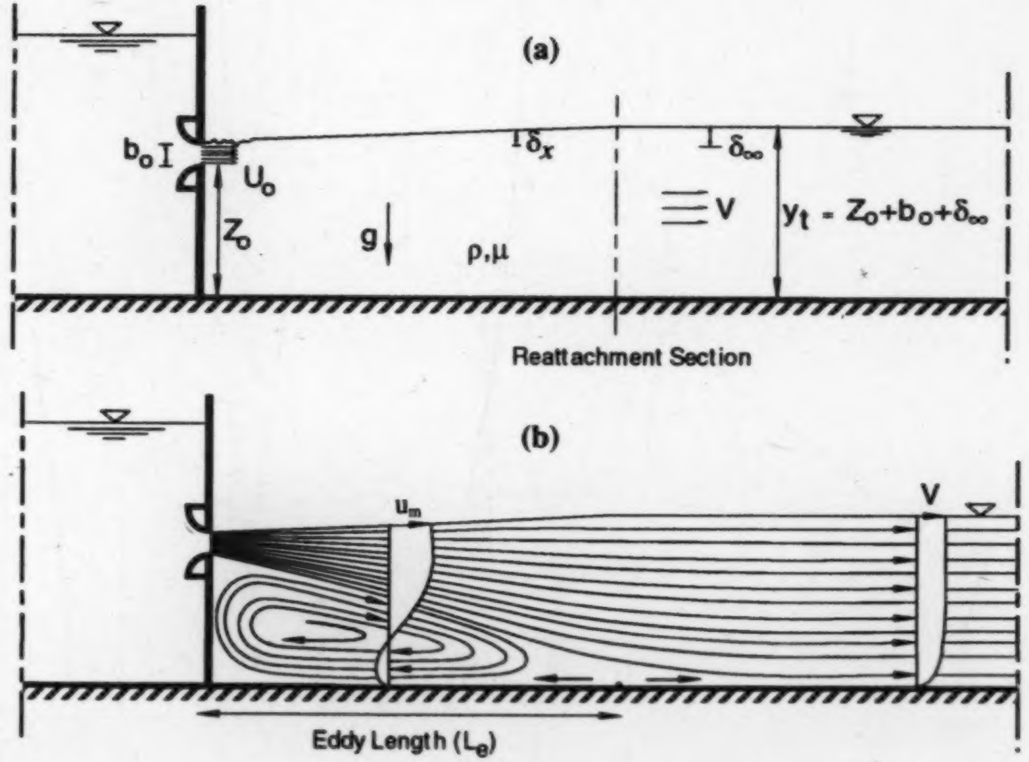
(a)
b_o
U_o
Z_o
δ_x
δ_∞
g
ρ,μ
V
$y_t = Z_o + b_o + \delta_\infty$
Reattachment Section
(b)
u_m
V
Eddy Length (L_e)

Fig. 5.1 (a) Definition sketch; (b) Flow pattern

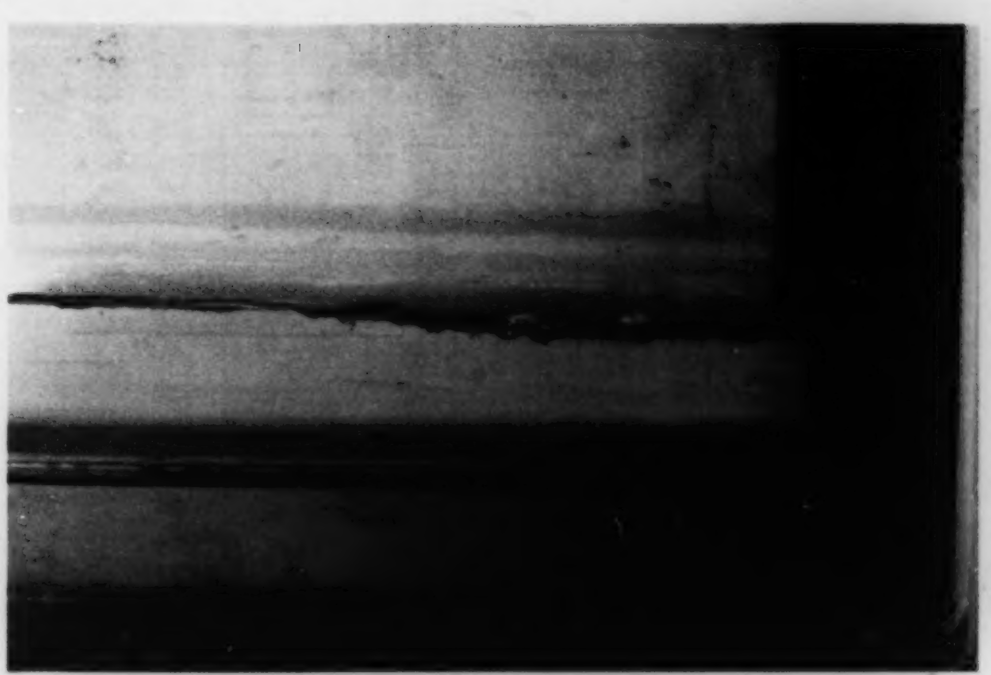

Fig. 5.2 Water surface elevation ($F_o = 4.0$, $Z_o/b_o = 10$)

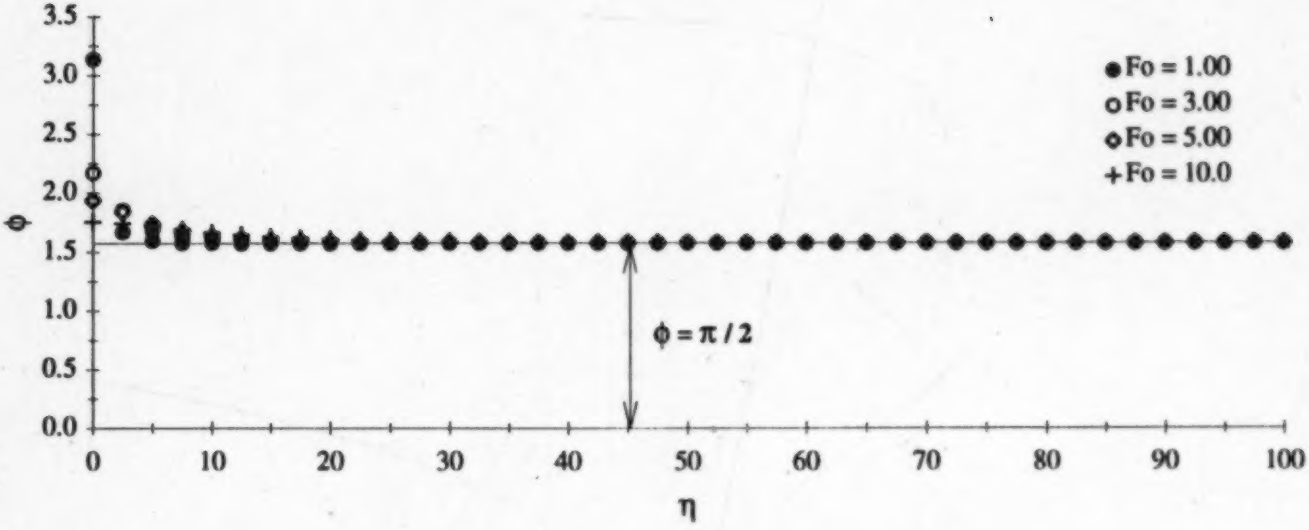

Fig. 5.3 Variation of (ϕ) with the offset ratio (η)

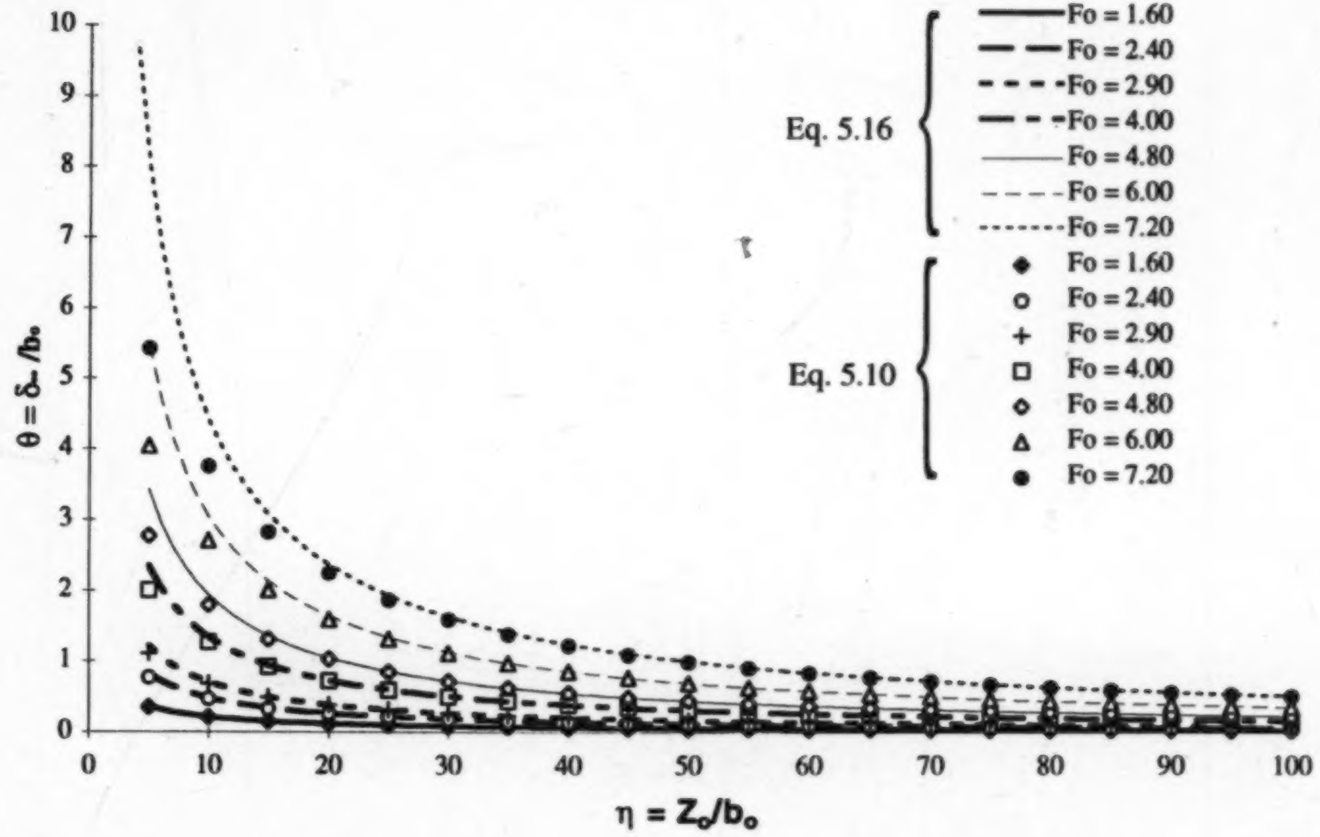

Fig. 5.4 Variation of (θ) with the offset ratio (η) for different Froude numbers

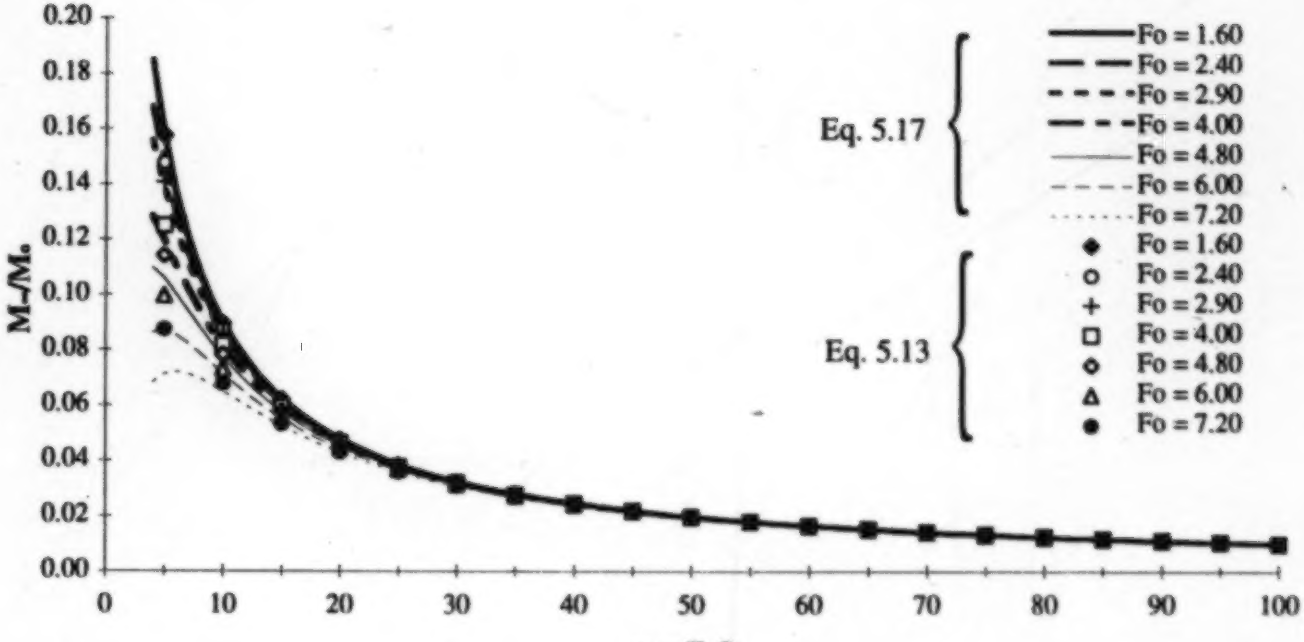

Fig. 5.5 Variation of (M_∞/M_o) with the offset ratio (η) for different Froude numbers

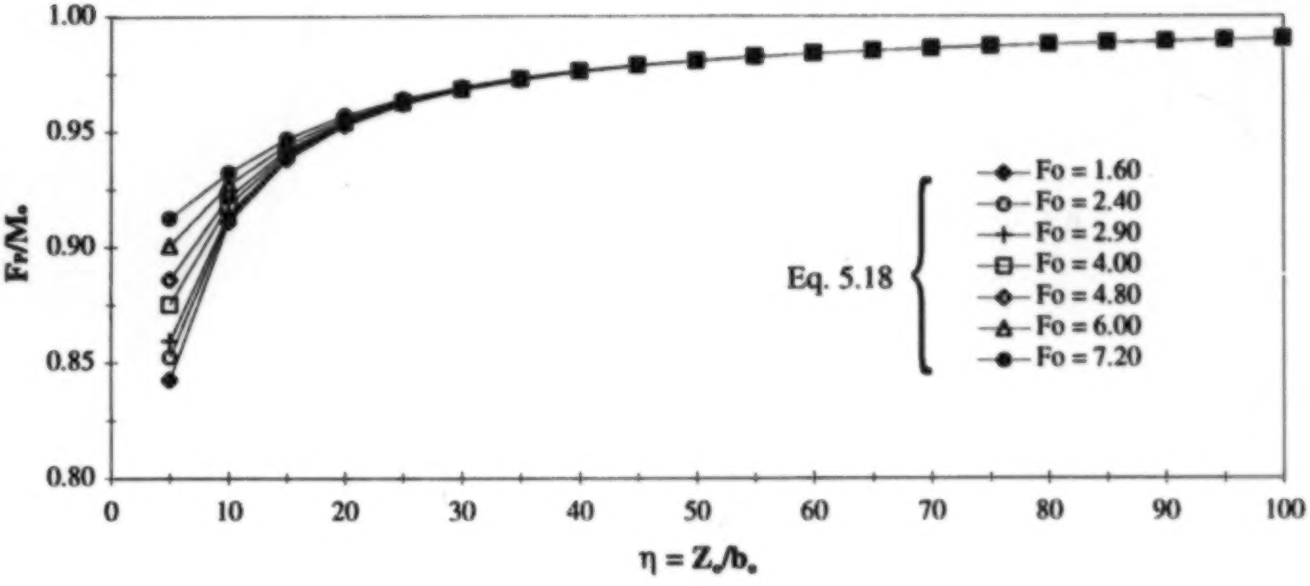

Fig. 5.6 Variation of (F_P/M_o) with the offset ratio (η) for different Froude numbers

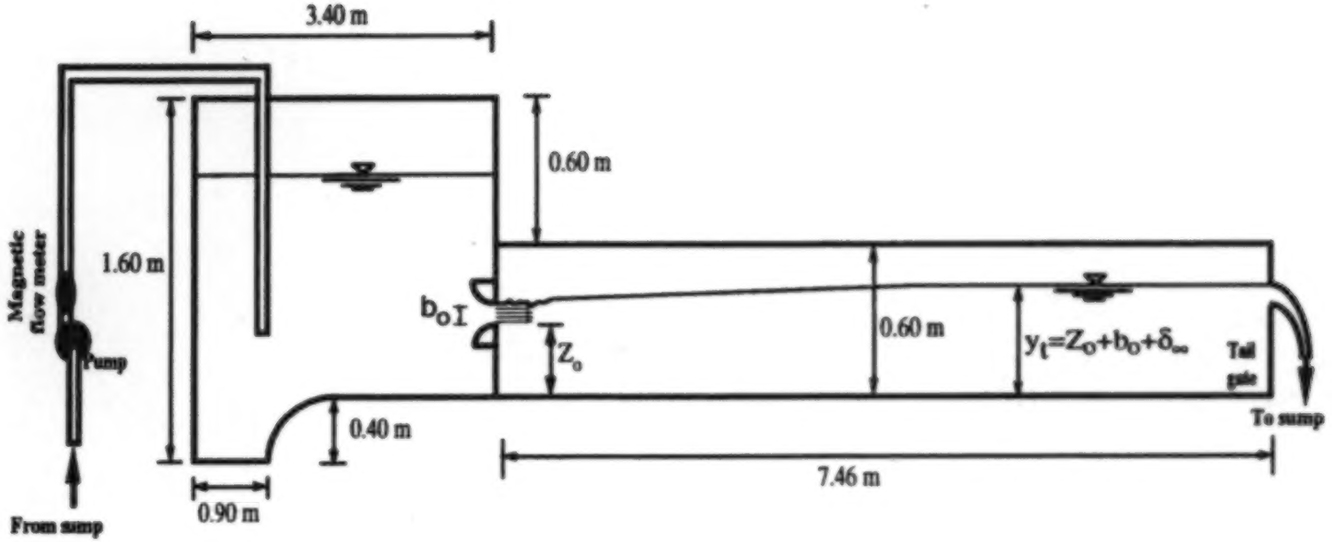
3.40 m
0.60 m
1.60 m
Magnetic flow meter
Pump
From sump
0.90 m
0.40 m
b_o
Z_o
0.60 m
$y_t = Z_o + b_o + \delta_\infty$
Tail gate
To sump
7.46 m

Fig. 5.7 Experimental flume

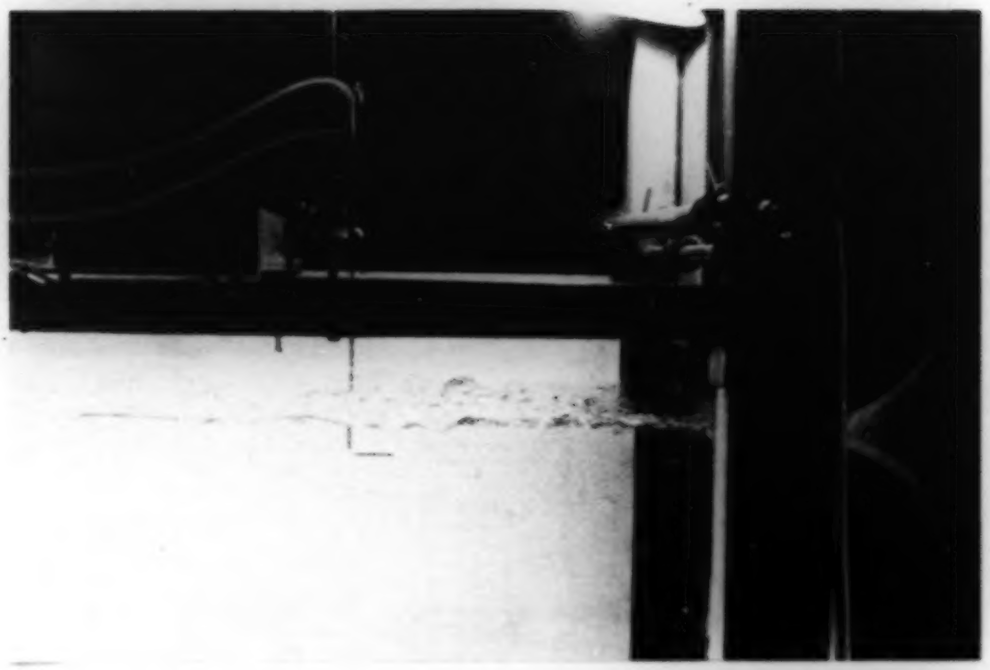

Fig. 5.8 Streamlined entrance to produce an uniform jet of thickness b_o

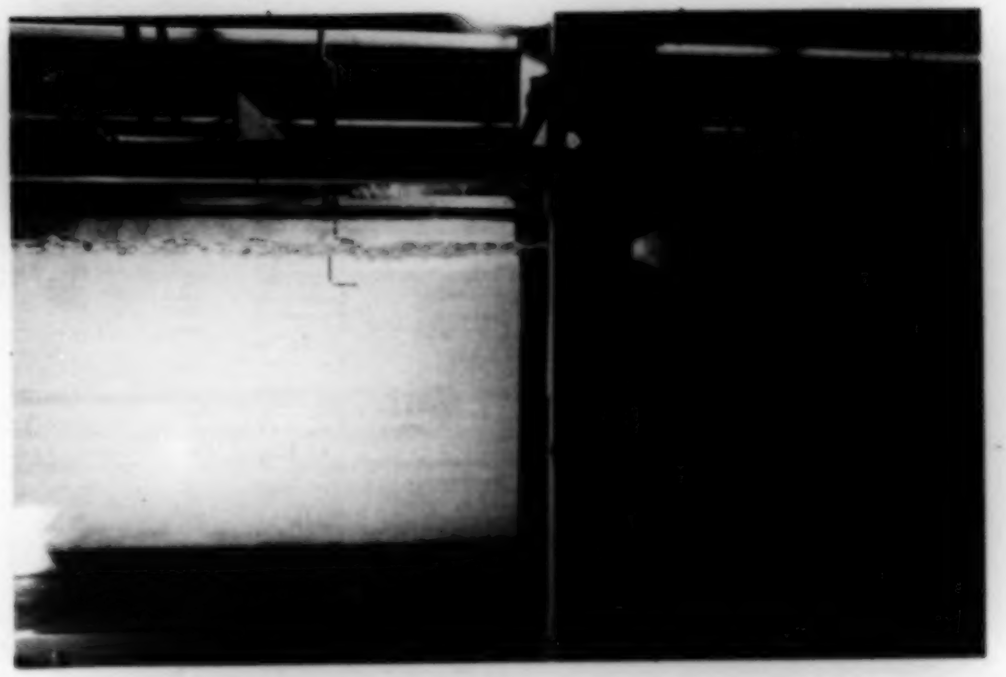

Fig. 5.9 False floor to produce an offset distance of Z_o

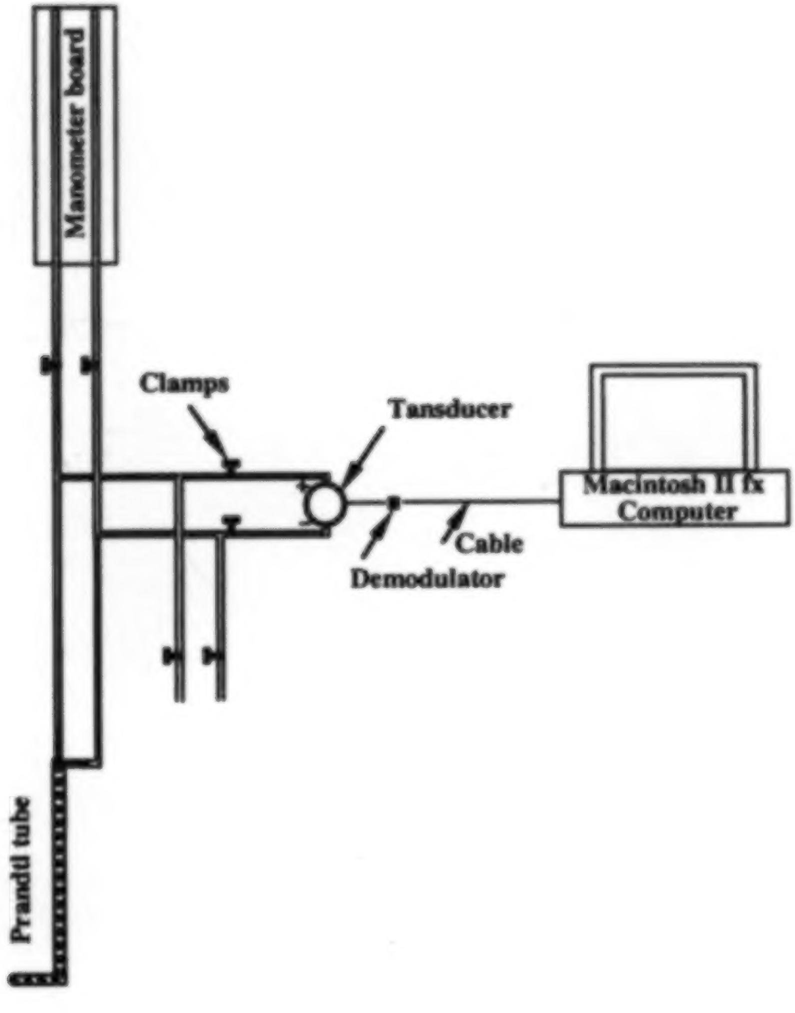
Manometer board
Clamps
Tansducer
Macintosh II fx Computer
Cable
Demodulator
Prandtl tube

Fig. 5.10 Prandtl tube

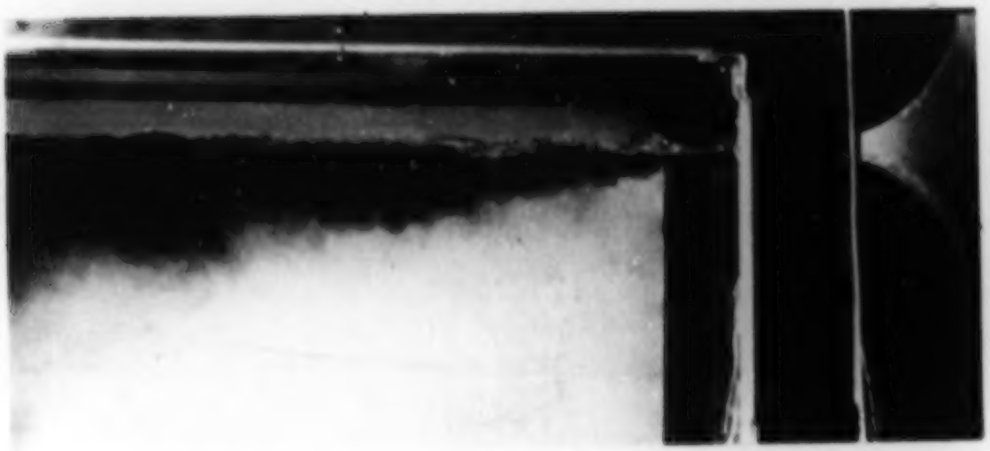

Fig. 5.11(a) Surface jet ($F_o = 7.20$, $Z_o/b_o = 100$)

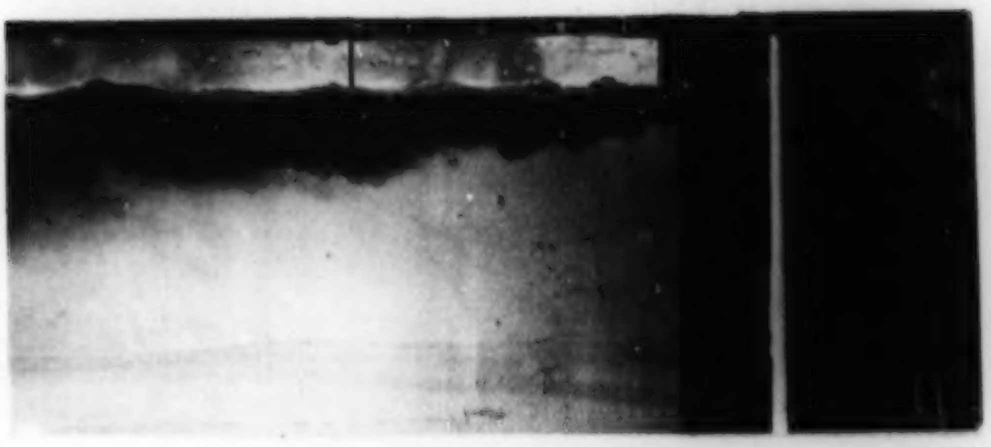

Fig. 5.11(b) Surface jet ($F_o = 4.80$, $Z_o/b_o = 50$)

Fig. 5.11(c) Surface jet ($F_o = 4.80$, $Z_o/b_o = 25$)

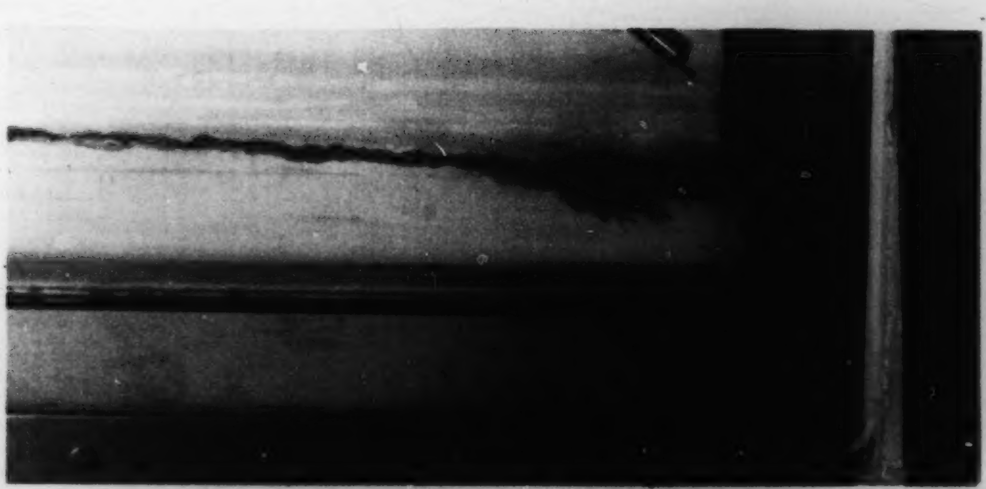

Fig. 5.11(d) Surface jet ($F_o = 4.00$, $Z_o/b_o = 10$)

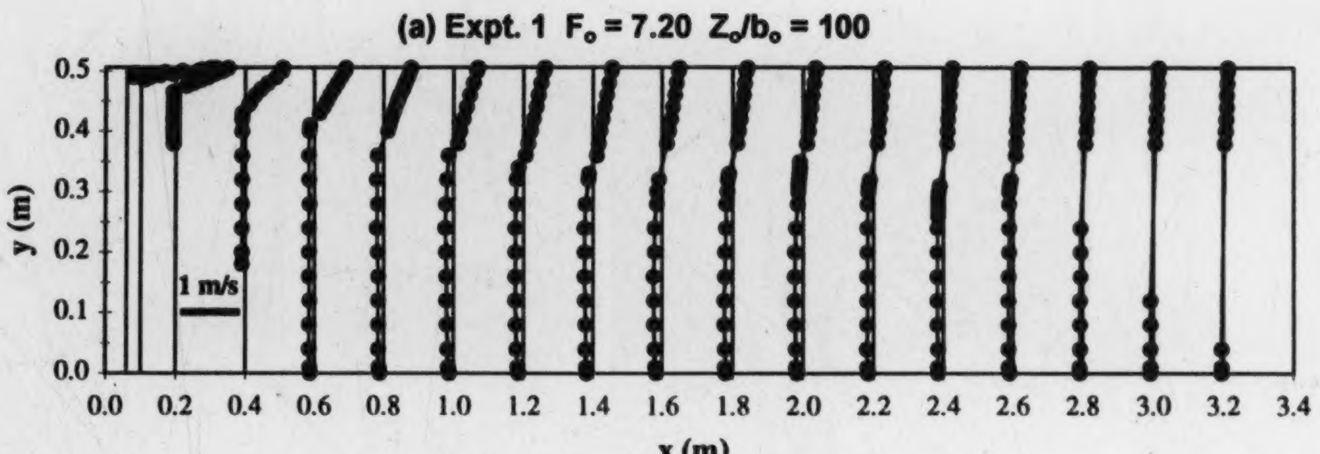
(a) Expt. 1 $F_o = 7.20$ $Z_o/b_o = 100$

Fig. 5.12(a) Typical velocity profiles (Expt. 1)

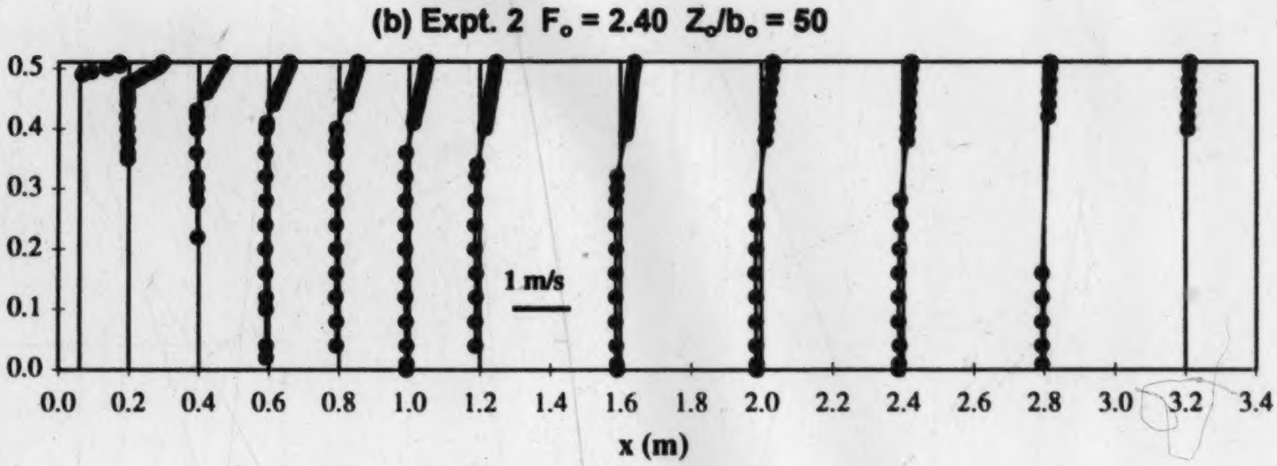

(b) Expt. 2 $F_o = 2.40$ $Z_o/b_o = 50$

Fig. 5.12(b) Typical velocity profiles (Expt. 2)

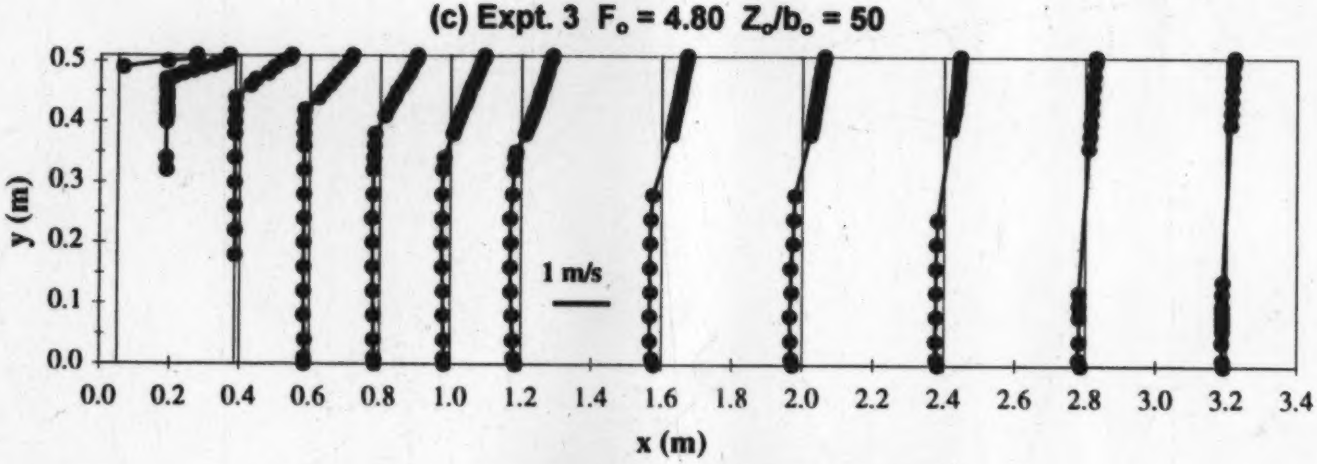

(c) Expt. 3 $F_o = 4.80$ $Z_o/b_o = 50$

Fig. 5.12(c) Typical velocity profiles (Expt. 3)

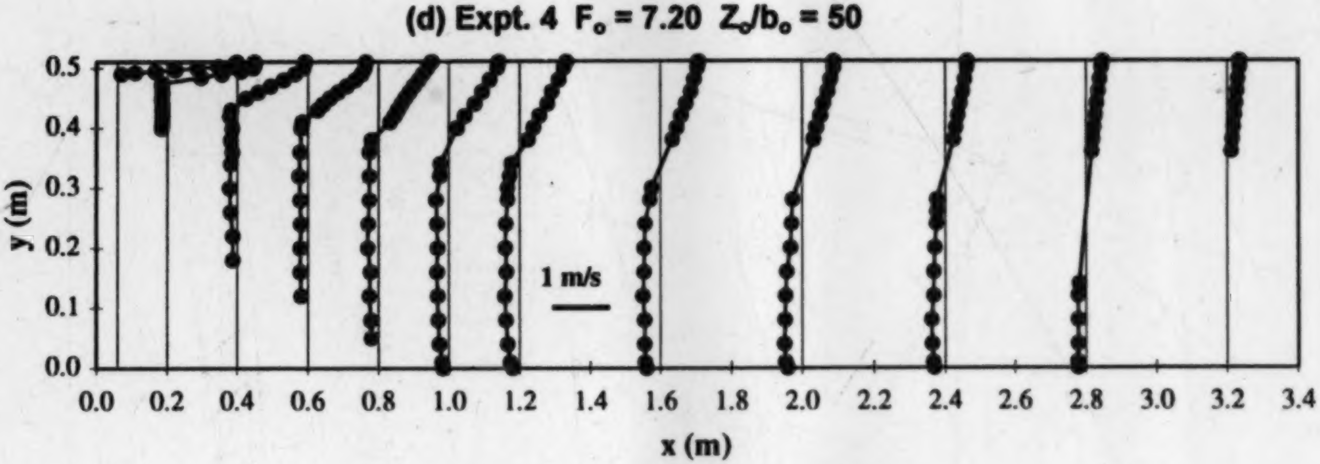

Fig. 5.12(d) Typical velocity profiles (Expt. 4)

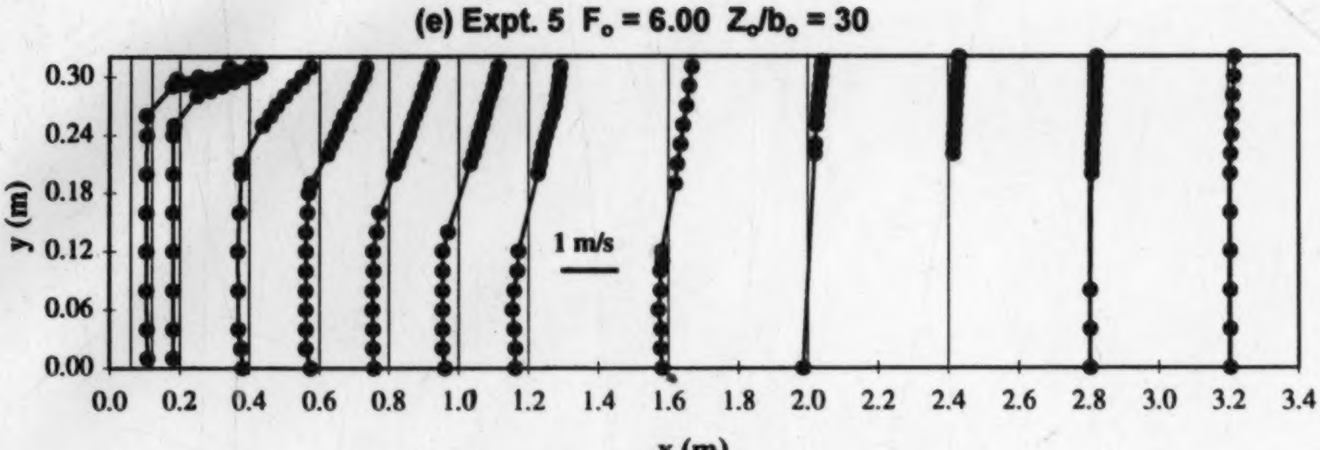
(e) Expt. 5 $F_o = 6.00$ $Z_o/b_o = 30$

Fig. 5.12(e) Typical velocity profiles (Expt. 5)

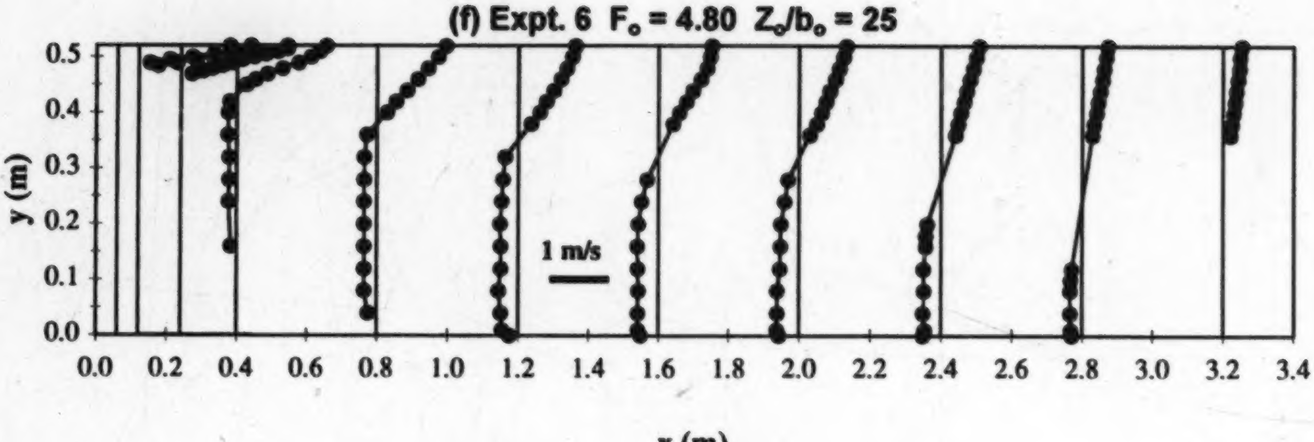

(f) Expt. 6 $F_o = 4.80$ $Z_o/b_o = 25$

Fig. 5.12(f) Typical velocity profiles (Expt. 6)

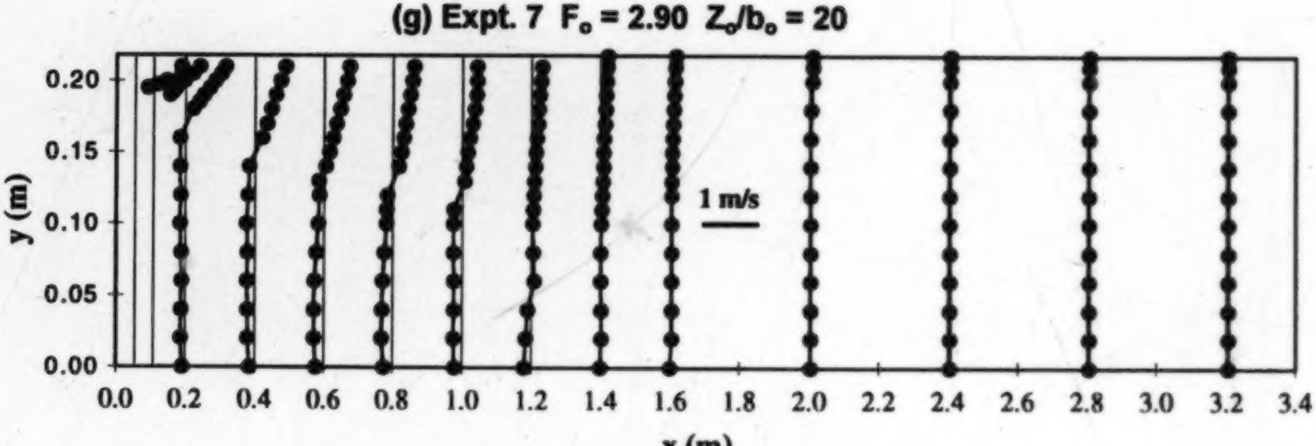

(g) Expt. 7 $F_o = 2.90$ $Z_o/b_o = 20$

Fig. 5.12(g) Typical velocity profiles (Expt. 7)

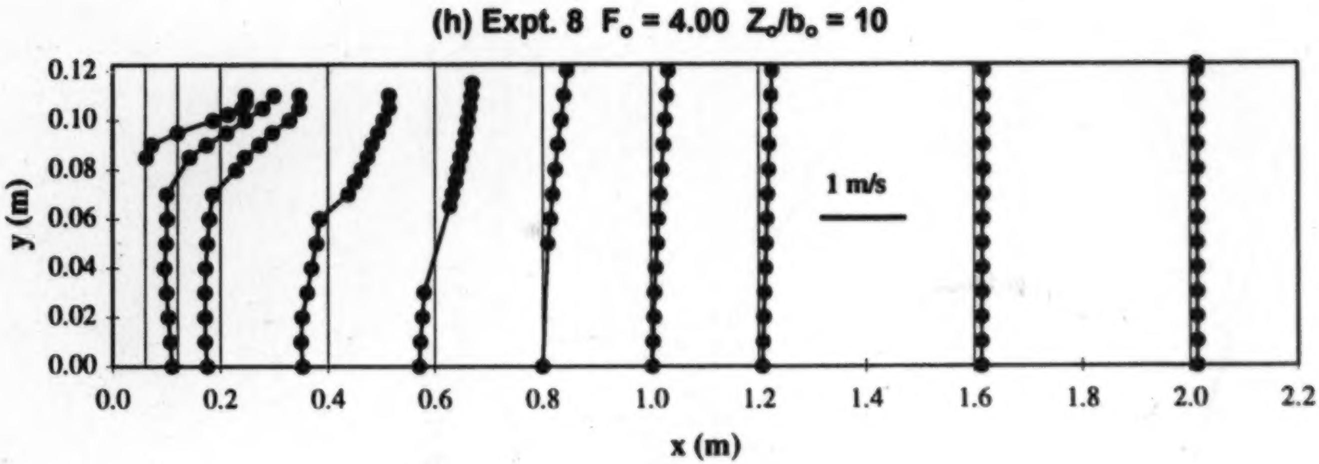

Fig. 5.12(h) Typical velocity profiles (Expt. 8)

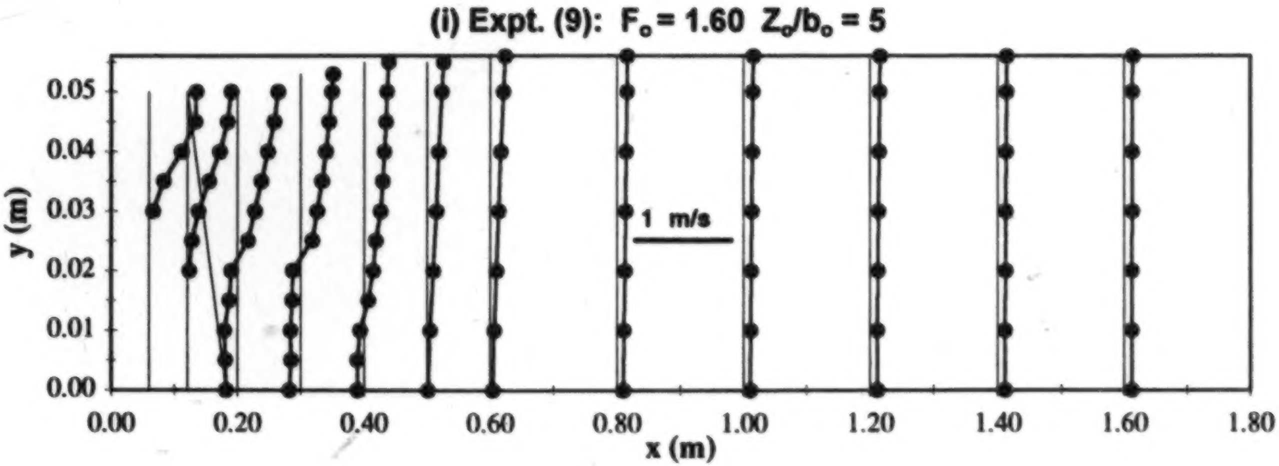
(i) Expt. (9): $F_o = 1.60$ $Z_o/b_o = 5$

Fig. 5.12(i) Typical velocity profiles (Expt. 9)

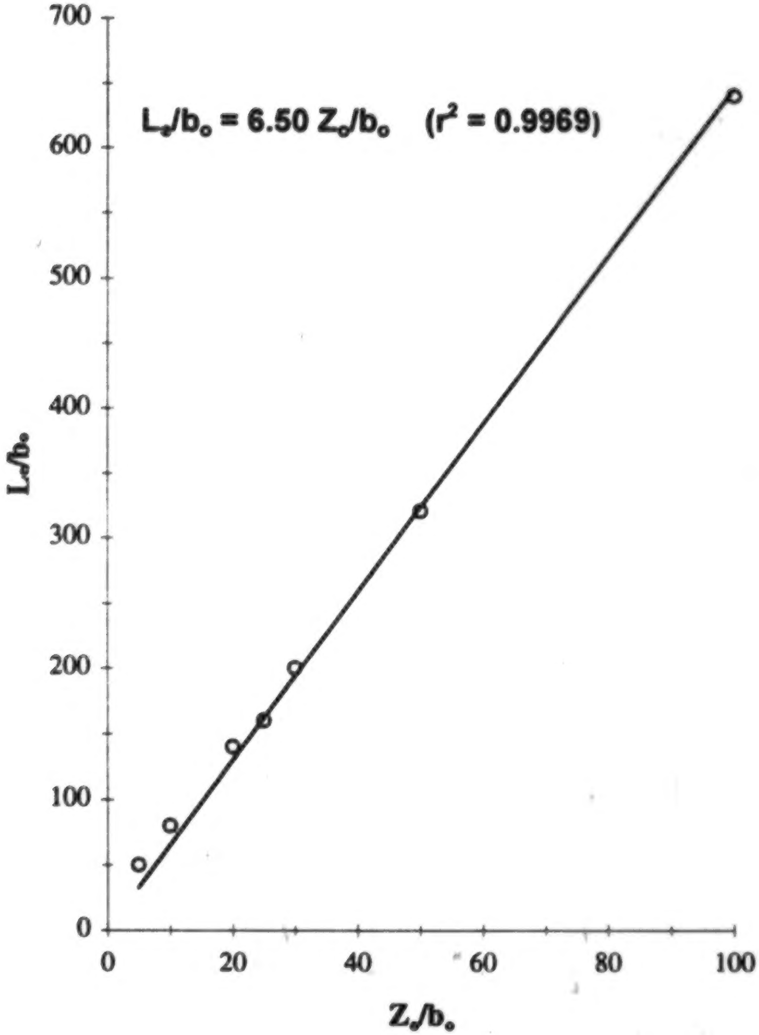

Fig. 5.13 Variation of the eddy length with the offset ratio

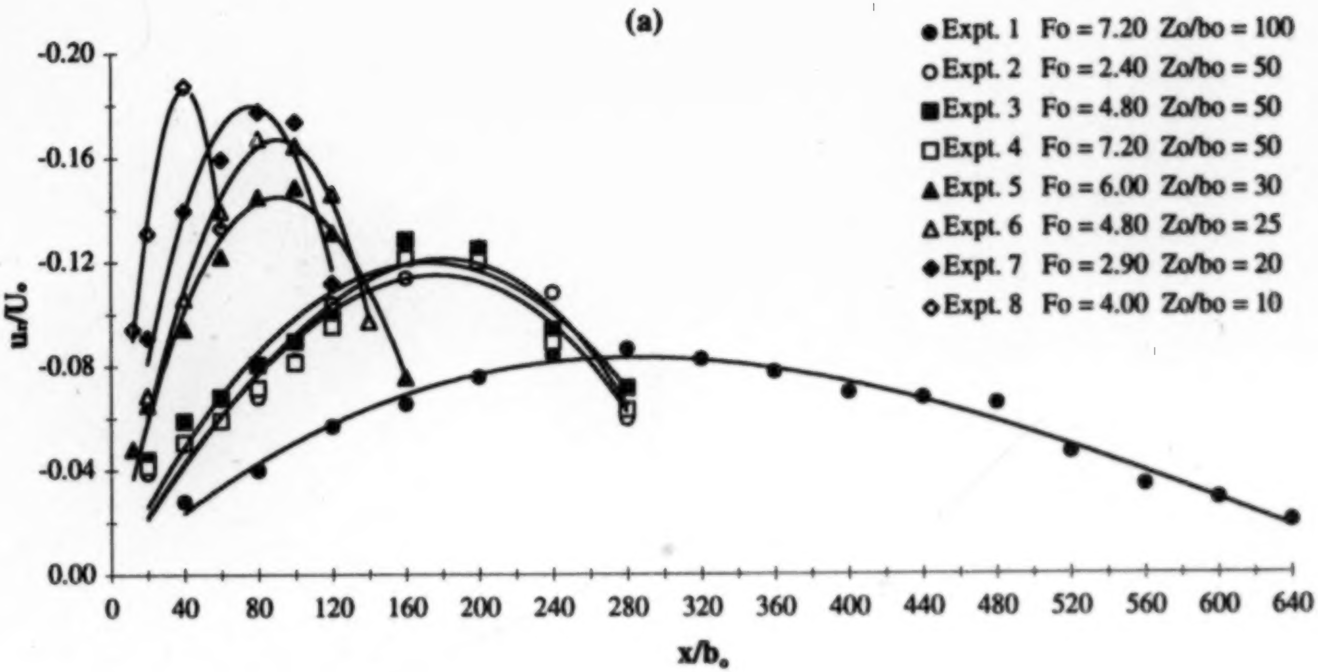

Fig. 5.14(a) Variation of the depth-averaged reverse velocity with distance

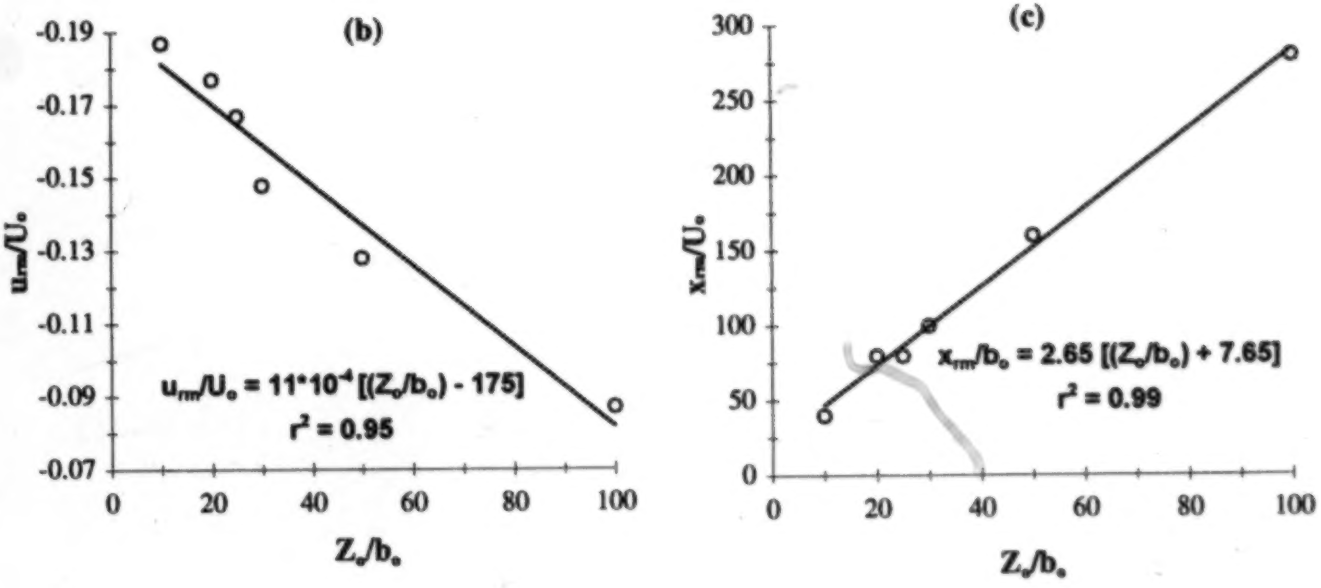

Fig. 5.14(b-c) Effect of the offset ratio on the magnitude and the location of the maximum reverse velocity

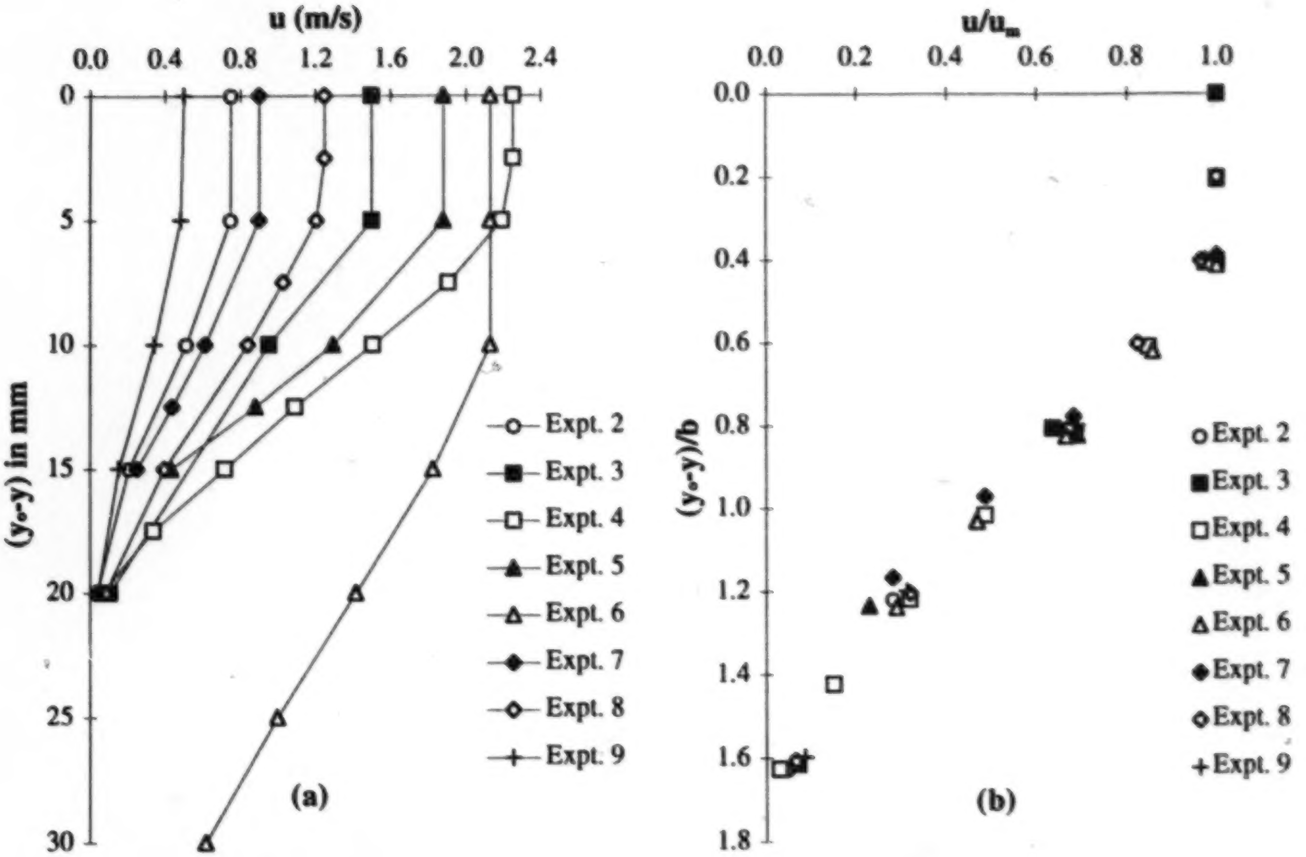

Fig. 5.15(a-b) Velocity distribution in partially-developed flow (x/bo = 6)
(a) Velocity profiles; and (b) Similarity profiles

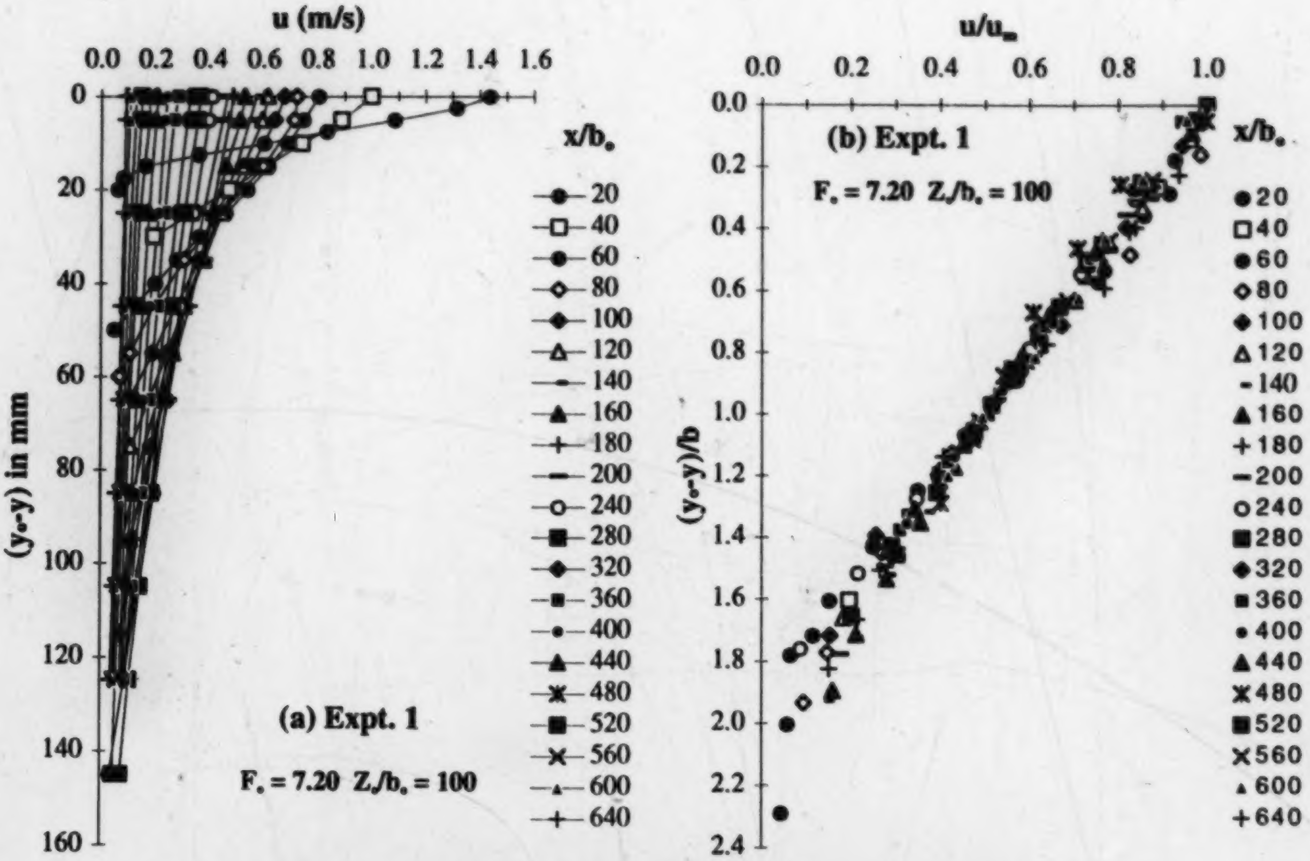

Fig. 5.16(a-b) Velocity distribution in fully-developed flow (Expt. 1)
(a) Velocity profiles; and (b) Similarity profile

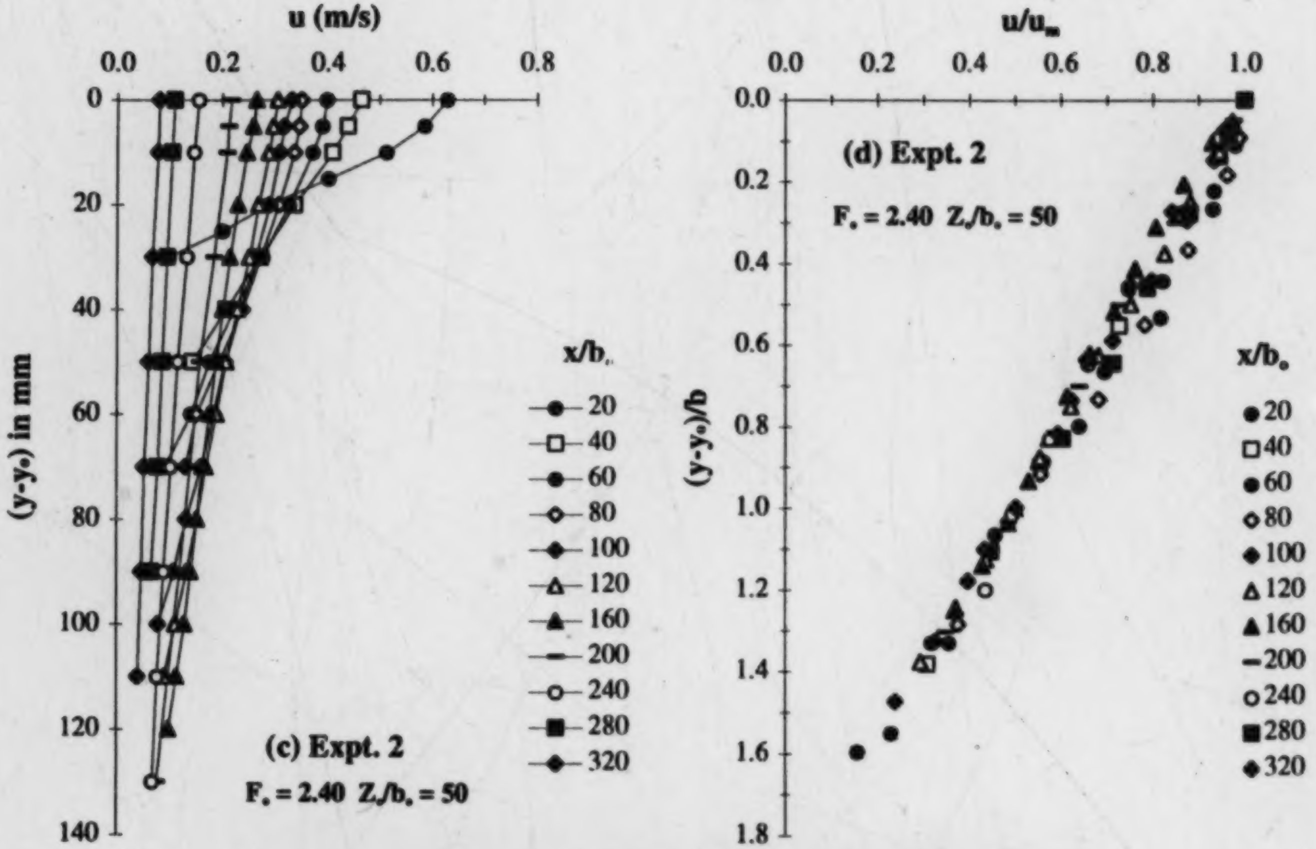

Fig. 5.16(c-d) Velocity distribution in fully-developed flow (Expt. 2)
(c) Velocity profiles; and (d) Similarity profile

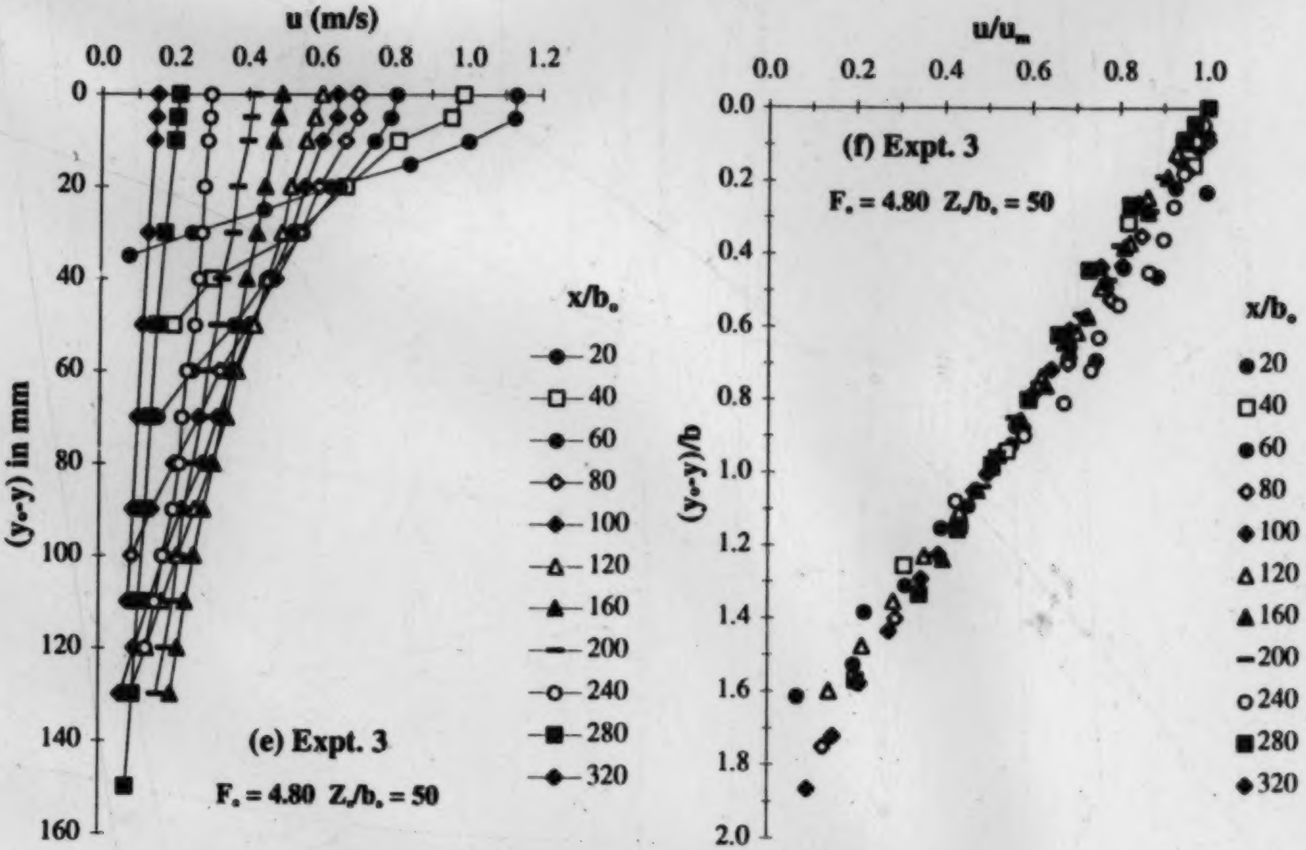

Fig. 5.16(e-f) Velocity distribution in fully-developed flow (Expt. 3)
(e) Velocity profiles; and (f) Similarity profile

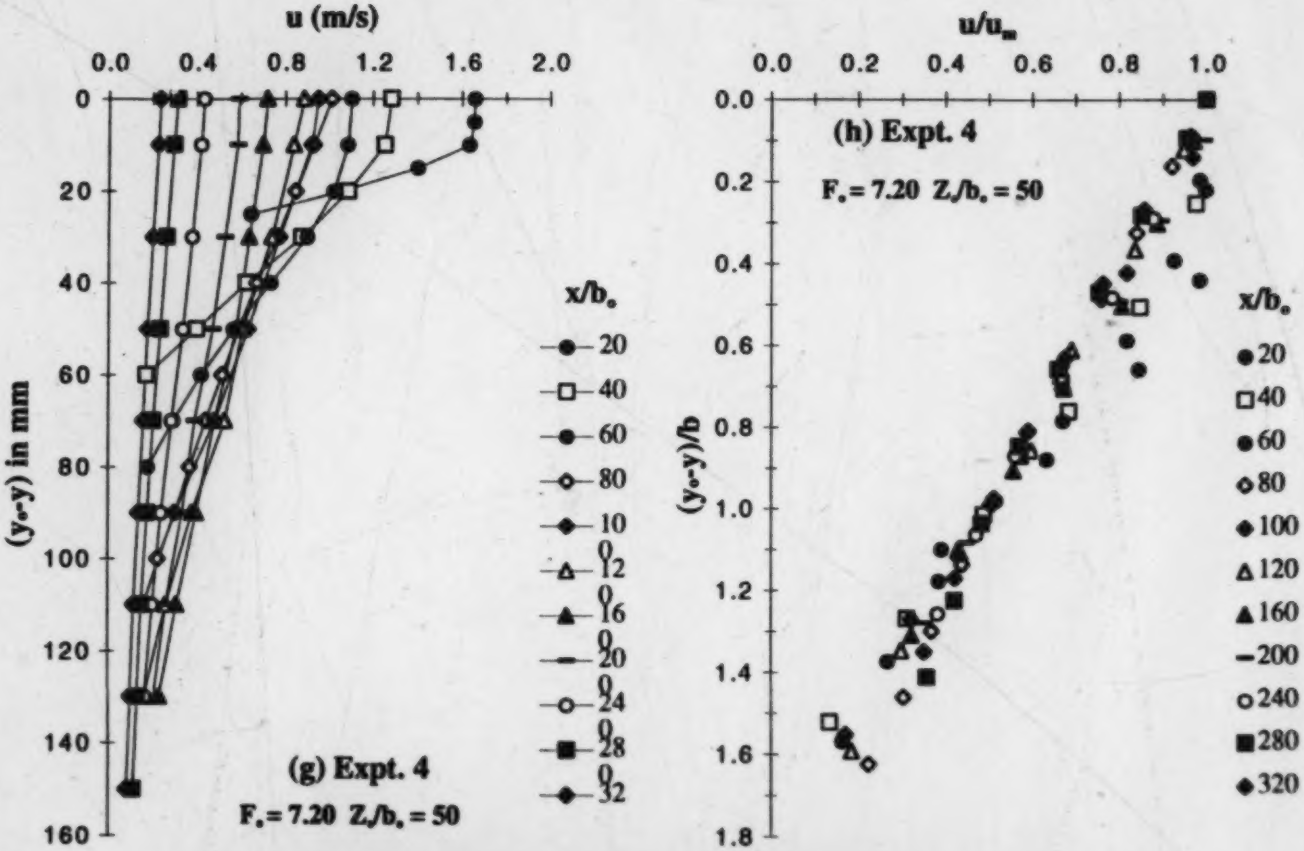

Fig. 5.16(g-h) Velocity distribution in fully-developed flow (Expt. 4)
(g) Velocity profiles; and (h) Similarity profile

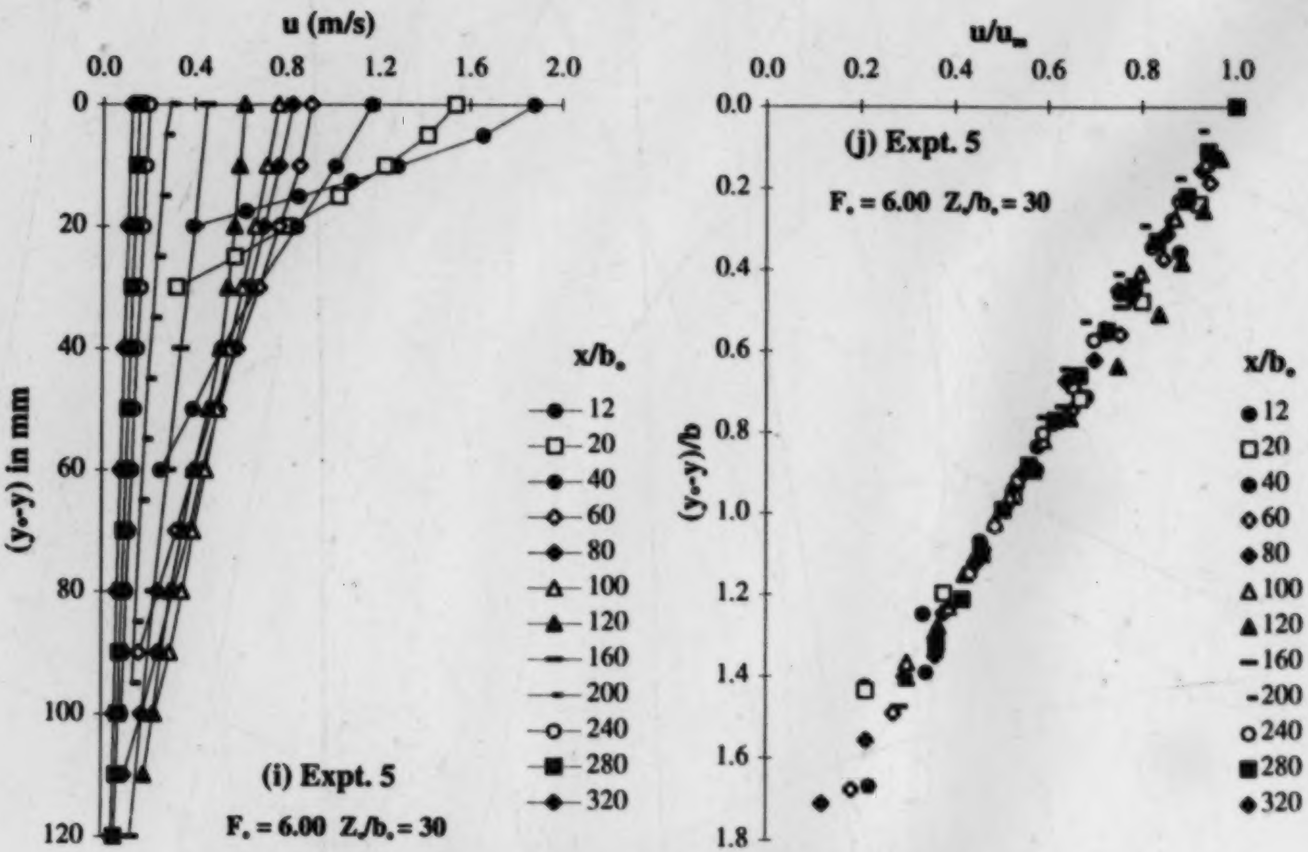

Fig. 5.16(i-j) Velocity distribution in fully-developed flow (Expt. 5)
(i) Velocity profiles; and (j) Similarity profile

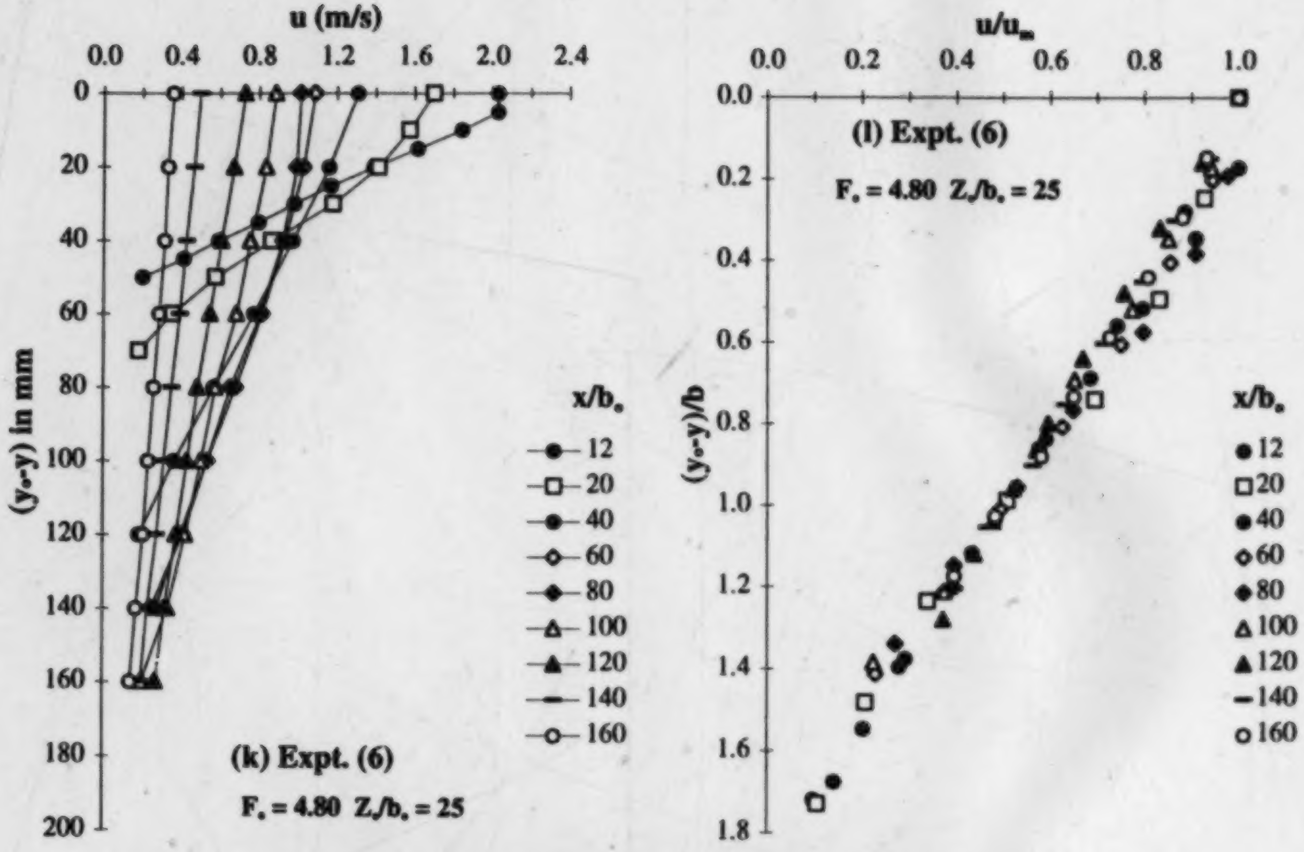

Fig. 5.16(k-l) Velocity distribution in fully-developed flow (Expt. 6)
(k) Velocity profiles; and (l) Similarity profile

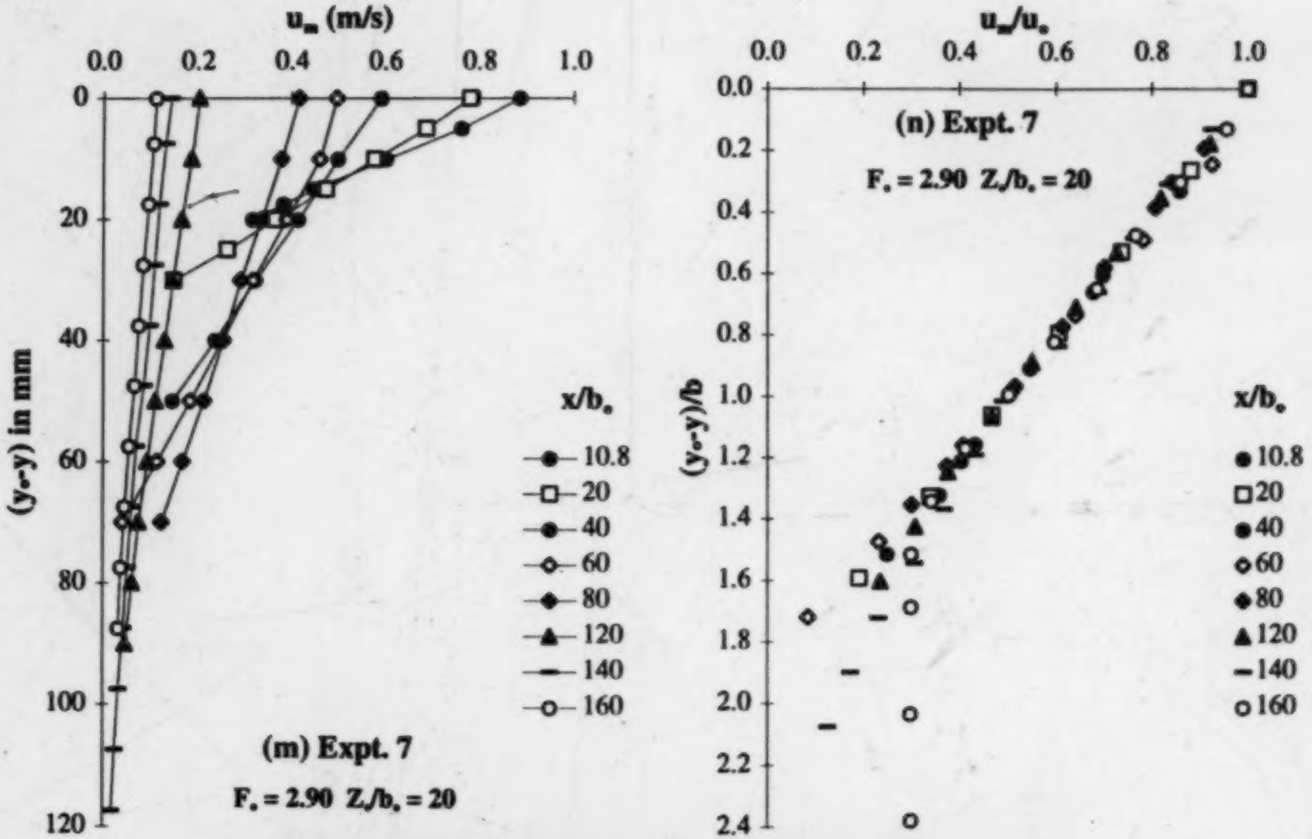

Fig. 5.16(m-n) Velocity distribution in fully-developed flow (Expt. 7)
(m) Velocity profiles; and (n) Similarity profile

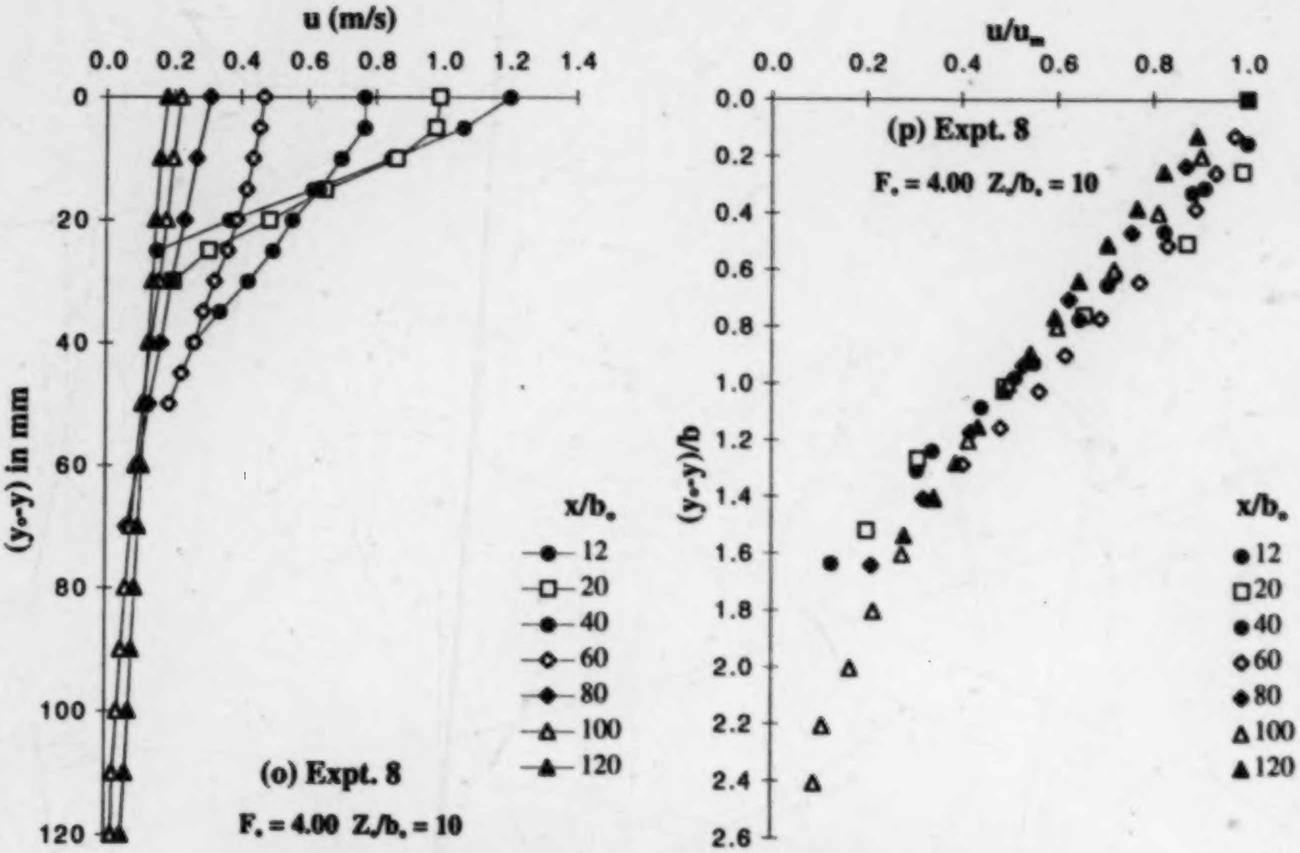

Fig. 5.16(o-p) Velocity distribution in fully-developed flow (Expt. 8)
(o) Velocity profiles; and (p) Similarity profile

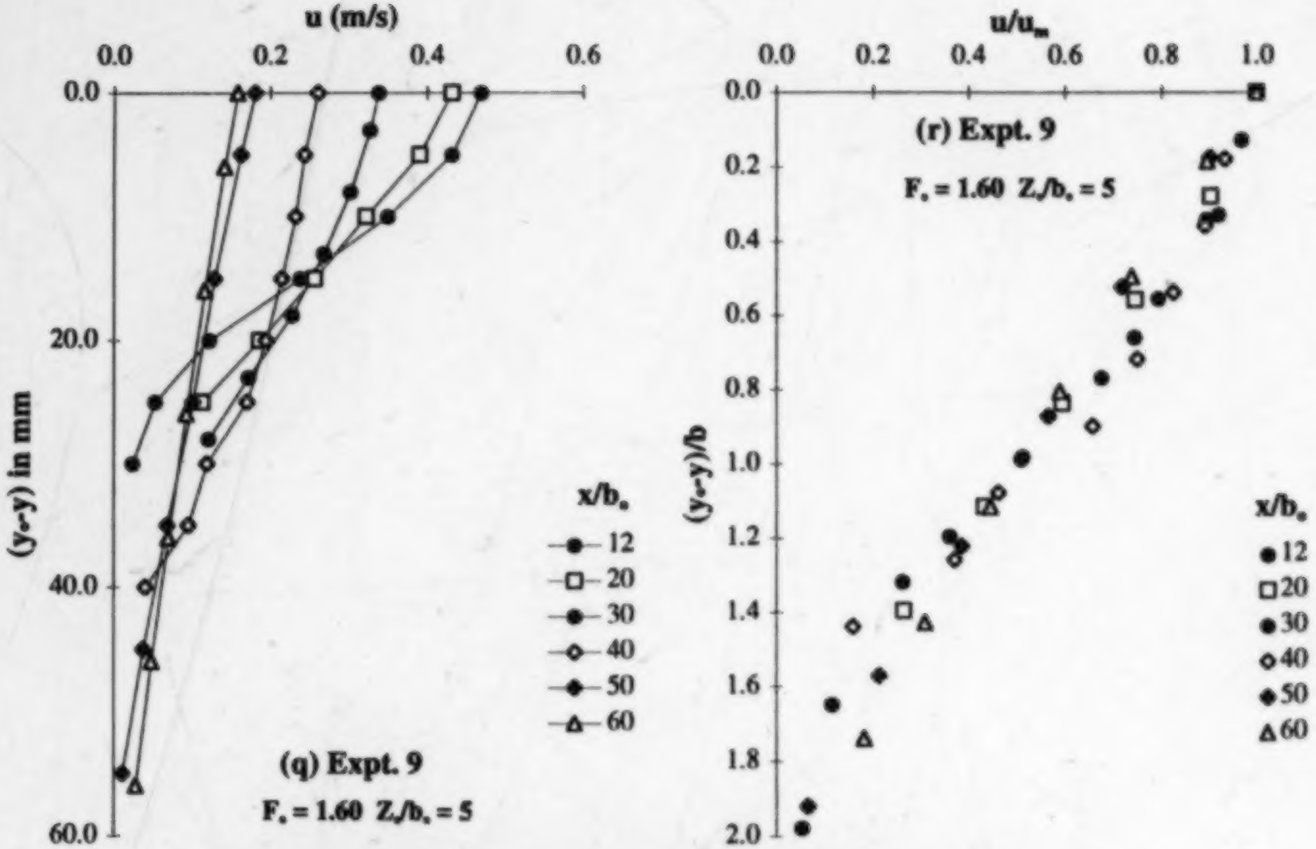

Fig. 5.16(q-r) Velocity distribution in fully-developed flow (Expt. 9)
(q) Velocity profiles; and (r) Similarity profile

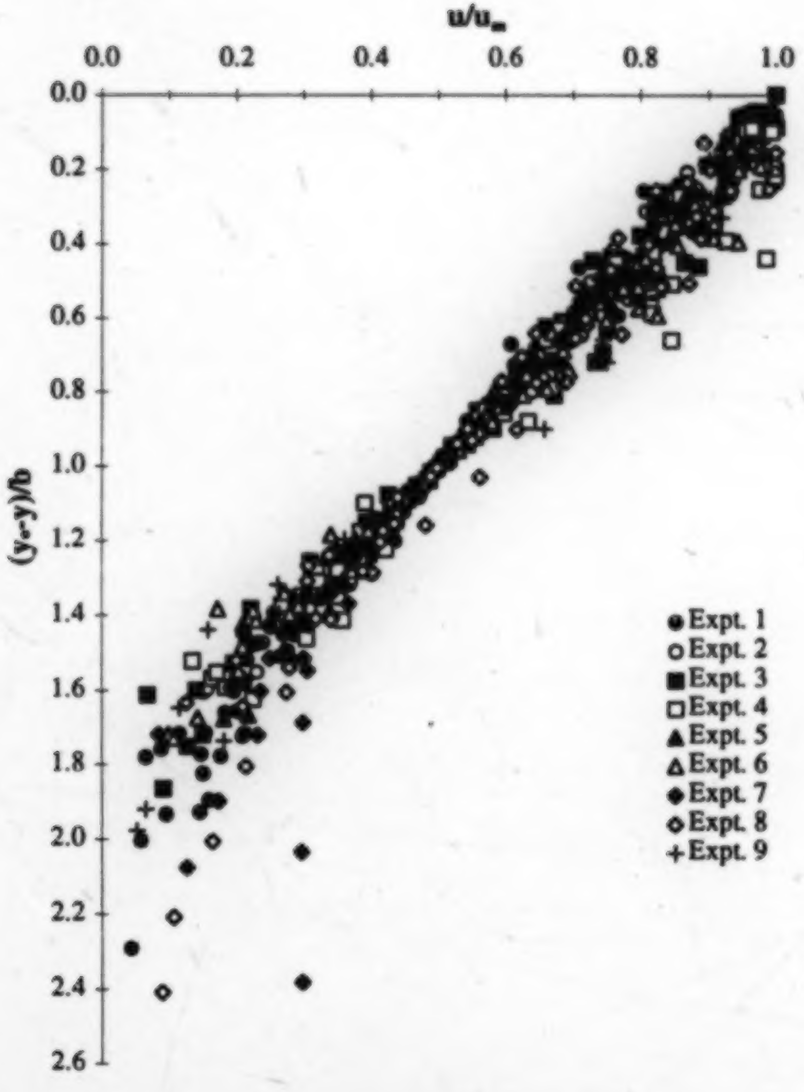

Fig. 5.17 Consolidated non-dimensional plot for the velocity distribution in the surface jet

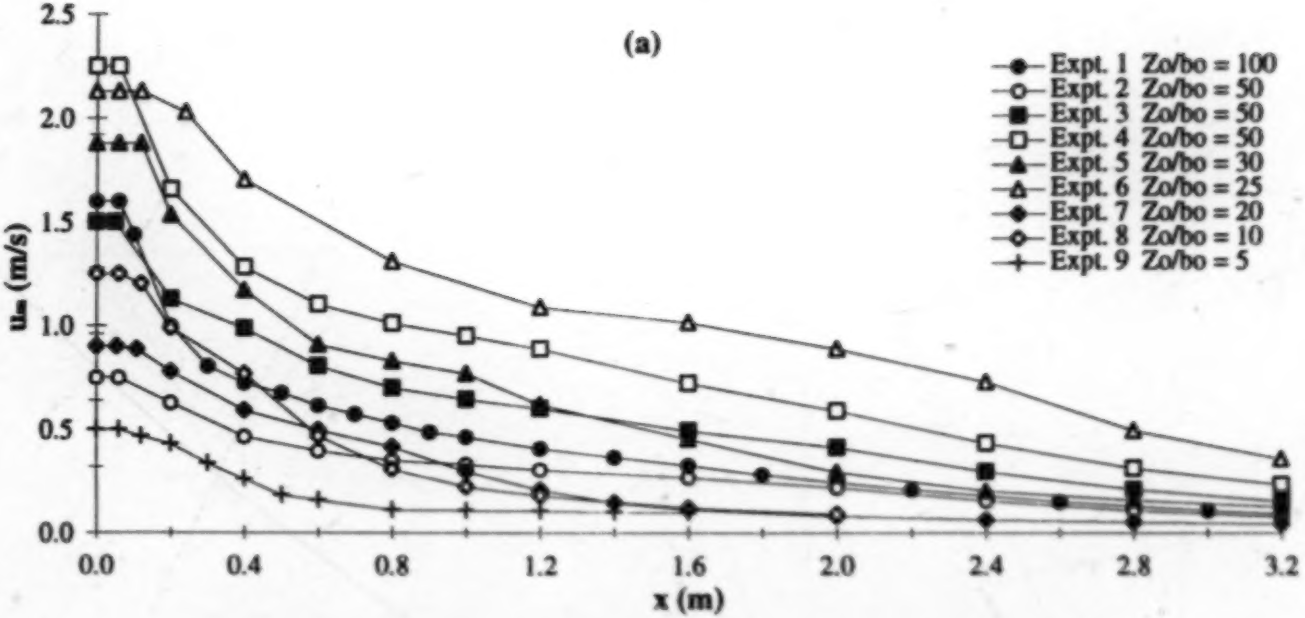

Fig. 5.18(a) Variation of the maximum jet velocity, u$_m$, with distance

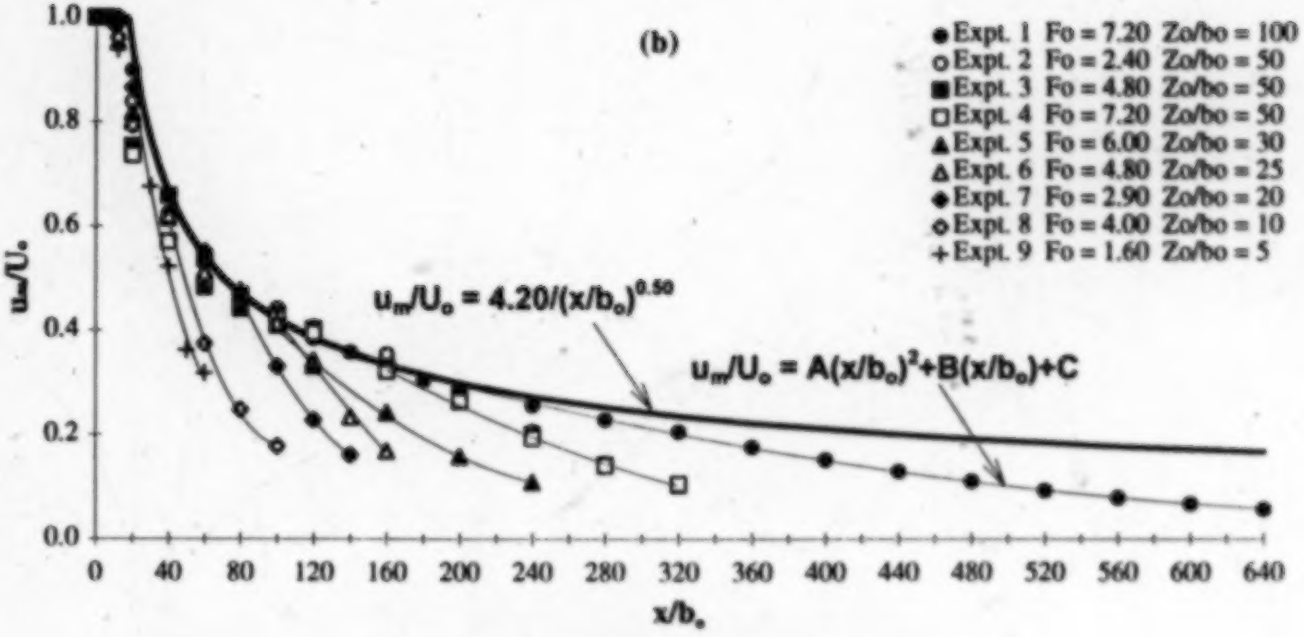

Fig. 5.18(b) Variation of u_m/U_o with x/b_o

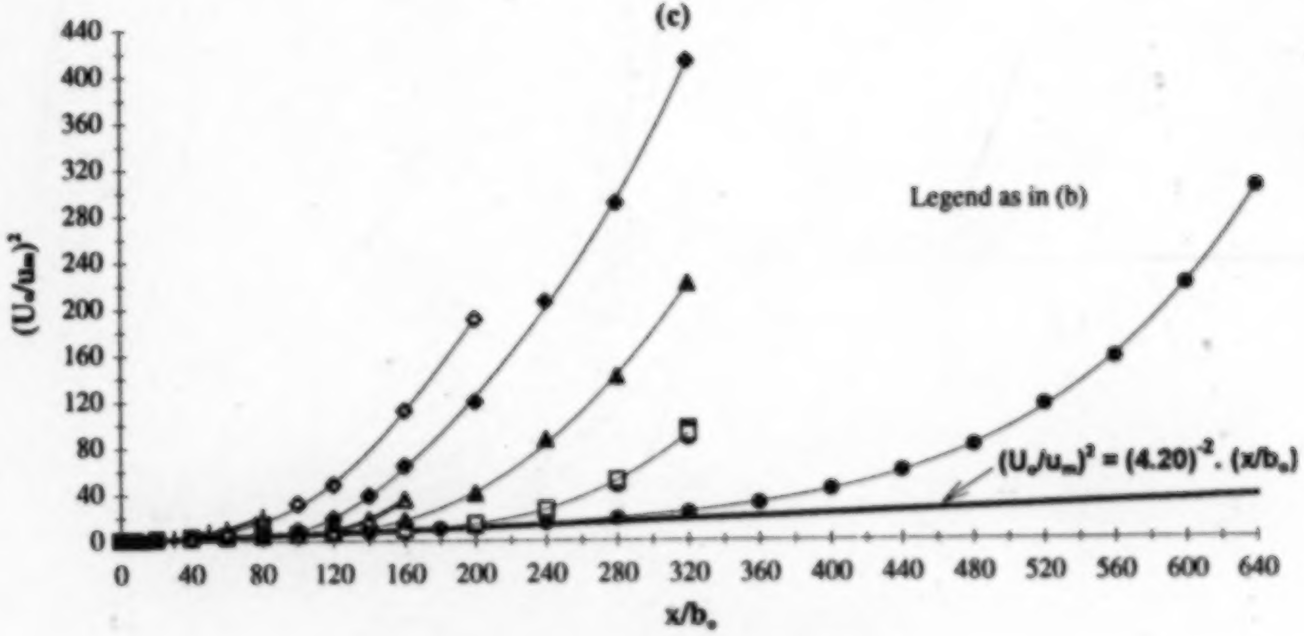

Fig. 5.18(c) Variation of $(U_o/U_m)^2$ with x/b_o

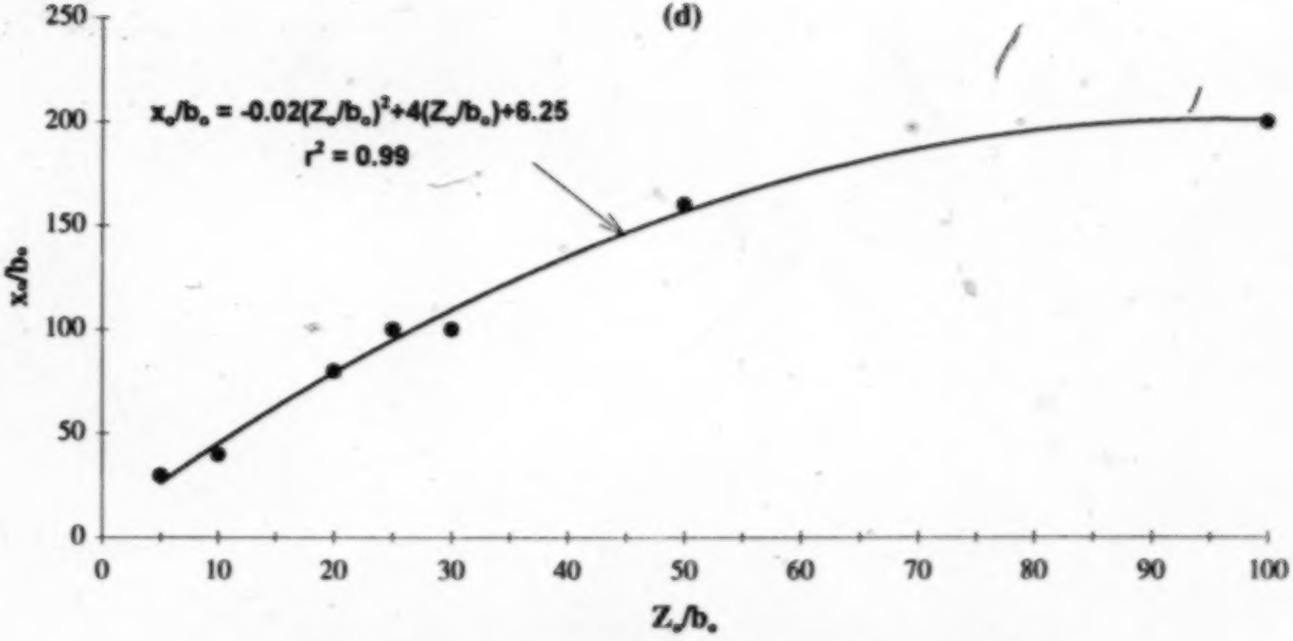

Fig. 5.18(d) Effect of the offset ratio on the breakdown distance

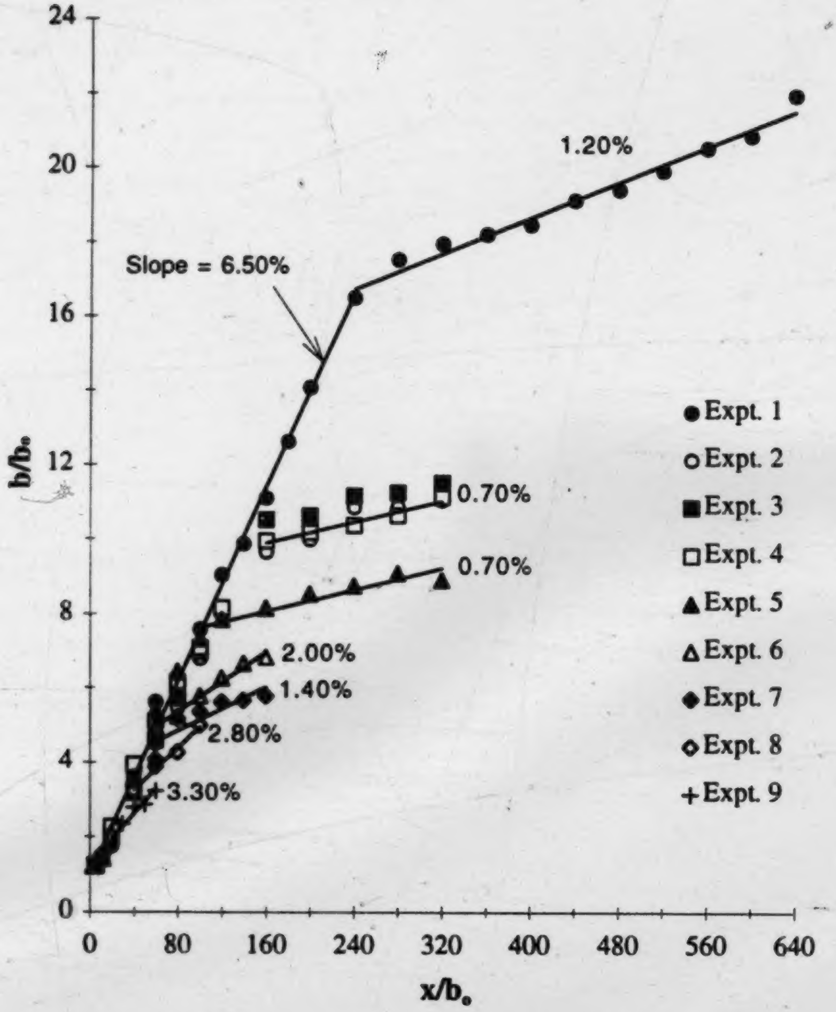

Fig. 5.19 Variation of the jet half-width with distance

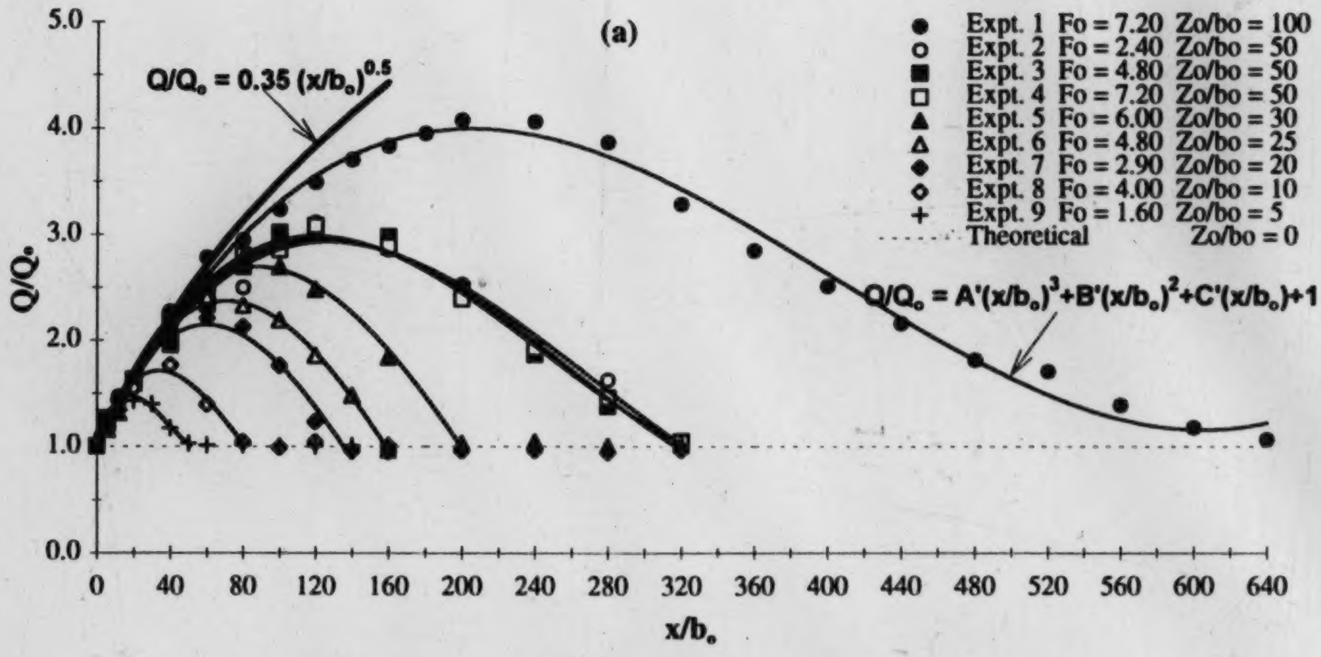

Fig. 5.20(a) Variation of the surface jet discharge with distance

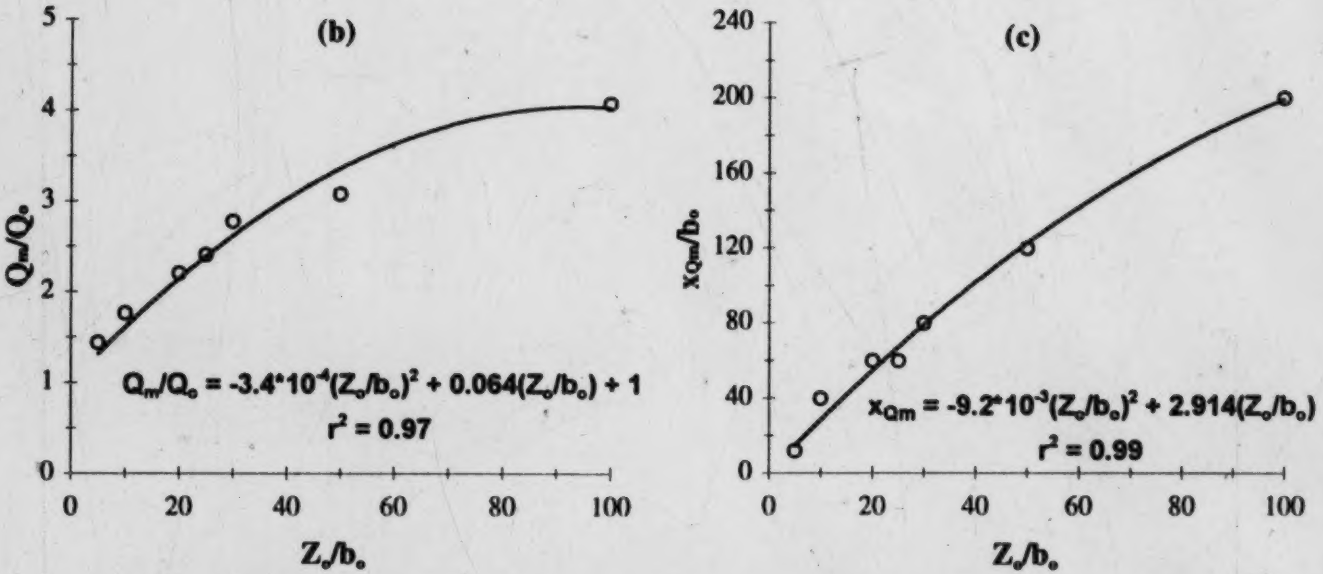

Fig. 5.20(b-c) Effect of Z_o/b_o on the magnitude and location of the maximum discharge

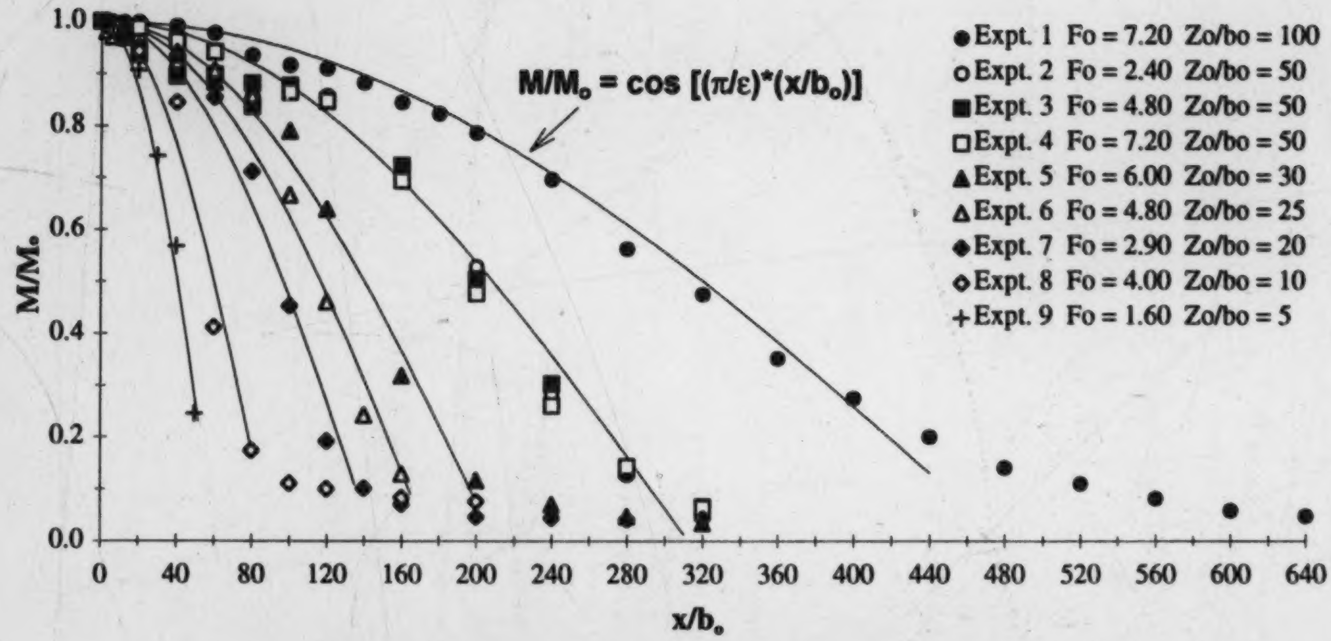

Fig. 5.21 Variation of the surface jet momentum flux with distance

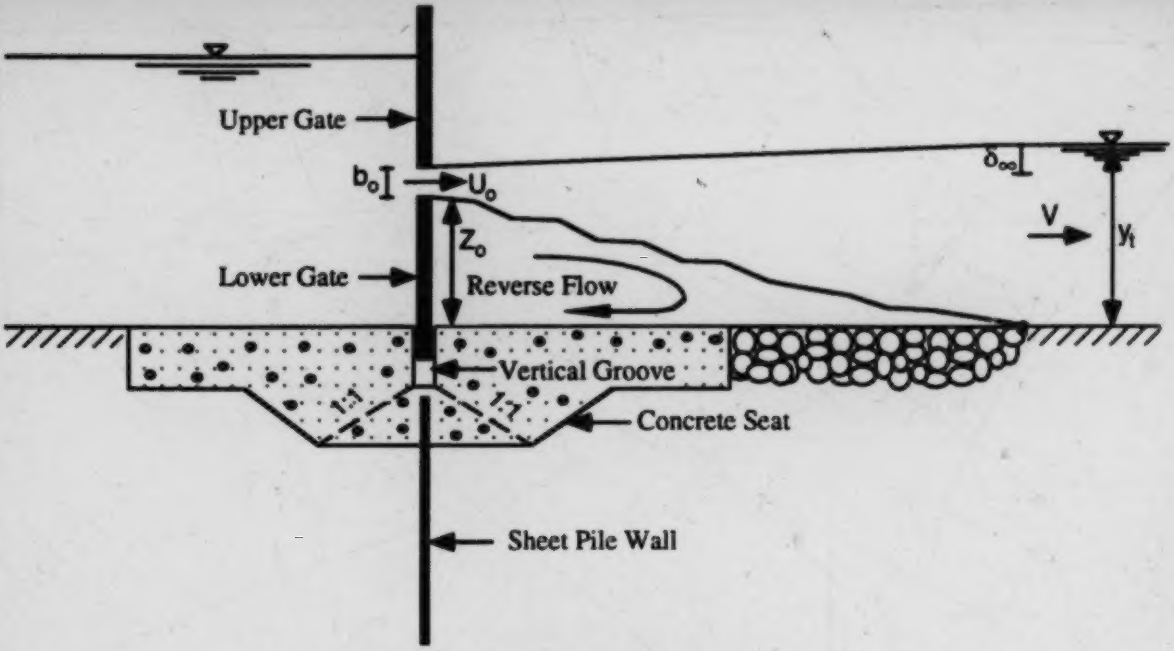
Upper Gate
b_o
U_o
δ_∞
V
y_t
Z_o
Lower Gate
Reverse Flow
Vertical Groove
1:1
1:1
Concrete Seat
Sheet Pile Wall

Fig. 5.22 Modified regulators

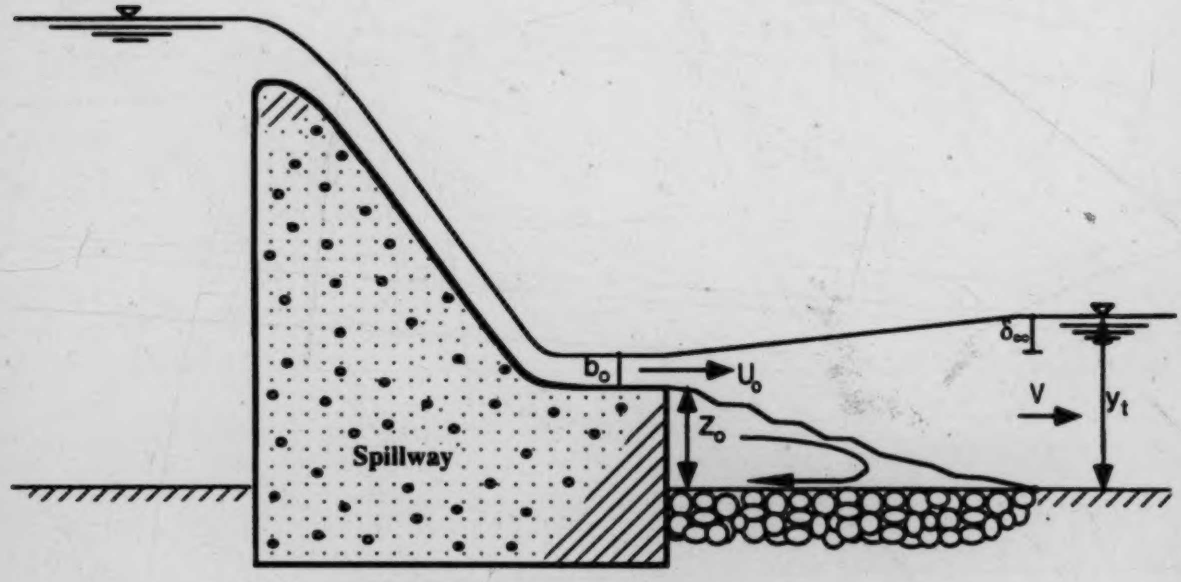
b_o
U_o
δ_∞
V
y_t
Z_o
Spillway

Fig. 5.23 Modified spillway

Chapter 6

Plane Turbulent Wall Jets in Shallow Tailwater*

6.1 Introduction

For turbulent jets discharged from slots or orifices in walls into large ambients at rest, it has been generally assumed (Albertson et al. (1950), Schlichting (1960), Rajaratnam (1976)) that the momentum flux would be preserved. In some experimental investigations (Miller and Comings (1957); Goldschmidt and Eskinazi (1966); Heskestad (1965) and Kotsovinos (1975)), it has been noticed that the momentum flux decayed to some extent at large distances from the origin of the jets. Kotsovinos (1978) noticed that the momentum flux could decay to about 80% of that at the source at a longitudinal distance equal to 100 b_o for plane turbulent jets where b_o is the slot width. Kotsovinos (1978) attributed this loss of momentum flux to the negative momentum carried by the entrained fluid which approached the jet at a angle of about $\pi/4$ radians from the forward direction of the jet. Based on an approximate integral analysis, Kotsovinos (1978) developed an equation to describe the variation of the momentum flux with the longitudinal distance from the nozzle producing the jet. Schneider (1985) attempted to explain this decay of momentum flux by combining the analysis of the jet with the flow in the region surrounding the jet. Schneider coupled the jet and the induced outer flow through momentum and volume balances.

Swean Jr. et al. (1989) studied the variation of momentum and mass fluxes as well as the growth for plane turbulent surface jets with limited depth of tailwater. They conducted 10 experiments to study the effect of the finite depth of tailwater on the characteristics of the surface jet and to observe the variation of the momentum and volume fluxes and the breakdown of the surface jet due to the limited depth of the ambient. They also used the experimental results of Vanvari and Chu (1974) and Rajaratnam and Humphries (1984). Their results showed a momentum decay and a break down (or variation from that of jets in infinite ambient) in the velocity and length scales due to the jet confinement. The study of Swean Jr. et al. (1989) provides a general understanding of the problem of turbulent jets with a finite depth of tailwater. However, their analysis did not consider the adverse pressure gradient in the momentum balance. As the depth of flow decreases in the vicinity of the gate, it is important to include the depression in the pressure force due to this decreasing depth.

---

*The main content of this chapter has been submitted to the Journal of Hydraulic Research of the International Association of Hydraulic Research for possible publication.

For plane turbulent wall (or bed) jets discharged into relatively deep tailwater, if the shear stress on the bed is neglected, it has been generally assumed (see for example: Rajaratnam 1976) that, as in the case of plane free jets, the momentum flux would be preserved. Since the plane wall jet model has been used to analyze a number of flows in hydraulic structures, wherein the tailwater depth may not even be very large, it was thought that it would be interesting and useful to study the variation of the momentum flux in a plane wall jet with a range of tailwater levels, including the effects of the bed friction.

The double-leaf gate energy dissipator was introduced in chapter 4 where the jet velocity and the momentum flux were found to decay rapidly. To understand the reasons behind this decay, it was important to study the behavior of plane turbulent jets, of simpler geometry, in shallow tailwater. In chapter 5, plane turbulent surface jet in shallow tailwater were presented. In this chapter, plane turbulent wall jets in shallow tailwater are presented.

This chapter presents the results of a theoretical and experimental investigation of plane turbulent wall jets with finite depth of tailwater, dealing with the growth of the jet, decay of the maximum velocity, the variation of the momentum and volume fluxes in the forward flow region of the wall jet, the variation of the shear stress on the bed and the effect of the depth of tailwater on these properties.

6.2 Theoretical Considerations

From the first glance, it might appear that the theoretical formulation of the plane wall jets is very similar to that of the plane surface jets with the only difference in the location of the nozzle. But there is a subtle difference related to the tailwater depth in the two problems which makes surface jets and wall jets distinguishable. In surface jets, the tailwater depth is divided into three parts which are, from bottom to top, the offset distance, the slot width and the rise of the water surface elevation above the upper edge of the slot (see Fig. 5.1(a)). The third factor, or the rise of the water surface elevation, is dependent on the jet thickness, the Froude number and the offset distance (see Eq. 5.5). The surface jet (by definition) issues from a slot with the water surface elevation exactly at the upper edge of the slot. Hence, any surface jet with a specific thickness, offset distance and Froude number can only form with a specific value of the tailwater depth. In other words, in the surface jet problem, the tailwater depth is dependent on the different characteristics of the jet. In the wall jet, the tailwater depth is an independent variable. In other words, a wall jet with a specific thickness and Froude number can form with an infinite number of tailwater depths. This subtle difference makes the theoretical formulation totally different in the two problems. In the surface jet problem, the tailwater depth was manipulated through its three components while in the wall jet it is treated as an independent variable.

Consider a plane turbulent wall jet of thickness b_0 with a flow rate per unit width of Q_0 and momentum flux per unit width of M_0 entering a rectangular channel, tangentially on its bed as shown in Fig. 6.1(a). Let U_0 be the velocity of the jet at the nozzle. The downstream control gate is adjusted so that the tailwater depth y_t is large enough to make the water level immediately downstream of the gate (housing the slot) horizontal. Taking the tailwater surface elevation as a reference, our experimental observations (presented later) show a depression, δ_w, in the water surface elevation at the gate (see Fig. 6.1(a-b) and Fig. 6.2). It appears that the depression in the water surface elevation at the vicinity of the wall is created to produce an adverse pressure gradient to drive the return flow above the wall jet, for the jet entrainment.

Assuming hydrostatic pressure distributions on the gate containing the slot and at the downstream section where the expanding wall jet attaches to the water surface and occupies the whole depth, and that the velocity distribution at the nozzle and the downstream section is uniform (see Fig. 6.1(b)), a theoretical analysis was performed and is presented herein.

6.2.1 Neglecting the bed shear stress

The continuity and the momentum equations could be written as

$$U_o b_o = V y_t \tag{6.1}$$

$$M_o - M_\infty = \gamma\delta_w(y_t - \delta_w) + 0.5\gamma\delta_w^{\ 2} \tag{6.2}$$

where V is the uniform velocity at the downstream section, M_∞ and M_o are, respectively, the momentum fluxes, per unit width, at the downstream section and at the nozzle, and γ is the weight per unit volume of water.

Multiplying Eq. 6.1 by $\rho U_o V$ where ρ is the mass density of water and rearranging, Eq. 6.1 is rewritten as

$$\frac{M_\infty}{M_o}=\frac{V}{U_o}=\frac{1}{y_t/b_o}=\frac{1}{\eta} \qquad (6.3)$$

where η is the tailwater depth ratio equal to y_t/b_o.

Dividing Eq. 6.2 by M_o and rearranging, Eq. 6.2 becomes

$$1-\frac{M_\infty}{M_o}=\frac{2\theta(\eta-\theta)+\theta^2}{2F_o^{\,2}} \qquad (6.4)$$

where θ is the depression ratio at the gate, equal to δ_s/b_o and F_o is the Froude number at the slot equal to $[U_o/(gb_o)^{0.5}]$ and g is the acceleration due to gravity.

Solving equations 6.3 and 6.4, we obtain a quadratic equation in θ

$$\eta\theta^2-2\eta^2\theta+2(\eta-1)F_o^{\,2}=0 \qquad (6.5)$$

The negative root of Eq. 6.5 was considered as the relevant solution which can be written as

$$\theta=\eta-\sqrt{\eta^2-2\left(\frac{\eta-1}{\eta}\right)F_o^{\,2}} \qquad (6.6)$$

Eq. 6.6 indicates that in submerged flows below the gate (either submerged jumps or wall jets), if the Froude number and the tailwater depth ratio are known, the drop in the water surface elevation at the gate can be predicted. According to Eq. 6.6, an increase in the Froude number F_o results in a larger drop in the water surface elevation at the gate and its vicinity which in turn creates a steeper water surface slope for driving a larger return flow.

If θ_f and η_f are the values of θ and η for the corresponding free hydraulic jump at the gate, it can be shown that

$$\theta_f = (\eta_f - 1) \tag{6.7}$$

Combining Eqs. 6.6 and 6.7 results in a quadratic equation, the solution of which can be written as

$$\eta_f = 0.5\left(\sqrt{1 + 8F_o^2} - 1\right) \tag{6.8}$$

This is the well-known Belanger equation.

If $F_{\delta w}$ is the reduction in the hydrostatic pressure force at the gate corresponding to a depression of δ_w in the water surface elevation, it can be shown that

$$\frac{F_{\delta w}}{M_o} = 1 - \frac{M_\infty}{M_o} = \frac{\eta - 1}{\eta} \tag{6.9}$$

6.2.2 Considering the bed shear stress

The integrated bed shear stress from the gate up to the section at which the wall jet surfaces can be expressed in terms of the inlet momentum flux as

$$F_\tau = \int_{x=0}^{x=Le} \tau \, dx = \varepsilon M_o \tag{6.10}$$

where F_τ is the integrated bed shear stress per unit width, τ is the bed shear stress at a distance x from the gate, ε is the shear force coefficient equal to F_τ/M_o and L_s is the distance from the gate to the section where the wall jet surfaces which may be referred to as the length of the recirculation region or surface eddy. The momentum balance equation can be written as

$$M_o - M_\infty - \varepsilon M_o = \gamma\delta_w(y_t - \delta_w) + 0.5\gamma\delta_w^{\,2} \tag{6.11}$$

Eq. 6.1 & Eq. 6.11 can be rearranged and solved together to finally give a quadratic equation in θ

$$\eta\theta^2 - 2\eta^2\theta + 2[(1-\varepsilon)\eta - 1]F_o^2 = 0 \tag{6.12}$$

The negative root of Eq. 6.12 was considered as the relevant solution and can be written as

$$\theta = \eta - \sqrt{\eta^2 - 2\left(\frac{\eta(1-\varepsilon)-1}{\eta}\right)F_o^{\,2}} \tag{6.13}$$

Eq. 6.13 is the general form of Eq. 6.6 with the bed shear stress taken into consideration. Substituting Eq. 6.7 in Eq. 6.13 results in a cubic equation

$$\eta_f^{\,3} - \left(1 + 2F_o^{\,2} - 2\varepsilon F_o^{\,2}\right)\eta_f + 2F_o^{\,2} = 0 \tag{6.14}$$

The above equation has three real roots. The following root is considered as the relevant solution

$$\eta_f = \frac{2}{\sqrt{3}}\sqrt{1+2F_o^2}\cos(\phi/3) \tag{6.15}$$

where ϕ is given by the equation

$$\phi = \tan^{-1}\left(\frac{\sqrt{\frac{4\left(1+2F_o^2-2\varepsilon F_o^2\right)^3}{27}-\left(2F_o^2\right)^2}}{-\left(2F_o^2\right)^2}\right) \tag{6.16}$$

Eq. 6.15 is the general equation of the free hydraulic jump and Eq. 6.8 (known as Belanger Equation) is a special case that is only valid when the bed shear stress is neglected. These equations, although of different forms, give the same results when the shear force coefficient ε is equal to zero.

It should be mentioned that the evaluation of M_∞/M_o is not affected by the consideration of the bed shear stress and is still represented by Eq. 6.3. With the inclusion of the bed shear stress, Eq. 6.9 becomes

$$\frac{F_{\delta w}}{M_o} = 1 - \frac{M_\infty}{M_o} - \frac{F_\tau}{M_o} = \frac{\eta(1-\varepsilon)-1}{\eta} = \frac{\eta-1}{\eta} - \varepsilon \tag{6.17}$$

Based on these theoretical formulations, the variation of θ, which is equal to the depression in the water surface elevation at the wall in terms of the slot width, with η =

y_t/b_o, is shown in Fig. 6.3(a) as solutions of Eq. 6.13 and Eq. 6.6, with and without considering the bed shear stress, respectively (ε equal to 0.15 and 0), for values of the Froude number varying from 2 to 10. Fig. 6.3(a) also shows the θ-η relationship for the free jump represented by Eq. 6.7. Fig. 6.3(a) shows that for any Froude number, the maximum value of θ occurs in the free jump when there is no submergence and that θ decreases after the jump gets submerged and η increases. The values of η at the intersections of Eq. 6.6 and Eq. 6.13 with the free jump line, for the different Froude numbers, are given by Eq. 6.8 and Eq. 6.15 respectively. In Fig. 6.3(a), for a given Froude number, the continuous line shows the variation of θ for $\varepsilon = 0.15$ whereas a string of symbols shows the corresponding variation for ε equal to zero. Fig. 6.3(a) shows that the inclusion of the bed shear stress reduces the water surface depression at the gate. This difference increased with the Froude number for a constant η and decreased as η increased for a constant Froude number.

In Fig. 6.3(b) three sets of curves are shown for Froude numbers equal to 10.0, 6.00 and 3.00 for several values of ε from 0 to 0.25. For a given η, the height of the spread between the set of curves including the string of points, increased with the Froude number, indicating the importance of considering the bed shear stress for relatively large Froude numbers. For a given Froude number, the corresponding height decreased as η increased, reaching almost zero for very large values of η, indicating the importance of the bed shear stress for relatively shallow tailwater.

Fig. 6.4(a-b) show the variation of the sequent depth ratio η_f, in a free hydraulic jump, with the Froude number F_o and the shear force coefficient ε, respectively. The curves in Fig. 6.4(a) were drawn for the shear force coefficient ε varying from 0.00 to 0.25, whereas the curves in Fig. 6.4(b) were drawn for three values of the Froude number of 10.0, 5.0 and 2.0. In Fig. 6.4(a), the bold line represents Eq. 6.8 (Belanger equation) and the white circles represent Eq. 6.15 (for $\varepsilon = 0.00$). Clearly, both equations gave identical results though they have different forms. All the other curves, in Fig. 6.4(a), represent Eq. 6.15 for different values of ε. While Fig. 6.4(a) shows that the deviation between Eq. 6.8 and Eq. 6.15 increases with the Froude number, Fig. 6.4(b) indicates the same for the increase in ε.

Eq. 6.3 is plotted in Fig. 6.5 to show the variation of the normalized momentum flux (M_w/M_0) with the tailwater depth ratio η. Fig. 6.5 shows that the momentum flux decays rapidly with η up to 30 after which the decrease is rather negligible. It was found that the minimum momentum flux, in terms of that at the nozzle, is equal to 0.04, 0.02, 0.013 and 0.01, respectively, for η equal to 25, 50, 75 and 100. Fig. 6.5 also shows the variation of the loss of hydrostatic pressure force at the gate due to the depression in the water surface in terms of the momentum flux at the slot with the tailwater depth ratio η with and without bed friction. It can be observed in Fig. 6.5 that the bed shear stress reduces ($F_{\delta w}/M_0$) by an amount of ε.

6.3 Dimensional Analysis

Considering the problem illustrated in Fig. 6.1(a), any property (m) of the flow can be expressed as a function of various parameters of the flow, fluid and channel dimensions as

$$m = f(U_o, g, b_o, y_t, \rho, \mu) \tag{6.18}$$

The above relation can be represented in a dimensionless form as follows

$$M = f'\left[\frac{U_o}{\sqrt{gb_o}}, \frac{\rho U_o b_o}{\mu}, \frac{y_t}{b_o}\right] \tag{6.19}$$

The above relation shows that any property of the flow can be expressed as a function of the Froude number, the Reynolds number and the tailwater depth ratio. For large values of the Reynolds number, $R = \rho U_o b_o/\mu$, where ρ and μ are respectively the mass density and dynamic viscosity of the fluid, viscosity is known to have negligible effects. Hence, Eq. 6.21 becomes

$$M = f''[F_o, \eta] \tag{6.20}$$

Eq. 6.20 shows that the main variables affecting the different characteristics of the flow are the Froude number and the tailwater depth ratio.

6.4 Experimental Study

6.4.1 Experimental arrangement

Plane turbulent wall jets were produced in a flume, 0.446 m wide, 0.60 m deep and 7.6 m long, with aluminum bottom and Plexiglas sides (see Fig. 6.6). Two pumps were used to supply the head-tank feeding the flume. The discharge was measured by a magnetic flow-meter located in the supply line. Water entered the flume under a sluice gate with a streamlined lip thereby producing an uniform jet with a thickness of b_o (see Fig. 6.7). A tailgate was used to control the tailwater depth in the flume.

A Prandtl tube with an external diameter of 3.0 mm was used to measure the time-averaged longitudinal velocity u (see Fig. 6.8). Velocity distributions of the forward and backward flows, were measured along vertical sections at different longitudinal distances from the nozzle producing the jet. The Prandtl tube was also used as a Preston tube for measuring the bed shear stress (Preston (1954); Patel (1965)). All of the measurements were taken in the middle third of the flume.

One transducer (Validyne model DP45-16 Northridge, Calif) was used in the experiments to measure the pressure difference indicated by the Prandtl tube. The output of the transducer was connected to a Macintosh IIfx computer. When the pressure difference was outside the transducer range (±25.4 mm), the pressure connections were switched to a manometer board (see Fig. 6.8). The computer displayed the results on a strip chart on the screen in real time. When the required number of samples (usually 5000) were recorded at each point with a sampling rate of 40 samples/s, the computer processed all the samples to obtain the mean value and the standard deviation for each variable and saved the results in an open file. The computer programs used in the experiments were written in LabView Language.

6.4.2 Experiments

Table 1 shows the primary details of the experiments of series A. The first two experiments were conducted for the present study and the results of experiments 3 to 6 (conducted in the same flume) were taken from Wu and Rajaratnam (1995). In these experiments, the tailwater depth ratio η was equal to 50, 50, 45, 35, 30 and 25 and the Froude number was equal to 8.0, 4.0, 5.5, 7.5, 7.5 and 7.5, respectively. The submergence factor (Rajaratnam, 1965) defined as $S = (y_t - y_2)/y_2 = (\eta/\eta_f - 1)$, ranged approximately between 2.00 to 9.00 where y_2 in Table 1 is the subcritical sequent depth for the hydraulic jump, obtained from the Belanger equation. The Reynolds number of the jet was in the range of 12500 to 42900. Figs. 6.9(a-d) show the wall jets produced with the tailwater depth ratio equal to 25, 30, 40 and 50 respectively.

A further series of experiments (series B) were conducted mainly to measure the drop in the water surface elevation at the gate, from that of the tailwater, as well as the length of the surface eddy. The series B experiments were conducted for Froude numbers equal to 2, 4, 6, 8, 10 with the tailwater depth ratio η varying from η_f to 50.

6.5 Experimental Results and Analysis

6.5.1 Eddy length

As soon as the jet issues from the slot, a recirculating flow region starts to develop above the jet (see Fig. 6.1(b)). If L_e is the length of the recirculating region (or the eddy length), it could be written that

$$L_e = f\left[U_o, b_o, g, \rho, \mu, y_t\right] \tag{6.21}$$

Using the Pi theorem, it can be shown that

$$\frac{L_e}{b_o} = f_1\left[\frac{y_t}{b_o}, \frac{U_o}{\sqrt{gb_o}}, \frac{\rho U_o b_o}{\mu}\right] \tag{6.22}$$

For large values of the Reynolds number, viscous effects may be neglected and Eq. 6.22 reduces to

$$\frac{L_e}{b_o} = f_2\left[\frac{y_t}{b_o}, F_o\right] \tag{6.23}$$

As the sequent-depth ratio η_f is a function of mainly the Froude number (Eq. 6.8), the above equation may be rewritten as

$$\frac{L_r}{b_o} = f_3[\eta, \eta_f] \qquad (6.24)$$

If Eq. 6.24 is rewritten as

$$\frac{L_r}{b_o} = 6\eta_f + k(\eta - \eta_f) \qquad (6.25)$$

Wherein the length of the free jump has been assumed to be equal to approximately 6 times the subcritical sequent depth and k is an empirical coefficient. The coefficient k was evaluated using the observations made in this study and those of Rajaratnam (1965) and was found to be equal to 4.0. Hence Eq. 6.25 can be written as

$$\frac{L_r}{b_o} - 6\eta_f = 4.0(\eta - \eta_f) \qquad (r^2 = 0.97) \qquad (6.26)$$

where r^2 is the correlation coefficient. The experimental results are shown plotted in Fig. 6.10 with $(L_r/b_o - 6\eta_f)$ versus $(\eta - \eta_f)$.

6.5.2 Velocity profiles

Figs. 6.11(a-f) show typical velocity fields along with the water surface profiles of the wall jets for experiment 1 to experiment 6 respectively. They show the velocity profiles in the forward as well as reverse flows at several sections with x/b_o varying from 6 to 200. In these figures, y is the distance above the bed. In Figs. 6.11(a-f), it may be noticed that the water surface in the vicinity of the gate is approximately horizontal and a rise in the water surface elevation may be observed further downstream. The depression in the tailwater elevation at the gate is also shown in Fig. 6.11(a-f). The strong shear layer that separates the forward and the backward flows is distinct in the six experiments. No velocity measurements could be taken within this layer. The section at which the jet surfaces was found using dye injection. The maximum reverse velocity, at any station, was found to occur at or very close to the water surface. The maximum reverse velocity for any experiment was found to occur at a distance of $L_e/2$ from the gate where L_e is the length of the surface eddy.

6.5.3 Wall jet

Returning to the discussion on the velocity field, velocity measurements in the forward flow clearly show the structure of the wall jet. To test for the similarity of the velocity profiles, the maximum velocity, u_m, at any station was chosen as the velocity scale. It occurs at a distance of δ above the bed where δ is the boundary layer thickness. The length scale, b, is equal to y where $u = 0.5u_m$ and $\partial u/\partial y < 0$ (see Fig. 6.1(c)). Figs. 6.12(a-b) show the velocity distributions and the similarity profiles in the developing flow region, which is the region between the slot and the end of the potential core. Fig. 6.12(b) shows the variation of u/u_m with y/b for a station located approximately in the middle of the developing region (at $x/b_o = 6$). Experiments 1, 2 and 3 showed similar distributions of the velocity profiles, at this station, in the developing flow region.

The velocity distributions and the similarity profiles in the fully-developed flow region ($x/b_o \geq 12$) are shown in Fig. 6.13(a-l) for experiment 1 to experiment 6, respectively which clearly show the wall jet features. In the similarity profiles, u_m and b were chosen as the velocity and length scales, respectively. Fig. 6.14 shows a consolidated plot of all the data for the six experiments. Although some velocity profiles were taken for larger values of x/b_o, these profiles were excluded as they were somewhat different from those shown in Fig. 6.13. A study of these profiles established that except for the sections far away from the nozzle (in the region where the water surface elevation begins to rise (see Fig. 6.11(a-f)), the velocity distributions are similar. The similarity profile follows that of the classical plane turbulent wall jet except near the upper end of the profile where it showed a linear distribution. This deviation, between the similarity profile of the present data and that of the classical wall jet profile, is possibly due to the interaction between the forward and the backward flows.

6.5.4 Velocity and length scales

Having found that the velocity profiles in the forward flow are similar, it is necessary to study the variation of the velocity scale, u_m, and the length scale, b, with the distance x. Fig. 6.15(a) shows the decay of the maximum velocity with the longitudinal distance from the nozzle. The maximum velocity at the nozzle was varied from 1.25 to 2.86 m/s and u_m was measured for x up to about 2.00 m. At the last section, the maximum velocity was in the range of 0.25-0.60 m/s. Fig. 6.15(b) shows the decay of the maximum velocity u_m at any section in terms of the velocity of the jet at the nozzle U_o with the normalized distance from the gate x/b_o. The decay of the maximum velocity shows the existence of two stages. The first stage represents the plane wall jet with large depth of tailwater and starts at the end of the development region. The decay of the normalized velocity scale in this region can be described by the following equation

$$\frac{u_m}{U_o} = \frac{4.00}{\sqrt{x/b_o}} \tag{6.27}$$

The coefficient in Equation 6.27 is larger than the value of 3.5 suggested for plane turbulent wall jets with large submergence (Rajaratnam 1976). The second stage of the velocity decay starts at a distance x_o from the gate, where the observations begin to deviate from the curve described Eq. 6.27 and the maximum velocity decays more rapidly. This behavior can be noticed more easily in Fig. 6.15(c) which shows the variation of $(U_o/u_m)^2$ with x/b_o where Eq. 6.27 would plot as a straight line. The decay of the maximum velocity in this second stage is linear and can be described by the equation

$$\frac{u_m}{U_o} = A\left(\frac{x}{b_o}\right) + B \qquad (6.28)$$

where B is a constant equal to 0.82 and A was found to be a function of the tailwater depth ratio $\eta = y_t/b_o$ and was described by the equation

$$A = 7 \cdot 10^{-5}(\eta - 100) \qquad (r^2 = 0.95) \qquad (6.29)$$

The value of x_o was also found to be a function of the tailwater depth ratio (see Fig. 6.15(d)) and is described by the equation

$$\left(\frac{x_o}{b_o}\right) = 2.85(\eta - 2.00) \qquad (r^2 = 0.995) \qquad (6.30)$$

These considerations show that as the tailwater depth ratio decreases, the length of the first stage of decay decreases and the maximum-velocity decay will be more rapid. It was also found that the Froude number does not have any significant effect on the velocity decay.

The growth of the length scale of the jet (or half-width) with distance is shown in Fig. 6.16. The growth rate was 0.076 for x/b_o up to about 120, which is somewhat larger than the value of 0.068 suggested by Rajaratnam (1976) for plane turbulent wall jets with large submergence. The growth rate of the jet half-width was found to change at a particular value of x/b_o. For experiments 1, 2 and 3, this breakdown occurred at x/b_o = 140, 140 and 120, respectively, whereas for experiments 4, 5 and 6 this breakdown was not clear. After the breakdown, the jet half-width grew with a rate of 0.20 in experiment 1 and 2 and 0.35 in experiment 3. It is interesting to note that the breakdown in the growth of the jet half-width (for at least the three experiments) and in the decay of the maximum-velocity occurred at the same location, x_o, which is described by Eq. 6.30.

6.5.5 Wall-jet discharge

For all the experiments, at every section where velocity observations were made, the forward flow rate Q and momentum flux per unit width M were calculated as the sum of the fluxes through thin strips (whose thicknesses varied from 2.5 to 25 mm). Fig. 6.17(a) shows the variation of the relative discharge Q/Q_o in the wall jet with distance x/b_o. A study of Fig. 6.17(a) shows that the relative discharge increases with the relative distance at the same rate as that of the wall jet with large tailwater up to a certain section and then deviates from it, to eventually reach the value of one. Secondly, the maximum value of the relative discharge decreases from about 4 for $y_t/b_o = 50$ to 2.5 for $y_t/b_o = 25$. If x_{Qm} is the longitudinal distance where the relative discharge reaches the maximum value, x_{Qm}/b_o was found to decrease from about 140 for y_t/b_o = 50 to about 65 for $y_t/b_o = 25$. The variation of Q/Q_o with x/b_o could be represented by the cubic equation

$$\frac{Q}{Q_o} = A'\left(\frac{x}{b_o}\right)^3 + B'\left(\frac{x}{b_o}\right)^2 + C'\left(\frac{x}{b_o}\right) + 1 \qquad (6.31)$$

where the coefficients A', B' and C' were found to be functions of the tailwater depth ratio, η as described by the following equations

$$A' = -0.43168 \bullet 10^{-10}\eta^4 + 0.68303 \bullet 10^{-8}\eta^3 - 0.40273 \bullet 10^{-6}\eta^2 + 0.10608 \bullet 10^{-4}\eta - 0.10802 \bullet 10^{-3}$$

$$(r^2 \neq 1.00) \qquad (6.32)$$

$$B' = 0.26089 \bullet 10^{-8}\eta^4 - 0.41366 \bullet 10^{-6}\eta^3 + 0.24496 \bullet 10^{-4}\eta^2 - 0.64942 \bullet 10^{-3}\eta + 0.66369 \bullet 10^{-2}$$

$$(r^2 = 1.00) \qquad (6.33)$$

$$C' = 0.58533 \bullet 10^{-7}\eta^4 - 0.91320 \bullet 10^{-5}\eta^3 + 0.51054 \bullet 10^{-3}\eta^2 - 0.11970 \bullet 10^{-1}\eta + 0.12740$$

$$(r^2 = 1.00) \qquad (6.34)$$

For a wall jet with a very large value of η, the variation of Q/Q_o with x/b_o should be independent of the tailwater depth ratio and for such a jet, Q/Q_o would be proportional to $(x/b_o)^{0.50}$. This equation is shown plotted in Fig. 6.17(a) with the value of the coefficient in this relation equal to 0.35.

Figs. 6.17(b-c) show linear variations of the maximum value of the relative flow Q_m/Q_o and the distance where this occurs x_{Qm}/b_o with the tailwater depth ratio η and these variations could be described by the equations

$$\frac{Q_m}{Q_o} = 0.058\eta + 1.00 \qquad (r^2 = 0.97) \qquad (6.35)$$

$$\frac{x_{Qm}}{b_o} = 2.77\eta \qquad (r^2 = 0.89) \qquad (6.36)$$

6.5.6 Bed shear stress

The integrated bed shear stress is one of the main forces involved in the momentum balance equation and it was essential to evaluate, experimentally, the bed shear stress and its scales. Fig. 6.18(a) shows the variation of the bed shear stress with distance. Fig. 6.18(b) shows the variation of the skin friction coefficient $C_{fo} = \tau/(\rho U_o^2/2)$ with x/b_o. At $x/b_o = 0$, C_{fo} was in the range of 0.006 to 0.007. A breakdown in the skin friction coefficient C_{fo} can be observed in Fig. 6.18(b) and this breakdown is very similar to that occurred in the maximum velocity decay (see Fig. 6.15(b-c)). The distance at which this breakdown occurred could also be described by Eq. 6.30. Fig. 6.18(c) shows a similarity profile where the maximum shear stress τ_m and b_τ, which is the distance between τ_m and $0.5\tau_m$, were chosen as the shear and length scales respectively. The distributions are quite similar up to a distance of $4b_\tau$ after which the similarity breaks down. The length scale b_τ was found to be a function of the tailwater depth, y_t and the Reynolds number, R and this relationship can be described by the equation

$$\frac{b_\tau}{y_t} = 6.10^{-6}R + 0.3 \qquad (r^2 = 0.97) \qquad (6.37)$$

Fig. 6.18(d) shows the variation of the shear force coefficient $\varepsilon_x = F_{\tau x} / M_o$ with x/b_o where ε_x and $F_{\tau x}$ are respectively the shear force coefficient and the integrated bed shear stress at a longitudinal distance x measured from the slot. The values of ε_x and $F_{\tau x}$, where $x = L_e$, would be ε and F_τ. At $x/b_o = 160$, the shear force coefficient ranged between 0.12-0.15 with an average value of 0.135. The variation of an average value of ε_x with x/b_o could be represented by the following equation

$$\varepsilon_x = -0.6635 \cdot 10^{-9}\left(\frac{x}{b_o}\right)^4 + 0.2717 \cdot 10^{-6}\left(\frac{x}{b_o}\right)^3 - 0.4125 \cdot 10^{-4}\left(\frac{x}{b_o}\right)^2 + 0.3198 \cdot 10^{-2}\left(\frac{x}{b_o}\right) \qquad (r^2 = 0.98) \qquad (6.38)$$

Fig. 6.19 shows a plot of Eq. 6.13 with θ against η for ε equal to 0.12 & 0.15 and for the Froude number equal to 10.0, 8.0, 6.0, 4.0 and 2.0 along with the experimental data of series B. In Fig. 6.19, the experimental observations of series B are well represented by Eq. 6.13 with ε in the range of 0.12-0.15.

6.5.7 Wall-jet momentum flux

It was mentioned earlier that the wall jet could lose a substantial portion of its momentum flux as it travels downstream when the depth of tailwater is relatively shallow, due to the entrainment of the recircultaing flow with opposite momentum. Fig. 6.20 shows the variation of the normalized momentum flux of the wall jet with the normalized distance from the nozzle for different tailwater depth ratios. Fig. 6.20 also shows that the losses in the normalized momentum flux are 0.980, 0.978, 0.971, 0.967 and 0.960 for tailwater depth ratios equal to 50, 45, 35, 30 and 25, respectively.

The momentum flux may be considered preserved for a distance of x_{M1}, measured from the gate, after which it starts to decay. If x_{M2} is the distance at which the momentum flux approaches zero, a simple function was found to describe the decay in the momentum flux and is written as

$$\frac{M}{M_o} = \cos\left[\left(\frac{x/b_o - x_{M1}/b_o}{x_{M2}/b_o - x_{M1}/b_o}\right)\pi/2\right] \tag{6.39}$$

It should be noted that for the range of η used in this study, the value of x_{M2}/b_o is approximately equal to the normalized eddy length L_e/b_o and hence Eq. 6.26 could be used to predict L_e/b_o for use in Eq. 6.39. Further, x_{M1}/b_o was found to increase from 50 for $\eta = 25$ to about 75 for $\eta = 50$ and the variation of x_{M1}/b_o with η can be described by the following equation

$$\frac{x_{M1}}{b_o} = -0.0181\eta^2 + 2.3855\eta \qquad (r^2 = 1.00) \tag{6.40}$$

It is interesting to see that the distance at which the momentum flux starts to decay, x_{M1}, is very close to the distance at which the relative discharge, Q/Q_o, deviates from the corresponding curve of the wall jets in deep tailwater (see Fig. 6.17(a)).

6.6 Conclusions

For turbulent wall jets in shallow tailwater, it has been shown theoretically and experimentally that the momentum flux in the forward flow region of the wall jet is not preserved. In the theoretical study, the momentum loss was evaluated at a section just downstream of the line of the jet attachment to the free surface. The depression in the water surface elevation and the loss in the hydrostatic pressure force at the wall were evaluated with and without the bed shear stress. The experimental results showed that the length of the return-flow region is dependent on the tailwater depth ratio and the Froude number. The velocity profiles in the wall jet were found to be similar, in the developing as well as in the developed regions. Two stages were seen to exist in the decay of the maximum velocity in the region of fully developed flow. The rate of the velocity decay in the first stage was independent of the relative depth of the tailwater whereas the faster rate in the second stage depended on it. The length of the first stage of decay was directly proportional to the tailwater depth ratio. The length scale of the jet grew at a rate of 0.076 in the early stage and the rate of growth was much larger in the second stage. The volume flux in the wall jet with limited tailwater was affected significantly. The momentum flux was preserved for a certain distance after which it decayed rapidly. The momentum decay was correlated with the tailwater depth ratio, the eddy length and the relative longitudinal distance. On the whole, the results from this study highlight the effect of limited tailwater depth on the behavior of plane turbulent wall jets.

6.7 References

Albertson, M. L., Dai. Y. B., Jensen, R. A. & Rouse, H. (1950). "Diffusion of submerged jets." Trans. ASCE, 115, 639-664.

Goldschmidt, V., and Eskinazi, S. (1966). "Two phase turbulent flow in a plane jet." Trans. ASME, Series E, J. Appl. Mech., 33(4), 735-747.

Heskestad, G. (1965). "Hot wire measurements in a plane turbulent jet." Trans. ASME, Series E, J. Appl. Mech., 32(4), 721-734.

Kotsovinos, N. E. (1975). "A study of the entrainment and turbulence in a plane turbulent jet." W. M. Keck Lab. Hydr. Water Resources, Calif. Inst. Tech. Rept. KH R-32.

Kotsovinos, N. E. (1978). "A note on the conservation of the axial momentum of a turbulent jet." J. Fluid Mech., 87(7), pp. 55-63.

Miller, D. R., and Comings, E. W. (1957). "Static pressure distribution in the free turbulent jet." J. Fluid Mech., 3(10), pp. 1-16.

Patel, V. C. (1965). "Calibration of the Preston tube and limitations on its use in pressure gradients." J. Fluid Mech., Vol. 23, pp. 185-208.

Preston, J. H. (1954). "The determination of turbulent skin friction by means of Pitot tubes." J. Royal Aero. Soc., Vol. 54, pp. 109-121.

Rajaratnam, N. (1965). "Flow below a submerged sluice gate as a wall jet problem." 2nd Australation Conf. on Hydraulics and Fluid Mechanics, Auckland, New Zealend.

Rajaratnam, N. (1976). Turbulent Jets. Elsevier Publishing Co, The Netherlands, 304p.

Rajaratnam, N., and Humphries, J. A. (1984). "Turbulent non-buoyant surface jet." J. Hydr. Res., 22(2), pp. 103-115.

Schlichting, H. (1960). "Boundary layer theory." 4th Edn. McGraw-Hill: New York.

Schneider, W. (1985). "Decay of momentum flux in submerged jets." J. Fluid Mech., 154(5), pp. 91-110.

Swean Jr, T. F., Ramberg, S. E., Plesniak, M. W. Stewart., M. B. (1989). "Turbulent surface jet in channel of limited depth." J. Hydr. Engrg., ASCE, 115(12), pp. 1587-1606.

Vanvari, M. R., and Chu, V. H. (1974). "Two-dimensional turbulent surface jets of low Richardson number." Tech. Report No. 74-2 [FML], Fluid Mech. Lab., Dept. of Civ. Engrg. and Appl. Mech., McGill Univ., Montreal, Canada.

Wu, S. and Rajaratnam, N. (1995). "Free jumps, submerged jumps and wall jets." J. Hydr. Res., 33(2), pp. 197-212.

Table 6.1. Primary details of experiments (series A)*

Expt. (1)	b_o (mm) (2)	W (mm) (3)	U_o (m/s) (4)	F_o (5)	y_t (mm) (6)	y_2 (mm) (7)	$\eta = y_t/b_o$ (8)	$S = \eta/\eta_f - 1$ (9)	R (x 10^3) (10)
1	10	446	2.50	8.0	500	108	50	3.63	25.00
2	10	446	1.25	4.0	500	52	50	8.68	12.50
3	10	446	1.72	5.5	440	73	45	5.04	17.20
4	15	446	2.86	7.5	530	151	35	2.51	42.90
5	15	446	2.86	7.5	460	151	30	2.05	42.90
6	15	446	2.86	7.5	390	151	25	1.59	42.90

* Experiments 3, 4, 5 and 6 were conducted by Wu and Rajaratnam (1995)

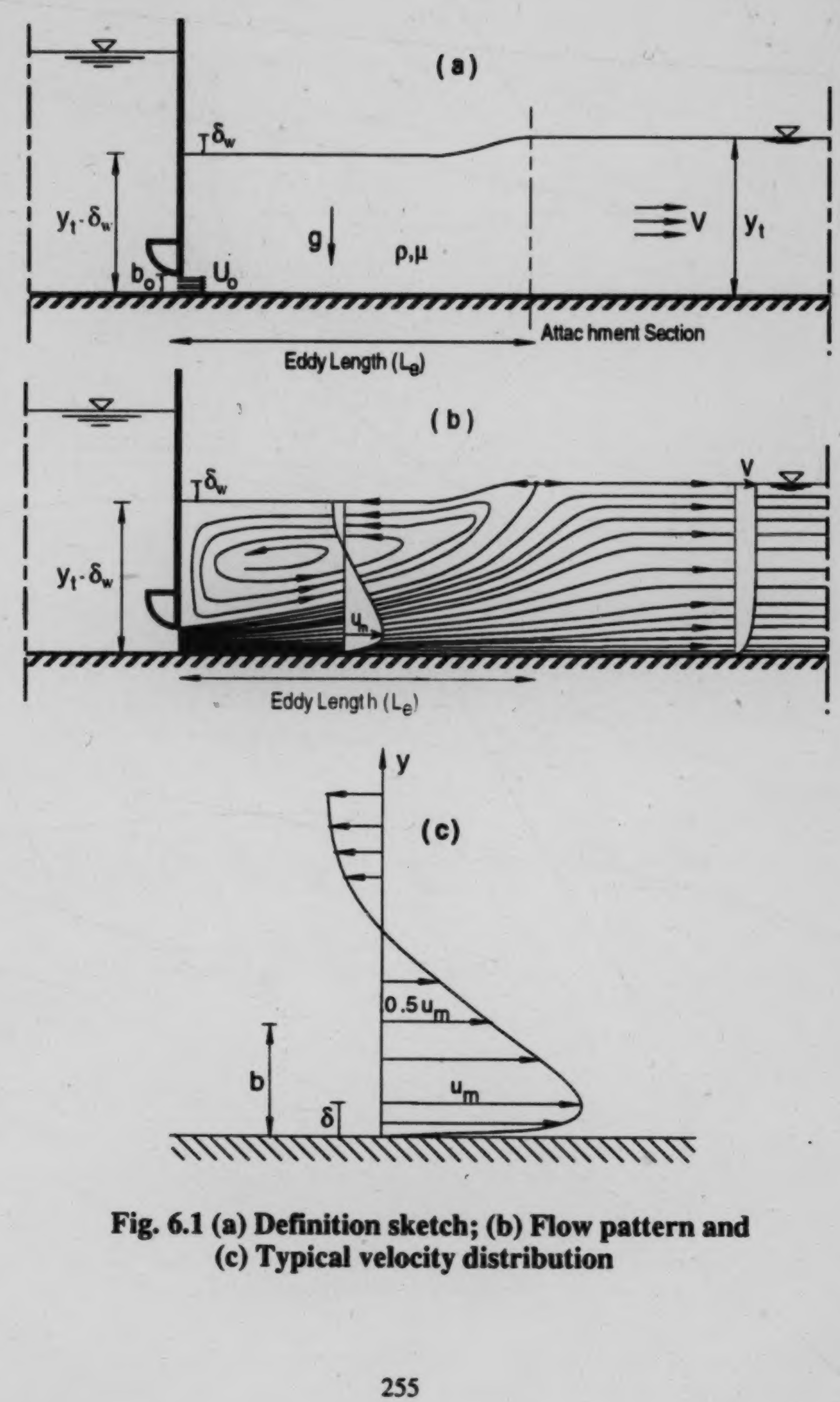
(a)
δw
yt - δw
bo
Uo
g
ρ,μ
V
yt
Attac hment Section
Eddy Length (Le)
(b)
δw
yt - δw
um
V
Eddy Length (Le)
y
(c)
0.5 um
b
um
δ

Fig. 6.1 (a) Definition sketch; (b) Flow pattern and (c) Typical velocity distribution

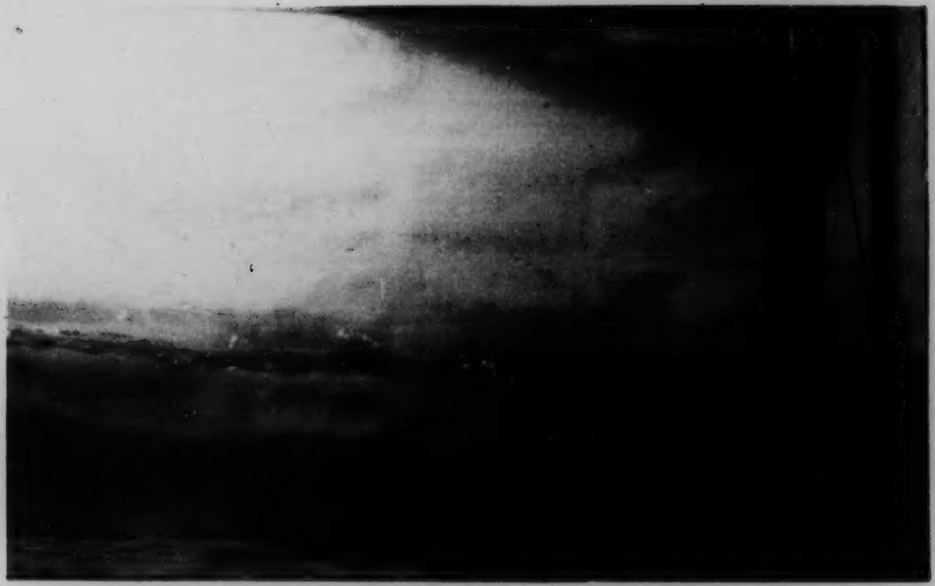

Fig. 6.2 Water surface elevation ($F_o = 8$, $y_t/b_o = 25$)

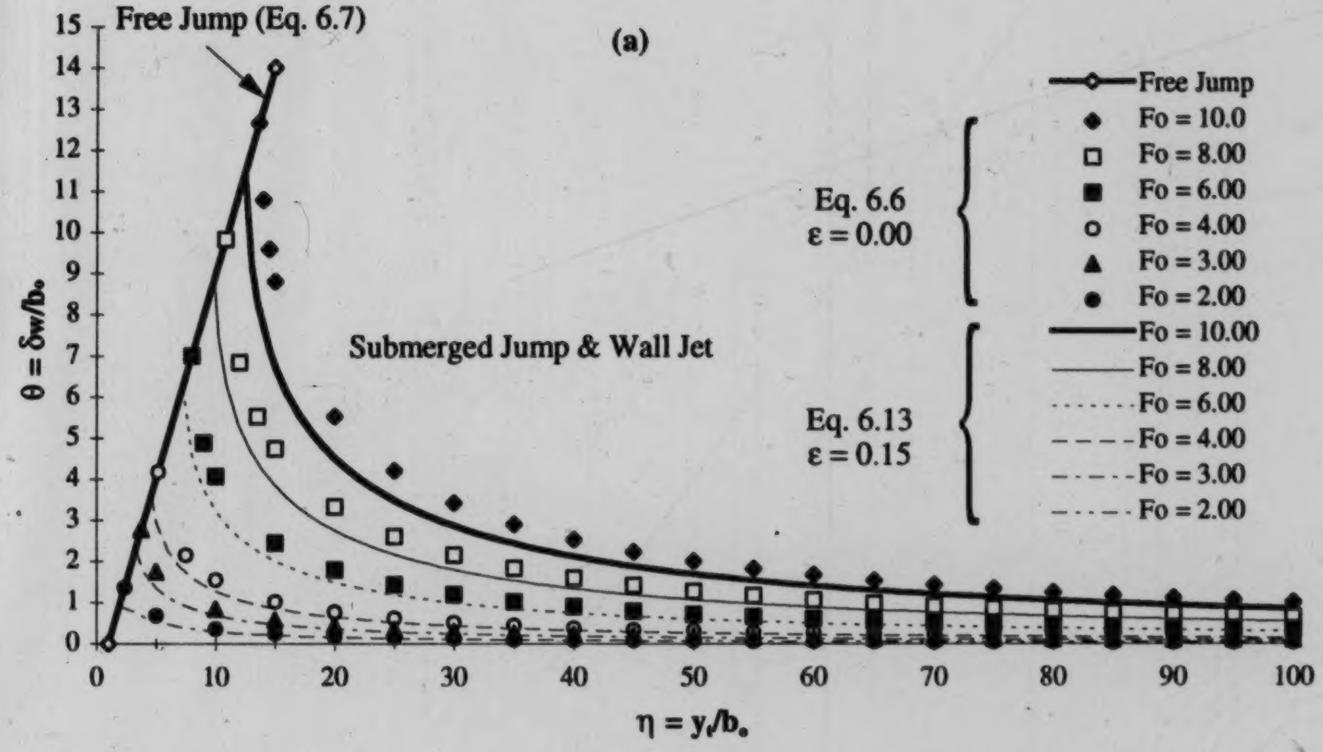

Fig. 6.3(a) Variation of θ with η for various Froude numbers F_o, with and without shear stress

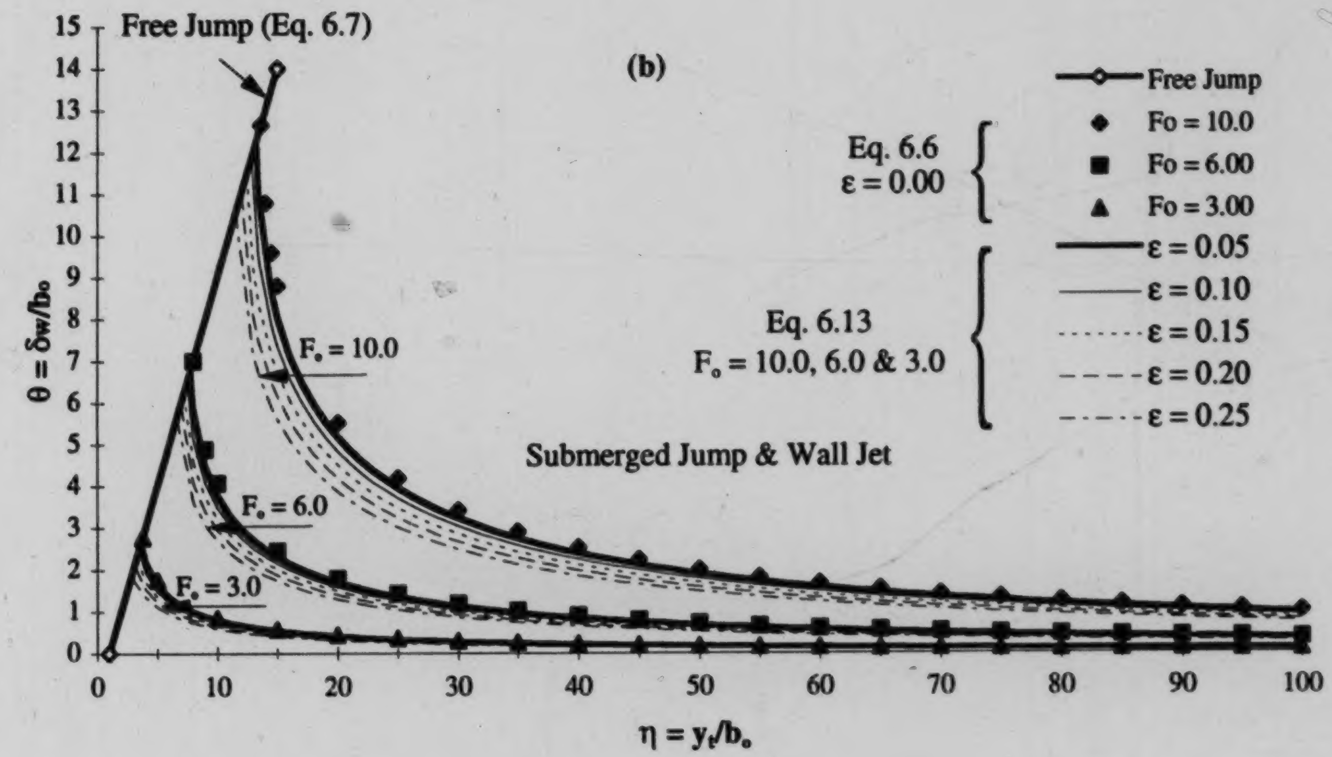

Fig. 6.3(b) Variation of θ with η for various shear coefficients ε

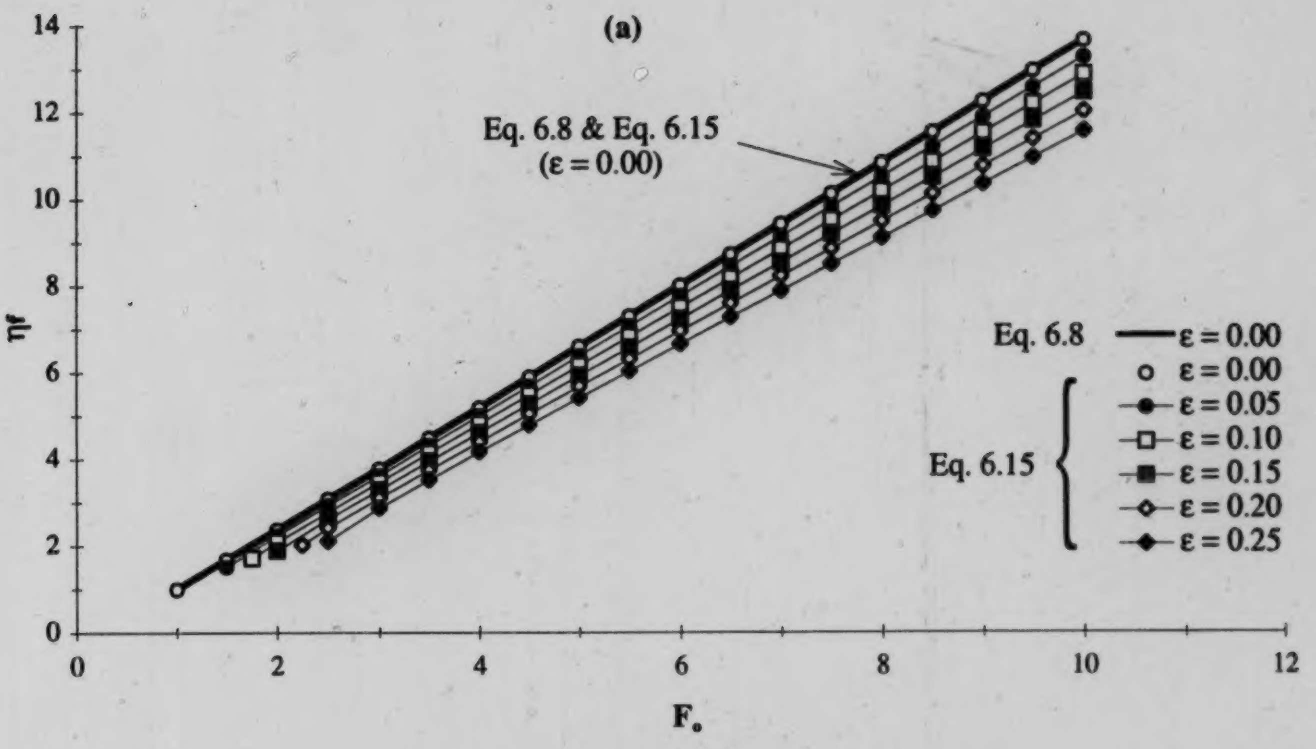

Fig. 6.4(a) Variation of η_f with F_o for various values of ε

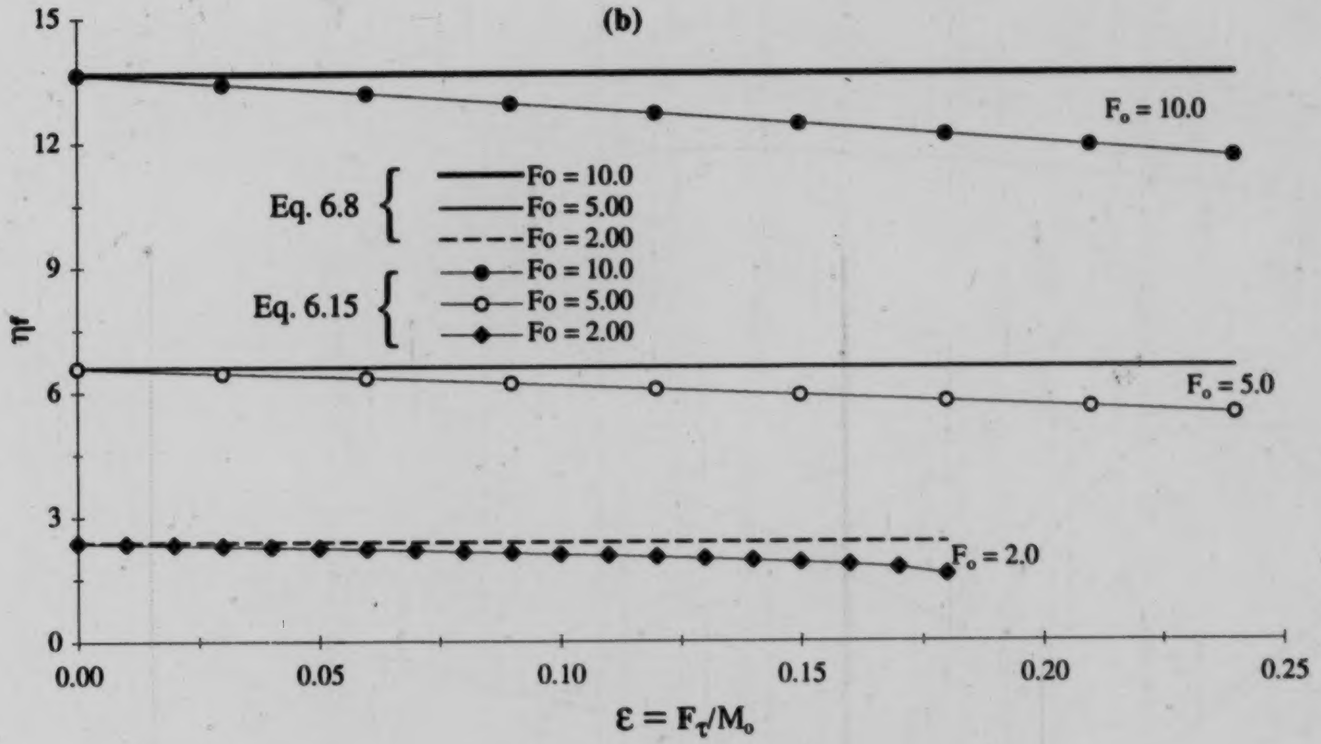

Fig. 6.4(b) Variation of η_r with ε for various values of F_o

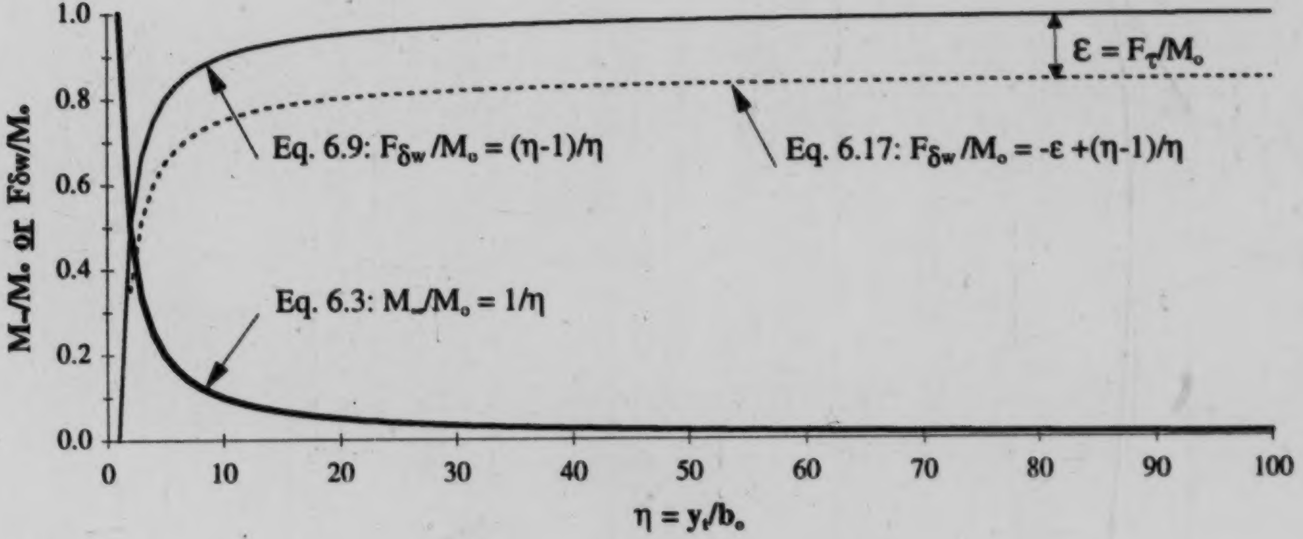

Fig. 6.5 Variation of ($M_{\sim}/M_o$) and ($F_{\delta w}/M_o$) with (η)

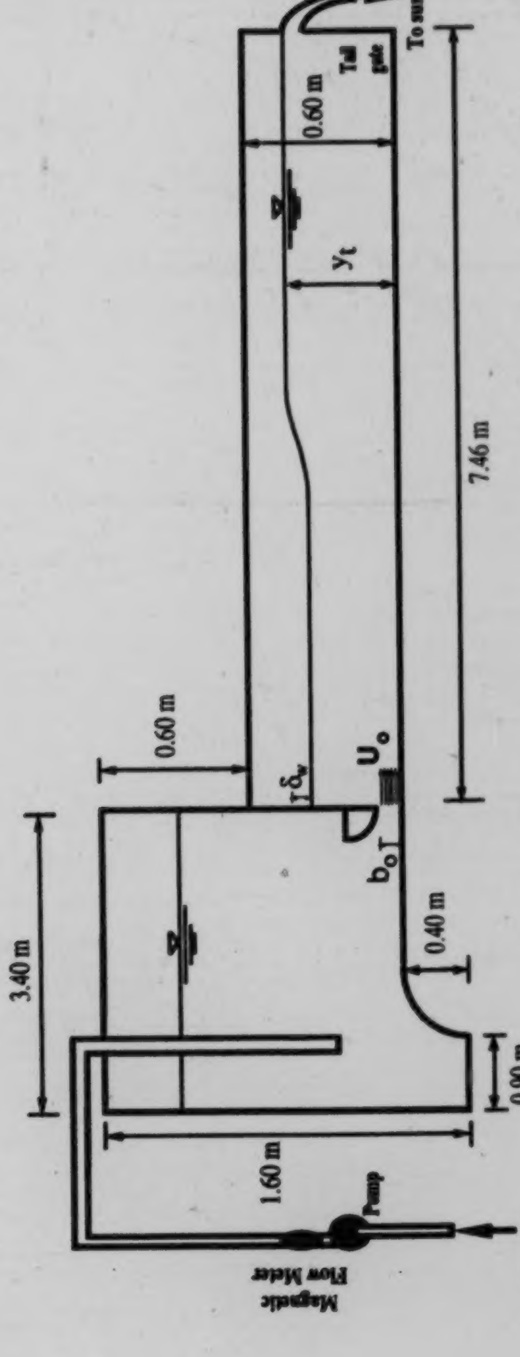
To sump
Tail gate
0.60 m
y_t
7.46 m
0.60 m
δ_w
U_o
b_o
0.40 m
3.40 m
0.90 m
1.60 m
Pump
Magnetic Flow Meter
From sump

Fig. 6.6 Experimental flume

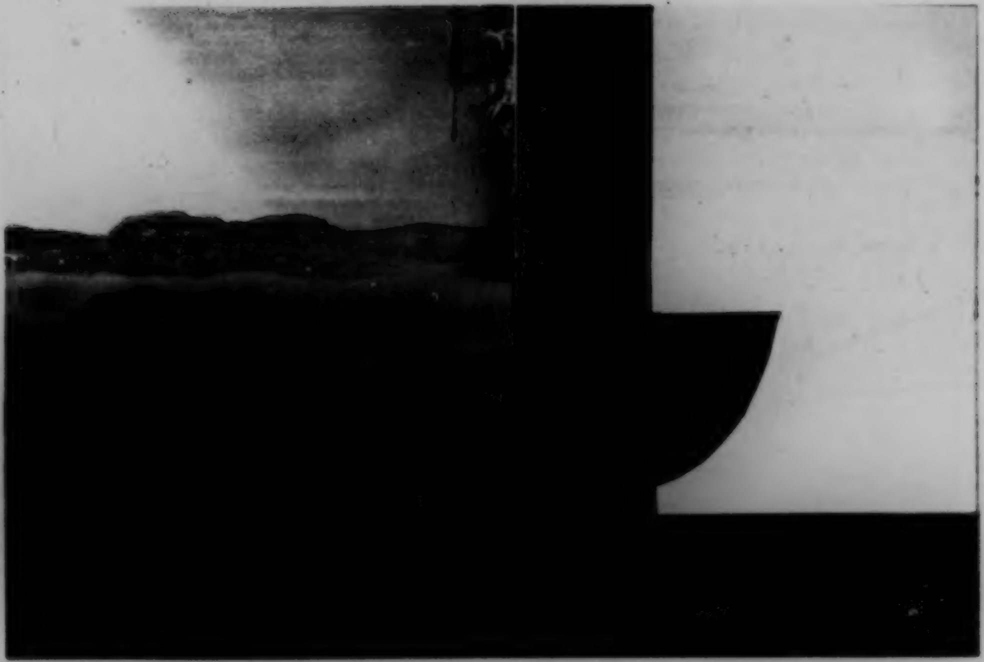

Fig. 6.7 Streamlined entrance to produce an uniform jet of thickness b_o

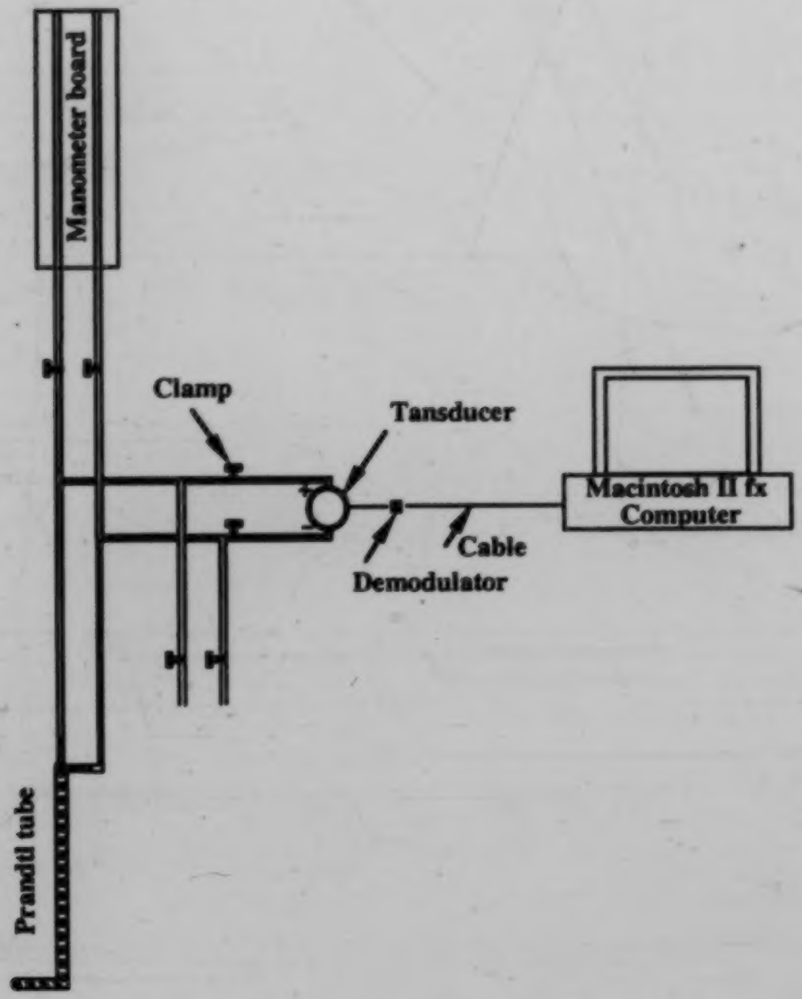
Manometer board
Clamp
Tansducer
+
-
Macintosh II fx Computer
Cable
Demodulator
Prandtl tube

Fig. 6.8 Prandtl tube

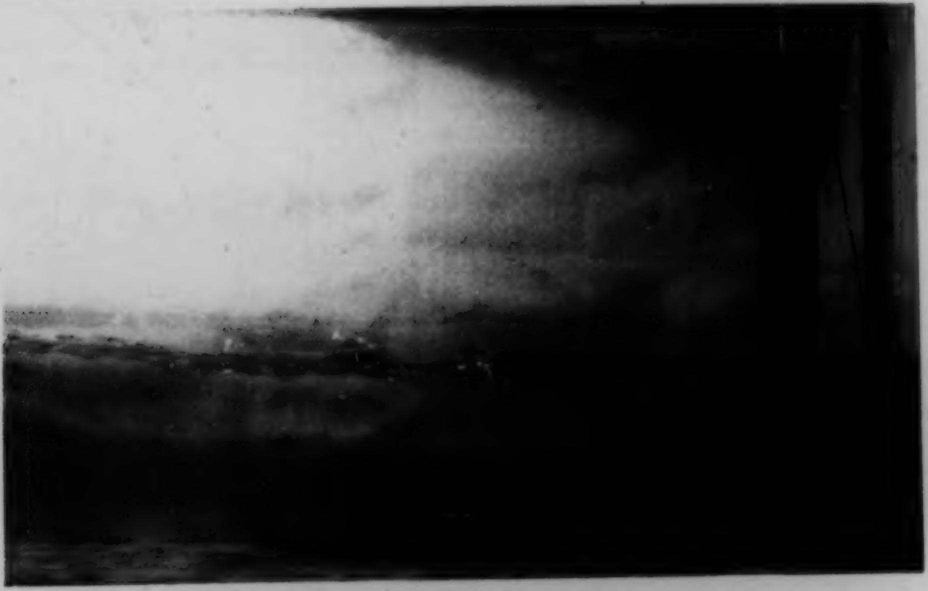

Fig. 6.9(a) Wall jet ($F_o = 8$, $y_t/b_o = 25$)

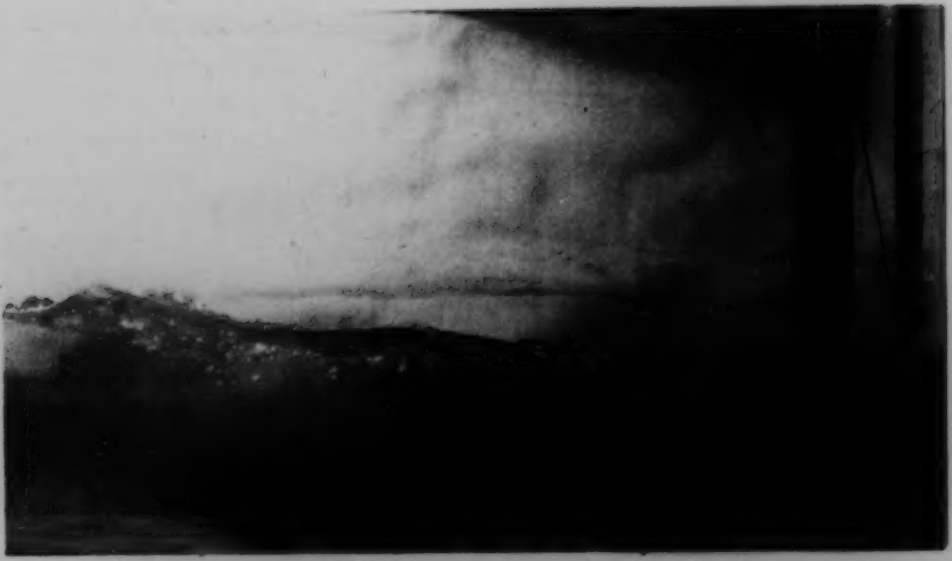

Fig. 6.9(b) Wall jet ($F_o = 8$, $y_t/b_o = 35$)

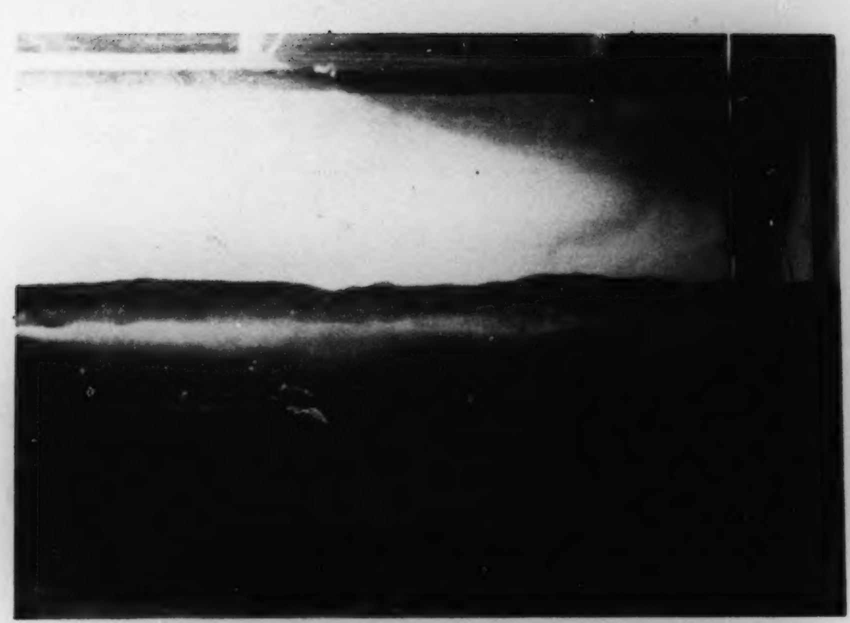

Fig. 6.9(c) Wall jet ($F_o = 8$, $y_t/b_o = 40$)

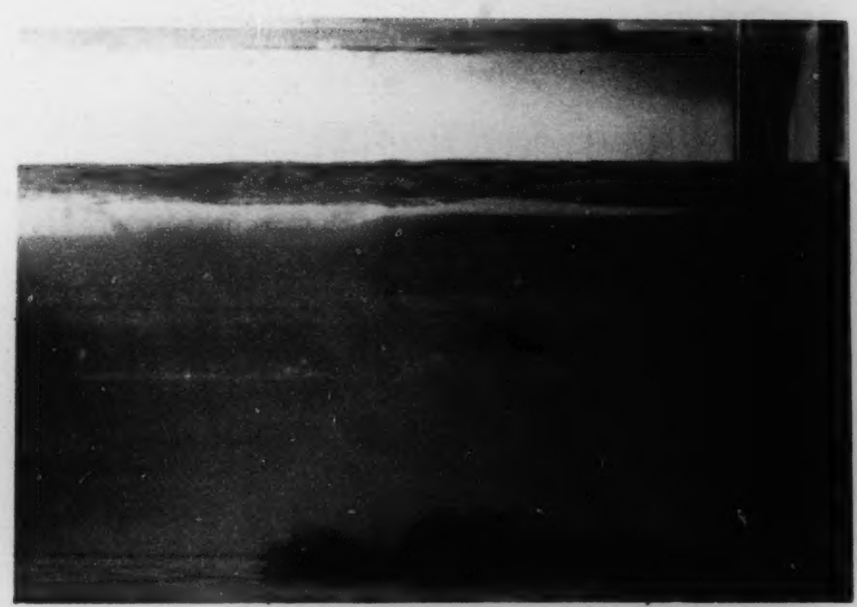

Fig. 6.9(d) Wall jet ($F_o = 8$, $y_t/b_o = 50$)

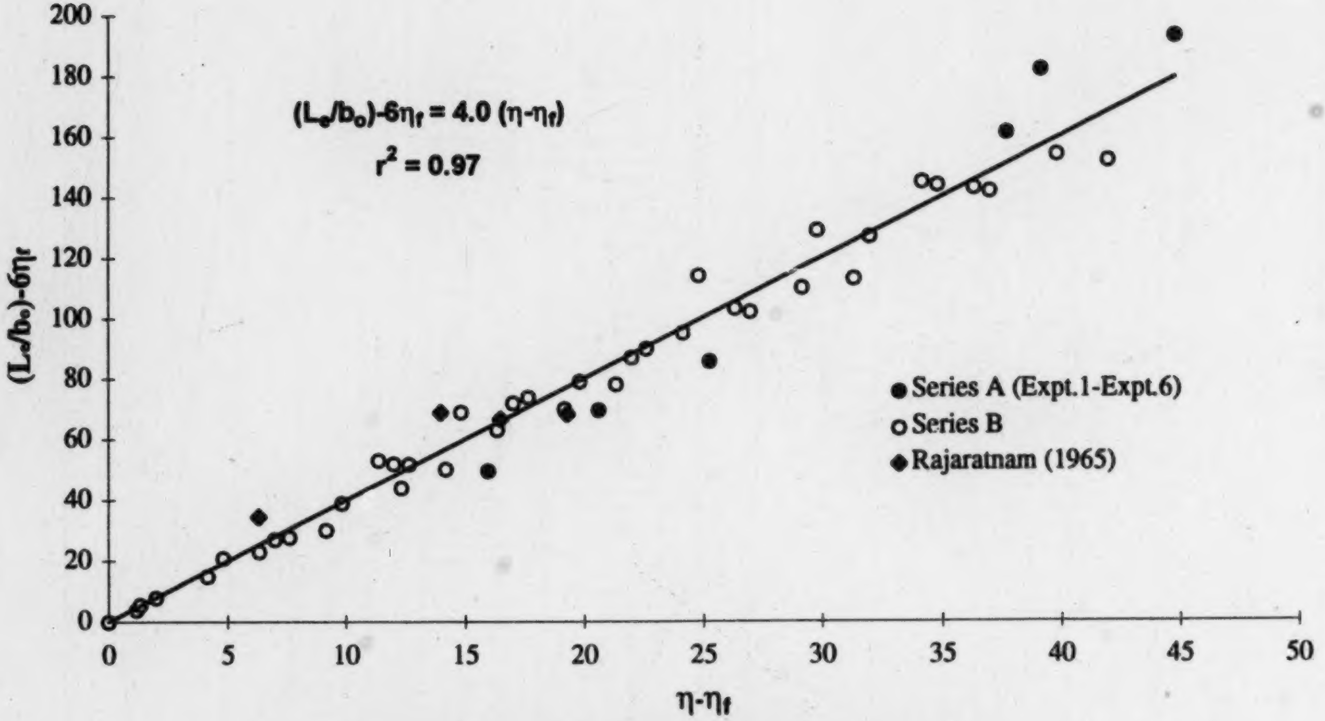

Fig. 6.10 Variation of the eddy length L_e/b_o with $(\eta-\eta_f)$

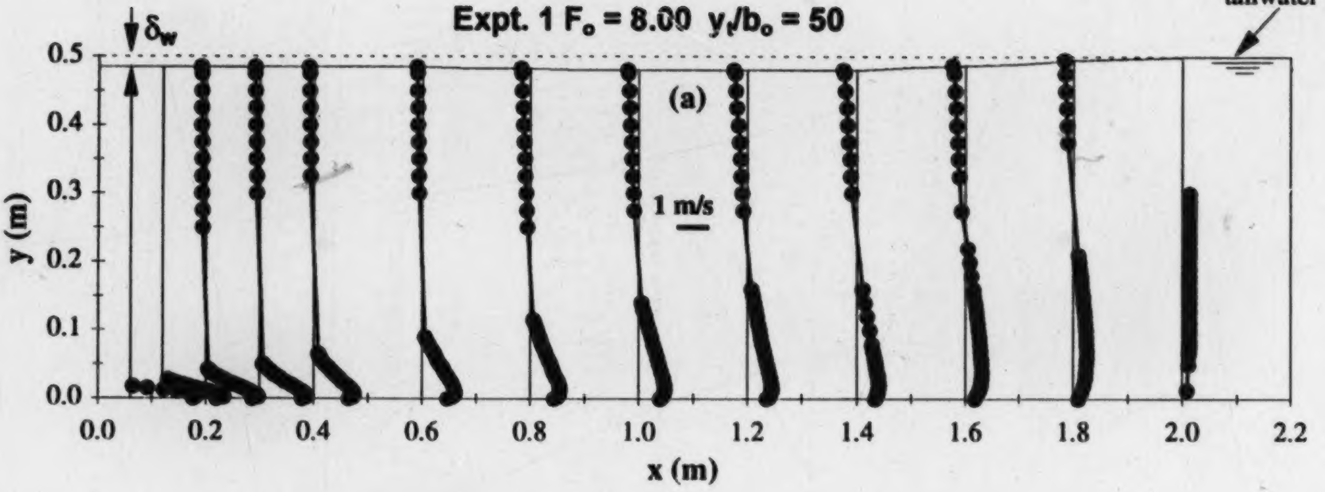

Fig. 6.11(a) Typical velocity fields of wall jets in shallow tailwaters (Expt. 1)

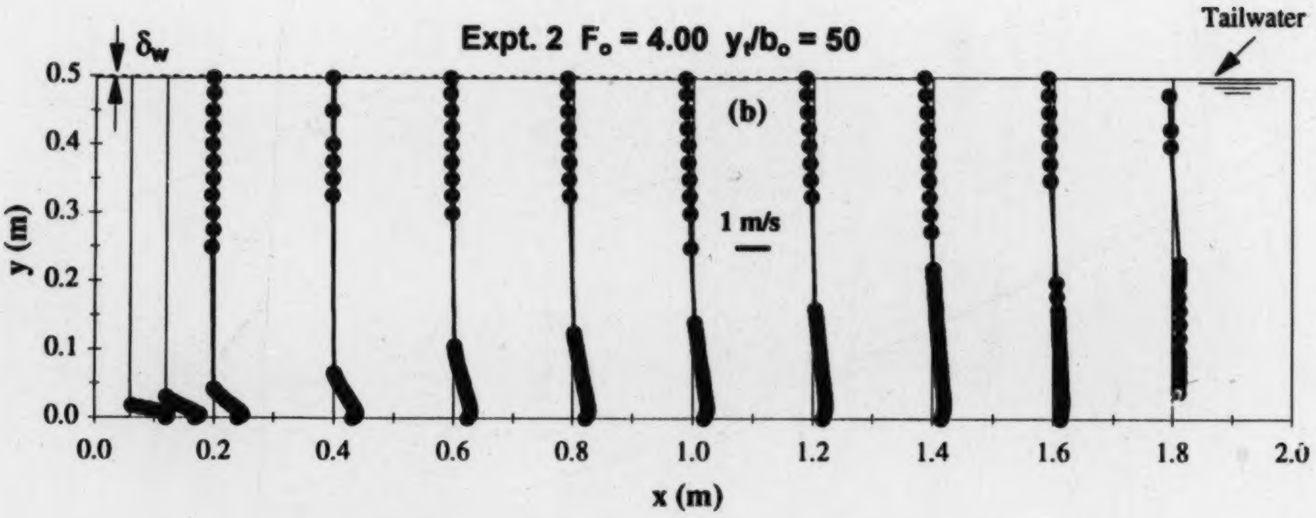

Fig. 6.11(b) Typical velocity fields of wall jets in shallow tailwaters (Expt. 2)

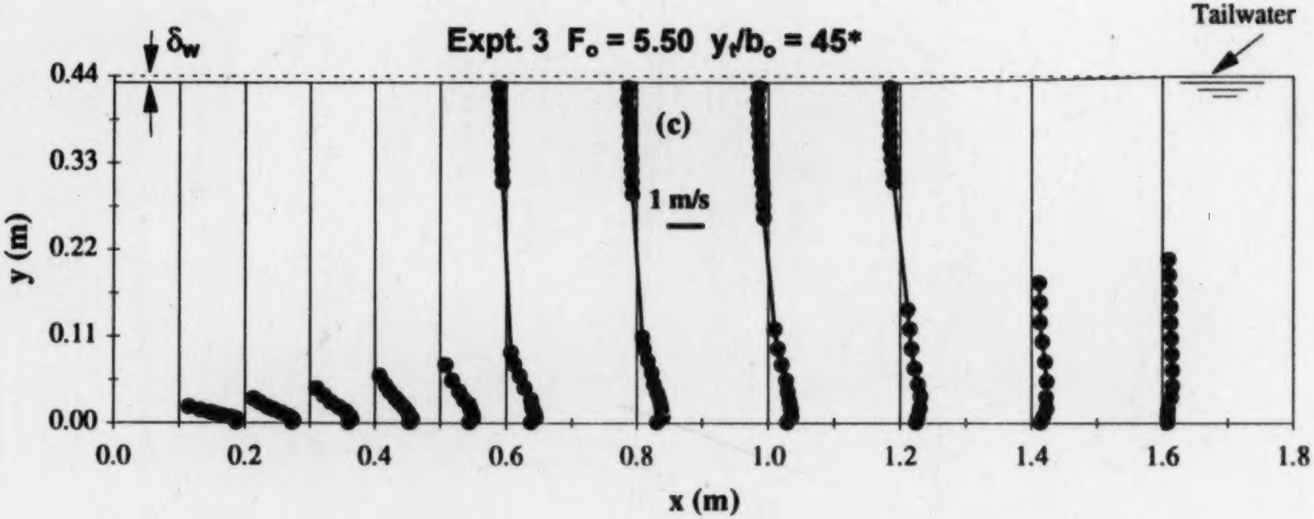

Fig. 6.11(c) Typical velocity fields of wall jets in shallow tailwaters (Expt. 3)
* Wu and Rajaratnam (1995)

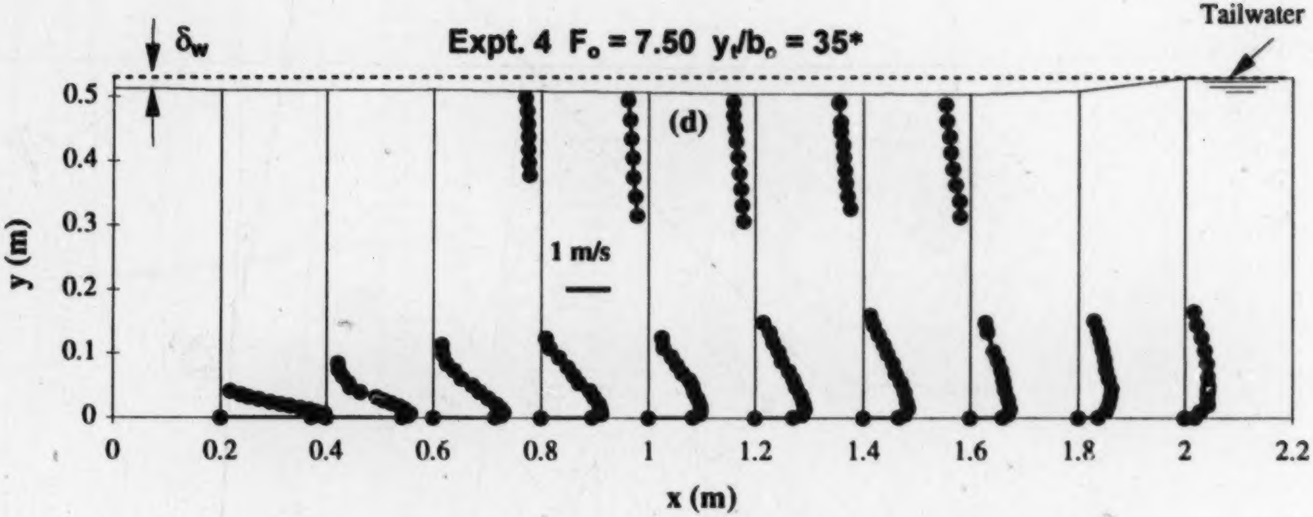

Fig. 6.11(d) Typical velocity fields of wall jets in shallow tailwaters (Expt. 4)
* Wu and Rajaratnam (1995)

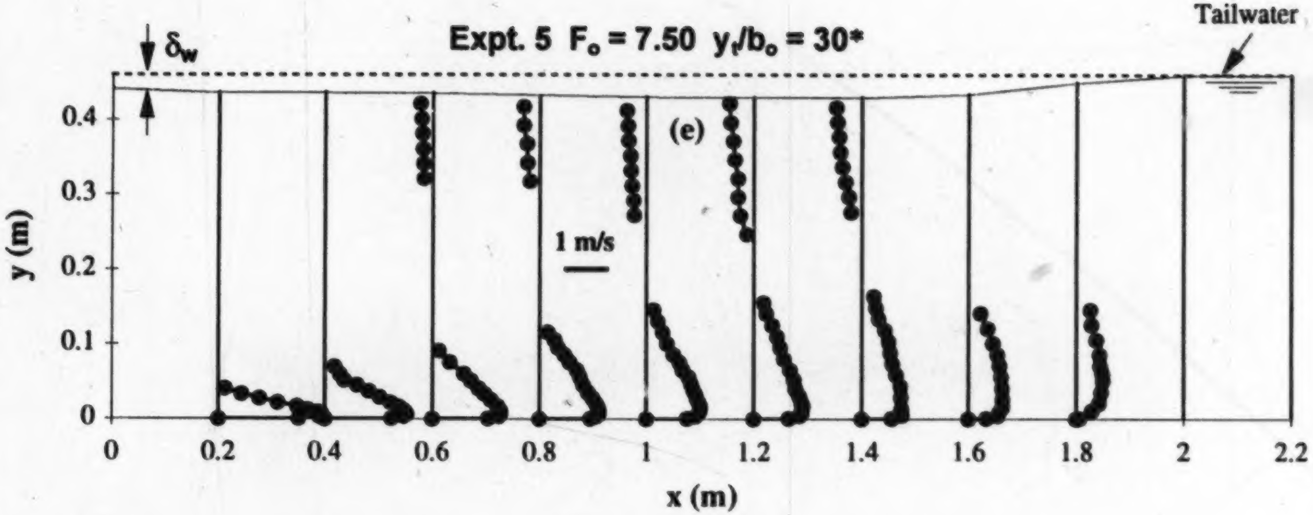

Fig. 6.11(e) Typical velocity fields of wall jets in shallow tailwaters (Expt. 5)
* Wu and Rajaratnam (1995)

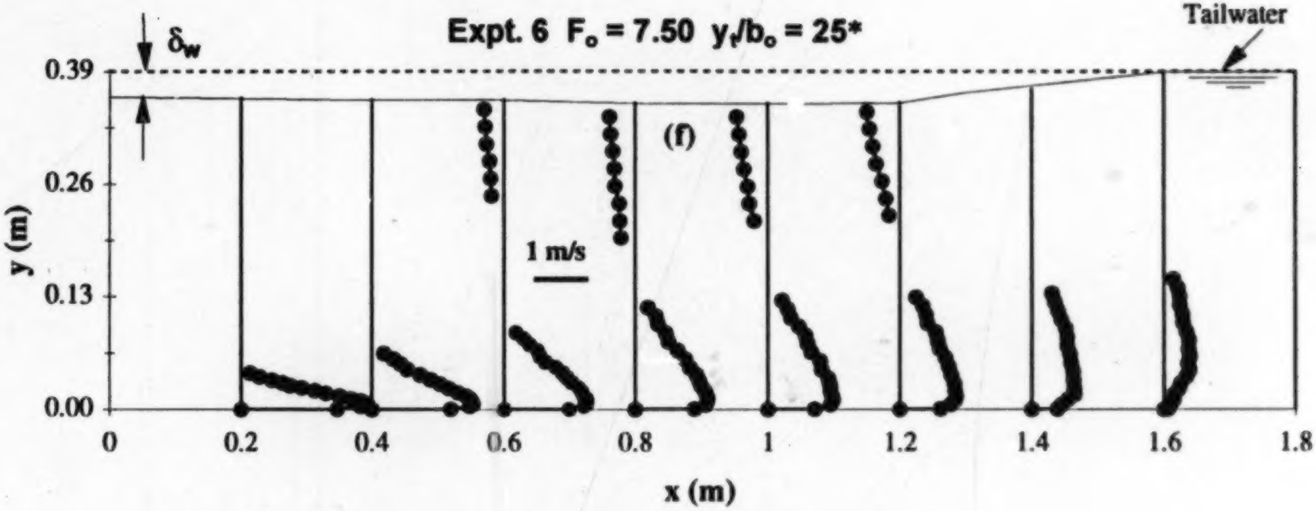

Fig. 6.11(f) Typical velocity fields of wall jets in shallow tailwaters (Expt. 6)
* Wu and Rajaratnam (1995)

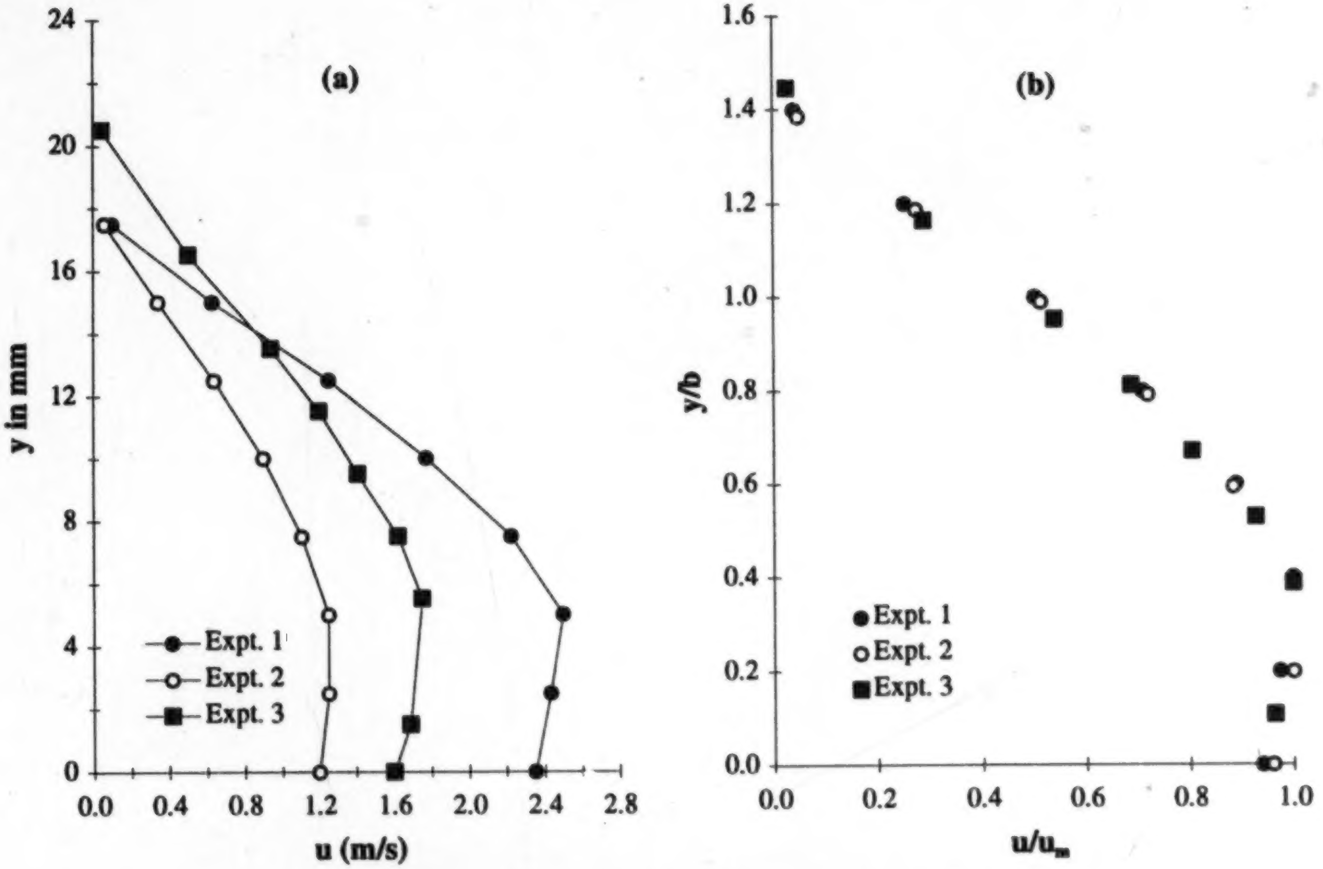

Fig. 6.12(a-b) Velocity distribution in partially-developed flow ($x/b_o = 6$)
(a) Velocity profiles; and (b) Similarity profile

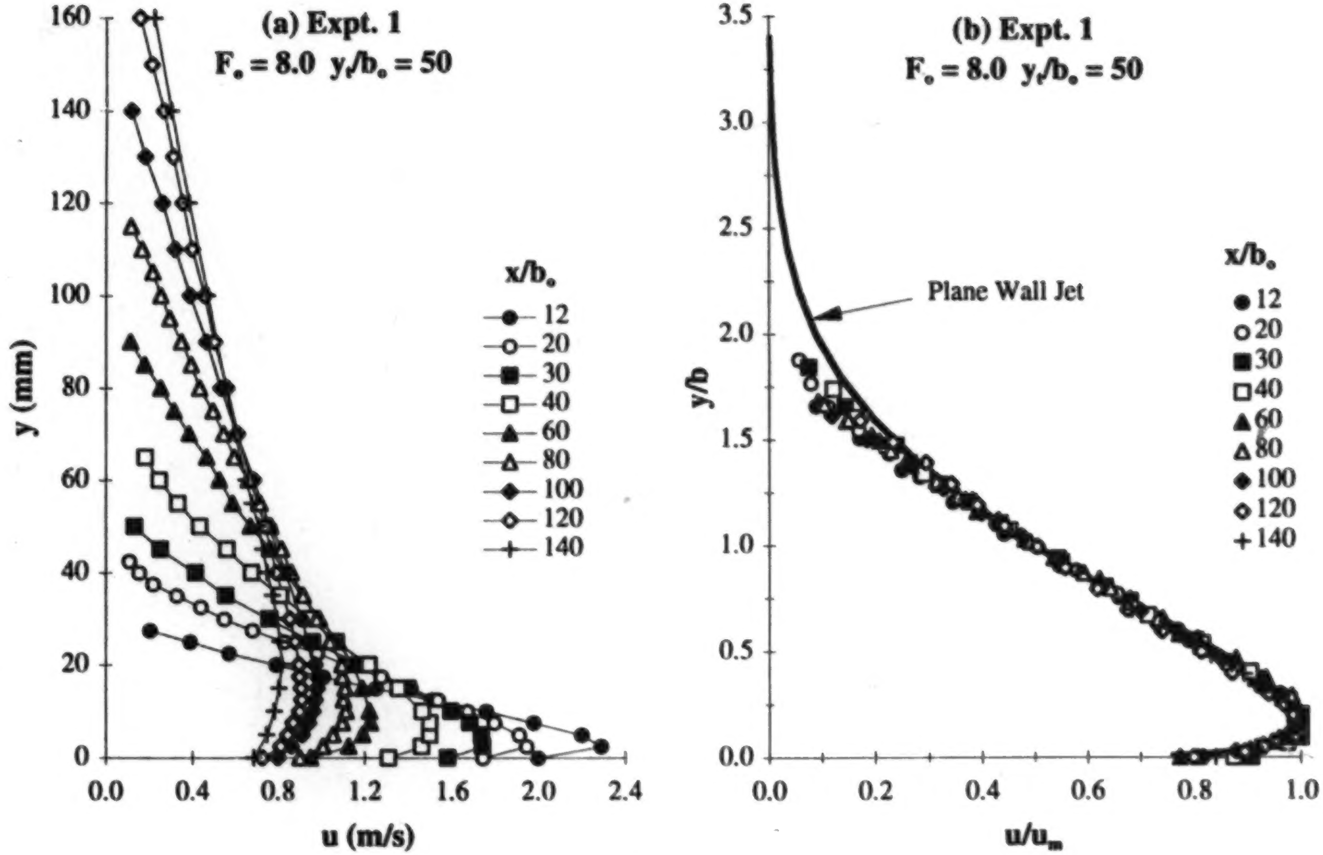

Fig. 6.13(a-b) Velocity distribution in fully-developed flow (Expt. 1)
(a) Velocity profiles; and (b) Similarity profile

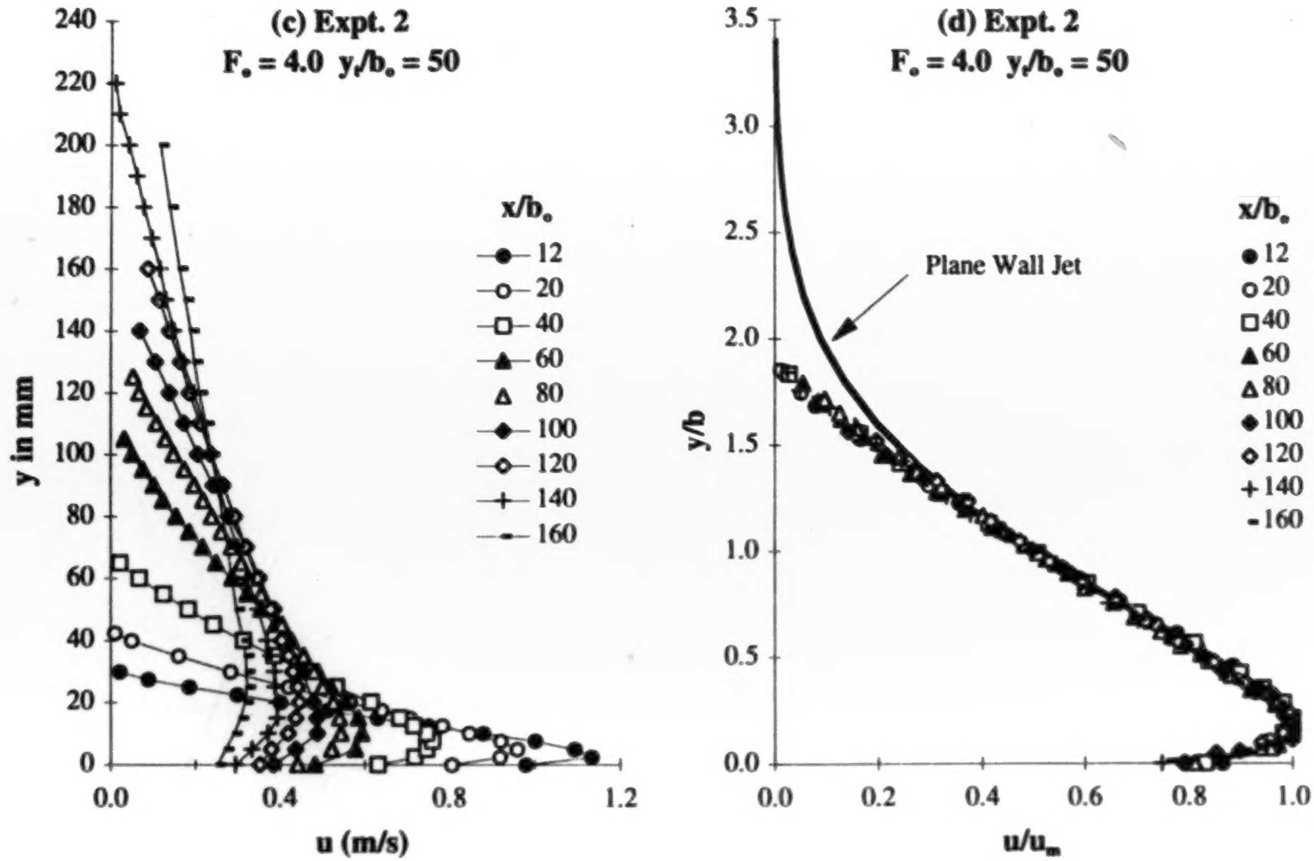

Fig. 6.13(c-d) Velocity distribution in fully-developed flow (Expt. 2)
(c) Velocity profiles; and (d) Similarity profile

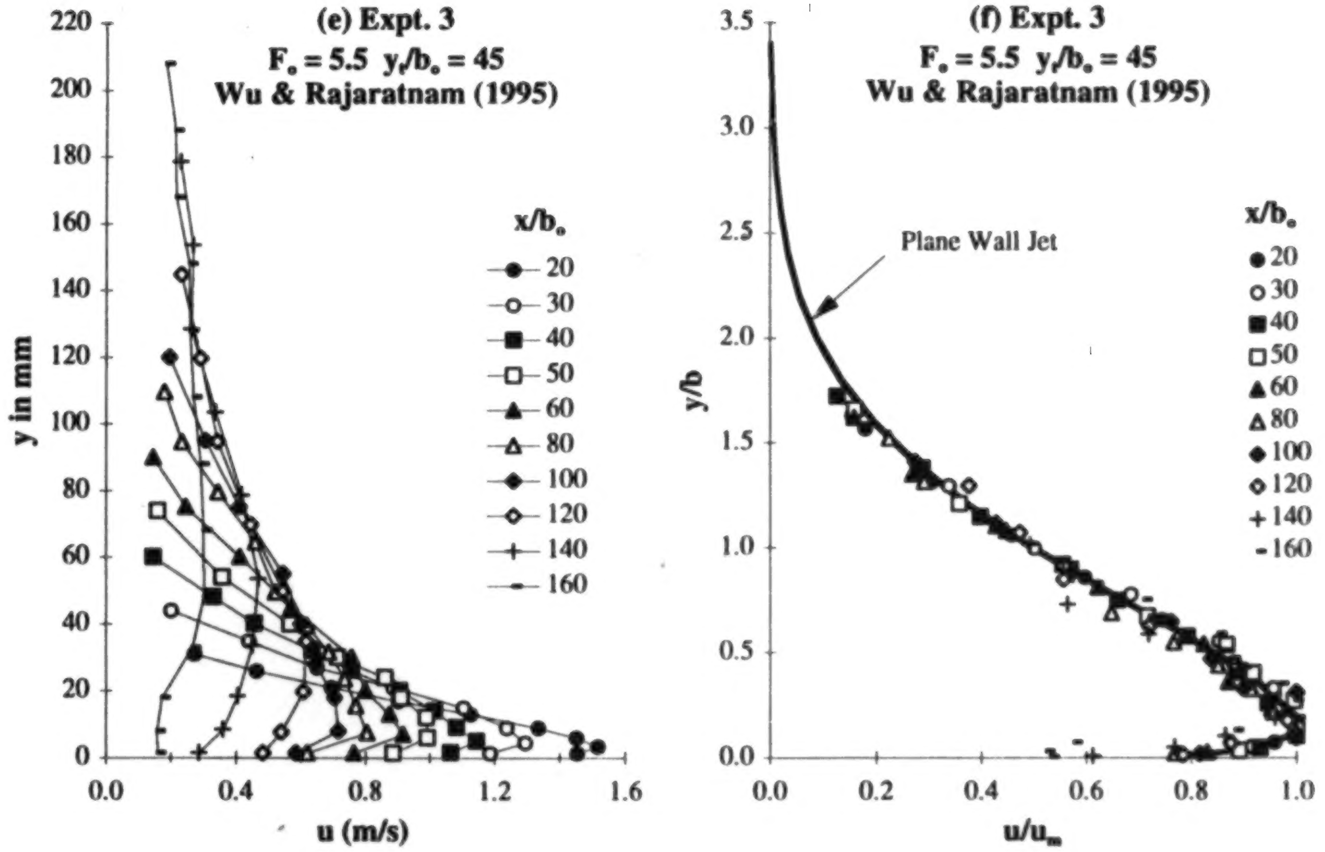

Fig. 6.13(e-f) Velocity distribution in fully-developed flow (Expt. 3)
(e) Velocity profiles; and (f) Similarity profile

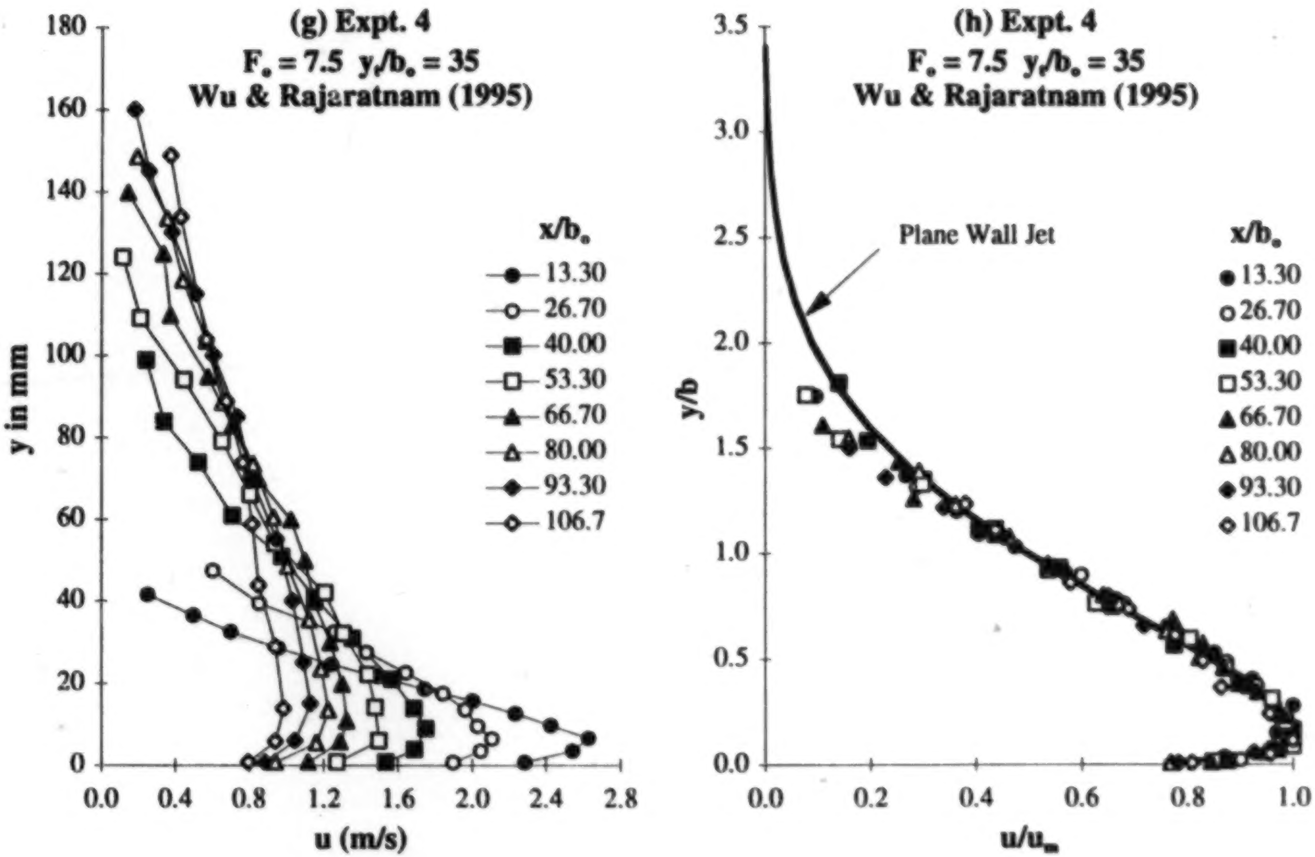

Fig. 6.13(g-h) Velocity distribution in fully-developed flow (Expt. 4)
(g) Velocity profiles; and (h) Similarity profile

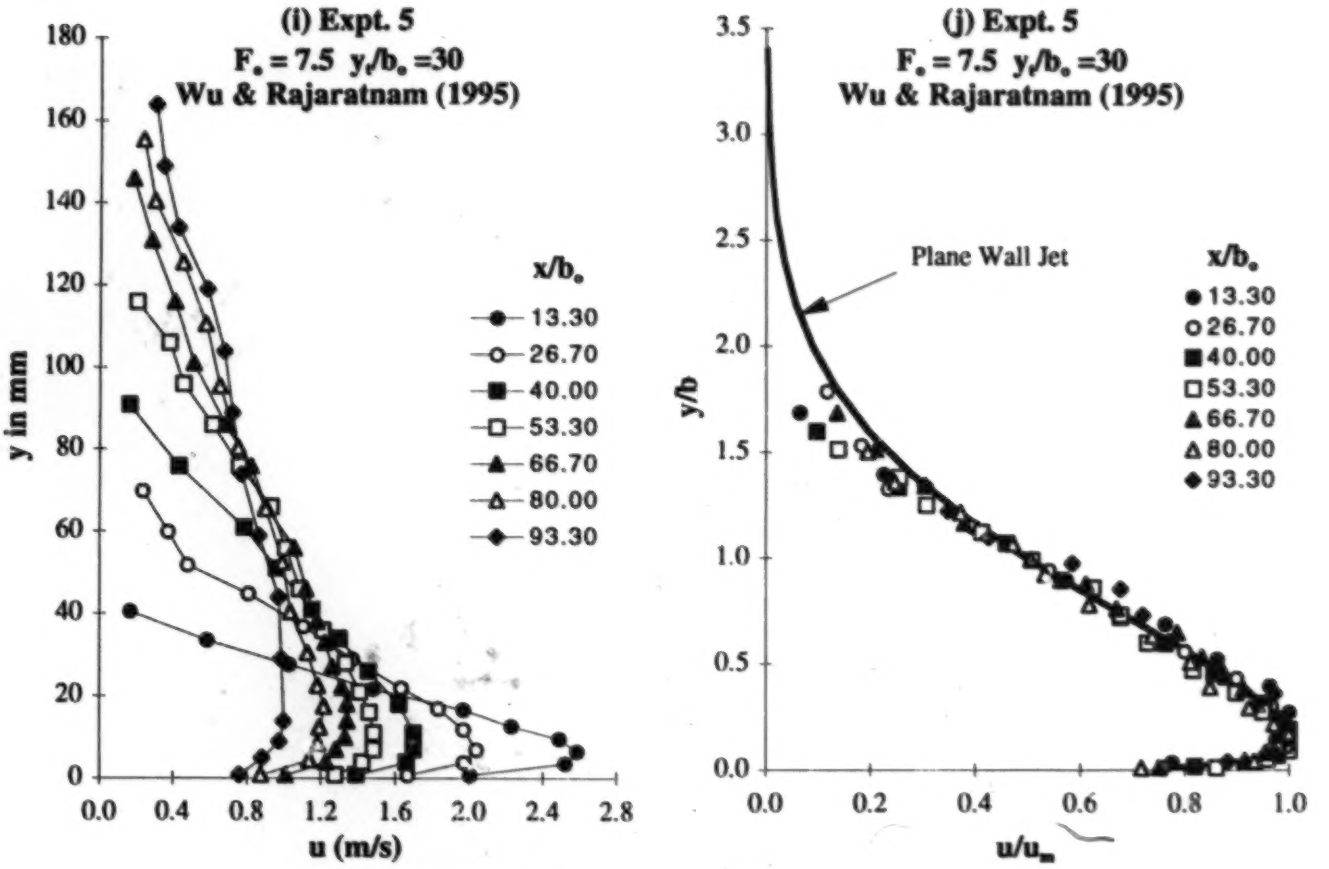

Fig. 6.13(i-j) Velocity distribution in fully-developed flow (Expt. 5)
(i) Velocity profiles; and (j) Similarity profile

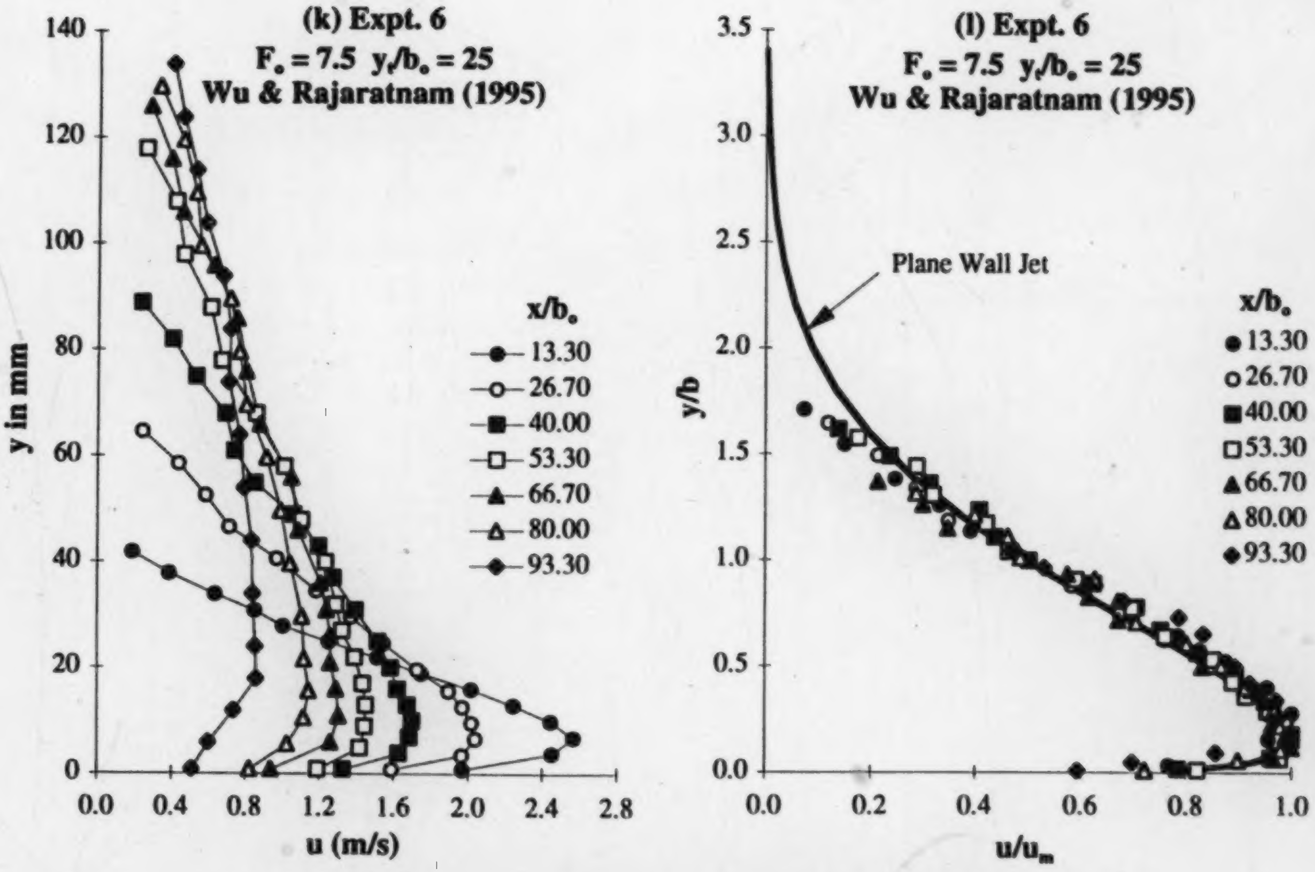
(k) Expt. 6
$F_o = 7.5$ $y_t/b_o = 25$
Wu & Rajaratnam (1995)

(l) Expt. 6
$F_o = 7.5$ $y_t/b_o = 25$
Wu & Rajaratnam (1995)

Fig. 6.13(k-l) Velocity distribution in fully-developed flow (Expt.6)
(k) Velocity profiles; and (l) Similarity profile

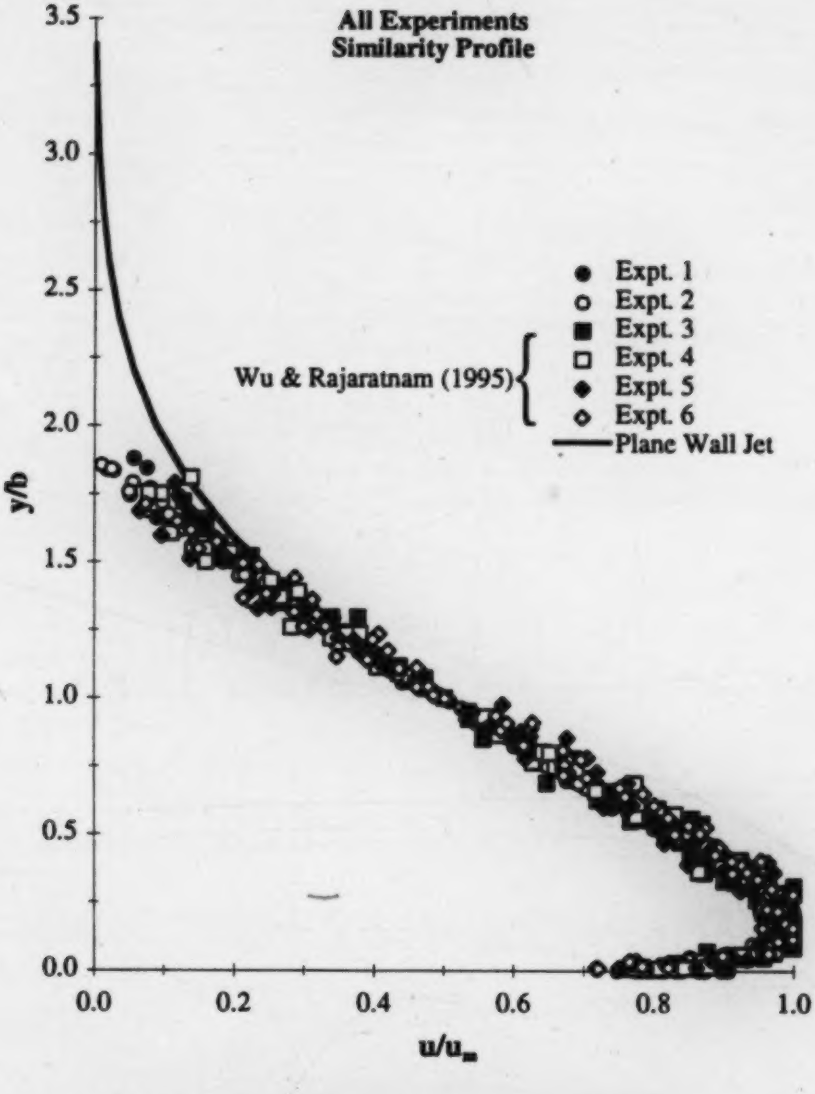

Fig. 6.14 Consolidated non-dimensional plot for the velocity distribution in the wall jet

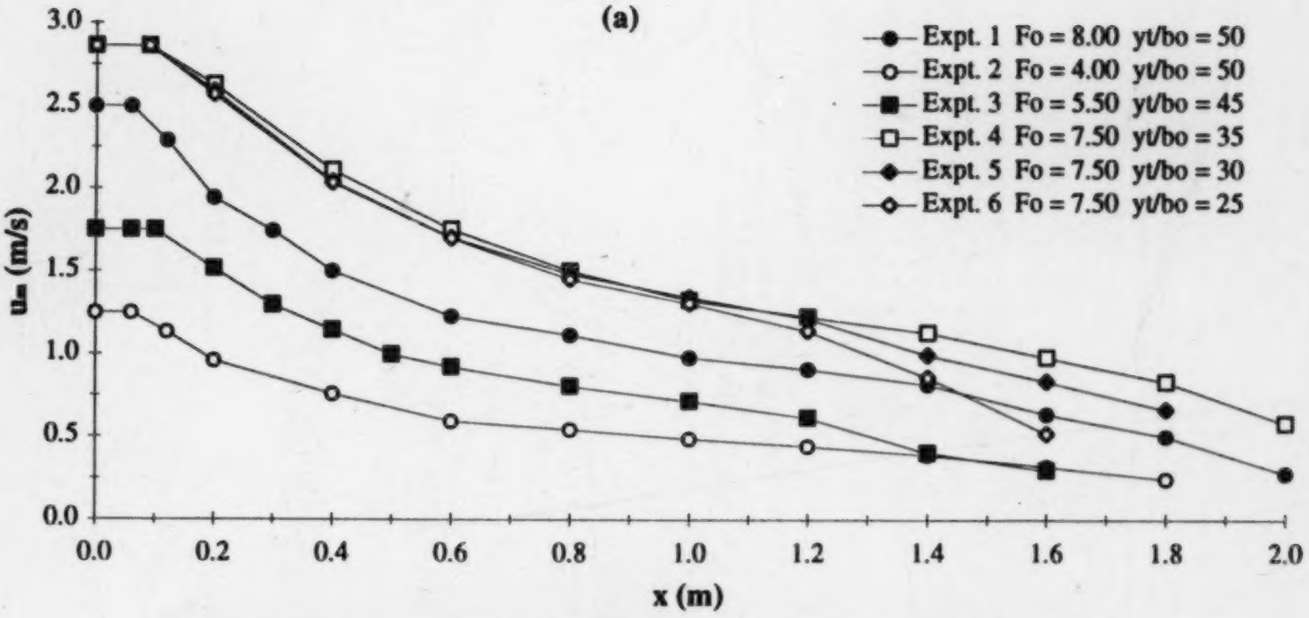

Fig. 6.15(a) Variation of the maximum jet velocity, u_m, with distance

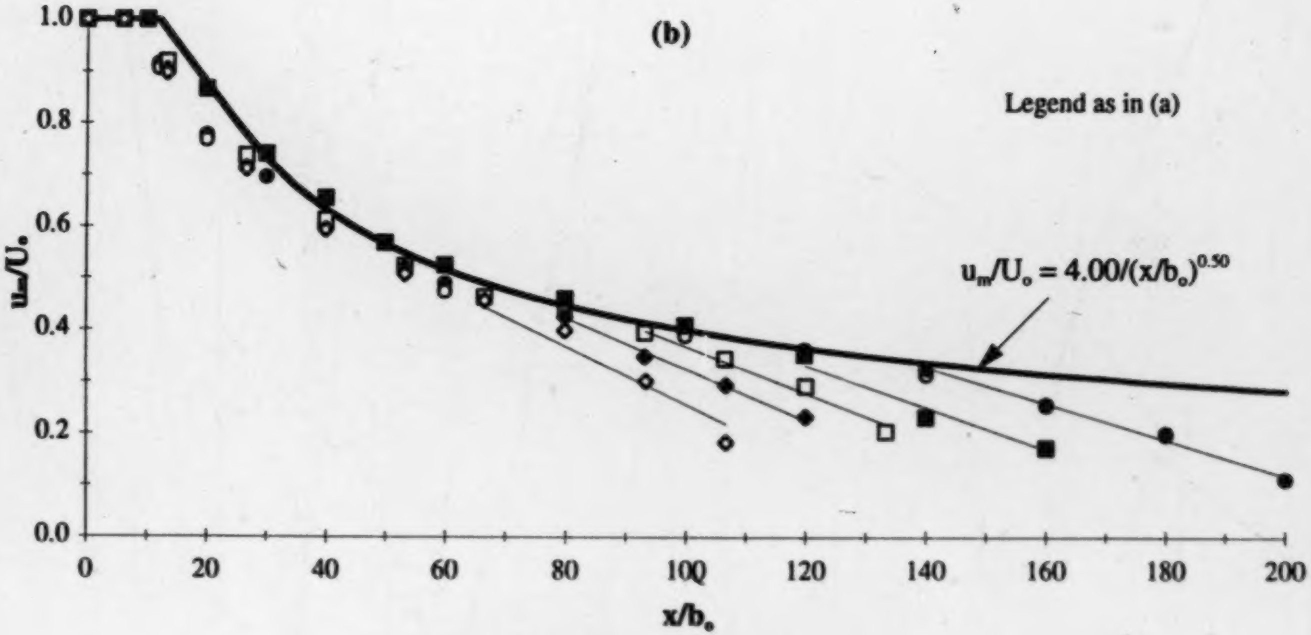

Fig. 6.15(b) Variation of u_m/U_o with x/b_o

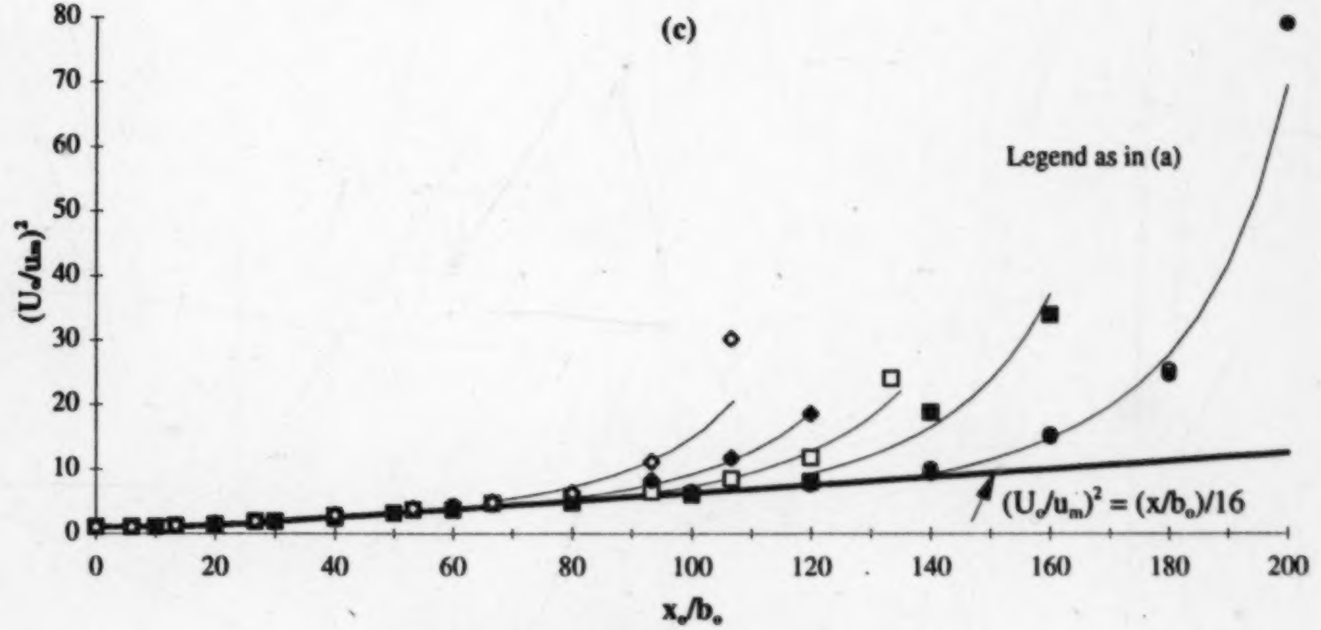

Fig. 6.15(c) Variation of $(U_o/U_m)^2$ with x/b_o

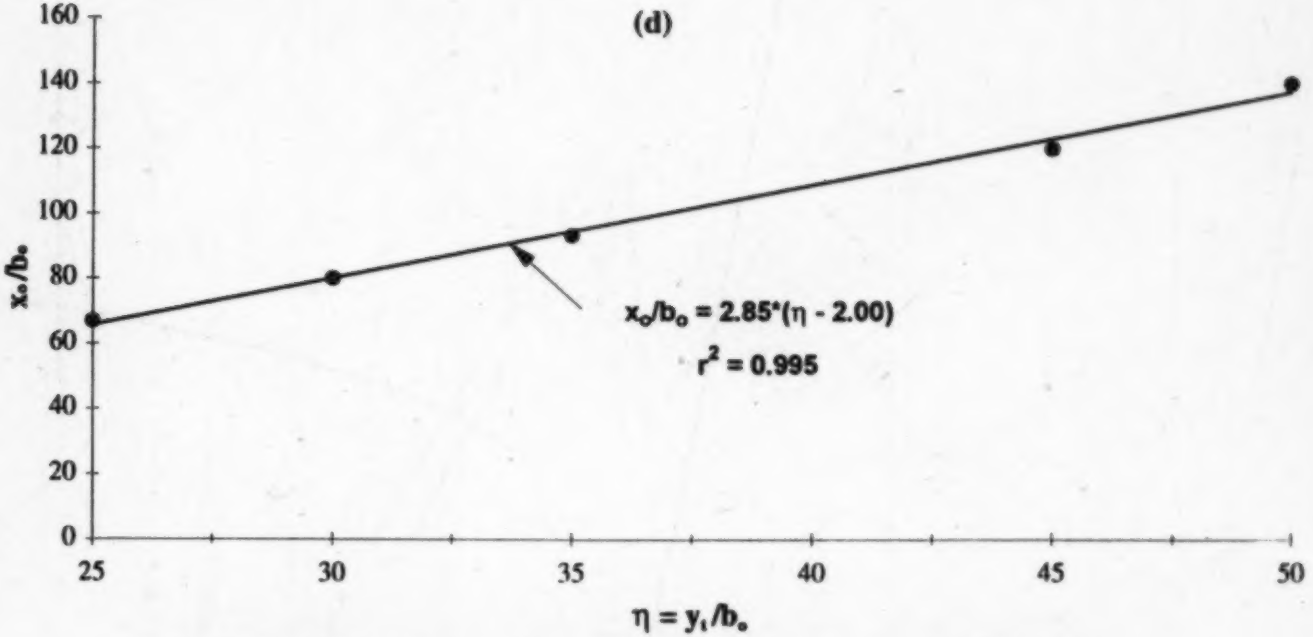

Fig. 6.15(d) Effect of the tailwater depth ratio on the breakdown distance

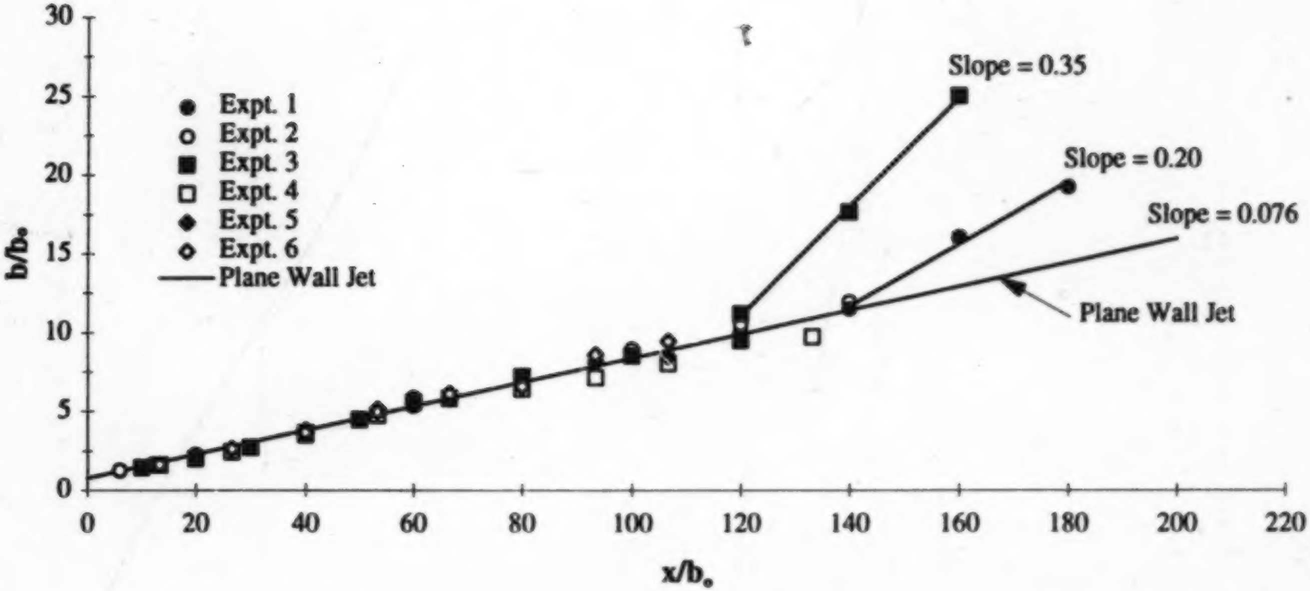

Fig.6.16 Variation of the jet half-width with distance

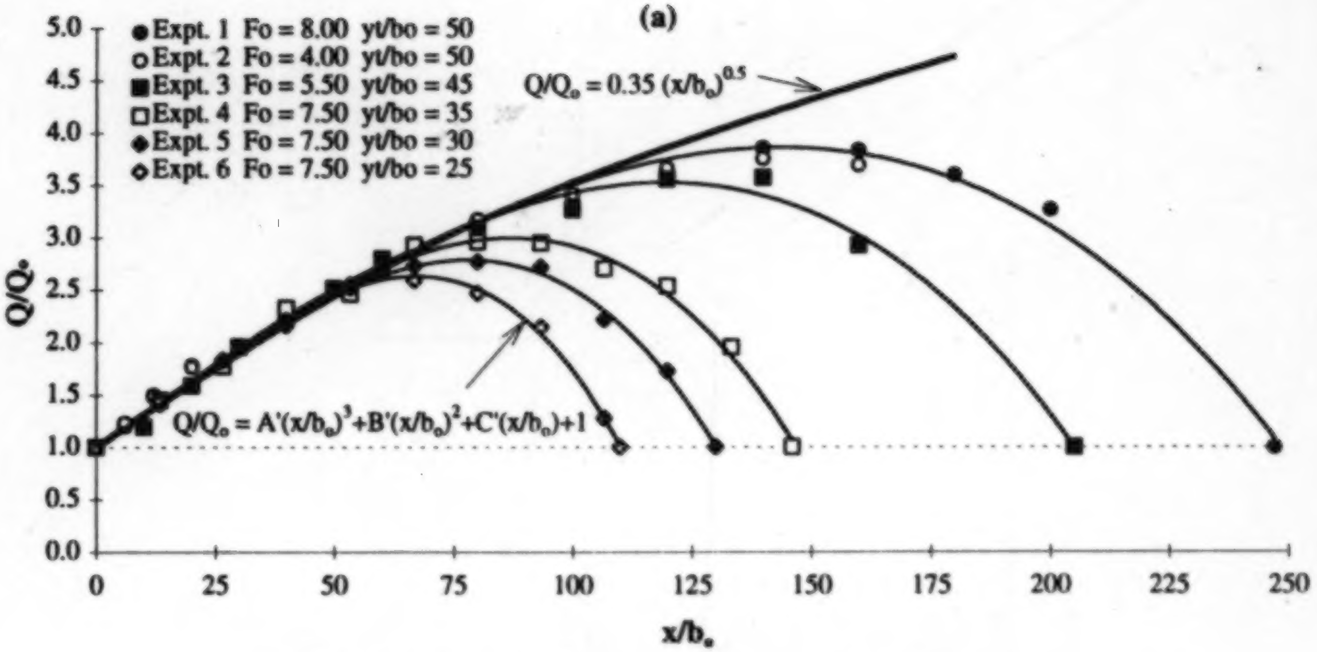

Fig. 6.17(a) Variation of the wall jet discharge with distance

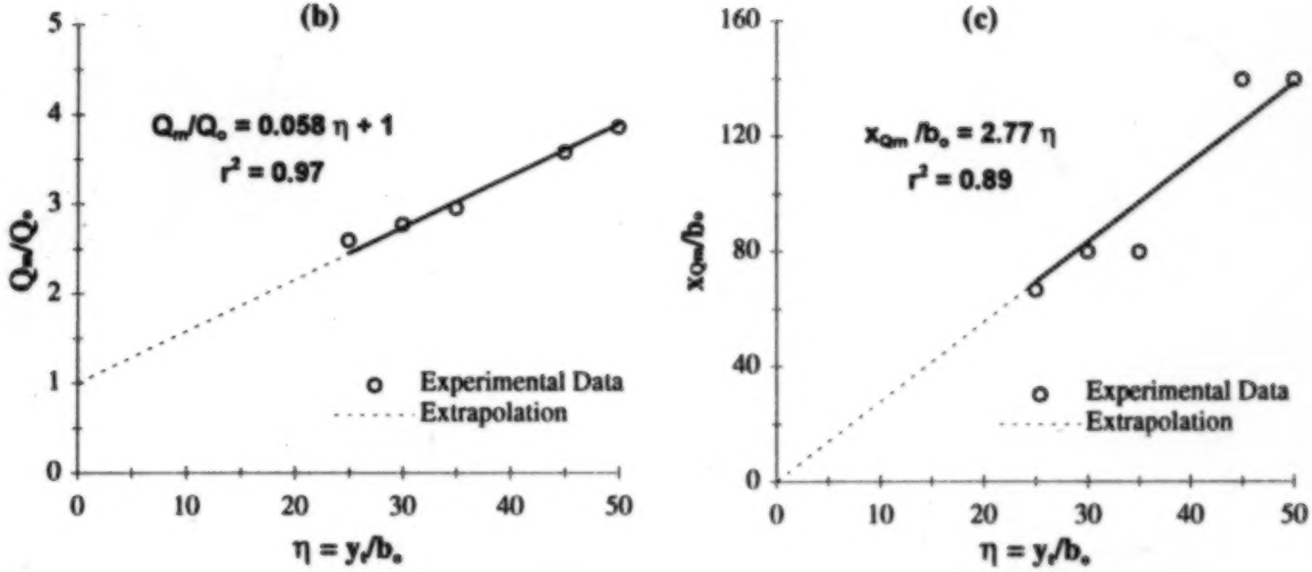

Fig. 6.17(b-c) Effect of y_t/b_o on the magnitude and location of the maximum discharge

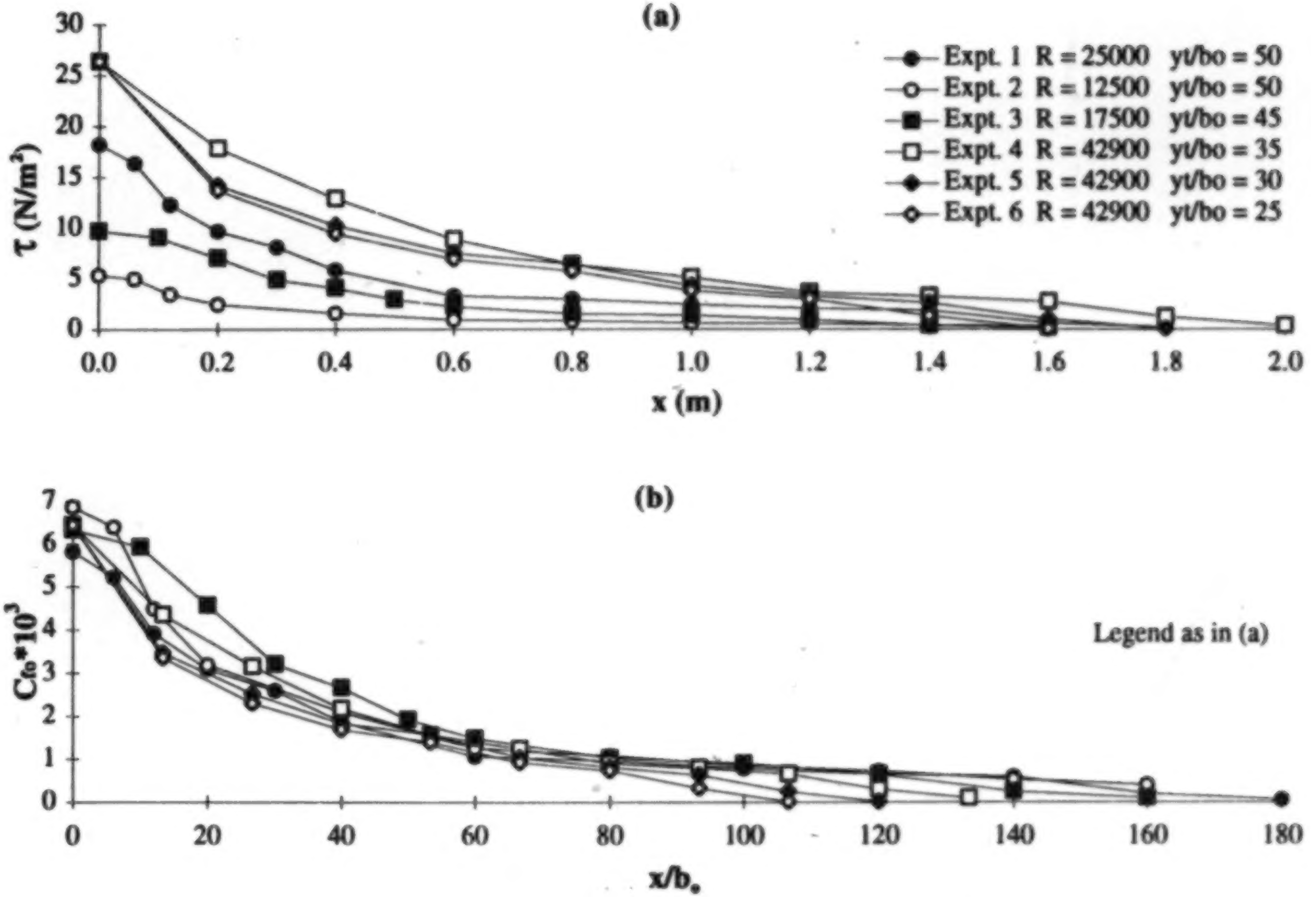

Fig. 6.18(a-b) Variation of the bed shear stress with distance

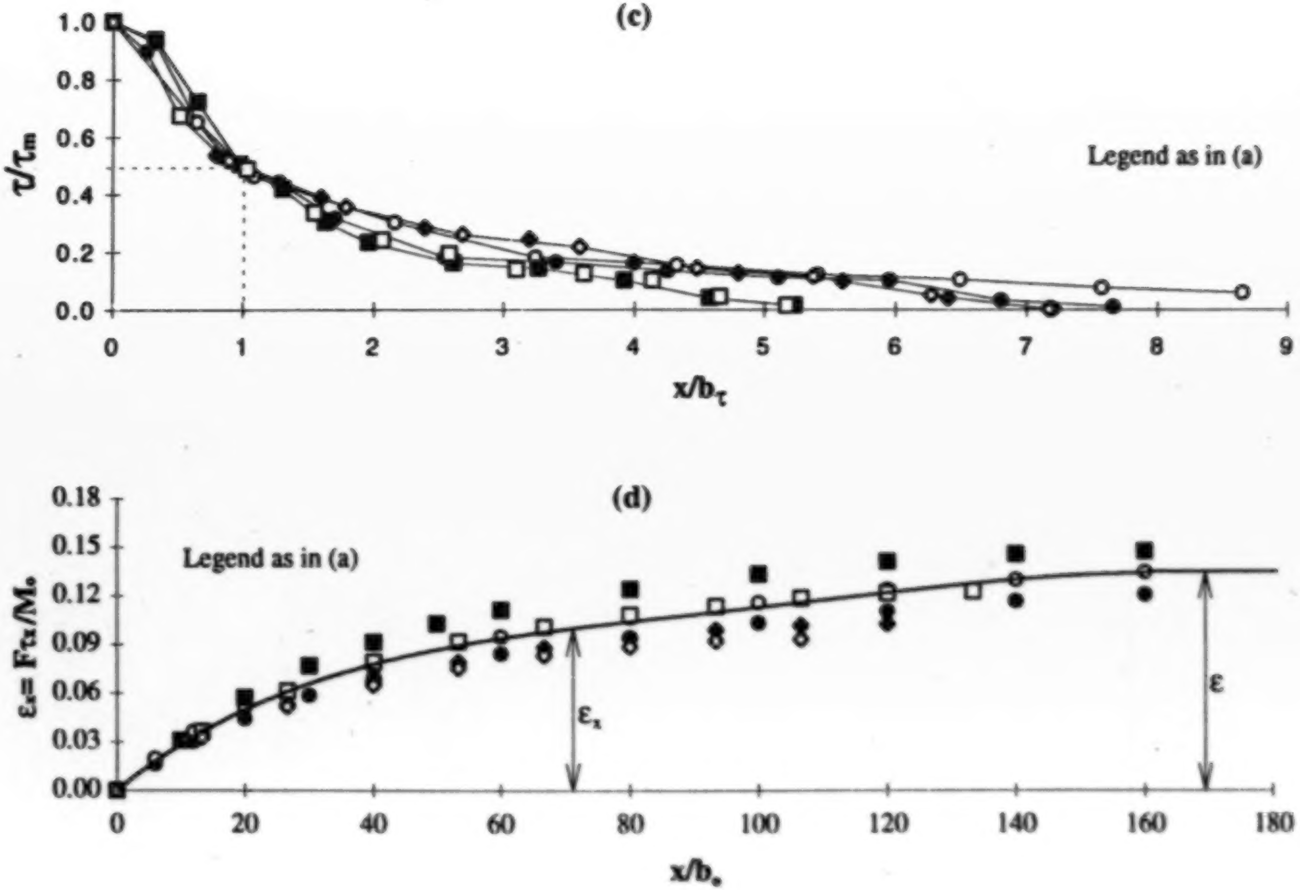

Fig. 6.18(c-d) Variation of the bed shear stress with distance

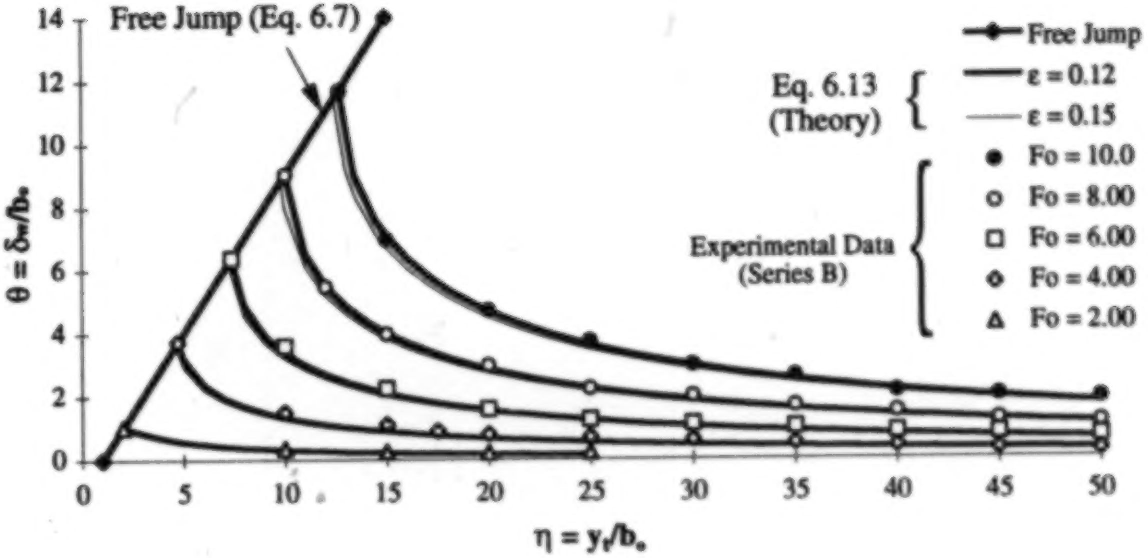

Fig. 6.19. Determination of the shear force coefficient ε

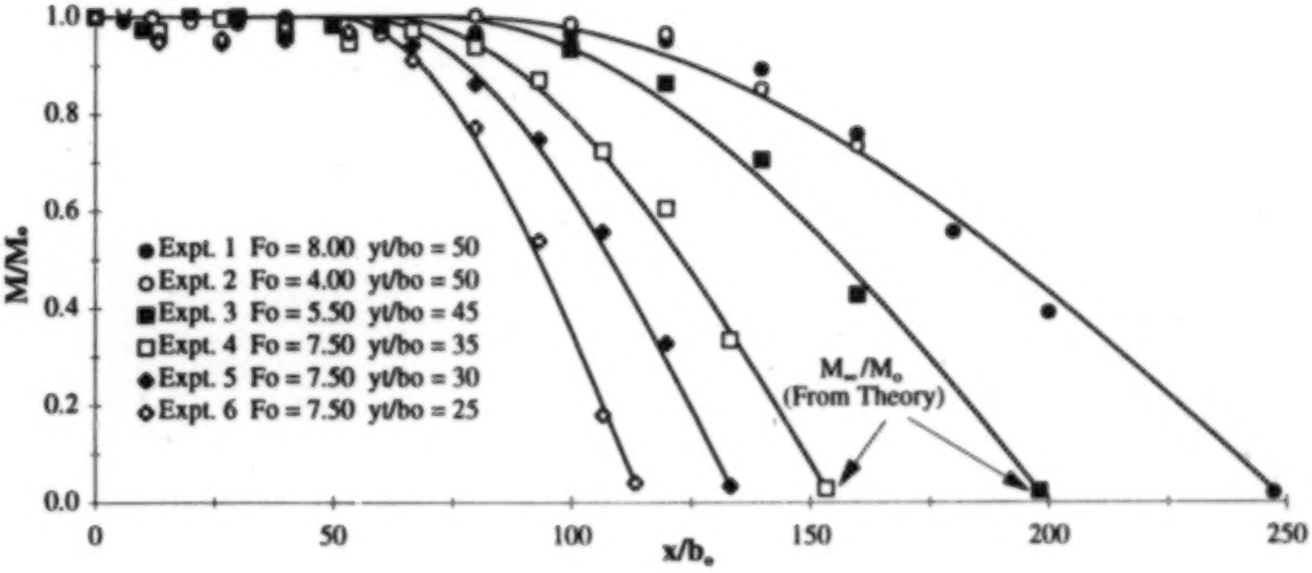

Fig. 6.20 Variation of the wall jet momentum flux with distance

Chapter 7

Conclusions and Recommendations

In the preceding three chapters, three studies have been presented on the behavior of turbulent jets in shallow tailwater. This chapter introduces a brief discussion on each of these contributions as well as recommendations for future research work.

Chapter 4 presented the results of an experimental study performed to introduce a new energy dissipator for use downstream of flow regulators. In the new design, a double-leaf gate is used where an inclined high-velocity jet issues between the two gates towards the free surface. In the double-leaf gate, the upper gate is located upstream of the lower one to create the opening which produces the inclined jet. The double-leaf gate is recommended for use in deeply submerged flow regulators where the discharge is independent of the location of the opening. Flow pattern A is recommended for design and can easily be achieved in flow regulators by keeping the opening, between the two gates, submerged and having side aeration to prevent jet oscillation.

The experimental work was performed mainly to study the decay of the maximum velocity and to compare it with that of free and submerged jumps. With a considerable submergence, the maximum velocity decays rapidly. The limited extent of the tailwater was the main reason for this enhanced decay. As soon as the jet issues from the slot, two recirculating flow regions, above the below the inclined jet, form and the return flow in these regions causes the momentum flux in the forward flow to decay significantly. The turbulent jet issues between the two gates towards the free surface and after striking the water surface proceeds as a surface jet. Shear stress on the bed is caused by the return flow which is relatively weak and hence, minor scour is anticipated downstream of the new dissipator. However, using an apron downstream of the prototype, or using an equivalent sheet pile wall, is still essential for percolation requirements.

Most of existing flow regulators have single-leaf gates (sluice gates). For the new design to be used in these regulators, an upward sloping sill may be installed under the gate. Few experiments were performed, in the present study, to investigate the behavior of the inclined jet with zero offset ratio. However, the design with the gate opening at the bed needs more experiments, especially for the effect of the inclination angle on jet stability. Also, a future study on the scour downstream of double-leaf gate energy dissipators is recommended. The main objective of such study would be to check for the possibility of using a relatively short apron, with a sheet pile wall driven under the gate, downstream of this type of dissipators.

Chapter 5 presented a comprehensive study of plane turbulent surface jets in shallow tailwater. This study may be considered as a special case of the inclined turbulent jet used in the double-leaf gate model, with the inclination angle and the submergence ratio are equal to zero. In the first study (the double-leaf gate) it has been found from the experimental results that the momentum flux in the forward flow decays significantly. As it has been generally assumed that the momentum flux in turbulent jets discharged into large ambients would be preserved, it was interesting to perform a theoretical and an experimental study of a turbulent jet, of a simple geometry, in shallow tailwater. The main objective of such study was to investigate the reasons causing the momentum of turbulent jets in shallow tailwater to decay rapidly and to study the effect of the relative tailwater on the different characteristics of turbulent jets.

In the theoretical study, expressions for the momentum loss and the piezometric-pressure increase were formulated at a section just downstream of the line of the jet attachment to the bed. Nine experiments covering a wide range of the Froude number and the offset ratio, were conducted. The experimental results showed that the length of the recirculating-flow region is about 6.50 times the offset distance. The velocity profiles in the surface jet were found to be similar, in the developing as well as in the developed flow regions. The maximum velocity was found to decay in two stages. In the first stage, the rate of decay was independent of the relative depth of tailwater whereas the faster rate in the second stage depended on it. The length of the first stage of decay was directly proportional to the offset ratio. The length scale of the jet grew at a rate of 0.065 in the early stage and the rate of growth was much smaller in the second stage. The variation of the volume flux in the surface jet was affected significantly by the tailwater depth ratio. The decay of the momentum flux in the surface jet, with the distance from the nozzle, was observed and correlated with the offset ratio and the relative longitudinal distance. The experimental observations of the momentum loss were found to be in agreement with theory. Empirical expressions for the above characteristics were developed.

This study has contributed to the theory of turbulent jets when the ambient fluid has a limited extent. A theoretical study of the momentum decay and the rise in the water surface elevation at any x-station, in the distance between the opening and the section at which the jet attaches to the bed, is challenging and needs further research. Surface jets in shallow tailwater could be used as the design element in what might be referred to as Surface Energy Dissipators. Experimental studies are needed, especially for the effect of relative tailwater on erosion downstream of these dissipators.

Chapter 6 presented a theoretical and a laboratory study of plane turbulent wall jets in shallow tailwater. After the completion of the first and second studies, it was interesting and useful to study the plane turbulent wall jets in a tailwater of limited extent. The combination of the three studies would make the subject, turbulent jets in shallow tailwater, more coherent and understandable.

The first thought implied that the two problems of surface and plane jets were very similar with the only difference in the location of the source discharge in both of them. But, the theoretical study revealed a subtle difference between the two problems regarding the tailwater depth in each of them. A surface jet with specific characteristics can be formed with only one value of the tailwater depth. On the other hand, a plane jet, having the same characteristics as the surface jet, can be formed with an infinite number of tailwater depths. This subtle difference made the theoretical approaches in the two problems quite different.

In the theoretical study, the momentum loss, in terms of the momentum at the nozzle, was evaluated at a section just downstream of the line of the jet attachment to the free surface. Also, the depression in the water surface elevation and the loss in the hydrostatic pressure force at the gate were evaluated with and without the inclusion of the bed shear stress. A general equation for the sequent depth ratio in free hydraulic jump with the inclusion of the bed shear stress, was also formulated. Experiments were conducted, for different Froude numbers and tailwater depth ratios, to measure the longitudinal velocity, the bed shear stress, the eddy length and the depression in the water surface elevation at the gate. The experimental results showed that the length of the return-flow region is dependent on the tailwater depth ratio and the Froude number. The velocity profiles in the wall jet were found to be similar, in the developing as well as in the developed flow regions. The maximum velocity in the fully developed flow region decayed in two stages. The rate of the velocity decay in the first stage was independent of the relative depth of tailwater while the length of this stage depended on it. In the second stage, the maximum velocity rate of decay was faster than that of the first stage and was affected by the relative tailwater. Empirical equations, in a non-dimensional form, for the effect of the relative tailwater on the discharge variation with distance, were developed. The integrated bed shear stress from the gate till the jet surfaced was estimated to be about 12%-15% of the momentum flux at the nozzle. The measured drops in the water surface elevation at the gate were compared with the corresponding values from theory where both, measurements and theory, gave almost the same results. Momentum flux was preserved for a certain distance after which it decayed rapidly. Momentum decay was correlated with the tailwater depth ratio, the eddy length and the relative longitudinal distance.

In conclusion, the results from this study have highlighted the effect of limited tailwater depth on the behavior of plane turbulent wall jets. Again, recommended for future research is a study of the effect of the relative tailwater on downstream scour. Also, it would be interesting to perform a theoretical study for the momentum decay at any x-station between the gate and the section where the jet surfaces.

Appendix

1. A Double-Leaf Gate for Energy Dissipation Below Regulators

1.1 Velocity Measurements along Vertical Sections at x-stations

Expt. 1

x = 50 cm

y (cm)	u (m/s)
0	0.398
1	0.377
2	0.370
4	0.349
6	0.251
8	0.164
11	-0.109
12	-0.135
14	-0.164
16	-0.189
18	-0.202
20	-0.211
22	-0.202
24	-0.204
25	-0.201
25.5	-0.177

x = 60 cm

y (cm)	u (m/s)
0	0.517
1	0.552
2	0.492
4	0.376
6	0.239
7	0.181
12	-0.157
14	-0.180
16	-0.214
18	-0.227
20	-0.229
22	-0.229
24	-0.233
25	-0.230
25.5	-0.222

x = 80 cm

y (cm)	u (m/s)
0	0.367
1	0.441
2	0.439
3	0.402
4	0.356
5	0.319
6	0.303
7	0.222
7.5	0.212
8	0.178
8.5	0.163
9	0.160
14	-0.123
16	-0.158
18	-0.187
20	-0.200
22	-0.212
24	-0.226
25	-0.214
25.5	-0.232

x = 100 cm

y (cm)	u (m/s)
0	0.207
1	0.269
2	0.285
3	0.279
4	0.251
5	0.228
6	0.223
7	0.217
8	0.178
9	0.159
10	0.146
17	-0.109
18	-0.107
20	-0.156
22	-0.150
24	-0.152
25	-0.153
25.5	-0.147

x = 120 cm

y (cm)	u (m/s)
4	0.128
5	0.128
6	0.140
7	0.125
8	0.126
9	0.117
10	0.112

Expt. 2

x = 30 cm

y (cm)	u (m/s)
21.5	0.164
22	0.188
22.5	0.264
23	0.317
23.5	0.345
24	0.429
24.5	0.453
25	0.485
25.5	0.493
26	0.476
26.5	0.481
27	0.495
27.5	0.504

x = 40 cm

y (cm)	u (m/s)
0	-0.0948
1	-0.1066
2	-0.0987
3	-0.0908
4	-0.0841
5	-0.0872
19	0.0893
19.5	0.1395
20	0.1671
20.5	0.2053
21	0.2331
21.5	0.2837
22	0.3675
22.5	0.3758
23	0.4223
23.5	0.466
24	0.4996
24.5	0.5484
25	0.5831
25.5	0.5982
26	0.6056
26.5	0.6153
27	0.6283
27.5	0.6382

x = 50 cm

y (cm)	u (m/s)
0	-0.1097
1	-0.1273
2	-0.1003
3	-0.0904
19	0.1194
19.5	0.1542
20	0.169
20.5	0.2188
21	0.2497
21.5	0.2806
22	0.3066
22.5	0.3383
23	0.3517
23.5	0.3991
24	0.4248
24.5	0.455
25	0.4669
25.5	0.494
26	0.4967
26.5	0.5045
27	0.5096
27.5	0.5145

x = 60 cm

y (cm)	u (m/s)
17.5	0.1942
18	0.1843
18.5	0.2007
19	0.2746
19.5	0.2717
20	0.2776
20.5	0.3185
21	0.3453
21.5	0.4025
22	0.3914
22.5	0.4664
23	0.4651
23.5	0.5118
24	0.5217
24.5	0.5514
25	0.5847
25.5	0.6063
26	0.6344
26.5	0.6518
27	0.6698
27.5	0.6718

x = 80 cm

y (cm)	u (m/s)
13	0.1812
14	0.1811
15	0.2265
16	0.2449
17	0.268
18	0.3098
19	0.3333
20	0.3472
21	0.4061
22	0.4461
22.5	0.4425
23	0.4667
23.5	0.497
24	0.5266
24.5	0.5377
25	0.5493
25.5	0.5786
26	0.5901
26.5	0.5951
27	0.5981
27.5	0.6072

x = 100 cm

y (cm)	u (m/s)
12	0.1537
13	0.1659
14	0.1921
15	0.2121
16	0.22
17	0.2641
18	0.2841
19	0.2783
20	0.3344
21	0.3666
22	0.3886
22.5	0.4041
23	0.4311
23.5	0.4374
24	0.4481
24.5	0.4823
25	0.4895
25.5	0.4822
26	0.5016
26.5	0.52
27	0.5428
27.5	0.55

x = 120 cm

y (cm)	u (m/s)
12.5	0.1515
13	0.1389
14	0.1572
15	0.1987
16	0.1848

17	0.201
18	0.232
19	0.243
20	0.275
21	0.282
22	0.310
23	0.349
24	0.354
25	0.363
25.5	0.401
26	0.400
26.5	0.403
27	0.412
27.5	0.422

x = 140 cm

y (cm)	u (m/s)
15.5	0.155
16	0.144
17	0.146
18	0.165
19	0.186
20	0.195
21	0.219
22	0.248
23	0.244
24	0.255
25	0.294
25.5	0.282
26	0.283
26.5	0.302
27	0.324
27.5	0.334

x = 160 cm

y (cm)	u (m/s)
19	0.119
20	0.117
21	0.147
22	0.169
23	0.168
24	0.190
25	0.208
25.5	0.204
26	0.212
26.5	0.230
27	0.242
27.5	0.255

x = 180 cm

y (cm)	u (m/s)
21.5	0.105
22	0.108
22.5	0.115
23	0.129
23.5	0.144
24	0.135
24.5	0.152
25	0.165
25.5	0.178
26	0.189
26.5	0.195
27	0.199
27.5	0.202

x = 200 cm

y (cm)	u (m/s)
23	0.087
23.5	0.089
24	0.102
24.5	0.110
25	0.105
25.5	0.119
26	0.152
26.5	0.162
27	0.165
27.5	0.166

Expt. 3

x = 30 cm

y (cm)	u (m/s)
0	-0.096
2	-0.113
4	-0.127
6	-0.130
8	-0.124
10	-0.134
12	-0.120
14	-0.135
16	-0.134
18	-0.125
20	-0.132
22	-0.125
24	-0.130
26	-0.128
28	-0.139
30	-0.133
32	-0.127
34	-0.115
36	-0.107
40	0.148
41	0.222
42	0.284
43	0.388
44	0.444
45	0.495
45.5	0.515
46	0.525
46.5	0.540
47	0.545
47.5	0.559
48	0.570

x = 40 cm

y (cm)	u (m/s)
0	-0.078
2	-0.108
4	-0.136
6	-0.128
8	-0.125
10	-0.123
12	-0.137
14	-0.135
16	-0.139
18	-0.143
20	-0.144
22	-0.154
24	-0.141
26	-0.142
28	-0.144
30	-0.131
32	-0.127
34	-0.104
39.5	0.152
40	0.179
41	0.240
42	0.293
43	0.387
44	0.436
45	0.502
45.5	0.535
46	0.571
46.5	0.591
47	0.603
47.5	0.612
48	0.626

x = 60 cm

y (cm)	u (m/s)
0	-0.095
1	-0.112
2	-0.130
4	-0.125
6	-0.119
8	-0.151
10	-0.148
12	-0.157
14	-0.157
16	-0.152
18	-0.151
20	-0.154
22	-0.151
24	-0.156
26	-0.159
28	-0.140
30	-0.127
32	-0.100
39	0.165
40	0.213
41	0.237
42	0.282
43	0.308
44	0.357
45	0.412
45.5	0.422
46	0.459
46.5	0.484
47	0.500
47.5	0.505
48	0.519

x = 80 cm

y (cm)	u (m/s)
0	-0.100
1	-0.131
2	-0.152
4	-0.156
6	-0.153
8	-0.156
10	-0.157
12	-0.166
14	-0.152
16	-0.167
18	-0.167
20	-0.159
22	-0.155
24	-0.152
26	-0.123
28	-0.115
39	0.183
40	0.237
41	0.239
42	0.278
43	0.300
44	0.343
45	0.365
45.5	0.398
46	0.410
46.5	0.429
47	0.449
47.5	0.461
48	0.480

x = 100 cm

y (cm)	u (m/s)
0	-0.115
1	-0.130
2	-0.145
4	-0.147
6	-0.154
8	-0.153
10	-0.173
12	-0.164
14	-0.161
16	-0.162
18	-0.165
20	-0.140
22	-0.152
23	-0.134
24	-0.135
25	-0.121
26	-0.117
37	0.136
38	0.161
39	0.165
40	0.203
41	0.224
42	0.248
43	0.263
44	0.286
45	0.323
45.5	0.347
46	0.373
46.5	0.369
47	0.385
47.5	0.402
48	0.423

x = 120 cm

y (cm)	u (m/s)

0	-0.094
1	-0.141
2	-0.130
4	-0.149
6	-0.166
8	-0.149
10	-0.157
12	-0.151
14	-0.157
16	-0.149
18	-0.136
20	-0.128
22	-0.124
24	-0.103
38	0.128
39	0.148
40	0.157
41	0.197
42	0.212
43	0.237
44	0.268
45	0.272
45.5	0.288
46	0.294
46.5	0.317
47	0.329
47.5	0.349
48	0.358

x = 140 cm

y (cm)	u (m/s)
0	-0.114
1	-0.126
2	-0.139
4	-0.132
6	-0.128
8	-0.147
10	-0.148
12	-0.137
14	-0.146
16	-0.142
18	-0.129
20	-0.102
22	-0.105
23	-0.105
38	0.119
39	0.131
40	0.141
41	0.177
42	0.187
43	0.203
44	0.224
45	0.244
45.5	0.253
46	0.276
46.5	0.284
47	0.296
47.5	0.305
48	0.311

x = 160 cm

y (cm)	u (m/s)
0	-0.099
1	-0.120
2	-0.122
4	-0.115
6	-0.123
8	-0.130
10	-0.124
12	-0.131
14	-0.133
16	-0.116
18	-0.102
20	-0.098
21	-0.094
22	-0.101
23	-0.104
40	0.126
41	0.133
42	0.167
43	0.174
44	0.181
45	0.203
45.5	0.212
46	0.229
46.5	0.239
47	0.249
47.5	0.256
48	0.269

x = 180 cm

y (cm)	u (m/s)
3	-0.102
4	-0.111
6	-0.105
8	-0.096
10	-0.108
12	-0.103
14	-0.100
16	-0.090
18	-0.078
41	0.108
42	0.121
43	0.139
44	0.147
45	0.160
45.5	0.164
46	0.174
46.5	0.185
47	0.195
47.5	0.204
48	0.213

x = 200 cm

y (cm)	u (m/s)
11	-0.127
45.5	0.136
46	0.142
46.5	0.152
47	0.144
47.5	0.152
48	0.156

Expt. 4

x = 30 cm

y (cm)	u (m/s)
2	-0.096
4	-0.107
6	-0.101
8	-0.114
10	-0.107
12	-0.124
14	-0.133
16	-0.127
18	-0.135
19	-0.126
20	-0.134
21	-0.132
22	-0.131
24	-0.136
25	-0.132
26	-0.134
27	-0.123
28	-0.123
29	-0.125
30	-0.122
31	-0.121
32	-0.115
34	-0.109
36	-0.115
38	-0.113
40	-0.104
43	0.189
44	0.228
45	0.278
46	0.316
47	0.337
48	0.362
49	0.359
50	0.370
50.5	0.347
51	0.342
51.5	0.351
52	0.332
52.5	0.316
53	0.286
53.5	0.269
54	0.266
54.5	0.253

x = 40 cm

y (cm)	u (m/s)
1	-0.091
2	-0.105
4	-0.108
6	-0.100
8	-0.100
10	-0.110
12	-0.106
14	-0.101
16	-0.111
18	-0.108
20	-0.118
22	-0.109
24	-0.109
26	-0.112
28	-0.111
30	-0.116
32	-0.118
34	-0.106
36	-0.113
38	-0.106
45	0.151
46	0.187
47	0.248
48	0.313
49	0.357
50	0.396
50.5	0.421
51	0.439
51.5	0.444
52	0.463
52.5	0.472
53	0.498
53.5	0.502
54	0.494

x = 60 cm

y (cm)	u (m/s)
1	-0.101
2	-0.119
4	-0.123
6	-0.134
8	-0.128
10	-0.136
12	-0.143
14	-0.152
16	-0.132
18	-0.128
20	-0.143
22	-0.147
24	-0.141
26	-0.139
28	-0.139
30	-0.145
32	-0.124
34	-0.119
35	-0.118
45	0.194
46	0.216
47	0.257
48	0.299
49	0.326
50	0.376
50.5	0.381
51	0.410
51.5	0.431
52	0.455
52.5	0.478
53	0.496
53.5	0.515
54	0.504

x = 80 cm

y (cm)	u (m/s)
0	-0.088
1	-0.119
2	-0.134

4	-0.140
6	-0.132
8	-0.148
10	-0.150
12	-0.148
14	-0.155
16	-0.156
18	-0.162
20	-0.163
22	-0.161
24	-0.150
26	-0.150
28	-0.133
30	-0.129
32	-0.112
33	-0.116
44	0.134
45	0.198
46	0.196
47	0.257
48	0.262
49	0.305
50	0.319
50.5	0.357
51	0.349
51.5	0.384
52	0.394
52.5	0.416
53	0.449
53.5	0.452
54	0.452

x = 100 cm

y (cm)	u (m/s)
0	-0.125
1	-0.139
2	-0.150
4	-0.154
6	-0.150
8	-0.160
10	-0.147
12	-0.155
14	-0.160
16	-0.168
18	-0.156
20	-0.163
22	-0.151
24	-0.149
26	-0.129
28	-0.123
30	-0.106
46	0.201
47	0.216
48	0.238
49	0.252
50	0.295
50.5	0.298
51	0.315
51.5	0.334
52	0.357
52.5	0.362
53	0.392
53.5	0.400
54	0.392

x = 120 cm

y (cm)	u (m/s)
1	-0.141
2	-0.142
4	-0.158
6	-0.145
8	-0.147
10	-0.162
12	-0.160
14	-0.161
16	-0.155
18	-0.152
20	-0.149
22	-0.131
24	-0.117
26	-0.122
43	0.124
44	0.170
45	0.147
46	0.179
47	0.184
48	0.206
49	0.230
50	0.247
50.5	0.270
51	0.276
51.5	0.299
52	0.282
52.5	0.317
53	0.307
53.5	0.342
54	0.326

x = 140 cm

y (cm)	u (m/s)
0	-0.111
1	-0.135
2	-0.151
4	-0.148
6	-0.145
8	-0.135
10	-0.149
12	-0.148
14	-0.150
16	-0.151
18	-0.140
20	-0.135
22	-0.119
23	-0.130
24	-0.113
25	-0.118
45	0.149
46	0.166
47	0.157
48	0.172
49	0.203
50	0.212
50.5	0.234
51	0.232
51.5	0.254
52	0.254
52.5	0.270
53	0.293
53.5	0.298
54	0.294

x = 160 cm

y (cm)	u (m/s)
0	-0.110
1	-0.132
2	-0.126
4	-0.128
6	-0.132
8	-0.127
10	-0.127
12	-0.136
14	-0.123
16	-0.128
18	-0.131
20	-0.121
22	-0.104
23	-0.102
45	0.114
46	0.120
47	0.135
48	0.155
49	0.192
50	0.183
50.5	0.200
51	0.197
51.5	0.210
52	0.216
52.5	0.209
53	0.234
53.5	0.224
54	0.242

x = 180 cm

y (cm)	u (m/s)
0	-0.099
1	-0.103
2	-0.103
4	-0.119
6	-0.100
8	-0.106
10	-0.111
12	-0.104
14	-0.105
16	-0.103
17	-0.109
48	0.125
49	0.136
50	0.154
50.5	0.145
51	0.186
51.5	0.175
52	0.179
52.5	0.171
53	0.200
53.5	0.201
54	0.203

x = 200 cm

y (cm)	u (m/s)
7	-0.08
8	-0.10
10	-0.10
12	-0.09
14	-0.10
15	-0.09
16	-0.09
48	0.10
49	0.11
50	0.15
50.5	0.16
51	0.14
51.5	0.14
52	0.139
52.5	0.163
53	0.168
53.5	0.196
54	0.189

Expt. 8

x = 35 cm

y (cm)	u (m/s)
0	-0.102
1	-0.157
2	-0.127
5	-0.153
8	-0.174
11	-0.172
14	-0.162
17	-0.170
20	-0.178
23	-0.164
25	-0.154
26	-0.116
33	0.215
34	0.261
35	0.358
36	0.437
37	0.504
38	0.562
39	0.589
40	0.602
41	0.629

x = 45 cm

y (cm)	u (m/s)
0	-0.115
1	-0.137
2	-0.160
5	-0.164
8	-0.195
11	-0.199
14	-0.200
17	-0.189
20	-0.214
23	-0.196
25	-0.146
26	-0.144
27	-0.149

30	0.116
32	0.200
34	0.283
36	0.403
38	0.496
39	0.529
40	0.553
41	0.588

x = 60 cm

y (cm)	u (m/s)
0	-0.139
1	-0.187
2	-0.191
5	-0.191
8	-0.198
11	-0.213
14	-0.208
17	-0.216
20	-0.210
23	-0.169
25	-0.106
26	-0.131
30	0.136
32	0.191
34	0.294
36	0.359
38	0.469
39	0.507
40	0.533
41	0.565

x = 80 cm

y (cm)	u (m/s)
0	-0.145
1	-0.178
2	-0.208
5	-0.190
8	-0.208
11	-0.208
14	-0.218
17	-0.218
20	-0.189
23	-0.165
24	-0.114
30	0.148
32	0.201
34	0.269
36	0.360
38	0.437
39	0.450
40	0.476
41	0.501

x = 100 cm

y (cm)	u (m/s)
0	-0.133
1	-0.174
2	-0.169
5	-0.170
8	-0.185
11	-0.176
14	-0.188
17	-0.182
20	-0.170
23	-0.124
31	0.152
32	0.176
34	0.260
36	0.297
38	0.362
39	0.392
40	0.420
41	0.454

x = 120 cm

y (cm)	u (m/s)
0	-0.120
1	-0.135
2	-0.132
5	-0.154
8	-0.151
11	-0.147
14	-0.152
17	-0.149
20	-0.145
22	-0.124
23	-0.117
32	0.140
34	0.163
36	0.210
38	0.281
39	0.304
40	0.327
41	0.353

x = 140 cm

y (cm)	u (m/s)
0	-0.103
1	-0.124
2	-0.128
5	-0.130
8	-0.144
11	-0.137
14	-0.122
17	-0.145
20	-0.131
23	-0.111
24	-0.090
25	-0.093
26	-0.087
27	-0.104
28	-0.077
29	-0.082
30	-0.074
33	0.094
34	0.130
36	0.182
38	0.205
39	0.252
40	0.283
41	0.308

x = 160 cm

y (cm)	u (m/s)
0	-0.089
1	-0.103
2	-0.092
5	-0.112
8	-0.120
11	-0.106
14	-0.112
17	-0.097
20	-0.101
23	-0.099
25	-0.100
27	-0.085
29	-0.060
32	0.102
33	0.104
34	0.121
36	0.158
38	0.176
39	0.220
40	0.235
41	0.292

x = 180 cm

y (cm)	u (m/s)
0	-0.064
1	-0.085
2	-0.082
5	-0.092
8	-0.096
11	-0.093
14	-0.084
17	-0.084
20	-0.106
23	-0.069
26	-0.068
29	-0.059
33	0.098
34	0.106
36	0.125
38	0.150
39	0.191
40	0.236
41	0.288

x = 200 cm

y (cm)	u (m/s)
1	-0.078
2	-0.081
5	-0.078
8	-0.083
11	-0.095
14	-0.074
17	-0.082
20	-0.076
23	-0.087
25	-0.064
27	-0.060
28	-0.059
30	0.085
32	0.074
34	0.079
36	0.128
38	0.138
39	0.145
40	0.204
41	0.289

Expt. 9

x = 35 cm

y (cm)	u (m/s)
1	-0.115
2	-0.111
2.5	-0.137
3	-0.141
4	-0.136
5	-0.150
6	-0.146
7	-0.136
8	-0.171
10	-0.149
12	-0.161
14	-0.152
16	-0.171
18	-0.161
20	-0.178
22	-0.179
24	-0.162
26	-0.146
28	-0.161
30	-0.159
32	-0.148
34	-0.154
36	-0.150
38	-0.137
40	-0.123
41	-0.126
42	-0.117
45.5	0.160
46	0.168
46.5	0.216
46.25	0.180
47	0.247
47.5	0.281
48	0.328
48.5	0.384
49	0.391
49.5	0.446
50	0.506
50.5	0.514
51	0.541
51.5	0.561
52	0.590
52.5	0.600
53	0.603
53.5	0.611
54	0.616
54.5	0.609
55	0.587

x = 45 cm

y (cm)	u (m/s)
1.5	-0.146
2	-0.156
3	-0.149
4	-0.129

5	-0.159	16	-0.171	22	-0.211	26	-0.209	44	0.249
6	-0.149	18	-0.208	24	-0.193	28	-0.196	44.5	0.275
8	-0.127	20	-0.189	26	-0.195	30	-0.188	45	0.249
10	-0.170	22	-0.181	28	-0.196	31	-0.172	45.5	0.281
12	-0.151	24	-0.186	30	-0.182	32	-0.153	46	0.264
14	-0.155	26	-0.189	32	-0.180	32.5	-0.145	46.5	0.321
16	-0.174	28	-0.171	34	-0.146	42.5	0.223	47	0.335
18	-0.157	30	-0.177	36	-0.143	43	0.199	47.5	0.345
20	-0.168	32	-0.178	43	0.185	43.5	0.224	48	0.335
22	-0.175	34	-0.150	43.5	0.196	44	0.233	48.5	0.373
24	-0.170	34.5	-0.151	44	0.221	44.5	0.266	49	0.391
26	-0.176	43.5	0.177	44.5	0.247	45	0.278	49.5	0.413
28	-0.161	44	0.175	45	0.263	45.5	0.298	50	0.432
30	-0.141	44.5	0.210	45.5	0.263	46	0.319	50.5	0.430
32	-0.164	45	0.236	46	0.297	46.5	0.318	51	0.453
34	-0.151	45.5	0.251	46.5	0.334	47	0.348	51.5	0.452
36	-0.142	46	0.287	47	0.337	47.5	0.372	52	0.481
37	-0.138	46.5	0.316	47.5	0.387	48	0.382	52.5	0.496
44.5	0.160	47	0.327	48	0.376	48.5	0.418	53	0.527
45.5	0.196	47.5	0.363	48.5	0.427	49	0.406	53.5	0.544
46	0.235	48	0.374	49	0.434	49.5	0.452	54	0.519
46.5	0.263	48.5	0.423	49.5	0.471	50	0.466	54.5	0.467
47	0.307	49	0.458	50	0.487	50.5	0.468	x = 120 cm	
47.5	0.341	49.5	0.461	50.5	0.489	51	0.502	y (cm)	u (m/s)
48	0.390	50	0.473	51	0.535	51.5	0.501	0.5	-0.182
48.5	0.422	50.5	0.530	51.5	0.563	52	0.526	1	-0.203
49	0.472	51	0.565	52	0.580	52.5	0.562	2	-0.183
49.5	0.511	51.5	0.587	52.5	0.602	53	0.585	3	-0.210
50	0.549	52	0.605	53	0.620	53.5	0.591	4	-0.199
50.5	0.588	52.5	0.633	53.5	0.636	54	0.570	6	-0.208
51	0.630	53	0.655	54	0.629	54.5	0.503	8	-0.210
51.5	0.667	53.5	0.647	54.5	0.595	x = 100 cm		10	-0.205
52	0.714	54	0.609	x = 80 cm		y (cm)	u (m/s)	12	-0.202
52.5	0.714	54.5	0.687	y (cm)	u (m/s)	3.5	-0.204	14	-0.203
53	0.741	x = 60 cm		1.5	-0.164	4	-0.202	16	-0.198
53.5	0.714	y (cm)	u (m/s)	2	-0.157	6	-0.202	18	-0.195
54	0.682	0.5	-0.1429	2.5	-0.183	8	-0.195	20	-0.180
x = 55 cm		1	-0.155	3	-0.168	10	-0.217	21	-0.176
y (cm)	u (m/s)	2.5	-0.1568	4	-0.171	12	-0.213	22	-0.182
0.5	-0.117	3	-0.1568	6	-0.182	14	-0.226	24	-0.168
1	-0.134	4	-0.1631	8	-0.215	16	-0.215	41	0.193
1.5	-0.133	6	-0.1644	10	-0.205	18	-0.226	41.5	0.204
2	-0.181	8	-0.172	12	-0.199	20	-0.206	43	0.222
4	-0.174	10	-0.176	14	-0.219	22	-0.197	43.5	0.227
6	-0.163	12	-0.1877	16	-0.230	24	-0.191	44	0.237
8	-0.155	14	-0.1905	18	-0.221	26	-0.180	44.5	0.240
10	-0.167	16	-0.1984	20	-0.224	42.5	0.211	45	0.295
12	-0.182	18	-0.1844	22	-0.223	43	0.221	45.5	0.299
14	-0.181	20	-0.1908	24	-0.211	43.5	0.227	46	0.306

46.5	0.312
47	0.311
47.5	0.321
48	0.309
48.5	0.333
49	0.373
49.5	0.365
50	0.376
50.5	0.402
51	0.405
51.5	0.439
52	0.450
52.5	0.469
53	0.465
53.5	0.470
54	0.464
54.5	0.437

x = 140 cm

y (cm)	u (m/s)
1	-0.172
2	-0.191
4	-0.203
6	-0.196
8	-0.200
10	-0.189
12	-0.188
14	-0.194
16	-0.179
18	-0.169
20	-0.173
42.5	0.223
43	0.203
43.5	0.231
44	0.212
44.5	0.219
45	0.232
45.5	0.220
46	0.234
46.5	0.234
47	0.259
47.5	0.266
48	0.315
48.5	0.291
49	0.301
49.5	0.320
50	0.316
50.5	0.332
51	0.347
51.5	0.376
52	0.360
52.5	0.394
53	0.390
53.5	0.390
54	0.431
54.5	0.401

x = 160 cm

y (cm)	u (m/s)
1	-0.177
2	-0.185
4	-0.171
6	-0.187
8	-0.175
10	-0.173
12	-0.186
14	-0.173
16	-0.163
17	-0.167
20	-0.145
41	0.165
43.5	0.189
44	0.203
44.5	0.197
45	0.204
45.5	0.201
46	0.221
46.5	0.226
47	0.233
47.5	0.253
48	0.249
48.5	0.280
49	0.277
49.5	0.288
50	0.282
50.5	0.317
51	0.311
51.5	0.291
52	0.342
52.5	0.293
53	0.346
53.5	0.341
54	0.379
54.5	0.365

x = 180 cm

y (cm)	u (m/s)
2	-0.163
4	-0.151
6	-0.153
8	-0.150
10	-0.15
12	-0.14
13	-0.15
16	-0.14
18	-0.14
43.5	0.18
44	0.20
45	0.17
45.5	0.18
46	0.18
46.5	0.23
47	0.20
47.5	0.18
48	0.22
48.5	0.24
49	0.23
49.5	0.24
50	0.23
50.5	0.25
51	0.27
51.5	0.29
52	0.29
52.5	0.29
53	0.28
53.5	0.32
54	0.33
54.5	0.32

x = 200 cm

y (cm)	u (m/s)
0	-0.113
2	-0.136
4	-0.149
6	-0.136
8	-0.124
10	-0.107
12	-0.120
14	-0.126
16	-0.114
42	0.138
41	0.159
41.5	0.139
42.5	0.136
43.5	0.163
44	0.172
44.5	0.180
45	0.157
45.5	0.190
46	0.191
46.5	0.192
47	0.172
47.5	0.196
48	0.199
48.5	0.192
49	0.221
49.5	0.219
50	0.242
50.5	0.257
51	0.249
51.5	0.274
52	0.272
52.5	0.289
53	0.267
53.5	0.305
54	0.297
54.5	0.314

Expt. 12

x = 40 cm

y (cm)	u (m/s)
0	-0.131
1	-0.170
2	-0.187
4	-0.179
7	-0.196
10	-0.221
13	-0.253
16	-0.256
19	-0.234
22	-0.251
25	-0.224
28	-0.253
31	-0.223
34	-0.218
37	-0.153
40	-0.146
46	0.191
47	0.235
48	0.363
49	0.438
50	0.547
51	0.632
52	0.714
53	0.754
54	0.780
55	0.780

x = 60 cm

y (cm)	u (m/s)
4	-0.258
6	-0.238
9	-0.286
12	-0.276
15	-0.296
18	-0.297
21	-0.301
24	-0.280
27	-0.254
29	-0.244
42	0.283
43	0.344
44	0.394
45	0.459
46	0.498
47	0.579
48	0.639
49	0.728
50	0.780
51	0.864
52	0.929
53	0.908
54	0.908

x = 80 cm

y (cm)	u (m/s)
0	-0.242
1	-0.275
2	-0.310
5	-0.326
8	-0.337
11	-0.336
14	-0.353
17	-0.343
20	-0.329
23	-0.330
26	-0.305
28	-0.258
30	-0.230
31	-0.206
39	0.234
40	0.276
41	0.284
42	0.368
43	0.371
44	0.442
45	0.506

46	0.530
47	0.550
48	0.594
49	0.631
50	0.670
51	0.754
52	0.780
53	0.792
54	0.792

x = 100 cm

y (cm)	u (m/s)
0	-0.230
1	-0.292
2	-0.298
5	-0.314
8	-0.320
11	-0.348
14	-0.334
17	-0.315
20	-0.315
23	-0.284
26	-0.245
27	-0.243
41	0.356
42	0.409
43	0.401
44	0.451
45	0.469
46	0.516
47	0.572
48	0.588
49	0.613
50	0.686
51	0.686
52	0.714
53	0.728
54	0.686

x = 120 cm

y (cm)	u (m/s)
0	-0.262
1	-0.273
2	-0.285
5	-0.297
8	-0.312
11	-0.291
14	-0.292
17	-0.296
20	-0.285
23	-0.264
24	-0.251
25	-0.250
26	-0.253
41	0.260
42	0.298
43	0.380
44	0.398
45	0.425
46	0.436
47	0.493
48	0.516
49	0.550
50	0.586
51	0.624
52	0.649
53	0.659
54	0.615

x = 140 cm

y (cm)	u (m/s)
0	-0.243
1	-0.268
2	-0.283
5	-0.289
8	-0.295
11	-0.281
14	-0.273
17	-0.259
20	-0.257
23	-0.242
24	-0.231
42	0.260
43	0.291
44	0.350
45	0.351
46	0.386
47	0.394
48	0.443
49	0.472
50	0.518
51	0.521
52	0.542
53	0.579
54	0.579

x = 160 cm

y (cm)	u (m/s)
0	-0.222
1	-0.258
2	-0.246
5	-0.264
8	-0.258
11	-0.251
14	-0.246
17	-0.221
20	-0.182
43	0.280
44	0.314
45	0.332
46	0.369
47	0.360
48	0.375
49	0.402
50	0.417
51	0.452
52	0.508
53	0.526
54	0.520

x = 180 cm

y (cm)	u (m/s)
0	-0.203
1	-0.241
2	-0.235
5	-0.219
8	-0.211
11	-0.214
14	-0.172
15	-0.178
16	-0.197
17	-0.177
18	-0.199
43	0.284
44	0.284
45	0.298
46	0.288
47	0.309
48	0.353
49	0.379
50	0.364
51	0.411
52	0.455
53	0.427
54	0.527

x = 200 cm

y (cm)	u (m/s)
0	-0.180
1	-0.193
2	-0.197
5	-0.187
8	-0.195
11	-0.185
14	-0.174
16	-0.140
43	0.240
44	0.269
45	0.274
46	0.285
47	0.289
48	0.310
49	0.321
50	0.329
51	0.345
52	0.374
53	0.386
54	0.391

Expt. 14

x = 40 cm

y (cm)	u (m/s)
43	0.182
44	0.169
45	0.202
46	0.229
47	0.300
48	0.340
49	0.381
50	0.437
51	0.452
52	0.478
53.5	0.497

x = 50 cm

y (cm)	u (m/s)
43	0.116
45	0.187
47	0.287
48	0.331
49	0.382
50	0.420
51	0.453
52	0.490
53	0.531
53.5	0.536

x = 60 cm

y (cm)	u (m/s)
41	0.100
43	0.145
45	0.224
47	0.300
49	0.386
51	0.463
53	0.521
53.5	0.545

x = 80 cm

y (cm)	u (m/s)
41	0.129
43	0.191
45	0.244
47	0.310
49	0.389
51	0.433
53	0.487
53.5	0.501

x = 120 cm

y (cm)	u (m/s)
39	0.095
41	0.157
43	0.203
45	0.255
47	0.275
49	0.326
51	0.365
53	0.408
53.5	0.409

x = 160 cm

y (cm)	u (m/s)
29	0.084
31	0.085
33	0.095
35	0.106
37	0.118
39	0.155
41	0.171
43	0.181
45	0.199
47	0.223
49	0.254
51	0.298
53	0.318
53.5	0.346

x = 200 cm

y (cm)	u (m/s)
36	0.077
38	0.110
40	0.128

42	0.122
44	0.147
46	0.183
48	0.246
50	0.215
52	0.258
53	0.256
53.5	0.264

x = 240 cm

y (cm)	u (m/s)
38	0.094
40	0.095
42	0.094
44	0.132
46	0.150
48	0.171
50	0.167
52	0.164
53	0.186
53.5	0.213

x = 280 cm

y (cm)	u (m/s)
38	0.074
40	0.084
42	0.082
44	0.097
46	0.107
48	0.118
50	0.157
52	0.133
53	0.158
53.5	0.181

Expt. 15

x = 50 cm

y (cm)	u (m/s)
0	-0.117
1	-0.144
4	-0.172
7	-0.161
10	-0.173
13	-0.167
16	-0.184
19	-0.176
22	-0.146
27	0.071
29	0.153
31	0.265
33	0.372
35	0.466
37	0.561
39	0.591

x = 65 cm

y (cm)	u (m/s)
0	-0.156
1	-0.174
4	-0.211
7	-0.201
10	-0.210
13	-0.220
16	-0.219
19	-0.195
22	-0.155
24	-0.129
27	0.151
29	0.240
31	0.295
33	0.379
35	0.445
37	0.534
39	0.585

x = 80 cm

y (cm)	u (m/s)
0	-0.202
1	-0.213
4	-0.233
7	-0.236
10	-0.210
13	-0.217
16	-0.211
19	-0.160
22	-0.127
23	-0.096
27	0.148
29	0.227
31	0.291
33	0.373
35	0.416
37	0.504
39	0.544

x = 120 cm

y (cm)	u (m/s)
0	-0.160
1	-0.175
4	-0.188
7	-0.191
10	-0.147
13	-0.153
16	-0.142
19	-0.127
20	-0.133
25	0.090
27	0.148
29	0.201
31	0.230
33	0.295
35	0.328
37	0.355
39	0.417

x = 160 cm

y (cm)	u (m/s)
0	-0.134
1	-0.132
4	-0.141
7	-0.143
10	-0.126
13	-0.127
16	-0.111
17	-0.102
18	-0.097
25	0.085
27	0.104
29	0.142
31	0.191
33	0.208
35	0.223
37	0.251
39	0.308

x = 200 cm

y (cm)	u (m/s)
0	-0.109
1	-0.117
4	-0.110
7	-0.111
9	-0.097
11	-0.103
14	-0.094
17	-0.097
20	-0.098
21	-0.090
27	0.114
29	0.122
31	0.139
33	0.143
35	0.169
37	0.188
39	0.202

x = 240 cm

y (cm)	u (m/s)
0	-0.101
1	-0.096
4	-0.095
7	-0.095
10	-0.090
13	-0.086
16	-0.084
19	-0.083
26	0.066
29	0.088
32	0.107
35	0.126
37	0.147
39	0.162

Expt. 16

x = 35 cm

y (cm)	u (m/s)
0	-0.157
1	-0.174
2	-0.172
4	-0.169
6	-0.172
8	-0.170
10	-0.158
12	-0.143
18	0.163
20	0.255
22	0.420
24	0.511
25	0.552
25.7	0.602

x = 50 cm

y (cm)	u (m/s)
0	-0.1696
2	-0.1917
4	-0.2177
6	-0.1588
8	-0.1569
10	-0.1197
17	0.1565
19	0.196
21	0.268
23	0.404
25	0.499
25.7	0.531

x = 70 cm

y (cm)	u (m/s)
0	-0.122
2	-0.125
4	-0.121
16	0.152
18	0.215
20	0.268
22	0.360
24	0.452
25	0.471
25.7	0.491

x = 100 cm

y (cm)	u (m/s)
16	0.139
18	0.174
20	0.198
22	0.226
24	0.295
25.7	0.351

x = 140 cm

y (cm)	u (m/s)
16	0.109
18	0.128
20	0.148
22	0.173
24	0.203
25.7	0.219

x = 180 cm

y (cm)	u (m/s)
18	0.080
20	0.099
22	0.117
24	0.127
25.7	0.133

x = 220 cm

y (cm)	u (m/s)
20	0.0747
22	0.0863
24	0.0988
25.7	0.1071

Expt. 17

x = 40 cm

y (cm)	u (m/s)
0	-0.304
2	-0.311
4	-0.316
6	-0.258
8	-0.218
9	-0.214
10	-0.191
11	-0.189
16	0.201
18	0.409
20	0.635
22	0.805
24	0.824
25.7	0.835

x = 50 cm

y (cm)	u (m/s)
0	-0.3172
2	-0.2981
4	-0.2579
6	-0.2063
15	0.2094
16	0.2716
18	0.4815
20	0.6329
22	0.8167
24	0.832
25.7	0.8346

x = 70 cm

y (cm)	u (m/s)
0	-0.188
2	-0.212
4	-0.179
14	0.182
16	0.267
18	0.326
20	0.405
22	0.488
24	0.540
25.7	0.566

x = 100 cm

y (cm)	u (m/s)
13	0.1494
15	0.1865
17	0.2299
19	0.2529
21	0.313
23	0.369
25.7	0.400

x = 120 cm

y (cm)	u (m/s)
14	0.141
16	0.191
18	0.259
20	0.237
22	0.293
24	0.313
25.7	0.336

x = 140 cm

y (cm)	u (m/s)
13	0.130
15	0.150
17	0.166
19	0.192
21	0.204
23	0.230
25.7	0.246

x = 180 cm

y (cm)	u (m/s)
0	0.088
2	0.109
4	0.122
6	0.119
8	0.106
10	0.103
12	0.091
14	0.109
16	0.125
18	0.147
20	0.164
22	0.185
25.7	0.201

x = 220 cm

y (cm)	u (m/s)
0	0.0445
2	0.0804
4	0.0996
6	0.1065
8	0.1068
10	0.1107
12	0.1085
14	0.1327
16	0.1173
18	0.1182
20	0.1489
22	0.1591
24	0.1754
25.7	0.1977

Expt. 18

x = 50 cm

y (cm)	u (m/s)
5	-0.230
8	-0.267
11	-0.272
14	-0.269
17	-0.240
20	-0.240
23	-0.233
26	-0.252
30	-0.222
33	-0.237
36	-0.238
42	0.197
44	0.337
46	0.521
48	0.754
50	0.820
52	0.886
54	0.908

x = 70 cm

y (cm)	u (m/s)
0	-0.230
1	-0.295
2	-0.255
5	-0.261
8	-0.295
11	-0.255
14	-0.256
17	-0.264
20	-0.273
23	-0.271
26	-0.265
29	-0.270
30	-0.272
31	-0.265
32	-0.275
38	0.211
40	0.330
42	0.433
44	0.570
46	0.660
48	0.720
50	0.806
52	0.840
54	0.882

x = 90 cm

y (cm)	u (m/s)
0	-0.226
1	-0.249
2	-0.286
5	-0.308
8	-0.291
11	-0.324
14	-0.327
17	-0.328
21	-0.329
24	-0.301
27	-0.272
30	-0.219
36	0.184
38	0.242
40	0.384
42	0.433
44	0.540
46	0.652
48	0.728
50	0.817
52	0.845
54	0.874

x = 110 cm

y (cm)	u (m/s)
0	-0.235
4	-0.316
8	-0.310
12	-0.325
16	-0.330
20	-0.325
24	-0.263
28	-0.233
29	-0.200
38	0.237
37	0.175
40	0.348
42	0.431
44	0.447
46	0.588
48	0.609
50	0.686
52	0.724
54	0.758

x = 140 cm

y (cm)	u (m/s)
0	-0.229
4	-0.266
8	-0.276
12	-0.277
16	-0.262
20	-0.241
22	-0.239
23	-0.231
37	0.187
38	0.224
40	0.299
42	0.368
44	0.425
46	0.515
48	0.545
50	0.591
52	0.639
53	0.647
54	0.659

x = 180 cm

y (cm)	u (m/s)
0	-0.1891
4	-0.2357
8	-0.2378
12	-0.2367
16	-0.2054
19	-0.1727
37	0.176
38	0.2104
40	0.2802
42	0.3426
44	0.3699
46	0.4107
48	0.4513
50	0.4961
52	0.5315
53	0.5493
54	0.5646

x = 220 cm

y (cm)	u (m/s)
0	-0.167

4	-0.1636
8	-0.1649
12	-0.1653
16	-0.1426
37	0.1767
38	0.2015
40	0.2467
42	0.2863
44	0.3066
46	0.3375
48	0.3657
50	0.3969
52	0.4257
53	0.4515
54	0.4712

x = 260 cm

y (cm)	u (m/s)
0	-0.155
4	-0.167
8	-0.169
12	-0.169
16	-0.159
36	0.177
38	0.202
40	0.233
42	0.255
44	0.278
46	0.295
48	0.310
50	0.328
52	0.346
53	0.363
54	0.373

Expt. 19

x = 50 cm

y (cm)	u (m/s)
2	-0.165
5	-0.192
8	-0.206
11	-0.218
14	-0.226
17	-0.247
20	-0.259
23	-0.247
26	-0.279
30	-0.260
38	0.207
40	0.388
42	0.551
44	0.728
46	0.767
48	0.817
50	0.817
52	0.847
54	0.884

x = 70 cm

y (cm)	u (m/s)
0	-0.127
1	-0.237
2	-0.227
5	-0.265
8	-0.297
11	-0.298
14	-0.320
17	-0.330
20	-0.317
23	-0.313
26	-0.299
29	-0.219
30	-0.244
36	0.197
38	0.310
40	0.465
42	0.594
44	0.780
46	0.919
48	0.991
50	1.052
52	1.093
54	1.100

x = 90 cm

y (cm)	u (m/s)
0	-0.254
1	-0.270
2	-0.315
5	-0.343
8	-0.330
11	-0.352
14	-0.344
17	-0.378
20	-0.352
23	-0.337
26	-0.323
29	-0.238
36	0.206
38	0.337
40	0.382
42	0.501
44	0.639
46	0.700
48	0.754
50	0.792
52	0.813
54	0.854

x = 110 cm

y (cm)	u (m/s)
0	-0.230
4	-0.350
8	-0.344
12	-0.362
16	-0.369
20	-0.349
24	-0.290
28	-0.235
29	-0.221
36	0.246
38	0.360
40	0.414
42	0.566
44	0.596
46	0.712
48	0.792
50	0.836
52	0.866
54	0.883

x = 140 cm

y (cm)	u (m/s)
0	-0.226
4	-0.276
8	-0.274
12	-0.293
16	-0.281
20	-0.302
22	-0.239
24	-0.218
26	-0.222
28	-0.170
36	0.195
38	0.262
40	0.327
42	0.405
44	0.458
46	0.560
48	0.662
50	0.705
52	0.724
54	0.754

x = 180 cm

y (cm)	u (m/s)
0	-0.168
4	-0.238
8	-0.245
12	-0.247
16	-0.215
20	-0.202
22	-0.166
24	-0.170
36	0.148
38	0.206
40	0.259
42	0.290
44	0.364
46	0.414
48	0.459
50	0.505
52	0.524
54	0.566

x = 220 cm

y (cm)	u (m/s)
0	-0.138
4	-0.146
8	-0.147
12	-0.151
16	-0.156
36	0.151
38	0.171
40	0.190
42	0.216
44	0.234
46	0.293
48	0.323
50	0.363
52	0.407
54	0.448

x = 260 cm

y (cm)	u (m/s)
0	-0.103
4	-0.100
8	-0.099
12	-0.101
16	-0.081
40	0.174
42	0.194
44	0.210
46	0.239
48	0.255
50	0.278
52	0.296
54	0.323

Expt. 20

x = 60 cm

y (cm)	u (m/s)
0	-0.134
1	-0.160
4	-0.204
8	-0.216
12	-0.224
16	-0.274
20	-0.259
24	-0.275
26	-0.265
28	-0.272
30	-0.208
32	-0.183
36	0.332
38	0.444
42	0.741
46	0.780
50	0.662
52	0.575
54	0.566

x = 80 cm

y (cm)	u (m/s)
0	-0.184
1	-0.223
4	-0.236
8	-0.304
12	-0.301
16	-0.306
20	-0.315
24	-0.333
28	-0.277
32	-0.161
38	0.198
42	0.472
44	0.589
46	0.655
48	0.714
50	0.767
52	0.829

54	0.829

x = 100 cm

y (cm)	u (m/s)
0	-0.235
1	-0.268
4	-0.309
8	-0.321
12	-0.313
16	-0.339
20	-0.332
24	-0.294
28	-0.260
32	-0.212
40	0.239
42	0.337
44	0.417
46	0.527
48	0.585
50	0.657
52	0.728
54	0.767

x = 120 cm

y (cm)	u (m/s)
0	-0.241
1	-0.304
4	-0.286
8	-0.321
12	-0.303
16	-0.315
20	-0.336
24	-0.309
26	-0.286
28	-0.280
30	-0.249
32	-0.206
42	0.245
44	0.317
46	0.398
48	0.511
50	0.610
52	0.687
54	0.683

x = 160 cm

y (cm)	u (m/s)
0	-0.235
1	-0.203
4	-0.239
8	-0.245
12	-0.254
16	-0.213
20	-0.219
24	-0.206
44	0.204
46	0.267
48	0.338
50	0.407
52	0.502
54	0.548

x = 200 cm

y (cm)	u (m/s)
0	-0.162
1	-0.166
4	-0.174
8	-0.177
12	-0.169
14	-0.190
46	0.204
48	0.224
50	0.254
52	0.299
54	0.354

x = 220 cm

y (cm)	u (m/s)
0	-0.136
1	-0.129
4	-0.139
8	-0.142
12	-0.139
14	-0.133
46	0.184
48	0.207
50	0.233
52	0.268
54	0.328

Expt. 21

x = 60 cm

y (cm)	u (m/s)
0	-0.226
1	-0.288
4	-0.286
8	-0.287
12	-0.311
16	-0.312
20	-0.293
24	-0.263
25	-0.230
26	-0.200
27	-0.160
32	0.278
36	0.605
40	0.829
44	0.727
46	0.598
48	0.480
50	0.411
52	0.316
54	0.313

x = 80 cm

y (cm)	u (m/s)
0	-0.255
1	-0.333
4	-0.319
8	-0.312
12	-0.356
16	-0.310
20	-0.316
24	-0.237
26	-0.191
32	0.168
34	0.224
36	0.324
38	0.440
40	0.515
42	0.573
44	0.638
46	0.656
48	0.647
50	0.607
52	0.578
54	0.550

x = 100 cm

y (cm)	u (m/s)
0	-0.231
1	-0.371
4	-0.354
8	-0.335
12	-0.335
16	-0.284
20	-0.245
24	-0.197
26	-0.166
34	0.161
36	0.238
38	0.284
40	0.366
42	0.450
44	0.470
46	0.504
48	0.535
50	0.551
52	0.571
54	0.584

x = 120 cm

y (cm)	u (m/s)
0	-0.207
1	-0.267
4	-0.277
8	-0.280
12	-0.266
16	-0.254
20	-0.257
22	-0.265
23	-0.275
24	-0.268
25	-0.249
34	0.132
36	0.163
38	0.171
40	0.228
42	0.261
44	0.309
46	0.373
48	0.444
50	0.478
52	0.508
54	0.547

x = 160 cm

y (cm)	u (m/s)
0	-0.201
1	-0.220
4	-0.204
8	-0.200
12	-0.196
16	-0.218
18	-0.208
19	-0.189
42	0.202
44	0.234
46	0.241
48	0.278
50	0.316
52	0.342
54	0.369

x = 200 cm

y (cm)	u (m/s)
0	-0.138
1	-0.158
4	-0.164
8	-0.167
12	-0.153
14	-0.142
16	-0.125
42	0.155
44	0.183
46	0.207
48	0.218
50	0.221
52	0.223
54	0.224

x = 220 cm

y (cm)	u (m/s)
1	-0.121
4	-0.130
8	-0.140
12	-0.142
16	-0.133
44	0.168
46	0.180
48	0.192
50	0.202
52	0.207
54	0.208

1.2 Velocity Measurements for the Inclined Jet

Expt. 3

$x/b_o = 9.12$ & $y/b_o = 32.90$

x (m)	y (m)	θ (deg.)	u (m/s)
0.1172	0.3140	30	0.325
0.1128	0.3165	30	0.562
0.1085	0.3190	30	0.611
0.1042	0.3215	30	0.822
0.0998	0.3240	30	0.936
0.0955	0.3265	30	1.018
0.0912	*0.3290*	*30*	*1.029*
0.0868	0.3315	30	0.959
0.0825	0.3340	30	0.912
0.0782	0.3365	30	0.812
0.0739	0.3390	30	0.763

$x/b_o = 11.62$ & $y/b_o = 34.65$

x (m)	y (m)	θ (deg.)	u (m/s)
0.1422	0.3315	30	0.514
0.1378	0.3340	30	0.542
0.1335	0.3365	30	0.615
0.1292	0.3390	30	0.775
0.1248	0.3415	30	0.802
0.1205	0.3440	30	0.820
0.1162	*0.3465*	*30*	*0.843*
0.1118	0.3490	30	0.812
0.1075	0.3515	30	0.794
0.1032	0.3540	30	0.726
0.0989	0.3565	30	0.672
0.0945	0.3590	30	0.636

$x/b_o = 14.12$ & $y/b_o = 36.15$

x (m)	y (m)	θ (deg.)	u (m/s)
0.1758	0.3415	30	0.417
0.1715	0.3440	30	0.477
0.1672	0.3465	30	0.522
0.1628	0.3490	30	0.565
0.1585	0.3515	30	0.678
0.1585	0.3515	30	0.666
0.1542	0.3540	30	0.704
0.1498	0.3565	30	0.739
0.1455	0.3590	30	0.752
0.1412	*0.3615*	*30*	*0.770*
0.1368	0.3640	30	0.766
0.1325	0.3665	30	0.731
0.1282	0.3690	30	0.713
0.1239	0.3715	30	0.678
0.1195	0.3740	30	0.645
0.1152	0.3765	30	0.603
0.1109	0.3790	30	0.560
0.1022	0.3840	30	0.492

$x/b_o = 16.62$ & $y/b_o = 37.90$

x (m)	y (m)	θ (deg.)	u (m/s)
0.2138	0.3515	30	0.3245
0.2095	0.3540	30	0.3944
0.2051	0.3565	30	0.4776
0.2008	0.3590	30	0.5112
0.1965	0.3615	30	0.4972
0.1922	0.3640	30	0.5502
0.1878	0.3665	30	0.5956
0.1835	0.3690	30	0.6146
0.1792	0.3715	30	0.6468
0.1748	0.3740	30	0.6566
0.1705	0.3765	30	0.6664
0.1662	*0.3790*	*30*	*0.6713*
0.1575	0.3840	30	0.6452
0.1489	0.3890	30	0.632
0.1402	0.3940	30	0.6106
0.1315	0.3990	30	0.5805
0.1142	0.4090	30	0.4841

$x/b_o = 19.12$ & $y/b_o = 39.40$

x (m)	y (m)	θ (deg.)	u (m/s)
0.2431	0.3640	30	0.2728
0.2345	0.3690	30	0.3434
0.2258	0.3740	30	0.376
0.2215	0.3765	30	0.3858
0.2172	0.3790	30	0.3961
0.2128	0.3815	30	0.491
0.2085	0.3840	30	0.5143
0.2042	0.3865	30	0.5143
0.1998	0.3890	30	0.5484
0.1912	*0.3940*	*30*	*0.5691*
0.1825	0.3990	30	0.5592
0.1739	0.4040	30	0.5581
0.1652	0.4090	30	0.5323
0.1565	0.4140	30	0.5245
0.1479	0.4190	30	0.4975

0.1392	0.4240	30	0.466

$x/b_o = 20.62$ & $y/b_o = 41.40$

x (m)	y (m)	θ (deg.)	u (m/s)
0.2928	0.3640	30	0.241
0.2841	0.3690	30	0.292
0.2755	0.3740	30	0.331
0.2668	0.3790	30	0.365
0.2581	0.3840	30	0.422
0.2495	0.3890	30	0.476
0.2408	0.3940	30	0.492
0.2322	0.3990	30	0.490
0.2235	0.4040	30	0.515
0.2148	0.4090	30	0.510
0.2062	*0.4140*	*30*	*0.528*
0.1975	0.4190	30	0.523
0.1889	0.4240	30	0.492
0.1802	0.4290	30	0.473
0.1629	0.4390	30	0.415

$x/b_o = 22.62$ & $y/b_o = 41.90$

x (m)	y (m)	θ (deg.)	u (m/s)
0.3128	0.3690	30	0.111
0.2955	0.3790	30	0.130
0.2868	0.3840	30	0.173
0.2781	0.3890	30	0.232
0.2695	0.3940	30	0.300
0.2608	0.3990	30	0.356
0.2522	0.4040	30	0.395
0.2435	0.4090	30	0.408
0.2348	0.4140	30	0.430
0.2262	0.4190	30	0.469
0.2089	0.4290	30	0.460
0.1915	0.4390	30	0.433
0.1742	0.4490	30	0.375

Expt.9

$x/b_o = 13.25$ & $y/b_o = 35.40$

x (m)	y (m)	θ (deg.)	u (m/s)
0.0554	0.3240	30	0.129
0.0803	0.3290	30	0.314
0.1248	0.3340	30	0.702
0.1162	0.3390	30	1.236
0.1075	*0.3440*	*30*	*1.413*
0.0989	0.3490	30	0.948
0.0902	0.3540	30	0.361

$x/b_o = 10.75$ & $y/b_o = 34.40$

x (m)	y (m)	θ (deg.)	u (m/s)
0.1845	0.3240	30	15.5
0.1758	0.3290	30	16
0.1672	0.3340	30	16.5
0.1585	0.3390	30	17
0.1498	0.3440	30	17.5
0.1412	0.3490	30	18
0.1325	*0.3540*	*30*	*18.5*
0.1239	0.3590	30	19
0.1152	0.3640	30	19.5
0.1065	0.3690	30	20
0.0979	0.3740	30	20.5
0.0892	0.3790	30	21

$x/b_o = 15.75$ & $y/b_o = 37.10$

x (m)	y (m)	θ (deg.)	u (m/s)
0.2095	0.3410	30	0.080
0.2008	0.3460	30	0.110
0.1922	0.3510	30	0.192
0.1835	0.3560	30	0.345
0.1748	0.3610	30	0.729
0.1662	0.3660	30	1.037
0.1575	*0.3710*	*30*	*1.298*
0.1489	0.3760	30	1.147
0.1402	0.3810	30	0.682

$x/b_o = 23.90$ & $y/b_o = 47.61$

x (m)	y (m)	θ (deg.)	u (m/s)
0.2991	0.4161	45	0.094
0.2891	0.4261	45	0.144
0.2691	0.4461	45	0.395
0.2591	0.4561	45	0.510
0.2491	0.4661	45	0.665
0.2391	*0.4761*	*45*	*0.707*
0.2291	0.4861	45	0.597
0.2191	0.4961	45	0.547
0.2091	0.5061	45	0.478

Expt.12

$x/b_o = 13.25$ & $y/b_o = 36.20$

x (m)	y (m)	θ (deg.)	u (m/s)
0.1498	0.3520	30	0.760
0.1412	0.3570	30	1.585
0.133	*0.3620*	*30*	*1.773*
0.1239	0.3670	30	0.813

$x/b_o = 25.41$ & $y/b_o = 47.31$

x (m)	y (m)	θ (deg.)	u (m/s)
0.2741	0.4531	45	0.501
0.2691	0.4581	45	0.633
0.2641	0.4631	45	0.735
0.2591	0.4681	45	0.952
0.2541	*0.4731*	*45*	*1.018*
0.2491	0.4781	45	0.987
0.2441	0.4831	45	0.988
0.2391	0.4881	45	0.862
0.2341	0.4931	45	0.840
0.2291	0.4981	45	0.762
0.2241	0.5031	45	0.630
0.2191	0.5081	45	0.599
0.2141	0.5131	45	0.554

$x/b_o = 29.41$ & $y/b_o = 51.06$

x (m)	y (m)	θ (deg.)	u (m/s)
0.3241	0.4806	45	0.658
0.3191	0.4856	45	0.640
0.3141	0.4906	45	0.726
0.3091	0.4956	45	0.868
0.3041	0.5006	45	0.886
0.2991	0.5056	45	0.923
0.2941	*0.5106*	*45*	*0.934*
0.2891	0.5156	45	0.854
0.2841	0.5206	45	0.708
0.2791	0.5256	45	0.657

Expt.14

$x/b_o = 0.81$ & $y/b_o = 14.95$

x (m)	y (m)	θ (deg.)	u (m/s)
0.0162	0.2790	30	0.154
0.0162	0.2840	30	0.285
0.0162	0.2890	30	0.447
0.0162	0.2940	30	0.728
0.0162	0.2952	30	0.860
0.0162	0.2970	30	0.979
0.0162	*0.2990*	*30*	*1.060*
0.0162	0.3040	30	1.040
0.0162	0.3090	30	0.920
0.0162	0.3140	30	0.597
0.0162	0.3190	30	0.285

$x/b_o = 3.31$ & $y/b_o = 16.45$

x (m)	y (m)	θ (deg.)	u (m/s)
0.0662	0.3040	30	0.134
0.0662	0.3090	30	0.281
0.0662	0.3140	30	0.501
0.0662	0.3190	30	0.720
0.0662	0.3240	30	0.892
0.0662	*0.3290*	*30*	*0.936*
0.0662	0.3340	30	0.875
0.0662	0.3390	30	0.688
0.0662	0.3440	30	0.547
0.0662	0.3490	30	0.401
0.0662	0.3540	30	0.308
0.0662	0.3590	30	0.240

$x/b_o = 5.81$ & $y/b_o = 17.70$

x (m)	y (m)	θ (deg.)	u (m/s)
0.1162	0.3090	30	0.1605
0.1162	0.3140	30	0.1594
0.1162	0.3190	30	0.1734
0.1162	0.3240	30	0.2526
0.1162	0.3290	30	0.354
0.1162	0.3340	30	0.4727
0.1162	0.3390	30	0.546
0.1162	0.3440	30	0.6631
0.1162	0.3490	30	0.7436
0.1162	*0.3540*	*30*	*0.763*
0.1162	0.3590	30	0.7602
0.1162	0.3640	30	0.6927
0.1162	0.3690	30	0.616
0.1162	0.3740	30	0.551
0.1162	0.3790	30	0.472
0.1162	0.3840	30	0.3835
0.1162	0.3890	30	0.3215
0.1162	0.3940	30	0.2863
0.1162	0.3990	30	0.2783

$x/b_o = 8.31$ & $y/b_o = 19.70$

x (m)	y (m)	θ (deg.)	u (m/s)
0.1662	0.3390	30	0.1137
0.1662	0.3440	30	0.1642
0.1662	0.3490	30	0.24
0.1662	0.3540	30	0.2971
0.1662	0.3590	30	0.36
0.1662	0.3640	30	0.4373
0.1662	0.3690	30	0.4854
0.1662	0.3740	30	0.554
0.1662	0.3790	30	0.632
0.1662	0.3840	30	0.673

0.1662	0.3890	30	0.704
0.1662	*0.3940*	*30*	*0.716*
0.1662	0.3990	30	0.708
0.1662	0.4035	30	0.680
0.1662	0.4090	30	0.630
0.1662	0.4140	30	0.560
0.1662	0.4190	30	0.507
0.1662	0.4240	30	0.455
0.1662	0.4290	30	0.411
0.1662	0.4340	30	0.375
0.1662	0.4390	30	0.318
0.1662	0.4440	30	0.279
0.1662	0.4490	30	0.260

$x/b_o = 10.81$ & $y/b_o = 21.45$

x (m)	y (m)	θ (deg.)	u (m/s)
0.2162	0.3690	30	0.411
0.2162	0.3790	30	0.421
0.2162	0.3890	30	0.520
0.2162	0.3990	30	0.643
0.2162	0.4090	30	0.723
0.2162	0.4190	30	0.740
0.2162	*0.4290*	*30*	*0.743*
0.2162	0.4390	30	0.738
0.2162	0.4490	30	0.715
0.2162	0.4590	30	0.690
0.2162	0.4690	30	0.643
0.2162	0.4790	30	0.600
0.2162	0.4890	30	0.568
0.2162	0.4990	30	0.534
0.2162	0.5090	30	0.495
0.2162	0.5190	30	0.468
0.2162	0.5240	30	0.463

$x/b_o = 13.31$ & $y/b_o = 23.95$

x (m)	y (m)	θ (deg.)	u (m/s)
0.2662	0.3990	30	0.423
0.2662	0.4090	30	0.425
0.2662	0.4190	30	0.458
0.2662	0.4290	30	0.519
0.2662	0.4390	30	0.568
0.2662	0.4490	30	0.600
0.2662	0.4590	30	0.655
0.2662	0.4690	30	0.669
0.2662	*0.4790*	*30*	*0.673*
0.2662	0.4890	30	0.668
0.2662	0.4990	30	0.656
0.2662	0.5090	30	0.641
0.2662	0.5190	30	0.602
0.2662	0.5290	30	0.532
0.2662	0.5390	30	0.456
0.2662	0.5490	30	0.424
0.2662	0.5590	30	0.396
0.2662	0.5690	30	0.395

Expt.16

$x/b_o = 0.81$ & $y/b_o = 14.33$

x (m)	y (m)	θ (deg.)	u (m/s)
0.0595	0.2615	30	0.204
0.0508	0.2665	30	0.168
0.0422	0.2715	30	0.420
0.0335	0.2765	30	0.930
0.0248	0.2815	30	1.057
0.0162	*0.2865*	*30*	*1.060*
0.0075	0.2915	30	1.010

$x/b_o = 3.31$ & $y/b_o = 16.58$

x (m)	y (m)	θ (deg.)	u (m/s)
0.1181	0.3015	30	0.2666
0.1095	0.3065	30	0.2905
0.1008	0.3115	30	0.4036
0.0922	0.3165	30	0.5868
0.0835	0.3215	30	0.7298
0.0748	0.3265	30	0.8745
0.066	*0.332*	*30*	*0.9590*
0.0575	0.3365	30	0.9447
0.0489	0.3415	30	0.8355
0.0402	0.3465	30	0.7106
0.0315	0.3515	30	0.5987
0.0229	0.3565	30	0.4677
0.0142	0.3615	30	0.4066
0.0056	0.3665	30	0.3600
0.0000	0.3715	30	0.3457

$x/b_o = 5.81$ & $y/b_o = 18.58$

x (m)	y (m)	θ (deg.)	u (m/s)
0.1681	0.3415	30	0.2975
0.1595	0.3465	30	0.3906
0.1508	0.3515	30	0.5899
0.1422	0.3565	30	0.7155
0.1335	0.3615	30	0.7418
0.1248	0.3665	30	0.7389
0.1162	*0.3715*	*30*	*0.7569*

0.1075	0.3765	30	0.7064
0.0989	0.3815	30	0.6476
0.0902	0.3865	30	0.6068
0.0815	0.3915	30	0.5204
0.0729	0.3965	30	0.4553
0.0642	0.4015	30	0.4186
0.0556	0.4065	30	0.3595
0.0469	0.4115	30	0.3421
0.0382	0.4165	30	0.2858
0.0296	0.4215	30	0.2725
0.0123	0.4315	30	0.2458

$x/b_o = 8.31$ & $y/b_o = 20.83$

x (m)	y (m)	θ (deg.)	u (m/s)
0.2788	0.3515	30	0.1929
0.2701	0.3565	30	0.2005
0.2614	0.3615	30	0.2174
0.2528	0.3665	30	0.2319
0.2441	0.3715	30	0.2520
0.2355	0.3765	30	0.2953
0.2268	0.3815	30	0.3295
0.2181	0.3865	30	0.4010
0.2095	0.3915	30	0.4357
0.2008	0.3965	30	0.4678
0.1922	0.4015	30	0.5270
0.1835	0.4065	30	0.5542
0.1748	0.4115	30	0.6052
0.1662	*0.4165*	*30*	*0.6106*
0.1575	0.4215	30	0.6005
0.1489	0.4265	30	0.5958
0.1402	0.4315	30	0.5704

0.1315	0.4365	30	0.5520
0.1229	0.4415	30	0.5061
0.1142	0.4465	30	0.4759
0.1056	0.4515	30	0.4552
0.0969	0.4565	30	0.4040
0.0882	0.4615	30	0.3843
0.0796	0.4665	30	0.3163
0.0709	0.4715	30	0.2800
0.0536	0.4815	30	0.2183

$x/b_o = 10.81$ & $y/b_o = 22.33$

x (m)	y (m)	θ (deg.)	u (m/s)
0.2941	0.4015	30	0.2568
0.2855	0.4065	30	0.2872
0.2768	0.4115	30	0.3110
0.2681	0.4165	30	0.3422
0.2595	0.4215	30	0.3824
0.2508	0.4265	30	0.3887
0.2422	0.4315	30	0.4280
0.2335	0.4365	30	0.4386
0.2248	0.4415	30	0.4342
0.2162	*0.4465*	*30*	*0.4501*
0.2075	0.4515	30	0.4499
0.1989	0.4565	30	0.4179
0.1902	0.4615	30	0.4041
0.182	0.467	30	0.3578
0.1729	0.4715	30	0.3408
0.1642	0.4765	30	0.3005
0.1556	0.4815	30	0.2909
0.1469	0.4865	30	0.2588
0.1382	0.4915	30	0.2289

1.3 Bed Shear Stress Measurements

Expt. 1

x (m)	τ (N/m^2)
0.13	-0.103
0.14	-0.107
0.16	-0.136
0.18	-0.193
0.20	-0.343
0.22	-0.445
0.24	-0.521
0.26	-0.571
0.28	-0.626
0.30	-0.799
0.32	-0.868
0.34	-0.885
0.36	-0.941
0.38	-0.745
0.40	-0.356
0.41	-0.256
0.46	0.389
0.48	0.666
0.50	0.970
0.52	1.186
0.54	1.216
0.56	1.253
0.58	1.311
0.60	1.272
0.62	1.119
0.64	1.039
0.66	1.030
0.68	0.950
0.70	0.891
0.72	0.863
0.74	0.767
0.76	0.720
0.78	0.724
0.80	0.628
0.82	0.524
0.84	0.510
0.86	0.422
0.88	0.468
0.90	0.393
0.92	0.372
0.94	0.310
0.96	0.301
0.98	0.201
1.00	0.224
1.02	0.127
1.04	0.177

Expt. 2

x (m)	τ (N/m^2)
0.40	-0.110
0.42	-0.152
0.44	-0.116
0.46	-0.127
0.48	-0.123
0.50	-0.156
0.52	-0.151
0.54	-0.154
0.56	-0.116
0.60	-0.108

Expt. 3

x (m)	τ (N/m^2)
0.60	-0.030
0.70	-0.052
0.75	-0.048
0.80	-0.054
0.90	-0.068
0.95	-0.078
1.00	-0.075
1.05	-0.079
1.10	-0.082
1.15	-0.081
1.20	-0.080
1.25	-0.076
1.30	-0.066
1.35	-0.060
1.40	-0.055
1.45	-0.053
1.50	-0.051
1.60	-0.032
1.70	-0.026

Expt. 4

x (m)	τ (N/m^2)
0.65	-0.051
0.70	-0.054
0.75	-0.063
0.80	-0.063
0.85	-0.073
0.90	-0.060
0.95	-0.069
1.00	-0.083
1.05	-0.083
1.10	-0.077
1.15	-0.075
1.20	-0.086
1.25	-0.087
1.30	-0.090
1.35	-0.090
1.40	-0.077
1.45	-0.082
1.50	-0.071
1.60	-0.082
1.70	-0.065
1.80	-0.053
1.90	-0.051

Expt. 5

x (m)	τ (N/m^2)
0.10	0.043
0.15	0.063
0.20	0.049
0.25	0.043
0.60	-0.109
0.65	-0.319
0.70	-0.556
0.75	-0.427
0.80	0.952
0.85	1.082
1.00	0.580
1.10	0.296
1.20	0.150

Expt. 6

x (m)	τ (N/m^2)
0.60	-0.179
0.65	-0.217
0.70	-0.285
0.75	-0.329
0.80	-0.272
0.85	-0.238
0.90	-0.185
0.95	-0.1441
1	-0.147
1.1	-0.1266
1.3	-0.1041
1.4	-0.1058
1.5	-0.0963

Expt. 7

x (m)	τ (N/m^2)
0.35	-0.105
0.40	-0.128
0.45	-0.199
0.50	-0.209
0.55	-0.224
0.60	-0.228
0.65	-0.224
0.70	-0.168

Expt.8

x (m)	τ (N/m^2)
0.30	-0.103
0.35	-0.101
0.40	-0.087
0.45	-0.091
0.50	-0.125
0.55	-0.120
0.60	-0.124
0.65	-0.115
0.70	-0.138
0.75	-0.123
0.80	-0.148
0.85	-0.143
0.90	-0.120
0.95	-0.118
1.00	-0.131
1.05	-0.110
1.10	-0.101
1.15	-0.094
1.20	-0.097
1.25	-0.087
1.30	-0.072
1.35	-0.071
1.40	-0.071
1.45	-0.078
1.50	-0.079
1.60	-0.043
1.70	-0.049
1.80	-0.039
1.90	-0.052
2.00	-0.031

Expt. 9

x (m)	τ (N/m^2)
0.30	-0.063
0.40	-0.063
0.50	-0.092
0.60	-0.102
0.70	-0.100
0.80	-0.118
0.90	-0.149
1.00	-0.157
1.10	-0.167
1.20	-0.156
1.30	-0.158
1.40	-0.145
1.50	-0.155
1.60	-0.154
1.70	-0.137
1.80	-0.121
1.90	-0.109
2.00	-0.088

Expt. 10

x (m)	τ (N/m^2)
0.90	-0.188
0.95	-0.392
1.00	-0.598
1.05	-0.770
1.10	-0.899
1.15	-0.938
1.20	-1.029
1.25	-0.853
1.30	-0.631
1.35	-0.582
1.40	-0.484

1.45	-0.429
1.50	-0.394
1.60	-0.303
1.70	-0.284
1.80	-0.231
1.90	-0.215
2.00	-0.215
2.10	-0.168
2.20	-0.137
2.30	-0.117

Expt. 11

x (m)	τ (N/m^2)
0.80	-0.189
0.85	-0.248
0.90	-0.271
0.95	-0.257
1.00	-0.250
1.05	-0.203
1.10	-0.207
1.15	-0.172
1.20	-0.157
1.25	-0.139
1.30	-0.138
1.35	-0.131
1.40	-0.127
1.45	-0.141
1.50	-0.128
1.55	-0.125

Expt. 12

x (m)	τ (N/m^2)
0.40	-0.130
0.50	-0.154
0.60	-0.176
0.70	-0.186
0.80	-0.217
0.90	-0.223
1.00	-0.226
1.10	-0.241
1.20	-0.214
1.30	-0.226
1.40	-0.200
1.50	-0.202
1.60	-0.183
1.70	-0.177
1.80	-0.183
1.90	-0.173
2.00	-0.143

Expt. 13

x (m)	τ (N/m^2)
0.15	-1.088
0.18	-1.233
0.20	-1.394
0.23	-1.534
0.25	-1.300
0.28	-0.730
0.28	-0.578
0.29	-0.347
0.30	0.618
0.33	1.579
0.35	2.021
0.38	2.158
0.40	2.277
0.43	2.157
0.45	2.087
0.50	1.830
0.55	1.517
0.60	1.251
0.65	0.970
0.70	0.759
0.80	0.336
0.90	0.181
1.00	0.154
1.10	0.160
1.20	0.078

Expt. 14

x (m)	τ (N/m^2)
0.70	-0.049
0.80	-0.054
0.90	-0.060
0.95	-0.066
1.00	-0.067
1.05	-0.073
1.10	-0.076
1.15	-0.084
1.20	-0.075
1.25	-0.076
1.30	-0.085
1.35	-0.084
1.40	-0.087
1.45	-0.095
1.50	-0.094
1.60	-0.087
1.70	-0.092
1.80	-0.081
1.90	-0.088
2.00	-0.076
2.10	-0.073
2.20	-0.058
2.30	-0.059
2.40	-0.058
2.50	-0.046
2.60	-0.040

Expt. 15

x (m)	τ (N/m^2)
0.50	-0.099
0.60	-0.109
0.70	-0.111
0.80	-0.116
0.90	-0.122
1.00	-0.121
1.10	-0.116
1.20	-0.114
1.30	-0.107
1.40	-0.106
1.50	-0.095
1.60	-0.087
1.70	-0.080
1.80	-0.075
1.90	-0.073

Expt. 18

x (m)	τ (N/m^2)
0.75	-0.250
0.80	-0.246
0.85	-0.258
0.90	-0.279
0.95	-0.261
1.00	-0.277
1.05	-0.284
1.10	-0.290
1.15	-0.299
1.20	-0.302
1.25	-0.305
1.35	-0.303
1.40	-0.300
1.45	-0.300
1.50	-0.282
1.55	-0.281
1.65	-0.279
1.70	-0.274
1.75	-0.243
1.80	-0.228
1.85	-0.201
1.90	-0.191
1.95	-0.187
2.00	-0.165
2.05	-0.164
2.10	-0.145
2.15	-0.134
2.20	-0.116
2.25	-0.129
2.30	-0.127
2.35	-0.117

Expt. 19

x (m)	τ (N/m^2)
0.60	-0.206
0.65	-0.242
0.70	-0.242
0.75	-0.262
0.80	-0.285
0.85	-0.298
0.90	-0.286
0.95	-0.305
1.00	-0.316
1.05	-0.322
1.10	-0.327
1.15	-0.322
1.20	-0.315
1.25	-0.306
1.30	-0.292
1.35	-0.280
1.40	-0.270
1.45	-0.253
1.50	-0.235
1.55	-0.220
1.60	-0.201
1.65	-0.187
1.70	-0.177
1.75	-0.160
1.80	-0.149
1.85	-0.140
1.90	-0.126
1.95	-0.116
2.00	-0.104
2.05	-0.099
2.10	-0.094
2.15	-0.087
2.20	-0.081
2.25	-0.074
2.30	-0.073

Expt. 20

x (m)	τ (N/m^2)
0.50	-0.140
0.60	-0.148
0.70	-0.172
0.80	-0.250
0.90	-0.248
1.00	-0.281
1.10	-0.275
1.20	-0.333
1.30	-0.285
1.40	-0.268
1.50	-0.252
1.60	-0.221
1.70	-0.193
1.80	-0.174
1.90	-0.136
2.00	-0.135
2.10	-0.111

Expt. 21

x (m)	τ (N/m^2)
0.35	-0.101
0.40	-0.133
0.50	-0.163
0.60	-0.235
0.70	-0.285
0.80	-0.319
0.90	-0.352
1.00	-0.370
1.10	-0.326
1.20	-0.282

Expt. 21 (Cont.)	
x (m)	τ (N/m²)
1.30	-0.239
1.40	-0.208
1.50	-0.173
1.60	-0.148
1.70	-0.127
1.80	-0.108
1.90	-0.088
2.00	-0.082

1.4 Variation of Velocity Scale, Length Scale, Jet Discharge and Momentum Flux with Distance

Expt. 1

x (m)	u_m (m/s)	x/b_o	u_m/U_o
0.00	1.430	0.00	1.000
0.50	0.398	55.56	0.278
0.60	0.552	66.67	0.386
0.65	0.448	72.22	0.313
0.70	0.418	77.78	0.292
0.75	0.379	83.33	0.265
0.80	0.441	88.89	0.308
0.85	0.310	94.44	0.217
0.90	0.262	100.00	0.183
0.95	0.203	105.56	0.142
1.00	0.285	111.11	0.199
1.05	0.140	116.67	0.098
1.20	0.140	133.33	0.098

Expt. 2

x (m)	u_m (m/s)	b_s (cm)	x/b_o	u_m/U_o	b_s/b_o
0.00	1.430	-	0.00	1.000	-
0.07	1.430	-	7.22	0.997	-
0.10	1.284	-	11.11	0.892	-
0.19	1.379	-	21.11	0.958	-
0.29	0.524	-	32.22	0.364	-
0.30	0.504	-	33.33	0.350	-
0.40	0.638	5.75	44.44	0.443	6.39
0.50	0.515	6.50	55.56	0.357	7.22
0.60	0.672	6.75	66.67	0.467	7.50
0.80	0.607	9.50	88.89	0.422	10.56
1.00	0.550	11.00	111.11	0.382	12.22
1.20	0.422	10.50	133.33	0.293	11.67
1.40	0.334	9.50	155.56	0.232	10.56
1.60	0.255	7.00	177.78	0.177	7.78
1.80	0.202	5.50	200.00	0.140	6.11
2.00	0.166	4.50	222.22	0.115	5.00

Expt. 3

x (m)	u_m (m/s)	u_r (m/s)	b_s (cm)	x/b_o	u_m/U_o	u_r/U_o	b_s/b_o	Q/Q_o	M/M_o
0.00	1.430	-	-	0.00	1.000	-	-	1.000	1.000
0.04	1.430	-	-	4.57	1.000	-	-	-	-
0.07	1.200	-	-	7.35	0.833	-	-	-	-
0.09	1.029	-	-	10.13	0.715	-	-	-	-
0.12	0.843	-	-	12.91	0.585	-	-	-	-
0.14	0.770	-	-	15.69	0.534	-	-	-	-
0.17	0.671	-	-	18.46	0.466	-	-	-	-
0.19	0.569	-	-	21.24	0.395	-	-	-	-
0.21	0.528	-	-	22.91	0.367	-	-	-	-
0.23	0.469	-	-	25.13	0.326	-	-	-	-
0.30	0.570	-0.125	-	33.33	0.396	-0.087	-	4.492	1.186
0.40	0.626	-0.130	5.75	44.44	0.435	-0.090	6.39	4.429	1.284
0.60	0.519	-0.138	6.40	66.67	0.361	-0.096	7.11	4.431	1.065
0.80	0.480	-0.147	7.00	88.89	0.334	-0.102	7.78	4.207	0.935
1.00	0.423	-0.145	7.50	111.11	0.294	-0.101	8.33	3.930	0.770
1.20	0.358	-0.138	7.40	133.33	0.249	-0.096	8.22	3.575	0.593
1.40	0.311	-0.128	7.50	155.56	0.216	-0.089	8.33	3.295	0.474
1.60	0.269	-0.114	6.80	177.78	0.187	-0.079	7.56	3.038	0.378
1.80	0.213	-0.099	7.20	200.00	0.148	-0.069	8.00	2.385	0.236
2.00	0.156	-0.092	8.00	222.22	0.109	-0.064	8.89	-	-

Expt. 4

x (m)	u_m (m/s)	u_r (m/s)	b_s (cm)	x/b_o	u_m/U_o	u_r/U_o	b_s/b_o	Q/Q_o	M/M_o
0.00	1.430	-	-	0.00	1.000	-	-	1.000	1.000
0.04	1.430	-	-	4.57	1.000	-	-	-	-
0.07	1.189	-	-	7.35	0.825	-	-	-	-
0.09	1.047	-	-	10.13	0.727	-	-	-	-
0.12	0.922	-	-	12.91	0.641	-	-	-	-
0.14	0.844	-	-	15.69	0.586	-	-	-	-
0.17	0.743	-	-	18.46	0.516	-	-	-	-
0.23	0.519	-	-	26.01	0.360	-	-	-	-
0.24	0.431	-	-	27.12	0.299	-	-	-	-
0.25	0.361	-	-	28.23	0.251	-	-	-	-
0.30	0.370	-0.121	-	33.33	0.257	-0.084	-	3.940	1.000
0.40	0.502	-0.108	-	44.44	0.348	-0.075	-	4.181	0.971
0.60	0.515	-0.132	6.50	66.67	0.358	-0.092	7.22	4.590	1.095
0.80	0.452	-0.139	7.50	88.89	0.314	-0.097	8.33	4.570	0.956
1.00	0.400	-0.146	7.50	111.11	0.278	-0.102	8.33	4.407	0.817
1.20	0.342	-0.146	9.50	133.33	0.237	-0.101	10.56	3.942	0.624
1.40	0.298	-0.136	8.50	155.56	0.207	-0.094	9.44	3.642	0.502
1.60	0.242	-0.123	8.00	177.78	0.168	-0.086	8.89	3.203	0.359
1.80	0.222	-0.106	8.00	200.00	0.154	-0.073	8.89	2.559	0.263
2.00	0.196	-0.093	5.50	222.22	0.136	-0.065	6.11	2.157	0.196

Expt. 5

x (m)	u_m (m/s)	x/b_o	u_m/U_o
0.00	2.14	0.00	1.000
0.85	0.51	94.44	0.238
0.90	0.58	100.00	0.269
0.95	0.57	105.56	0.266
1.00	0.48	111.11	0.225
1.05	0.51	116.67	0.240
1.10	0.44	122.22	0.206
1.15	0.41	127.78	0.192
1.20	0.36	133.33	0.166
1.25	0.29	138.89	0.137
1.30	0.25	144.44	0.117
1.35	0.25	150.00	0.118
1.40	0.18	155.56	0.082
1.45	0.15	161.11	0.068

Expt. 8

x (m)	u_m (m/s)	u_r (m/s)	b_s (cm)	x/b_o	u_m/U_o	u_r/U_o	b_s/b_o	Q/Q_o
0.00	2.140	-	-	0.00	1.000	-	-	1.000
0.35	0.629	-0.153	6.50	38.89	0.294	-0.071	7.22	3.054
0.45	0.588	-0.170	7.00	50.00	0.275	-0.079	7.78	3.373
0.60	0.565	-0.180	7.00	66.67	0.264	-0.084	7.78	3.418
0.80	0.501	-0.185	7.00	88.89	0.234	-0.087	7.78	3.305
1.00	0.454	-0.167	8.00	111.11	0.212	-0.078	8.89	2.989
1.20	0.353	-0.139	7.00	133.33	0.165	-0.065	7.78	2.652
1.40	0.308	-0.111	6.00	155.56	0.144	-0.052	6.67	2.718
1.60	0.292	-0.098	5.00	177.78	0.136	-0.046	5.56	2.474
1.80	0.288	-0.082	4.00	200.00	0.135	-0.038	4.44	2.226
2.00	0.289	-0.077	2.00	222.22	0.135	-0.036	2.22	2.109

Expt. 9

x (m)	u_m (m/s)	u_r (m/s)	b_s (cm)	x/b_o	u_m/U_o	u_r/U_o	b_s/b_o	Q/Q_o	M/M_o
0.00	2.140	-	-	0.00	1.000	-	-	1.000	1.000
0.04	2.140	-	-	4.57	1.000	-	-	-	-
0.07	1.839	-	-	7.35	0.858	-	-	-	-
0.09	1.533	-	-	10.13	0.716	-	-	-	-
0.12	1.345	-	-	12.91	0.628	-	-	-	-
0.14	1.118	-	-	15.69	0.522	-	-	-	-
0.17	0.983	-	-	18.46	0.459	-	-	-	-
0.22	0.730	-	-	24.90	0.341	-	-	-	-
0.23	0.768	-	-	26.01	0.358	-	-	-	-
0.24	0.657	-	-	27.12	0.307	-	-	-	-
0.26	0.602	-	-	28.79	0.281	-	-	-	-
0.27	0.536	-	-	30.45	0.250	-	-	-	-
0.28	0.518	-	-	31.56	0.242	-	-	-	-
0.29	0.520	-	-	32.68	0.243	-	-	-	-
0.35	0.616	-0.151	-	38.89	0.287	-0.071	-	4.293	1.000
0.45	0.741	-0.155	5.00	50.00	0.346	-0.073	5.56	4.450	1.028
0.55	0.680	-0.171	6.00	61.11	0.318	-0.080	6.67	4.340	0.919
0.60	0.636	-0.175	7.00	66.67	0.297	-0.082	7.78	4.270	0.846
0.80	0.591	-0.192	8.00	88.89	0.276	-0.090	8.89	4.230	0.779
1.00	0.544	-0.206	8.00	111.11	0.254	-0.096	8.89	3.768	0.639
1.20	0.470	-0.194	9.50	133.33	0.219	-0.091	10.56	3.409	0.499
1.40	0.431	-0.187	10.00	155.56	0.201	-0.087	11.11	2.934	0.393
1.60	0.379	-0.173	10.50	177.78	0.177	-0.081	11.67	2.791	0.329
1.80	0.329	-0.148	-	200.00	0.154	-0.069	-	2.381	0.244
2.00	0.314	-0.128	11.00	222.22	0.146	-0.060	12.22	2.061	0.201

Expt. 12

x (m)	u_m (m/s)	u_r (m/s)	b_s (cm)	x/b_o	u_m/U_o	u_r/U_o	b_s/b_o	Q/Q_o	M/M_o
0.00	3.090	-	-	0.00	1.000	-	-	1.000	1.000
0.04	3.026	-	-	4.57	0.976	-	-	-	-
0.07	2.466	-	-	7.35	0.796	-	-	-	-
0.09	2.209	-	-	10.13	0.712	-	-	-	-
0.12	1.969	-	-	12.91	0.635	-	-	-	-
0.14	1.773	-	-	15.69	0.572	-	-	-	-
0.17	1.511	-	-	18.46	0.487	-	-	-	-
0.19	1.140	-	-	21.24	0.368	-	-	-	-
0.26	1.018	-	-	28.79	0.328	-	-	-	-
0.27	0.738	-	-	29.90	0.238	-	-	-	-
0.29	0.675	-	-	32.12	0.218	-	-	-	-
0.40	0.780	-0.206	-	44.44	0.252	-0.066	-	3.951	1.000
0.60	0.929	-0.273	9.00	66.67	0.300	-0.088	10.00	4.280	0.855
0.80	0.792	-0.299	10.50	88.89	0.256	-0.096	11.67	4.317	0.736
1.00	0.728	-0.295	12.75	111.11	0.235	-0.095	14.17	3.853	0.603
1.20	0.659	-0.278	12.00	133.33	0.213	-0.090	13.33	3.589	0.509
1.40	0.579	-0.265	11.00	155.56	0.187	-0.086	12.22	3.282	0.409
1.60	0.526	-0.239	11.50	177.78	0.170	-0.077	12.78	2.711	0.307
1.80	0.455	-0.204	12.00	200.00	0.147	-0.066	13.33	2.317	0.227
2.00	0.391	-0.181	12.00	222.22	0.126	-0.058	13.33	2.039	0.171

Expt. 14

x (m)	u_m (m/s)	b_s (cm)	x/b_o	u_m/U_o	b_s/b_o
0.00	1.060	-	0.00	1.000	-
0.02	1.060	-	0.81	1.000	-
0.07	0.936	-	3.31	0.883	-
0.12	0.763	-	5.81	0.720	-
0.17	0.716	-	8.31	0.676	-
0.22	0.743	-	10.81	0.701	-
0.27	0.673	-	13.31	0.635	-
0.40	0.497	-	20.00	0.469	-
0.50	0.536	-	25.00	0.506	-
0.60	0.545	6.50	30.00	0.514	3.25
0.80	0.501	8.50	40.00	0.472	4.25
1.20	0.409	10.5	60.00	0.386	5.25
1.60	0.346	12.5	80.00	0.326	6.25
2.00	0.264	13.50	100.00	0.249	6.75
2.40	0.213	11.50	120.00	0.201	5.75
2.80	0.181	11.5	140.00	0.171	5.75

Expt. 15

x (m)	u_m (m/s)	u_r (m/s)	b_s (cm)	x/b_o	u_m/U_o	u_r/U_o	b_s/b_o
0.00	1.060	-	-	0.00	1.000	-	-
0.05	1.060	-	-	2.50	1.000	-	-
0.10	0.850	-	-	5.00	0.802	-	-
0.20	0.660	-	-	10.00	0.623	-	-
0.30	0.520	-	-	15.00	0.491	-	-
0.40	0.480	-	-	20.00	0.453	-	-
0.50	0.591	-0.160	7.00	25.00	0.558	-0.151	3.50
0.65	0.585	-0.187	8.00	32.50	0.552	-0.176	4.00
0.80	0.544	-0.190	8.50	40.00	0.513	-0.180	4.25
1.20	0.417	-0.157	9.75	60.00	0.394	-0.148	4.88
1.60	0.308	-0.124	9.75	80.00	0.290	-0.117	4.88
2.00	0.202	-0.103	12.50	100.00	0.190	-0.097	6.25
2.40	0.162	-0.091	10.50	120.00	0.153	-0.086	5.25

Expt. 16

x (m)	u_m (m/s)	b_s (cm)	x/b_o	u_m/U_o	b_s/b_o	Q/Q_o	M/M_o
0.00	1.060	-	0.00	1.000	-	1.000	1.000
0.02	1.060	-	0.81	1.000	-	-	-
0.07	0.959	-	3.31	0.905	-	-	-
0.12	0.757	-	5.81	0.714	-	-	-
0.17	0.611	-	8.31	0.576	-	-	-
0.22	0.450	-	10.81	0.425	-	-	-
0.35	0.602	4.95	17.50	0.568	2.48	1.490	0.564
0.50	0.531	4.70	25.00	0.500	2.35	1.552	0.518
0.70	0.491	6.70	35.00	0.463	3.35	1.435	0.443
1.00	0.351	7.70	50.00	0.331	3.85	1.106	0.244
1.40	0.219	9.70	70.00	0.206	4.85	1.000	0.137
1.80	0.133	8.70	90.00	0.125	4.35	1.000	0.084
2.20	0.107	7.70	110.00	0.101	3.85	1.000	0.067
2.60	0.092	8.70	130.00	0.087	4.35	1.000	0.058

Expt. 17

x (m)	u_m (m/s)	b_s (cm)	x/b_o	u_m/U_o	b_s/b_o	Q/Q_o	M/M_o
0.00	1.590	-	0.00	1.000	-	1.000	1.000
0.02	1.590	-	0.81	1.000	-	-	-
0.04	1.590	-	2.06	1.000	-	-	-
0.07	1.339	-	3.31	0.837	-	-	-
0.12	1.065	-	5.81	0.666	-	-	-
0.17	0.890	-	8.31	0.556	-	-	-
0.22	0.643		10.81	0.402		-	-
0.40	0.835	7.70	20.00	0.522	3.85	1.838	0.640
0.50	0.835	7.70	25.00	0.522	3.85	1.753	0.610
0.70	0.566	9.20	35.00	0.354	4.60	1.528	0.360
1.00	0.400	9.70	50.00	0.250	4.85	1.021	0.170
1.20	0.336	10.70	60.00	0.210	5.35	1.000	0.140
1.40	0.246	12.70	70.00	0.154	6.35	1.000	0.103
1.80	0.201	13.70	90.00	0.125	6.85	1.000	0.084
2.20	0.198	13.70	110.00	0.124	6.85	1.000	0.082

Expt. 18

x (m)	u_m (m/s)	u_r (m/s)	b_s (cm)	x/b_o	u_m/U_o	u_r/U_o	b_s/b_o	Q/Q_o	M/M_o
0.00	2.130	-	-	0.00	1.000	-	-	1.000	1.000
0.04	2.126	-	-	2.06	1.000	-	-	-	-
0.07	1.744	-	-	3.31	0.820	-	-	-	-
0.12	1.595	-	-	5.81	0.750	-	-	-	-
0.17	1.526	-	-	8.31	0.718	-	-	-	-
0.26	1.319	-	-	12.95	0.620	-	-	-	-
0.50	0.908	-0.245	8.50	25.00	0.427	-0.115	4.25	3.192	0.909
0.70	0.882	-0.267	12.00	35.00	0.415	-0.125	6.00	3.509	0.971
0.90	0.874	-0.288	12.00	45.00	0.411	-0.135	6.00	3.237	0.887
1.10	0.758	-0.282	13.50	55.00	0.356	-0.132	6.75	3.187	0.757
1.40	0.659	-0.253	13.00	70.00	0.310	-0.119	6.50	2.811	0.581
1.80	0.565	-0.213	14.00	90.00	0.266	-0.100	7.00	2.402	0.425
2.20	0.471	-0.161	14.00	110.00	0.222	-0.075	7.00	1.963	0.290
2.60	0.373	-0.164	14.00	130.00	0.175	-0.077	7.00	1.982	0.232

Expt. 19

x (m)	u_m (m/s)	u_r (m/s)	b_s (cm)	x/b_o	u_m/U_o	u_r/U_o	b_s/b_o	Q/Q_o	M/M_o
0.000	2.130	-	-	0.00	1.000	-	-	1.000	1.000
0.004	2.130	-	-	0.21	1.002	-	-	-	-
0.046	1.982	-	-	2.31	0.932	-	-	-	-
0.146	1.549	-	-	7.31	0.729	-	-	-	-
0.196	1.357	-	-	9.81	0.638	-	-	-	-
0.246	1.160	-	-	12.31	0.545	-		-	-
0.296	0.998	-	-	14.81	0.469	-	-	-	-
0.346	0.807	-	-	17.31	0.380	-	-	-	-
0.500	0.804	-0.230	13.00	25.00	0.378	-0.108	6.50	2.838	0.715
0.600	1.000	-0.269	12.00	30.00	0.470	-0.126	6.00	3.085	0.967
0.900	0.924	-0.320	13.00	45.00	0.435	-0.150	6.50	3.405	0.987
1.100	0.883	-0.305	13.75	55.00	0.415	-0.143	6.88	3.298	0.913
1.400	0.754	-0.250	13.00	70.00	0.354	-0.117	6.50	2.881	0.681
1.800	0.566	-0.206	12.00	90.00	0.266	-0.097	6.00	2.504	0.445
2.200	0.448	-0.148	12.00	110.00	0.211	-0.069	6.00	1.902	0.267
2.600	0.323	-0.097	14.00	130.00	0.152	-0.045	7.00	1.523	0.154

Expt. 20

x (m)	u_m (m/s)	u_r (m/s)	b_s (cm)	x/b_o	u_m/U_o	u_r/U_o	b_s/b_o	Q/Q_o	M/M_o
0.000	2.130	-	-	0.00	1.000	-	-	1.000	1.000
0.004	2.130	-	-	0.21	1.000	-	-	-	-
0.034	2.120	-	-	1.71	0.996	-	-	-	-
0.084	1.871	-	-	4.21	0.879	-	-	-	-
0.134	1.587	-	-	6.71	0.745	-	-	-	-
0.184	1.393	-	-	9.21	0.654	-		-	-
0.239	1.209	-	-	11.96	0.568	-	-	-	-
0.289	1.087	-	-	14.46	0.510	-	-	-	-
0.339	0.981	-	-	16.96	0.461	-	-	-	-
0.389	0.889	-	-	19.46	0.417	-	-	-	-
0.439	0.768	-	-	21.96	0.361	-	-	-	-
0.489	0.660	-	-	24.46	0.310	-	-	-	-
0.539	0.611	-	-	26.96	0.287	-	-	-	-
0.559	0.592	-	-	27.96	0.278	-	-	-	-
0.600	0.780	-0.223	-	30.00	0.366	-0.105	-	3.227	0.788
0.800	0.829	-0.264	-	40.00	0.389	-0.124	-	3.638	0.943
1.000	0.767	-0.288	11.00	50.00	0.360	-0.135	25.00	4.049	0.972
1.200	0.683	-0.286	8.50	60.00	0.321	-0.134	30.00	4.113	0.880
1.600	0.548	-0.227	8.00	80.00	0.257	-0.106	40.00	3.265	0.560
2.000	0.354	-0.173	12.00	100.00	0.166	-0.081	50.00	2.474	0.274
2.200	0.328	-0.136	11.00	110.00	0.154	-0.064	55.00	2.122	0.218

Expt. 21

x (m)	u_m (m/s)	υ_r (m/s)	b_s (cm)	x/b_o	u_m/U_o	u_r/U_o	b_s/b_o	Q/Q_o	M/M_o
0.000	2.130	-	-	0.00	1.000	-	-	1.000	1.000
0.004	2.130	-	-	0.21	1.000	-	-	-	-
0.034	2.055	-	-	1.71	0.966	-	-	-	-
0.084	1.736	-	-	4.21	0.817	-	-	-	-
0.134	1.464	-	-	6.71	0.689	-	-	-	-
0.184	1.275	-	-	9.21	0.600	-		-	-
0.234	1.044	-	-	11.71	0.491	-	-	-	-
0.284	0.939	-	-	14.21	0.442	-	-	-	-
0.334	0.921	-	-	16.71	0.433	-	-	-	-
0.384	0.800	-	-	19.21	0.376	-	-	-	-
0.434	0.761	-	-	21.71	0.358	-	-	-	-
0.484	0.707	-	-	24.21	0.332	-	-	-	-
0.534	0.664	-	-	26.71	0.312	-	-	-	-
0.600	0.709	-0.260	-	30.00	0.333	-0.122	-	4.417	0.982
0.800	0.578	-0.292	-	40.00	0.272	-0.137	-	4.984	0.903
1.000	0.584	-0.280	16.00	50.00	0.275	-0.131	8.00	4.950	0.907
1.200	0.547	-0.260	12.00	60.00	0.257	-0.122	6.00	5.164	0.886
1.600	0.369	-0.205	13.00	80.00	0.174	-0.096	6.50	3.886	0.450
2.000	0.224	-0.150	19.00	100.00	0.105	-0.070	9.50	2.828	0.199
2.200	0.208	-0.133	18.00	110.00	0.098	-0.063	9.00	2.629	0.171

2. Plane Turbulent Surface Jets in Shallow Tailwater

2.1 Velocity Measurements along Vertical Sections at x-stations

Expt. 1

x = 10 cm	
y (cm)	u (m/s)
48.5	0.063
48.75	0.084
49	0.166
49.25	0.360
49.5	0.601
49.75	0.834
50	1.085
50.25	1.315
50.5	1.439

x = 20 cm	
y (cm)	u (m/s)
38	-0.042
39	-0.045
40	-0.049
41	-0.047
42	-0.049
43	-0.042
44	-0.041
45	-0.041
46	-0.045
46.5	-0.050
47.5	0.196
48	0.332
48.5	0.473
49	0.603
49.5	0.742
50	0.889
50.5	1.000

x = 40 cm	
y (cm)	u (m/s)
18	-0.062
20	-0.068
24	-0.068
28	-0.069
32	-0.061
36	-0.061
40	-0.065
42	-0.064
43	-0.060
44.5	0.069
45	0.107
46	0.195
47	0.309
48	0.442
49	0.598
50	0.71
50.5	0.72

x = 60 cm	
y (cm)	u (m/s)
0	-0.083
1	-0.091
4	-0.096
8	-0.097
12	-0.091
16	-0.094
20	-0.097
24	-0.094
28	-0.091
32	-0.093
36	-0.097
40	-0.088
41	-0.075
43	0.113
44	0.176
45	0.245
46	0.309
47	0.380
48	0.447
49	0.525
50	0.594
50.5	0.615

x = 80 cm	
y (cm)	u (m/s)
0	-0.069
1	-0.090
4	-0.099
8	-0.098
12	-0.102
16	-0.104
20	-0.112
24	-0.128
28	-0.114
32	-0.128
36	-0.111
40	0.085
41	0.113
42	0.149
43	0.189
44	0.229
45	0.267
46	0.309
47	0.372
48	0.414
49	0.463
50	0.513
50.5	0.531

x = 100 cm	
y (cm)	u (m/s)
0	-0.086
1	-0.098
4	-0.117
8	-0.125
12	-0.132
16	-0.129
20	-0.143
24	-0.149
28	-0.143
32	-0.123
36	-0.089
38	0.082
40	0.128
42	0.185
44	0.249
46	0.310
48	0.379
50	0.446
50.5	0.464

x = 120 cm	
y (cm)	u (m/s)
0	-0.094
1	-0.113
4	-0.131
8	-0.145
12	-0.158
16	-0.151
20	-0.155
24	-0.153
28	-0.150
32	-0.131
34	-0.096
36	0.036
38	0.088
40	0.142
42	0.198
44	0.245
46	0.292
48	0.342
50	0.397
50.5	0.408

x = 140 cm	
y (cm)	u (m/s)
0	-0.127
1	-0.132
4	-0.142
8	-0.149
12	-0.158
16	-0.163
20	-0.166
24	-0.163
28	-0.142
32	-0.100
33	-0.084
36	0.073
38	0.106
40	0.146
42	0.188
44	0.226
46	0.265
48	0.309
50	0.356
50.5	0.365

x = 160 cm	
y (cm)	u (m/s)
0	-0.120
1	-0.134
4	-0.148
8	-0.154
12	-0.156
16	-0.164
20	-0.154
24	-0.145
28	-0.110
30	-0.103
32	-0.064
38	0.084
40	0.134
42	0.173
44	0.202
46	0.243
48	0.279
50	0.317
50.5	0.328

x = 180 cm	
y (cm)	u (m/s)
0	-0.126
1	-0.137
4	-0.144
8	-0.149
12	-0.150
16	-0.143
20	-0.139
24	-0.120
28	-0.117
30	-0.104
32	-0.093
33	-0.068
38	0.088
40	0.118
42	0.151
44	0.179
46	0.209
48	0.236
50	0.266
50.5	0.282

x = 200 cm	
y (cm)	u (m/s)
0	-0.112
1	-0.127
4	-0.133
8	-0.153
12	-0.155
16	-0.156
20	-0.151
24	-0.131
28	-0.101
30	-0.092
31	-0.090
32	-0.083
33	-0.071
34	-0.061
35	-0.054
38	0.079
40	0.105
42	0.131
44	0.158
46	0.181
48	0.212

50	0.235
50.5	0.242

x = 220 cm

y (cm)	u (m/s)
0	-0.105
1	-0.114
4	-0.118
8	-0.113
12	-0.118
16	-0.117
20	-0.117
24	-0.115
28	-0.111
30	-0.106
31	-0.095
32	-0.071
38	0.071
40	0.094
42	0.115
44	0.134
46	0.156
48	0.178
50	0.202
50.5	0.208

x = 240 cm

y (cm)	u (m/s)
0	-0.102
1	-0.104
4	-0.103
8	-0.114
12	-0.116
16	-0.116
20	-0.112
24	-0.112
26	-0.104
27	-0.107
28	-0.102
29	-0.106
30	-0.097
31	-0.072
38	0.071
40	0.084
42	0.097
44	0.108
46	0.126
48	0.143
50	0.178
50.5	0.178

x = 260 cm

y (cm)	u (m/s)
0	-0.063
1	-0.086
4	-0.086
8	-0.084
12	-0.090
16	-0.083
20	-0.071
24	-0.075
28	-0.070
30	-0.080
31	-0.064
32	-0.044
36	0.045
38	0.058
40	0.071
42	0.084
44	0.099
46	0.114
48	0.127
50	0.145
50.5	0.149

x = 280 cm

y (cm)	u (m/s)
0	-0.059
1	-0.069
4	-0.061
8	-0.058
12	-0.054
16	-0.049
20	-0.046
24	-0.044
38	0.051
40	0.063
42	0.076
44	0.088
46	0.100
48	0.112
50	0.125
50.5	0.128

x = 300 cm

y (cm)	u (m/s)
0	-0.047
1	-0.047
4	-0.047
8	-0.044
12	-0.048
38	0.045
40	0.054
42	0.066
44	0.077
46	0.083
48	0.093
50	0.103
50.5	0.108

x = 320 cm

y (cm)	u (m/s)
0	-0.033
1	-0.032
4	-0.031
38	0.038
40	0.048
42	0.059
44	0.071
46	0.076
48	0.086
50	0.090
50.5	0.092

Expt. 2

x = 6 cm

y (cm)	u (m/s)
49	0.036
49.5	0.211
50	0.515
50.5	0.750
51	0.750

x = 20 cm

y (cm)	u (m/s)
35	-0.023
36	-0.023
38	-0.024
40	-0.031
42	-0.038
44	-0.031
45	-0.027
46	-0.035
47	-0.032
47.5	-0.029
48	0.098
48.5	0.200
49	0.287
49.5	0.402
50	0.514
50.5	0.586
51	0.629

x = 40 cm

y (cm)	u (m/s)
22	-0.028
28	-0.031
30	-0.036
32	-0.035
36	-0.041
40	-0.043
42	-0.045
43	-0.042
46	0.143
47	0.208
48	0.272
49	0.337
50	0.409
50.5	0.439
51	0.465

x = 60 cm

y (cm)	u (m/s)
2	-0.048
4	-0.047
10	-0.052
12	-0.050
16	-0.054
20	-0.056
24	-0.052
28	-0.050
32	-0.056
36	-0.052
40	-0.048
41	-0.041
44	0.092
45	0.142
46	0.176
47	0.223
48	0.276
49	0.327
50	0.372
50.5	0.391
51	0.398

x = 80 cm

y (cm)	u (m/s)
4	-0.044
8	-0.047
12	-0.057
16	-0.053
20	-0.051
24	-0.053
28	-0.052
32	-0.051
36	-0.051
38	-0.053
40	-0.051
44	0.132
45	0.152
46	0.194
47	0.239
48	0.274
49	0.307
50	0.337
50.5	0.346
51	0.350

x = 100 cm

y (cm)	u (m/s)
0	-0.048
1	-0.046
4	-0.049
8	-0.060
12	-0.070
16	-0.071
20	-0.069
24	-0.073
28	-0.066
32	-0.071
36	-0.058
41	0.079
42	0.108
43	0.132
44	0.161
45	0.184
46	0.206
47	0.236
48	0.264
49	0.290
50	0.310
50.5	0.318
51	0.332

x = 120 cm

y (cm)	u (m/s)
4	-0.080
8	-0.079
12	-0.071
16	-0.076
20	-0.092
24	-0.092
28	-0.087

32	-0.069
34	-0.056
40	0.090
41	0.112
42	0.133
43	0.152
44	0.169
45	0.189
46	0.208
47	0.229
48	0.252
49	0.269
50	0.289
50.5	0.298
51	0.305

x = 160 cm

y (cm)	u (m/s)
0	-0.0701
1	-0.0745
4	-0.0897
8	-0.0934
12	-0.0923
16	-0.0998
20	-0.0901
24	-0.0963
28	-0.0829
30	-0.0803
32	-0.0687
39	0.0985
40	0.1137
41	0.1286
42	0.1405
43	0.1523
44	0.1629
45	0.1761
46	0.19
47	0.2021
48	0.2146
49	0.2308
50	0.2472
50.5	0.2589
51	0.2658

x = 200 cm

y (cm)	u (m/s)
0	-0.0855
1	-0.0896
4	-0.1002
8	-0.1024
12	-0.0959
16	-0.1092
20	-0.0979
24	-0.0854
28	-0.0809
38	0.0758
40	0.0971
42	0.1198
44	0.1388
46	0.1577
48	0.1847
50	0.2085
50.5	0.2125
51	0.2175

x = 240 cm

y (cm)	u (m/s)
0	-0.096
1	-0.086
4	-0.077
8	-0.094
12	-0.094
16	-0.092
20	-0.073
24	-0.057
28	-0.061
38	0.067
40	0.076
42	0.089
44	0.102
46	0.116
48	0.133
50	0.146
51	0.155

x = 280 cm

y (cm)	u (m/s)
1	-0.0436
4	-0.0415
8	-0.0482
12	-0.0453
16	-0.0448
42	0.0655
44	0.0775
46	0.0857
48	0.0956
50	0.1049
51	0.1088

x = 320 cm

y (cm)	u (m/s)
40	0.040
42	0.048
44	0.053
46	0.060
48	0.068
50	0.078
51	0.080

Expt. 3

x = 6 cm

y (cm)	u (m/s)
49	0.106
50	0.953
50.5	1.500
51	1.500

x = 20 cm

y (cm)	u (m/s)
32	-0.065
34	-0.069
40	-0.070
41	-0.064
42	-0.062
43	-0.069
44	-0.061
45	-0.067
46	-0.068
47	-0.069
47.5	0.077
48	0.250
48.5	0.444
49	0.626
49.5	0.840
50	1.000
50.5	1.125
51	1.129

x = 40 cm

y (cm)	u (m/s)
18	-0.081
22	-0.085
26	-0.090
30	-0.092
34	-0.096
38	-0.090
40	-0.091
42	-0.081
44	-0.088
46	0.199
47	0.305
48	0.536
49	0.667
50	0.808
50.5	0.954
51	0.986

x = 60 cm

y (cm)	u (m/s)
0	-0.097
1	-0.095
4	-0.091
8	-0.107
12	-0.108
16	-0.108
20	-0.102
24	-0.102
28	-0.102
32	-0.108
36	-0.106
38	-0.107
40	-0.103
42	-0.094
44	0.158
45	0.252
46	0.366
47	0.453
48	0.550
49	0.650
50	0.745
50.5	0.788
51	0.805

x = 80 cm

y (cm)	u (m/s)
0	-0.096
1	-0.110
4	-0.114
8	-0.119
12	-0.132
16	-0.140
20	-0.139
24	-0.144
28	-0.127
32	-0.130
34	-0.113
36	-0.106
38	-0.097
41	0.089
42	0.142
43	0.204
44	0.272
45	0.327
46	0.406
47	0.476
48	0.545
49	0.595
50	0.666
50.5	0.700
51	0.700

x = 100 cm

y (cm)	u (m/s)
0	-0.109
1	-0.116
4	-0.123
8	-0.126
12	-0.133
16	-0.154
20	-0.158
24	-0.148
28	-0.153
32	-0.141
34	-0.113
38	0.059
39	0.096
40	0.136
41	0.178
42	0.225
43	0.282
44	0.321
45	0.367
46	0.414
47	0.464
48	0.519
49	0.556
50	0.603
50.5	0.643
51	0.645

x = 120 cm

y (cm)	u (m/s)
0	-0.097
1	-0.143
4	-0.148
8	-0.166
12	-0.180
16	-0.187
20	-0.180
24	-0.187
28	-0.148
32	-0.130

34	-0.114
35	-0.089
38	0.084
39	0.130
40	0.172
41	0.214
42	0.261
43	0.306
44	0.346
45	0.373
46	0.422
47	0.454
48	0.494
49	0.519
50	0.558
50.5	0.583
51	0.601

x = 160 cm

y (cm)	u (m/s)
0	-0.138
1	-0.185
4	-0.213
8	-0.217
12	-0.209
16	-0.218
20	-0.202
24	-0.191
28	-0.159
38	0.195
39	0.214
40	0.234
41	0.258
42	0.283
43	0.311
44	0.336
45	0.356
46	0.377
47	0.399
48	0.425
49	0.447
50	0.471
50.5	0.483
51	0.492

x = 200 cm

y (cm)	u (m/s)
0	-0.1774
1	-0.2033
4	-0.2123
8	-0.2265
12	-0.2012
16	-0.2124
20	-0.1617
24	-0.1553
28	-0.1318
38	0.155
39	0.1789
40	0.201
41	0.215
42	0.2305
43	0.2546
44	0.278
45	0.2941
46	0.3189
47	0.3303
48	0.3589
49	0.3715
50	0.3994
50.5	0.4057
51	0.4134

x = 240 cm

y (cm)	u (m/s)
0	-0.119
1	-0.150
4	-0.156
8	-0.152
12	-0.150
16	-0.151
20	-0.134
24	-0.113
39	0.127
40	0.153
41	0.174
42	0.201
43	0.219
44	0.224
45	0.238
46	0.258
47	0.268
48	0.275
49	0.282
50	0.290
50.5	0.296
51	0.299

x = 280 cm

y (cm)	u (m/s)
-0.08	0
1	-0.124
4	-0.1107
8	-0.1093
10	-0.1108
12	-0.1065
36	0.0729
38	0.0912
40	0.1078
42	0.1252
44	0.1397
46	0.1543
48	0.1744
50	0.2006
50.5	0.2054
51	0.2118

x = 320 cm

y (cm)	u (m/s)
0	-0.0515
1	-0.0737
4	-0.0785
6	-0.0711
7	-0.0735
8	-0.0705
9	-0.0738
10	-0.0712
12	-0.0666
14	-0.0619
40	0.0796
42	0.0921
44	0.1047
46	0.1158
48	0.1289
50	0.1446
50.5	0.1486
51	0.1532

Expt. 4

x = 6 cm

y (cm)	u (m/s)
49	0.067
49.25	0.339
49.5	0.717
49.75	1.091
50	1.505
50.25	1.906
50.5	2.190
50.75	2.250
51	2.250

x = 20 cm

y (cm)	u (m/s)
40	-0.095
41	-0.090
42	-0.090
43	-0.092
44	-0.090
45	-0.096
46	-0.092
47	-0.099
47.5	-0.096
48.5	0.647
49	1.049
49.5	1.401
50	1.633
50.5	1.656
51	1.657

x = 40 cm

y (cm)	u (m/s)
18	-0.0862
22	-0.0864
26	-0.1269
30	-0.1484
34	-0.1265
36	-0.0981
38	-0.1231
40	-0.0984
42	-0.134
43	-0.1111
45	0.1724
46	0.3993
47	0.6265
48	0.8772
49	1.0868
50	1.2528
51	1.2828

x = 60 cm

y (cm)	u (m/s)
12	-0.1201
16	-0.1436
20	-0.1402
24	-0.1335
28	-0.1418
32	-0.1576
36	-0.1414
40	-0.117
41	-0.1008
43	0.1807
44	0.2949
45	0.4235
46	0.5678
47	0.7381
48	0.9004
49	1.0205
50	1.085
51	1.1018

x = 80 cm

y (cm)	u (m/s)
5	-0.132
8	-0.137
12	-0.166
16	-0.150
20	-0.202
24	-0.185
28	-0.169
32	-0.171
36	-0.169
38	-0.127
41	0.226
42	0.307
43	0.372
44	0.442
45	0.517
46	0.594
47	0.674
48	0.767
49	0.849
50	0.930
51	1.010

x = 100 cm

y (cm)	u (m/s)
0	-0.103
1	-0.123
4	-0.172
8	-0.200
12	-0.202
16	-0.219
20	-0.211
24	-0.220
28	-0.238
32	-0.170
34	-0.153
40	0.162
42	0.304
44	0.483
46	0.635
48	0.777

50	0.920
51	0.950

x = 120 cm

y (cm)	u (m/s)
0	-0.12
1	-0.1698
4	-0.2186
8	-0.2496
12	-0.275
16	-0.2392
20	-0.2635
24	-0.2539
28	-0.2267
30	-0.2183
32	-0.1812
34	-0.15
38	0.1632
40	0.2641
42	0.3805
44	0.5294
46	0.6113
48	0.7412
50	0.8404
51	0.8859

x = 160 cm

y (cm)	u (m/s)
0	-0.259
1	-0.289
4	-0.293
8	-0.301
12	-0.326
16	-0.312
20	-0.309
24	-0.287
28	-0.193
30	-0.162
38	0.232
40	0.313
42	0.401
44	0.484
46	0.581
48	0.639
50	0.700
51	0.720

x = 200 cm

y (cm)	u (m/s)
0	-0.270
1	-0.315
4	-0.329
8	-0.317
12	-0.312
16	-0.289
20	-0.222
24	-0.200
28	-0.176
38	0.207
40	0.264
42	0.338
44	0.393
46	0.473
48	0.529
50	0.587
51	0.591

x = 240 cm

y (cm)	u (m/s)
0	-0.2048
1	-0.224
4	-0.2445
8	-0.2483
12	-0.2104
16	-0.2089
20	-0.1897
24	-0.1582
26	-0.1536
28	-0.1555
38	0.1656
40	0.2038
42	0.2425
44	0.289
46	0.3393
48	0.3804
50	0.4198
51	0.4329

x = 280 cm

y (cm)	u (m/s)
0	-0.1453
1	-0.1489
4	-0.1449
8	-0.1448
12	-0.1397
14	-0.1277
36	0.1118
38	0.1317
40	0.1512
42	0.1782
44	0.2061
46	0.236
48	0.266
50	0.299
51	0.313

x = 320 cm

y (cm)	u (m/s)
36	0.082
38	0.099
40	0.118
42	0.139
44	0.159
46	0.179
48	0.202
50	0.226
51	0.235

Expt. 5

x = 6 cm

y (cm)	u (m/s)
29.5	0.432
29.75	0.880
30	1.296
30.5	1.880
31	1.880

x = 12 cm

y (cm)	u (m/s)
1	-0.073
4	-0.086
8	-0.094
12	-0.094
16	-0.094
20	-0.096
24	-0.091
26	-0.095
29	0.395
29.25	0.626
29.5	0.853
29.75	1.081
30	1.282
30.5	1.655
31	1.880

x = 20 cm

y (cm)	u (m/s)
1	-0.125
4	-0.124
8	-0.128
12	-0.121
16	-0.129
20	-0.124
24	-0.122
25	-0.107
28	0.324
28.5	0.578
29	0.808
29.5	1.028
30	1.229
30.5	1.415
31	1.535

x = 40 cm

y (cm)	u (m/s)
0	-0.125
2	-0.158
4	-0.208
8	-0.210
12	-0.218
16	-0.188
20	-0.155
21	-0.157
25	0.256
26	0.397
27	0.524
28	0.676
29	0.846
30	1.013
31	1.170

x = 60 cm

y (cm)	u (m/s)
0	-0.158
2	-0.253
4	-0.253
6	-0.252
8	-0.258
10	-0.252
12	-0.258
14	-0.252
16	-0.225
18	-0.197
19	-0.162
22	0.165
23	0.246
24	0.326
25	0.403
26	0.483
27	0.591
28	0.685
29	0.769
30	0.858
31	0.908

x = 80 cm

y (cm)	u (m/s)
0	-0.271
2	-0.300
4	-0.295
6	-0.307
8	-0.303
10	-0.281
12	-0.298
14	-0.220
16	-0.175
20	0.099
21	0.176
22	0.244
23	0.312
24	0.382
25	0.438
26	0.509
27	0.580
28	0.644
29	0.707
30	0.769
31	0.829

x = 100 cm

y (cm)	u (m/s)
0	-0.2555
2	-0.2994
4	-0.2985
6	-0.2955
8	-0.2969
10	-0.2956
12	-0.2959
14	-0.1951
21	0.2298
22	0.2981
23	0.3525
24	0.3976
25	0.4533
26	0.5049
27	0.5532
28	0.6118
29	0.6678
30	0.7172
31	0.7672

x = 120 cm

y (cm)	u (m/s)
0	-0.244

2	-0.253
4	-0.270
6	-0.299
8	-0.274
10	-0.203
12	-0.182
20	0.186
21	0.226
22	0.261
23	0.301
24	0.353
25	0.401
26	0.464
27	0.519
28	0.548
29	0.576
30	0.599
31	0.619
x = 160 cm	
y (cm)	u (m/s)
0	-0.113
2	-0.148
4	-0.134
6	-0.189
8	-0.150
10	-0.155
11	-0.117
12	-0.128
19	0.127
21	0.175
23	0.230
25	0.287
27	0.342
29	0.402
31	0.452
x = 200 cm	
y (cm)	u (m/s)
0	-0.077
22	0.135
23	0.148
25	0.171
26	0.186
27	0.199
28	0.220
29	0.237
30	0.259
31	0.273
31.5	0.296
x = 240 cm	
y (cm)	u (m/s)
22	0.088
23	0.099
24	0.109
25	0.119
26	0.132
27	0.142
28	0.152
29	0.167
30	0.178
31	0.191
32	0.202
x = 280 cm	
y (cm)	u (m/s)
0	0.030
4	0.030
8	0.030
20	0.057
21	0.066
22	0.073
23	0.080
24	0.089
25	0.098
26	0.106
27	0.115
28	0.124
29	0.132
30	0.142
31	0.149
32	0.159
x = 320 cm	
y (cm)	u (m/s)
0	0.045
4	0.045
8	0.045
12	0.045
16	0.045
20	0.046
22	0.056
24	0.069
26	0.081
28	0.095
30	0.113
32	0.127
Expt. 6	
x = 6 cm	
y (cm)	u (m/s)
49	0.618
49.5	0.998
50	1.417
50.5	1.826
51	2.130
51.5	2.130
52	2.130
x = 12 cm	
y (cm)	u (m/s)
48.5	0.368
49	0.725
49.5	1.084
50	1.409
50.5	1.757
51	2.010
51.5	2.130
52	2.130
x = 24 cm	
y (cm)	u (m/s)
47	0.202
47.5	0.413
48	0.593
48.5	0.798
49	0.980
49.5	1.169
50	1.391
50.5	1.617
51	1.846
51.5	2.030
52	2.030
x = 40 cm	
y (cm)	u (m/s)
16	-0.116
24	-0.158
28	-0.143
32	-0.142
36	-0.162
40	-0.165
42	-0.139
45	0.183
46	0.355
47	0.578
48	0.864
49	1.180
50	1.416
51	1.577
52	1.701
x = 80 cm	
y (cm)	u (m/s)
4	-0.169
8	-0.237
12	-0.240
16	-0.239
20	-0.237
24	-0.239
28	-0.239
32	-0.240
36	-0.189
40	0.187
42	0.366
44	0.568
46	0.773
48	0.971
50	1.159
52	1.309
x = 120 cm	
y (cm)	u (m/s)
0	-0.160
1	-0.307
4	-0.320
8	-0.365
12	-0.323
16	-0.322
20	-0.338
24	-0.307
28	-0.282
32	-0.246
38	0.250
40	0.410
42	0.537
44	0.680
46	0.816
48	0.930
50	1.028
52	1.088
x = 160 cm	
y (cm)	u (m/s)
0	-0.342
1	-0.387
4	-0.392
8	-0.381
12	-0.392
16	-0.401
20	-0.376
24	-0.314
28	-0.216
38	0.275
40	0.401
42	0.536
44	0.655
46	0.807
48	0.920
50	0.989
52	**1.012**
x = 200 cm	
y (cm)	u (m/s)
0	-0.381
1	-0.419
4	-0.412
8	-0.412
12	-0.365
16	-0.349
20	-0.343
24	-0.265
28	-0.203
36	0.200
38	0.332
40	0.424
42	0.506
44	0.577
46	0.686
48	0.754
50	0.835
52	0.886
x = 240 cm	
y (cm)	u (m/s)
0	-0.3384
1	-0.3158
4	-0.3439
8	-0.3247
12	-0.3302
16	-0.2888
18	-0.2876
20	-0.2574
36	0.271
38	0.3191
40	0.3785
42	0.4327
44	0.4864
46	0.5507
48	0.6064
50	0.6718
52	0.7278
x = 280 cm	

y (cm)	u (m/s)
0	-0.190
1	-0.209
4	-0.218
8	-0.222
10	-0.212
12	-0.189
36	0.196
38	0.231
40	0.278
42	0.313
44	0.353
46	0.395
48	0.428
50	0.465
52	0.496

x = 320 cm

y (cm)	u (m/s)
36	0.142
38	0.173
40	0.208
42	0.232
44	0.260
46	0.289
48	0.315
50	0.334
52	0.358

Expt. 7

x = 6 cm

y (cm)	u (m/s)
19.5	0.253
19.75	0.438
20	0.615
20.5	0.000
21	0.000

x = 12 cm

y (cm)	u (m/s)
19	0.3172
19.25	0.3831
19.5	0.4469
20	0.601
20.5	0.7612
21	0.8859

x = 20 cm

y (cm)	u (m/s)
0	-0.053
2	-0.085
4	-0.075
6	-0.070
8	-0.081
10	-0.098
12	-0.087
14	-0.096
16	-0.094
18	0.150
18.5	0.264
19	0.365
19.5	0.473
20	0.576
20.5	0.687
21	0.780

x = 40 cm

y (cm)	u (m/s)
0	-0.098
2	-0.135
4	-0.135
6	-0.140
8	-0.128
10	-0.151
12	-0.120
14	-0.101
16	0.148
17	0.238
18	0.323
19	0.413
20	0.498
21	0.591

x = 60 cm

y (cm)	u (m/s)
0	-0.154
2	-0.186
4	-0.189
6	-0.180
8	-0.150
10	-0.109
12	-0.089
13	-0.091
14	0.042
15	0.116
16	0.185
17	0.253
18	0.318
19	0.389
20	0.459
21	0.496

x = 80 cm

y (cm)	u (m/s)
0	-0.174
2	-0.214
4	-0.203
6	-0.194
8	-0.162
10	-0.118
11	-0.119
12	-0.096
14	0.125
15	0.169
16	0.215
17	0.255
18	0.292
19	0.336
20	0.378
21	0.416

x = 100 cm

y (cm)	u (m/s)
0	-0.146
2	-0.162
4	-0.157
6	-0.157
8	-0.160
10	-0.162
11	-0.152
13	0.053
14	0.084
15	0.121
16	0.163
17	0.215
18	0.253
19	0.283
20	0.293
21	0.297

x = 120 cm

y (cm)	u (m/s)
0	-0.133
2	-0.103
4	-0.066
6	0.057
8	0.039
10	0.031
11	0.045
12	0.048
13	0.063
14	0.077
15	0.096
16	0.113
17	0.131
18	0.149
19	0.167
20	0.188
21	0.204

x = 140 cm

y (cm)	u (m/s)
0	0.000
2	0.011
4	0.011
6	0.011
8	0.010
10	0.018
11	0.025
12	0.033
13	0.044
14	0.053
15	0.062
16	0.071
17	0.087
18	0.099
19	0.110
20	0.120
21	0.133
21.75	0.144

x = 160 cm

y (cm)	u (m/s)
0	0.000
2	0.029
4	0.031
6	0.033
8	0.034
10	0.034
12	0.034
13	0.034
14	0.038
15	0.046
16	0.057
17	0.067
18	0.077
19	0.086
20	0.097
21	0.108
21.75	0.113

x = 200 cm

y (cm)	u (m/s)
0	0.032
2	0.032
4	0.033
6	0.032
8	0.032
10	0.032
12	0.033
14	0.033
16	0.040
18	0.051
20	0.066
21	0.075
21.75	0.082

x = 240 cm

y (cm)	u (m/s)
0	0.036
2	0.037
4	0.036
6	0.036
8	0.037
10	0.037
12	0.036
14	0.037
16	0.038
18	0.045
20	0.054
21	0.059
21.75	0.063

x = 280 cm

y (cm)	u (m/s)
0	0.038
2	0.038
4	0.039
6	0.039
8	0.039
10	0.038
12	0.038
14	0.038
16	0.038
18	0.039
20	0.041
21	0.047
21.75	0.053

x = 320 cm

y (cm)	u (m/s)
0	0.040
2	0.040
4	0.040
6	0.040

8	0.040
10	0.040
12	0.041
14	0.040
16	0.040
18	0.040
20	0.040
21	0.042
21.75	0.044

Expt. 8

x = 6 cm

y (cm)	u (m/s)
8.5	0.013
9.0	0.083
9.5	0.400
10.0	0.841
10.3	1.029
10.5	1.205
10.8	1.250
11.0	1.250

x = 12 cm

y (cm)	u (m/s)
0.0	-0.063
1.0	-0.086
2.0	-0.114
3.0	-0.133
4.0	-0.155
5.0	-0.136
6.0	-0.121
7.0	-0.132
8.5	0.151
9.0	0.367
9.5	0.615
10.0	0.847
10.5	1.062
11.0	1.202

x = 20 cm

y (cm)	u (m/s)
0.0	-0.165
1.0	-0.1922
2.0	-0.1912
3.0	-0.1921
4.0	-0.1794
5.0	-0.1639
6.0	-0.1334
7.0	-0.0932
8.0	0.1981
8.5	0.3042
9.0	0.4862
9.5	0.6499
10.0	0.8635
10.5	0.9805
11.0	0.9905

x = 40 cm

y (cm)	u (m/s)
0.0	-0.314
1.0	-0.333
2.0	-0.318
3.0	-0.248
4.0	-0.194
5.0	-0.135
6.0	-0.097
7.0	0.259
7.5	0.338
8.0	0.422
8.5	0.495
9.0	0.553
9.5	0.632
10.0	0.697
10.5	0.767
11.0	0.767

x = 60 cm

y (cm)	u (m/s)
0.00	-0.194
1.00	-0.181
2.00	-0.155
3.00	-0.134
6.50	0.188
7.00	0.225
7.50	0.263
8.00	0.289
8.50	0.323
9.00	0.361
9.50	0.389
10.00	0.416
10.50	0.437
11.00	0.456
11.50	0.468

x = 80 cm

y (cm)	u (m/s)
5.0	0.065
6.0	0.098
7.0	0.129
8.0	0.163
9.0	0.193
10.0	0.233
11.0	0.268
12.0	0.308

x = 100 cm

y (cm)	u (m/s)
0.0	0.020
1.0	0.024
2.0	0.037
3.0	0.048
4.0	0.061
5.0	0.076
6.0	0.092
7.0	0.110
8.0	0.132
9.0	0.159
10.0	0.179
11.0	0.200
12.0	0.221

x = 120 cm

y (cm)	u (m/s)
0.0	0.050
1.0	0.061
2.0	0.070
3.0	0.078
4.0	0.088
5.0	0.098
6.0	0.107
7.0	0.116
8.0	0.127
9.0	0.138
10.0	0.148
11.0	0.161
12.0	0.180

x = 160 cm

y (cm)	u (m/s)
0.0	0.091
1.0	0.092
2.0	0.094
3.0	0.097
4.0	0.099
5.0	0.102
6.0	0.104
7.0	0.107
8.0	0.109
9.0	0.111
10.0	0.113
11.0	0.115
12.0	0.118

x = 200 cm

y (cm)	u (m/s)
0.00	0.098
1.00	0.098
2.00	0.098
3.00	0.099
4.00	0.098
5.00	0.099
6.00	0.099
7.00	0.099
8.00	0.099
9.00	0.098
10.00	0.098
11.00	0.098
12.00	0.099
12.25	0.091

Expt. 9

x = 6 cm

y (cm)	u (m/s)
3	0.043
3.5	0.156
4	0.345
4.5	0.487
5	0.500

x = 12 cm

y (cm)	u (m/s)
2	0.025
2.5	0.054
3	0.123
3.5	0.239
4	0.349
4.5	0.432
5	0.469

x = 20 cm

y (cm)	u (m/s)
0	-0.120
0.5	-0.124
1	-0.137
1.5	-0.086
2	-0.061
2.5	0.114
3	0.187
3.5	0.256
4	0.322
4.5	0.390
5	0.432

x = 30 cm

y (cm)	u (m/s)
0	-0.119
0.5	-0.098
1	-0.104
1.5	-0.088
2	-0.079
2.5	0.122
3	0.173
3.5	0.228
4	0.268
4.5	0.302
5	0.327
5.3	0.338

x = 40 cm

y (cm)	u (m/s)
0	-0.072
0.5	-0.071
1	-0.044
1.5	0.041
2	0.097
2.5	0.120
3	0.171
3.5	0.195
4	0.215
4.5	0.232
5	0.243
5.5	0.261

x = 50 cm

y (cm)	u (m/s)
0	0.012
1	0.039
2	0.070
3	0.102
4	0.130
5	0.163
5.5	0.181

x = 60 cm

y (cm)	u (m/s)
0	0.029
1	0.049
2	0.071
3	0.094
4	0.117
5	0.142
5.6	0.159

x = 80 cm

y (cm)	u (m/s)
0	0.070
1	0.076
2	0.085

3	0.092
4	0.099
5	0.106
5.6	0.111
x = 100 cm	
y (cm)	u (m/s)
0	0.073
1	0.079
2	0.083
3	0.090
4	0.096
5	0.104
5.6	0.108
x = 120 cm	
y (cm)	u (m/s)
0	0.076
1	0.080
2	0.086
3	0.091
4	0.095
5	0.101
5.6	0.104
x = 140 cm	
y (cm)	u (m/s)
0	0.080
1	0.084
2	0.088
3	0.089
4	0.093
5	0.097
5.6	0.100
x = 160 cm	
y (cm)	u (m/s)
0	0.084
1	0.086
2	0.089
3	0.091
4	0.093
5	0.095
5.6	0.096

2.2 Variation of Velocity Scale, Length Scale, Jet Discharge and Momentum Flux with Distance

Expt. 1

x (m)	u_m (m/s)	u_r (m/s)	b (m)	x/b_o	u_m/U_o	u_r/U_o	b/b_o	Q/Q_o	M/M_o
0.00	0.000	-	-	0	1.000	-	-	1.000	1.000
0.06	1.600	-	0.007	12	1.000	-	1.382	1.472	0.999
0.10	1.439	-	0.009	20	0.899	-	1.746	1.624	0.999
0.20	1.000	-0.045	0.019	40	0.625	-0.028	3.741	2.273	0.992
0.30	0.805	-	0.028	60	0.503	-	5.611	2.784	0.978
0.40	0.724	-0.064	0.031	80	0.453	-0.040	6.204	2.948	0.935
0.50	0.678	-	0.038	100	0.424	-	7.571	3.236	0.916
0.60	0.615	-0.091	0.045	120	0.385	-0.057	9.030	3.492	0.911
0.70	0.572	-	0.049	140	0.358	-	9.857	3.702	0.883
0.80	0.531	-0.105	0.055	160	0.332	-0.065	11.074	3.829	0.845
0.90	0.486	-	0.063	180	0.304	-	12.597	3.950	0.823
1.00	0.464	-0.121	0.070	200	0.290	-0.076	14.056	4.071	0.786
1.20	0.408	-0.134	0.082	240	0.255	-0.084	16.478	4.057	0.696
1.40	0.365	-0.138	0.087	280	0.228	-0.087	17.498	3.860	0.562
1.60	0.328	-0.132	0.090	320	0.205	-0.083	17.926	3.280	0.475
1.80	0.282	-0.124	0.091	360	0.176	-0.078	18.168	2.845	0.352
2.00	0.242	-0.111	0.092	400	0.151	-0.070	18.438	2.509	0.274
2.20	0.208	-0.108	0.095	440	0.130	-0.068	19.085	2.159	0.201
2.40	0.178	-0.105	0.097	480	0.111	-0.065	19.378	1.816	0.141
2.60	0.149	-0.075	0.099	520	0.093	-0.047	19.884	1.711	0.111
2.80	0.128	-0.055	0.102	560	0.080	-0.034	20.492	1.393	0.083
3.00	0.108	-0.046	0.104	600	0.068	-0.029	20.827	1.182	0.059
3.20	0.092	-0.032	0.110	640	0.058	-0.020	21.922	1.066	0.048

Expt. 2

x (m)	u_m (m/s)	u_r (m/s)	b (m)	x/b_o	u_m/U_o	u_r/U_o	b/b_o	Q/Q_o	M/M_o
0.00	0.750	-	-	0	1.000	-	-	1.000	1.000
0.06	0.750	-	0.012	6	1.000	-	1.230	1.246	1.000
0.20	0.629	-0.029	0.019	20	0.839	-0.039	1.879	1.569	0.965
0.40	0.465	-0.038	0.036	40	0.620	-0.050	3.616	2.041	0.914
0.60	0.398	-0.050	0.045	60	0.531	-0.067	4.512	2.441	0.900
0.80	0.350	-0.051	0.055	80	0.467	-0.068	5.451	2.500	0.856
1.00	0.332	-0.062	0.068	100	0.442	-0.082	6.788	2.928	0.877
1.20	0.305	-0.078	0.080	120	0.407	-0.104	7.988	3.112	0.858
1.60	0.266	-0.085	0.096	160	0.354	-0.114	9.639	2.855	0.725
2.00	0.218	-0.094	0.100	200	0.290	-0.125	9.974	2.524	0.529
2.40	0.155	-0.081	0.108	240	0.207	-0.108	10.827	1.863	0.282
2.80	0.109	-0.045	0.109	280	0.145	-0.060	10.850	1.627	0.127
3.20	0.080	-	0.110	320	0.107	-	11.014	1.019	0.064

Expt. 3

x (m)	u_m (m/s)	u_r (m/s)	b (m)	x/b_o	u_m/U_o	u_r/U_o	b/b_o	Q/Q_o	M/M_o
0.00	1.500	-	-	0	1.000	-	-	1.000	1.000
0.05	1.500	-	0.012	5	1.000	-	1.239	1.262	0.991
0.20	1.129	-0.066	0.022	20	0.753	-0.044	2.170	1.630	0.941
0.40	0.986	-0.088	0.032	40	0.658	-0.059	3.184	1.958	0.895
0.60	0.805	-0.102	0.046	60	0.536	-0.068	4.583	2.336	0.897
0.80	0.700	-0.120	0.057	80	0.467	-0.080	5.707	2.690	0.881
1.00	0.645	-0.134	0.070	100	0.430	-0.089	6.967	3.015	0.877
1.20	0.601	-0.147	0.081	120	0.401	-0.098	8.122	3.062	0.847
1.60	0.492	-0.192	0.105	160	0.328	-0.128	10.489	2.970	0.723
2.00	0.413	-0.187	0.106	200	0.276	-0.125	10.593	2.477	0.504
2.40	0.299	-0.141	0.111	240	0.199	-0.094	11.128	1.863	0.302
2.80	0.212	-0.107	0.112	280	0.141	-0.071	11.229	1.376	0.136
3.20	0.153	-0.069	0.115	320	0.102	-0.046	11.480	1.050	0.066

Expt. 4

x (m)	u_m (m/s)	u_r (m/s)	b (m)	x/b_o	u_m/U_o	u_r/U_o	b/b_o	Q/Q_o	M/M_o
0.00	2.250	-	-	0	1.000	-	-	1.000	1.000
0.06	2.250	-	0.012	6	1.000	-	1.230	1.240	0.987
0.20	1.657	-0.093	0.023	20	0.736	-0.041	2.274	1.603	0.987
0.40	1.283	-0.114	0.039	40	0.570	-0.051	3.941	2.209	0.962
0.60	1.102	-0.133	0.051	60	0.490	-0.059	5.099	2.521	0.941
0.80	1.010	-0.161	0.062	80	0.449	-0.071	6.155	2.799	0.837
1.00	0.950	-0.183	0.071	100	0.422	-0.081	7.084	2.850	0.864
1.20	0.886	-0.214	0.082	120	0.394	-0.095	8.161	3.075	0.847
1.60	0.720	-0.273	0.099	160	0.320	-0.121	9.926	2.878	0.693
2.00	0.591	-0.270	0.102	200	0.262	-0.120	10.156	2.389	0.476
2.40	0.433	-0.200	0.103	240	0.192	-0.089	10.346	1.927	0.260
2.80	0.313	-0.142	0.106	280	0.139	-0.063	10.615	1.457	0.142
3.20	0.235	-	0.111	320	0.104	-	11.104	1.036	0.063

Expt. 5

x (m)	u_m (m/s)	u_r (m/s)	b (m)	x/b_o	u_m/U_o	u_r/U_o	b/b_o	Q/Q_o	M/M_o
0.00	1.880	-	-	0	1.000	-	-	1.000	1.000
0.06	1.880	-	0.012	6	1.000	-	1.214	1.154	0.977
0.12	1.880	-0.090	0.014	12	1.000	-0.048	1.404	1.312	0.972
0.20	1.535	-0.122	0.021	20	0.816	-0.065	2.089	1.592	0.954
0.40	1.170	-0.177	0.036	40	0.623	-0.094	3.597	2.217	0.941
0.60	0.908	-0.229	0.054	60	0.483	-0.122	5.363	2.604	0.883
0.80	0.829	-0.272	0.064	80	0.441	-0.145	6.426	2.779	0.839
1.00	0.767	-0.279	0.073	100	0.408	-0.148	7.310	2.689	0.789
1.20	0.619	-0.246	0.078	120	0.329	-0.131	7.829	2.473	0.638
1.60	0.452	-0.142	0.081	160	0.241	-0.075	8.134	1.837	0.318
2.00	0.296	-	0.085	200	0.157	-	8.523	1.024	0.116
2.40	0.202	-	0.087	240	0.108	-	8.730	1.042	0.070
2.80	0.159	-	0.091	280	0.084	-	9.075	1.001	0.047
3.20	0.127	-	0.089	320	0.067	-	8.892	1.013	0.033

Expt. 6

x (m)	u_m (m/s)	u_r (m/s)	b (m)	x/b_o	u_m/U_o	u_r/U_o	b/b_o	Q/Q_o	M/M_o
0.00	2.130	-	-	0	1.000	-	-	1.000	1.000
0.06	2.130	-	0.024	3	1.000	-	1.210	1.159	0.979
0.12	2.130	-	0.025	6	1.000	-	1.265	1.217	0.970
0.24	2.030	-	0.029	12	0.953	-	1.454	1.403	0.969
0.40	1.701	-0.146	0.040	20	0.799	-0.069	2.022	1.622	0.936
0.80	1.309	-0.225	0.072	40	0.614	-0.106	3.580	2.152	0.923
1.20	1.088	-0.297	0.099	60	0.511	-0.139	4.949	2.412	0.906
1.60	1.012	-0.356	0.104	80	0.475	-0.167	5.222	2.325	0.857
2.00	0.886	-0.350	0.115	100	0.416	-0.164	5.771	2.187	0.665
2.40	0.728	-0.311	0.125	120	0.342	-0.146	6.246	1.852	0.460
2.80	0.496	-0.206	0.133	140	0.233	-0.097	6.638	1.480	0.241
3.20	0.358	-	0.136	160	0.168	-	6.817	0.967	0.128

Expt.7

x (m)	u_m (m/s)	u_r (m/s)	b (m)	x/b_o	u_m/U_o	u_r/U_o	b/b_o	Q/Q_o	M/M_o
0.00	2.130	-	-	0	1.000	-	-	1.000	1.000
0.06	2.130	-	0.024	3	1.000	-	1.210	1.159	0.979
0.12	2.130	-	0.025	6	1.000	-	1.265	1.217	0.970
0.24	2.030	-	0.029	12	0.953	-	1.454	1.403	0.969
0.40	1.701	-0.146	0.040	20	0.799	-0.069	2.022	1.622	0.936
0.80	1.309	-0.225	0.072	40	0.614	-0.106	3.580	2.152	0.923
1.20	1.088	-0.297	0.099	60	0.511	-0.139	4.949	2.412	0.906
1.60	1.012	-0.356	0.104	80	0.475	-0.167	5.222	2.325	0.857
2.00	0.886	-0.350	0.115	100	0.416	-0.164	5.771	2.187	0.665
2.40	0.728	-0.311	0.125	120	0.342	-0.146	6.246	1.852	0.460
2.80	0.496	-0.206	0.133	140	0.233	-0.097	6.638	1.480	0.241
3.20	0.358	-	0.136	160	0.168	-	6.817	0.967	0.128

Expt. 8

x (m)	u_m (m/s)	u_r (m/s)	b (m)	x/b_o	u_m/U_o	u_r/U_o	b/b_o	Q/Q_o	M/M_o
0.00	1.250	-	-	0	1.000	-	-	1.000	1.000
0.06	1.250	-	0.012	6	1.000	-	1.245	1.270	0.982
0.12	1.202	-0.117	0.015	12	0.961	-0.094	1.528	1.427	0.977
0.20	0.991	-0.164	0.020	20	0.792	-0.131	1.972	1.551	0.943
0.40	0.767	-0.234	0.032	40	0.614	-0.187	3.228	1.767	0.844
0.60	0.468	-0.166	0.039	60	0.374	-0.133	3.884	1.395	0.412
0.80	0.308	-	0.043	80	0.247	-	4.258	1.042	0.174
1.00	0.221	-	0.050	100	0.177	-	4.982	0.989	0.111
1.20	0.180	-	0.078	120	0.144	-	7.793	1.044	0.100
1.60	0.118	-	-	160	0.094	-	-	1.000	0.084
2.00	0.091	-	-	200	0.072	-	-	0.964	0.076

Expt. 9

x (m)	u_m (m/s)	u_r (m/s)	b (m)	x/b_o	u_m/U_o	u_r/U_o	b/b_o	Q/Q_o	M/M_o
0.000	0.9012	-	-	0	1.000	-	-	1.000	1.000
0.054	0.9012	-	0.013	5	1.000	-	1.286	1.162	0.982
0.108	0.8859	-	0.015	11	0.983	-	1.513	1.338	0.966
0.200	0.7799	-0.082	0.019	20	0.865	-0.091	1.883	1.569	0.944
0.400	0.5914	-0.126	0.033	40	0.656	-0.140	3.300	2.044	0.935
0.600	0.4962	-0.144	0.041	60	0.551	-0.159	4.069	2.207	0.854
0.800	0.4155	-0.160	0.052	80	0.461	-0.177	5.167	2.124	0.711
1.000	0.2969	-0.157	0.053	100	0.329	-0.174	5.346	1.760	0.453
1.200	0.2044	-0.101	0.056	120	0.227	-0.112	5.612	1.231	0.192
1.400	0.1442	-	0.057	140	0.160	-	5.660	0.958	0.102
1.600	0.1125	-	0.058	160	0.125	-	5.775	0.951	0.071
2.000	0.0824	-	-	200	0.091	-	-	0.958	0.047
2.400	0.0629	-	-	240	0.070	-	-	0.965	0.044
2.800	0.0529	-	-	280	0.059	-	-	0.942	0.041
3.200	0.0444	-	-	320	0.049	-	-	0.964	0.044

NOTE TO USERS

Page(s) not included in the original manuscript are unavailable from the author or university. The manuscript was microfilmed as received.

352

This reproduction is the best copy available.

UMI

3. Plane Turbulent Wall Jets in Shallow Tailwater

3.1 Velocity Measurements along Vertical Sections at x-stations

Expt. 1

x = 6 cm

y (cm)	u (m/s)
0	2.352
0.25	2.434
0.5	2.500
0.75	2.226
1	1.773
1.25	1.253
1.5	0.632
1.75	0.101

x = 12 cm

y (cm)	u (m/s)
0	2.00
0.25	2.29
0.5	2.20
0.75	1.98
1	1.76
1.25	1.51
1.5	1.25
1.75	1.01
2	0.79
2.25	0.57
2.5	0.39
2.75	0.20

x = 20 cm

y (cm)	u (m/s)
0	1.745
0.25	1.946
0.5	1.911
0.75	1.798
1	1.673
1.25	1.537
1.5	1.412
1.75	1.276
2	1.124
2.25	0.981
2.5	0.829
2.75	0.683
3	0.550
3.25	0.441
3.5	0.330
3.75	0.219
4	0.155
4.25	0.110
25	-0.119
27.5	-0.124
30	-0.128
32.5	-0.133
35	-0.139
37.5	-0.143
40	-0.148
42.5	-0.153
45	-0.158
47.5	-0.161
48.5	-0.170

x = 30 cm

y (cm)	u (m/s)
0	1.581
0.25	1.744
0.5	1.738
0.75	1.683
1	1.595
1.5	1.399
2	1.187
2.5	0.958
3	0.756
3.5	0.557
4	0.416
4.5	0.250
5	0.132
30	-0.108
32.5	-0.112
35	-0.124
37.5	-0.131
40	-0.146
42.5	-0.153
45	-0.162
47.5	-0.179
48.5	-0.186

x = 40 cm

y (cm)	u (m/s)
0	1.309
0.25	1.461
0.5	1.498
0.75	1.498
1	1.464
1.5	1.355
2	1.221
2.5	1.069
3	0.948
3.5	0.813
4	0.677
4.5	0.563
5	0.435
5.5	0.333
6	0.246
6.5	0.181
32.5	-0.108
35	-0.119
37.5	-0.122
40	-0.138
42.5	-0.142
45	-0.153
47.5	-0.162
48.5	-0.179

x = 60 cm

y (cm)	u (m/s)
0	0.951
0.25	1.128
0.5	1.193
0.75	1.228
1	1.222
1.5	1.189
2	1.146
2.5	1.078
3	0.990
3.5	0.911
4	0.835
4.5	0.764
5	0.672
5.5	0.590
6	0.529
6.5	0.469
7	0.385
7.5	0.317
8	0.255
8.5	0.180
9	0.115
30	-0.110
32.5	-0.123
35	-0.135
37.5	-0.148
40	-0.160
42.5	-0.173
45	-0.186
47.5	-0.197
48.5	-0.209

x = 80 cm

y (cm)	u (m/s)
0	0.900
0.25	1.008
0.5	1.055
0.75	1.098
1	1.115
1.25	1.102
1.5	1.110
1.75	1.099
2	1.096
2.5	1.041
3	0.979
3.5	0.917
4	0.860
4.5	0.817
5	0.767
5.5	0.718
6	0.661
6.5	0.597
7	0.548
7.5	0.499
8	0.435
8.5	0.396
9	0.351
9.5	0.297
10	0.255
10.5	0.216
11	0.167
11.5	0.117
25	-0.107
27.5	-0.131
30	-0.154
32.5	-0.179
35	-0.202
37.5	-0.227
40	-0.242
42.5	-0.267
45	-0.298
47.5	-0.323
48.25	-0.350

x = 100 cm

y (cm)	u (m/s)
0	0.800
0.25	0.861
0.5	0.911
0.75	0.941
1	0.961
1.25	0.971
1.5	0.980
1.75	0.980
2	0.970
2.5	0.939
3	0.906
4	0.835
5	0.757
6	0.686
7	0.608
8	0.536
9	0.468
10	0.392
11	0.321
12	0.261
13	0.181
14	0.116
27.5	-0.157
30	-0.191
32.5	-0.215
35	-0.239
37.5	-0.269
40	-0.298
42.5	-0.315
45	-0.343
47.5	-0.373
48	-0.391

x = 120 cm

y (cm)	u (m/s)
0	0.7264
0.25	0.8121
0.5	0.8448
0.75	0.8682
1	0.8994
1.25	0.9084
1.5	0.9054
1.75	0.8976
2	0.8956
2.5	0.8798
3	0.8530
4	0.7906
5	0.7392
6	0.6725
7	0.6134

8	0.5618
9	0.5061
10	0.4578
11	0.4016
12	0.3551
13	0.3111
14	0.2675
15	0.2116
16	0.1565
27.5	-0.1348
30	-0.1769
32.5	-0.214
35	-0.2459
37.5	-0.2833
40	-0.3222
42.5	-0.3672
45	-0.4097
47.5	-0.4462
48	-0.4862
x = 140 cm	
y (cm)	u (m/s)
0	0.6859
0.5	0.7472
1	0.7824
1.5	0.8046
2	0.8167
2.5	0.8099
3	0.7943
3.5	0.7743
4	0.7498
4.5	0.7292
5	0.7104
5.5	0.6789
6	0.6531
7	0.6012
8	0.5577
10	0.4737
12	0.3868
14	0.3014
16	0.2252
30	-0.1692
32.5	-0.2077
35	-0.2407
37.5	-0.2863
40	-0.3236
42.5	-0.3612
45	-0.404
47.5	-0.4445
48	-0.4859
x = 160 cm	
y (cm)	u (m/s)
0	0.376
0.25	0.412
0.5	0.437
0.75	0.477
1	0.505
1.25	0.546
1.5	0.553
1.75	0.573
2	0.604
2.5	0.612
3	0.636
4	0.638
5	0.631
6	0.616
7	0.588
8	0.565
9	0.537
10	0.517
11	0.483
12	0.452
13	0.424
14	0.387
15	0.351
16	0.321
18	0.252
20	0.181
22	0.117
27.5	-0.131
32.5	-0.219
35	-0.241
37.5	-0.277
40	-0.313
42.5	-0.335
45	-0.377
47.5	-0.416
48.75	-0.462
x = 180 cm	
y (cm)	u (m/s)
0	0.190
1	0.309
2	0.385
3	0.441
4	0.469
5	0.495
6	0.503
7	0.504
8	0.497
9	0.482
10	0.463
11	0.449
12	0.434
13	0.405
14	0.379
15	0.363
16	0.340
17	0.310
18	0.289
19	0.260
20	0.229
21	0.199
37.5	-0.209
40	-0.233
42.5	-0.255
45	-0.277
47.5	-0.298
49.5	-0.328
x = 200 cm	
y (cm)	u (m/s)
1.25	0.1822
5	0.2393
6.5	0.2642
7	0.2625
7.5	0.2728
8	0.2767
8.5	0.2776
9.5	0.2745
10	0.2792
11	0.2786
12	0.2787
13	0.2797
14	0.2775
15	0.2795
16	0.2801
17	0.2799
18	0.2768
19	0.2783
20	0.2777
21	0.2803
22	0.2813
23	0.2808
24	0.28
25	0.2796
26	0.279
27	0.2799
28	0.2781
29	0.2722
30	0.2705
x = 240 cm	
y (cm)	u (m/s)
0	-0.1085
1	-0.1072
2	-0.1017
3	-0.1116
4	-0.1211
5	-0.1041
6	-0.1352
35	0.1321
37.5	0.1289
40	0.1399
42.5	0.2045
45	0.2017
47.5	0.1882
0.5	0.2307
Expt. 2	
x = 6 cm	
y (cm)	u (m/s)
0	1.2
0.25	1.25
0.5	1.25
0.75	1.1068
1	0.9004
1.25	0.6412
1.5	0.3441
1.75	0.0609
x = 12 cm	
y (cm)	u (m/s)
0	0.9805
0.25	1.1339
0.5	1.0951
0.75	1.0018
1	0.8800
1.25	0.7504
1.5	0.6304
1.75	0.5105
2	0.4019
2.25	0.3005
2.5	0.1862
2.75	0.0896
3	0.0211
x = 20 cm	
y (cm)	u (m/s)
0	0.806
0.25	0.919
0.5	0.960
0.75	0.920
1	0.847
1.25	0.784
1.5	0.707
1.75	0.640
2	0.564
2.5	0.420
3	0.284
3.5	0.160
4	0.050
4.25	0.011
25	-0.031
27.5	-0.036
30	-0.040
32.5	-0.046
35	-0.052
37.5	-0.055
40	-0.062
42.5	-0.066
45	-0.071
47.5	-0.075
49.75	-0.087
x = 40 cm	
y (cm)	u (m/s)
0	0.632
0.25	0.718
0.5	0.746
0.75	0.760
1	0.746
1.25	0.716
1.5	0.683
2	0.616
2.5	0.532
3	0.459
3.5	0.386
4	0.314
4.5	0.242
5	0.183
5.5	0.125
6	0.067
6.5	0.022
32.5	-0.051
35	-0.057
37.5	-0.059
40	-0.064

45	-0.070
49.75	-0.075

x = 60 cm

y (cm)	u (m/s)
0	0.483
0.5	0.578
1	0.594
1.5	0.585
2	0.556
2.5	0.519
3	0.489
3.5	0.456
4	0.426
4.5	0.391
5	0.356
5.5	0.323
6	0.288
6.5	0.249
7	0.218
7.5	0.185
8	0.155
8.5	0.123
9	0.102
9.5	0.076
10	0.050
10.5	0.033
30	-0.059
32.5	-0.061
35	-0.071
37.5	-0.078
40	-0.084
42.5	-0.094
45	-0.110
47.5	-0.119
49.75	-0.128

x = 80 cm

y (cm)	u (m/s)
0	0.442
0.5	0.522
1	0.544
1.5	0.541
2	0.527
2.5	0.501
3	0.480
3.5	0.456
4	0.427
4.5	0.406
5	0.378
5.5	0.357
6	0.327
6.5	0.308
7	0.286
7.5	0.262
8	0.239
8.5	0.219
9	0.197
9.5	0.174
10	0.149
10.5	0.130
11	0.109
11.5	0.086
12	0.068
12.5	0.053
32.5	-0.115
35	-0.127
37.5	-0.141
40	-0.153
42.5	-0.170
45	-0.184
47.5	-0.201
49.75	-0.214

x = 100 cm

y (cm)	u (m/s)
0	0.385
0.5	0.438
1	0.488
1.5	0.486
2	0.479
3	0.452
4	0.419
5	0.387
6	0.353
7	0.321
8	0.279
9	0.243
10	0.206
11	0.174
12	0.139
13	0.105
14	0.069
25	-0.079
30	-0.097
32.5	-0.114
35	-0.131
37.5	-0.159
40	-0.171
42.5	-0.194
45	-0.213
47.5	-0.233
49.75	-0.255

x = 120 cm

y (cm)	u (m/s)
0	0.354
0.5	0.380
1	0.419
1.5	0.438
2	0.446
2.5	0.443
3	0.430
3.5	0.421
4	0.404
5	0.378
6	0.347
7	0.319
8	0.294
9	0.265
10	0.237
11	0.211
12	0.186
13	0.166
14	0.139
15	0.115
16	0.087
32.5	-0.049
35	-0.078
37.5	-0.101
40	-0.136
42.5	-0.162
45	-0.193
47.5	-0.223
49.9	-0.254

x = 140 cm

y (cm)	u (m/s)
0	0.295
0.5	0.334
1	0.373
1.5	0.394
2	0.394
2.5	0.389
3	0.387
3.5	0.379
4	0.370
5	0.348
6	0.325
7	0.300
8	0.276
9	0.254
10	0.237
11	0.219
12	0.196
13	0.171
14	0.149
15	0.130
16	0.116
17	0.096
18	0.077
19	0.061
20	0.042
21	0.019
22	0.010
27.5	-0.0658
30	-0.0894
32.5	-0.1063
35	-0.121
37.5	-0.1499
40	-0.1613
42.5	-0.1897
45	-0.211
47.5	-0.2541
50	-0.2992

x = 160 cm

y (cm)	u (m/s)
0	0.252
0.5	0.271
1	0.292
1.5	0.307
2	0.318
2.5	0.322
3	0.322
3.5	0.319
4	0.314
5	0.298
6	0.287
7	0.277
8	0.264
9	0.253
10	0.238
11	0.223
12	0.209
13	0.197
14	0.188
15	0.175
16	0.162
18	0.138
20	0.116
35	-0.110
37.5	-0.123
40	-0.136
42.5	-0.149
45	-0.160
47.5	-0.172
50	-0.190

x = 160 cm

y (cm)	u (m/s)
4	0.224
5	0.221
6	0.238
7	0.240
8	0.240
9	0.240
10	0.235
12	0.248
14	0.240
16	0.247
18	0.234
20	0.236
21	0.235
22	0.227
23	0.226
40	-0.074
42.5	-0.086
47.5	-0.133

Expt. 3*

x = 10 cm

y (m)	u (m/s)
0.002	1.687
0.006	1.750
0.008	1.624
0.010	1.410
0.012	1.203
0.014	0.943
0.017	0.507
0.021	0.047

x = 20 cm

y (m)	u (m/s)
0.002	1.454
0.004	1.516
0.006	1.452
0.009	1.335
0.013	1.128

0.017	0.904
0.021	0.694
0.026	0.463
0.031	0.272

x = 30 cm

y (m)	u (m/s)
0.002	1.187
0.005	1.295
0.009	1.239
0.015	1.105
0.021	0.887
0.027	0.649
0.035	0.439
0.044	0.201

x = 40 cm

y (m)	u (m/s)
0.002	1.066
0.005	1.145
0.009	1.084
0.014	1.015
0.020	0.908
0.026	0.755
0.032	0.635
0.040	0.457
0.048	0.329
0.060	0.146

x = 50 cm

y (m)	u (m/s)
0.002	0.887
0.006	0.994
0.012	0.990
0.018	0.912
0.024	0.863
0.030	0.713
0.040	0.566
0.054	0.357
0.074	0.159

x = 60 cm

y (m)	u (m/s)
0.002	0.763
0.007	0.919
0.013	0.877
0.020	0.801
0.030	0.758
0.045	0.570
0.060	0.411
0.075	0.247
0.090	0.146

x = 80 cm

y (m)	u (m/s)
0.002	0.619
0.008	0.805
0.016	0.770
0.024	0.737
0.032	0.686
0.040	0.617
0.050	0.521
0.065	0.460
0.080	0.345
0.095	0.235
0.110	0.181

x = 100 cm

y (m)	u (m/s)
0.002	0.584
0.008	0.716
0.018	0.704
0.028	0.644
0.040	0.599
0.055	0.545
0.075	0.410
0.095	0.306
0.120	0.196

x = 120 cm

y (m)	u (m/s)
0.002	0.484
0.008	0.540
0.020	0.607
0.035	0.617
0.050	0.545
0.070	0.444
0.095	0.343
0.120	0.292
0.145	0.233

x = 140 cm

y (m)	u (m/s)
0.002	0.286
0.009	0.359
0.019	0.405
0.034	0.449
0.054	0.468
0.079	0.417
0.104	0.336
0.129	0.264
0.154	0.268
0.179	0.230

x = 160 cm

y (m)	u (m/s)
0.002	0.160
0.008	0.157
0.018	0.173
0.033	0.266
0.048	0.301
0.068	0.300
0.088	0.292
0.108	0.270
0.128	0.258
0.148	0.256
0.168	0.216
0.188	0.213
0.208	0.185

Expt. 4*

x = 20 cm

y (m)	u (m/s)
9E-04	2.285
0.004	2.546
0.007	2.628
0.010	2.425
0.013	2.235
0.016	2.005
0.019	1.745
0.022	1.492
0.025	1.244
0.029	0.956
0.033	0.699
0.037	0.500
0.042	0.252

x = 40 cm

y (m)	u (m/s)
9E-04	1.900
0.004	2.048
0.007	2.108
0.01	2.031
0.014	1.964
0.018	1.844
0.023	1.644
0.028	1.433
0.033	1.262
0.04	0.855
0.048	0.604
0.055	0.559
0.065	0.421
0.075	0.304
0.085	0.300

x = 60 cm

y (m)	u (m/s)
9E-04	1.535
0.004	1.691
0.009	1.751
0.014	1.686
0.021	1.569
0.031	1.356
0.041	1.153
0.051	0.977
0.061	0.710
0.074	0.525
0.084	0.341
0.099	0.243
0.114	0.216

x = 80 cm

y (m)	u (m/s)
9E-04	1.273
0.006	1.499
0.014	1.478
0.022	1.440
0.032	1.308
0.042	1.207
0.054	0.940
0.066	0.804
0.079	0.654
0.094	0.446
0.109	0.211
0.124	0.117

x = 100 cm

y (m)	u (m/s)
9E-04	1.119
0.006	1.289
0.011	1.325
0.02	1.302
0.03	1.236
0.04	1.151
0.05	1.100
0.06	1.024
0.07	0.849
0.083	0.709
0.095	0.577
0.11	0.373
0.125	0.336
0.14	0.146

x = 120 cm

y (m)	u (m/s)
9E-04	0.942
0.005	1.162
0.013	1.226
0.023	1.189
0.035	1.123
0.048	1.007
0.06	0.931
0.073	0.822
0.088	0.657
0.103	0.569
0.118	0.443
0.133	0.358
0.148	0.195

x = 140 cm

y (m)	u (m/s)
9E-04	0.885
0.006	1.046
0.015	1.130
0.025	1.094
0.04	1.033
0.055	0.946
0.07	0.811
0.085	0.736
0.1	0.607
0.115	0.511
0.13	0.383
0.145	0.258
0.16	0.180

x = 160 cm

y (m)	u (m/s)
9E-04	0.795
0.006	0.941
0.014	0.983
0.029	0.940
0.044	0.850
0.059	0.815
0.074	0.764
0.089	0.678
0.104	0.568
0.134	0.430
0.149	0.373

x = 180 cm

y (m)	u (m/s)
9E-04	0.502
0.011	0.701
0.021	0.764
0.033	0.813
0.046	0.835
0.061	0.748
0.076	0.691

0.091	0.661
0.106	0.610
0.121	0.549
0.136	0.486
0.151	0.385
x = 200 cm	
y (m)	u (m/s)
0.000	0.000
0.001	0.251
0.010	0.383
0.020	0.571
0.030	0.564
0.040	0.576
0.045	0.576
0.050	0.584
0.065	0.558
0.085	0.545
0.105	0.490
0.125	0.404
0.145	0.292
0.165	0.226
Expt. 5*	
x = 20 cm	
y (m)	u (m/s)
9E-04	2.007
0.004	2.522
0.007	2.586
0.010	2.491
0.013	2.230
0.017	1.972
0.022	1.482
0.028	1.028
0.034	0.583
0.041	0.169
x = 40 cm	
y (m)	u (m/s)
9E-04	1.669
0.004	1.975
0.007	2.041
0.012	1.972
0.017	1.835
0.022	1.633
0.029	1.367
0.037	1.102
0.045	0.805
0.052	0.479
0.06	0.373
0.07	0.237
x = 60 cm	
y (m)	u (m/s)
9E-04	1.393
0.004	1.663
0.007	1.699
0.011	1.700
0.018	1.621
0.026	1.455
0.034	1.297
0.041	1.150
0.051	0.957
0.061	0.781
0.076	0.431
0.091	0.164
x = 80 cm	
y (m)	u (m/s)
9E-04	1.279
0.004	1.424
0.007	1.485
0.011	1.485
0.016	1.461
0.021	1.409
0.028	1.333
0.036	1.211
0.046	1.083
0.056	1.006
0.066	0.926
0.076	0.754
0.086	0.612
0.096	0.456
0.106	0.379
0.116	0.205
x = 100 cm	
y (m)	u (m/s)
9E-04	1.008
0.004	1.228
0.007	1.281
0.01	1.329
0.014	1.341
0.018	1.340
0.022	1.311
0.027	1.259
0.033	1.223
0.038	1.178
0.046	1.117
0.056	1.053
0.066	0.897
0.076	0.819
0.086	0.678
0.101	0.509
0.116	0.408
0.131	0.282
0.146	0.182
x = 120 cm	
y (m)	u (m/s)
9E-04	0.874
0.004	1.137
0.008	1.185
0.012	1.193
0.017	1.218
0.022	1.182
0.03	1.125
0.04	1.034
0.052	0.987
0.065	0.898
0.08	0.751
0.095	0.649
0.11	0.574
0.125	0.453
0.14	0.300
0.155	0.238
x = 140 cm	
y (m)	u (m/s)
9E-04	0.757
0.005	0.880
0.009	0.974
0.014	0.997
0.029	0.983
0.044	0.969
0.059	0.860
0.074	0.767
0.089	0.717
0.104	0.674
0.119	0.583
0.134	0.425
0.149	0.348
0.164	0.304
x = 160 cm	
y (m)	u (m/s)
9E-04	0.441
0.004	0.718
0.009	0.767
0.016	0.837
0.026	0.838
0.041	0.829
0.056	0.806
0.071	0.766
0.086	0.710
0.101	0.594
0.121	0.464
0.141	0.288
x = 180 cm	
y (m)	u (m/s)
9E-04	0.076
0.011	0.396
0.021	0.563
0.036	0.618
0.051	0.664
0.061	0.646
0.071	0.599
0.086	0.584
0.106	0.492
0.126	0.374
0.146	0.355
Expt. 6*	
x = 20 cm	
y (m)	u (m/s)
9E-04	1.968
0.004	2.453
0.007	2.567
0.01	2.446
0.013	2.243
0.016	2.014
0.019	1.743
0.022	1.512
0.025	1.249
0.028	1.003
0.031	0.850
0.034	0.634
0.038	0.385
0.042	0.189
x = 40 cm	
y (m)	u (m/s)
9E-04	1.589
0.004	1.965
0.007	2.035
0.01	2.016
0.013	1.966
0.016	1.892
0.02	1.725
0.025	1.544
0.03	1.370
0.035	1.184
0.041	0.969
0.047	0.710
0.053	0.583
0.059	0.434
0.065	0.242
x = 60 cm	
y (m)	u (m/s)
9E-04	1.330
0.004	1.629
0.007	1.682
0.01	1.696
0.013	1.670
0.016	1.618
0.02	1.583
0.025	1.515
0.031	1.393
0.037	1.274
0.043	1.195
0.049	1.059
0.055	0.850
0.061	0.741
0.068	0.691
0.075	0.530
0.082	0.401
0.089	0.235
x = 80 cm	
y (m)	u (m/s)
9E-04	1.192
0.005	1.420
0.009	1.444
0.013	1.452
0.017	1.432
0.022	1.389
0.027	1.324
0.032	1.289
0.04	1.234
0.048	1.102
0.058	1.011
0.068	0.857
0.078	0.671
0.088	0.610
0.098	0.462
0.108	0.417
0.118	0.255
x = 100 cm	
y (m)	u (m/s)
9E-04	0.941
0.006	1.261
0.011	1.307

0.016	1.293	y (m)	u (m/s)	0.12	0.455	0.094	0.676	0.053	0.482
0.021	1.258	9E-04	0.825	0.13	0.327	0.104	0.585	0.061	0.521
0.026	1.260	0.006	1.026	x = 140 cm		0.114	0.527	0.069	0.492
0.031	1.239	0.011	1.118	y (m)	u (m/s)	0.124	0.456	0.08	0.498
0.036	1.208	0.016	1.142	9E-04	0.511	0.134	0.401	0.09	0.448
0.046	1.085	0.022	1.117	0.006	0.600	x = 160 cm		0.1	0.387
0.056	1.047	0.03	1.106	0.012	0.736	y (m)	u (m/s)	0.11	0.371
0.066	0.877	0.04	1.040	0.018	0.860	9E-04	0.083	0.12	0.315
0.076	0.803	0.05	0.989	0.024	0.854	0.005	0.116	0.13	0.312
0.086	0.751	0.06	0.914	0.034	0.840	0.011	0.196	0.14	0.273
0.096	0.625	0.07	0.805	0.044	0.834	0.017	0.200	0.15	0.183
0.106	0.454	0.08	0.766	0.054	0.791	0.023	0.298		
0.116	0.392	0.09	0.716	0.064	0.767	0.03	0.337		
0.126	0.279	0.1	0.554	0.074	0.708	0.038	0.451		
x = 120 cm		0.11	0.527	0.084	0.716	0.045	0.511		

* Wu and Rajaratnam (1995)

3.2 Bed Shear Stress Measurements

Expt. 1

x (m)	τ (N/m^2)
0.00	18.223
0.06	16.353
0.12	12.282
0.20	9.652
0.30	8.112
0.40	5.827
0.60	3.326
0.80	3.023
1.00	2.464
1.20	2.082
1.40	1.884
1.60	0.634
1.80	0.201

Expt. 2

x (m)	τ (N/m^2)
0.00	5.371
0.06	5.000
0.12	3.511
0.20	2.494
0.40	1.634
0.60	0.982
0.80	0.841
1.00	0.660
1.20	0.569
1.40	0.416
1.60	0.321

Expt. 3

x (m)	τ (N/m^2)
0.00	9.704
0.10	9.093
0.20	7.005
0.30	4.902
0.40	4.063
0.50	2.946
0.60	2.270
0.80	1.577
1.00	1.386
1.20	0.987
1.40	0.397
1.60	0.154

Expt. 4

x (m)	τ (N/m^2)
0.00	26.398
0.20	17.798
0.40	12.874
0.60	8.875
0.80	6.404
1.00	5.117
1.20	3.669
1.40	3.275
1.60	2.711
1.80	1.221
2.00	0.398

Expt. 5

x (m)	τ (N/m^2)
0.00	26.398
0.20	14.176
0.40	10.272
0.60	7.488
0.80	6.454
1.00	4.272
1.20	3.338
1.40	2.608
1.60	1.034
1.80	0.055

Expt. 6

x (m)	τ (N/m^2)
0.00	26.398
0.20	13.695
0.40	9.419
0.60	6.910
0.80	5.717
1.00	3.796
1.20	3.019
1.40	1.328
1.60	0.063

3.3 Variation of Velocity Scale, Length Scale, Jet Discharge and Momentum Flux with Distance

Expt. 1

x (m)	u_m (m/s)	b (m)	x/b_o	u_m/U_o	b/b_o	Q/Q_o	M/M_o
0.00	2.50	-	0	1.000	-	1.000	1.000
0.06	2.50	1.25	6	1.000	1.250	1.204	0.992
0.12	2.29	1.66	12	0.916	1.657	1.486	1.000
0.20	1.95	2.26	20	0.778	2.262	1.779	1.000
0.30	1.74	2.71	30	0.697	2.714	1.955	0.987
0.40	1.50	3.73	40	0.599	3.735	2.281	1.000
0.60	1.23	5.35	60	0.491	5.354	2.659	0.965
0.80	1.12	6.90	80	0.446	6.901	3.084	0.968
1.00	0.98	8.67	100	0.392	8.671	3.347	0.964
1.20	0.91	10.06	120	0.363	10.064	3.603	0.949
1.40	0.82	11.50	140	0.327	11.504	3.854	0.891
1.60	0.64	16.07	160	0.255	16.069	3.834	0.758
1.80	0.50	19.27	180	0.201	19.266	3.599	0.558
2.00	0.28	-	200	0.113	-	3.268	0.392

Expt. 2

x (m)	u_m (m/s)	b (m)	x/b_o	u_m/U_o	b/b_o	Q/Q_o	M/M_o
0.00	1.25	-	0	1.000	-	1.000	1.000
0.06	1.25	1.26	6	1.000	1.264	1.231	1.017
0.12	1.13	1.63	12	0.907	1.632	1.496	0.998
0.20	0.96	2.29	20	0.768	2.292	1.767	0.991
0.40	0.76	3.54	40	0.608	3.543	2.179	0.971
0.60	0.59	5.86	60	0.475	5.863	2.790	0.965
0.80	0.54	7.28	80	0.436	7.284	3.176	1.002
1.00	0.49	8.97	100	0.390	8.966	3.418	0.985
1.20	0.45	10.53	120	0.356	10.531	3.663	0.964
1.40	0.39	11.95	140	0.315	11.953	3.758	0.851
1.60	0.32	16.05	160	0.258	16.048	3.693	0.734
2.50	0.25	-	224	0.198	-	1.000	-

Expt. 3

x (m)	u_m (m/s)	b (m)	x/b_o	u_m/U_o	b/b_o	Q/Q_o	M/M_o
0.00	1.750	-	0	1.000	-	1.000	1.000
0.10	1.750	0.014	10	1.000	1.418	1.191	0.974
0.20	1.516	0.020	20	0.866	1.978	1.587	1.010
0.30	1.295	0.027	30	0.740	2.700	1.958	1.002
0.40	1.145	0.035	40	0.654	3.490	2.221	0.964
0.50	0.994	0.045	50	0.568	4.462	2.512	0.982
0.60	0.919	0.056	60	0.525	5.558	2.793	0.980
0.80	0.805	0.072	80	0.460	7.199	3.089	0.949
1.00	0.716	0.085	100	0.409	8.506	3.263	0.931
1.20	0.617	0.112	120	0.352	11.160	3.552	0.861
1.40	0.405	0.176	140	0.231	17.624	3.571	0.703
1.60	0.301	0.250	160	0.172	25.000	2.927	0.427

Expt. 4

x (m)	u_m (m/s)	b (m)	x/b_o	u_m/U_o	b/b_o	Q/Q_o	M/M_o
0.00	2.860	-	0	1.000	-	1.000	1.000
0.20	2.860	0.024	13	1.000	1.587	1.446	0.972
0.40	2.628	0.036	27	0.919	2.408	1.771	0.996
0.60	2.108	0.055	40	0.737	3.643	2.328	0.984
0.80	1.751	0.071	53	0.612	4.719	2.461	0.947
1.00	1.499	0.087	67	0.524	5.804	2.924	0.971
1.20	1.325	0.096	80	0.463	6.396	2.955	0.937
1.40	1.226	0.107	93	0.429	7.109	2.942	0.869
1.60	1.130	0.120	107	0.395	8.031	2.702	0.721
1.80	0.983	0.142	120	0.344	9.467	2.534	0.603
2.00	0.835	0.145	133	0.292	9.697	1.951	0.334

Expt. 5

x (m)	u_m (m/s)	b (m)	x/b_o	u_m/U_o	b/b_o	Q/Q_o	M/M_o
0.00	0.000	-	0	0.000	-	1.000	1.000
0.20	2.586	0.024	13	0.904	1.603	1.411	0.953
0.40	2.041	0.039	27	0.714	2.604	1.834	0.946
0.60	1.700	0.057	40	0.594	3.796	2.161	0.952
0.80	1.485	0.077	53	0.519	5.112	2.516	0.967
1.00	1.341	0.087	67	0.469	5.770	2.732	0.942
1.20	1.218	0.103	80	0.426	6.895	2.769	0.861
1.40	0.997	0.122	93	0.349	8.133	2.717	0.747
1.60	0.838	0.126	107	0.293	8.418	2.217	0.556
1.80	0.664	0.142	120	0.232	9.467	1.724	0.326

Expt. 6

x (m)	u_m (m/s)	b (m)	x/b_o	u_m/U_o	b/b_o	Q/Q_o	M/M_o
0.00	2.86	-	0	1.000	-	1.000	1.000
0.20	2.567	0.024	13	0.898	1.631	1.430	0.948
0.40	2.035	0.039	27	0.712	2.613	1.822	0.955
0.60	1.696	0.055	40	0.593	3.665	2.209	0.979
0.80	1.452	0.075	53	0.508	4.993	2.550	0.970
1.00	1.307	0.092	67	0.457	6.133	2.593	0.910
1.20	1.142	0.099	80	0.399	6.568	2.468	0.771
1.40	0.860	0.129	93	0.301	8.571	2.144	0.538
1.60	0.521	0.141	107	0.182	9.426	1.275	0.180